**Cloud Publications**
International Journal of Advanced Remote Sensing and GIS
2014, Volume 3, Issue 1, pp. 580-591, Article ID Tech-138
ISSN 2320 - 0243

Research Article | Open Access

# Groundwater Quality Mapping using Remote Sensing and GIS – A Case Study at Thuraiyur and Uppiliapuram Block, Tiruchirappalli District, Tamilnadu, India

**Pandian M., and Jeyachandran N.**

Centre for Remote Sensing, Bharathidasan University, Khajamalai Campus, Tiruchirappalli, Tamil Nadu, India

Correspondence should be addressed to Pandian M., mahapandian@hotmail.com

Publication Date: 26 May 2014

Article Link: http://technical.cloud-journals.com/index.php/IJARSG/article/view/Tech-138



**Abstract** Ground water is the major source in India not only for domestic use, but also for agriculture and industrial sector. At present scenario, 85% of domestic water requirement in rural areas, 55% of irrigation water requirement of farmers, 50% of domestic water requirement in urban areas and 50% of process water requirement of industries are met by ground water. Ground water is tapped for the past two decades due to increasing demand of water and mismanagement of water resource. This leads to water scarcity. Ground water level has been falling rapidly day by day. It is very essential to start investigations oriented towards the ground water quantification and qualification which are the basic to form plans for its exploitation, management and conservation. In the present study, the authors have carried out detailed studies by using Survey of India Topographic sheet No (57 O/4) on 1:50,000 scale and Remotely sensed image data from IRS ID (LISS III) (false colour composite (FCC) of bands 321 (rgb), and Landsat 7 ETM (Enhanced Thematic Mapper) (false colour composite (FCC) of bands 457 (RGB), were visually interpreted for tone, texture, size, shape, relief, drainage pattern, vegetation association, and other factors. Field studies were also conducted and corrections were made accordingly to maps of geology, lineaments, and hydromorphogeology. Well inventory, well yield, water table level and groundwater samples were collected during field study. Finally ArcGIS tools were used for analyzing and displaying the spatial data for investigating the ground water quality information.

**Keywords** *Groundwater; Remote Sensing; ETM; Hydromorphogeology; GIS*

## 1. Introduction

Many consequences of unsustainable groundwater use are increasingly evident in several parts of the world due to ever-increasing population, urbanization and intensified human activities, and the main concern is how to maintain sustainable groundwater supply on a long-term basis. In India 90% of the rural and nearly 30% of the urban populations depend on groundwater for meeting their drinking and domestic requirements. Unfortunately, water scarcity and over-exploitation of groundwater resources are common in several parts of India. In view of growing water scarcity and

the adverse impact of global climate change on water resources, it is imperative that groundwater be used efficiently, equitably, and in an ecologically sound manner for both present and future generations so as to ensure sustainable utilization of this vital resource. Groundwater, being a hidden natural resource, is not amenable to direct observations and, hence, exploration or assessment of this resource plays a pivotal role in determining locations of water supply and monitoring wells, and in controlling groundwater pollution. Test drilling and stratigraphy analysis are the most reliable and standard methods for determining the location and thickness of aquifers and other subsurface formations, quality of groundwater, physical/ hydraulic characteristics of aquifers, etc., in a basin. However, such an approach for groundwater investigation is very costly, time-consuming and requires skilled manpower in developing nations. Alternatively, geophysical techniques and fracture-trace analysis can be used for exploring groundwater. In the era of information technology, modern technologies such as remote sensing (RS) and geographic information systems (GIS), coupled with geophysical surveys are very helpful for the evaluation of groundwater resources in a basin. The RS technology, with its advantages of spatial, spectral and temporal availability of data covering large and inaccessible areas within a short time, has emerged as a powerful tool for the assessment, monitoring and management of groundwater resources. The hydro-geologic interpretation of satellite data has been proved to be a valuable survey tool in areas of the world where little geologic and cartographic information exists or is not accurate as well as in inaccessible regions of the world. Since remote sensors cannot detect groundwater directly, the occurrence of groundwater is judged from different surface features derived from satellite imagery such as geomorphology, soil, land use/land cover, topographic slope, surface water bodies, etc., which act as indicators of groundwater existence. In addition, surface geophysical techniques are non-invasive and relatively less time-consuming, and offer cost-effective alternatives for obtaining information about subsurface formations and groundwater [1; 3; 8].

## 2. Study Area

The study area, Thuraiyur and Uppiliapuram block, Tiruchirappalli district, Tamilnadu. Their search work is to make a groundwater potential and groundwater quality assessment using GIS, based on the remote sensing and available physico-chemical data from 76 locations in Thuraiyur and Uppiliapuram block of Tiruchirappalli district. Data being used Landsat ETM data (Path 143 and Row 52); Water quality data from CGWB; Soil Map from NBSS & LUP Nagpur Survey of India Toposheet No 58I/7,8,11,12, latitude $78^{o}$ 28'to $78^{o}$ 45'E, longitude $11^{o}$ 5'to $11^{o}$ 20'N. Software used Arc GIS 9.3.1 surfer 9.0.

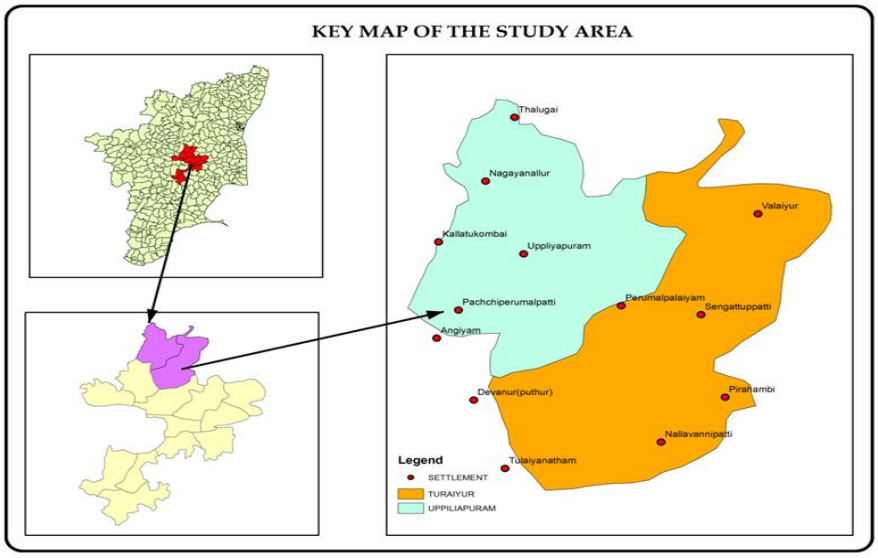


***Figure 1:*** *Study Area*

## 3. Materials and Methods

Acquisition of Remote sensing and Hydrogeochemical data in order to demarcate groundwater potential zones and ground water quality map in the study area, a multi-parametric dataset comprising satellite data, conventional maps and field data were used. Landsat ETM data were used. Toposheets covering the study area were collected from the Survey of India (SOI). The soil map of the study area was collected from the National Bureau of Soil Science and Land Use Planning (NBSS and LUP). The following schematic diagram shows the methodology of the present work [2].

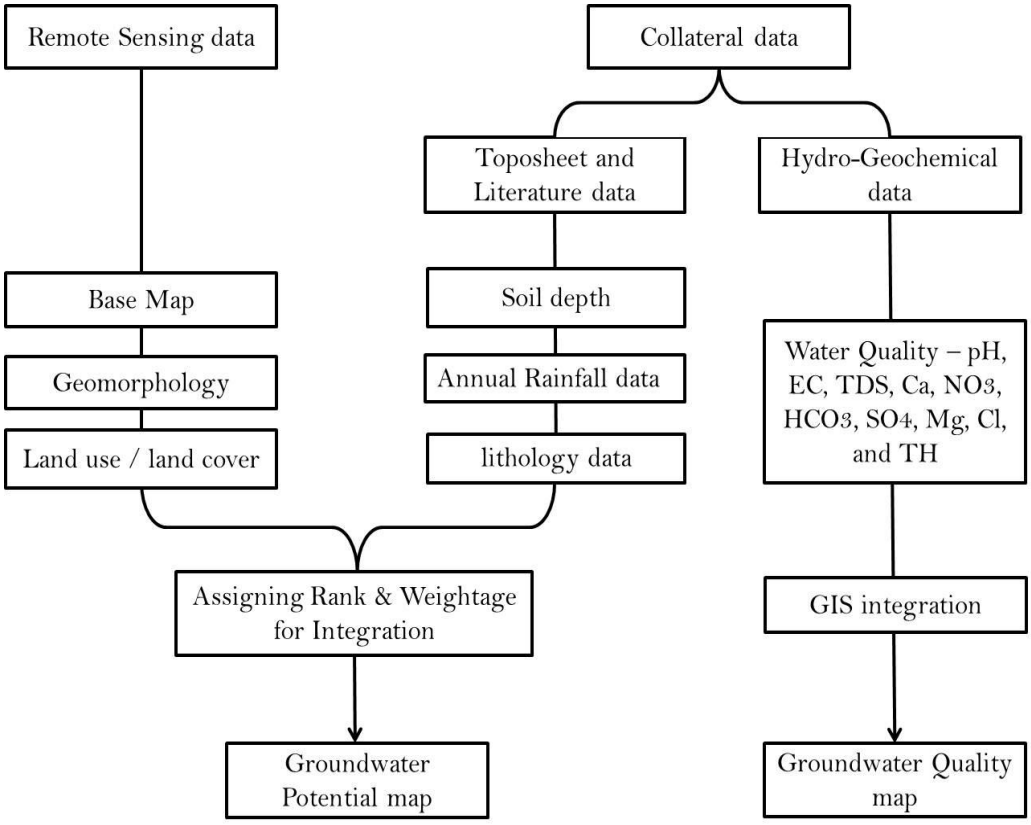


***Figure 2:*** *Flow Chart*

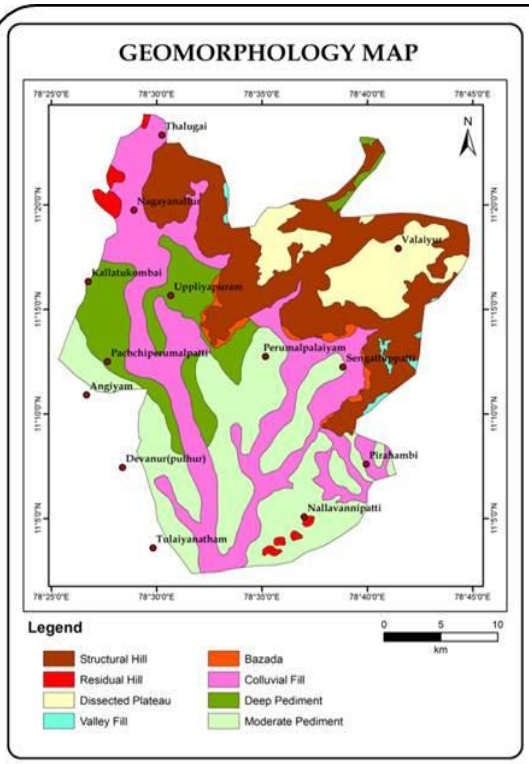


**Figure 3:** *Geomorphology*

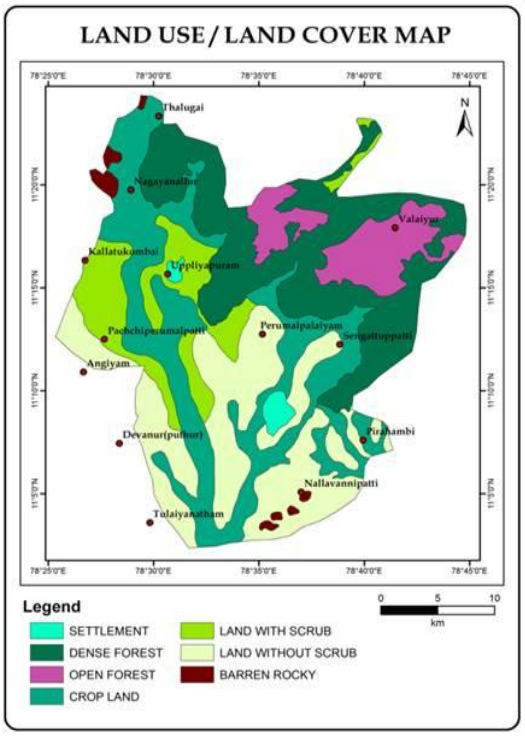


**Figure 4:** *Landuse/Landcover*

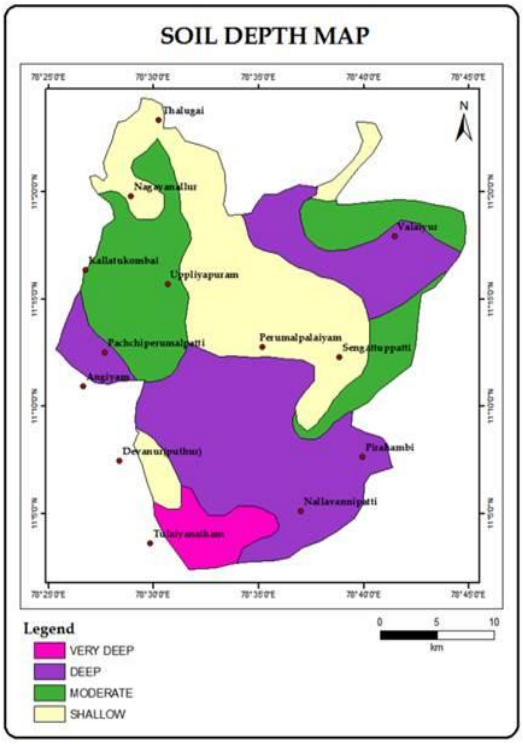


**Figure 5:** *Soil Depth*

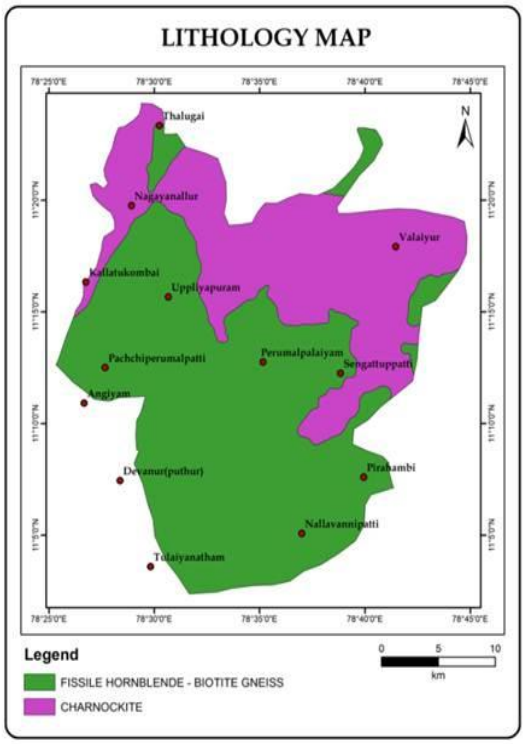


**Figure 6:** *Lithology*

***Figures 3; 4; 5 and 6:*** *Geomorphology; Landuse/ Landcover and Soil Depth and Lithology*

***Table 1:*** *Assigning Weightage and Ranks to the Thematic Layers*

| S. No. | Themes / Weightages | Ranks | | |
|---|---|---|---|---|
| | | 3 | 2 | 1 |
| 1 | Rainfall /5 | Nil | 850 – 900mm (T.W. -10) | 800-850mm (T.W.-8) |
| 2 | Land Use / Land Cover/4 | Crop Land (T.W.- 12) | Open Forest, Land With Scrub, Dense Forest (T.W.- 8) | Barren Rocky, Settlement, Land Without Scrub (T.W.- 4) |
| 3 | Geomorphology /3 | Bazada, Colluvial Fill (T.W.-15) | Dissected Plateau, Deep Pediment, Valley Fill (T.W.-10) | Residual Hill, Structural Hill And Moderate Pediment (T.W.-5) |
| 4 | Soil Depth/2 | Very Deep, Deep (T.W.- 6) | Moderate (T.W.-4) | Shallow (T.W.-2) |
| 5 | Lithology /1 | Nil | Fiddile Hornblende-Biotite Gneiss (T.W.-2) | Charnockite (T.W.-1) |

## 4. Water Quality Mapping

Water samples (13 Nos.) are collected from shallow aquifers for chemical analysis. After chemical analysis, all the results obtained are shown in Table 2 and compare with drinking water set by Bureau of Indian Standard (BIS). The range of chemical parameters in the study area is summarized below [3].

***Table 2:*** *Geochemical Analyzed Data of the Collected Samples in and Around the Study Area*

| Location | E.C | PH | Ca | Mg | Na+k | $HCo_3$ | $Co_3$ | Cl | $No_3$ | $So_4$ | TDS |
|---|---|---|---|---|---|---|---|---|---|---|---|
| Valaiyur | 2260 | 8.3 | 17.84 | 36.47 | 416.7 | 427.09 | 60 | 389.63 | 0 | 96.06 | 1240 |
| Tulaiyanatham | 1810 | 8.4 | 81.36 | 60.78 | 228.93 | 244.05 | 90 | 283.39 | 0 | 192.12 | 1029 |
| Nallavannipatti | 1810 | 8.3 | 100.2 | 36.47 | 152.12 | 1189.7 | 150 | 1098.9 | 61.99 | 398.66 | 3916 |
| Pirahambi | 1700 | 8.5 | 46.09 | 37.69 | 274.97 | 366.08 | 89.71 | 265.86 | 14.03 | 0 | 907 |
| Devanu (puthur) | 1950 | 8.4 | 82.97 | 38.05 | 284.94 | 427.09 | 27 | 319.04 | 9.15 | 129.2 | 1115 |
| Angiyam | 2340 | 8.3 | 17.84 | 85.1 | 455.28 | 305.06 | 120 | 425.38 | 62 | 144.09 | 1376 |
| Sengattupatti | 700 | 8.6 | 56.11 | 26.74 | 273.74 | 488.1 | 90 | 212.69 | 0 | 28.82 | 953 |
| Pachchiperumalpatti | 700 | 8.3 | 18.04 | 21.88 | 98.85 | 170.84 | 30 | 77.98 | 1202 | 28.82 | 370 |
| Perumalpalaiyam | 570 | 707 | 26.05 | 6.08 | 92.84 | 128.13 | 0 | 106.35 | 23.56 | 408 | 321 |
| Uppliyapuram | 450 | 7.2 | 14.03 | 1022 | 99.52 | 57.35 | 0 | 70.54 | 27.95 | 47.55 | 285 |
| Kallatukombai | 2350 | 8.6 | 140.28 | 36.47 | 363.33 | 98.23 | 14.7 | 602.62 | 62 | 144 | 1453 |
| Nagayanallur | 580 | 7.7 | 48.1 | 13.37 | 53.7 | 128 | 0 | 113.43 | 0 | 24.02 | 318 |
| Thalugai | 570 | 707 | 26.05 | 6.08 | 92.84 | 128.13 | 0 | 106.35 | 23.56 | 4.8 | 321 |

***Table 3:*** *Quality of Groundwater based on Electrical Conductivity*

| EC(µS/cm) | Water Class | Representing Wells | Total No of Wells |
|---|---|---|---|
| <250 | Excellent | 9,11 | 2 |
| 250-750 | Good | 1,4,5,6and10 | 5 |
| 750-2000 | Permissible | 2,3,7,8 | 4 |
| 2000-3000 | Doubtful | Nil | Nil |
| >3000 | Unsuitable | Nil | Nil |

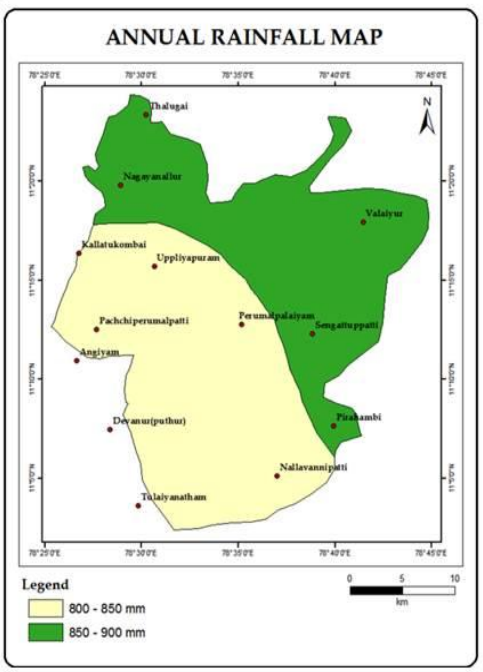


**Figure 7:** *Annual Rainfall*

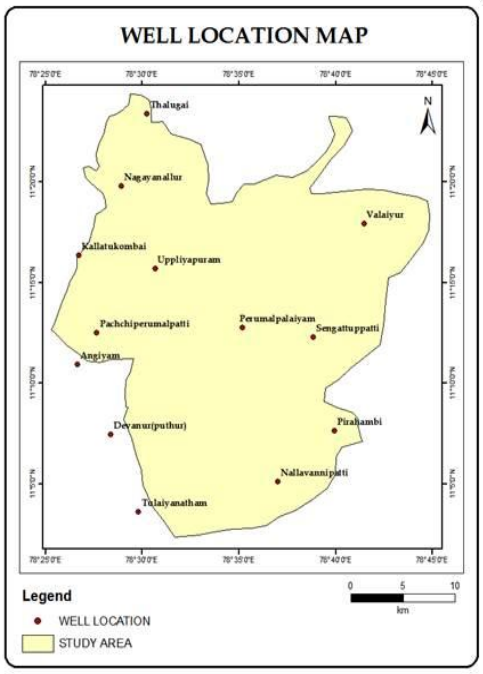


**Figure 8:** *Well Location*

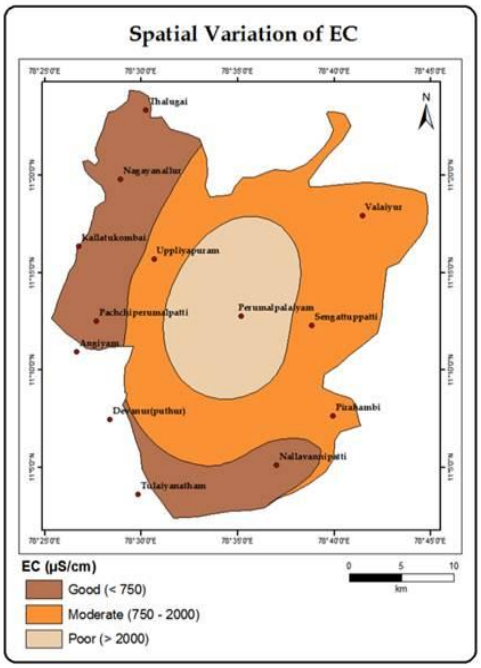


**Figure 9:** *Spatial Variation of EC*

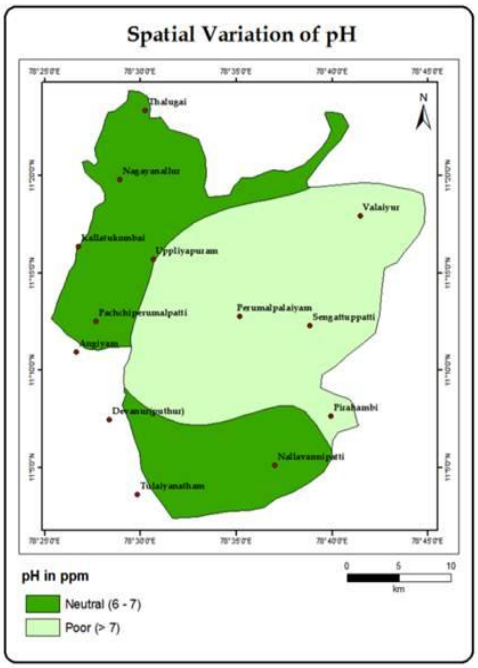


**Figure 10:** *Spatial Variation of pH*

***Figures 7; 8; 9 and 10:*** *Annual Rainfall; Well Location; Spatial Variation of EC and Spatial Variation of P*H

***Table 4:*** *Suitability of Drinking Quality for Calcium Ions*

| Concentration of Ca | Suitable Zone |
|---|---|
| <30ppm | Good |
| 30-120ppm | Moderate |
| >120ppm | Poor |

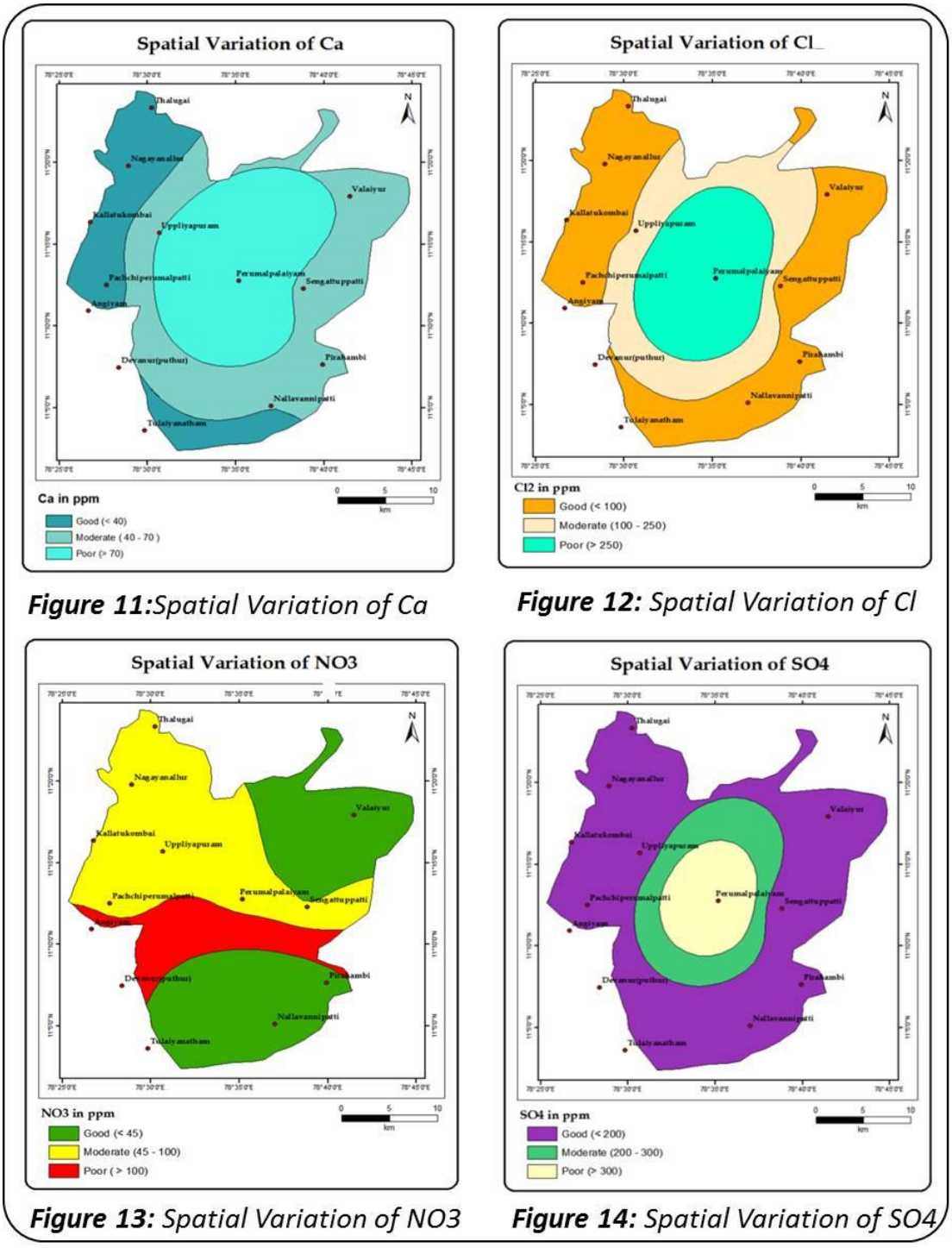


**Figure 11:** *Spatial Variation of Ca*

**Figure 12:** *Spatial Variation of Cl*

**Figure 13:** *Spatial Variation of NO3*

**Figure 14:** *Spatial Variation of SO4*

***Figures 11; 12; 13 and 14:*** *Spatial Variation of Ca; Spatial Variation of Cl; Spatial Variation of NO3and Spatial Variation of SO4*

***Table 5:*** *Suitability of Drinking Quality for Chloride Ions*

| Concentration of Chloride | Suitable Zone |
|---|---|
| <100ppm | Good |
| 100-250ppm | Moderate |
| >250ppm | Poor |

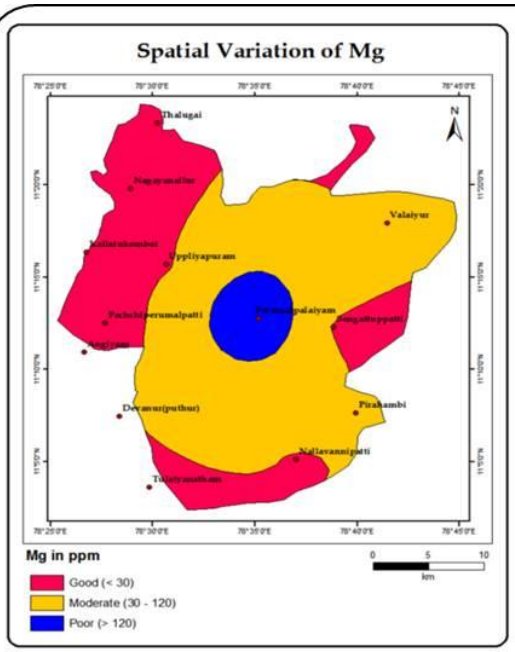


**Figure 15:** *Spatial Variation of Mg*

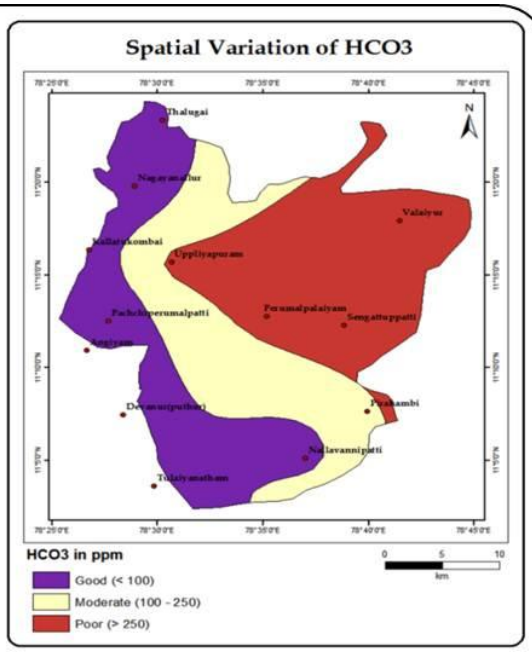


**Figure 16:** *Spatial Variation of HCO3*

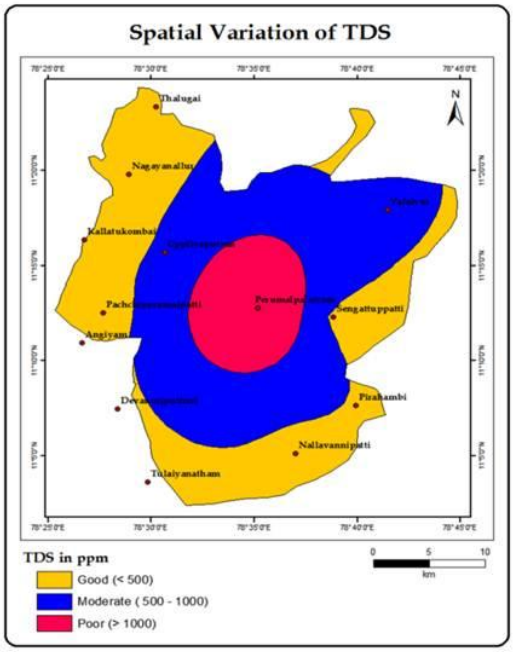


**Figure 17:** *Spatial Variation of TDS*

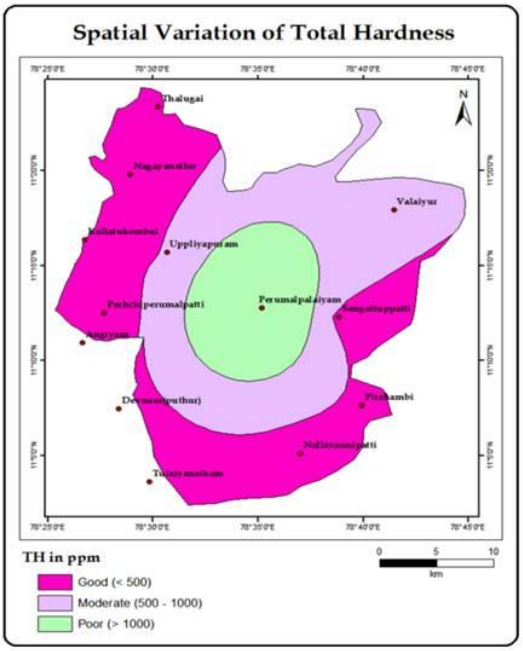


**Figure 18:** *Spatial Variation of Total Hardness*

***Figures 15; 16; 17 and 18:*** *Spatial Variation of Mg; Spatial Variation of HCO3; Spatial Variation of TDS and Spatial Variation of Total Hardness*

***Table 6:*** *Suitability of Drinking Quality for Mg*

| Concentration of Mg | Suitable Zone |
|---|---|
| <30ppm | Good |
| 30-120ppm | Moderate |
| >120ppm | Poor |

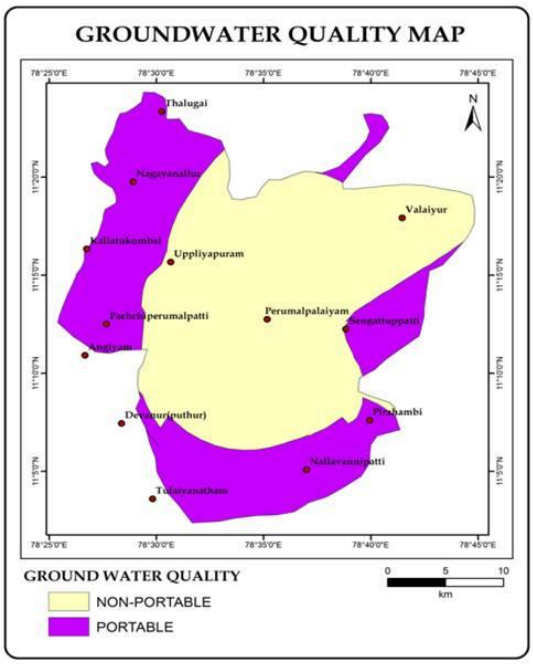


***Figure 19:*** *Groundwater Quality Map*

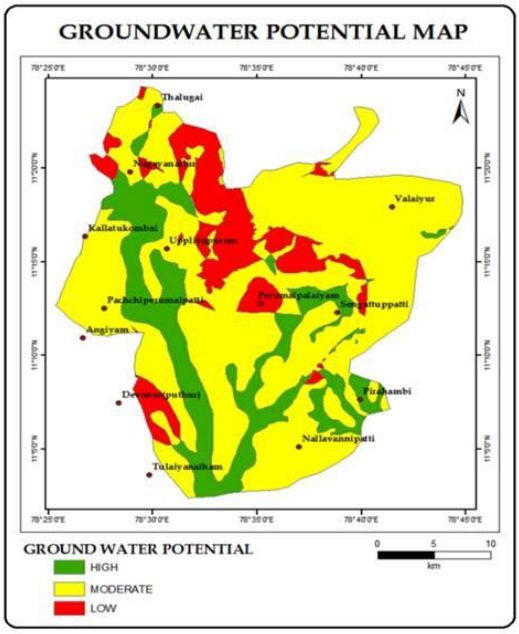


***Figure 20:*** *Groundwater Potential Map*

***Figures 19 and 20:*** *Ground Water Quality Map and Ground Potential Map*

***Table 7:*** *Suitability of Drinking Quality for HCO3*

| Concentration of $HCO_3$ | Suitable Zone |
|---|---|
| <100ppm | Poor |
| 100-250ppm | Moderate |
| >250ppm | Good |

## 5. Results and Discussion

Groundwater quality was essential for drinking and domestic purposes and Ground Water Quality maps are also very useful in assessing the usability of the water for different purposes. Similarly, the spatial distribution of chloride, total hardness, total dissolved solids distribution and nitrate concentrations in study area are generated. Finally, by integrating the entire above maps groundwater quality map was prepared and has been classified.

### Electrical Conductivity (EC)

Electrical Conductivity can be defined as the ability of a solution to conduct an electric current and measured in micro mhos /cm and reported at 25°C. Electrical Conductivity is a function of concentration of ions, charge and ionic mobility Electrical Conductivity is approximately indicative of ionic strength. The EC in the study area ranges from <250 to >3000 and the area has been classified as 5 classes as shown in Table 3 and Figure 9. [4], [5], [6]

### pH

The pH is a numerical scale which express the degree of acidity or alkalinity of solution and represented by the equation $pH= \log 1/aH^{+}= -\log aH^{+}$ or in other words pH may be defined as negative logarithmic of Hydrogen ion concentration. In study area, the overall range of pH in ground water varies from <7.2 to >70 and the area has been classified as 5 classes as shown in Figure 10. [4], [6]

### Calcium (Ca)

The calcium is a major constituent of various rocks. Calcium minerals associated with sodium, aluminum, silica, sulphate, carbonate and Fluoride. Maximum permissible limit for calcium is <40 mg/l. Maximum concentration in ground water is >70 mg/l and the study area has been classified as 5 classes as shown in Table 4 and Figure 11. [4], [5]

### Chloride (Cl)

Chloride is one of the most common constituent in groundwater and very stable as compared to other ions like $SO_4$, $HCO_3$, and $NO_3$ etc. It varies from <100 to >250 and the area has been classified as 5 class as shown in Table 5 and Figure 12.[4], [5], [7]

### Nitrate ($NO_3$)

Nitrate is one of the important pollution related parameter. Nitrate is the end product of the aerobic oxidation of nitrogen compounds. Mainly it is contributed by nitrogenous fertilizers, decomposition of organic matter in the soil, fixation of nitrogen by bacteria etc. Human and animal excreta may also add nitrate to water by bacterial decomposition. For drinking water maximum permissible limit of nitrate is 45 mg/l as per BIS 1991-Rev-2007. In the study area, maximum concentration of Nitrate in ground water is recorded from the Valayur and Nallavannipatti. The range of Nitrate ranges from <45 to >100 and the area has been classified as 5 classes as shown in Figure 13. [5], [7]

### Sulphates ($SO_4$)

Sulphates was classified in to three ranges (0-200 mg/l, 200-300 mg/l and >300 mg/l) and based on these ranges the spatial variation map for sulphates has been obtained and presented in Figure 14. Sulphate of water samples ranges from 0 to 408 mg/l. From the spatial variation map, it was

observed that Northern part of the study area, the sulphates value is in the poor range (>300 mg/l). For the Southern part of the study area, sulphate value is in the moderate and good range. [4], [6]

**Magnesium (Mg)**

Magnesium also is one of the abundant elements in rocks. It causes hardness in water. Magnesium concentration of water samples ranges from 6.08 to 85.1 mg/l. The spatial variation map for magnesium has been obtained and presented in Table 6 and Figure 15. From the spatial variation map, it was observed that Northern part of the study area, the magnesium concentration is in the poor range. The most part of the study area has moderate range and only smaller portion is having good range [5; 6].

**Bicarbonate ($HCO_3$)**

Bicarbonate (HCO3) concentration of water samples ranges from 57.35 to 488.1 mg/l. The spatial variation map for Bicarbonate has been obtained and presented in Table 7 and Figure 16. From the spatial variation map, it was observed that most part of the study area is in moderate and poor range and only smaller portion is having good range [6].

**Total dissolved solids (TDS)**

Total Dissolved Solids is a measure of organic and inorganic substances which are in suspended condition in a liquid. TDS of 500 mg/L or lesser is desirable for drinking water and varies from 50 mg/L to 200 mg/L for industrial use Total dissolved solids in water could be controlled by reverse osmosis, electro dialysis, exchange and solar distillation process (Figure 17) [5; 6; 7].

**Total hardness (TH)**

Total Hardness of water is the capacity to neutralize soap and is mainly caused by carbonates and bicarbonates of calcium, magnesium. In study area, Maximum concentration in ground water is >1000 mg/l and Minimum concentration in ground water is <500 mg/l and the study area has been classified as 5 classes as shown in Figure 18, [5; 6; 7].

## 6. Conclusion

After the overlay of critical parameters for portable and non-portable zones in study area, the final Ground-water Quality Map derived shows only a small region in the North-Western and Southern part of the study area where the groundwater is portable. Similarly, high groundwater potential of the study area also lies in the North-Western and Southern part. This justifies that ground water quality depends on the amount of the natural recharge.

## Acknowledgement

Author is highly thankful to the head of the department, Centre for Remote Sensing, Bharathidasan University, Tiruchirappalli, India for their kind help in providing reference data and valuable suggestion.

## References

[1] K., Jha Madan, Alivia Chowdhury, V.M., Chowdary, and Stefan Peiffer. Groundwater Management and Development by Integrated Remote Sensing and Geographic Information Systems: Prospects and Constraints. Water Resource Manage. 2007. 21; 427-467.

[2] M., Azizur Rahman, Bernd Rusteberg, R.C., Gogu, J.P., Lobo Ferreira, and Martin Sauter. *A New Spatial Multi-Criteria Decision Support Tool for Site Selection for Implementation of Managed Aquifer Recharge*. Journal of Environmental Management. 2012. 99; 61-75.

[3] T., Subramani, S. Krishnan, and P.K., Kumaresan. *Study of Groundwater Quality with GIS Application for Coonoor Taluk in Nilgiri District*. International Journal of Modern Engineering Research. 2012. 2 (3) 586-592.

[4] N., Karthikeyan, A., Saranya, and M.C., Sashikkumar. *Spatial Analysis of Groundwater Quality for Virudhunagar District, Tamil Nadu Using GIS*. International Journal of Remote Sensing & Geoscience. 2013. 2 (4). 23-30.

[5] Environmental Protection Administration, R.O.C., Taiwan. Environmental Water Quality Information. http://wq.epa.gov.tw/WQEPA/Code/Business/Vocabulary.aspx?Languages=en.

[6] P., Balakrishnan, Abdul Saleem and N.D., Mallikarjun. *Groundwater Quality Mapping using Geographic Information System (GIS): A Case Study of Gulbarga City, Karnataka, India*. African Journal of Environmental Science and Technology. 2011. 5 (12) 1069-1084.

[7] A., Thangavelu. *Mapping the Groundwater Quality in Coimbatore city, India based on Physico-Chemical Parameters.* IOSR Journal of Environmental Science, Toxicology and Food Technology 2013. 3 (4) 32-40,

[8] Renji Remesan and R.K., Panda, 2008: *Remote Sensing and GIS Application for Groundwater Quality and Risk Mapping*. The 3rd International Conference on Water Resources and Arid Environments (2008) and the 1st Arab Water Forum.

**Cloud Publications**
International Journal of Advanced Remote Sensing and GIS
2014, Volume 3, Issue 1, pp. 506-515, Article ID Tech-149
ISSN 2320 - 0243

Research Article | Open Access

# Accuracy Analysis of Digital Outcrop Models Obtained from Terrestrial Laser Scanner (TLS)

**Reginaldo Macedônio da Silva[1,2], Maurício Roberto Veronez[1,2], Francisco Manoel Wohnrath Tognoli[1,2], Marcelo Kehl de Souza[1,2] and Leonardo Campos Inocêncio[1,2]**

[1]VizLab - Advanced Visualization Laboratory - Vale do Rio dos Sinos University (UNISINOS), São Leopoldo-RS, Brazil
[2]Graduate Program in Geology, Vale do Rio dos Sinos University (UNISINOS), São Leopoldo-RS, Brazil

Correspondence should be addressed to Reginaldo Macedônio da Silva, macedonios@unisinos.br

Publication Date: 1 April 2014

Article Link: http://technical.cloud-journals.com/index.php/IJARSG/article/view/Tech-149



**Guest Editor-in-Chief: Dr. Maurício Roberto Veronez**
***(This article belongs to the Special Issue "Application of Geotechnology in Urban Planning")***

**Abstract** The analysis, description and interpretation of outcrops are mainly based on field activities from which geoscientists can make observations, descriptions and sketches in field books as well as acquisition of digital photographs and different measurements with compass and other equipaments. The development of geotechnologies in the last decade has been crucial in obtaining geological data directly in digital format and has contributed to save time and to better integrate the various types of data. The aim of this work is to quantify the error positional of outcrop mapped by the LIDAR technique. Data acquisition was performed by the Terrestrial Laser Scanner supported by georeferenced points with a GNSS-GPS receiver. Using field data, it was possible to generate the Digital Outcrop Model (DOM), which permitted accurate visualization, measurement, and interpretation of geological characteristics. It was observed that the differences were not significant between the control data, measured with Total Station, and data acquired with a Terrestrial Laser Scanner (TLS). The interpretations allowed us to model the position of the top of a coal bed using interpolation between two of the outcrop walls. A field validation was performed to ensure the quality of the methodology proposed for this type of analysis. Thus, we conclude that DOMs obtained from TLS have high correlation coefficient in comparison with standard methods (*e.g.* Total Station), supporting high accuracy in this type of models independently of the access conditions in the outcrop.
**Keywords** *Digital Outcrop Models; Geological Interpretation; GPS; Terrestrial Laser Scanner*

## 1. Introduction

The increasing advance of the geotechnologies has generated new opportunities in the field of geosciences. Since the 2000's the use of digital mapping technologies has grown considerably, in

particular the use of Terrestrial Laser Scanner (TLS) (Xu *et al.*, 2001; Bellian *et al.*, 2005; Alfarhan *et al.*, 2008). This technique has substituted the old-fashioned photographic mosaics routinely used for visualization and interpretation of large outcrops and has supported a number of different approaches about digital outcrop modeling. The Laser Scanning is capable to acquire georeferenced 3D data by means of mobile mirror or prisms and a laser beam and provide accurate data for topographic reconstructions and digital models.

The use of TLS in studies of outcrops has expanded in the last years due to the facility and fastness to acquire precise georeferenced data. The topics of interest are quite diverse, including methodological approaches (Bellian *et al.*, 2005; Abellán *et al.,* 2006; Enge *et al*., 2007; Buckley *et al.*, 2008; Ferrari *et al.,* 2012), reservoirs (Pringle *et al.,* 2004; Phelps & Kerans, 2007; Jones *et al.,* 2008; Rotevatn *et al*., 2009; Enge & Howell, 2010; Fabuel-Perez *et al.*, 2009, 2010), fractured rocks (Bellian *et al.,* 2007; Olariu *et al.,* 2008; Jones *et al.,* 2009; Zahm & Hennings, 2009; Souza *et al.,* 2013), erosion rates (Wawrzyniec *et al.,* 2007), synthetic seismic model (Janson *et al.,* 2007), orientation of basaltic lava flows (Nelson *et al.,* 2011) and classification of spectral patterns (Inocencio *et al.,* 2014).

Georeferenced database are close-dependent of the Global Navigation Satellite System (GNSS). The quality of such data are directly related with the positional quality of the tridimensional digital outcrop models generated from data derived from TLS. This fact is particularly important because a digital outcrop model might be a product of different database (e.g., ground penetration radar, terrestrial laser scanner, total station etc). Thus, geoscientists must consider accuracy as a fundamental criteria of integration among different database in order to generate high-quality 3D models. The goal of this study is to quantify the positional error associated with data acquired with TLS and to discuss its impact on the quality of 3D geological models.

## 2. Materials and Methods

The database comprises an outcrop located in the municipality of Mariana Pimentel, Rio Grande do Sul State, southern Brazil. In the Morro do Papaleo crops out a coal-bearing succession of the Rio Bonito Formation, Lower Permian of the Paraná Basin (Figure 1). It is located among the geodetic coordinates (latitude $30^0$18’10”S and $30^0$18’40”S, longitude $51^0$28’20”W and $51^0$38’20”W), datum WGS-84. This outcrop represents an abandoned kaolin quarry with a good exposure of different rocks such as fossiliferous siltstone, carbonaceous siltstone, kaolinic pebbly mudstone and coarse to conglomeratic sandstone (Figure 2).

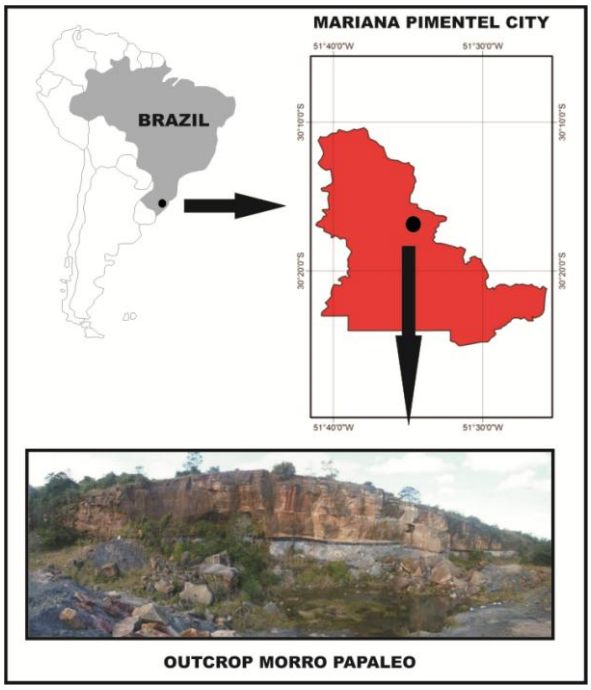


***Figure 1:*** *Location of Study Area*

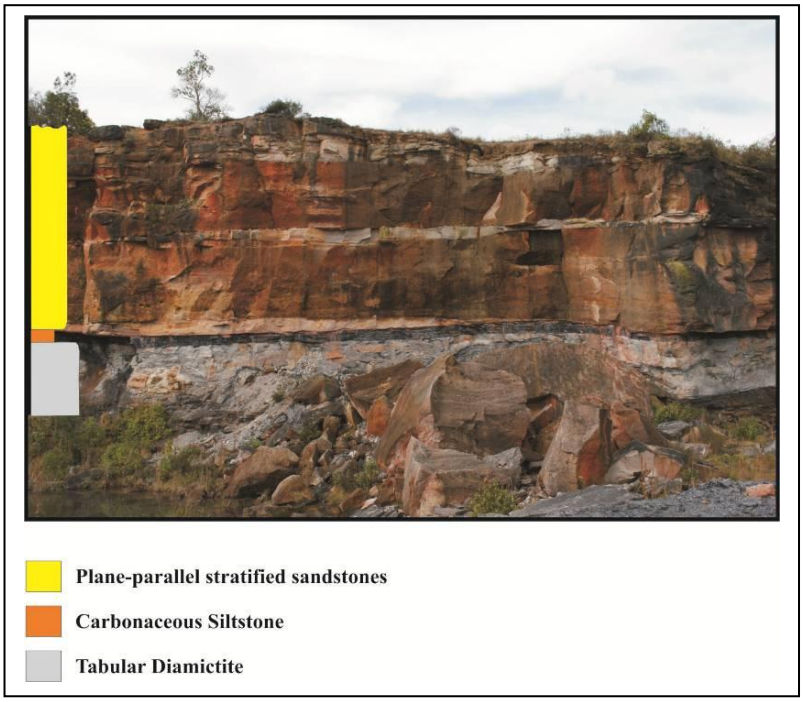


***Figure 2:*** *Part of the West Side of Morro Papaléo Outcrop in Mariana Pimentel City. Note the lithological log*

One geodetic mark which served as support for the georeferencing of the point clouds obtained by TLS was firstly implanted on the top of the outcrop. Two georeferenced points were tracked with Hyper-RTK GNSS equipment using the geodetic mark as a reference. These georeferenced points (Table 1) were used as a support for measuring coordinates of several points in the outcrop using Total Station Leica Viva TS-15 and also to calculate the positional error.

***Table 1:*** *Plane Coordinates in UTM Projection of the Surveying Support Points, Central Meridian at 51°W - SIRGAS2000 Reference System (Geocentric Reference System for the Americas)*

| UTM COORDINATES | | | |
|---|---|---|---|
| POINTS | E (m) | N (m) | Ellipsoidal height – h (m) |
| P1 | 438125,808 | 6646812,115 | 136,775 |
| P2 | 438135,602 | 6646873,338 | 137,468 |

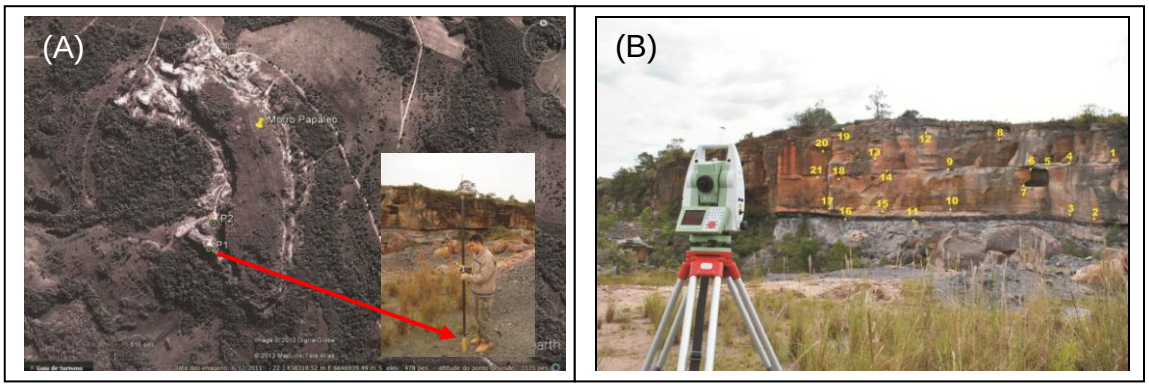


***Figure 3:*** *Geodetic Data Acquisition in the Outcrop. (A) Tracking of points P1 and P2 with the Use of GNSS-RTK. (B) Points Measured with Total Station*

As a criterion for selection of points, color contrast and unequivocal physical characteristics on the outcrop were chosen for measurements. This procedure was crucial to identify the same points in the point cloud. We measured a total of 21 points of the outcrop surface, as illustrated in the Figure 3. These coordinates were used as a parameter for determining the positional quality of the studied outcrop. The TLS Leica Scanner Station C10 was used to acquire the point cloud with a resolution ranging between 2mm and 4cm (Figure 4).

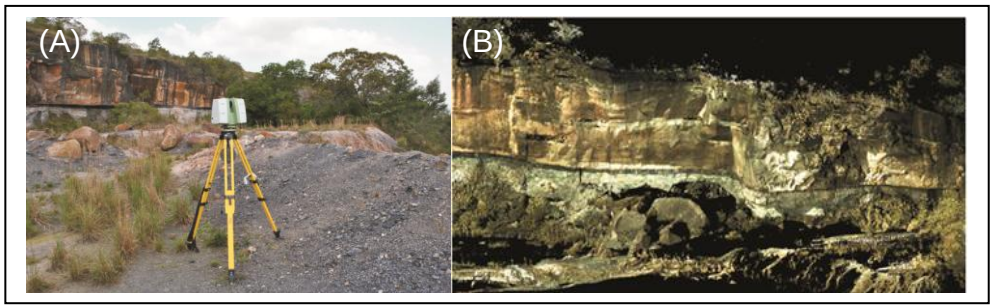


***Figure 4:*** *Digital representation of the Morro Papaléo Outcrop. (A) TLS Leica Scann Station C10. (B) Point cloud acquired with the TLS*

## 4. Results and Discussion

Field data ware processed in the software Cyclone. In this step, a number of unnecessary data were removed of the point cloud, especially vegetation and fallen rocks in front of the outcrop. The field data were georeferenced with 21 control points this process allowed to analyze the positional error. Table 2 shows the results obtained from the coordinates of the 21 points measured with both total station and the TLS.

***Table 2:*** *Plane Coordinates in UTM Projection of the Surveying Support Points, Central Meridian at 51°W - SIRGAS2000 Reference System (Geocentric Reference System for the Americas)*

| | Total Station | | | TLS point cloud | | | ERROR |
|---|---|---|---|---|---|---|---|
| **ID** | **E (m)** | **N (m)** | **h (m)** | **E (m)** | **N (m)** | **h (m)** | **LINEAR (m)** |
| **1** | 438167,809 | 6646815,668 | 145,5616 | 438167,8500 | 6646815,7100 | 145,5600 | 0,059 |
| **2** | 438168,0484 | 6646817,345 | 140,3815 | 438168,0100 | 6646817,3000 | 140,3800 | 0,059 |
| **3** | 438169,1769 | 6646819,65 | 140,8100 | 438169,1800 | 6646819,6300 | 140,7900 | 0,029 |
| **4** | 438169,6515 | 6646818,151 | 147,5608 | 438169,6500 | 6646818,1300 | 147,5600 | 0,021 |
| **5** | 438171,0883 | 6646822,08 | 145,7361 | 438171,0400 | 6646822,0600 | 145,6500 | 0,101 |
| **6** | 438170,5994 | 6646823,688 | 145,6885 | 438170,6500 | 6646823,6400 | 145,6800 | 0,070 |
| **7** | 438170,5904 | 6646824,459 | 144,0473 | 438170,5800 | 6646824,4500 | 144,0400 | 0,015 |
| **8** | 438169,8187 | 6646826,621 | 149,0989 | 438169,8300 | 6646826,5900 | 149,1000 | 0,033 |
| **9** | 438166,8273 | 6646831,059 | 145,8373 | 438166,8100 | 6646831,0700 | 145,8400 | 0,021 |
| **10** | 438167,2303 | 6646831,05 | 141,5598 | 438167,2200 | 6646831,0600 | 141,5400 | 0,024 |
| **11** | 438165,6669 | 6646834,704 | 140,4017 | 438165,6900 | 6646834,6900 | 140,4000 | 0,027 |
| **12** | 438164,475 | 6646832,524 | 149,4687 | 438164,4900 | 6646832,5400 | 149,4700 | 0,022 |
| **13** | 438163,7205 | 6646838,55 | 147,1102 | 438163,7200 | 6646838,5200 | 147,1100 | 0,030 |
| **14** | 438163,8878 | 6646837,122 | 145,3689 | 438163,9400 | 6646837,1200 | 145,3500 | 0,056 |
| **15** | 438164,0082 | 6646837,468 | 141,3125 | 438164,0100 | 6646837,4600 | 141,3100 | 0,009 |
| **16** | 438164,0356 | 6646842,716 | 140,6971 | 438164,0500 | 6646842,7200 | 140,6900 | 0,016 |
| **17** | 438163,2926 | 6646844,521 | 141,7660 | 438163,3000 | 6646844,5100 | 141,7600 | 0,014 |
| **18** | 438163,8241 | 6646843,506 | 145,2157 | 438163,8300 | 6646843,5000 | 145,2200 | 0,009 |
| **19** | 438163,7537 | 6646843,073 | 151,1475 | 438163,6900 | 6646843,1000 | 151,1300 | 0,071 |
| **20** | 438163,6816 | 6646845,826 | 148,7649 | 438163,6600 | 6646845,8300 | 148,7600 | 0,023 |
| **21** | 438164,191 | 6646847,502 | 145,9879 | 438164,2000 | 6646847,4500 | 145,9600 | 0,059 |
| | | | | | **Mean** | | **0,037** |
| | | | | | **Standard Deviation** | | **0,025** |
| | | | | | **Variance** | | **0,001** |

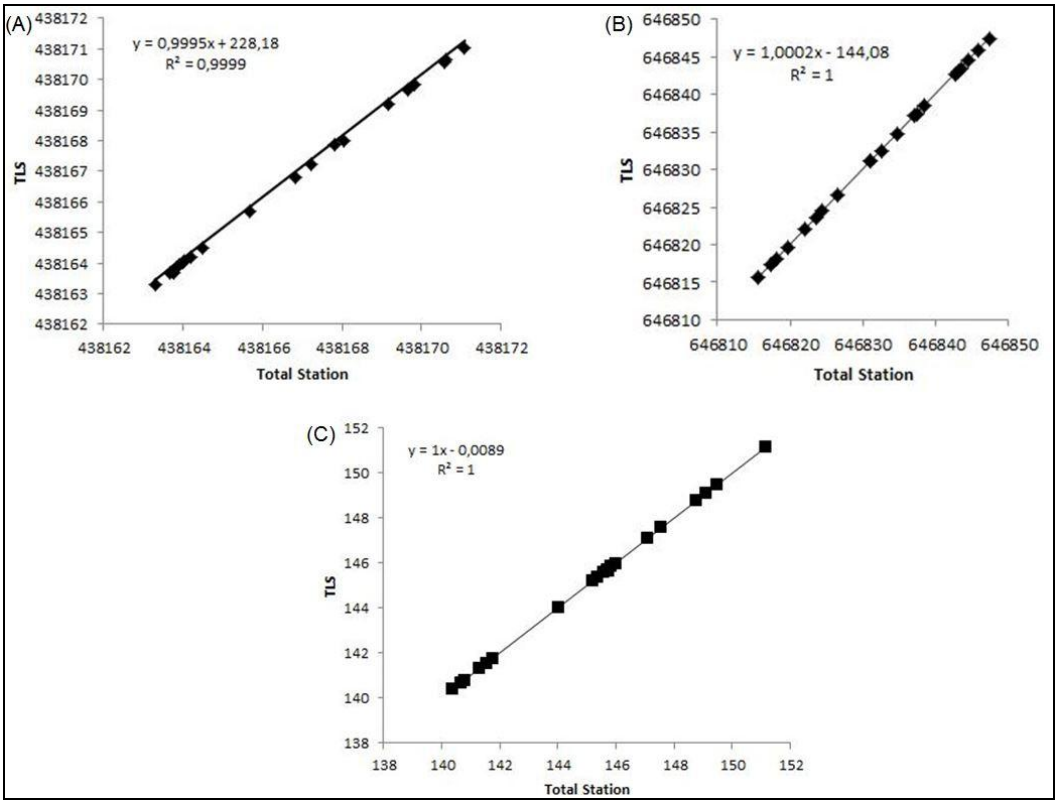


***Figure 5:*** *Comparison between the Measured Coordinates with Total Station and TLS to East (A), North (B), and Height (C)*

The Figure 5 shows a high correlation coefficient if compared with the measured coordinates, East (Figure 5A), North (Figure 5B), Height (Figure 5C) obtained with total station and TLS. The level of reliability of the Chi-Square test was done with 95% and results show that differences were not significative between the control data and those acquired with TLS.

Based on the digital outcrop model (Figure 6), measurements such as height, length and thickness were obtained. Furthermore, it was possible to identify important geological features such as bed geometry, lithology, sedimentary structures, fractures and faults. The field work was fundamental to identify and describe these features before identifying them directly on the point cloud or digital outcrop model.

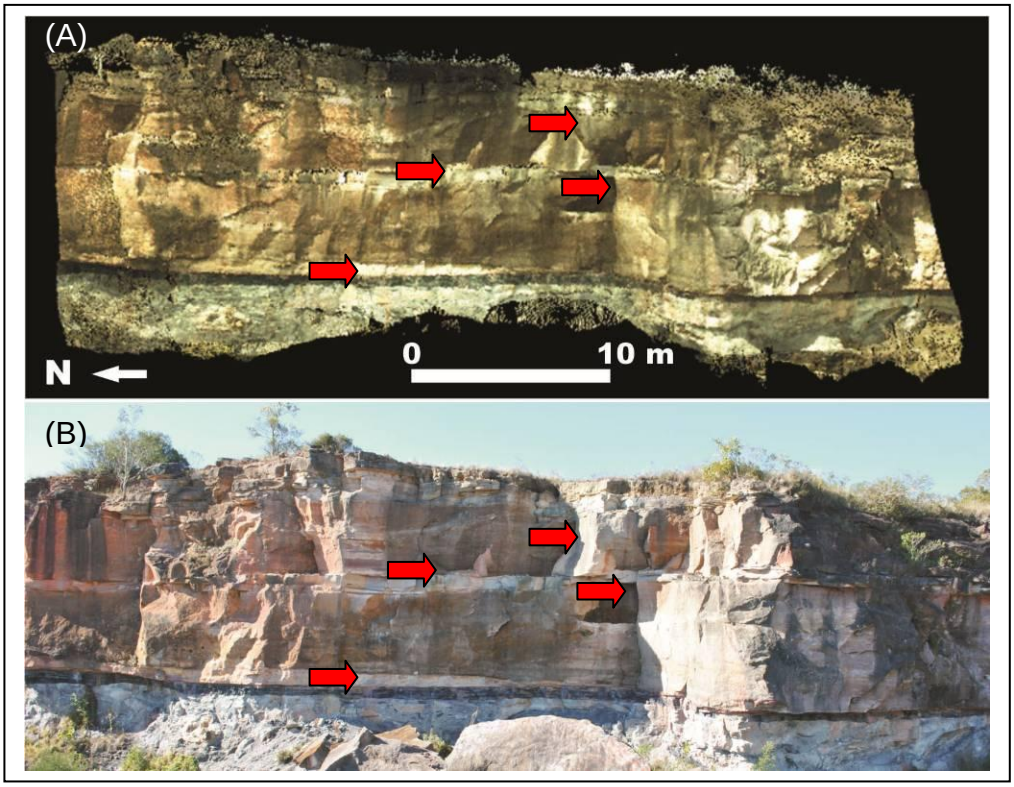


***Figure 6:*** *Digital Outcrop Model. (A) Comparison between Photomosaic and Digital Outcrop Model. (B) Note the Deformation of the Compound Photographs. Red Arrows Show Features Seen in Both Images*

The interpretation based directly on the DOM results in tridimensional geological interpretations expressed by 3D lines (vectors), as shown in the Figure 7. It is possible to observe the top of the carbonaceous siltstone both in digital outcrop models and field information (Figure 7). This vector was used as a parameter to generate the surface model using data obtained from the two faces of the outcrop, the west side (7A) and east side (7B). The coal bed generated by interpolation in modeling softwares (7C and 7D) can be integrated with other data, such as GPR (Ground Penetration Radar), total station, GNSS and other geophysics data.

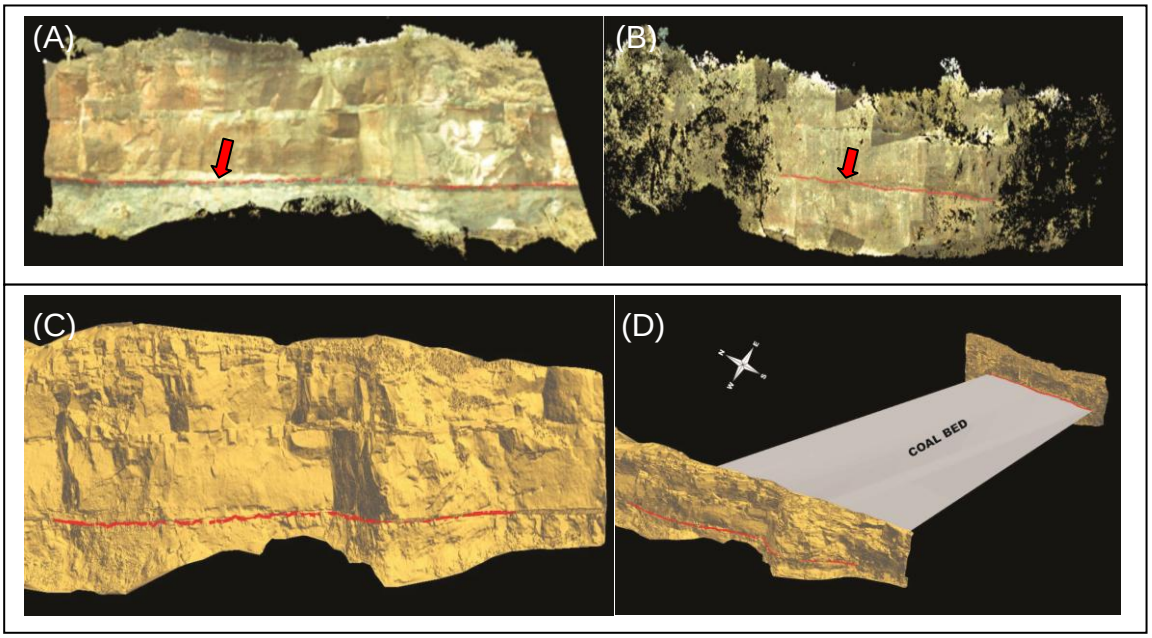


***Figure 7:*** *Coal Bed Seen in both the West and East Side of the Outcrop. (A, B) Point Cloud of the Outcrop with the Interpretation of the Coal Bed on the West Side (A) And East Side (B). (C) The Coal Bed Generated from the Interpretation in Point Cloud. (D) Triangulation of the Point Cloud (West Side) With the Interpretation of the Coal Bed*

## 5. Conclusions

This study has shown that LIDAR is an efficient technique for geological purposes. DOMs are efficient tools for assisting in the fieldwork planning as well as in the subsequent interpretation activities. The high resolution of the point cloud allows measurements of different geological features such as bed thickness, clast size, and fracture orientation. It was determined low values of standard deviation and variance between the control data, measured with Total Station, and those measured with TLS.

The geological interpretations are still limited because most of them are performed in CAD-based conventional softwares for manipulation and processing of the point clouds. Consequently, few tools are available for interpretation purposes and they seldom are developed considering the needs of geological studies. Moreover, large amounts of data have been an additional problem because of the central processing unit (CPU) limitations.

The development of computational routines both in hardware as in software are crucial to optimize the processing and interpretation of DOMs. A multidisciplinary research group involving Geology, Engineering and Graphic Computers has been working to improve data acquisition and processing of 3D visualization techniques, interpretation of geological features, and integration of the interpreted DOMs with different types of modeling software. High accuracy in the data acquisition will warrant the quality of the database that will be integrated with different data (e.g., GPR, total station, seismic etc) in multi-scalar approaches that can range from millimeters to hundred of meters.

## Acknowledgments

The authors would like to thank the Private Graduate Program (PROSUP) of CAPES, Bureau for the Qualification of Higher Education Students. This project was financially supported by FAPERGS, project "Modelos Digitais de Afloramentos como ferramenta na análise e interpretação geológica" (ARD– Process 10/0477-0) and FINEP (Financiadora de Estudos e Projetos), project “MODA-

Modelagem Digital de Afloramentos Usando GPU" (MCT/FINEP– Pré-Sal Cooperativos ICT–Empresas 03/2010).

## References

Abellán, A., Vilaplana, J.M., Martínez, J. *Application of a Long-Range Terrestrial Laser Scanner to a Detailed Rockfall Study at vall de núria (eastern pyrenees, Spain).* Eng Geol. 2006. 88 (3-4) 136-48.

Alfarhan, M., White, L., Tuck, D., Aiken, C. *Laser Rangefinders and ArcGIS Combined with Three-Dimensional Photorealistic Modeling for Mapping Outcrops in the Slick Hills, Oklahoma***.** Geosphere. 2008. 4 (3) 576-587.

Bellian, J.A., et al. *Digital Outcrop Models: Applications of Terrestrial Scanning Lidar Technology in Stratigraphic Modeling*. Journal of Sedimentary Research. 2005. 75; 166-176.

Bellian, J.A., Jennette, D.C., Kerans, C., Gibeaut, J., Andrews, J., Yssldyk, B., and Larue, D., 2002: *3-Dimensional Digital Outcrop Data Collection and Analysus Using Eye-Safe Laser (LIDAR) Technology: American Association of Petroleum Geologists (AAPG).* Search and Discovery Article 40056. http://www.searchanddiscovery.net/documents/beg3d/index.htm.

Buckley, S.J., et al. *Terrestrial Laser Scanning in Geology: Data Acquisition Processing and Accuracy Considerations.* Journal of the Geological Society, London. 2008. 165 (3) 625-638.

Enge, H.D., and Howell, J.A. *Impact of Deltaic Clinothems on Reservoir Performance: Dynamic Studies of Reservoir Analogs from the Ferron Sandstone Member and Panther Tongue, Utah.* AAPG Bulletin, February 1, 2010. 94 (2) 139-161.

Enge, H.D., Buckley, S.J., Rotevatn, A., Howell, J.A. *From Outcrop to Reservoir Simulation Model: Workflow and Procedures*. Geosphere, 2007 3 (6) 469-490.

Fabuel-Perez, I., et al. *A New Approach for Outcrop Characterization and Geostatistical Analysis of a Low-Sinuosity Fluvial-Dominated Succession Using Digital Outcrop Models: Upper Triassic Oukaimeden Sandstone Formation, Central High Atlas, Morocco*. AAPG Bulletin. 2009. 93; 795-827.

Fabuel-Perez, I., Hodgetts, D., Redfern, J. *Integration of Digital Outcrop Models (DOMs) and High Resolution Sedimentology - Workflow and Implications for Geological Modelling: Oukaimeden Sandstone Formation, High Atlas (Morocco).* Petroleum Geoscience, 2010. 16 (2) 133-154.

Ferrari, F., et al. *Visualização e Interpretação de Modelos Digitais de Afloramentos Utilizando Laser Scanner Terrestre.* Geociências (São Paulo. Online). 2012. 31; 79-91.

Inocencio, L.C., Veronez, M.R., Tognoli, F.M.W., Souza, M.K., Silva, R.M., Gonzaga J.R., L., Silveira, C.L.B. *Spectral Pattern Classification in Lidar Data for Rock Identification in Outcrops*. The Scientific World Journal. 2014. 2014; 1-10.

Janson, X., Kerans, C., Bellian, J.A., Fitchen, W. *Three-dimensional Geological and Synthetic Seismic Model of Early Permian Redeposited Basinal Carbonate Deposits, Victorio Canyon, West Texas*. AAPG Bulletin, October 1, 2007; 91 (10) 1405-1436.

Jones, R.R., Mccaffrey, K.J.W., Imber, J., Wightman, R., Smith, S.A.F., Holdsworth, R.E., Clegg, P., Paola, N. De, Healy, D., Wilson, R.W. *Calibration and Validation of Reservoir Models: The Importance*

*of High Resolution, Quantitative Outcrop Analogues*. Geological Society, London, Special Publications, January 1, 2008. 309 (1) 87-98.

Jones, R.R., Kokkalas, S., Mccaffrey, K.J.W. *Quantitative Analysis and Visualization of Nonplanar Fault Surfaces Using Terrestrial Laser Scanning (LIDAR)--The Arkitsa Fault, Central Greece, as a Case Study.* Geosphere. 2009; 5 (6) 465-482.

Nelson, C.E., Jerram, D.A., Hobbs, R.W., Terrington, R., Kessler, H. *Reconstructing Flood Basalt Lava Flows in Three Dimensions Using Terrestrial Laser Scanning*. Geosphere. 2011. 7 (1) 87-96.

Olariu, M.I., Ferguson, J.F., Aiken, C.L.V., Xu, X. *Outcrop Fracture Characterization Using Terrestrial Laser Scanners: Deep-water Jackfork Sandstone at Big Rock Quarry, Arkansas*. Geosphere. 2008. 4 (1) 247-259.

Phelps, R.M., and Kerans, C. *Architectural Characterization and Three-Dimensional Modeling of a Carbonate Channel Levee Complex: Permian San Andres Formation, Last Chance Canyon, New Mexico, U.S.A.* Journal of Sedimentary Research. 2007. 77 (11) 939-964.

Pringle, J.K., et al. *Virtual Geological Outcrops-Fieldwork and Analysis Made Less Exhaustive?* Geology Today. 2004. 20; 67-72.

Rotevatn, A., et al. *Overlapping Faults and Their Effect on Fluid Flow in Different Reservoir Types: A LIDAR-based Outcrop Modeling and Flow Simulation Study.* AAPG Bulletin. 2009. 93; 407-427–11.

Souza, M.K., Veronez, M.R., Tognoli, F.M.W., Silveira J.R., L.G., Inocencio, L.C., Silva, R.M.; Modena, R.C.C. *Terrestrial Laser Scanning: Application for Measuring of Structures Information in Geological Outcrops.* International Journal of Advanced Remote Sensing and GIS. 2013. 2 (1) 260-270.

Wawrzyniec, T.F., McfaddeN, L.D., Ellwein, A.; Meyer, G., Scuderi, L., Mcauliffe, J., Fawcett, P. *Chronotopographic Analysis Directly from Point-Cloud Data: A Method For Detecting Small, Seasonal Hillslope Change, Black Mesa Escarpment, NE Arizona*. Geosphere. 2007. 3 (6) 550-567.

Xu, X., Bhattacharya, J.B., Davies, R.K., Aitken, C.L.V. *Digital Geologic Mapping of the Ferron Sandstone, Muddy Creek, Utah, With GPS an Reflectorless Laser Rangefinders*. GPS Solutions. 2001. 5; 15-23.

Zahm, C.K., and Hennings, P.H. *Complex Fracture Development Related to Stratigraphic Architecture: Challenges for Structural Deformation Prediction, Tensleep Sandstone at the Alcova anticline, Wyoming.* Journal The American Association of Petroleum Geologists. Geological Society of América. Geosphere. 2009. 3 (11) 1427-1446.

**Cloud Publications**
International Journal of Advanced Remote Sensing and GIS
2014, Volume 3, Issue 1, pp. 433-445, Article ID Tech-188
ISSN 2320 - 0243

Cloud Publications

**Research Article** **Open Access**

# Evaluating the Thermal Spatial Distribution Signature for Environmental Management and Vegetation Health Monitoring

**Anibal Gusso[1,5], Mauricio Roberto Veronez[2], Fernanda Robinson[3], Vanessa Roani[3], and Rafaela Christ Da Silva[4]**

[1]Department of Environmental Engineering, University of Vale do Rio dos Sinos (UNISINOS), São Leopoldo-RS, CP275, Brazil
[2]Graduate Program in Geology, University of Vale do Rio dos Sinos (UNISINOS), São Leopoldo-RS, CP275, Brazil
[3]Undergraduate Program in Environmental Management, University of Vale do Rio dos Sinos (UNISINOS), São Leopoldo-RS, CP275, Brazil
[4]Undergraduate Program in Geology, University of Vale do Rio dos Sinos (UNISINOS), São Leopoldo-RS, CP275, Brazil
[5]Center for Remote Sensing and Meteorological Researches, Federal University of Rio Grande do Sul (UFRGS), Porto Alegre, Brazil

Correspondence should be addressed to Anibal Gusso, anibalg@unisinos.br

Publication Date: 21 January 2014

Article Link: http://technical.cloud-journals.com/index.php/IJARSG/article/view/Tech-188



**Guest Editor-in-Chief: Dr. Maurício Roberto Veronez**
***(This article belongs to the Special Issue "Application of Geotechnology in Urban Planning")***

**Abstract** An accurate evaluation of the environment while cities are still growing economically is highly necessary for reliable assessment of ecosystem conditions. This research evaluates a comparison between the pattern of Land Surface Temperature (LST) distribution and Enhanced Vegetation Index 2 (EVI-2) during the summer season as an indicator of development conditions in an Area of Environmental Protection (AEP) that is under pressure from the surrounding urban environment in São Leopoldo, Brazil. A TSDS (Thermal Spatial Distribution Signature) procedure using Thermal infrared (TIR) data obtained from Landsat-5 Thematic Mapper (TM) was applied to evaluate vegetation coverage conditions. A set of six images were used to analyze vegetation development of an AEP between 1985 and 2009. Our analysis suggests that there is a strong relationship between the spatial distributions of LST and its pattern of vegetation coverage conditions. The LST variance exhibited differences in the two studied periods. A decreasing trend was observed in the variance averages from 1.04 to 0.35, which is associated to higher LST occurrences and a wider range of LST distribution in the first period than in the second. The results indicate that the LST distribution variance close to 1.0 can be associated with several level of vegetation degradation. In addition, a variance below 0.5, inside the studied AEP during summertime, is associated with better conditions of vegetation

coverage. In this manner, the TSDS procedure was considered a simple yet effective procedure for the timely diagnosis of AEP.
**Keywords** *Land Surface Temperature; TSDS; Remote Sensing; Area of Environmental Protection; Wetland; Vegetation Coverage*

## 1. Introduction

In the 19th century, civilization initiated a powerful transformation of land use cover without precedent that is strongly related to the high acceleration of industrialization. In recent decades, excessive local demands on environmental systems became global in scope (Brown, 2010). Since then, frequently, the processes of soil occupation have been demonstrated to be in disagreement with the concepts of sustainable development. In this scenario, legislative processes are an indispensable means for defining priority uses of land use (Fragomeni, 2005). However, the monitoring of local environmental problems and planning is perceived, increasingly, as an institutional and governmental tool to introduce the principles of sustainable development. The (SEMMAM Report, 2007) was established by the Administration of the São Leopoldo municipality and University of Vale do Rio dos Sinos to obtain a realistic diagnosis of environmental problems and soil occupation surveys in relevant Areas of Environmental Protection. Environmental problems herein refer to any human-induced damage to the physical environment inside Areas of Environmental Protection (AEP) but mainly indicate degradation of vegetated coverage resulting from estate pressure, unfair waste management or any other unintended side-effect due to human activity.

This research explores the development of a quantitative methodology for the evaluation of the general physical conditions of vegetated land cover based on the monitoring of Land Surface Temperature (LST) distribution in an AEP.

It is well known that shade trees and even small plants for land cover, such as shrubs and grass, help cool the urban environment (Bell et al., 2008). Furthermore, urban green space is always beneficial to mitigating urban heat islands and the evapotranspiration process generated by trees and vegetation in cities can cool the air by using the surrounding urban environment heat from the air to evaporate water (Li et al., 2011). The LST is closely related to the distribution of land use and land cover (LULC) characteristics (Weng et al., 2004; Gusso, 2013) and the physical conditions and properties of the vegetation types and surrounding urban environment are key factors that determine LST distribution (Chudnovsky et al., 2004).

The Landsat series satellites collected several years of data in the thermal spectral band, and the launch of LDCM (Landsat Data Continuity Mission) on February 11th, 2013, carrying the Thermal Infrared Sensor (TIRS), will extend the Land sat data archive from the earlier missions, thus allowing long-term studies (Irons et al., 2012).

A literature review has indicated that thermal satellites with high temporal resolution data are able to generate accurate classifications of environmental parameters (Kogan et al., 2002) and agricultural vegetation conditions (Silva et al., 2005; Gusso, 2013). This paper takes this method a step further, combining applicability of medium spatial resolution satellite imagery and providing an objective methodology for the monitoring of wetlands using thermal satellite data that can be used by decision makers and planners for environmental diagnosis. The objective in this work is to evaluate a LST-based procedure using medium resolution sensor images to obtain an accurate assessment of vegetation conditions in wetland AEPs. TSDS can assist the management of local and regional environmental protected areas further by providing reliable spatial information regarding natural vegetation conditions.

## 2. Study Area

This study covers an AEP of 445 ha located between the following coordinates (51º13'39"W, 29º49'48"S) and (51º01'14"W, 29º38'59"S) as shown in Figure 1. Approximately 72% of the wetlands in the state have an area smaller than 100 ha (Rolon and Maltchick, 2006). São Leopoldo has a total area of 10,700 ha, and it is located in a highly urbanized area in Rio Grande do Sul State (Figure 1). According to the (IBGE, 2012), the city has an estimated population of 193,403 inhabitants, with most of them (98%) located in the urban area.

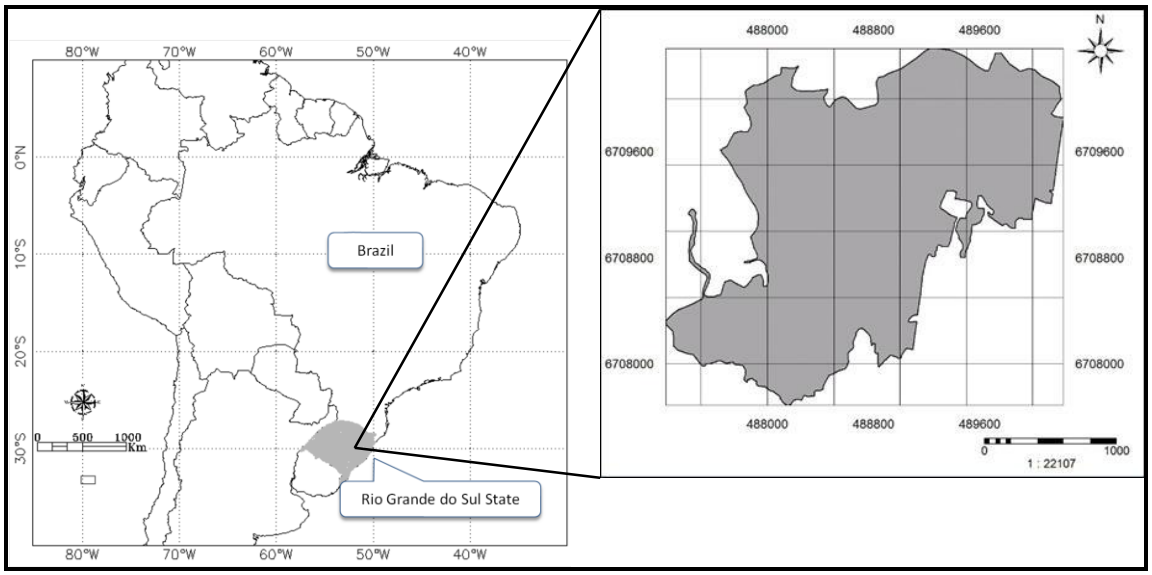


***Figure 1:*** *São Leopoldo Municipality in Rio Grande do Sul State, Brazil, and the AEP*

São Leopoldo municipality is located in the lower part of the basin over an extensive plain configuration, consisting of wetlands and floodplains, and its economy is mainly based on the transformation industry, in particular the processing of leather for shoe manufacturers (Teixeira, 2002).

The municipality has an average elevation of 26 m above sea level and occupies approximately 2.95% of the drainage area at the Rio dos Sinos basin (Nascimento, 2001). A moist subtropical mid-latitude climate prevails in this region with four well-defined seasons and an average annual temperature of 19.7ºC, varying between 12 and 26°C, with an absolute minimum of -0.7°C and a maximum of 40.4°C. The accumulated average rainfall during the year is 1538 mm with no dry period (Köppen, 1948). The studied AEP is covered by Landsat scene path/row 221-081.

## 3. Material and Methods

### 3.1. Satellite Imagery and Data Set

The data sources used for the LST distribution analysis included the

i. Monthly rainfall data of three surrounding meteorological stations, covering the period (October to December), before satellite measurements in January obtained from the Database for Meteorological Research of the Instituto Nacional de Meteorologia (Brazil, 2013). These data were used to validate LST and EVI-2 occurrence.

ii. Climate logical normal of accumulated rainfall from October to December.

iii. Landsat-5 TM images distributed in Brazil by the Instituto Nacional de Pesquisas Espaciais (INPE: www.dgi.inpe.br).

iv. Shuttle Radar Topography Mission (SRTM) data, which was used to generate a slope map with 30 m spatial resolution, according to (Rabus et. al. 2003). These data were used to identify the proper location of wetlands inside the studied area.

v. Wetlands vegetation definition and classification according to IBGE was used to compare and evaluate the obtained results to the present natural vegetation.

vi. Thematic map with vector delineation available for AEP obtained from SEMMAM Project-Report.

vii. Geo location reference images from National Aeronautics and Space Administration-Global Land Survey (http://landsat.gsfc.nasa.gov/).

This is composed by cloud free images and geo-referencing metrics with good quality were used. This latter product was used to provide accurate geo-registration on a per-pixel-basis of the selected images as presented in Table 1.

***Table 1:*** *Selected Landsat-5 TM Imagery for the Monitoring of the Studied Area*

| Year | Path/Row | Data Quality |
|---|---|---|
| | 221/081 | |
| First Period | | |
| 1985 | 6February | Ok |
| 1986 | 24 January | Ok |
| 1991 | 6 January | Ok |
| Second Period | | |
| 2004 | 11 February | Ok |
| 2007 | 2 January | Ok |
| 2009 | 7 January | Ok |

### 3.2. Imagery Calibration and Data Generation

The Landsat-5 TM images were fully calibrated and corrected to generate reflectance and LST values, according to Landsat Calibration Documents (Chander, 2009). Typically, correction includes atmospheric- and sensor-related parameters and thus leads to the derivation of physical units such as reflectance (Schroeder et.al. 2006). Considering the strict sense, full image correction involves both applications of absolute calibration coefficients for sensor and related parameters of atmospheric correction to derive estimates of surface reflectance (Chander, 2009). In this work, the first step was to convert the digital numbers (DN) into radiance and then to reflectance, according to the calibration parameters of (Rabus and Eineder, 2003) and LST (Markham and Barker, 1987). To accurately transform DN into reflectance, the images were also atmospherically corrected according to (Chavez, 1996) for which the data necessary to perform the atmospheric correction in the visible bands 1-5 can be obtained from the image itself (Sobrino et al., 2004). Variations of atmospheric conditions are spatially and temporally significant (Chander et al., 2009). Thus, as quality control, imagery data were submitted to atmospheric condition criteria, and water vapor content, which requires that no image have atmospheric contamination effects above 60 DN in the blue band, was used. Subsequently, reflectance's values from Bands 3 and 4 were used to generate EVI-2 data according to equation 1 from (Jiang et al., 2008).

EVI-2 is a two-band version of EVI that has been developed for sensors without a blue band (Jiang et al., 2008). It retains sensitivity and linearity as EVI for high LAI canopies but does not rely on the

usually poor quality blue band (Liu et al., 2012). According to the EVI-2 approach, although it is computed without a blue band, it remains equivalent to the EVI. In this way, EVI-2 calculation (Equation 1) can be used as an acceptable substitute of EVI over atmospherically corrected pixels (Jiang et al., 2008). NIR and Red are the obtained reflectance in the near-infrared and red bands of Landsat-5 TM, respectively.

$$EVI2 = 2.5 * \frac{NIR - Red}{NIR + 2.4 * Red + 1} \quad \text{Equation (1)}$$

For the thermal analysis, from band 6, after converting the digital numbers (DN) into absolute radiance values, LST is computed from at-satellite brightness temperatures (i.e., blackbody temperature) under the assumption of unity emissivity and using pre-launch calibration constants (Weng et al., 2009; Chander et al., 2009). Then, LST is corrected to non-unity surface emissivity according to the formulation of (Markham and Barker, 1987) which, however, does not perform corrections to atmospheric effects (absorption and emissions along path) because of the difficulty with estimating water vapor content from thermal detection in the mono-window band 6 (Qin et al., 2001; Ma et al., 2010). Further numerous factors need to be quantified to assess LST retrieval from satellite thermal data, including sensor radiometric calibrations (Wukelic et al., 1989), atmospheric correction (Cooper and Asrar, 1989; Chavez, 1996), surface emissivity correction (Allen et al., 2002) and physically driven conditions of land coverage (Gusso, 2013). The conversion of the detected thermal radiation to brightness temperature (Chander et al., 2009) is given by Equation 2. After that, LST is obtained by correcting radiating surface temperature to the surface emissivity (ε), which is the ratio of the thermal energy radiated by the surface to the thermal energy radiated by a blackbody at the same temperature (Allen et al., 2002). The accurate retrieval of LST from thermal spectral bands also requires an accurate estimate of emissivity from surface coverage (Gusso et al., 2007). The emissivity of the surface is controlled by factors such as water content, chemical composition, structure and roughness (Andersen, 1997). The emissivity ε depends on the Leaf Area Index (LAI) as given by Equation 3 (Allen et al., 2002) as follows:

$$LST = \frac{K2}{\ln\left(\frac{\varepsilon_{NB} * K1}{L} + 1\right)} \quad \text{Equation (2)}$$

$$\varepsilon_{NB} = 0.97 + 0.0033 * LAI \quad \text{Equation (3)}$$

Where LST is the emissivity-corrected surface temperature (Kelvin); K1 is the calibration constant 1 (607.76); K2 is the calibration constant 2 (1260.56); L is the blackbody radiance of thermal band 6, and $\varepsilon_{NB}$ is the emissivity factor, which depends on surface coverage type. When LAI<3.0, $\varepsilon_{NB}$ = 0.98 because increased water content in vegetation actually increases emissivity capacity.

### 3.3. TSDS Concept: LST and Biophysical Descriptors

The concept for the AEP assessment procedure developed in this study is referred to as Thermal Spatial Distribution Signature (TSDS). TSDS is based on the concept that vegetation mitigates higher values of LST occurrences; therefore, when considering the same study area, the impervious surface or degraded vegetation coverage leads to a wider range of temperatures distribution.

As a first approach, the vegetation index values of natural vegetation cover were evaluated during the summer season. Leaves and branches reduce the amount of solar radiation that reaches the area below the canopy of a tree or plant. In the summer season, generally 10 to 30 percent of the sun's energy reaches the area below a tree, with most of it being absorbed by leaves and used for photosynthesis and some being reflected back into the atmosphere. During the winter season, the

sunlight transmitted through a tree can be much wider— 10 to 80 percent— because trees losing their leaves allow more sunlight through (Huang et al., 1990).

For any surface material, certain internal properties, such as heat capacity, thermal conductivity and inertia, play important roles in governing the temperature of a body at equilibrium with its surroundings (Campbell, 2002).

Thermal responses for vegetation can be highly varied as a function of the biophysical properties of the vegetation itself as well (Bottyán and Unger, 2003; Weng et al., 2004). These thermal properties vary with soil type and moisture content (Sandholt et al., 2002). Dry, bare, and low-density soils, for example, have been linked to high LST as a result of relatively low thermal inertia (Sandholt et al., 2002). This is because the emissivity of soils, or sparsely vegetated areas, is a function of soil moisture conditions and soil density (Valor and Caselles, 1996; Gusso et.al., 2007).

In surface areas characterized by fraction of vegetation cover, thermal properties from non-vegetated surface areas can largely influence the surrounding measurements of LST through the thermal processes related to direct interception of sunlight. In this way, it is expected that degraded or sparsely vegetated areas are not able to cool the surrounding sensible heat by means evapotranspiration, which leads to a spread in the range of LST occurrences by increasing statistical indicators in terms of the variance of distribution toward higher LST values in a histogram. Thus, in this study, we only used summer season imagery to detect the most pronounced values of LST because of the heating effect associated with surface coverage.

The LST obtained from satellite imagery is, strictly speaking, a measure of “skin” temperature or surface radiometric energy (kinetic) emitted from the land surface and is related to the thermal infrared (TIR) radiation rather than air temperature (Qin et al., 2001; Gusso et al., 2007), which is more commonly used in physiological studies (Sims et al., 2008). The relationship between thermal characteristics of surface and vegetation indices has been extensively documented in the literature (Nemani et al., 1993; Lambin & Ehrlich, 1996; Sandholt et al., 2002; Kogan et al., 2002; Sims et al., 2008; Schelenker and Roberts, 2009; Carmo-Silva et al., 2012; Gusso, 2013).

The LST and vegetation index relationship has been used by (Kogan et al., 2002) for studies of the role of LST in global vegetation coverage dynamics and precipitation. (Lambin and Ehrlich, 1996) have used the relationship to analyze land cover dynamics with correlations between NDVI, brightness temperature and precipitation over the globe, and (Gusso, 2013) used it to evaluate drought impacts over agriculture in Rio Grande do Sul State, Brazil.

Many studies have observed a negative relationship between LST and vegetation indices. In the USA, (Nemani et al., 1993) used remotely sensed data to estimate surface moisture and identified a strong negative relationship between NDVI and LST over all present biomes, including grassland and forests. Given this and considering that temperature is closely related to physiological activities of vegetation cover, LST can be a useful measure of physiological activity of the top canopy leaves when leaf cover is great enough to not be affected by soil surface temperature (Sims et al., 2008).

Typically, simplified models that describe Land Use and Cover Change (LUCC) can provide a link between LST and physical spatial distribution. However, further statistical analysis plays an important role in linking LST to the surface characteristics (Bottyán and Unger, 2003). In addition, LST is highly variable through time, which does not allow comparing absolute values in a simplified conceptual approach. It is important to note that the studied AEPs in the early period (in the 1980s) were under different physically driven conditions of surface and vegetation coverage as compared with the most recent period. In this context, the challenge in the monitoring of environmental system is the same proposed by (Wilson et al., 2003), who searched for evidence of “to what extent changes in vegetation

vigor and surrounding physical conditions detected by remote sensing can actually reveal the natural environment conditions?" Using this conceptual approach, the TSDS procedure consists of the analysis and interpretation of statistical data associated to LUCC that leads to spatial and temporal variation of LST distribution.

### 3.4. Validation of TSDS

In this validation step, to partially determine the LST relation to biophysical descriptors, we compared LST values on a per-pixel-basis to EVI-2 data. The performance of the TSDS was validated by means of the analysis of LST distribution in relation to the vegetation index EVI-2 data. This analysis relates the LST to the vegetated land coverage capacity to perform evapotranspiration processes.

It is well-known that in drought-free years, well-developed vegetation reflects only a small portion of incident solar radiation in the visible band of spectrum because of chlorophyll absorption properties and other plant pigments that absorb sunlight (Gusso and Ducati, 2012). In the NIR, plants reflect much more because of a scattering effect caused by the internal structure and water content of leaves (Jensen, 2007).

By considering the bioclimatic conditions of natural vegetation cover in wetland areas, it became clear that the challenge is to understand what represents vegetation development, as it is expected that soil moisture tends to produce different spectral behavior in the reflectance bands. Background contamination can actually promote imbalance in the relation between bands 3 and band 4 (EVI-2 calculation), potentially leading to decreases in the resulting EVI-2 values under the influence of wetland areas. Thus, we compared accumulated rainfall to the climatologically normal data in the period from October to December, before satellite measurements (in January), to detect river flood occurrences that could result in low EVI-2 values from one period to another, masking the actual vegetation coverage conditions.

Figure 2 presents the rainfall deviation from the climatologically normal inside the AEP in 1984 and 2006, which is related to Landsat images on February 6, 1985 (first period), and January 2, 2007 (second period), respectively, indicating that soil moisture conditions in the different studied periods are similar. Rainfall data also indicate a slight water deficit for both periods (1984 and 2006), which reduces the possibility of a trend effect of background contamination from soil moisture.

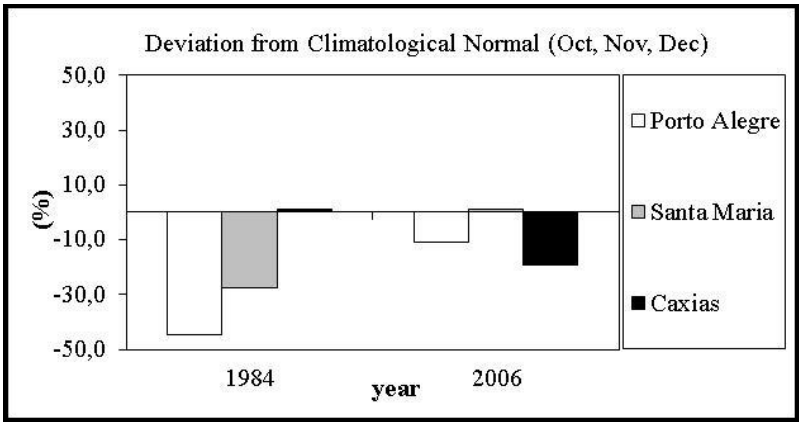


***Figure 2:*** *Deviation from Climatologically Normal of Accumulated Rainfall in the Period October to December of 1984 and 2006*

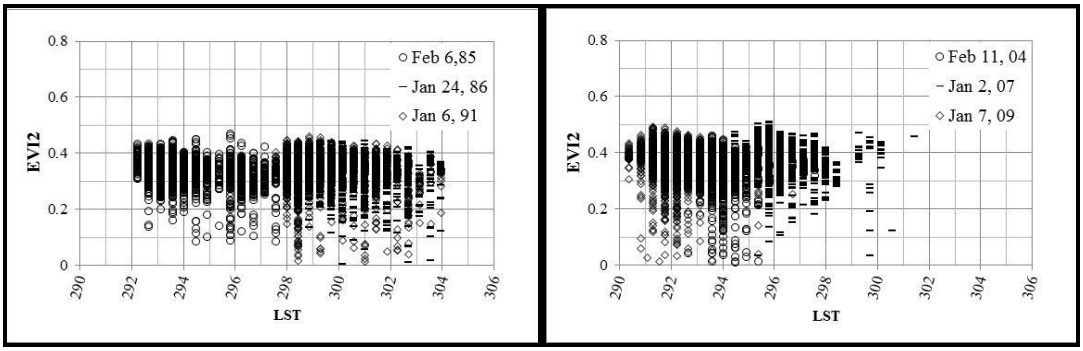


***Figure 3:*** *Scatter gram of LST against EVI-2 from Landsat-5 TM Covering the Area of Environmental Protection in the (A) First Period and (B) Second Period*

## 4. Results and Discussion

The validation step, which compares the obtained results of TSDS estimates with obtained from EVI-2 for natural vegetation cover evaluation, indicated that the two estimates are in good agreement. The distribution of LST and EVI-2 inside the AEP, as shown in Figure 3, revealed a wider range of LST in the first period than in second one. This result is in agreement with the expected inverse mathematical relation based on the physical assumption that LST and EVI-2 data, at a given pixel, vary inversely over time.

Regarding the LST distribution, in the first period, LST is distributed from 292 to 304 Kelvin ($\Delta$LST= 12 K), whereas in the second period, most of the data are between 290 and 298 Kelvin ($\Delta$LST= 8K), as shown. Although daily weather variations of temperatures can actually mask the range of LST distribution, a slight increase in the EVI-2 values reaching 0.5 units is associated with the second period in Figure 3, which also suggests a slight improvement in vegetation health coverage.

Figure 4 presents bar-chart diagrams for the six dates monitored for the AEP between 1985 and 2009. It is also important to note that intra-period variances are in agreement. The variance values were between 1.11 and 0.95, in the first period, and between 0.27 and 0.39 in the second period, as shown in Figure 5. This result indicates that the LST distribution adheres to the evaluated physical concept of vegetation coverage in the two different studied periods. The average of variances obtained from LST distribution analysis is 1.04 in the first period and 0.35 in the second period. It is possible to observe in Figure 4a, 4c and 4e a specific configuration of LST distribution characterized by a bimodal distribution. These results indicate that the LST distribution variance is close to 1.0 in the studied AEP during summertime and can be associated with some level of vegetation degradation. In addition, a variance below 0.5 is associated with better vegetation coverage conditions.

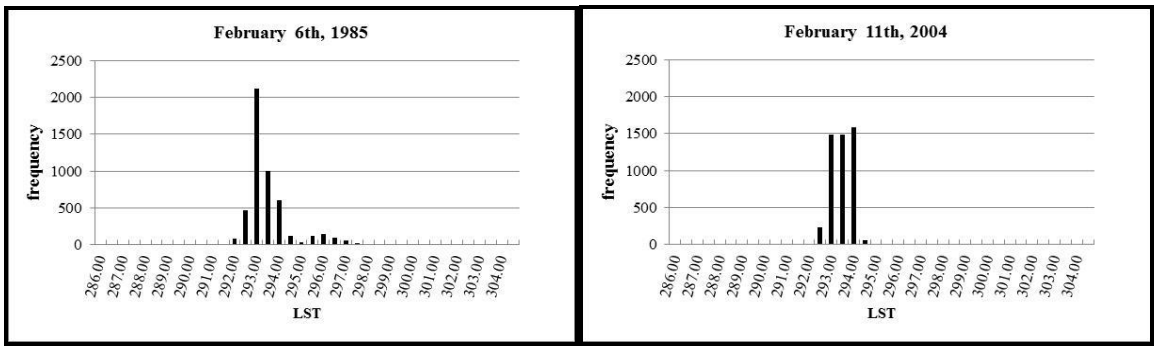

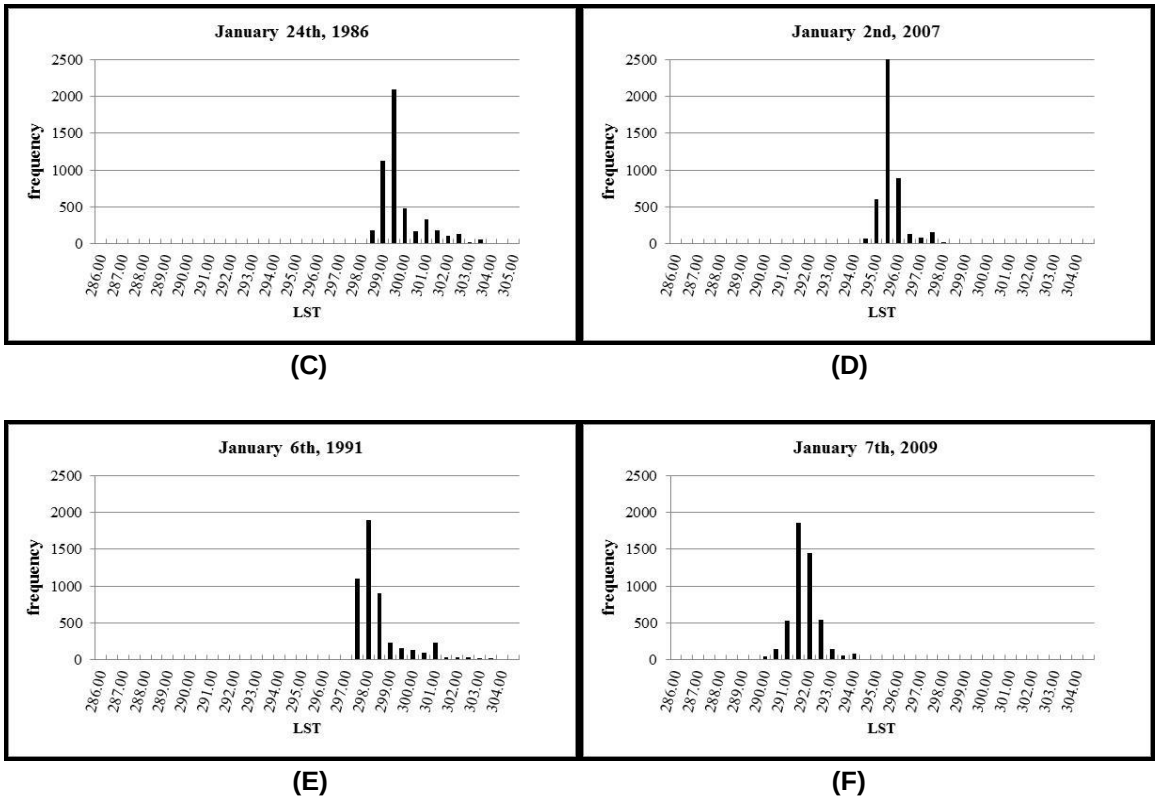


***Figure 4:*** *Estimated LST Distribution in the AEP for the First Period (A, C, E) and the Second Period (B, D, F)*

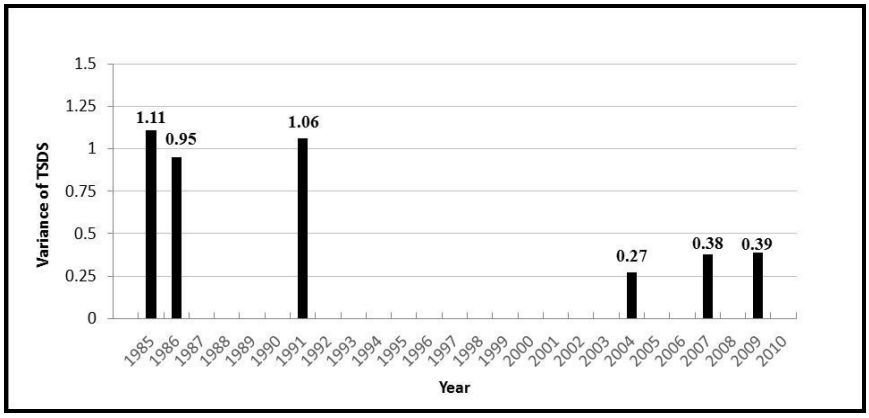


***Figure 5:*** *Variance of LST Distribution inside the AEP in the Two Periods from 1985 to 2009*

## 5. Conclusion

The analysis of vegetation coverage conditions using the LST distribution indicated that in the first period, a wider range of LST is associated with higher fractions of impervious surfaces or degraded vegetation conditions. The results indicate that LST distribution variance below 0.5, inside the studied AEP during summertime, is associated with better vegetation coverage conditions. In addition, a variance close to 1.0 can be associated with some level of vegetation degradation. Thus, the TSDS procedure based on LST distribution analysis was demonstrated to be an objective and consistent methodology for the evaluation of the general vegetation coverage conditions inside Areas of Environmental Protection.

Our results suggest that the vegetation conditions and AEP coverage grew substantially after January 6, 1991. Because of the simplified analysis process used in TSDS and the computation resources needed, it is a timesaving procedure and is less vulnerable to analyst image interpretation skills and subjectivity.

This study also demonstrates that even when not considering geological and pedological questions in the study as related to estate pressure, the municipality urban development appears to be in agreement with the AEPs boundaries even before the implementation of the State Law Code for Environment in Rio Grande do Sul defined on August 3, 2000 (*CódigoEstadual de MeioAmbiente do Estado do Rio Grande do Sul – Lei Estadual nº 11.520, de 3 de agosto de 2000*), as there was no detected expansion toward the studied AEP.

Finally, the TSDS procedure is not species-specific and is therefore useful for application to the analysis of several other vegetation types. We expect that the use of TSDS analysis applied to another ecoregions, under different natural vegetation conditions and climate, can generate good results. In this context, the launch of the LDCM (Landsat Data Continuity Mission) on February 11, 2013, and TSDS can further assist the management of local and regional environmental protected areas by providing reliable spatial information on natural vegetation conditions.

## Acknowledgments

We wish to thank the Vale do Rio dos Sinos University (UNISINOS) and National Aeronautical and Space Administration (NASA) for the Landsat-5 TM data and the Image Processing Division at the Instituto Nacional de Pesquisas Espaciais (INPE) for the Landsat-5 TM data distribution in Brazil. We also wish to specially thank the Conselho Nacional de DesenvolvimentoCientífico e Tecnológico (CNPq) for their support.

## References

Brown L. *World on the Edge*. W. W. Norton & Company. 2010. 325.

Fragomeni A.L.M. *Parques Industriais Ecológicos como Instrumento de Planejamento e Gestão Ambiental Cooperativa.* 2005.

SEMMAM-Report. *Implantação De Um Sistema De Informação Geográfica Como Ferramenta No Diagnóstico Ambiental Do Município De São Leopoldo/RS*. 2007. 14.

Bell R., et al. *Reducing Urban Heat Islands: Compendium of Strategies-Trees and Vegetation.* 2008.

Li J., et al. *Impacts of Landscape Structure on Surface Urban Heat Islands: A Case Study of Shanghai, China.* Remote Sensing of Environment. 2011. 115; 3249-3263.

Weng Q., et al. *Estimation of Land Surface Temperature–Vegetation Abundance Relationship for Urban Heat Island Studies.* Remote Sensing of Environment. 2004. 89; 467-483.

Gusso A. *Integração de Imagens NOAA/AVHRR: Rede de Cooperação para Monitoramento Nacional da Safra de Soja*. Rev. Ceres [Online]. 2013. 60 (2) 194-204.

Chudnovsky A., et al. *Diurnal Thermal Behavior of Selected Urban Objects using Remote Sensing Measurements.* Energy and Buildings. 2004. 36 (11) 1063-1074.

Irons J.R., et al. *The Next Landsat Satellite: the Landsat Data Continuity Mission*. Remote Sensing of Environment. 2012. 122; 11-21.

Kogan F.N. *World Droughts in the New Millennium from AVHRR-based Vegetation Health Indices*. Eos Trans. 2002. 83; 557-564.

Silva B.B., et al. *Balanço De Radiação Em Áreas Irrigadas Utilizando Imagens Landsat 5–TM*. Revista Brasileira de Meteorologia. 2005. 20 (2) 243-252.

Rolon A.S. and Maltchik L. *Environmental Factors as Predictors of Aquatic Macrophyte Richness and Composition in Wetlands of Southern Brazil*. Hydrobiologia. 2006. 556; 221-231.

Nascimento C.E.G. *Verificação De Critérios Técnicos Para Seleção De Áreas Aptas A Disposição Final De Resíduos Sólidos Urbanos No Município De São Leopoldo–RS.* 2001.

Teixeira M.B. *Plano Ambiental De São Leopoldo: Estruturas Institucionais, Legislação, Planejamento E Proteção Ambiental*. MTC. 2002. 1; 128.

Köppen W. *Climatologia: con un Estúdio de los Climas de la Tierra*. Fondo de Cultura Econômica. 1948. 466.

IBGE–Instituto Brasileiro de Geografia e Estatística. http://www.ibge.gov.br/english/ (accessed on July 2nd, 2012).

Rabus B.M. and Eineder A.R.R. *The Shuttle Radar Topography Mission—a New Class of Digital Elevation Models Acquired by Space Borne Radar*. Photogram. Eng. Remote Sensing. 2003. 57; 241-262.

Chander G., et al. *Summary of Current Radiometric Calibration Coefficients for Landsat MSS, TM, ETM+, and EO-1 ALI Sensors.* Remote Sens. Environ. 2009. 113; 893-903.

Schroeder et al. *Radiometric Correction of Multi-Temporal Landsat Data for Characterization of Early Successional Forest Patterns in Western Oregon.* Remote Sensing of Environment. 2006. 103; 16-26.

Markham B.L. and Barker J.L. *Thematic Mapper Band pass Solar Exoatmospherical Irradiances.* Int. Journal of Remote Sensing. 1987. 8 (3) 517-523.

Chavez Jr. P.S. *Image-Based Atmospheric Correction—Revisited and Improved.* Photogram. Eng. Remote Sensing. 1996. 62; 1025-1036.

Sobrino J.A., et al. *Land Surface Temperature Retrieval from LANDSAT TM 5.* Remote Sensing of Environment. 2004. 90 (4) 434-440.

Jiang Z., et al. *Development of a Two-Band Enhanced Vegetation Index without a Blue Band*. Remote Sensing of Environment. 2008. 112; 3833-3845.

Liu et al. *Assessment of Vegetation Indices for Regional Crop Green LAI Estimation from Landsat Images over Multiple Growing Seasons.* Remote Sensing of Environment. 2012. 123; 347-358.

Weng Qi. *Thermal Infrared Remote Sensing for Urban Climate and Environmental Studies: Methods, Applications, and Trends.* ISPRS Journal of Photogrammetric and Remote Sensing. 2009. 64; 335-344.

Qin Z., et al. *A Mono-Window Algorithm for Retrieving Land Surface Temperature from Landsat TM Data and its Application to the Israel–Egypt Border Region.* International Journal of Remote Sensing. 2001. 22 (18) 3719-3746.

Ma Y., et al. *Coupling Urbanization Analyses for Studying Urban Thermal Environment and its Interplay with Biophysical Parameters Based on TM/ETM+ Imagery.* 2010.

Wukelic G.E., et al. *Radiometric Calibration of Landsat Thematic Mapper Thermal Band.* Remote Sensing of Environment. 1989. 28; 339-347.

Cooper D.I. and Asrar G. *Evaluating Atmospheric Correction Models for Retrieving Surface Temperatures from the AVHRR Over A Tall Grass Prairie*. Remote Sensing of Environment. 1989. 27; 93-102.

Allen R.G., et al. *Surface Energy Balance Algorithms for Land (SEBAL)*. Advanced Training and User´s Manual. 2002. 1; 97.

Gusso A., et al. *Mapeamento Da Temperatura Da Superfície Terrestre Com Uso Do Sensor NOAA/AVHRR.* Pesquisa Agropecuária Brasileira. 2007. 42; 231-237.

Andersen H.S. *Land Surface Temperature Estimation Based on NOAA-AVHRR Data during the HAPEX-Sahel Experiment*. Journal of Hydrology. 1997. 189; 788-814.

Huang J., et al. *The Wind-Shielding and Shading Effects of Trees on Residential Heating and Cooling Requirements. ASHRAE Winter Meeting*. American Society of Heating, Refrigerating and Air-Conditioning Engineers. 1990.

Campbell J.B. *Introduction to Remote Sensing*. The Guilford Press. 2002. 3.

Bottyán Z. and Unger J. *A Multiple Linear Statistical Model for Estimating the Mean Maximum Urban Heat Island.* Theoretical and Applied Climatology. 2003. 75 (3-4) 233-243.

Sandholt L., et al. *A Simple Interpretation of the Surface Temperature/Vegetation Index Space for Assessment of Surface Moisture Status.* Remote Sensing of Environment. 2002. 79; 213-224.

Valor E. and Cassells V. *Mapping Land Surface Emissivity from NDVI: Application to European, African, and South American Areas.* Remote Sensing of Environment. 1996. 57 (3) 167-184.

Sims D.A., et al. *A New Model of Gross Primary Productivity for North American Ecosystems Based Solely on the Enhanced Vegetation Index and Land Surface Temperature from MODIS*. Remote Sensing of Environment. 2008. 112; 1633-1646.

Nemani R., et al. *Developing Satellite-Derived Estimates of Surface Moisture Status*. Journal of Applied Meteorology. 1993. 32; 548-557.

Lambin E.F. and Ehrlich D. *Combining Vegetation Indices and Surface Temperature for Land-Cover Mapping at Broad Spatial Scales*. International Journal of Remote Sensing. 1995. 16; 573-579.

Schlenker W. and Roberts M. *Nonlinear Temperature Effects Indicate Severe Damages to U.S. Crop Yields Under Climate Change.* Proceedings of the National Academy of Sciences. 2009. 106; 15594-15598.

Carmo-Silva A.E., et al. *Decreased $CO_2$ Availability and Inactivation of Rubisco Limit Photosynthesis in Cotton Plants under Heat and Drought Stress in the Field*. Environmental and Experimental Botany. 2012. 83; 1-11.

Wilson et al. *Evaluating Environmental Influences of Zoning in Urban Ecosystems with Remote Sensing.* Remote Sensing of Environment. 2003. 86; 303-321.

Gusso and Ducati. *Algorithm for Soybean Classification Using Medium Resolution Satellite Images.* Remote Sens. 2012. 4; 3127-3142.

Jensen J.R. *Remote Sensing of the Environment: An Earth Resource Perspective*. 2007. 592.

National Aeronautics and Space Administration–NASA. *Landsat Data*. http://landsat.gsfc.nasa.gov/ (accessed on 5 December 2011).

Brazil, Banco de Dados Meteorológicos para Ensino e Pesquisa do Instituto Nacional de Meteorologia (BDMEP-INMET). http://www.inmet.gov.br/portal/index.php?r=bdm ep/bdmep (accessed on 30th March 2013).

**Cloud Publications**
International Journal of Advanced Remote Sensing and GIS
2014, Volume 3, Issue 1, pp. 476-485, Article ID Tech-209
ISSN 2320 - 0243

Case Study | Open Access

# Application of Geographical Information System in Urban Management and Planning: A Case Study of Kulgaon-Badlapur, Dist-Thane, Maharashtra

**Syed Aasif Farooqi and Sohieb Gazali**

Department of Environment and Remote Sensing, Srinagar, Jammu & Kashmir, India

Correspondence should be addressed to Syed Aasif Farooqi, s.aasif723@gmail.com

Publication Date: 15 February 2014

Article Link: http://technical.cloud-journals.com/index.php/IJARSG/article/view/Tech-209



**Abstract** The project enclosed, is about GIS application in urban management and planning. The client for this project is KBMC (Kulgaon– Badlapur Municipal Council). Urban Planning is a technical and political process concerned with the control of the use of land and design of the urban environment, including transportation networks, to guide and ensure the orderly development of settlements and communities. Project will provide the new updated and more correct data of the town with the help of GIS. This project will also provide the new improved base maps of the town, which will consist of every feature like footprints of the buildings, the project will definitely help in improving the infrastructure of the city. The project has completed using CAD & GIS software like AutoCAD, Arc GIS and Arc View.

**Keywords** *KBMC; Development; GIS; Urban Planning; Software's; Municipal Council*

## 1. Introduction

Geographical Information System (GIS) is defined as computer system that can hold and use different data describing happening on the earth's surface. Its is set of tools for collecting storing, retrieving, transforming and displaying spatial data from the real world for a particular set of purposes. When applied in a municipal context GIS becomes Municipal Information system (MIS) and used as planning tool in urban planning and development control. Applying GIS based municipal information tools can lead to solution of these data management problems. GIS does not work in isolation rather it combines hardware, software and people together to achieve its performance [1] (*Arnof, 1995*).

Geographic Information System (GIS) technology has found its way into many Corporations/Councils across the world. Many local governments now rely on GIS technology as a support tool to design development plans to make important decisions. The nature of GIS and its overwhelming use and reliance on computer technology can run contrary to the data, skills, and training found in many municipalities. In the light of tremendous pressure of rapid development in the urban areas, many

municipal authorities generate large urban dataset of urban information from development planning applications. Irrespective of development control pressure and the fluid nature in which planning applications are submitted at the municipal authorities, data has to be maintained and managed well all the times to allow for an efficient urban development control process [7].

## 2. Study Area of the Project

The study area of the project is small 12 towns of Kulgaon-Badlapur Municipal Council **(**KBMC) in Thane district near Mumbai city. KBMC in its jurisdiction has the area of about 35.68 sq. Kms [(13.78 sq mile), elevation 44 m (144 ft)], which is split into 34 wards & 13 Operating Zones. This project involves extensive field survey and data collection. Project is done for mapping and calculating legal and illegal properties in the city, for calculating the total tax earn from those properties, planning for development of the transport, now and in the future, management and planning of the town.

Badlapur was a village which turned into a new developed town. It is also known as Kulgaon – Badlapur. It is only 5 kms from the railway station. People from congested areas of nearby cities tends to move toward badlapur town as it provides pleasant environment, beautiful location, affordable real estate price, beautiful landscape and quiet neighborhood along with a proximity to Mumbai by local trains. Now Badlapur city encompasses the old Badlapur village, Kulgaon, Manjarli, Belavali, Katrap and many other small villages.

### 2.1. Government and Politics

*Badlapur* name was formed by combination of two name's 'Badla' and 'pur'. Balda in Marathi means 'change' and 'pur' is suffix commonly used to name the village or town. Badlapur name was formed because it was a travel route from Konkan to Gujrat via Surat. The town was famous for its rich horse breeds and Shivaji Maharaj and his warriors used to change their horses at the town in anticipation of the difficult climb through the Konkan area. Badlapur was recognized as a town for the first time in 1971 as a municipal town in the Ulhasnagar Tehsil. Badlapur was surrounded by twelve villages: - Badlapurgaon, Shirgaon, Katrap, Jeweli, Kharvai, Sonivali, Arenjad, Valivali, Manjarli, Mankivali, Kulgaon, and Belavali.

Badlapur Municipal Council was a separate gram panchayat before 1983 and became a Municipal Corporation on 2nd October 1983 as part of Kalyan-Dombivali-Ambernath and Badlapur Municipal Corporation. It was found that the formation of the corporation was geographically improper and many questions were raised by public personalities and objected its formation as Municipal Corporation. Thus, in 1992 Badlapur and Ambernath Municipal Councils were formed. Badlapur Municipal Council was rewarded by "Presidential Silver Medal of India" for its commendable efforts and achievements. Badlapur Municipal Council was declared as B-class municipal council based on the population which was approximately 52,000 as per 1991 census [2].

### 2.2. Collaborative-Strategic-Goal-Oriented-Programming (CoSGOP)

CoSGOP has been developed as a logical framework to help develop the community based approach for tackling urban distress and to support large-scale regeneration. It has been applied in European cross-border policy programming, as well as in local and regional development programs with good results. It offers a decision-making process which is inclusive, competitive and sustainable. As such it promotes collaboration between stakeholders and their integration into a strategy which is cross-cutting and allows partners to develop consensus on the scope and distribution of urban distress and program of area-based regeneration. In addition to this, it draws particular attention to the goals of the program and participation required between stakeholders to agree them. The scope and distribution of urban distress and goals of the area-based regeneration program, CoSGOP provides a way of

logically framing the improvement process and a means of communicating the aims and objectives between stakeholders.

The generic goals of this program are to represent the main outcomes expected from the community-based approach to tackling urban distress and area-based regeneration. CoSGOP is a process model on the contrary than a planning method. It provides a framework for communication and joint decision-making in a structured process characterized by feed-back loops. In this sense, it facilitates a joint learning process of all the stakeholders involved [4].

### 2.3. Information Data Flow

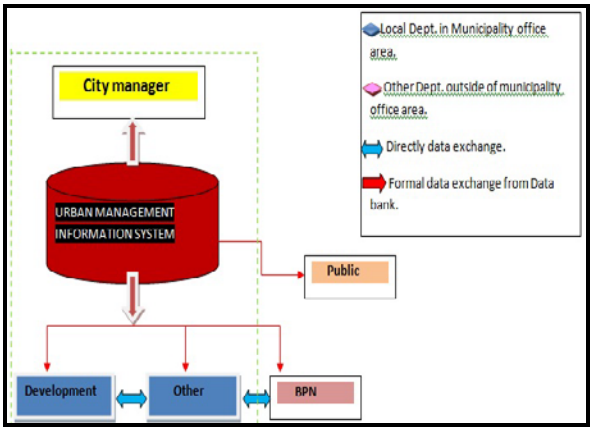


***Figure 1:*** *The Existing Condition*

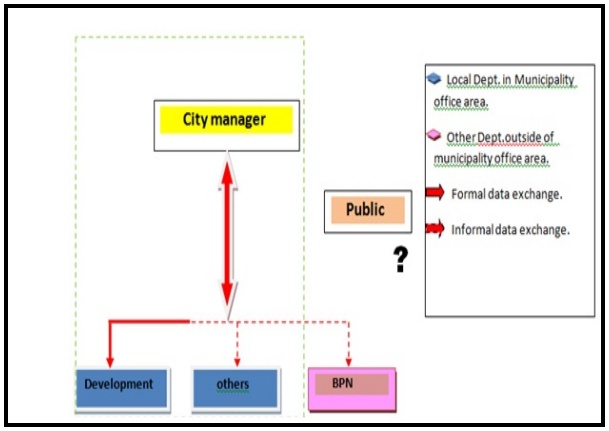


***Figure 2:*** *The Ideal Condition*

## 3. Objectives

The objectives that are expected to achieve through the course of this study are, to integrate remote sensing, GIS and non-spatial data and to bring them on a common plat-forum viz e-GIS, to share the resources generated from the study using a common plat-forum for better planning and optimization of the resources and at same time to quantify the shortcoming of spatial data integration.

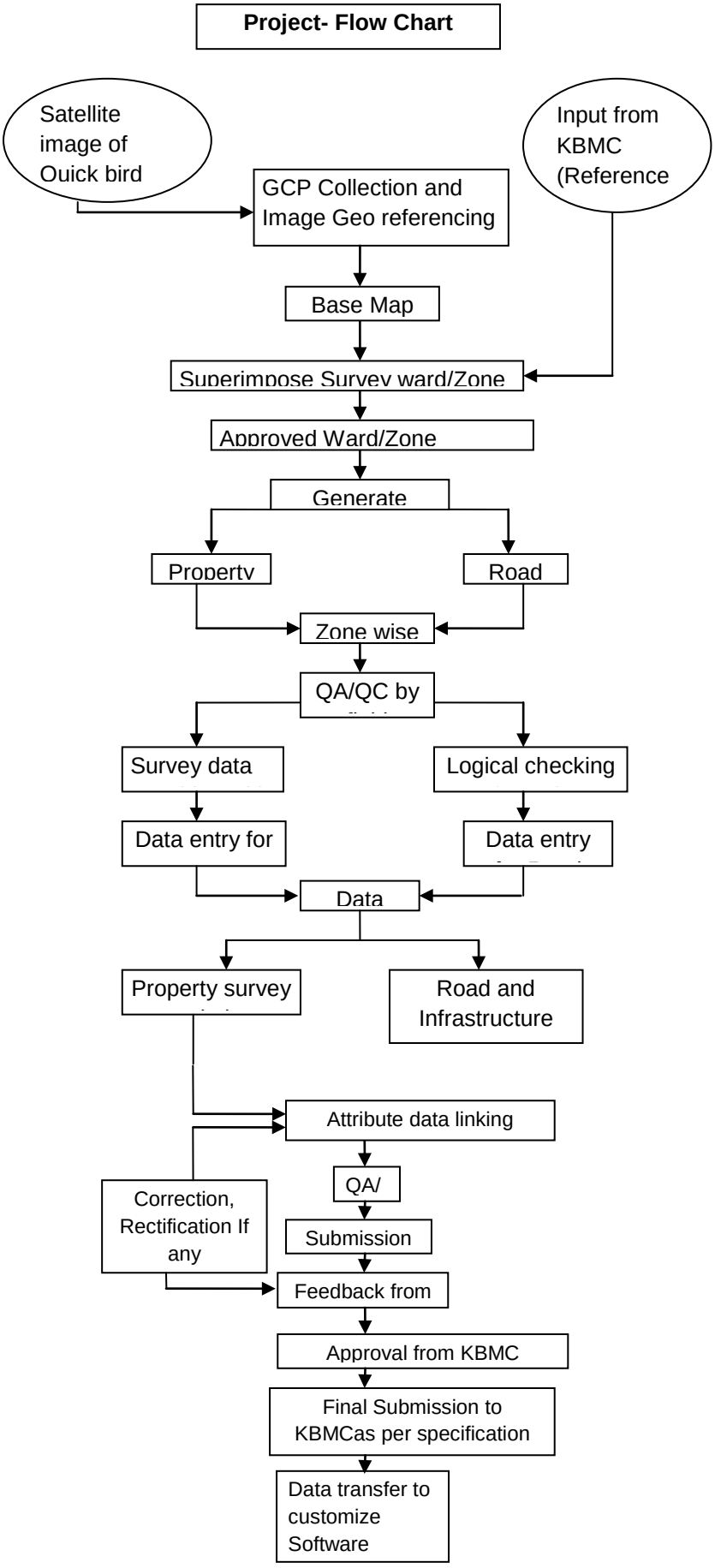
Project- Flow Chart
Satellite image of Quick bird
Input from KBMC (Reference
GCP Collection and Image Geo referencing
Base Map
Superimpose Survey ward/Zone
Approved Ward/Zone
Generate
Property
Road
Zone wise
QA/QC by
Survey data
Logical checking
Data entry for
Data entry
Data
Property survey
Road and Infrastructure
Attribute data linking
QA/
Correction, Rectification If any
Submission
Feedback from
Approval from KBMC
Final Submission to KBMCas per specification
Data transfer to customize Software

## 4. Methodology

Research methodology involves means and methods of conducting the research. It includes the procedure used in data collection and analysis.

Infrastructure, utilities and the newly constructed building features are digitized from satellite imagery. The photos are also attached for additional supporting information and to verify the work. The non-spatial data such as land information, building information and utility services information are collected during the field survey. All The available data are linked together in Arc View and Arc Map platform. Research methodologies are described in relevant headings:

### 4.1. Digitization

In this process Digitization of the polygon features like buildings, line features like Roads and Railways, Engineering or point features like street lights, manholes, shoulder drains etc was carried out. When digitization of these buildings was carried out, at the same time plot boundaries are also marked. All this digitization was carried out using AutoCAD. This is also called as feature extraction. Side by side plot boundary is also digitized. Because it is necessary to take the plot boundaries.

This feature extraction is important for verification and marking of the features on the actual site.

### 4.2. Creation of the Base Maps

From those digitized drawings base maps of the buildings were created. These maps were used for site verification. Parcel and house data maps were produced from the digitization of the satellite imagery, at the scale of 1: 500. The map sheet was digitized in AutoCAD using the sheet corner to control the digitization and facilitates joining adjacent map sheets together. The updating of buildings, parcels were made from “Quick Bird“ satellite imagery.

The other spatial data map of road network was also prepared from the image, and supported with recent field verification [6].

### 4.3. Verification of the Base Maps

Base maps of the buildings were then sending to the site for verification. On those maps all the updating according to the conditions on the site were made. At the same time, survey team also marked Ward boundary and Zone boundary on those maps, because for taking final output it is necessary to digitize Ward and Zone boundary. Plot boundaries which are digitized initially on the satellite image are also checked and if necessary those are corrected.

### 4.4. Data Collection (Non-Spatial Data)

The non – spatial data collected are land data records. The land data are used to guide for the revenue collection of parcel by parcel information of owners, building permit data that has building information, addressed data that has a house numbers and road names information and utilities data which has information for payment calculation of utilities services. Data collection is the main work in the project. It is the most tedious work of the project [6].

### 4.5. Data Integration (Spatial and Non – Spatial Integration)

The user – interface data integration developed in Arc View, interfaces parcels, building, infrastructure, utilities and satellite image, photos of buildings and owners and associated non – spatial data. Data

Integration consists of the work of removing error from the work they entered data. Integration means entering newly updated data and removing errors from the old data or removing incorrect data. It also consists of editing and merging all the data. The application has helped to make a spatial query for parcel, building, utilities services of owners.

Data integration is very important since it is the first step for output data. If data entered at the time of data integration is correct then there will be no need to enter data again after verification by revenue inspector [6, 8].

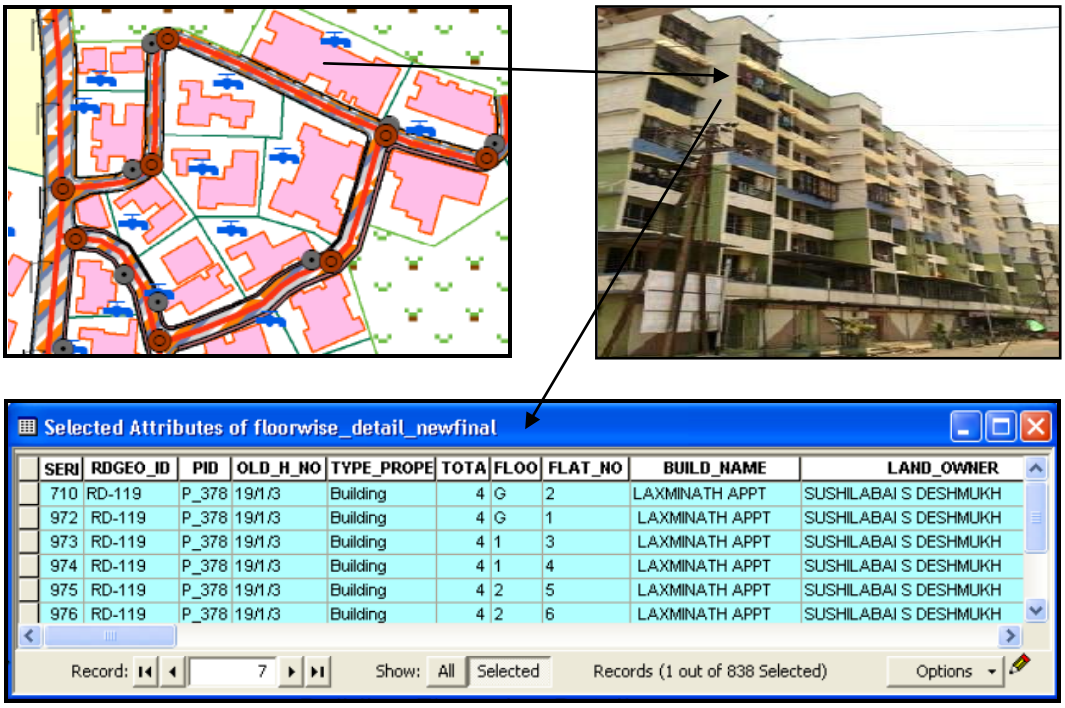


***Figure 3:*** *Property Survey*

### 4.5.1. Integration of Data with GIS System

The finalized data after getting all the approvals from KBMC and the external agency are integrated into the GIS system developed for KBMC. As we have done all the process in the software of Autodesk map, it is compatible with all the leading GIS formats. Hence data can be provided in the format as desired by KBMC [8].

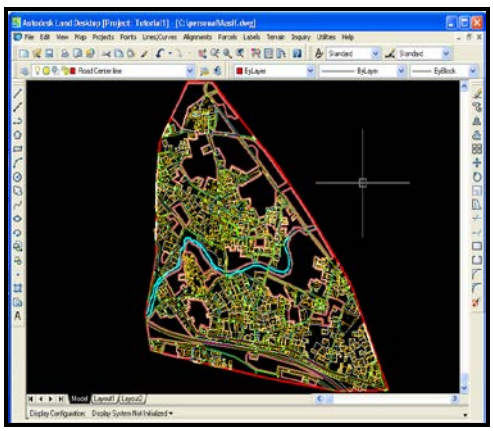

***Auto CAD Map 2008***

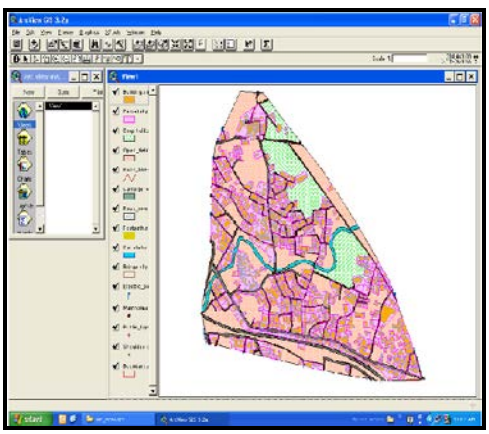

***Arc View 3.2***

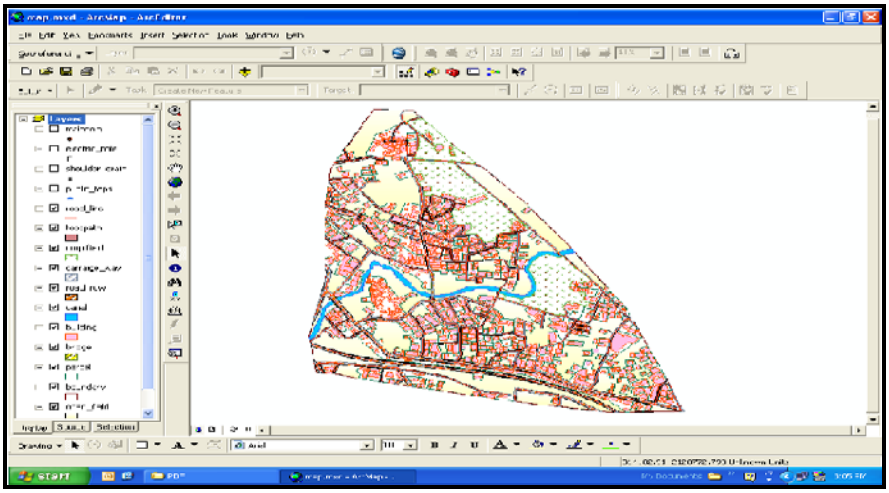

*ArcMap 9.2*

## 5. Software Development

Software development for various purposes in the project is carried out by the software department. The computer language used for the software development is VB (Visual Basic).

Various small software's like data entry software for various features and one software for e-Taxpaying is prepared. These software's act as the front end of the database where as MS-Access act as a back end.

### ➢ Screens for Data Entry for Various Features

***Entry Screen for Property Data***

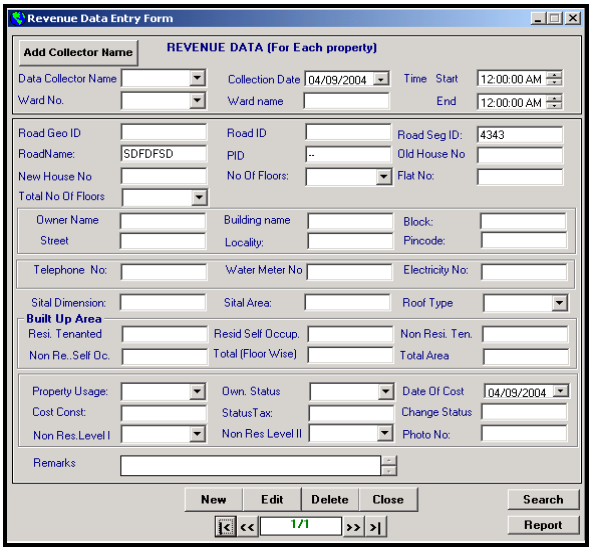


***Data Entry Screen for Cross Drainage***

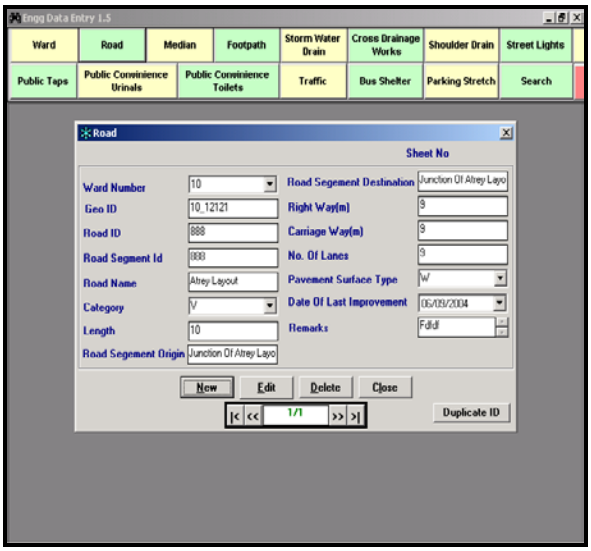

***Data Entry Screen for Road***

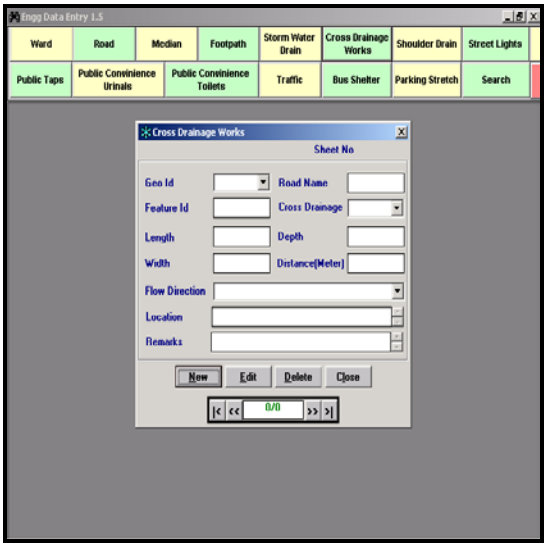


***Data Entry Screen for Street Lights***

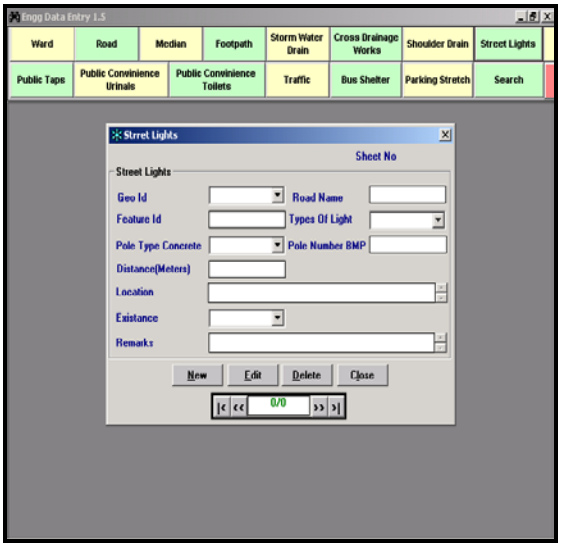


## 6. Software & Data

### 6.1. Software Used

AutoCAD Autodesk 2004, Arc View 3.2, Arc Map 9.2, Data Entry Software, MS- Access.

### 6.2. Data Used

*Quickbird* satellite was successfully launched in 2001. Quickbird, having high spatial resolution space borne sensor is capable of panchromatic imaging at 0.61 cm. The sensor also has 4 multispectral bands with resolutions of 2.44 m at nadir. Among all the VHR (Very High Resolution) satellites having an extended archive, Quick Bird possesses the one with the best resolution. The imagery can sufficiently distinguish man-made features on the landscape and serve as an excellent base map for GIS applications.

- Launch date: 18$^{th}$ October 2001
- Orbit: 97,2°, sun synchronous
- Orbital altitude: 450 km
- Viewing angle: Max +/- 30° off-nadir
- Equator crossing time: 10.30 am solar time
- Revisit time: 2,4 to 5,9 days depending on latitude
- Swath width: 16,5 km at nadir
- Minimum order size: 25 km² (archive) and 1800 USD (new acquisition) for Standard and Ortho-rectified product
- Resolution

| Resolution |
|---|
| 0,61 m (panchromatic) at nadir |
| 2,44 m (multispectral) at nadir |
| 0,72 m (panchromatic) at 25° off-nadir |
| 2,88 m (multispectral) at 25° off-nadir |
| 23 m CE90% for Basic and Standard products |
| 12,7 m CE90% for Ortho-rectified products |

- Geo-vocational accuracy (without GCP)
- Spectral range

| Spectral Range |
|---|
| 0,45 – 0,90 µm (panchromatic) |
| 0,45 – 0,52 µm (band 1 – blue) |
| 0,52 – 0,60 µm (band 2 – green) |
| 0,63 – 0,69 µm (band 3 –red) |
| 0,76 – 0,90 µm (band 4 – near infrared) |

- Standard acquisition window new imagery: 90 days
- Tasking: Standard, Priority and Rush tasking possible
- Radiometric resolution: 11 bits per pixel
- Product types: Basic, Standard, Ortho-rectified, Stereo are available
- Price: Pricing per km²
- Area of Interest: Irregular polygon (max 999 vertices and minimum width of 3 km)

## 7. Results

It will become easy to acquire information about any property [5].

Infrastructure development will become more powerful.

(i). Project will provide facility of online taxation.
(ii). As it will provide the facility to find optimum path, in case of emergency services, facilities can be provided faster.
(iii). For PWD department, it will become easy to maintain roads line and to monitor road life.
(iv). In case of Slums, facilities can be improved. Provision for new facilities can be done.
(v). Drainage system can be monitor and improve.
(vi). Marking of green belt area, can give the information about vegetated area in the town.
(vii). Town also has a river. So, there is always a danger of flood. With the help of this project, flood prone can be marked, as well as buffer zone around the river can also be marked.
(viii). In case of any disaster, estimation about loss of property as well as human life will become easy.
(ix). Documentation about any purpose related to urban management become easier.

## 8. Conclusions and Recommendations

Bringing the information together for planning and management activities certainly provide broader vision. Through this study the main aim was to develop a preliminary e-GIS plat forum that will showcase the ability of e-geographical information system for optimization of resources in a most excellent form. The e-GIS plat-forum will become a conceptual model for achieving better planning, good urban governance and management to the whole areas of city which may require further working. Once the application become functional, it is necessary a training part for daily operational activity. Security offices and other stakeholders could be more useful these integrated application as well as the introduction of e-geographical information system in governmental system is surely going to benefit the people in variety of ways [3, 5].

## References

[1] Aronoff S., 1990: *Geographical Information Systems: A Management Perspective*. WDL Publications, Ottawa, Canada.

[2] *Census Commission of India*. On 2004-06-16. Retrieved 2008-11-01.

[3] Subash S. and Arun Padaki., 2003: *Enterprise GIS for Municipalities –An Integrated Approach*, Map India Conference 2003

[4] LUDA E-compendium: Handbook E4 *Annex 1 & Annex 2.*

[5] K.J. Madadock 2001: Report on *Municipal Taxation,* in Particular Land Tax Procedures of KMC.

[6] M. Sigdel. 2001: Presented Paper on *Land Surveying in Nepal* upon the Request of Katmandu Valley Mapping Program.

[7] Costly Chanza, 2003: A *GIS based Municipal Information System for Management of Urban Development Control Process.*

[8] Tika Ram Adhikari and Purushottam Singh. *Urban Management Decisions Integrating Spatial and Non-Spatial Data.*

[9] Taylor Nigel, 2007: *Urban Planning Theory since 1945*, London, Sage.

**Cloud Publications**
International Journal of Advanced Remote Sensing and GIS
2014, Volume 3, Issue 1, pp. 486-498, Article ID Tech-222
ISSN 2320 - 0243

Cloud Publications

**Research Article** **Open Access**

# Evaluation of ASTER Images for Characterization and Mapping of Volcanic Rocks (Basalts)

**Paulo Roberto Markoski and Silvia Beatriz Alves Rolim**

CEPSRM/UFRGS, Centro Estadual De Pesquisas em Sensoriamento Remoto e Meteorologia – Federal University of Rio Grande do Sul State, Brazil

Correspondence should be addressed to Silvia Beatriz Alves Rolim, silvia.rolim@ufrgs.br

Publication Date: 14 March 2014

Article Link: http://technical.cloud-journals.com/index.php/IJARSG/article/view/Tech-222



**Guest Editor-in-Chief: Dr. Maurício Roberto Veronez**
***(This article belongs to the Special Issue "Application of Geotechnology in Urban Planning")***

**Abstract** The objective of this work was to evaluate the potential of hyperspectral classification techniques in the Advanced Spaceborne Thermal Emission and Reflection Radiometer (ASTER) reflectance data (visible to short wave infrared region) and spatial resolution (15 and 30 m), to map volcanic rocks in Ametista do Sul Region, Rio Grande do Sul State, Brazil. This region is one of the most important amethyst mineralization of the World. The spectral behavior of these rocks is similar to shadows and soils when interpreted with traditional digital classification techniques and multispectral sensors, like TM-Landsat, CCD-CBERS, etc. As an alternative was applied hyperspectral image processing technique (Spectral Angle Mapper - SAM) to identify and discriminate basalt rocks occurrence in mixed pixels. Due to vegetation around and covering some outcrops and the pixel spatial resolution, it was not possible to extract a basalt endmember directly into the ASTER image, being used so an endmember from NASA spectral library. To compare SAM results with traditional classification techniques were applied the Maximum Likelihood (MaxVer) algorithm. The SAM technique produced better results than MaxVer, but the error persisted, even in a lesser proportion, in mixed pixels with "Shadows", "Soils" and "Basalt" classes.
**Keywords** *Classification Methods; MaxVer; SAM; Spectral Analysis*

## 1. Introduction

The Remote Sensing and auxiliary computing techniques are important tools used for identification, geological mapping and mineral exploration. These tools aim the spectral discrimination of targets. To accomplish this discrimination is important to know about the spectral behavior through the observation of diagnostic features that express the physical and chemical composition of each target. One way to perform this study is to use orbital sensors that allow working with an adequate spatial and spectral scale.

It´s difficult to perform a digital classification closer of the scene reality because the radiance recorded by a sensor may be a result of the mixture of many materials inside the pixel, added by the atmospheric scattering.

The radiance recorded by a sensor in a pixel may be a mixture of many materials, hampering a digital classification closer the scene reality. Traditional classification methods, such as MaxVer and Minimum Distance [26], use to be applied by prior knowledge of the targets by collecting training samples. Spectral classification methods are also applied by a prior knowledge of the targets, but implying a supervised classification based on sampling and analysis of spectral signatures and their comparison with the image pixels spectra. Such signatures can be obtained collecting *endmembers (*defined as spectrally "pure" features*)* on the image, measuring in laboratories or field with a spectroradiometer, or searching in spectral libraries. The classification by spectral analysis allows decompose each pixel by its correlation with the material that composes it (spectrum) in a direct way, establishing location and, sometimes, sub-pixel composition [30].

In this context, this study aims to evaluate the potential of hyperspectral classification techniques in the Advanced Spaceborne Thermal Emission and Reflection Radiometer (ASTER) [1] images to map and identify volcanic rocks extracted from amethyst mines in Ametista do Sul region, north of Rio Grande do Sul State, Brazil (Figure 1.1).

The basalt rock is very dark, compact, sometimes with cavities and some crystals developed on the solid mass formed by minerals rich in iron and magnesium. It is a basic igneous rock composed mainly of fine grains of plagioclase feldspar enriched with calcium and pyroxene. Some others minerals such as olivine, magnetite and apatite can be present in the rock.

### 1.1. Study Area

The study area is located in north of Rio Grande do Sul State, Brazil, City of Ametista do Sul (Figure 1.1). This region is the largest amethyst producer in the world.

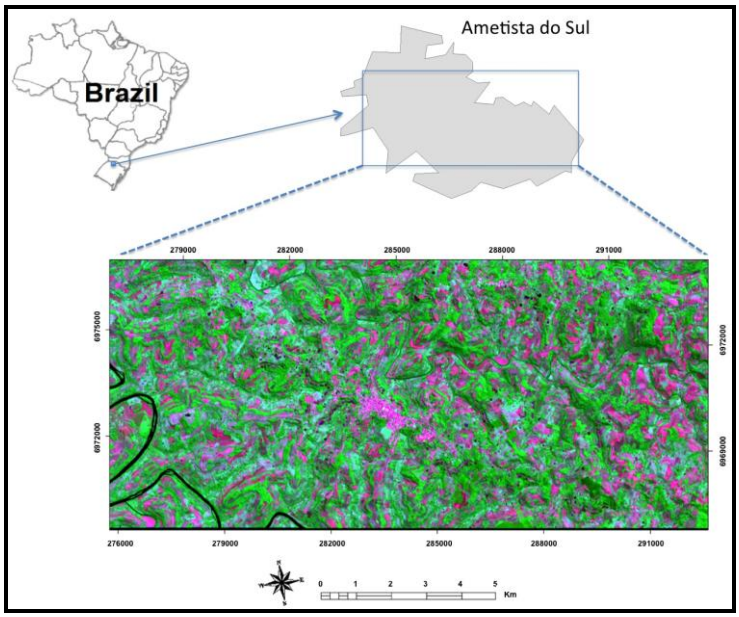


***Figure 1.1:*** *Study Area*

The basalt is extracted into the mountain during de mining process and deposited outside, where large stacking of rocks is formed (Figure 1.2). These stacks are many times smaller than ASTER pixel size

(VNIR - 15 meters and SWIR – 30 meters). Thus, the pixel composition becomes a mixing of materials, hampering its identification and mapping.


***Figure 1.2:*** *Photos of Amethyst Mining Residues/Basalt*

## 2. Mapping Methods

### 2.1. Traditional Method: MaxVer Algorithm

MaxVer or Maximum Likelihood is a statistical classification method that considers the weighting of the distances between averages classes values using statistical parameters. To be accurate enough, MaxVer needs a number of "pixels" for each training group (more than 30). The training groups define the classes scatter diagram and their probability distributions, considering the normal probability distribution for each training class [7]. The classification limits are defined from points of same classification probability for all classes. This classification method assumes that the user knows previously the analyzed area and the distribution of the classes. In this way, when performed the classification, selection of training samples can be as efficient as possible [7]. The Equation (1) defines the Maximum Likelihood algorithm:

$$g_j(x) = -\frac{1}{2}(x - m_j)^t \sum_j^{-1}(x - m_j) - \frac{1}{2} ln \left|\sum_j\right| (1) + \ln P(\omega_j) \qquad (1)$$

Where:
m=Vector of means
Σ= Covariance matrix
ω= Occurrence probability of each class

This is the traditional method most commonly used to obtain informational classes from remote sensing images. The spectral distribution of land use classes is considered to be Gaussian or normal, i.e., objects belonging to the same class will present spectral response close to the average values for that class. To obtain satisfactory results is necessary to choose a fairly large number of pixels for each training sample class, and these present a statistical distribution close to the normal distribution [7].

Another important factor to effectiveness results is to obtain a reasonably accurate estimate of the mean vector and covariance matrix for entire spectral class, which also depends the number of pixels included in the training samples [28].

### 2.2. Spectral Method: Spectral Angle Mapper (SAM)

The spectral classification methods were originally developed for hyperspectral data. The process of image acquisition in contiguous bands allows deriving a spectral reflectance curve, named "imaging spectroscopy" and "Hyperspectral remote sensing" [29]. The goal of imaging spectroscopy is quantitatively measure the spectral signature of the components of the Earth system from calibrated spectra, acquired from images, useful in scientific research and remote sensing applications [22].

This spectral classifications method has provided satisfactory results not only in its application to hyperspectral data, but also in data obtained by multispectral sensors like ASTER [27; 11; 8; 22].

The spectral classification methods can be divided in total pixel detection and sub-pixel scale. The total pixel detection is restricted to map the distribution of the material in its percentage prevalence into the pixel; otherwise it will not be detected. Examples of these classification techniques: Binary Enconding [14]; Tricorder / Tetracorder and its variation Spectral Feature Fitting - SFF [6] and Spectral Angle Mapper - SAM [20]. Mapping sub-pixel scale, the feature is not mapped by predominance into the pixel, but for its occurrence, even small. It is established, hence, a relative estimation of abundance, distribution and occurrence of the target material component, outlining a mixture of materials inside each pixel, expressed in their spectral behavior. Examples of techniques associated with this concept: Linear Spectral Unmixing - LSU [25] Matched Filtering and Mixture Tuned Matched Filtering - MTMF [5; 2; 17].

The SAM technique [20] allows fast mapping of the similarity between the pixel spectra and the reference spectra. The reference spectra can be extracted in laboratory, field or extracted from the image. This method assumes that the image data was converted to surface reflectance. The algorithm determines the spectral similarity between two spectra calculating the angle formed between them, treating them as vectors in a space of dimensionality corresponding to the number of bands (nb) (Equation 2).

$$\emptyset = Cos^{-1}\left[\frac{\sum_{i=1}^{n} t_i\, r_i}{\sqrt{\sum_{i=1}^{n} t_i^2 \sum_{i=1} r_i^2}}\right] \qquad (2)$$

Where:
$n$ = number of spectral bands
$t$ = reflectance of the pixel spectra
$r$ = reflectance of the reference spectra

This similarity measured is insensitive to gain factors because the angle between two vectors is invariant in relation to the vectors lengths. Laboratory spectra can be directly compared to pixels reflectance spectra, which inherently have a gain factor related to unknown illumination effects due to topography [20]. As a result, a classified image is created, showing the best fit for each pixel, subject to a limit specified by the user. Additionally, “rule” images are provided showing the angular distance (in radians) between each spectra image and each reference spectra. The black pixels in the "rule" image present low spectral angles values, and therefore more similar to the spectra of *end members*. For best viewing, these images are inverted and the smaller angles appear in a clear tone.

## 3. Method

In this paper were evaluated two classification techniques: algorithm MaxVer and the SAM technique. The reason why were chosen these two techniques is the fact that they have been successfully used in other studies of soil and rocks and the possibility to compare different classification approaches:

traditional classification methods (MaxVer) versus spectral Methods (SAM). An ASTER image, Level 1B (Figure 1.3) was used to test and perform the techniques. A total of 16 points of volcanic rocks exposition area was collected to check the classification/mapping accuracy (Figure 1.3).

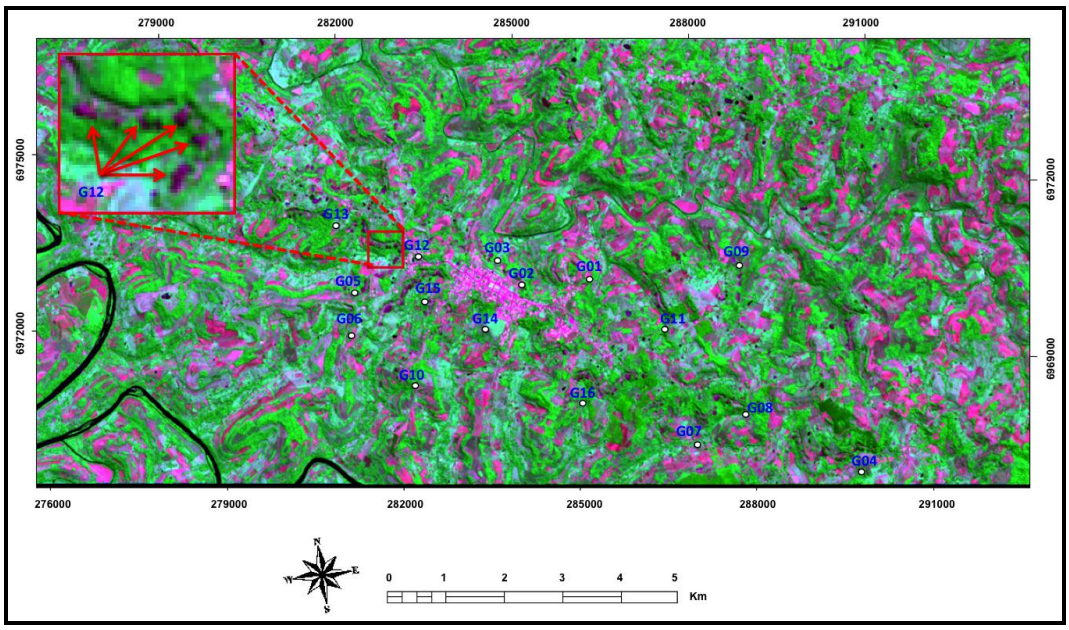


***Figure 1.3:*** *Aster Color Composition R (2), G (3), B (1) with the Amethyst Mining Points Distribution, Collected by GPS*

### 3.1. Image Processing

To perform both classifications methods an ASTER Level 1B image was employed. First, the image was submitted to crosstalk effect correction through the software Crosstalk [10]. This problem affect the dispersion of the incident light in the band 4, which is reflected on the focal plane of SWIR bands, producing, for example, appearance of "ghosts" at the interface between land and water surfaces [18]. After that, a SWIR bands spatial re-sampling was performed, artificially, increasing its resolution to 15 m, thus, allowing the composition with VNIR bands in an image database with nine spectral bands. This data set were submitted to atmospheric correction through the Atmospheric Moderate Resolution Radiance and Transmittance Model (MODTRAN), implemented on the algorithm Fast Line-of-sight Atmospheric Analysis of Spectral Hypercube (FLAASH) and converted to apparent reflectance. FLAASH is a first-principles atmospheric correction tool that corrects wavelengths in the visible through near-infrared and shortwave infrared regions, up to 3 µm [9].

FLAASH starts from a standard equation for spectral radiance at a sensor pixel, $L$, that applies to the solar wavelength range (thermal emission is neglected) and flat, Lambertian materials or their equivalents. The equation is as follows:

$$L = \left(\frac{A\rho}{1-\rho_e S}\right) + \left(\frac{B\rho_e}{1-\rho_e S}\right) + L_a \qquad (3)$$

Where:

$\rho$ is the pixel surface reflectance

$\rho_e$ is an average surface reflectance for the pixel and a surrounding region

$S$ is the spherical albedo of the atmosphere

$L_a$ is the radiance back scattered by the atmosphere

$A$ and $B$ are coefficients that depend on atmospheric and geometric conditions but not on the surface. Each of these variables depends on the spectral channel; the wavelength index has been omitted for simplicity. The first term in Equation (3) corresponds to radiance that is reflected from the surface and travels directly into the sensor, while the second term corresponds to radiance from the surface that is scattered by the atmosphere into the sensor. The distinction between $\rho$ and $\rho_e$ accounts for the adjacency effect (spatial mixing of radiance among nearby pixels) caused by atmospheric scattering. To ignore the adjacency effect correction, set $\rho_e = \rho$. However, this correction can result in significant reflectance errors at short wavelengths, especially under hazy conditions and when strong contrasts occur among the materials in the scene [9].

The values of $A$, $B$, $S$ and $L_a$ are determined from MODTRAN4 calculations that use the viewing and solar angles and the mean surface elevation of the measurement, and they assume a certain model atmosphere, aerosol type, and visible range. The values of $A$, $B$, $S$ and $L_a$ are strongly dependent on the water vapor column a27, which is generally not well known and may vary across the scene. To account for unknown and variable column water vapor, the MODTRAN4 calculations are looped over a series of different column amounts, and then selected wavelength channels of the image are analyzed to retrieve estimated amounts for each pixel. Specifically, radiance averages are gathered for two sets of channels: an absorption set centered at a water band (typically 1130 nm) and a reference set of channels taken from just outside the band. A lookup table for retrieving the water vapor from these radiances is constructed [9].

For images that do not contain bands in the appropriate wavelength positions to support water retrieval (for example, Landsat or SPOT), the column water vapor influence is determined by the user-selected atmospheric model. After the water retrieval is performed, Equation (3) is solved for the pixel surface reflectance in all of the sensor channels. The solution method involves computing a spatially averaged radiance image $L_e$, from which the spatially averaged reflectance $\rho_e$ is estimated using the approximate equation:

$$L_e = \left( \frac{(A + B)\rho_e}{1 - \rho_e S} \right) + L_a \qquad (4)$$

Spatial averaging is performed using a point-spread function that describes the relative contributions to the pixel radiance from points on the ground at different distances from the direct line of sight. For accurate results, cloud-containing pixels must be removed prior to averaging. The cloudy pixels are found using a combination of brightness, band ratio, and water vapor tests, as described by [23].

To perform the atmospheric correction in this work, the following image conditions were considered:

a) Elevation of study area (550 m);
b) Aerosol levels (visibility: 40 km, rural model). In the Initial Visibility field, is used an estimate of the scene visibility in kilometers (40 to 100 km for clear conditions; 20 to 30 km for moderate haze and 15 km or less for thick haze). Rural model represents aerosols in areas not strongly affected by urban or industrial sources.
c) Atmospheric model (Mid-Latitude Summer). For the best results, must be select a model whose standard column water vapor a27 is similar to, or somewhat greater than, that expected for the scene.

If no water vapor information is available, the model may be selected based on a seasonal-latitude surface described by [9].

After the atmospheric correction, the classification was performed using the MaxVer algorithm. Were selected six classes: Soil 1, Soil 2, Native Forest, Agriculture, Basalt and Shadow. The interest classes for this work are Shadow, Soils and Basalt. The others were used only to improve the classifier accuracy. For each class were selected a number of pixels greater than 30. After the image classified, geometric correction was performed to compare with the basalt points collected in field.

The following processes were performed to SAM Technique. Due to the small size of the areas with basalt exposition (usually less than one pixel - 15m ASTER), the spectral signature of reference (endmember) cannot be extracted in the ASTER image. As Basalt endmember was employed a spectral signature from the Jonh Hopkins University Spectral Library, available in: http://speclib.jpl.nasa.gov. Before processing the SAM technique, the spectral signature was resampled to nine bands ASTER VNIR/SWIR subsystems resolutions (Figure 3.1). A similarity angle of 0.05 radians was used to perform the technique.

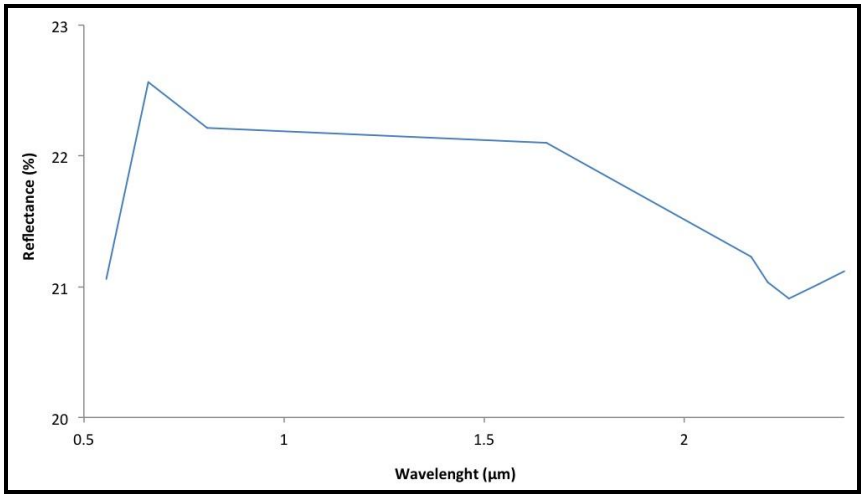


***Figure 3.1:*** *Reflectance Spectra of Basalt endmember Extracted from Jonh Hopknis University Spectral Library and Resampled to ASTER VNIR/SWIR Resolution*

## 4. Results

### 4.1. MaxVer Processing

The ASTER image was classified into six classes: Soil 1, Soil 2, Native Forest, Agriculture, Basalt and Shadow. Figure 4.1 presents the classification results.

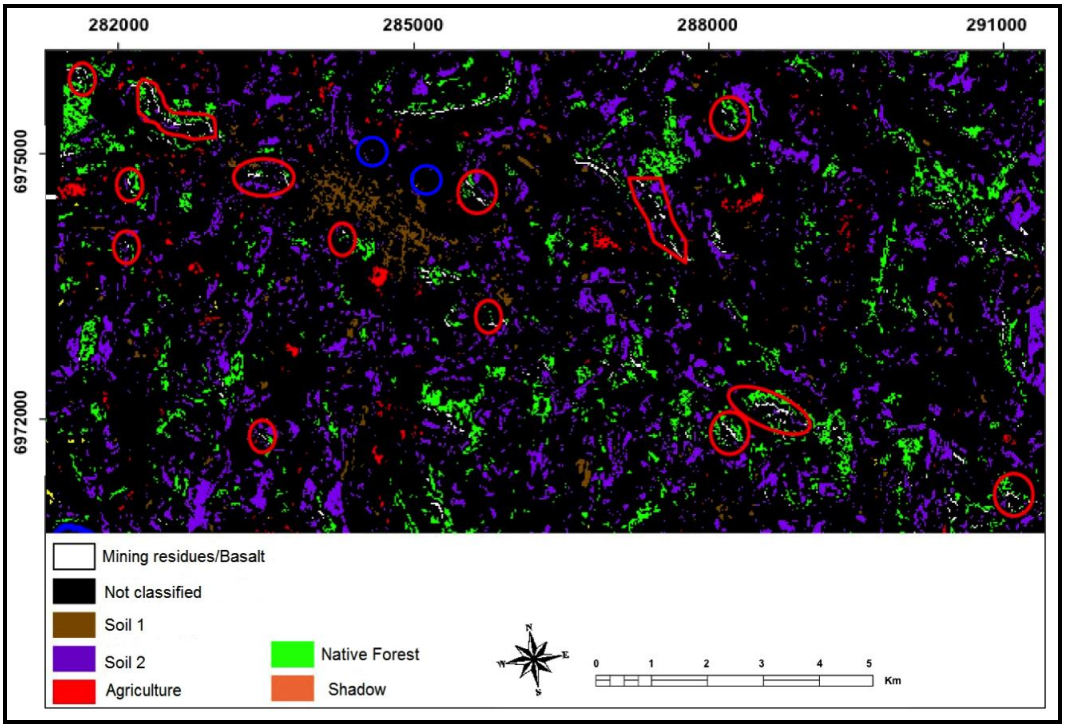


***Figure 4.1:*** *MaxVer Classification Results*

The MaxVer algorithm classified correctly fourteen of sixteen basalt points (G02 and G03 not classified - blue circles). There is a large occurrence of vegetation closer the mines/basalt, especially native forest, hampering the classification. Due to shaded areas in the visible region, is easily confused with the basalt. These two points were not classified, presumably because they were located in very small mines, where the stacks of basalt are smaller, being strongly influenced by other targets reflectance, such as bare soil or shadow. The main problem found with MaxVer algorithm was the mixture produced between "shadow" "Soils and "basalt" classes. Several shaded areas were classified as “basalt” even when have no occurrence of them. This can be seen in Figure 4.2. In the classification result, the “Shadow” class included several pixels classified as basalt (white color).

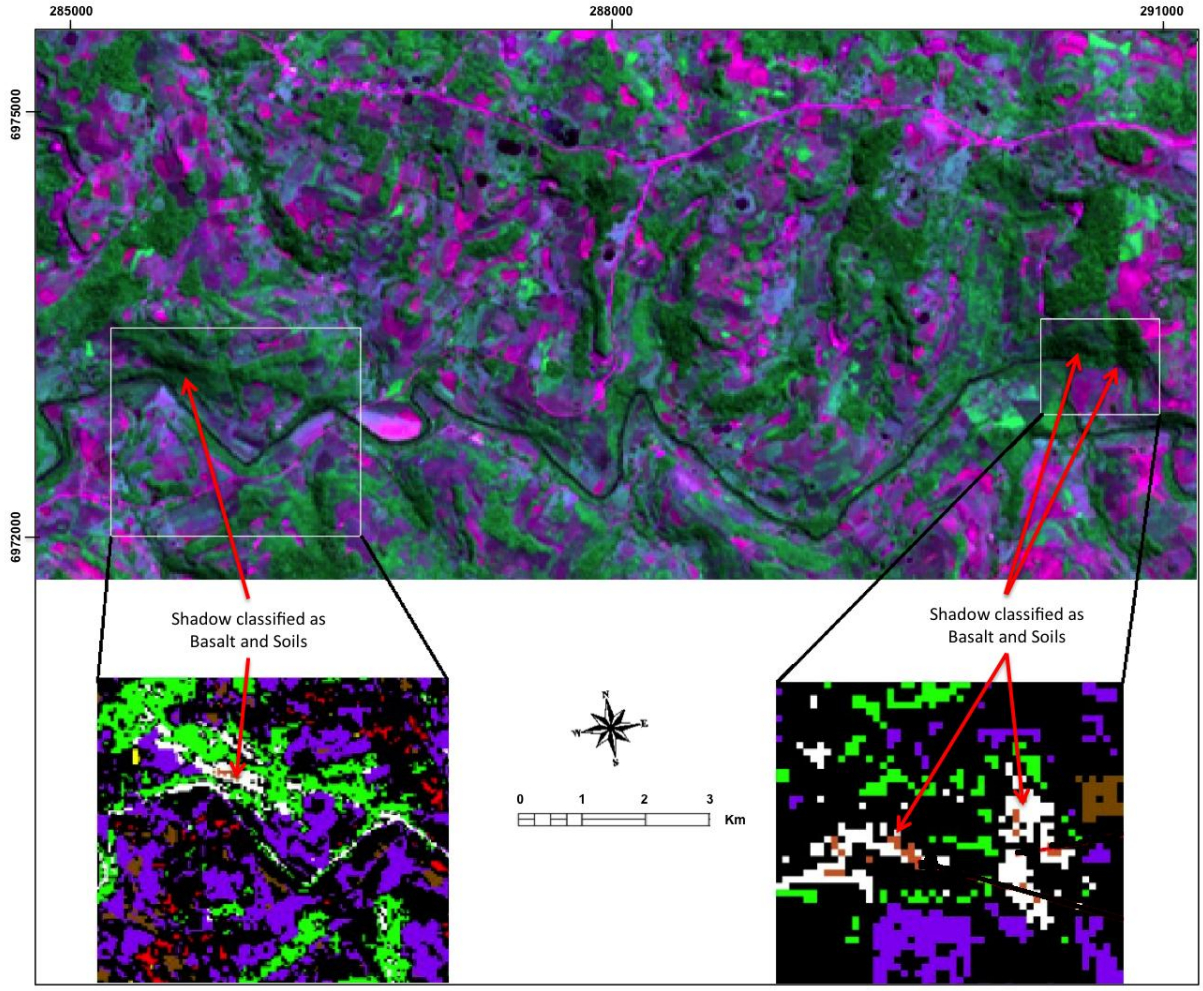


***Figure 4.2:*** *Misclassification between "Soils", "Shadow" and "Basalt" Classes. Shadow Pixels were classified as Basalt and Soils*

## 4.2. SAM Processing

The result of SAM technique processing is presented in Figure 4.3 (rule image). The lighter pixels are those with greatest similarity with the basalt spectral signature, that is, the clearer, more likely to be a pure pixel class.

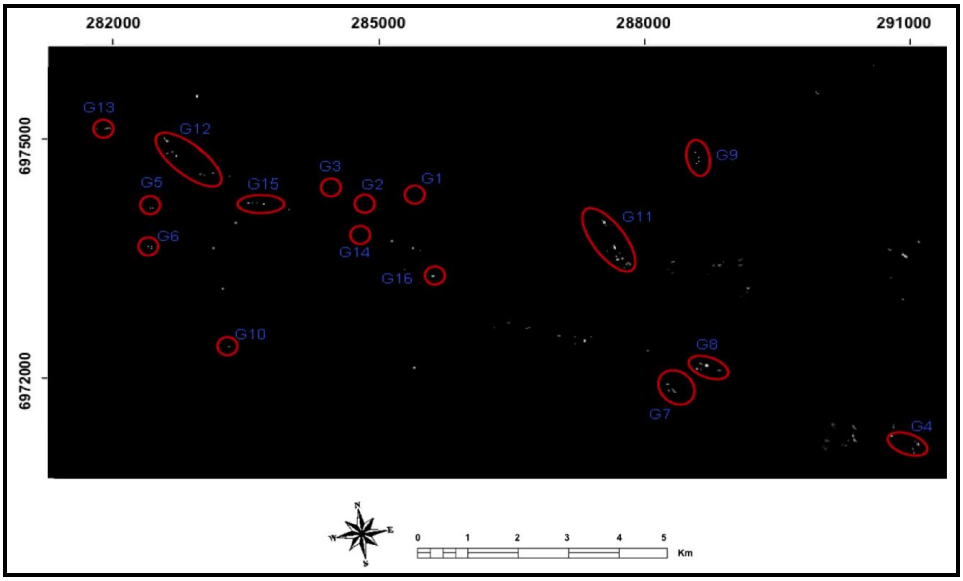


***Figure 4.3:*** *SAM Result*

The basalt points G1, G2, G3 and G14 did not show similarity with the spectral *endmember* mainly due to the reduced amount of basalt present at these areas, smaller than one pixel (15 m – VNIR, 30 m - SWIR). Most of the polygons has pixels with white color saturated indicating the basalt occurrence and hence, the mines. The figure also shows other areas identified as basalt that were not mapped by GPS, indicating the presence of other mines.

The advantage using this technique over conventional classification techniques is that it has greater control over the results. Based on the image "rule", filters can be applied over the pixels with the highest probability of belong the study class, whereas in the other classification techniques, the pixels are classified according to a range of values, which are similar.

Classification with reference spectra extracted directly from images always tend to have better results because factors such as lighting conditions, particles and aerosols, the spectral influence of other targets are already associated with the image and consequently the spectral curve. Due to the small size of basalt areas (usually less than one pixel at 15m ASTER) spectral signature of reference cannot be extracted in the ASTER image because the same had not totally pure pixels.

## 5. Conclusions

The results showed that ASTER images can be employed for mineral characterization, in the study case, the basalt extracted from amethysts mining.

The algorithm MaxVer produced satisfactory results. The main problem was the mixing (error) between Shadow, Soils and Basalt classes.

The SAM technique has achieved better results than MaxVer, being able to identify the pixels with greater spectral similarity. Even areas where basalt occurrence was small, sometimes lower than one pixel, the technique could identify the basalt spectral influence, of course, with a lower similarity value.

The forest native present beside the mines has great influence on the pattern detection process and extraction of reference spectra. Therefore, to generate reference spectra that are more pure and reliable, large areas should be chosen, where the vegetation and shadow influence are smaller.

The low spectral contrast of basalt in VNIR/SWIR region (Figure 3.1) is a factor that influences the classifications results. Due to the small intensity of diagnostic features, basalt may by easily mix with other classes like shadow and soils. A better approach to study this kind of rock may be employing emissivity data on thermal infrared region (8 - 12µm). In this region, the quartz, a mineral that compounds basalts rocks, has more intensity spectral features, also known as restrahlen bands, while other classes like soils, vegetation and shaded areas tend to behave like a gray body.

## References

[1] Abrams, M., and Hook, S.J., 2002: *Aster User Handbook: Advanced Spaceborne Thermal Emission and Reflection Radiometer.* USA: NASA/Jet Propulsion Laboratory, California Institute of Technology. 2; 135.

[2] Boardman, J.W., Kruse, F.A., and Green, R.O., 1995: *Mapping Target Signatures via Partial Unmixing of AVIRIS Data*. In: Summaries, Fifth JPL Airborne Earth Science Workshop. JPL Publication 95-1. 1; 23-26.

[3] Breunig, F.M., 2008: *Dados De Reflectância E Emissividade Do Sensor ASTER/Terra Aplicados Ao Estudo De Solos Quartzosos*. Dissertação de Mestrado. INPE.

[4] Carvalho junior, O, A., Carvalho, A.P.F., Meneses, P.R., Guimarães, R.F., and Martins, E.S. *Análise de imagens hiperespectrais pelo método Multiple Endmember Spectral misture Analysis (MESMA) em depósito supergênico de níquel*. Revista Brasileira de Geociências. 2003. 33 (1).

[5] Chen, J.Y., and Reed, I.S. *A Detection Algorithm for Optical Targets in Clutter.* IEEE Trans. on Aerosp. Electron. Syst. 1987. AES-23 (1).

[6] Clark, R.N., and Swayze, G.A., 1995: *Mapping Minerals, Amorphous Materials, Environmental Materials, Vegetation, Water, Ice, and Snow, and Other Materials: The USGS Tricorder Algorithm*. In Summaries of the Fifth Annual JPL Airborne Earth Science Workshop, JPL Publication 95-1. 39-40.

[7] Crósta, A.P., 1993: Processamento Digital de Imagens de Sensoriamento Remoto, Campinas, SP, UNICAMP, ed. rev.

[8] Ducart, D.F., Crósta, A.P., and Souza Filho, C.R. *Mapeamento De Alteração Hidrotermal No Distrito De Los Menucos, Argentina, Por Meio De Imagens Multiespectrais ASTER*. In: Simp. Bras. de Sens. Rem., Goiânia, INPE/SELASR. 2005. 12; 4057-4064.

[9] ENVI User Guide, 2009: Atmospheric Correction Module: QUAC and FLAASH User's Guide. Version 4.7.

[10] ERSDAC (Earth Remote Sensing Data Analysis Center), 2003: *The Crosstalk Correction Software User's Guide*. 21.

[11] Galvão, L.S., Almeida-Filho R., and Ícaro, V. *Spectral Discrimination of Hidrotermally Altered Materials using ASTER Short-Wave Infrared Bands: Evaluation in a Tropical Savannah Environment.* International Journal of Applied Earth Observation and Geoinformation. 2005. 7; 107-114.

[12] Gao, B.C., Hiedebrecht, K.B., and Goetz, A.F.H. *Derivation of Scaled Surface Reflectance are from AVIRIS Data*. Remote Sensing of Environment. 1993. 44; 165-178.

[13] Goetz, A.F.H. *The Spectral Image Processing System (SIPS) - Interactive Visualization and Analysis of Imaging Spectrometer Data*: *Remote Sensing of Environment*. Special Issue on AVIRIS. May-June 1993. 44; 145-163.

[14] Goetz, A.F.H., Vane, G., Solomon, J.E., and Rock, B.N. *Imaging Spectrometry for Earth Remote Sensing.* Science. 1985. 228; 1147-1153.

[15] Goetz, A.F.H. *The Spectral Image Processing System (SIPS) – Interactive Visualization and Analysis of Imaging Spectrometer Data.* Remote Sensing Environment. 1993. 44; 145-163.

[16] Green, A.A., Bermam, M., Switzer, P., and Craig, M.D. *A Transformation for Ordering Multispectral Data in Terms of Image Quality with Implications for Noise Removal*. IEEE Transactions on Geosciences and Remote Sensing. 1988. 26 (1) 65-74.

[17] Harsanyi, J.C., and Chang, C. *Hyperspectral Image Classification and Dimensionality Reduction: an Orthogonal Subspace Projection Approach.* IEEE Transactions on Geosciences and Remote Sensing. 1994. 32; 779-785.

[18] Iwasaki, A., and Tonooka, H. *Validation of a Crosstalk Correction Algorithm for ASTER/SIWR*. IEEE Transactions on Geosciences and Remote Sensing. 2005. 43 (12) 2747-2751.

[19] Kalinowski, A., and Oliver, S. 2004: *ASTER Mineral Index Processing Manual*. Ed. Geosciences Australia.

[20] Kruse, F.A., Lefkof, A.B., Boardman, J.W., Heiedbrechet, K.B., Shapiro, A.T., Barloon, P.J., and Goetz, A.F.H. *The Spectral Image Processing System (SIPS) – Interactive Visualization and Analysis of Imaging Spectrometer Data*. Remote Sensing Environment. 1993. 44; 145-163.

[21] Matthew, M.W., S.M. Adler-Golden, A. Berk, S.C. Richtsmeier, R.Y. Levine, L.S. Bernstein, P.K. Acharya, G.P. Anderson, G.W. Felde, M.P. Hoke, A. Ratkowski, H.H. Burke, R.D. Kaiser, and D.P. Miller. *Status of Atmospheric Correction Using a MODTRAN4-based Algorithm*. SPIE Proceedings, Algorithms for Multispectral, Hyperspectral, and Ultraspectral Imagery VI. 2000. 4049; 199-207.

[22] Nunes, G.M., Souza Filho, C.R., and Ferreira, L.G. *Caracterização De Fisionomias Vegetais Em Área De Floresta Tropical Através De Análises Espectrais Em Dados E Produtos Do Sensor ASTER,* In: Simp. Bras. de Sens. Rem., Florianópolis, INPE. 2007. 13; 6497-6504.

[23] Nunes, G.M., 2008: *Sensoriamento Remote Aplicado Na Análise Da Cobertura Vegetal Das Reservas De Desenvolvimento Sustentável Amanã E Mamirauá*. Tese de Doutorado, IAG-Unicamp.

[24] Richards, J.A., 1993: *Remote Sensing Digital Image Analysis*. Springer, Heidelberg, New York.

[25] Smith, M.O., and Adams, J.B. *Interpretation of AIS Images of Cuprites, Nevada, Using Constrains of Spectral Mixtures*. In: Airborne Imaging Spectrometer Data Analysis Workshop. Pasadena, CA. Proceedings, JPL Publ. 1985. 85-41, 62-68.

[26] Schowengerdt, R.A., 2007: *Remote Sensing: Models and Methods for Image Processing.* Third Edition. Academic Press. 509.

[27] Souza Filho, C.R., Tápia, C.H., Crósta, A.P., and Xavier, R.P., 2003: *Infrared Spectroscopy and ASTER Imagery Analysis of Hidrotermal Alteration Zones at the Quellaveco Porphyry-Cooper Deposit, Southern Peru*. In: Proceedings of the American Society of Photogrammetry and Remote Sensing (ASPRS), Annual Conference – Technology: Converging at the Top of the World. 1-12.

[28] SULSOFT, Guia do ENVI em Português. Disponível em: <http://www.envi.com.br>. Acesso em: 06/07/2013.

[29] Van der Meer, F., 2000: *Imaging Spectrometry Geological Applications.* In: The Encyclopedia of Analytical Chemistry, Meyers R.A. (Ed.), John Wiley & Sons Ltd., Sussex, U.K. 8601-8638.

[30] Vicente, L.E., 2007: *Caracterização De Sistemas Ambientais Tropicais Complexos Utilizando Análise Sistêmica E Classificação Hiperespectral De Dados Do Sensor ASTER (Advanced Spaceborne Thermal Emission And Reflection Radiometer)*. Tese de Doutorado, IAG-Unicamp.

**Cloud Publications**
International Journal of Advanced Remote Sensing and GIS
2014, Volume 3, Issue 1, pp. 467-475, Article ID Tech-223
ISSN 2320 - 0243

Research Article | Open Access

# Space Technology in Transport Disaster Search and Rescue Operation: the Challenge for Africa

**J.J. Dukiya**

Department of Transport Management Technology, Federal University of Technology, Minna, Nigeria

Correspondence should be addressed to J.J. Dukiya, duksat2000@futminna.edu.ng, duksat2000@yahoo.co.uk

Publication Date: 30 January 2014

Article Link: http://technical.cloud-journals.com/index.php/IJARSG/article/view/Tech-223



**Abstract** Science and technological advancement is not so pronounced in any sector globally as in the transport sector that is obvious since the first Ford's Model Ts vehicle in 1908 which has metamorphosis into the present day hybrid vehicles. But the towering environmental hazard accompanying these developments is of major concern. Disasters are sometimes natural, human-induced or both. But the long time-lag between the occurrence of mishap and the rescue operation carried out is the major factor responsible for the great loses of life and properties especially in the developing countries like Nigeria with high road and air accident records. This paper is aimed at exploring the critical role of space technology in the provision of timely and qualitative information that facilitates the works of the disaster management agencies especially in critical decision making for better preparedness as a challenge for African countries. The analysis reveals that GIS and RS is the pivot on which a timely SAR revolve, and that the present status of most African countries' SAR operations is obsolete, disjointed and none real-time based. It is therefore recommended that a more dynamic synergy and coordinated SAR operation that leverage on remote sensing techniques be developed.

**Keywords** *Environment Hazards; Rescue Operation; Remote Sensing and Transportation*

## 1. Introduction

Human imperfection in its entire ramification often leads to natural or man-induced hazards and vehicular crashes that call for one search and rescue operation or the other. Human intrusion into the space began when the first Russians launch Sputnik-1 into space on October 4, 1957 and the first man (Yuri Gagarin) was launched into space on April 12, 1961 when he orbited the earth for just 108 minutes. Environmental hazard can be in the high sea, in the air, or on the earth surface. The more we probe into any of these earth spheres, the more we are exposed to accident of different degrees. The method of rescue operation carried out depends to a large extent on the technological know-how at that point in time in a giving society.

Although much can be said to have been achieved in the area of science and technology especially in communication, transportation and space exploration; but human imperfection in all these field are glaring with the rate of crashes which do result in loss of life and property in the national and international project investments. For instance, SEASAT, launched on 28 June 1978 operated for only 105 days due to power failure. On January 28, 1986, the greatest tragedy in space flight occurred when the Shuttle Challenger exploded in the air 73 seconds after it was launched. The seven members of the crew including a civilian space teacher Christa Mc Auliffe were all killed. Also, in November 2010 and just in july, 2013, Russia lost bilions of dollars in the rocket lounch failure.

### 1.1. Aims and Objectives

The aim of this paper is to explore the critical role of space technology in the provision of timely and qualitative information that facilitates the works of the disaster management agencies especially in critical decision making for better preparedness as a challenge for African countries. The objectives include:

a. Examine the experiences of UN Agencies and other specialist that used remote sensing data for transport disaster management;
b. Review various hazards that often plague human ingenuity under the various transport modes;
c. Examine some of the African countries SAR operational structure and techniques, and
d. Assess the link between the applications of remote sensing data and ground control stations, and the associated benefits arising from effective spectrum management.

## 2. General Hazards in Various Spheres of the Earth

Hazards that plague man-kind in the various spheres are either natural or man-induced following the school of thought of environmental possibility as against determinism. The intrusion of man into the spheres as a result of technological advancement has trigger lots of mishaps that tend to overwhelm the existing combating system as revealed in the following incidences.

### 2.1. Water Related Hazard

The great water bodies like the oceans, rivers, and lakes have been a major support to human survival in different ways. The key activities in these water bodies are animal and fish hunting, off-shore mining (crude oil), sea bed exploration and marine transport. All this activities are not free of one hazard or the other that involve the loss of both human life and properties. Flooding activities in the form of tsunamis that ravage most coastal cities globally like that of India flash flood in June, 2013 leaving 65,000 people stranded and 5,000 people unaccounted for. African countries like Nigeria have her own share in 2012.

### 2.2. Atmospheric (Air) Related Hazard

Another major hazard that plagues space exploration and aviation industry is the issue of power failure and malfunctioning of spacecraft and other related causes.

Whenever aviation mishap is discussed in Nigeria, three important years would always bring back reminiscences of fresh mourning and agonies to some individuals. Dates such as July 11, 1991 when the nation lost 247 pilgrims who were on their way home from Jeddah, Saudi-Arabia; September 26, 1992 in which a generation of young military officers (about 163) perished at Ejigbo at the out-skirt of Lagos and November 7, 1996 a day the nation recorded a casualty figure of 143 lives through plane crash. Also the case of DC-9 commercial plane, owned by Sosoliso Airlines, that was carrying 75 school children (aged between 12 and 16) home for the Christmas holidays and staffs of Loyola Jesuit

School in Abuja were among the 103 people that crashed in Port Harcourt (Midweek Concord [1]; National Concord [2]).

Another one was ADC airlines flight to Sokoto in which the spiritual leader of Nigerian Muslims; his Eminent Mohammadu Maccido and his son, a senator, and other northern leaders were among the 104 people crashed near Abuja; see Figure 1 for the relics.

At Somalia, an Ethiopian military aircraft carrying ammunition crash-landed at Mogadishu's international airport, bursting into flames and killing four of the six crew members. Somalia's aviation record is among the worst on the continent that has a history of plane disasters; see Figure 2 for the relics (Abdi and Feisal) [3].


***Figure 1:*** *ADC Airline to Sokoto Crash*
Source: BBC News

***Figure 2:*** *Plane Crash at Mogadishu's International Airport*
Source: BBC News

## 2.3. Land Related Hazard

Land related hazard include fire accidents, road traffic crash etc. Loss of lives and destruction of various sources of livelihood (properties) as a result of road accidents is unquantifiable as reveal by the pages of daily newspapers and network programmes, see Figure 3 and 4 for such instances. For instance, no fewer than 22 people lost their lives in an auto accident which occurred on Kwanar-K of road, about 62 kilometres from Kano, on Wednesday as a result of tyre burst. The accident occurred a week after the state was thrown into mourning following the death of 22 members of a family in another road accident on Gwarzo road, Kano State.

***Figure 3:*** *100 Nigerians Burnt to Death in Trailer Tanker Fire Accident (June, 2012)*

***Figure 4:*** *Multiple Trailer Carnage Burnt by Petrol Tanker Accident*

Science can predict the activities of weather and climate, wave and wave actions, but less of how to predict whether a particular trip will crash midway of a journey or a particular stroke will cause a wild-fire and also lack the necessary up to date technique to respond to those incidences.

From the foregoing discussion on areas of environmental hazard and disasters, the question then is "what are the effective techniques of rescue operation that can mitigate the total loss of life and properties in all this occurrences. Space Technology is the worldwide accepted panacea to environmental hazard surveillance and mitigation technique as will be discussed in this paper.

## 3. Space Technology and Search/Rescue Operation

The alarming rate of environmental hazard at the three spheres of human activities (hydrosphere, lithosphere and atmosphere) have agitated the mind of experts in space operation technology that calls for series of national and international summits on natural and human-induced environmental hazards among which are:

The World Telecommunication Development Conference 2006 (WTDC-06) - Resolution 34 focused on the role of telecommunications/information and communication technology in early warning and mitigation of disasters and humanitarian assistance. While Plenipotentiary Conference 2006 (PP-06) - Resolution 136 focused on the use of telecommunications/information and communication technologies for monitoring and management in emergency and disaster situations for early warning, prevention, mitigation and relief.

The World Radio-communication Conference 2007 (WRC-07) recognizes that the radio frequency spectrum is a critical resource for remote sensing and environmental management, particularly in the search and rescue operation. Also in the international workshop on crew Safety and Rescue held at Le Bourget on 7 June 1987 which brought together more than 150 space professionals including engineers, astronauts and managers; jointly organized by AAAF, AIAA and ESA focused on the complementary of ground based and space-based rescue systems and the importance of the response time to an emergency.

The Global Maritime Distress and Safety System (GMDSS) as an internationally agreed-upon set of safety procedures to rescue distressed ships, boats and aircraft. While the International Mobile Satellite Organization (INMARSAT) is a satellite system under the International Mobile Satellite Organization (IMSO) is an intergovernmental organization that oversees certain public satellite safety and security communication services provided via the satellites, see Figure 5 for the map of the member countries where more than 50% of African countries are yet to be members compared to other continents of the world.

***Figure 5:*** *Inmarsat Member States as at 2013*
**Source:** International Mobile Satellite Organization.png

### 3.1. Remote Sensing Operation Missions Techniques

It will be necessary at this juncture to give a general view of the definition of Remote Sensing (RS) technology as "an act of observing and measuring an object or phenomenon by the use of electromagnetic sensors placed on a fixed or moving vehicle without physical contact. It operates with four components via: energy source, radiant interaction with the earth surface, interaction with the atmosphere and the final detection by the sensors" (Alexandre [4]) with this definition, the uniqueness of remote sensing technique in environmental issues like SAR includes the following:

a) Real-time data-information collection;
b) Potential for direct Electro-transmission to receiving stations and action areas;
c) Comparatively low-cost of large area coverage;
d) Ability to operate day and night via thermal infrared and microwave sensors.

Remote sensing application in SAR operation can be seen as space digital data technology assemblage. Sensors like the Scatterometer and Radiometer and even Radar series can be placed in special aircraft as done by companies like Motorola Inc or placed on space borne satellite launched by various countries space research centres like; Russian-COSMOS-1500, U.S-SKYLAB, GEOSAT, IKONOS, France-SPOT-5, QUIKBIRD and even the Nigeria-Sat-X etc. While SAR operation is an amalgamation of different but related professions' technical knowhow like the Remote sensing scientist, Naval force, Air force, Police, Road safety, Red Cross, Fire service, etc. for disaster management and mitigations.

There are series of air space missions that are oriented to search and rescue activities. For instance, COSPAS/SARSAT is a joint international Search and Rescue Satellite Aided Tracking System established and operated in January 1986 (ESA [5]).

In the case of fire related search and rescue operation, the infrared scanning system can penetrate through smoke while the line scanner system can map fire and locate their hot spots. After the first hand notification, the smokejumper reaches the fire site by helicopter parachute as used in a fire incidence at Nezperce forest in Northern Idaho (Trevett [6]).

### 3.2. Operation on the High Sea

In the search and rescue operation on the high sea, remote-sensing technique has proved vital and indispensable for fruitful operation. Satellites such as Seasat, launched on 28 June 1978 were the first satellites with a scatterometer (after tests on Skylab). Seasat was also equipped with a Radar Altimeter and the Scanning Multichannel Microwave Radiometer (SMMR) (Dalati [7]). Microwave sensors generally have the ability to penetrate through the water bodies and reveal water bed materials. See Figure 6 and 7 for space based rivers and high sea search and rescue operations.

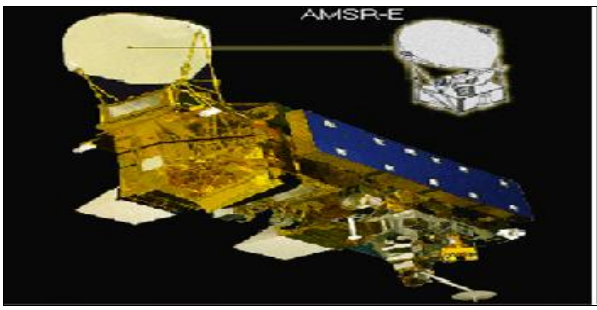


***Figure 6:*** *Satellite-based Flood Assessment*
**Source:** Dartmouth Flood Observatory College

***Figure 7:*** *Danish Air Force S-61A with Its Rescue Swimmer*

## 4. Africa Initiatives in Rescue Operation Mission

African countries bordering the Atlantic and Indian Ocean have some MOU on maritime rescue regional grouping with major countries heading each group. The South Africa sub-regional group appears to be more organized and more pro-active than others like Nigeria sub-grouping, see Figure 8 for the maritime grouping.

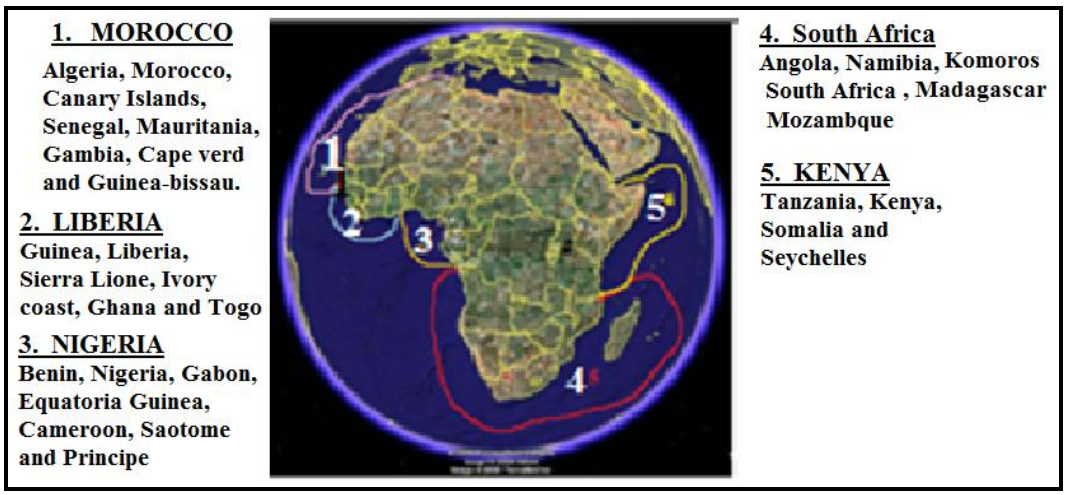


***Figure 8:*** *Regional Maritime Rescue Coordination Centre (MRCC) for Africa*
**Source:** After Botes A. (Head of Maritime SAR operation)

### 4.1. South Africa Position

South Africa is the only country that has a relatively coordinated search and rescue organization called South Africa Search and Rescue Organization (SASAR). It is made up of representatives from government departments, commercial and voluntary organizations which are signatories to SASAR which are able to contribute service and facilities.

### Ghana Position

The Ghana Maritime Authority (GMA) is mandated to coordinate maritime Search and Rescue activities in collaboration with other relevant agencies. National Maritime SAR Coordinating Centre at Tema is to be linked to the Regional Maritime SAR Coordinating Centre in Monrovia, Liberia to provide effective search and rescue coverage for the countries in the sub region. The GMA has concluded bilateral arrangements with the United Kingdom Hydrographic Office (UKHO) to publish hydrographic and safety information covering the Ghanaian coast on navigational charts for dissemination to ships (GMA [8]).

The country is to establish a Vessel Traffic Management Information System (VTMIS). The Contract Agreement for the project was signed on February 9, 2011 between the Ghana Maritime Authority/Ministry of Transport and ELTEL Networks Corporation of Finland. The VTMIS consists of the following among other things:

a. An integrated system comprising of eight (8) Remote Sensor Sites to be sited along the entire coast of Ghana from Keta to Half Assini.
b. Three (3) Remote Base Stations (RBS) along the Volta Lake (for the inland waterways).

### 4.2. Nigeria Position

Nigeria that is often referred to as the giant of Africa is yet to fully organize a well-coordinated space technology based search and rescue operation. For instance, how can one explain the episode of the Bellview Airlines crash on Saturday at about 20.45 (19.45 GMT) on its way to Abuja from Lagos that was first reported found on Sunday morning by a police helicopter search team near Kishi, Oyo state, 400 km (320 miles) from Lagos; was later found at Lissa in Ogun state, about 50 km (30 miles) from Lagos. According to (Yusuf and Ikechiji [9]) a vast country like Nigeria has only one search and rescue helicopter that is parked in the "Office of the Presidency".

It was after much air mishaps in the country that the Federal Airport Authority (FAA) began to talk of the establishment of search and rescue service in the country. Some of the facilities in the country lack proper coordination, see Figure 9 for an air crash simulation exercise undertaken by NEMA and other relevant agencies at the Murtala Muhammed airport Abuja, but after display what next?

***Figure 9:*** *Air Craft Hazard Simulated with NEMA Helicopter at Abuja, Nigeria*

The question is how many underwater breathing apparatus (SCUBA, surface-supplied air, re-breathers, etc.) are available for water divers in the country? In fact, it just in the year 2013 that the Nigerian Air Force (NAF) signed a Memorandum of Understanding (MOU) with the Nigerian Maritime Administration and Safety Agency (NIMASA) in the fight against crime in the nation's coastal waters (Nigercom Network [10]; National Concord [11, 12]; Ronald [13]; NEMA [14]).

## 5. Conclusion

From the ongoing discussion on search and rescue operation and the billions of naira been lost in various hazards and mishaps due to improper coordination of agencies and lack of up-to-date space technology equipments in most African countries SAR, the policy makers need to be fully sensitized on the need to fund and enhance the capacity building of the relevant rescue agencies.

### 5.1. The Way Forward

A functional SAR is not unachievable if there is a political will. Although political instability quagmire is a major monster against the progress of African countries, the following recommendations are some of the panacea to the ailing SAR operation in the continent:

a. A budgetary allocation should be established at all level to finance the activities of those agencies and units.

b. The National Emergency Management Agency (NEMA) at the central level should be the coordinator and the superior commander of the allied agencies through special signal networking.
c. NEMA should have a legislative power to call upon allied agencies and departments that are signatory to SAR mission when their support services are required.
d. There should be hierarchical regional, states, local government and municipal disaster emergency coordinating units with relatively up-to-date Radar system and communication equipments to respond to issue within their jurisdiction or send distress call to NEMA.
e. The Unified Command structure should issues operation orders and mission assignments to activate responses based on the scope and magnitude of the threat or incident as indicated in the proposed organizational structure (see Figure 10). The coordinating centre is to establish communication links with support agencies and regional coordinators which will provide the relevant agency and other stakeholders with Situation Status (SITSTAT) and Resource Status (RESTAT) as required, (COES, 1999).

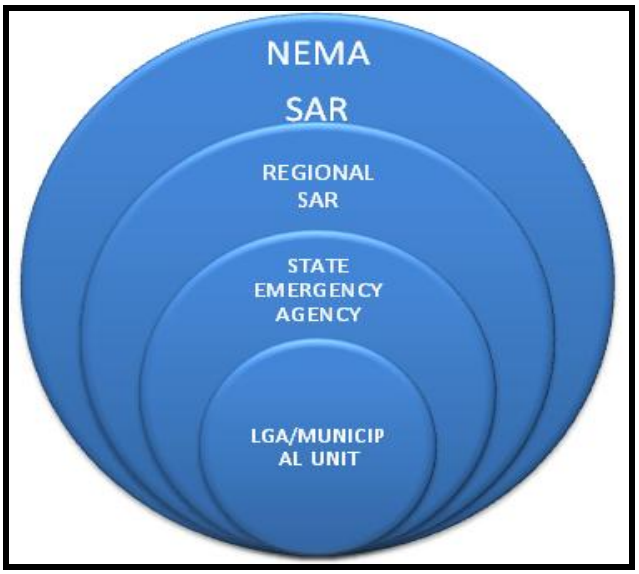


***Figure 10:*** *Organizational Structure of National SAR*

## References

[1] Midweek Concord, Wednesday, December 4, 1996. 3.

[2] National Concord, Tuesday, December 17, 1997. 11.

[3] Abdi Sheikh and Feisal Omar. Military Plane Bursts Into Flames at Mogadishu Airport. August 09 2013, 14:53. http//www.bdlive.co.za/Africa/africanews/2013/08/09.

[4] Alexandre VASSILIEV. The Role of Remote Sensing in Disaster Management, Paper Presented at the Workshop Organized in Geneva, 10-11, December, 2007.

[5] ESA. Reach for the Skies in ESA's. Quarterly Publication on Space Transportation System No. 7, 1992.

[6] Trevett J.W. *Imaging Radar for Resources Survey*. Chapman and Hall, USA. 205-251.

[7] Dalati M., 2000: Lineaments on Landsat Images-Detection, and Tectonic Significance in North Western Depressions of Syria. Proceedings of XIX International Congress for Photogrammetry and Remote Sensing, ISPRS, Volume XXXIII, Part B7/1, Amsterdam, Netherlands, 301-308.

[8] Ghana Maritime Authority's Rescue Activities. http://www.ghanamaritime.org/en/services/search-and-rescue-activites.php.

[9] Yusuf Alli and Ikechiji. Nigeria Has Only One Helicopter for Search and Rescue, 2008. http://thenationonlineng.com/dynamicpage.asp?id=51265 (Accessed on 25th November, 2012).

[10] Nigercom Network. SAR Committee Seeks Oil Majors' Cooperation in Tackling Maritime Mishaps. allafrica.com (19 February, 2010).

[11] National Concord Monday, December 23, 1996. 16.

[12] National Concord, December 22, 1997. 1-2.

[13] Ronald Mutum. Air Force Partners NIMASA on War against Crude Oil Theft. DialyTrust. 26 of August, 2013.

[14] NEMA Annual Report. National Emergency Management Agency, the Presidency, Abuja, Nigeria. 2012. 124-139.

[15] California Office of Emergency Services (COES). Search and Rescue Model Operating Plan, A Guide for State and Local Government, 1999.

**Cloud Publications**
International Journal of Advanced Remote Sensing and GIS
2014, Volume 3, Issue 1, pp. 446-466, Article ID Tech-228
ISSN 2320 - 0243

Research Article | Open Access

# An Experimental Comparison of Line Generalization Algorithms in GIS

**Younis Saida Saeedrashed**

Department of Civil Engineering, University of Gaziantep, Gaziantep, Turkey

Correspondence should be addressed to Younis Saida Saeedrashed, younus.saida.69@gmail.com

Publication Date: 23 January 2014

Article Link: http://technical.cloud-journals.com/index.php/IJARSG/article/view/Tech-228



**Abstract** During the process of "Digitizing" which requires execute of huge amount of sequential vertices and segments for creating layers that are in vector base, cartographers face two main problems which are; the quality of presented data and the file size. Despite that the process of line generalization is a superior solution to overcome these two problems, it produces errors such as spike, line-crossing, line-coincident, and polygon knot in the topological structures of lines being generalized. Geometric data that have complex topological structure can be simplified and smoothed by applying four types of techniques based algorithms, which are; Nth Point, Jenks, Point Remove, and Bend Simplify. In this paper, through an experimental comparison study, it is proved that the bend simplify algorithm is the best approach amongst four types of algorithms applied to line generalization that preserves the quality of the line being generalized and reduce the file size moderately.
**Keywords** *Geographical Information Systems (GIS); Algorithms; Line Generalization*

## 1. Introduction

GIS–based generalization became the more applicable approach among cartographers, enabling them to manipulate and process spatial data more effectively than before. One of the essential tasks of implementing a GIS-based solution for generalization is the automation of generalization process that used to be done manually by experienced cartographers (Lee and Hardy, 2005).

Generalization can be used for deriving small scale maps from large scale maps that are in high resolution and accuracy. It requires geo processing algorithms and problem solving, which are performed at the topology level before feature symbolization. From the moment objects are generalized, geographical objects undergo changes in their geometry and, from these, significant changes may occur in the topological or none topological relations among the elements. Nevertheless, according to McMaster, the generalization process must try to preserve the consistency of topological matters (Dal Santo et al., 2007).

There are four significant individual components of automated generalization, which are: simplification, smoothing, displacement, and enhancement. Simplification may be described as the elimination of unwanted detail. Specifically, simplifications algorithms identify and eliminate superfluous coordinate pairs by applying a variety of mathematical criteria, such as angular deviation or distance between points (McMaster, 1987). In this study some techniques are experimented using methods of algorithms such as: Point Remove, Bend Simplify, Nth and Jenks to discover some aspects of “Automated Generalization” that can be applied on some data before and after implementing each of aforementioned methods. Generalization results in changes or displacement of data points from their original positions. Part of the displacement can be minimized by carefully choosing algorithms and parameters, executing generalization operations in a certain order (Muller et al., 1995).

This paper concerns the evaluating of different types of algorithms methods according to the obtained results. The main objective of this experiment is to determine relatively the best method amongst these four types of algorithms based on two criteria which are the file size of the produced feature classes (vector layers) and the quality of the topographic structures of the poly-line being generalized.

## 2. Methodology

### 2.1. Selected Feature Class

The shape-file which is titled "Gower" has been selected in order to be processed by four types of practical algorithms methods. The properties of this shape file such as file size, length of the digitized poly-line, and the number of vertices are investigated and recorded as a baseline of the applied tests. Figure 1 shows the selected feature class "Gower" and the part of the poly-line which subjected to the Generalization process.

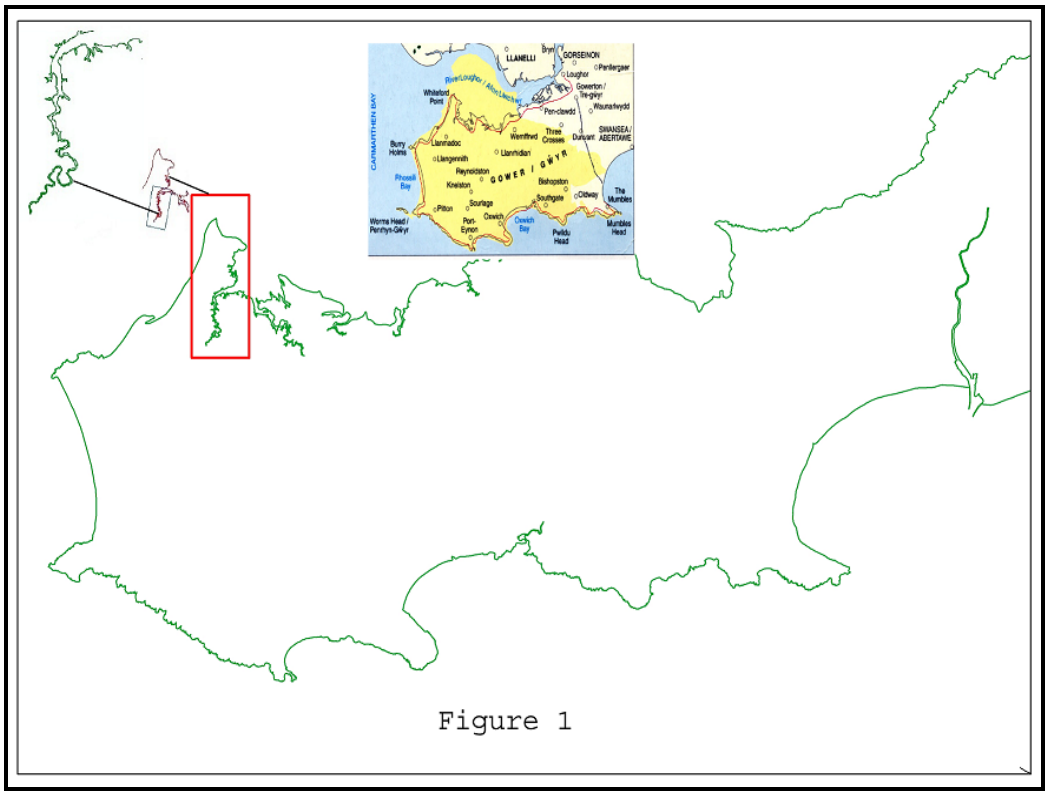


Figure 1

***Figure 1:*** *Gower-Poly-line (Boundary of Western Region of South Wales, UK)*

### 2.2. Concept of Line Generalization

In map simplification, algorithms are applied to digital files to remove unwanted detail, to select or emphasize particular items, or to clarify by removing visual clutter. Most simplification algorithms incorporate some mechanism to control the amount of detail that is removed (McMaster et al., 1991)

### 2.3. Line Simplification

Line simplification is the process of removing some of redundant distributed points along the poly-lined based on an algorithmic calculations. “Simplification” is the process of eliminating unwanted detail. However, some important factors should be taken into consideration while cartographers perform generalization process: reality, map purpose, map scale, quality and quantity of available data, audience, condition of use, and graphic limits (Robinson et al., 1995). As the amount of simplification increases, the degree of sub optimality increases in absolute terms but declines in relative terms when compared to the entire distribution of possible distortion values (Veregin, 1999).

### 2.4. Line Smoothing

Line smoothing is the processes of adding up points (additional vertices) to the rough poly-line for smoothing it. This process is essential to smooth sharp angles in lines to improve aesthetic or cartographic quality. Figure 2 shows both simplification and smoothing processes.

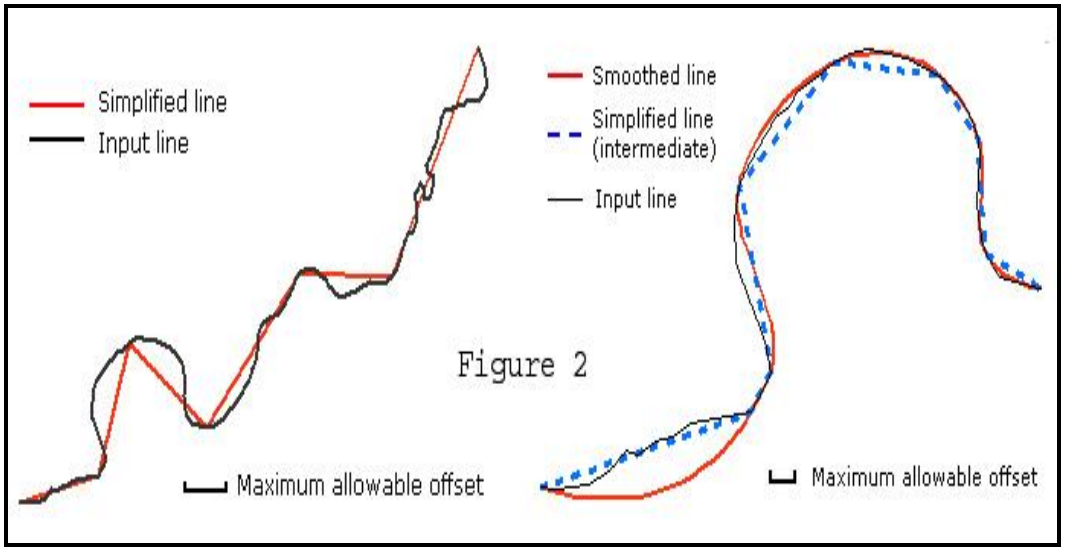


***Figure 2:*** *Principle of Simplification and Smoothing*

### 2.5. Produced Errors in Line Simplification

Generally, there are two types of data errors: inherent errors embedded in the source of data and operational errors introduced by users during data input, storage, analysis, and output. Inherent errors can be avoided by using the right kind of data. While, operational errors can be prevented by quality control and training (U.M. Shamsi, 2005).

Errors can be removed either manually which is time consuming and requires skilled cartographers, or automatically which is a more accurate and time saving process. In these experiments, introduced errors during the line simplification process have been removed automatically, since both Point Remove and Bend Simplify are provided by a function that enables the cartographers to perform the

correction process while the operation is carrying on. On the contrary, the first two applied approaches: Nth Point and Jenks are not provided by the capability of automated removing errors.

The process of removing points and smoothing lines is a sensitive application that should be performed with an intensive care. Especially, in regions where the poly-line itself has an opposite direction, approximately very close and parallel to each other, as the case in the selected sample, Figure 3 indicates such case. The reason is that the simplification process for removing points in such regions is quite possible to produce errors like Line-coincident, Spike, Line-crossing, and Polygon knot. Also, it is possible to find more than one type of errors successively within a specific region along the poly-line.

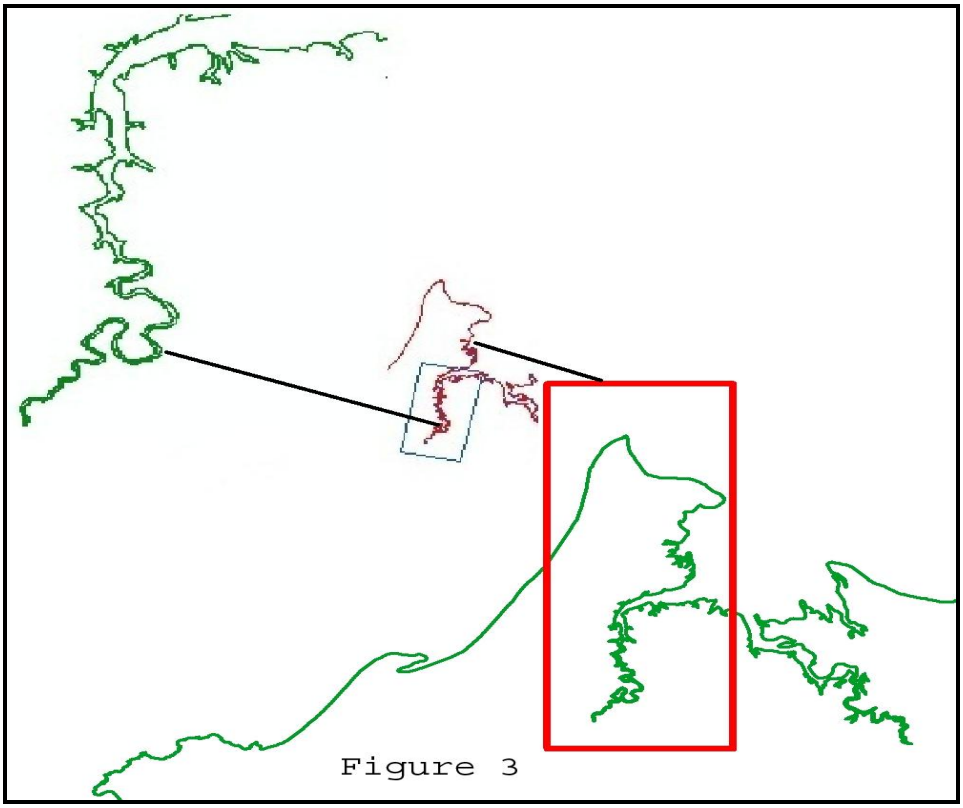


***Figure 3:*** *Selected Region for Applying Methods of Algorithm*

There are four types of errors that produce from the simplification process which are: A-Line-coincident Error, B- Spike Error, C- Line-crossing Error, and D- Polygon Knot Error. Figure 4 illustrate these types. Line-coincident Error is a the error generated after performing simplification process where the two part of the same poly-line join each other alongside specific portion and they separates from each other in the other parts. Spike Error generated after performing simplification process where the poly-line intersect itself within a very small distance between two successive points creating a sharp spine. Line-crossing Error emerges after performing simplification process where the poly-line intersects itself in a specific point. Polygon Knot Error occurs after performing simplification process where the poly-line intersect itself into two successive points that are far from each other creating closed region that looks like polygon.

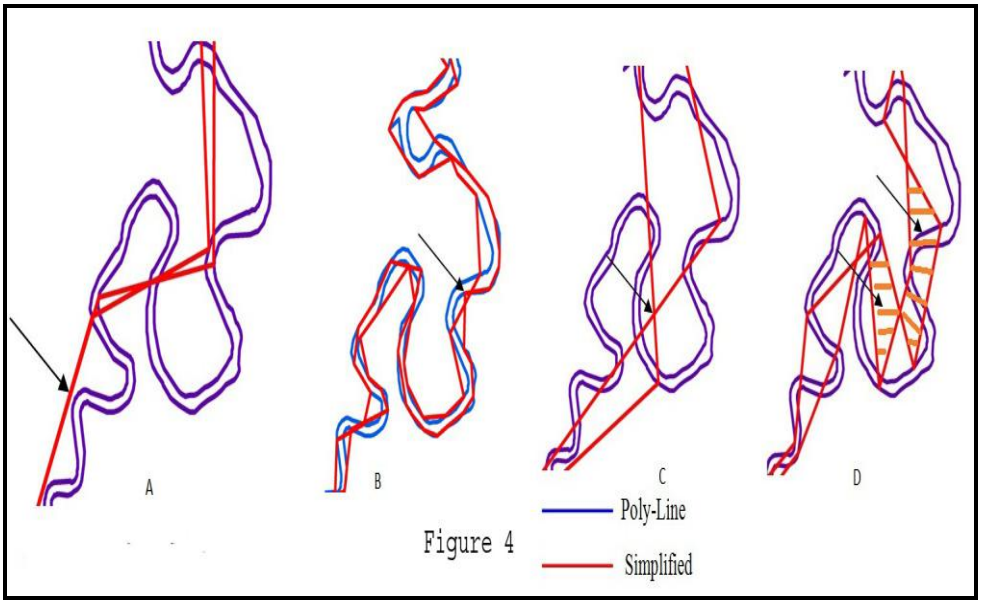


***Figure 4:*** *Produced Types of Errors from Simplification Process*

### 2.6. Produced Errors in Line Smoothing

There are two types of applied algorithms used for smoothing poly-lines which are PAEK method and BEZIER-INTERPOLATION method. Usually, smoothing process causes a displacement of poly-line from its original location and an increase of vertices because of smoothing requirement.

The PAEK (Polynomial Approximation with Exponential Kernel) method smoothes lines based on a smoothing tolerance. Each smoothed line may have more vertices than its source line. The Smoothing Tolerance parameter controls the length of a "moving" path used in calculating the new vertices. The shorter the length the more detail that will be preserved and the longer the processing time (ESRI).

In the PAEK process, topological errors such as Line-coincident, Spike, Line-crossing and polygonal do not occur. Only some displacements form the original poly-line occurs. That is because the number of vertices for the smoothed poly-line becomes greater than that the original poly-line have had. There is a direct proportional between the parameters and the displacement of the smoothed poly-line. Usually, lower parameter (degree of simplification) produces less displacement. Figure 5 illustrate this.

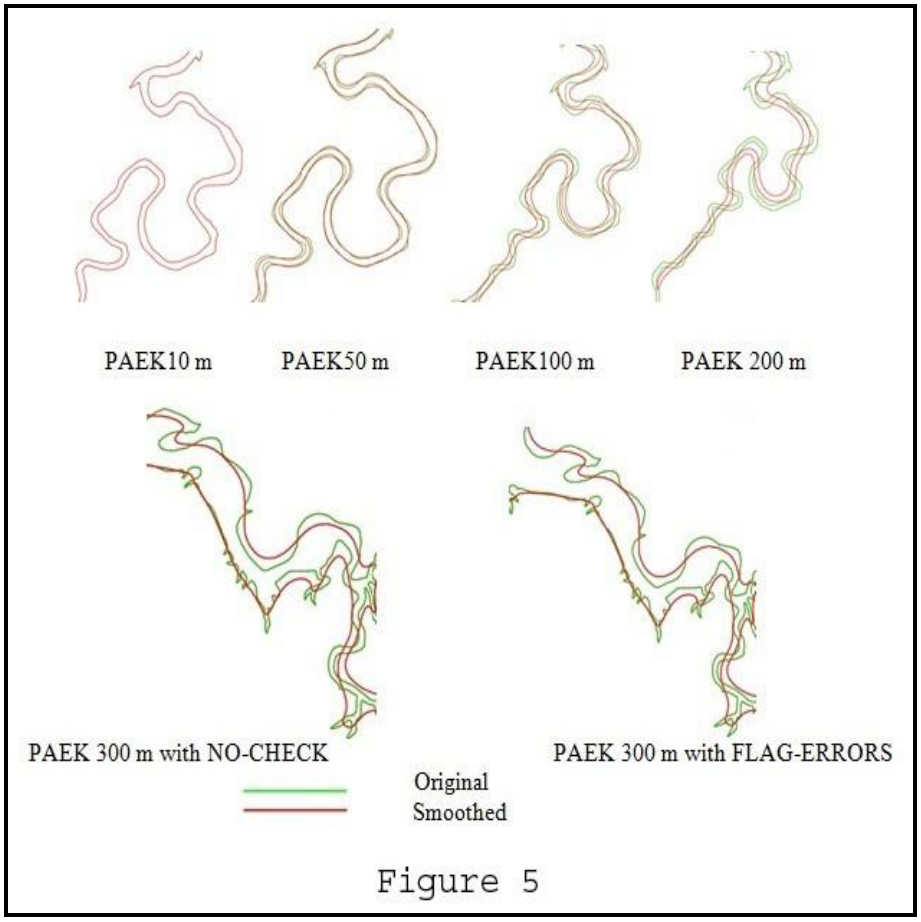


***Figure 5:*** *PAEK Smoothing*

Table 1 indicates that there is an inverse proportional between the parameters and the number of vertices of the smoothed poly-line. This means that less parameter produces less displacement with the high increase in vertices.

***Table 1:*** *Produced Vertices after Smoothing Process; Original Line Vertices = 18475*

| Parameter (Smoothing Tolerance) in Meters | No. of Vertices |
|---|---|
| 10 | 89838 |
| 50 | 30455 |
| 100 | 17326 |
| 200 | 9381 |
| 300 with Handling Topological Errors (NO-CHECK) | 6443 |
| 300 with Handling Topological Errors (FLAG ERRORS) | 6443 |

The BEZIER_INTERPOLATION method smoothes lines without using a tolerance by creating Bezier curves to match the input lines. If the output is a shape file, the Bezier curves will be approximated, since true Bezier curves cannot be storied in shape files (ESRI).

In the BEZIER process, topological errors such as Line-coincident and Spike do not occur, while errors such as Line-crossing and Polygon Knot are quite possible, as shown in Figure 6.

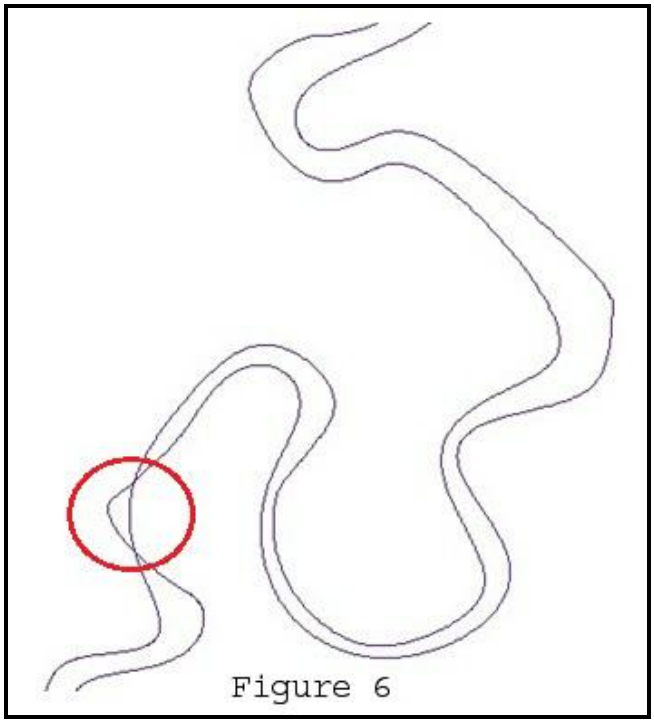


***Figure 6:*** *BEZIER Smoothing*

On the other hand, the change of the parameters values does not affect on the number of vertices of the poly-line being smoothed. Only, there is a very limited change in the number of vertices because of the smoothing process not because of changing parameters. Although, on rare occasions, some very minor displacement might occur, this can be neglected as shown in Figure 7.

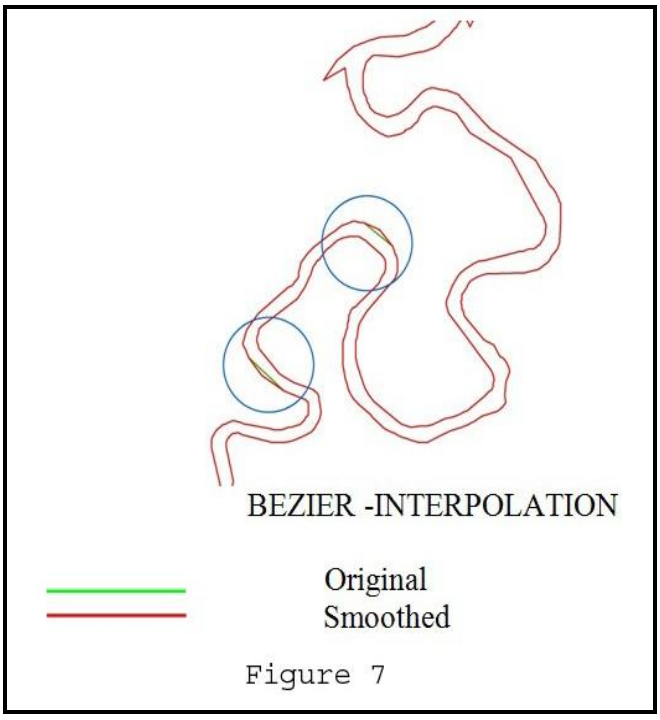


***Figure 7:*** *BEZIER-INTERPOLATION*

## 3. Methods of Line Simplification

### 3.1. Nth Point Method

This method is applied through a GUI-based visual basic program which designed specifically for processing both Nth Point and Jenks algorithm. The GUI shows the number of vertices (points) of the poly-line before and after simplification process.

This method is called Point Elimination Algorithm. In this process, the first coordinate point will be taken and every Nth point there after (e.g. 2nd, 4th, 6th etc). The larger the value of N, the greater will be the simplification (Robinson et al., 1995). These routines are very computationally efficient, but they are unacceptable for accurate mapping applications (Taylor, 2005).

In this test, the number of vertices (spots) of poly-line is 18475 and the obtained results from this method are listed in the Table 2.

***Table 2:*** *Produced Vertices after Nth Point Process; Original Line Vertices = 18475*

| Parameter (N Tolerance) in Meters | $N^{th}$ Point Algorithm |
|---|---|
| 10 | 1848 |
| 30 | 616 |
| 40 | 462 |
| 40 (Remove Topological Errors) | 462 |
| 80 | 231 |
| 80 (Remove Topological Errors) | 231 |
| 150 | 124 |
| 150 (Remove Topological Errors) | 124 |

Figure 8 shows the topological errors introduced by Nth Point simplification. It can be noticed that the topological errors, such as Line-coincident (10, 40, 80), Spike (10), Line-crossing (80, 150), and polygonal knot (30, 40) have been produced. This program does not include removal errors capability.

Table 2 indicates that there is an inverse proportional between the parameters and the number of the points that have been removed.

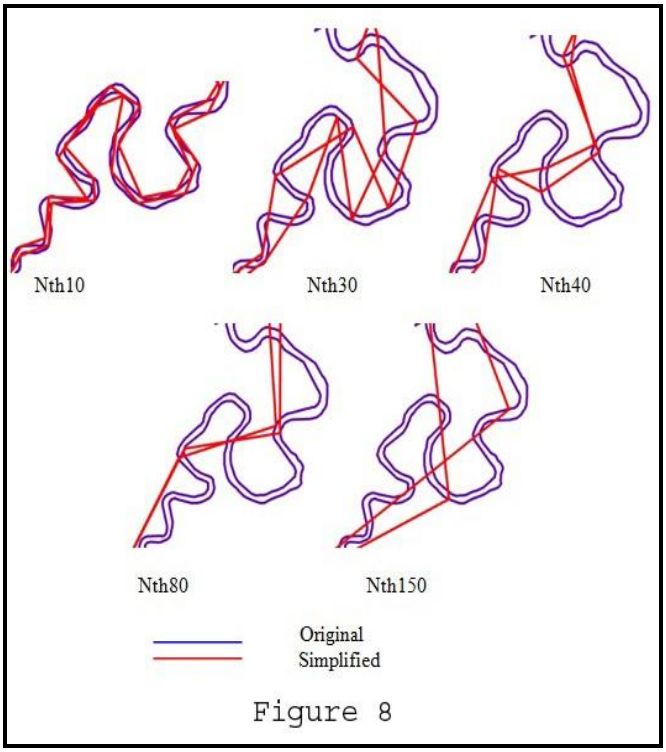


***Figure 8:*** *Topological Errors Produced by N$^{th}$ Point Simplification*

### 3.2. Jenks Method (Perpendicular Distance Algorithm)

G. Taylor stated that “This method calculates the perpendicular distance from a line connecting two co-ordinate pairs to an intermediate co-ordinate pair, as shown in Figure. First, the three points being considered are selected (**a, b, c**) and the tolerance t is set for simplification. Second, a line is defined between points **a** and **c**, the first and third coordinate pair. A perpendicular is calculated from this line to the point **b**, the intermediate co-ordinate pair. If the length of this perpendicular is greater than the tolerance **t**, the point is retained and becomes the first of the next three points selected (**b, c, d**). If the length is less than **t**, the point **b** is rejected and the next three points considered are **a, c,** and **d**. This algorithm is efficient in computer processing time and generally produces good results in application, but not in every case. Unsatisfactory, line simplification occurs with this algorithm when it is applied to curving lines consisting of many co-ordinate pairs". Figure 9 illustrate this method.

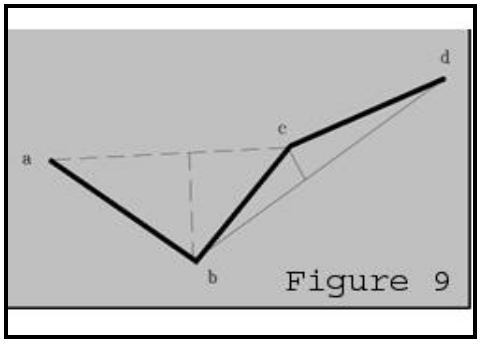


***Figure 9:*** *Adapted from Line Simplification Algorithms (Taylor, 2005)*

The number of vertices (spots) of poly line is 18475 and the obtained results from this method are listed in the Table 3.

***Table 3:*** *Produced Vertices after Jenks Process; Original Line Vertices = 18475*

| Parameter (Jenks Tolerance) in Meters | Jenks Algorithm |
|---|---|
| 10 | 5188 |
| 30 | 1495 |
| 40 | 1169 |
| 40 (Remove Topological Errors) | 1169 |
| 80 | 1012 |
| 80 (Remove Topological Errors) | 1012 |
| 150 | 1012 |
| 150 (Remove Topological Errors) | 1012 |

Figure 10 shows the topological errors introduced by Jenks simplification. Also in this process, topological errors, such as Line-coincident (10, 30), Line-crossing (40), Spike (10) and polygonal knot (80, 150), can be noticed for the same aforementioned reason.

Table 3 indicates that there is an inverse proportional between the parameters and the number of the points that have been removed.

The above applied method was repeated to perform Jenks Algorithm and the results were as illustrated in Figure 10.

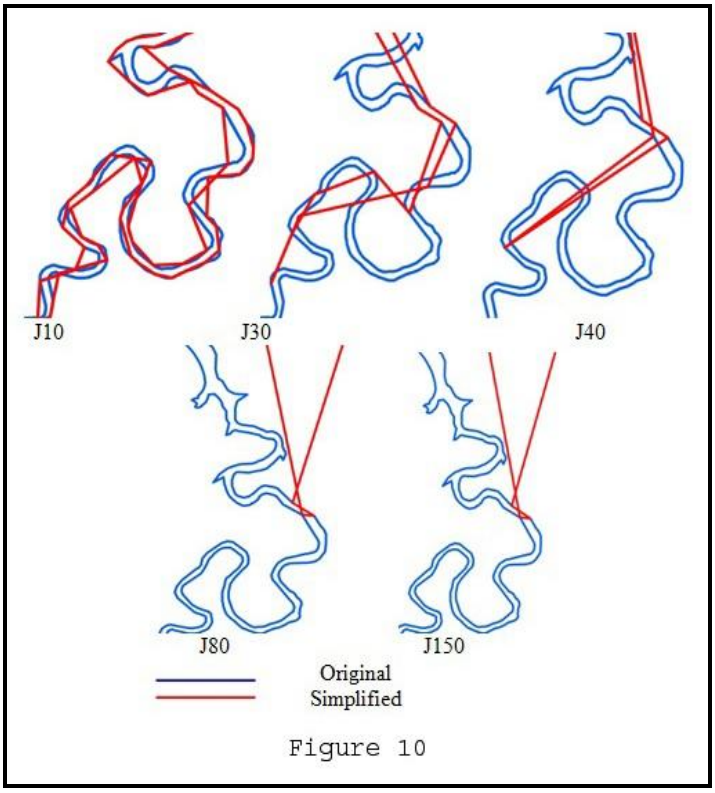


***Figure 10:*** *Topological Errors Introduced by Jenks Simplification Method*

### 3.3. Douglas and Peucker (Point Remove) Method

This method is applied through a Generalization tool which embedded into the ArcGIS tool box. In contrary with the previous two methods, this tool included the capability to perform check for topological errors and removing them.

This method is called Douglas and Peucker Algorithm. In this process the entire line, or specified line segment are considered (UNI-ZH, 1999, p.18). Point **c** has the greatest perpendicular distance to line **ab**. The elimination of points between points **a** and **c**, because no perpendicular exceeds the threshold, and the retention of point **d**, because it's perpendicular distance to line **cb** does exceed the threshold (Robinson, 1995:466). The method is illustrated in Figure 11 A.

(G. Taylor, 2005) has explained this method in more detail as it illustrated in Figure 11 B. The first point **a** is selected as the anchor point and the last point **b** is selected as the float point. The maximum perpendicular distance **fc**, from the digitized points to the line **ab** is compared with the tolerance distance **td**. If **fc>td**, then **c** becomes the new float point. Then, the maximum perpendicular distance from points to **ac**, says **ed**, is compared with **td**. If **ed > td**, then **d** becomes the new floating point, **c** is saved in the first position on a stack, or else **d** is selected as the new anchor point and all points between **a** and **d** are discarded. In this fashion the program processes the entire line, backing up onto the stack as necessary, until all intermediary points are within the corridor, or there are no intermediary points. The last float point now becomes the anchor and the first co-ordinate pair is taken from the stack to become the new float point.

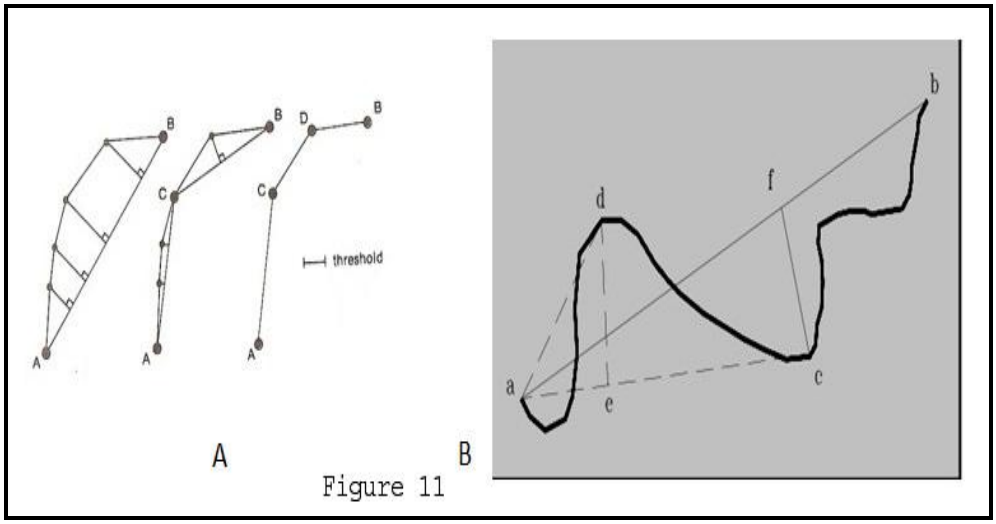


***Figure 11 A and B:*** *Adapted from Elements of Cartography and Line simplification Algorithms*

(Veregin, 2000) performed a detailed study on positional errors induced by line specification by using Douglas and Peucker Method, which showed that error can be modeled at an aggregate level using cumulative frequency curves and their confidence limits. This made it possible to identify the level of simplification that eliminates the largest number of vertices while still attaining a specific positional accuracy standard. The Douglas and Peuker Algorithm tries to preserve directional trend in a line using a tolerance factor which may be varied according to the amount of simplification required (Taylor, 2005).

The point remove method is faster than the bend simplify method. It removes redundant vertices. It can be used for data compression or coarser simplification, especially when data is well-known. The angularity (sharp corners) of the resulting line will increase significantly as the tolerance increase, so the line may become less aesthetically pleasing. Point remove produces rougher and more simplified results than bend simplify (ESRI). Figure 12 A and B illustrated both Point Remove and Bend Simplify methods.

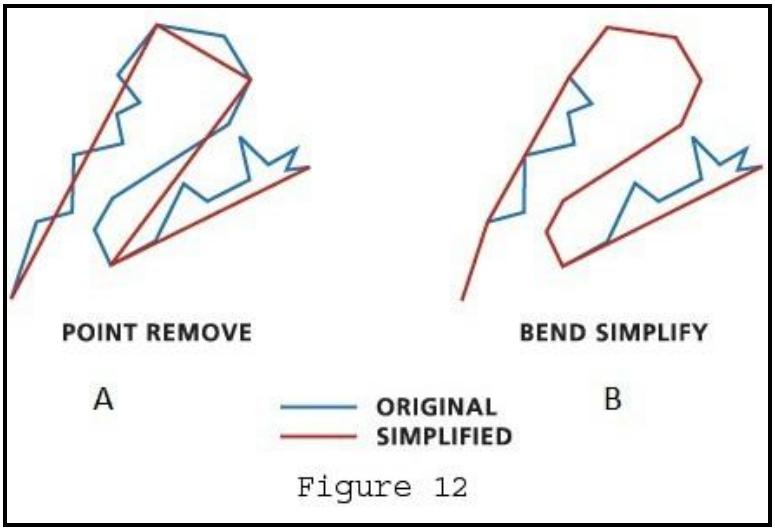


***Figure 12:*** *Sample of Point Remove and Bend Simplify Algorithm, Adapted from ESRI*

Table 4 indicates that there is an inverse proportional between the parameters and the number of the points that have been removed. The number of vertices (spots) of poly line is 18475 and the obtained results from this method are listed in the Table 4.

***Table 4:*** *Produced Vertices after Douglas and Peucker Process; Original Line Vertices = 18475*

| Parameter (Simplification Tolerance/ Maximum Allowable Offset) in Meters | Point Remove Algorithm |
|---|---|
| 10 | 2351 |
| 30 | 1028 |
| 40 | 781 |
| 40 (Remove Topological Errors) | 801 |
| 80 | 401 |
| 80 (Remove Topological Errors) | 449 |
| 150 | 212 |
| 150 (Remove Topological Errors) | 242 |

Figure 13 shows the topological errors introduced by Douglas and Peucker (Point Remove) simplification method and the data before and after processing. In this process topological errors such as Line-coincident (80), Spike (80), Line-crossing (80, 150), and polygonal knot (40) have been removed by checking specified box for activating this operation. This correction process was achieved while the generalization process was in progress. In this case, it can be noticed that the number of points after performing this operation is greater than the number of points without removing topological errors; this means that the correction process requires some more additional points.

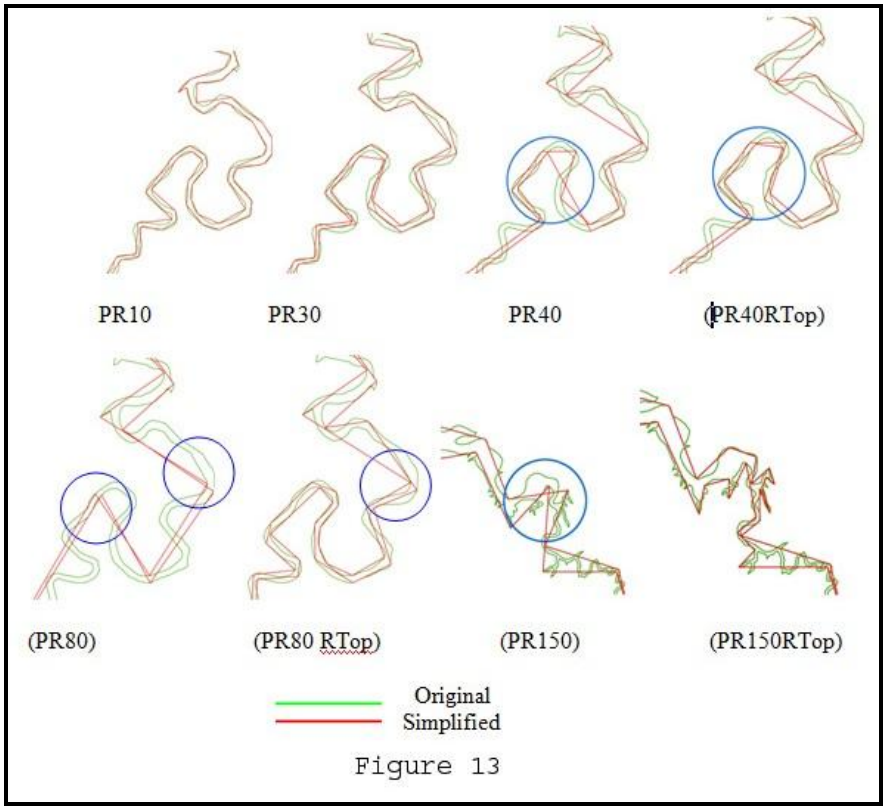


***Figure 13:*** *Topological Errors Introduced by Point Remove Simplification Method*

### 3.4. Bend Simplify Method

This method is called Wang Algorithm. In this method, arc recognition techniques will be applied, which analyzes arc characteristics and eliminates the most meaningless ones (Santo et al., 2007). This method produces results that are more faithful to the original and more aesthetically pleasing. It operates by eliminating insignificant bends along lines (ESRI).

The number of Vertices (Spots) of original line is 18475 and the obtained results from this method are listed in the Table 5, which indicates that there is an inverse proportional between the parameters and the number of the points that have been removed.

***Table 5:*** *Produced Vertices after Bend Simplify Process; Original Line Vertices = 18475*

| Parameter (Simplification Tolerance/ Reference Baseline) in Meters | Bend Simplify Algorithm |
|---|---|
| 10 | 14393 |
| 30 | 9325 |
| 40 | 7975 |
| 40 (Remove Topological Errors) | 7975 |
| 80 | 4914 |
| 80 (Remove Topological Errors) | 4998 |
| 150 | 3177 |
| 150 (Remove Topological Errors) | 3399 |

Figure 14 shows the topological errors introduced by Bend Simplify method and the data before and after processing. By applying the same approach as before, topological errors such as Line-crossing (150) and polygonal knot (80) have been removed by checking the specified box for activating errors

removing process. It can be noticed that the number of points after performing this operation is greater than the number of points without removing topological errors. This means that the correction processes during bend simplify application requires some more additional points, as well.

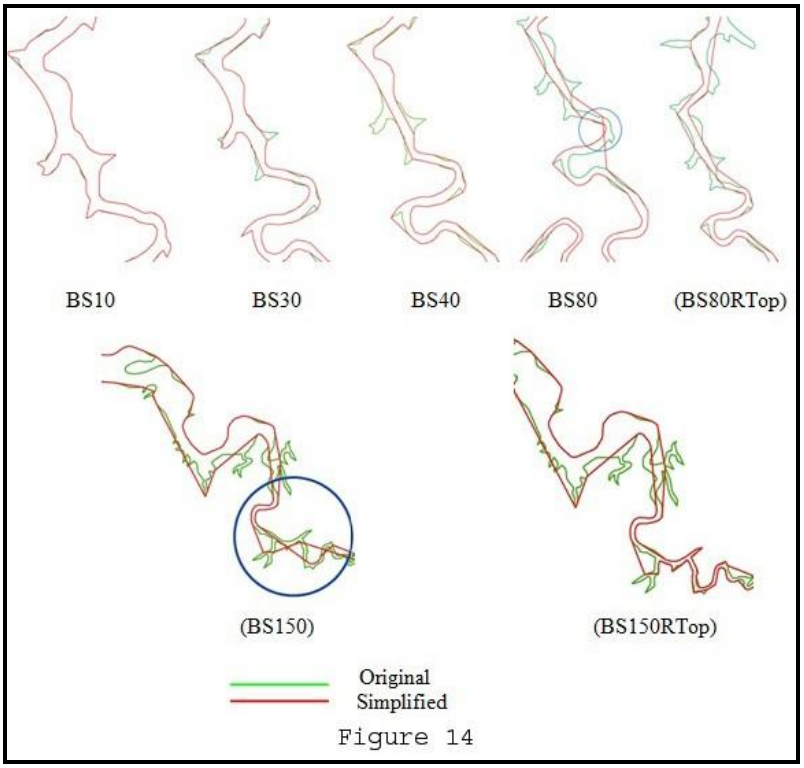


***Figure 14:*** *Topological Errors Introduced by Bend Simplify Method*

### 3.5. Software and Hardware

The computational tests are conducted to make comparisons between four methods of algorithms. This will assist in indicating potential capabilities of applied algorithms in the line simplification process. In these experiments, the following line simplification algorithms described in Section are used.

"Gower", a poly-line shape-file was used as a baseline of the required tests. Properties of the file under processing is investigated and recorded so as to be used for further required analysis. ArcGIS10 software and its add-in tools (ET Geo Wizards, and Easy Calculators 5.0) have been used to perform these tests. PC which has the specifications: 2.5 GHz of CPU and 6 GB of RAM have been used for utilizing the software.

## 4. Results and Discussion

### 4.1. Properties of Feature Class

The first step of this test commence with the investigation of properties of the original shape file which is poly-line feature class and the properties of the produced polygon from this file through the conversion process. "Gower" as a poly-line feature is converted to polygon feature using ET Geo Wizards for performing the required calculations. It can be noticed that the file specifications have not been changed during the converting process and the average segment length of polygon and the average segment length of poly-line are equal, as shown in Table 6 which indicate that the converted file has retained most of its properties.

***Table 6:*** *Specification of Original Poly-Line and Original Polygon*

| Specifications | Original Poly-line | Original Polygon |
|---|---|---|
| File Name | Gower | Gower |
| Format Type: | Shape-file | Shape-file |
| File Size of Original Poly-line | $F_{opl}$ = 289 kb | |
| File Size of Original Polygon: | | $F_{op}$ = 289 kb |
| Feature Type | Poly-line | Polygon |
| Length of poly-line | $L_{pl}$ = 192, 632.080132 m | |
| Perimeter of original polygon | | $P_{op}$ = 192, 632.080132 m |
| Area of original polygon | | $A_{op}$ = 247,259,043.356 Sqm |
| No. of Vertices | $v_o$ = 18,476 | $v_o$ = 18,476 |
| Average Segment Length of poly-line | $ASL_{pl} = L_{pl} / v_o$ = 10.426 m | |
| Average Segment Length of Polygon | | $ASL_{pg} = P_{op} / v_o$ = 10.426 m |

### 4.2. Definition and Equations

In order to evaluate the performance of each algorithm, the following measurements have been included into the table: average segment length, parameter, file size, time, number of vertices, vertices reduction percentage, files size reduction percentage, perimeter of polygon, area of polygon, areal displacement.

| Term | Symbol | Equation/ Measurement | Definition |
|---|---|---|---|
| Segment | S | Distance unit | It is a part of a line that is bounded by two distinct end points, and contains every point on the line between its end points. When the end points both lie on a curve such as a circle, a line segment is called a chord (of that curve). |
| Parameter (Tolerance) | t | Distance unit | It is a provided simplification/ smoothing tolerance value which determines the degree of simplification. It will be set equal to or greater than the minimum allowable spacing between graphic elements. It has an effective influence on the line simplification/ smoothing. |
| Time | T | Time unit | It is a manually recorded time (in seconds) for implementing simplification or smoothing process using stopwatch. |
| File Size | $F$ | Capacity unit | It is an occupied capacity of file (in kilobyte) which can be investigated through windows explorer. |
| Number of vertices | $v$ | Dimensionless | It is a countable point objects which can be calculated by using Easy Calculator 5.0 program. |
| Length of poly-line | $L_{pl}$ | Distance unit | It is a total distance between the start point and endpoint of a line. |
| Perimeter of polygon | $P_p$ | Distance unit | It is a perimeter of a polygon that obtained from the converted poly-line by using ET Geo Wizards tool. |
| Area of polygon | $A_p$ | Area unit | It is an area that obtained from the converted poly-line by using ET Geo Wizards tool. |

| | | | |
|---|---|---|---|
| Average segment length of poly-line | $ASL_{pl}$ | $ASL_{pl} = L_{pl} / v$ | It is the measured average length of poly-line which can be calculated by dividing the length of the poly-line over the number of vertices. |
| Average segment length of polygon | $ASL_{pg}$ | $ASL_{pg} = P_p / v$ | It is the measured average length of polygon which can be calculated by dividing the perimeter of the polygon over the number of vertices. |
| Displaced perimeter | $D_p$ | $D_p = P_{op} - P_p$ | It is the measured displaced perimeter of polygon which can be calculated by subtracting the perimeter of the polygon that produced after performing simplification process based on the entered tolerance values from the perimeter of the original polygon. |
| Displaced Area | $D_a$ | $D_a = A_{op} - A_p$ | It is the measured displaced area of polygon which can be calculated by subtracting the area of the polygon that produced after performing simplification process based on the entered tolerance values from the area of the original polygon. |
| File Size Reduction | $F_r$ | $F_r = 100 - (\frac{F}{F_{op}} \times 100)$ | It is the percentage of file size that has been reduced. It can be calculated based on corresponding equation. Where $F$ the file is size after simplification and $F_{op}$ is the file size of the original polygon in KB. |
| Vertices Reduction | $V_r$ | $V_r = 100 - (\frac{v}{v_o} \times 100)$ | It is the percentage of vertices (points) that have been removed. It can be calculated based on corresponding equation. Where $v$ is the number of vertices after simplification and $v_o$ is the number of vertices of the original polygon. |

## 5. Evaluation and Discussion

Point Remove and Bend Simplify are performed to simplify poly-lines by removing extraneous bends while preserving essential shape.

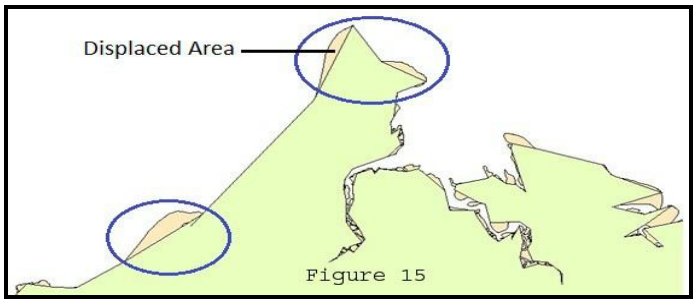


***Figure 15:*** *Displacement of Area Produced by Nth Simplification Method*

In this test, introduced errors during the line simplification process have been removed automatically, since both Douglas-Peucker and Bend Simplify methods are provided by a function that enables the cartographers to perform the correction process while the operation in progress. On the contrary, the first two applied methods: Nth Point and Jenks are not provided by the capability of automated removing errors.

Table 7 includes all required numerical data which have been recorded in the basis of ascending change of parameters for performing comparisons with the other applied algorithms later. The main reason of applying and evaluating these methods are selecting the best method that reduces file size and at the same time preserves the quality of produced map through the less displacement of area. Figure 15 shows a sample of areal displacement that has been shaped after using Nth Point Algorithm with the (Parameter = 50 m).

***Table 7:*** *Nth Point Method Results*

| Parameter (Simplified Tolerance) (m) t | Approx. Time (sec) T | File Size (kb) $F$ | File Size Reduction (%) $F_r$ | No. of Vertices $v$ | Vertices Reduction (%) $V_r$ | Perimeter of Polygon (m) $P_p$ | Displaced perimeter (m) $D_p$ | Average Segment Length of Polygon (m) $ASL_{pg}$ | Area of Polygon ($m^2$) $A_p$ | Displaced area ($m^{2)}$ $D_a$ |
|---|---|---|---|---|---|---|---|---|---|---|
| 1 | 3.56 | 289 | 0 % | 18475 | 0.00% | 192632.080132 | 0 | 10.42663 | 247259043.356 | 0 |
| 3 | 2.63 | 97 | 66.43% | 6159 | 66.66% | 181112.4617 | 11519.61843 | 29.40615 | 247215167.014 | 43876.342 |
| 7 | 2.57 | 42 | 85.46% | 2640 | 85.71% | 171172.60796 | 21459.47217 | 64.83811 | 247364227.898 | -105184.542 |
| 10 | 2.39 | 30 | 89.61% | 1848 | 90% | 165531.706285 | 27100.37385 | 89.57343 | 247170773.383 | 88269.973 |
| 20 | 2.29 | 15 | 94.80% | 924 | 95% | 152038.083294 | 40593.99684 | 164.5434 | 246990944.388 | 268098.968 |
| 30 | 2.19 | 10 | 96.53% | 616 | 96.67% | 144355.682898 | 48276.39723 | 234.3436 | 248413775.849 | -1154732.493 |
| 40 | 2.15 | 8 | 97.23% | 462 | 97.50% | 138605.98238 | 54026.09775 | 300.0129 | 248407837.212 | -1148793.856 |
| 50 | 2.09 | 6 | 97.92% | 370 | 98% | 135617.581518 | 57014.49861 | 366.534 | 249886028.074 | -2626984.718 |
| 60 | 2.02 | 5 | 98.26% | 308 | 98.33% | 132217.630529 | 60414.4496 | 429.278 | 250129334.757 | -2870291.401 |
| 70 | 2.0 | 5 | 98.26% | 264 | 98.57% | 128815.315478 | 63816.76465 | 487.9368 | 251031471.092 | -3772427.736 |
| 80 | 1.97 | 4 | 98.61% | 231 | 98.75% | 128337.327538 | 64294.75259 | 555.5728 | 250262996.35 | -3003952.994 |
| 90 | 1.95 | 4 | 98.61% | 206 | 98.89% | 124344.041431 | 68288.0387 | 603.6119 | 252678572.864 | -5419529.508 |
| 100 | 1.91 | 4 | 98.61% | 185 | 99% | 121371.634576 | 71260.44556 | 656.0629 | 252362507.587 | -5103464.231 |

Table 8 indicates that the corresponding displacement of area to the same parameters which are repeated for all applied methods have only positive signs in this case, which means that the area of original polygon is greater than the area of produced area being processed.

***Table 8:*** *Jenks Method Results*

| Parameter (Simplified Tolerance) (m) t | Approx. Time (sec) T | File Size (kb) $F$ | Size Reduction (%) $F_r$ | No. of Vertices $v$ | Vertices Reduction (%) $V_r$ | Perimeter of Polygon (m) $P_p$ | Displacement Perimeter (m) $D_p$ | Average Segment Length of Polygon (m) $ASL_{pg}$ | Area of Polygon ($m^2$) $A_p$ | Displaced area ($m^{2)}$ $D_a$ |
|---|---|---|---|---|---|---|---|---|---|---|
| 1 | 4.28 | 276 | 4.49% | 17595 | 4.77% | 192441.631516 | 190.448616 | 10.93729 | 247259030.451 | 12.905 |
| 3 | 3.87 | 211 | 26.98% | 13441 | 27.25% | 190964.071136 | 1668.008996 | 14.20758 | 247255435.354 | 3608.002 |
| 7 | 3.21 | 117 | 59.51% | 7459 | 59.63% | 185122.874177 | 7509.205955 | 24.81873 | 247220210.266 | 38833.09 |
| 10 | 3.04 | 82 | 71.62% | 5188 | 71.92% | 179360.739343 | 13271.34079 | 34.57223 | 247185573.749 | 73469.607 |
| 20 | 2.74 | 38 | 86.85% | 2361 | 87.22% | 162879.642042 | 29752.43809 | 68.98757 | 247193569.981 | 65473.375 |
| 30 | 2.71 | 24 | 91.69% | 1495 | 91.91% | 150034.367259 | 42597.71287 | 100.3574 | 246936428.351 | 322615.005 |
| 40 | 2.69 | 19 | 93.42% | 1169 | 93.67% | 141343.560611 | 51288.51952 | 120.9098 | 245689292.414 | 1569750.94 |
| 50 | 2.55 | 17 | 94.11% | 1050 | 94.32% | 135916.066761 | 56716.01337 | 129.4439 | 245663517.24 | 1595526.12 |
| 60 | 2.52 | 17 | 94.11% | 1014 | 94.51% | 135362.244096 | 57269.83604 | 133.4933 | 245397731.956 | 1861311.4 |
| 70 | 2.47 | 16 | 94.46% | 1012 | 94.52% | 135184.536564 | 57447.54357 | 133.5816 | 245397246.927 | 1861796.43 |
| 80 | 2.35 | 16 | 94.46% | 1012 | 94.52% | 135184.536564 | 57447.54357 | 133.5816 | 245397246.927 | 1861796.43 |
| 90 | 2.32 | 16 | 94.46% | 1012 | 94.52% | 135184.536564 | 57447.54357 | 133.5816 | 245397246.927 | 1861796.43 |
| 100 | 2.25 | 16 | 94.46% | 1012 | 94.52% | 135184.536564 | 57447.54357 | 133.5816 | 245397246.927 | 1861796.43 |

Table 9 indicates that most obtained displacement of areas by applying Douglas and Peucker method gave approximately the same number of figures that have negative signs.

***Table 9:*** *Point Remove Method Results*

| Parameter (Simplified Tolerance) (m) t | Approx. Time (sec) T | File Size (kb) $F$ | File Size Reduction (%) $F_r$ | No. of Vertices $v$ | Vertices Reduction (%) $V_r$ | Perimeter of Polygon (m) $P_p$ | Displacement Perimeter (m) $D_p$ | Average Segment Length of Polygon (m) $ASL_{pg}$ | Area of Polygon ($m^2$) $A_p$ | Displaced area ($m^{2)}$ $D_a$ |
|---|---|---|---|---|---|---|---|---|---|---|
| 1 | 5.42 | 136 | 52.94% | 8686 | 52.99% | 192033.793317 | 598.286815 | 22.10843 | 247258912.373 | 130.983 |
| 3 | 5.52 | 81 | 71.97% | 5133 | 72.22% | 190789.585724 | 1842.494408 | 37.16922 | 247254061.622 | 4981.734 |
| 7 | 5.62 | 47 | 83.73% | 2986 | 83.84% | 187991.895443 | 4640.184689 | 62.95777 | 247265941.436 | -6898.08 |
| 10 | 5.64 | 37 | 87.19% | 2350 | 87.28% | 186190.460444 | 6441.619688 | 79.22998 | 247260080.943 | -1037.587 |
| 20 | 5.66 | 22 | 92.38% | 1384 | 92.51% | 180571.451585 | 12060.62855 | 130.4707 | 247234956.899 | 24086.457 |
| 30 | 5.71 | 17 | 94.11% | 1040 | 94.37% | 176373.133015 | 16258.94712 | 169.5896 | 247238418.576 | 20624.78 |
| 40 | 5.75 | 13 | 95.50% | 800 | 95.67% | 171575.460844 | 21056.61929 | 214.4693 | 247268814.026 | -9770.67 |
| 50 | 5.79 | 11 | 96.19% | 668 | 96.38% | 168644.727365 | 23987.35277 | 252.4622 | 247261372.168 | -2328.812 |
| 60 | 6.63 | 9 | 96.88% | 561 | 96.96% | 165231.53966 | 27400.54047 | 294.5304 | 247335475.88 | -76432.524 |
| 70 | 7.05 | 8 | 97.23% | 497 | 97.31% | 162324.666938 | 30307.41319 | 326.609 | 247342561.636 | -83518.28 |
| 80 | 7.19 | 8 | 97.23% | 448 | 97.58% | 160454.95196 | 32177.12817 | 358.1584 | 247425155.915 | -166112.559 |
| 90 | 6.92 | 7 | 97.57% | 384 | 97.92% | 157613.242206 | 35018.83793 | 410.4512 | 247543131.756 | -284088.4 |
| 100 | 6.79 | 6 | 97.92% | 341 | 98.15% | 155704.004112 | 36928.07602 | 456.61 | 247459615.801 | -200572.445 |

Table 10 indicates that the obtained displacement of areas by applying Bend Simplify method are all have negative signs which is quite opposite to the recorded results in Table 7. This means that in this case, the area of original polygon is less than the area of produced area being processed.

***Table 10:*** *Bend Simplify Method Results*

| Parameter (Simplified Tolerance) (m) t | Approx. Time (sec) T | File Size (kb) $F$ | File Size Reduction (%) $F_r$ | No. of Vertices $v$ | Vertices Reduction (%) $V_r$ | Perimeter of Polygon (m) $P_p$ | Displacement Perimeter (m) $D_p$ | Average Segment Length of Polygon (m) $ASL_{pg}$ | Area of Polygon ($m^2$) $A_p$ | Displaced area ($m^{2)}$ $D_a$ |
|---|---|---|---|---|---|---|---|---|---|---|
| 1 | 5.43 | 289 | 0% | 18472 | 0.00% | 192632.079668 | 0.000464 | 10.42833 | 247259043.465 | -0.108999997 |
| 3 | 5.63 | 267 | 7.61% | 17041 | 7.77% | 192478.385373 | 153.6948 | 11.29502 | 247259212.278 | -168.922 |
| 7 | 5.64 | 240 | 16.95% | 15298 | 17.20% | 192217.383831 | 414.6963 | 12.56487 | 247259623.262 | -579.906 |
| 10 | 5.67 | 226 | 21.79% | 14391 | 22.11% | 191708.375881 | 923.7043 | 13.32141 | 247260500.179 | -1456.823 |
| 20 | 5.60 | 178 | 38.40% | 11380 | 38.41% | 187681.831893 | 4950.248 | 16.49225 | 247273454.695 | -14411.339 |
| 30 | 5.38 | 146 | 49.48% | 9323 | 49.54% | 183045.9184 | 9586.162 | 19.6338 | 247290961.031 | -31917.675 |
| 40 | 5.57 | 125 | 56.74% | 7971 | 56.86% | 179065.509062 | 13566.57 | 22.46462 | 247308913.761 | -49870.405 |
| 50 | 6.23 | 108 | 62.62% | 6865 | 62.84% | 174699.205955 | 17932.87 | 25.44781 | 247335970.866 | -76927.51 |
| 60 | 6.05 | 96 | 66.78% | 6088 | 67.05% | 171421.763308 | 21210.32 | 28.15732 | 247355625.268 | -96581.912 |
| 70 | 6.23 | 86 | 70.24% | 5477 | 70.36% | 167794.593218 | 24837.49 | 30.63622 | 247376674.958 | -117631.602 |
| 80 | 6.40 | 79 | 72.66% | 4997 | 72.95% | 164235.646378 | 28396.43 | 32.86685 | 247375654.096 | -116610.74 |
| 90 | 6.02 | 72 | 75.08% | 4576 | 75.23% | 162692.867845 | 29939.21 | 35.55351 | 247344765.837 | -85722.481 |
| 100 | 6.05 | 68 | 76.47% | 4311 | 76.67% | 161054.368548 | 31577.71 | 37.35893 | 247381806.803 | -122763.447 |

Through graphing Tables 7, 8, 9, and 10 we can conclude the following; Figure 16 shows charts that produced from these four tables.

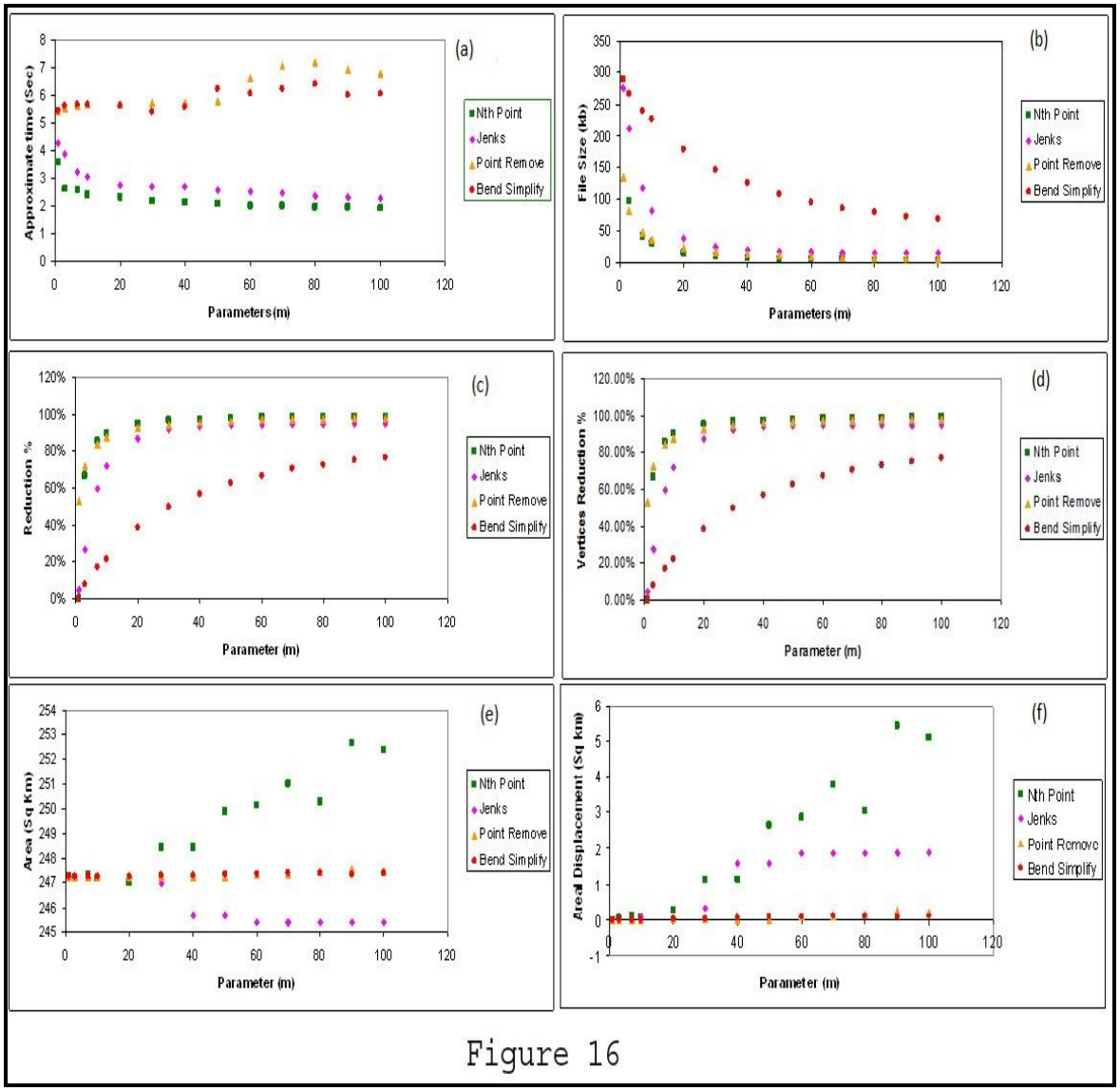


***Figure 16:*** *Charts Representing Tables 7-10: Relationship between (a) Parameter-Time, (b) Parameter-File Size (c) Parameter- File Size Reduction (d) Parameter-Point Reduction, (e) Parameter-Produced Area, (f) Point Reduction-Areal Displacement*

Figure 16-a show that the required time for performing line simplification using Douglas and Peucker and Bend Simplify algorithms has increased relatively in punctuated shape with an increasing of simplifying parameters. As opposed to this, required time for implementing Nth Point and Bend Simplify has decreased slowly with the increase of parameters. This explains that Bend Simplify and Point Remove processes require more time than nth point and Jenks because of the additional required time for removing topological errors.

Figure 16-b shows that the size of files decreases with increasing of simplifying parameters. Nth point, Jenks, and Point Remove algorithms lead to rapid reduction of file size. While the Bend Simplify algorithm leads to graduate reduction of file size. This explains that the bend simplify algorithm eliminates less spots.

Figure 16-c shows that the percentage of reduced file size by using Nth Point, Jenks, and Douglas and Peucker reaches to 90% around 20 m simplifying parameter. While it reaches to 40% at the same parameter by using Bend Simplify Algorithm. This proves that the Bend Simplify Algorithm eliminates less spots and its reduction is more moderate compared to the other applied algorithms.

Figure 16-d shows that the percentage of eliminated spots according to applied parameters reaches to 90% around 20 m simplifying parameter. While it reaches to 40% at the same parameter by using Bend Simplify Algorithm. In comparing between Figure 16-c and Figure 16-d, perfect compatibility can be deduced between the file size reduction and point reduction.

Areal displacement is a measurement factor of topological change. The less areal displacement, the more conserve are of topology and vice versa. Figure 16-e shows that the Bend Simplify is the most one that preserves topological structure the closest to prototype. Figure 16-f shows the relationship between the areal displacement and the percentage of point reduction. It can be deduced that the Bend simplify method reduce less spots and keep areal displacement in the lowest level compared to the other applied algorithms. Thus it is more acceptable than the other algorithms for performing the line simplification process.

## 6. Conclusions

Generalization is an important process for creating layers that have acceptable quality and file size. There are different types of algorithms that can be used for performing generalization process, but the obtained results differ from one method to another. In comparison between produced lines and original lines using such types of algorithms, we can conclude that Duglas-Peucker and Wang are better than Nth Point and Jenks. In both methods, topological errors can be removed and both are more acceptable by cartographers topologically. On the other hand, Wang Algorithm is more accurate than Douglas-Peucker Algorithm, since it conserves topological structure and eliminates fewer points.

It can be deduced from this experiment that the Bends Simplify Algorithm is the best method that can be applied by cartographers for performing generalization processes. This is because, it conserves a topology which is very close to the original one, thus, areal displacement is too small compared to the other algorithm methods, moreover it has moderate reduction in both file size and eliminated vertices, and finally, it eliminates less spots.

## References

Dal Santo M.A., Oliveira F.H., and Wosny G.C., 2007: *Algorithms for Automated Line Generalization in GIS*, UDESC University, Brazil.

ESRI, Desktop Help 10.0-Simplify Line (Cartography).
http://help.arcgis.com/en/arcgisdesktop/10.0/help/index.html#//007000000010000000

Lee D. and Hardy P., 2005: *Automating Generalization-tools and Models,* Cartographic Conference (ICC2005), Spain.

McMaster R.B. *Automated Line Generalization*. Journal of Cartographica. 1987. 24 (2) 74-111.

Muller et al., 1995: *GIS and Generalization-Methodology and Practice*, Taylor & Francis Ltd, UK.

Robinson et al., 1995: *Elements of Cartography*, Wiley & Sons, USA.

Shamsi U.M., 2005: *GIS Applications for Water, Wastewater, and Storm water Systems*, CRC, USA.

UNI-ZH, 1999: *Selection of Basic Algorithms.* Report DD 2, ESPRIT/LTR/24939.
Taylor G., 2005: *Line Simplification Algorithms*. University of Glamorgan. UK.

Veregin H. *Line Simplification, Geometric Distortion, and Positional Error.* Int. J. Geog. Inf. and Geovis. 1999. 36 (1) 25-39.

Veregin H. *Quantifying Positional Error Induced by Line Simplification*. International Journal of Geographical Information Science. 2000. 14 (2) 113-130.

**Cloud Publications**
International Journal of Advanced Remote Sensing and GIS
2014, Volume 3, Issue 1, pp. 569-579, Article ID Tech-229
ISSN 2320 - 0243

Cloud Publications

Research Article | Open Access

# Analysis of Hyperion Satellite Data for Discrimination of Banded Magnetite Quartzite in Godumalai Hill, Salem District, Tamil Nadu, India

**S. Aravindan[1] and B. Poovalinga Ganesh[2]**

[1]Department of Earth Sciences, Annamalai University, Annamalai Nagar, Tamil Nadu, India
[2]Center for Research and Development, PRIST University, Vallam, Thanjavur, Tamil Nadu, India

Correspondence should be addressed to S. Aravindan, aravindan_rs@yahoo.com

Publication Date: 23 May 2014

Article Link: http://technical.cloud-journals.com/index.php/IJARSG/article/view/Tech-229



**Abstract** In order to determine mineralogy of rock and soil samples, reflectance and emittance spectroscopy in the near-infra red and short-wave infra-red is used extensively and found to be inexpensive. Hyper spectral remote sensing satellite data are found to be prospective to deliver in depth physico-chemistry like mineralogy, chemistry, morphology of the earth's surface. Therefore hyper spectral data is useful for mapping potential host rocks, alteration assemblages and mineral characteristics. In the present study EO-1, Hyperion data had been used for delineating magnetite mineral in Godumalai hill, Salem region, Tamil Nadu, India. The requirements for extracting magnetite from Hyperion images is to be first compensated for atmospheric effects using flag mask correction, cross track illumination correction and FLAASH model. Minimum Noise Fractionation transformation was applied to reduce the data noise and for extracting the extreme pixels. Some pure pixel end member for the target mineral and backgrounds were used in this study to account for the Spectral Angle Mapping & matched filtering techniques and the arrived results were validated with field study. Those mapping techniques have proved that the magnetite mineral can be mapped with high precaution by Hyperion preprocessing adopting methods.
**Keywords** *Hyper Spectral Analysis; Magnetite; Spectral Angle Mapping; Matched Filtering*

## 1. Introduction

The hyper spectral sensors represent one of the most important technological trends in remote sensing. Hyperion sensors have 242 contiguous spectral bands to sample the electromagnetic spectrum from 400 to 2,400 nanometer (visible to short wave infrared) wave length. Hyper spectral Remote Sensing or Imaging Spectroscopy are concerned with the measurement, analysis & interpretation of spectra acquired from a region or part of the Earth by an airborne or satellite sensor (Gupta, 2003). Each mineral has a unique reflectance and absorption pattern across different wavelength region. So, each mineral can be identified by their unique absorption and reflectance

property. Geological remote sensing is performed through the atmospheric windows where Hyperion uses two atmospheric windows as VNIR and SWIR regions for mapping surface mineralogy as these wavelengths are highly sensitive to a wide range of diagnostic EMR interactions with rock materials. In particular,

1) The mineral-spectral features in the VNIR region were largely related to the transfer of electrons between energy levels of constituent elements, especially the transition metals Fe, Mn and Cr (Hunt et al., 1971).
2) The mineral-spectral features in the SWIR were largely related to the overtones and combination tones in vibrations of octahedral coordinated captions (typically Al, Fe and Mg) bonded with OH groups (Hunt et al., 1968).

Banded iron formations occur in many parts of the world and have been described under a variety of names such as banded hematite quartzite, banded magnetite quartzite, Calico rock, ironstone, itabirite, jasper bars, jaspilite, ribbon rock, striped magnetite jasper, taconite, zebra rock and so on. Iron ores occurs in different geological formations practically in different states of India, economically workable deposits is found to occur in Precambrian banded iron formations of Jharkhand, Orissa, Chhattisgarh, Goa, Karnataka, Tamil Nadu and Andhra Pradesh.

In Tamil Nadu, there are extensive bands of magnetite quartzite in Salem and Trichirappalli districts (King and Foote, 1864; Holland, 1892; Middlemiss, 1896). They form a series of ridges and hillocks like Kanjamalai, Godumalai, Tirthamalai and Kollimalai, many of those peaks are about 1000 m high (Aiyangar, 1941; Krishnan and Aiyangar 1944).

The primary aim and objectives of the present work is to study and analyze the spectral signatures of magnetite deposits in the Godumalai hill and to find out the application of hyper spectral remote sensing techniques in mapping magnetite mineral of the study area. The study area Godumalai region lies between north latitude 78°18’ to 78°24’ and east longitude from 11°38’ to 11°42’ in part of Salem district of Tamil Nadu state, India and the hill has a structural trend in east-west direction (Figure 1).

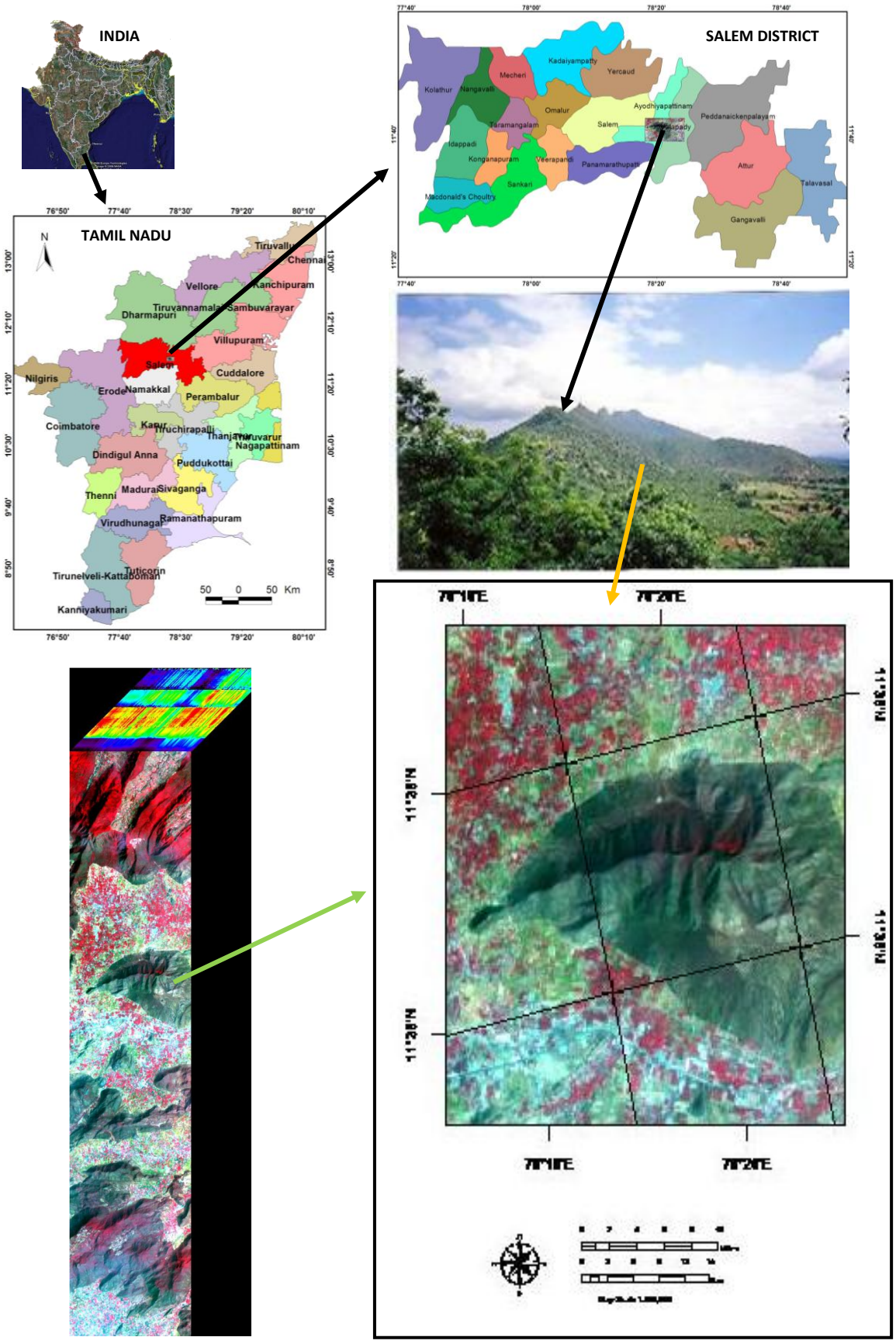


***Figure 1:*** *Study Area Godumalai Hill Shown in Hyperion Image (R40, G30 & B20) with 3D Cube (242 Band Data)*

Geologically the ores are found in rocks of different ages throughout the Precambrian by far most importantly they comprise magnetite deposits in the study area. Metamorphism in those areas has converted hematite into magnetite and the jasper into quartz. These ore bodies are found in the Salem and Trichirapalli districts of Tamil Nadu (Krishnan, 1964). The study area consists of mixed rock types namely gneisses, charnockite, magnetite quartzite and the study area is about 50 sq. km.

## 2. Data Used and Methodology

Hyperion data of onboard EO-1 satellite acquired on 14.02.2010 was used for this study. The Hyperion was a push-broom Image with 242 bands, 10 nm band widths covering the spectrum from 400 nm – 2400 nm. ASD field spectroradiometer was used, 45 rock samples collected from the field with different composition of magnetite quartzite samples and with different grain size and ancillary data of geology map obtained from Geological survey of India was used for field study. The detailed methodology adopted here is given in Figure 2.

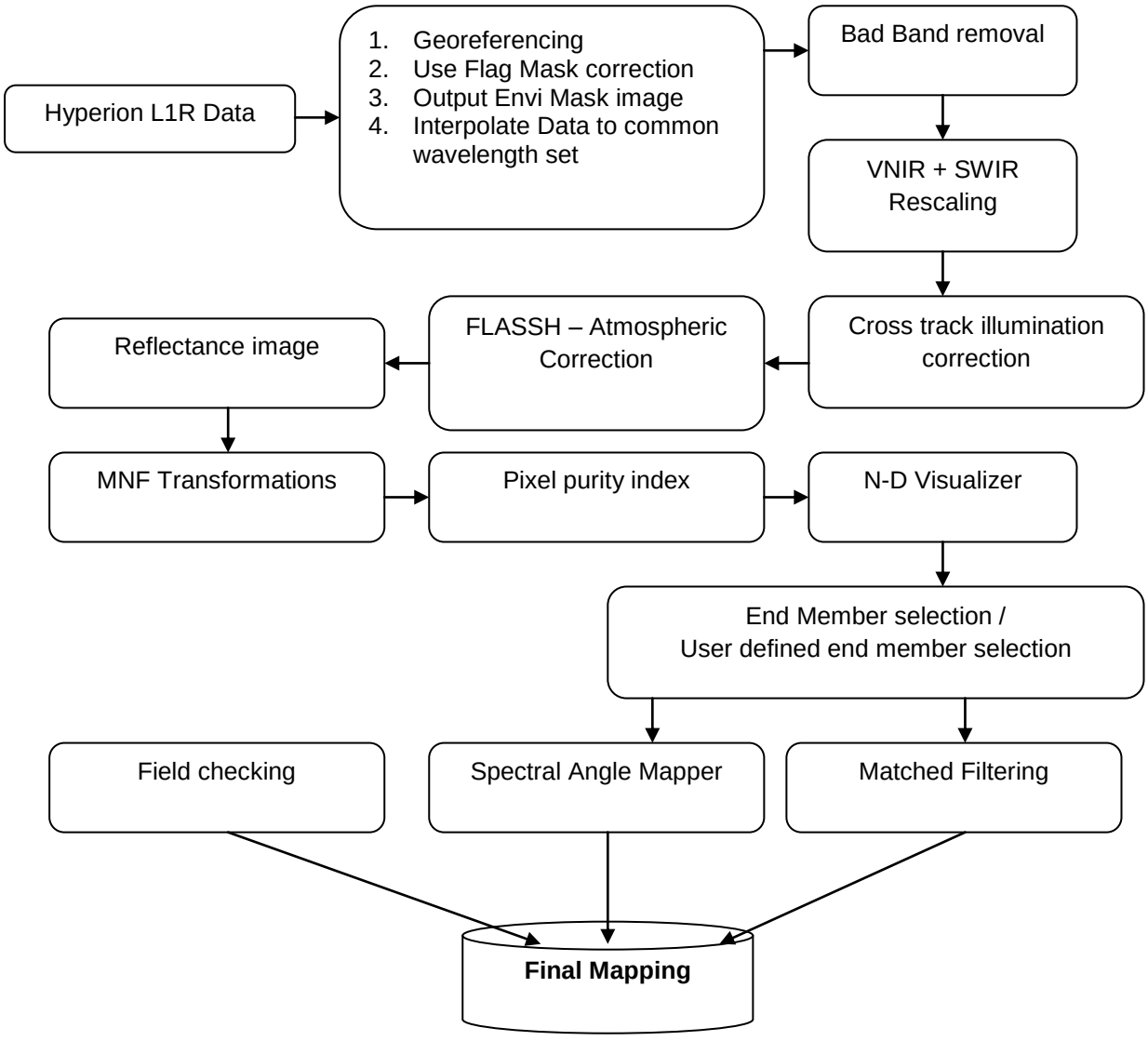


***Figure 2:*** *Processed Data Flow for Mapping Magnetite Mineral Deposits*

Data Pre-Processing of Hyperion L-1R data require several phases of pre-processing to enable different hyper spectral analysis technique for production of mineral index maps.

The apparent strips frequently found in several bands to reduce the errors caused by the de stripping effect were reduced by screening all spectral bands and manually rejected a total of 88 bands with apparent stripping effects from VNIR to SWIR spectral range. Thus in total 158 bands were taken for the present study. 3D Cube in Figure 1 shows the study area Godumalai hill in Hyperion image (R40, G30 & B20) with a 3D Cube (242 band data) Hyperion L1R Data 1. 2. 3. 4. Georeferencing using Flag Mask correction Output Envi Mask image Interpolates Data to a common wavelength set with bad Band removal of VNIR + SWIR rescaling Reflectance image of FLASSH – Atmospheric Correction Cross track illumination correction MNF Transformation, Pixel purity index n-D Visualizer of End Member selection/User defined end member selection Field checking Spectral Angle Mapper, Matched Filtering of Final Mapping is shown in Figure 2. Processing flows for mapping magnetite mineral deposits with rescaling the L1R digital values represent absolute radiance values stored as 16-bit signed integer. To get that sensor radiance value, the data must be rescaled. The scaling factors, 40 for VNIR band and 80 for SWIR bands detailed descriptions were mentioned in EO-1 User Guide, 2003. Accordingly, Cross-Track Illumination corrections were applied to remove the variations in the cross-track illumination on image (Envi user guide, 2003). Cross track illumination variations may be due to shifting effects of sensor, off set of instrument scanning or other non-uniform illumination effects. A polynomial function is fit to the mean value which is used to remove the variation in Atmospheric Correction. In order to obtain the correct and fruitful results, hyper spectral data should be preprocessed though the data has its own ability to discriminate the surface materials especially in geological aspects. Owing to the atmospheric gases and aerosols, atmospheric or radiometric corrections are required. Different gases in the atmosphere absorb or transmit the light which depends on the respective wavelength of the energy. Atmospheric correction of hyper spectral data is therefore an obligation for radiance to reflect conversion. Hyperion data carry the influence of a number of external factors, which masks the fine spectral features of ground objects. The factors are due to

1) Effects of the solar irradiance curve;
2) Atmosphere and Topography: The effect of the solar irradiance curve arises from the fact that solar radiation intensity peaks at 0.48 μm and the radiation intensity drops off towards longer wavelengths, therefore the effects of solar irradiance is not uniform throughout the image. Atmospheric effects arise due to the fact that the Hyperion image data are collected over a wide wavelength range, which includes atmospheric windows as well as atmospheric absorption and scattering. Topographic effects arise due to local landscape orientation. Above factors must be adequately normalized in order to compute ground reflectance values in different channels. In order to retrieve the surface reflectance and to study the surface reflectance properties atmospheric effects has to be removed. This is referred to as atmospheric correction and was applied to Hyperion data set. Atmospheric correction was achieved by using ENVI's fast line-of-sight atmospheric analysis of hyper spectral-cubes (FLAASH) model. Necessary parameters for the FLAASH were determined from the metadata of the image files. The scaling factors, 40 for VNIR and 80 for SWIR bands has a detailed descriptions mentioned in EO–1 user Guide 2003. Accordingly cross– Track illumination corrections were applied to remove the variations in the cross-track illumination on image units (Envi User Guide, 2003). An ASCII file was prepared for each band of the selected 158 bands, with a scaling factor of 40 for the first 43 bands of VNIR and 80 for the rest SWIR bands and provided as the scale factor file for the FLAASH to convert the DN values of the L1 data in to the units of radiance. Parameters used for the atmospheric correction is provided below in the Table 1. The results after the FLAASH atmospheric correction on the Hyperion image is shown with the respective spectral profiles in the Figure 3.1 and Figure 3.2 below with Spectral profile (Z-profile) Vegetation pixel, a) before Atmospheric corrections and b) after Atmospheric corrections with FLAASH.

***Table 1:*** *Parameters used in the FLAASH Atmospheric Correction*

| | | | |
|---|---|---|---|
| Scene Canter Location | 11.68E and 78.34N | Initial Visibility | 30 Km |
| Sensor Altitude | 705Km | Spectral Polishing | Yes |
| Ground elevation | 0.6 Km | Width (no of bands) | 9 |
| Pixel Size | 30m | Wavelength Recalibration | No |
| Flight date | 14-Feb-2010 | Aerosol scale height | 2.00Km |
| Flight time | 20:42:42 | $Co_2$ mixing ratio (ppm) | 390 ppm |
| Atmospheric Model | Tropical | Use adjacency correction | Yes |
| Water retrieval | Yes | Modtran Resolution | 15 $cm^{-1}$ |
| Water absorption feature | 1135 nm | Modtran Multiscatter Model | Scaled DISORT |
| Aerosol model | Urban | No of Disort streams | 8 |
| Aerosol retrieval | None | Output reflectance scale factor | 10000 |

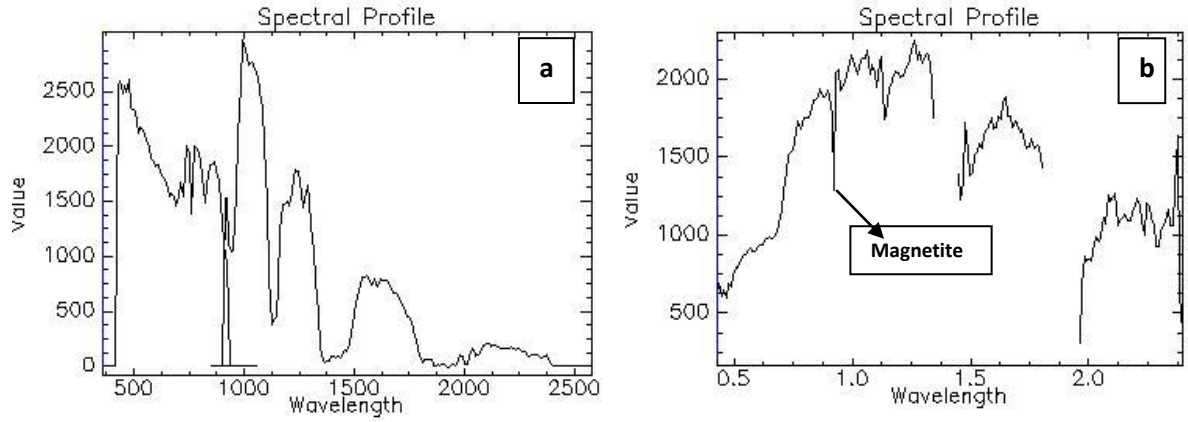


***Figure 3.1:*** *Spectral Profile (Z-profile) Magnetite pixel* ***a)*** *before Atmospheric Corrections and* ***b)*** *after Atmospheric Corrections with FLAASH*

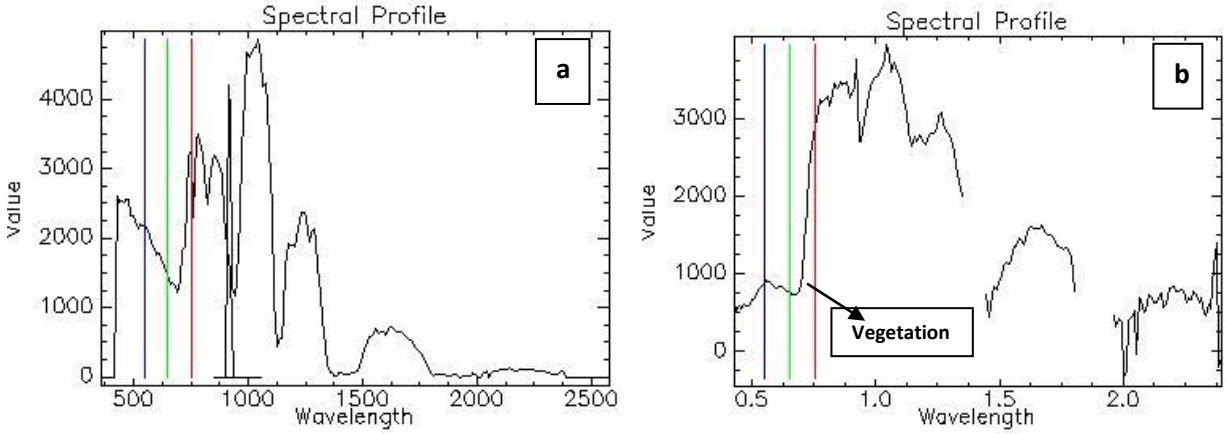


***Figure 3.2:*** *Spectral Profile (Z-profile) Vegetation Pixels,* ***a)*** *Before Atmospheric Corrections and* ***b)*** *After Atmospheric Corrections with FLAASH*

In general the spectral absorption peak for the magnetite is 0.9 to 1.1 µm and fall, in VNIR bands in 0.48 to 0.52 µm region. The Hyperion image after FLASSH atmospheric correction has clearly showed the absorption peak at 0.49 and 0.9 µm (Poovalinga Ganesh et al., 2012). In order to cross check as well as to understand the vegetation influences in the retrieved spectral absorption. The vegetation spectra were separately identified and taken into account highly in following classification procedures.

### 2.1. Hyperspectral Analysis

For this research, minimum noise fraction transformation (for Reduction of spectral data), pixel purity index (to retrieve the spectrally pure pixel values), and subsequently n-dimensional visualizer (to determine the end member) were applied to hyper spectral satellite datasets to map the magnetite mineral deposits. Details about these techniques are discussed as follows.

The approach of SAM was employed to identify the magnetite deposits. Finally, the Matched filtering technique was used to target the magnetite deposits.

### 2.2. MNF Transformation

MNF transformations determine the inherent dimensionality of image data to disintegrate noise in the data and to diminish the computational requirements for further process. This MNF take place in two-step process. The results of first step is to transform the spatial data in which the noise has unit variance and without band-to-band correlations. The second step result is the standard principal components transformation of the noise-whitened data.

***Figure 4:*** *MNF Hyperion Pseudo Color Image of Godumalai Hill*

### 2.3. Pixel Purity Index

Pixel purity index (PPI) is a means to determine automatically the relative purity of the pixels from the higher order. A MNF Eigen image uses the convex geometry argument (Boardman, 1993). A PPI image was created by repeatedly projected MNF images into random unit vector in a dimensional scatter plots in which the digital number (DN) of each pixel corresponded to the total number of times that the pixel was judged as extreme in all projections.

### 2.4. N-Dimensional Visualizer

Further step is to refine the most spectrally pure end members derived from the two- dimensional PPI image and more importantly to label them with specific end member types. Thus each end members had assigned with specific mineral type by examined visually the selected pixels and grouped (Boardman et al., 1994). This could be achieved through the field knowledge about the study area.

### 2.5. Spectral Angle Mapping

Spectral angle mapper (SAM) is a procedure that determines the similarity between a pixel and each of the reference spectra based on the calculation of the "spectral angle" between them (Boardman et al., 1994). It had been treating both the known and unknown spectra as vectors and calculated the spectral angle between them. A smaller angle differences between the two spectra and the pixels were identified as the fixed class else as a separate class. This classification carried following equation (ENVI Tutorials, 2002) and easily achieved through the ENVI software.

$$\alpha = \cos^{-1}\left[\frac{\vec{t} * \vec{r}}{\|\vec{t}\| * \|\vec{r}\|}\right] \qquad \text{Eq. 1}$$

### 2.6. Matched Filtering

Matched Filtering (MF) is a mapping technique to find the abundances of user-defined end member using a partial immixing (ENVI User's Guide, 2008). Matching filtering techniques maximize the response of known spectra and suppress the response of the composite unknown spectra, thus matching with known signature. Matched filtering assists us to detect known minerals easily from the study area and it does not require more knowledge about the field while there will be a chances of false minerals mapping for the presence of ambiguity spectral values. This attempt also tries to validate the earlier approach of SAM analysis and delineate the magnetite deposits as exact as possible.

## 3. Results and Discussion

The atmospherically corrected reflectance image was transformed linearly by using MNF transformation. There were first 10 MNF bands contains most of the spectral information. Then, pixel purity index techniques employed to determine the pure pixels in the hyperion satellite image. The spectra of pure pixels were plotted on the n-dimensional scatter plot to retrieve the end members. The end member is analyzed using spectral angle mapper and matched filtering technique is used to identify the magnetite minerals. SAM identifies most of the magnetite and float ores deposits used as end members accurately. The advantage of SAM was attributed to the fact that SAM determines the similarity of two spectra based on calculating the "spectral angle" between them. The angle or direction of the spectral vectors where determined by the "color" of the material. If color increases, SAM can identify them. The spectral angle used for magnetite mapping for the study is 0.10radian. The matched filtering technique maximized the magnetite abundances and suppresses the background features. Here, the SAM & MF ratio image (Figure 5a and 5b) identified most accurately the magnetite abundances within the study area. The MTMF image showing exposed magnetite quartzite deposits in the presence of top of the hill in red color and floats ores abundance near to gneissic rocks and foot hill region in yellow color. Rest of the other classified features such as scrub, vegetation, harvested land and settlement are mapped for the purpose to differentiate the features and enhance the magnetite deposits from the other interferences.

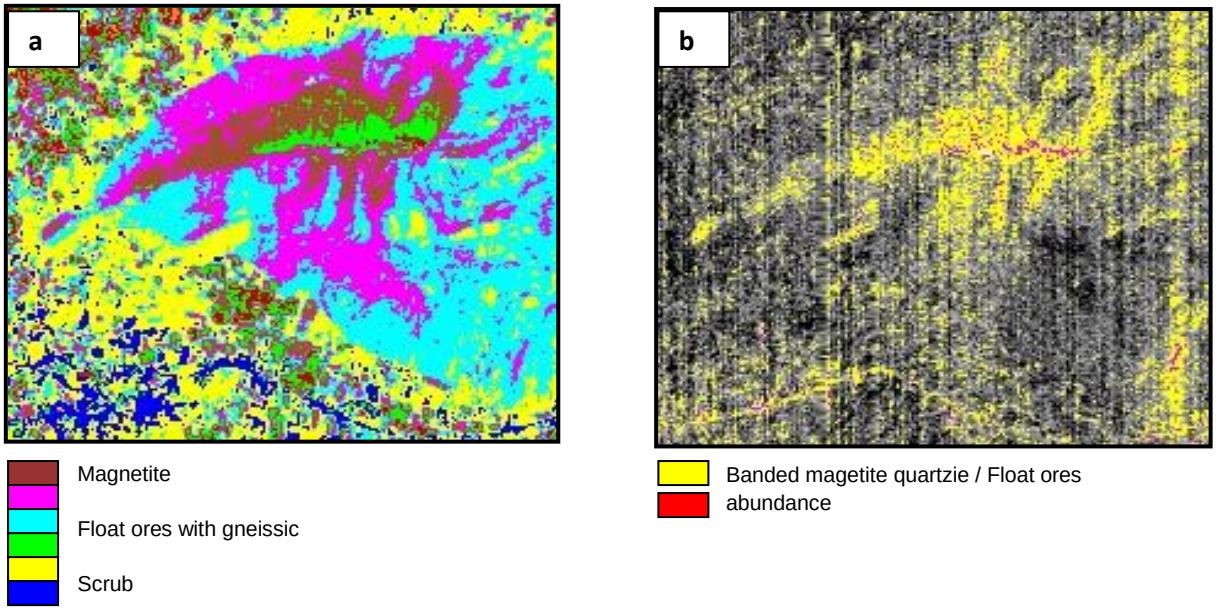


***Figure 5a:*** *SAM Classified Image Showing the Magnetite Deposits and Other Features*
***Figure 5b:*** *MTMF Image Showing Magnetite Mineral Abundance in Red Color and Gneissic Mixed with Iron Ores / Float Ores Abundance in Yellow Color*

In order to improve the classification accuracy and make the result reliable, the results of SAM classification was implemented in confusion matrix with reference to user ROI end members where known pixel locations are found in the image, cross checked with published geology map and field check. Accuracy of the classification in percentage is given in Table 2.

***Table 2:*** *Result of Confusion Matrix in % for SAM Classified Features with User ROI end Member's Datasets*

| Class | Production Accuracy (%) | User Accuracy (%) |
|---|---|---|
| Magnetite | 28.57 | 40 |
| Vegetation | 92.42 | 100 |
| Harvested Land | 82.84 | 77.78 |
| Settlement | 75 | 99.71 |
| Hill Gneiss | 84.89 | 92.84 |
| Scrub | 96.16 | 91.04 |
| Overall Accuracy | 0.84507 | 84.51% |
| Kappa Coefficient | 0.8045 | |

Result of Confusion matrix in % for SAM Classified features with user ROI end member's datasets Class Production. Accuracy (%) of Magnetite is 28.57/40, Vegetation - 92.42 / 100, Harvested Land - 82.84 / 77.78, Settlement - 75 / 99.71, Hill & Gneisses - 84.89 / 92.84, Scrub - 96.16 / 91.04, Overall Accuracy level are 0.84507 / 84.51%, Kappa Coefficient is 0.8045, Iron ore (Magnetite) was mapped to 40% accuracy and remaining features were mapped with more than 75% accuracy. This is due to the iron ore pixels which are unable to discriminate well from associated geological features and other land use / land cover features in the satellite image due to presence of overlapping pixels and less spatial resolution of satellite data. The overall accuracy percentage was 84.51%. Thus the highly discriminating features or non-overlapped pixel features which can be easily mapped with high accuracy due to its high spectral resolution.

## 4. Conclusion

Comparing the results with the field check and geology map of the study area, it illustrates usefulness of Hyperion data for identifying mineral abundances and mapping the geology of natural features.

Hyperion data covering the study area were analyzed using several hyper spectral image analysis techniques, which have demonstrated their potentiality in identifying magnetite deposits since spectral absorption peak has clearly showed magnetite regions after FLAASH correction and pure end members were able to be retrieved from the satellite data without any ambiguity. Limitations of the hyperion imagery is apparent strips could be view in the several important absorption bands and low signal-to-noise ratio. Within the 242 spectral bands, only 158 bands were used because of overlap between the VNIR and SWIR focal planes and FLASSH atmospheric correction model was performed well within those spectral bands. The SAM and MF techniques have proved that magnetite can be mapped through these techniques with high precaution of Hyperion preprocessing adoption methods. The classification accuracy can be increased further in the study area by refining the procedure in pure pixel selection process or by employing spectral end members from field spectral data or from spectral library as satellite data has high spectral resolution.

## Acknowledgement

Authors are thankful to LP-DAAC, USA for providing the facility to order the data as well as provided data for downloading freely. Authors wish to thank their respective institutions for their moral support in providing infrastructure facilities. Authors are also thankful to Dr. S. Rajendran, Sultan Qaboos University, Oman for given valuable guidance to improve the quality of the research.

## References

Aiyangar, N.K.N. 1941: *Preliminary Report on the Iron Ores of the Salem District*. Madras, Rept. to Govt. of. Madras, G.O. No. 1781.

Boardman, J.W., 1993: *Automating Spectral Unmixing of AVIRIS Data Using Convex Geometry Concepts.* In: Realmuto VJ (Ed.). Summaries of the 4th Annual JPL Air-Borne Geosciences Workshop, JPL Publication 93-26, Pasadena, CA. 1; 11-14.

Boardman, J.W., and Kruse, F.A., 1994: *Automated Spectral Analysis: A Geological Example Using AVIRIS Data, North Grapevine Mountains, Nevada.* In: Erim (Ed.) Proc. 10th Thematic Conference on Geological Remote Sensing, San Antonio, TX, 9-12 May. 407-418.

ENVI Tutorials. 2002: Research Systems, Inc., Boulder.

EO-1, 2003: User Guide, Version 2.3.

Gupta, R.P., 2003: *Remote Sensing Geology*. Second Ed, Springer-Verlag, Berlin. 250-258.

Hunt, G.R., and Vincent, R.K. *The Behavior of Spectral Features in the Infrared Emission from Particulate Surfaces of Various Grain Sizes*. J Geographical Research. 1968. 73 (18) 6039-6046.

Hunt, G.R., Salisbury, J.W., and Lehnoff, C.J. *Visible and Near Infrared Spectra of Minerals and Rocks: III.* Oxides and Ox hydroxides, Modern Geology. 1971. 2; 195-205.

Holland, T.H., 1892: *Preliminary Reports on the Iron Ores and Iron Industries of Salem District*. Records of the Geological Survey of India. 25; 136-159.

ITT Visual Information Solutions, 2008: ENVI User's Guide, Version 4.5.

King Foote, R.B., 1864: *Geological Structures on Parts of the Districts of Salem, Thiruchirapallit, Tanjore and South Arcot in the Madras Presidency*. Mem Geol Surv Ind. 4; 223-386.

Krishnan, M.S., and Aiyengar, N.K.N. 1944: *The Iron Ore Deposits of Salem and Thiruchirapallit District.* Geo Surv India, Bull Series on Econ Geol. 1-64.

Middlemiss, C.S., 1896: *Notes on the Ultrabasic Rocks and Derived Minerals of Chalk (Magnesite) Hills and Other Localities near Salem*. Madras. Rec Geol Surv Ind XXIX. 31-38.

Poovalinga Ganesh, B., Aravindan, S., Raja, S., and Thirunavukkarasu, A. *Hyperspectral Satellite Data (Hyperion) Preprocessing– A Case Study on Banded Magnetite Quartzite in Godumalai Hill, Salem, Tamil Nadu, India.* Arabian J Geosci. 2013, 6 (9) 3249-3256.

Raja, S., Aravindan S., Thirunavukkarasu, A., Alaguraja, P., and Poovalinga Ganesh, B. *Processing and Analyzing Advanced High Resolution Satellite Data for Identifying Iron Ore Deposits of Precambrian Age*. Int. Journal of Advances in Remote Sensing and GIS. 2012. 1 (1) 59-75.

**Cloud Publications**
International Journal of Advanced Remote Sensing and GIS
2014, Volume 3, Issue 1, pp. 499-505, Article ID Tech-236
ISSN 2320 - 0243

Research Article | Open Access

# Land Use-Land Cover Change Detection Using Remote Sensing and GIS Techniques; Solapur District of Maharashtra, India

**P.R. Patekar and R.R. Patil**

School of Earth Sciences, Solapur University, Solapur, Maharashtra, India

Correspondence should be addressed to P.R. Patekar, punamrpatekar@gmail.com; prof.r.r.patil@ gmail.com

Publication Date: 29 March 2014

Article Link: http://technical.cloud-journals.com/index.php/IJARSG/article/view/Tech-236



**Abstract** Land use-land cover study is vital as it deals with how people are using the land. Remote Sensing and Geographical Information System (GIS) are well accepted and more dependable advance techniques to detect change in land use and land cover pattern by providing more reliable direct quantitative information. Therefore in the present study an attempt is made on Solapur district to bring out the quantitative information through the study of satellite imageries purchased in the department and those freely available at Global Land Cover Forecasting (GLCF) site. The results obtained through this study using imageries of 1992, 2000 and 2012 of Solapur district are presented.
**Keywords** *Remote Sensing; GIS; Land Use/Land Cover; Change Detection*

## 1. Introduction

Considering potential of Geographical information study many attempts has been made to utilize this techniques for scientific thematic mapping by Geographers, Hydrologists, Geologists, Geomorphologist, Planners from municipality Corporation, Maharashtra Board Electrical Boards, Public Work Department and collectorates of every district. In the present attempt the studies are carried out to know the landuse and land cover from Talukas of Solapur district. This study is planned with an aim to use for the qualitative and quantitative data generated for correlative it for site suitability of Great Indian Bustard from Solapur district.

### 1.2. Study Area

Solapur district a wildly known drought prone district of Maharashtra extends geographically from $17^0$8' to $18^0$33' North latitude to $74^0$36' to $76^0$26' East longitude. It is well connected by road, rail & airways from Bombay, Hyderabad & Bangalore. Location map of the district is given in Figure 1.

## 2. Objectives

The study is aimed to bring out vital information on geographical situation through past. The land use and land cover spatial changes will be discerned using remotely sensed data. On the basis of availability of images it is plan of to bring out the temporal changes in land use pattern from 1992 to 2012 by preparing respective thematic maps.

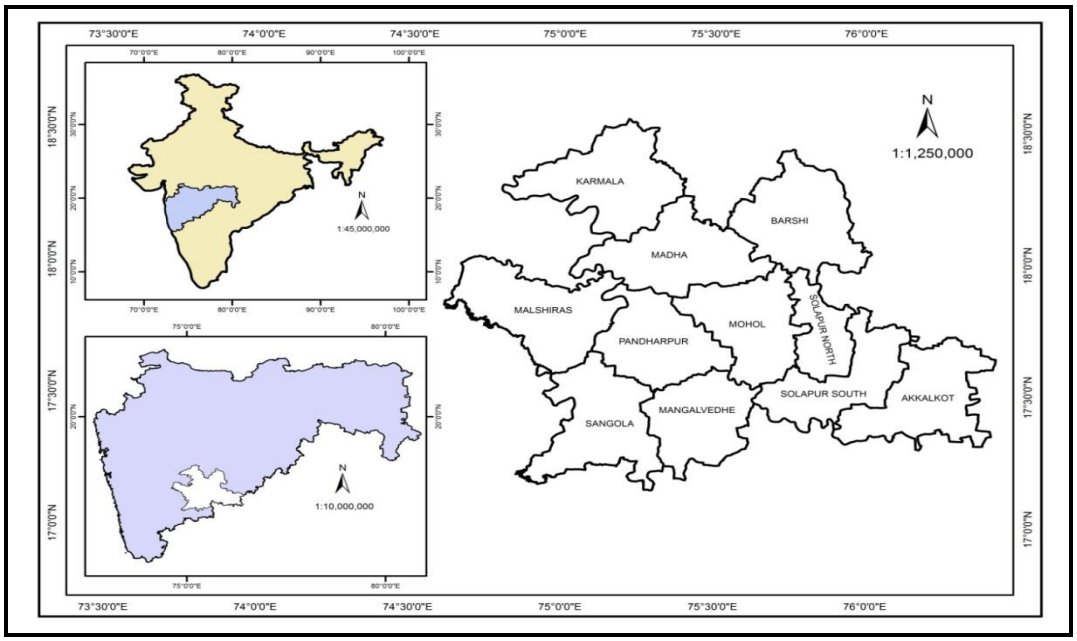


***Figure 1:*** *Location Map of Study Region*

## 3. Methodology

Systematic study plan was completed in two steps where in first includes supervised classification of TM 1992 (30 m), ETM+ 2000 (30 m) & LISS3 2012 (23.5 m) images while the second will encompass change detection analysis. The flow chart of the methodology attempted is given in Figure 2.

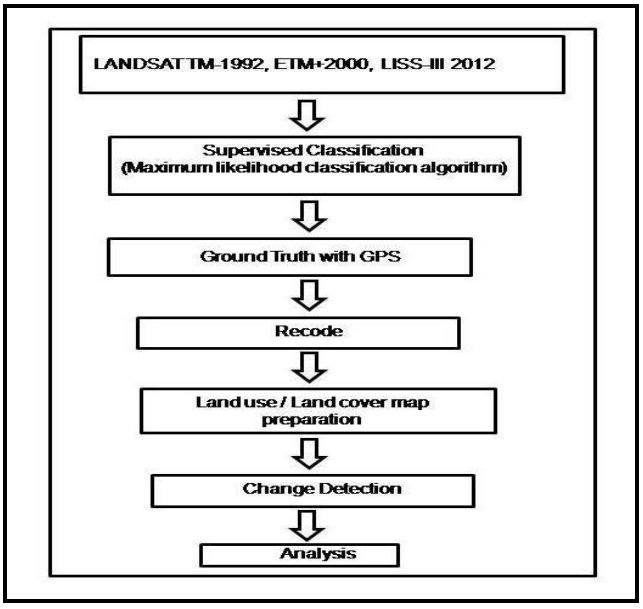


***Figure 2:*** *Flow Chart of Methodology*

All images collected from TM (1992), ETM+ (2000), and LISS-III (2012) where chronologically arranged and were subjected to supervised classification. An attempt was made to classify the images under five classes viz. Agriculture, Water body, Fallow land, Shrub land & Settlement. Out of the available modes of supervised classification Maximum likelihood classification algorithm technique is used considering its potential and suitability in the study planned. In this method care was taken to define signatures of each class after defining the signatures for each land cover category. The software uses those signatures to classify the remaining pixels. The classified land use/ land cover images were taken for ground truth. Ground truth was conducted by using GPS (Global Positioning System) and land use class was corrected by using recode technique, wherever it was needed based on the ground truth information. Considering the suitability of satellite data various satellite data used are tabulated along with their details in Table 1.

***Table 1:*** *Detail of Satellite Data used to Create Land use/ Land Cover Map*

| Satellite | Sensor | Path/Row | Year | Resolution |
|---|---|---|---|---|
| LANDSAT | TM | 145/47&48<br>146/47&48 | December 1992 | 30 m |
| LANDSAT | ETM+ | 145/47&48<br>146/47&48 | December 2000 | 30 m |
| IRS | LISS 3 | 96/60<br>97/60&98/60 | January 2012 | 23.5 m |

## 4. Results and Discussion

The study of the contour and morphology suggest that maximum area under water body is resulted to Karmala, Pandharpur, Sangola, Barshi and Akkalkot Talukas because of river and lake availability, whereas Karmala, Madha, Mohol, and Malshiras are beneficiary Talukas of Ujjani dam. Maximum settlements are found in North Solapur, South Solapur & Pandharpur Talukas which can be attributed to industrial and educational development. There is shrub land and fallow land noteworthy in whole Solapur district which may be due to the lack of water availability and lack of adaption of advance techniques in agriculture. Shrub land covered maximum area lies in Sangola and Malshiras Talukas due to the hilly region exibited by contour diferences and slope along which shallow soil cover is found**.** Maximum area occupied by agriculture in Pandharpur and Mangalwedha may be because of soil suitability as well as water availability in these Talukas. Madha, Karmala and Mohol are most beneficiaries of Ujjani dam due to rejuanation of Sina River by canal which pramoted maximum area under agriculture.

Major noteworthy changes between study periods are exhibited by agriculture and shrub land because the shrub land is converted into agriculture day by day due to the addaption of advance technique in agriculture. The area under settlement is increased due to population growth influenced by workers in agricultureal and allied industry. Solapur is a drought prone area so there is no major change in water body in study period of twenty year.

The result obtained through the study of imageries to evolve change in the land use and land cover of Solapur district are evaluated from twenty years of study period i.e. 1992, 2000, 2012. Land use-land cover of 1992 is presented in Figure 3 and Figure 4. Status of land use in the year 2000 is shown in Figure 5 and Figure 6. Whereas landuse status of year 2012 present in Figure 7 and Figure 8. Taluka wise landuse/ landcover status of 1992, 2000 and 2012 is tabulated in Table 2, Table 3 and Table 4 respectively.

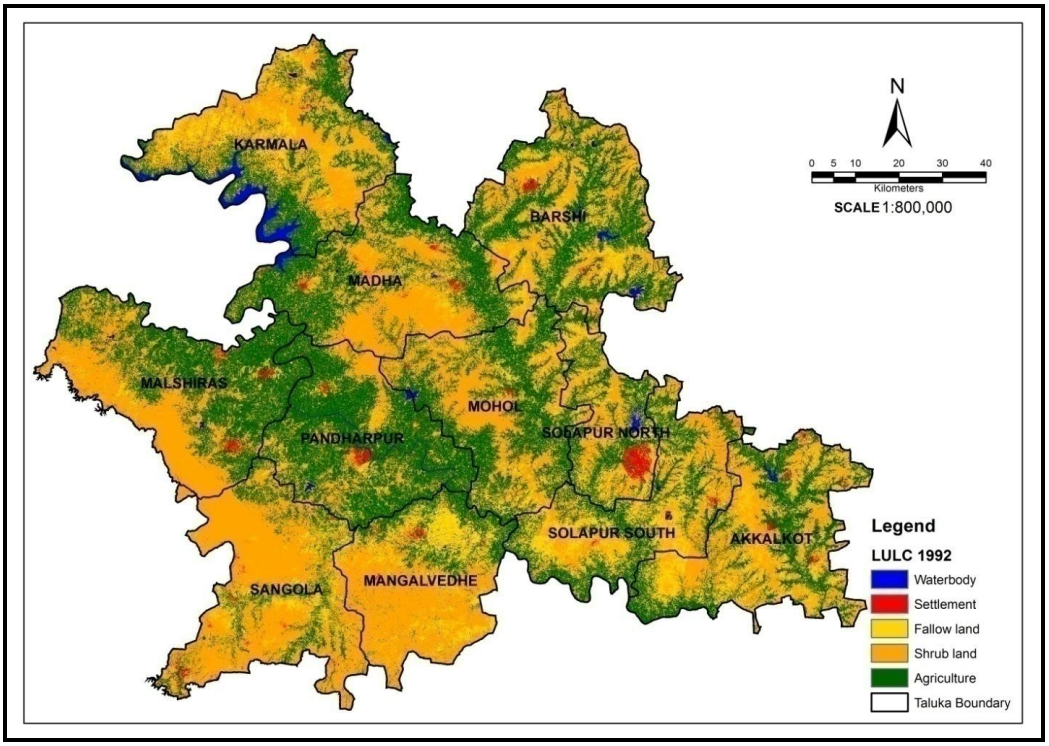


***Figure 3:*** *Taluka Wise Land Use / Land Cover of Solapur District Year 1992*

***Table 2:*** *Taluka Wise Land Use / Land Cover of Solapur District Year 1992*

| Taluka Name | Agriculture | Shrub land | Fallow land | Settlement | Water body | Total |
|---|---|---|---|---|---|---|
| Akkalkot | 487 | 482 | 387 | 19 | 32 | 1407 |
| Barshi | 576 | 552 | 355 | 15 | 47 | 1545 |
| Karmala | 466 | 537 | 416 | 17 | 159 | 1595 |
| Madha | 569 | 509 | 377 | 14 | 36 | 1505 |
| Malshiras | 665 | 786 | 90 | 22 | 41 | 1604 |
| Mohol | 499 | 599 | 184 | 16 | 22 | 1320 |
| N.Solapur | 201 | 256 | 145 | 62 | 20 | 684 |
| Pandharpur | 807 | 305 | 106 | 29 | 44 | 1291 |
| S.Solapur | 379 | 375 | 386 | 25 | 26 | 1191 |
| Sangola | 339 | 819 | 301 | 14 | 44 | 1517 |
| Mangalwedha | 431 | 622 | 86 | 19 | 24 | 1182 |
| **Total** | **5419** | **5842** | **2833** | **252** | **495** | **14841** |

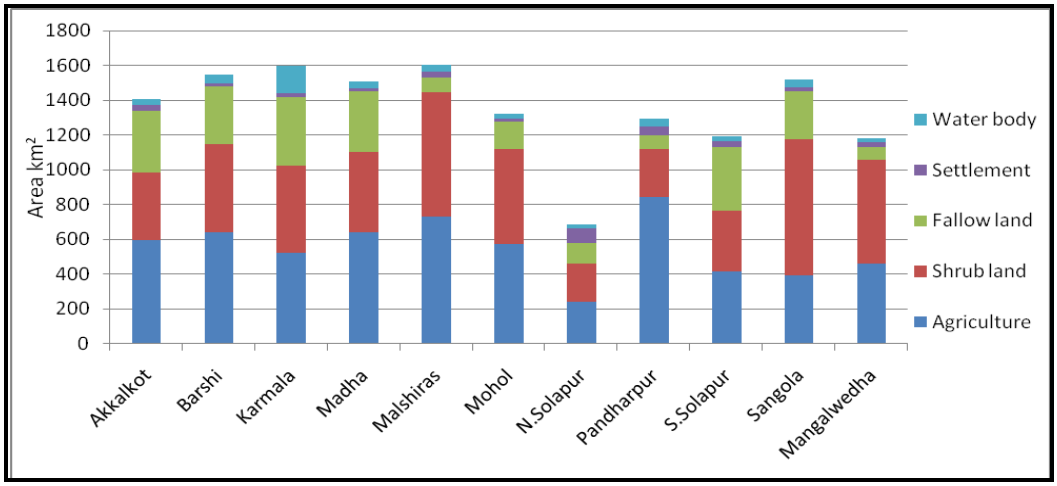


***Figure 4:*** *Taluka Wise Land Use / Land Cover of Solapur District Year 1992*

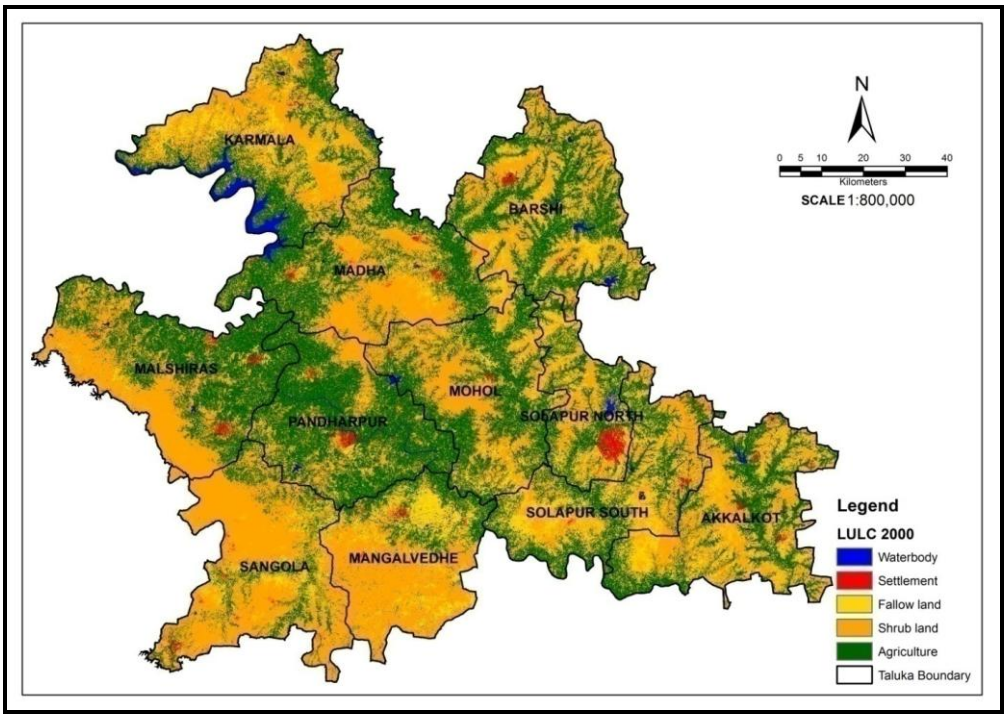


***Figure 5:*** *Land Use / Land Cover of Solapur District Year 2000*

***Table 3:*** *Taluka Wise Land Use / Land Cover of Solapur District Year 2000*

| Taluka Name | Agriculture | Shrub land | Fallow land | Settlement | Water body | Total |
|---|---|---|---|---|---|---|
| Akkalkot | 508 | 465 | 379 | 25 | 30 | 1407 |
| Barshi | 603 | 534 | 342 | 21 | 45 | 1545 |
| Karmala | 490 | 527 | 400 | 24 | 154 | 1595 |
| Madha | 594 | 496 | 361 | 22 | 32 | 1505 |
| Malshiras | 715 | 742 | 79 | 30 | 38 | 1604 |
| Mohol | 509 | 594 | 175 | 19 | 23 | 1320 |
| N.Solapur | 220 | 242 | 133 | 68 | 21 | 684 |
| Pandharpur | 822 | 294 | 96 | 36 | 43 | 1291 |
| S.Solapur | 402 | 365 | 370 | 29 | 25 | 1191 |
| Sangola | 357 | 810 | 290 | 18 | 42 | 1517 |

| | | | | | | |
|---|---|---|---|---|---|---|
| Mangalwedha | 452 | 603 | 77 | 26 | 24 | 1182 |
| **Total** | **5672** | **5672** | **2702** | **318** | **477** | **14841** |

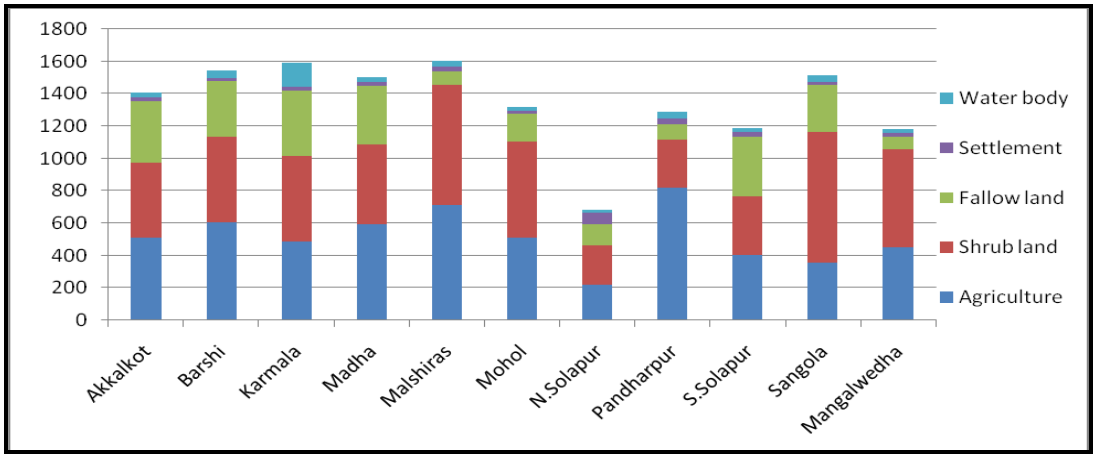


***Figure 6:*** *Taluka Wise Land Use / Land Cover of Solapur District Year 2000*

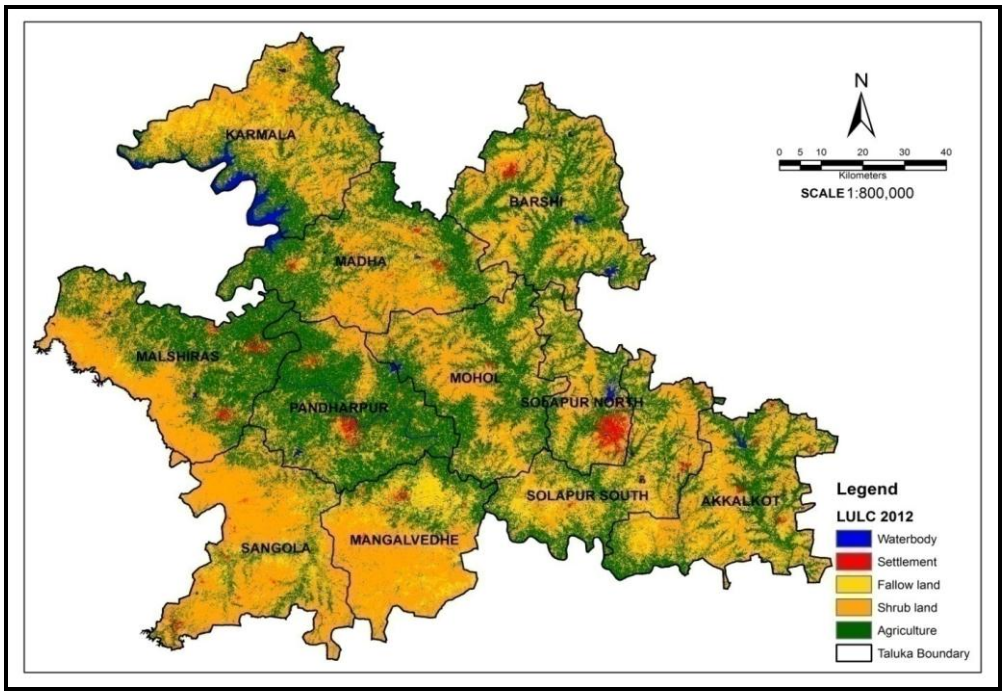


***Figure 7:*** *Land Use / Land Cover of Solapur District Year 2012*

***Table 4:*** *Taluka Wise Land Use / Land Cover of Solapur District Year 2012*

| Taluka Name | Agriculture | Shrub land | Fallow land | Settlement | Water body | Total |
|---|---|---|---|---|---|---|
| Akkalkot | 594 | 392 | 354 | 35 | 32 | 1407 |
| Barshi | 643 | 503 | 331 | 22 | 46 | 1545 |
| Karmala | 525 | 501 | 389 | 24 | 156 | 1595 |
| Madha | 641 | 461 | 349 | 19 | 35 | 1505 |
| Malshiras | 731 | 717 | 84 | 31 | 41 | 1604 |
| Mohol | 574 | 544 | 158 | 20 | 24 | 1320 |
| N.Solapur | 242 | 218 | 122 | 81 | 21 | 684 |
| Pandharpur | 843 | 279 | 78 | 49 | 42 | 1291 |
| S.Solapur | 414 | 349 | 365 | 38 | 25 | 1191 |

| | | | | | | |
|---|---|---|---|---|---|---|
| Sangola | 393 | 785 | 275 | 19 | 45 | 1517 |
| Mangalwedha | 462 | 598 | 68 | 30 | 24 | 1182 |
| **Total** | **6062** | **5347** | **2573** | **368** | **491** | **14841** |

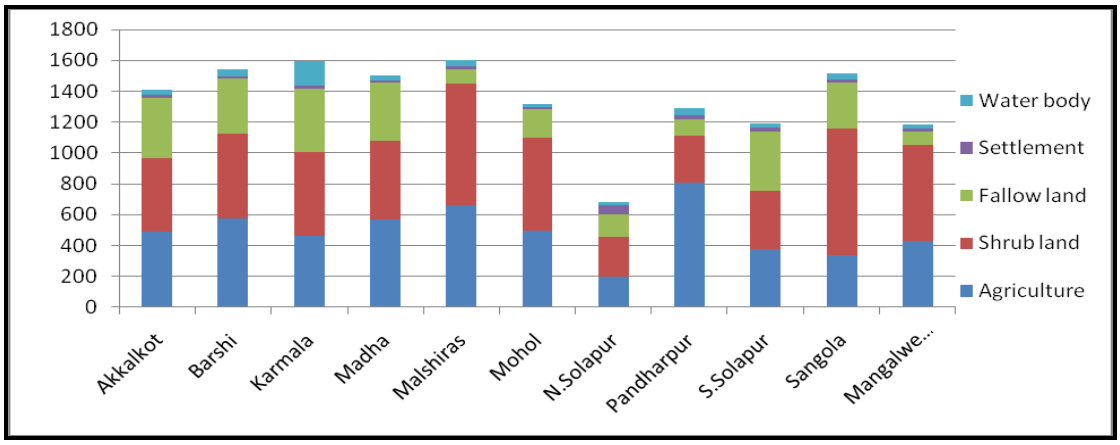


***Figure 8:*** *Taluka Wise Land Use / Land Cover of Solapur District Year 2012*

## 5. Conclusion

In the present study, highlight the role of land use change modeling in providing the required information to plan and manage the study area. The data so generated land use/ land cover is essential for the planning and implementation of land use schemes based on human need and welfare. This study corroborate that Remote Sensing & Geographical Information System has the unique capability to detect land use changes quickly and accurately thus serves as dependable tool for managers or planner involved in developmental activity.

## References

[1] Phukan, P., Thakuriah, G., and Saikia, R. *Land use Land Cover Change Detection Using Remote Sensing and GIS Techniques - A Case Study of Golaghat District of Assam, India*. International Research Journal of Earth Sciences. 2013. 1 (1) 11-15.

[2] Manonmani, R., and Mary Divya Suganya G. *Remote Sensing and GIS Application in Change Detection Study in Urban Zone Using Multi Temporal Satellite*. International Journal of Geomatics & Geosciences. 2010. 1 (1).

**Cloud Publications**
International Journal of Advanced Remote Sensing and GIS
2014, Volume 3, Issue 1, pp. 544-552, Article ID Tech-237
ISSN 2320 - 0243

Case Study | Open Access

# Urban Growth Using Shannon's Entropy: a Case Study of Rohtak City

**Bijender Singh**

Department of Geography, I.G. University, Meerpur, Rewari, Haryana, India

Correspondence should be addressed to Bijender Singh, sbijender@gmail.com

Publication Date: 30 April 2014

Article Link: http://technical.cloud-journals.com/index.php/IJARSG/article/view/Tech-237



**Abstract** With an extensive history dating back to antiquity urban development, human-induced climate change is one of the most important areas of human induced environment transformation. The study makes use of Shannon's Entropy with the help of Geographic Information System (GIS) and Remote Sensing technique. Rohtak city is located amidst fertile agricultural lands; the city has undergone rapid expansion during the recent past. The study spread over a period 38 years. On the basis of Survey of India Toposheet and satellite images, built up cover of Rohtak was classified for different time periods. Data used in the present study are the Survey of India Toposheet, LANDSAT TM 1989, IRS P6 LISS-IV PAN (mono) 2005, image acquired from Google earth 2011, and Census of India. The growth rate of built-up area was around three times more than population growth rate during 1989-2002. The growth rate in built-up area was 24.14 percent and population growth rate was 14.47 percent during 2002-2005. On the basis of these data urban growth are examined with the help of Shannon's Entropy and found the sprawl direction.
**Keywords** *Remote Sensing; Shannon's Entropy; Urban Growth; Rohtak City*

## 1. Introduction

In the Report of the United Nations (2003) it is estimated that in the next thirty years, almost all global population will be concentrated in urban areas. Such as Europe and North America in the more developed parts of the world, the level of urbanization is very high, and almost 50 percent at the global population lives in urban areas. This percentage, according to several estimates is expected to rise yet further in future decades. In 1800, only 3 percent of the world population lived in urban areas. By 1900, i.e. over next hundred years this figure went up to almost 14 percent only. Further, there were only 12 cities with 1 million or more inhabitants at the onset of last century. However, by 1950, 30 percent of the world population lives in urban centers, and the number of cities with more than 1 million people were 83. The world has experienced fast urban growth in recent decades. In 2000, nearly 47 percent of the world population lived in urban areas. Now, with over 1 million population cities are as many as 411. Less developed countries, 40 percent of residents live in urban areas, while more developed

countries, about 76 percent are urban. Rapid urbanization in many developing countries is low even today. It is expected that 60 percent of the world population will be urban by 2030, and that most urban growth will occur in less developed countries (Population Research Bureau, 2005:19).

In developing countries, urbanization is a phenomenon that has become increasingly intense in the past decade. India has most of the features of urbanization like developing countries. Total number of towns has grown from 1827 to 5161 during 1901 to 2001. The total size of urban population has increased from 2.58 crores 1901 to 28.53 crore in 2001. During 1921-31 to until 1951 an annual growth rate of urban population in India has a faster pace. After that a sharp decreased in growth of urban population in the decade 1951-61. During the 1961-71 and 1971-81 urban growth rate reached up to the current level of 2.7 percent. During the decade 1951-61 the growth rate of urban area decrease because a large number of cities declassification as a result of sticker definition of urban centers at the time of 1961 Census. In India, the number of million cities has increased to 5 million in 1951 to 23 in 1991 and 35 in 2001. At the time of 2001 Census, 37 percent of total urban population resides in these million plus cities.

Haryana, after its formation as a separate state in 1966, and particularly since the 1970s has experienced a marked acceleration in its urbanization process. The number of Class-I urban centers in the state has increased from just 4 in 1971 to as many as 19 in 2001. In 2001, 66.69 percent of the urban population in the state lived in Class- I towns.

## 2. Study Area

Rohtak city is located on the intersection of 28°54′ N latitude and 76°35′ E longitude, at a distance of 75 kilometers to the north-west of Delhi, the National Capital of India. Rohtak is the administrative headquarters of a district and a tehsil by the same name. The national capital of India has the only Metropolis city in the northern region of the country. Rohtak city is situated in the National Capital Region (NCR). According to The Regional Plan 2021 of NCR, Rohtak city has identifies the regional centre with the population of ranging from 3 lakh to 10 lakh.

Due to its location in the close vicinity of the National Capital, the urban landscape of Rohtak has undergone change from time to time. According to the Census of India 2011, Rohtak city is the third largest city of Haryana state. Rohtak is a Class–I city with a population of 3, 73, 133 at the time of 2011 census. In 2010, Municipal Committee of Rohtak was up-graded to Municipal Corporation (MC). According to the MC limit the total area of the city was 11039.15 hectares in 2010.

## 3. Data Based and Methodology

The present study is spread over a period of 38 years (1973 to 2011). The study is based on remote sensing and GIS techniques in conjunction with secondary data have been adopted in the study. The data related to remote sensing are handled with the help of Erdas Imagine 10 and related to GIS with the help ArcGIS Desktop 10.0 respectively. The lists of data used in the study are the Survey of India Toposheet No. H 53 D/9 and H 43 W9 at the scale of 1:50,000, LANDSAT TM 1989 (Landsat TM: path 158, row 40, 18/5/1989) downloaded from the Global Land Cover Facility (http://glcf.umiacs.umd.edu/), IRS ID LISS-III 2002 (IRS LISS III: path 95, row 51, 15/02/2002), IRS P6 (Resourcesat–1) LISS-IV PAN (mono) 2005, Image acquired from Google earth, 2011 (20/09/2011) and Census of India.

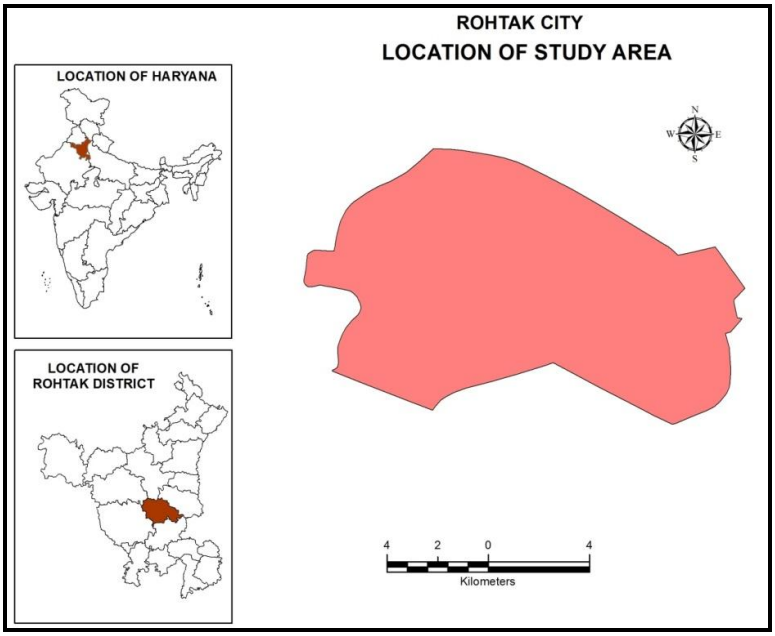


***Figure 1:*** *Location Map of Study Area*

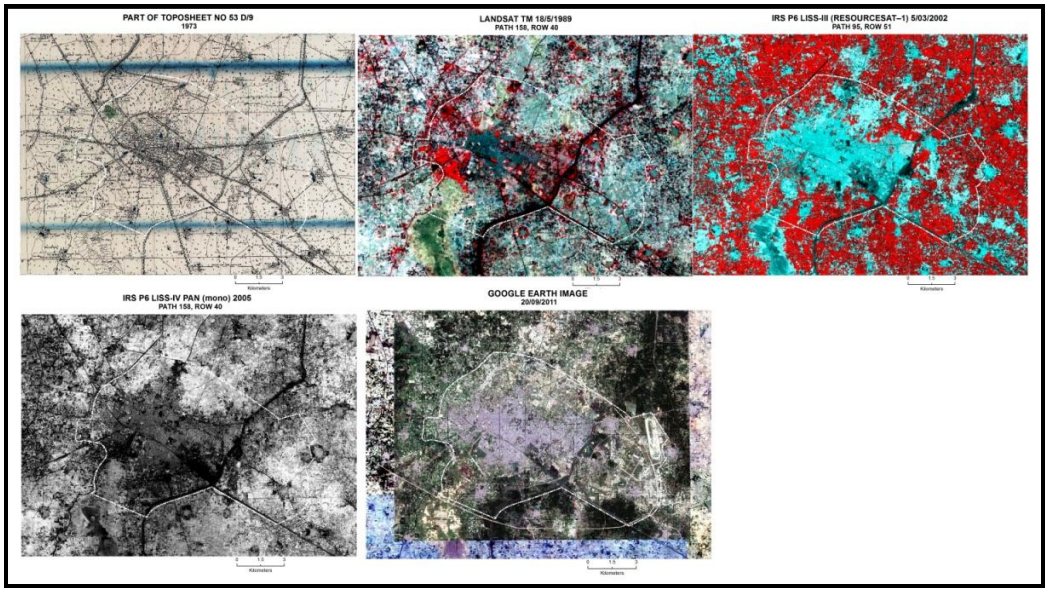


***Figure 2:*** *Topographical Map and Satellite Images of the Study Area*

Toposheet no. H 53 D/9 (Survey of India) at the scale of 1:50,000 have been used as a reference to perform geometric correction using Erdas Imagine 10.0 software. Approximately, 60 ground control points (GCPs) were selected in order to register the images to the Universal Transverse Mercator (UTM) coordinate system in 43 North Zone and WGS 84 Datum. The Toposheet used as a reference to perform reference to four times satellite data i.e. for Landsat TM, IRS LISS III, IRS PAN, and acquired from Google earth. The both toposheet and Google earth image have been classified by the visual interpretation. The Municipal committee of Rohtak became Municipal Corporation in 2010. Therefore, the latest MC limit of Rohtak, 2010 has been used to analyze the growth of the city.

**Shannon's Entropy**

One of the measures commonly used due to its toughness in urban sprawl measurement is *Shannon's entropy* (Yeh and Li, 2001). It measures the patterns of built-up area either dispersed or concentrated over time (Yeh and Li, 2001). Entropy calculation is based on computation of area. It is measured with the help of a combination of remote sensing (RS), geographic information system (GIS) and photogrammetric techniques (Sudhira et al., 2004)

The Entropy (E) value could be calculated using following formula.

$$\sum_{i}^{n} \mathrm{Pi} \cdot \log\left(\frac{1}{\mathrm{Pi}}\right) \qquad (1)$$

Pi Xi/$\sum_{i}^{n} xi$ is the observed value in the $i^{th}$ zone in a total of n zones.

n represents total number of zones/wards

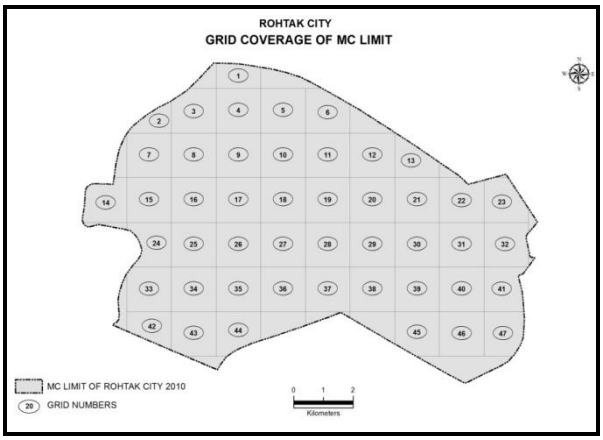


***Figure 3:*** *MC limit of Rohtak Divide into Grids*

Entropy value ranges from 0 to log (n). In the present case, log (n) is 1.672. Entropy value closer to zero represents compact distribution of urban growth, while values closer to 'log n' represent dispersed distribution of sprawl. Values of entropy near to 'log n' reveal the dispersion of built -up area, which indicates the occurrence of urban growth and heterogeneity of land uses (Punia and Singh, 2012). In this study, Shannon's entropy has been used to quantify the patterns of urban growth. Shannon's entropy is used to measure the degree of spatial concentration or dispersion (homogeneity) of a geophysical variable (built-up area) among 'n' spatial units/ wards (Jat et al., 2008).

## 4. Urban Sprawl Analysis

It is important to note that comparison of an area in a time series data required a same spatial unit. Also, it is useful in the case of Rohtak using *entropies* for different time period data. The boundary of municipal wards and limits in Rohtak City has undergone change over time. To resolve this problem the latest MC boundary of Rohtak city has been taken as base for different time data in the present study. Therefore, the MC boundary has been divided into 1.5 kilometres by 1.5 kilometres grids (as shown in Figure 2). Forty seven grids cover the entire MC area of Rohtak city.

Generally, it is suggested that the urban sprawl is affected by access to road network and distance from city centre. In the present case entropy calculated based on the distance decay properties of urban sprawl. The influences of these location factors were measured with the help of buffer in GIS.

The aim of the present study is to depict pattern of urban sprawl in Rohtak city. Therefore, this study of trends of urban built-up area is required to get temporary data. In this work, Survey of India (SOI) Toposheet published in 1973 and Landsat TM 1989, IRS-1D LISS -III 2002, IRS P6 (RESOURCESAT 1), LISS -IV Pan (mono) 2005 and Google Earth 2011 image acquired from Google Earth has been used to detect changes in urban built-up areas. Using these data of built up area over a period of time shows the changing trend in the pattern.

***Table 1:*** *Built-up Area and Population Change in Rohtak City (1973-2011)*

| Years | Built-up Area (in Hectares) | Change in Built-up Area from Previous Year | Percent Change over the Previous Year | Estimated/Census Population | Percent Change over the Previous Year | |
|---|---|---|---|---|---|---|
| 1973 | 399.82 | - | - | 128956 | - | - |
| 1989 | 649.07 | 249.25 | 62.34 | 206230 | 77274 | 59.92 |
| 2002 | 1409 | 759.93 | 117.08 | 302425 | 96194.9 | 46.64 |
| 2005 | 1609.67 | 200.67 | 14.24 | 325969 | 23544.3 | 7.79 |
| 2011 | 1998.2 | 388.53 | 24.14 | 373133* | 47163.6 | 14.47 |

Census population for the year 2011

**Source**: i) Based on SOI toposheet for the year of 1973 and satellite data 1989, 2002, 2005, 2011 respectively

Table 1 presents data on built-up area and total population of Rohtak city for the year 1973 to 2011. Built-up area is calculated from SOI for 1973 and Satellite data for 1989, 2002, 2005 and 2011. Total built-up area of Rohtak city was 399.82 hectare in 1973. At that time the estimated population of the city was 1, 28,956.

Built-up area became 649.07 hectare at the time of 1989 and recording a growth rate more than 60 percent as compared to 1973. In the same time the growth of population increased at the rate of 59.92 percent. This implied that growth in built-up area was in commensurate with growth in population of the city as the gap between the two rates was not that large. During the period between 1973 and 1989 Tilyar Lake was developed for tourism purpose in the eastern side of the city on the highway connecting Rohtak with Delhi. The lake is spread over an area of 132 acres (0.53 $km^2$) area and forms an integral part of the tourist setup, making it one of the greenest stretches in the adjoining area.

The growth rate of built-up area and population worked out to be 117.08 and 46.64 percent respectively at the time of 2002. Growth rate of built-up area was around three times more than population growth rate during 1989-2002. It shows that the city grew more in the form of horizontal expansion than vertical one. Lots of new residential areas have come into existence during this time. Although, the city has expanded in all direction, the main growth was along the eastern parts of the city along National Highway No. 10 (Singh, 2013).

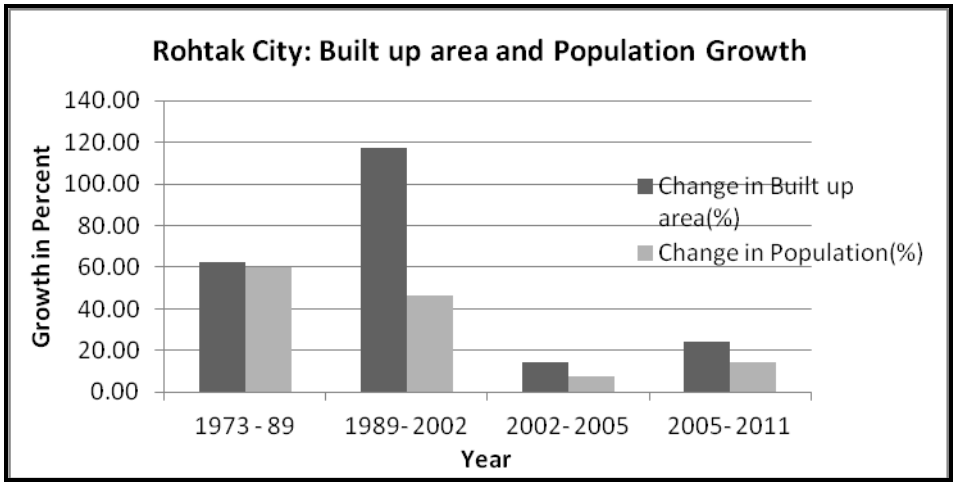


***Figure 4:*** *Build up Area and Population Growth*

In this direction an industrial area was developed by the Haryana State Industrial and Infrastructure Development Corporation Limited (HSIIDC). During 2002-2005 a growth rate of 14 percent was recorded in the built-up area while population grew at the rate of only 7.79 percent only. This indicates that the growth of the city is more of horizontal expansion continued to exist. The built-up area of the city has become 1998.2 hectares and population 3, 73,133 at the time of 2011. Thus, growth rate in built-up area was 24.14 percent and population growth rate was 14.47 percent during the period of 2005-2011. During this period, several residential, institutional, industrial areas have been developed in the city. During the same time HSIIDC has developed an Industrial Model Township (IMT) on the eastern side of the city. Several industries/companies are developing its units in Industrial Model Township (IMT) area, for instance, Asian Paints Limited, Maruti Suzuki's Research and Development Plant, Hitech Plastics Limited and Footwear Design and Development Institute. In the northern side of the city many institutions have come up like Institute of Fashion Design, Film & TV, Fine Arts and Communication, Industrial Training Institute. The Haryana Urban Development Authority (HUDA) is developing the Rajiv Gandhi Sports Complex in Sector-6 also on the northern side of the city.

The city has experienced a growth of built-up area by almost five times while the population of the city has barely trebled during the 1973 to 2011. The growth rate of built-up area has doubled than the growth rate of population in nearly four decades i.e. 1973 to 2011. It showed that growth of the city is mainly horizontal at the cost of surrounding fertile agricultural land. Also, the growth of built-up area in the city shows that it is not demand driven. It is striking to note that as much as 37 percent of the addition in the geographical area of city during the period has occurred over less than a decade between 2002 and 2011.

The entropy used for measure the sprawl of the city and was calculated for the 47 grids that cover the municipal limit of the city. The upper limit for the value of Shannon's entropy in the present case could be 1.672 i.e. equal to log n ('n' is the number of grids i.e. 47). During the study period, relatively lower value of Shannon's entropy (0.921) in the year 1973 and largest value of Shannon's entropy (1.319) in the year 2011. It indicates that at the time of 1973 the built-up area was distributed compact and homogeneous in the core. Also, it is noted that the entropy values have continuously increased during the study period (1973 to 2011). Entropy values 0.921 in 1973, 1,031 in 1989, 1,230 in 2002, 1,278 in 2005 and 1,319 in 2011 are reached. Be close to the upper limit of log n, 1.672 i.e. show the degree of dispersion of the built-up area. This increase in entropy increase in the built-up area indicates the scattered distribution.

***Table 2:*** *Rohtak City: Shannon's Entropy Value*

| Years | Value of Shannon's entropy |
|---|---|
| 1970 | 0.921 |
| 1989 | 1.031 |
| 2002 | 1.230 |
| 2005 | 1.278 |
| 2011 | 1.319 |

**Source:** Computed by Author from SOI Toposheet and Satellite Data

It is found that in the early years of 1970s the almost built up area was exit in the first 20 grids. In these grids, 10 grids account around 96 percent of the total built up area of the city. With the passage of time the share of built-up area in 10 grids gradually decline from 96 percent in 1973, 92 percent in 1989, 78 percent in 2002, 73 percent and 2005 and finally 66 percent in 2011. Obviously the spread was more conspicuous during the last decade. In other words, while for the year 1973, there were as many as 31 grids without any built-up area, the corresponding figure for 2011 is only 10. The number of such grids for the years 1989, 2002 and 2005 was 20, 29 and 33 respectively. This is indicative of the pace of dispersal of built-up area in the city during the recent past.

In the present study, grid-wise area has been considered as the geophysical variable, which enables determination of urban growth. Shannon's entropy analysis results for 5 time-points (1973, 1989, 2002, 2005 and 2011) are presented in Table 2.

## 5. Spatial Pattern of Urban Sprawl

Shannon's entropy has been determined to understand the spatial pattern of urban growth of the city. Shannon's entropy has been calculated for all the grids taking each grid as an individual spatial unit. Built-up area has been used as a variable of Shannon's entropy to find out that the pattern of land development in these grids whether compact built-up dominated or it is dispersed/ homogenous. The temporal change of spatial patterns of urban development can be easily measured from the change in entropy. The increase in the value of the entropy indicates that there is an increase in urban sprawl and development tends to be more dispersed. As already mention earlier, the city has been divided into 47 grids. After that Shannon's Entropy has been calculated for each grid. Shannon's entropy values were assigned to the respective central point of the grid. Shannon Entropy interpolation methods have been used to show the smooth pattern of urban sprawl. It is used with the help of centriods of each grid using ArcGIS (ESRI product) software extension Spatial Analyst Tools. Interpolation method has applied for Shannon's entropy values for all five sets of data time period (i.e. 1973, 1989, 2002, 2005 and 2011).

Based on the interpolation of Entropy value the shape of city shown in Figure 5 like an ellipse in year 1973. The major axes of ellipse are mainly following the major road transport routes of the city. Major axis follows the National Highway No. 10 which connects Delhi to Hisar and passes through the heart of the city. Similarly minor axis follows the National Highway Nos. 71 and 71A. Figure 5 also shows that the value of Shannon's entropy index decreases towards the outskirts of the city. The central parts of the city which contain higher Entropy values are enclosed by circles of higher values of entropy, and as one move away from the centre the values tend to decline towards the outer part of the city.

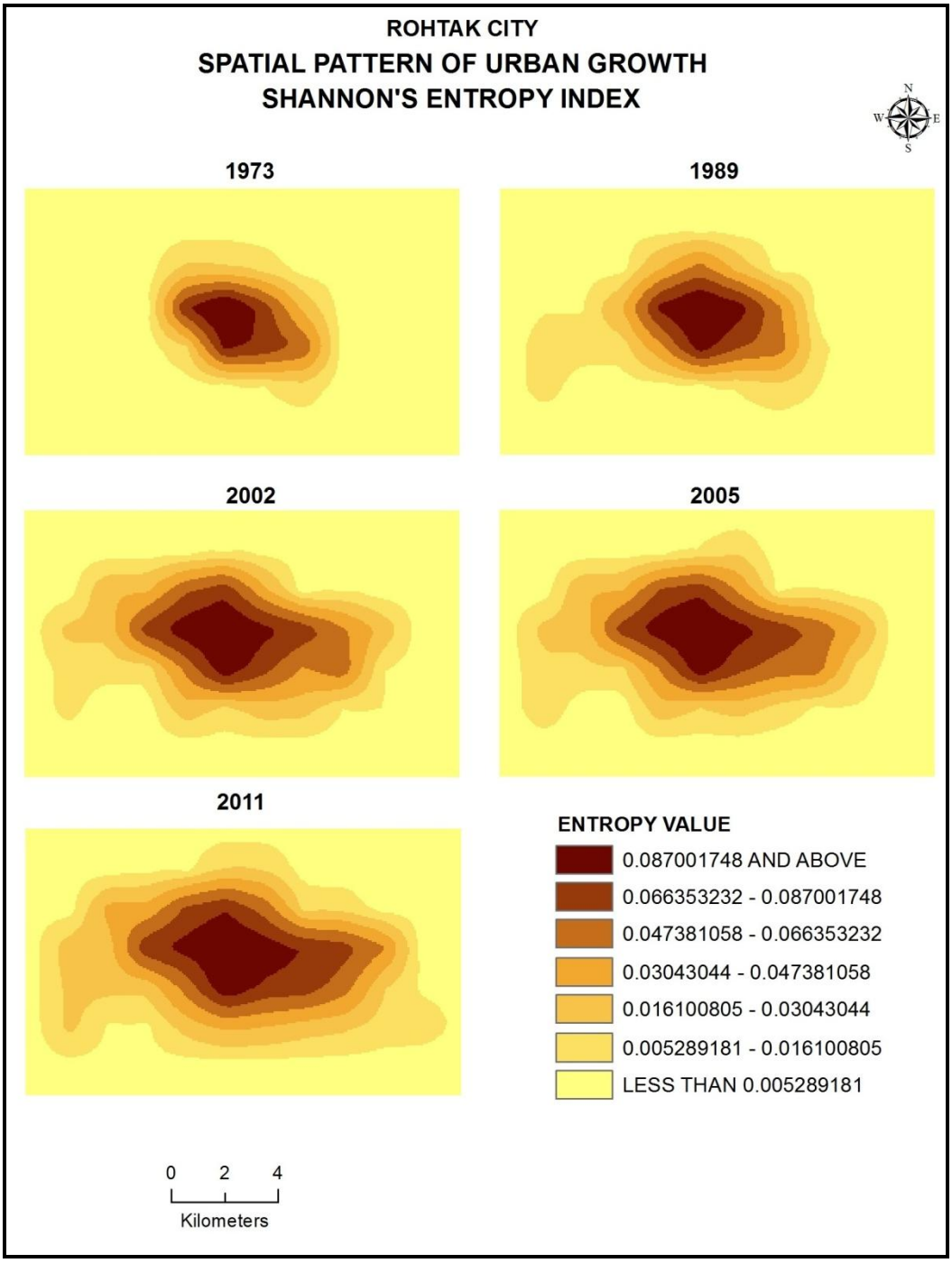


***Figure 5:*** *Spatial Pattern of Urban Sprawl*

The outer parts of the city are enclosed by circles of gradually declining value of Shannon's Entropy. This shape has persisted up to the year 1989. In the year 2002 some notches in the outer part of the city come up, and continue up to 2011. The shape of the city based on Entropy value in year 1973 is very similar to the one that emerges from the Rohtak Development Plan 2025 developed by Department of Town and Country Planning, Haryana. During the periods under study it is found that the major direction of the expansion of the city is towards the eastern parts. It is the impact of National Capital Territory of Delhi. As already mention earlier, the major extension of the city is in the eastern side mainly because planned residential sectors developed by HUDA have come up in this side. Moreover, the growth directions are more prominent in eastern and northern side after the year 2005.

The growth in MC limits of the city that has extended much faster than before because of political factor. The growth of the city become faster and beyond the Jawahar Lal Nehru Feeder Canal in the year 2005. At the same time Industrial Model Township (IMT) has been developed between National Highway No. 10 (towards Delhi) and State Highway No. 18 (towards Sonipat).

## 6. Conclusion

The method of Shannon's Entropy with the help of Geographic Information System (GIS) and Remote Sensing technique is very useful tool for measuring urban sprawl. The measurement of urban sprawl is very useful for future urban planning at local and global level. The calculated Shannon's entropy for built up area of the study area confirms that the development is highly dispersed as the entropy for 2011 is 1.319. It shows that rate of urban growth of Rohtak city is quite high and needs proper management to attain sustainable development. It also showed that the horizontal growth is very high than the population growth of the city. The city is located in the fertile agricultural land so the government should monitor the growth of the city for proper management of land in a particular use of a category.

## References

Jat, M.K., Garg, P.K., and Khare, D. *Modeling of Urban Growth using Spatial Analysis Techniques: A Case Study of Ajmer City (India).* International Journal of Remote Sensing. 2008. 29 (2) 543-567.

Population Research Bureau, 2005: Human Population: Fundamental of Growth, Patterns of World Urbanisation. Population Reference Bureau, Inc., Washington, DC.

Punia, M., and Singh, L. *Entropy Approach for Assessment of Urban Growth: A Case Study of Jaipur, India.* Indian Society of Remote Sensing. 2012. 40 (2) 231-244.

Singh, B., 2013: *Urban Sprawl and Land Transformation of Rohtak City: A Study Using Remote Sensing and GIS Techniques.* Ph.D. Thesis, Department of Geography, Maharshi Dayanand University, Rohtak.

Sudhira, H.S., Ramachandra, T.V., and Jagadish, K.S. *Urban Sprawl: Metrics, Dynamics and Modelling Using GIS.* International Journal of Applied Earth Observation and Geoinformation. 2004. 5; 29-39.

United Nations, 2003: *Worlds Urbanization Prospects*. The 2003 Revision, New York.

Yeh, A.G.O., and Li, X. *Measurement and Monitoring of Urban Sprawl in a Rapidly Growing Region Using Entropy*. Photogrammetric Engineering and Remote Sensing. 2001. 67; 83-90.

**Cloud Publications**
International Journal of Advanced Remote Sensing and GIS
2014, Volume 3, Issue 1, pp. 739-747, Article ID Tech-241
ISSN 2320 - 0243

Cloud Publications

**Research Article** **Open Access**

# Comprehensive Wastewater Analysis and its Management in Some Part of Nagpur City, Maharashtra, India using SRTM DEM, GIS and Remote Sensing Approach

**Sushil S. Umbarkar[1], B.S. Manjare[1] and I.M. Daberao[2]**

[1]Department of Geology, RTM Nagpur University, Nagpur, Maharashtra, India
[2]GSDA, Solapur, Maharashtra, India

Correspondence should be addressed to Sushil S. Umbarkar, sushilumbarkar2007@yahoo.co.in

Publication Date: 20 November 2014

Article Link: http://technical.cloud-journals.com/index.php/IJARSG/article/view/Tech-241



**Abstract** Remote Sensing (RS) and Geographical Information System (GIS) and SRTM DEM have been used by as an effective and powerful method. These information and visual analytical tools have been widely applied to improve monitoring and conservation of water resources and calculate changes in environmental conditions. This study comprises in two main parts. The first part covers the Nag River and Pioli River sub basins in Nagpur. These basins were analyzed in an Arc GIS 10.2 (Ver.) by using concerning spatial data and considering water pollution parameters, population density, capacity and number of treatment plants, and etc. The Nag river sub basin was selected as the study area based on population density, generated wastewater, distribution and type of wastewater treatment plants, population served, treatment capacity and treated wastewaters, which are gained as the study area as a result of GIS queries analysis, was inspected by using remote sensing technology. Hence, relationship between land use and land cover categories, watershed and water quality parameters were interpreted by using remote sensing and GIS techniques. The geospatial information from the remote sensing data provides more effective solution for sustainable environment development. In common consensus that the progress of spatial data analysis (DSA) is a key to sustainable land management with economic and urban development.
**Keywords** *Wastewater; Change Detection; Urbanisation; Sustainable Development*

## 1. Introduction

Sewerage is part of the city planning in the technical terms because the size and the network of the system are strongly related to the spatial location of the population and its density. GIS base provides an integrative platform for urban planning and sewerage system planning exercise, thus an attempt has been made to apply the technology of GIS, SRTM DEM and Remote Sensing in the planning of sewerage infrastructure. The development and maintenance of a comprehensive sewer system inventory should be regarded as an essential undertaking for all sewerage authorities. Urban land

cover/land use changes are very dynamic in nature and have to be monitored at regular intervals for sustainable environment development. Remote sensing data, which is extremely essential for monitoring urban expansion and change detections studies (Lo, 1981; Mukherjee, 1987; & Quarmby & Cushine, 1989).

## 2. Database and Methodology

### 2.1. Data Used

Fallowing data were used for the analysis;

***Table 1:*** *Satellite Images Information*

| Satellite | Sensor | Path/Raw | Date of Pass |
|---|---|---|---|
| IRS - P6 (ResourceSat1) | LISS III | 198 / 62 | 1 Oct. 2000<br>12 Oct. 2006 |
| Space Shuttle Endeavor | WRS-2<br>C-band<br>X-band | 185/185 | 12 Oct. 2006 |

**SRTM DEM**

For given study, SRTM DEM was used and resample at a grid resolution of 90 m. The positional accuracy is within the sub pixel range when compared with 1:50,000 toposheets (Figure 2) which is down load from the web.

**Toposheet**

Survey of India toposheet No. 55 O/4 covers the part of entire Nagpur city, Maharashtra. Scale of this toposheet is 1:50000. Contour interval is of 20 meters.

***Table 2:*** *A Characteristic of ResourceSat - 1 LISS III Image*

| | Characteristics | LISS III |
|---|---|---|
| 1. | Spatial resolution (m) | 23.5 |
| 2. | Swath (km) | 141 |
| 3. | Swath steering range (Deg.) | -- |
| 4. | Spectral bands<br>Band 1 (Green)<br>Band 2 (Red)<br>Band 3 (NIR)<br>Band 4 (SWIR) | <br>0.52 – 0.59<br>0.62 – 0.68<br>0.77 – 0.86<br>1.55 – 1.70 |
| 5. | Repetitive Coverage | 24 days |
| 6. | No. of quantization levels | 7 |
| 7. | SNR at saturation radiance | >128 |
| 8. | Integration Time | 3.5528 (2,3,4)10.6584 (5) |

## 2.2. Tools Used

- Erdas imagine 9.1
- Geomatica 8.3
- Arcview 3.2
- Arc GIS 9.3

## 3. Study Area

The study area lies in Survey of India toposheet No. 55 O/4 bounded by the Latitudes $20^0$35' to $21^0$44 N and $78^0$15' to $79^0$40' E Longitudes. For the present wastewater management studies the area covers the approximately 40 $km^2$ area. The district is bounded by Chhindwara District of Madhya Pradesh on the North Bhandara District on the east, Chandrapur District of South and Wardha and Amravati District of Maharashtra on the West side. (Figure 1 & Figure 2).

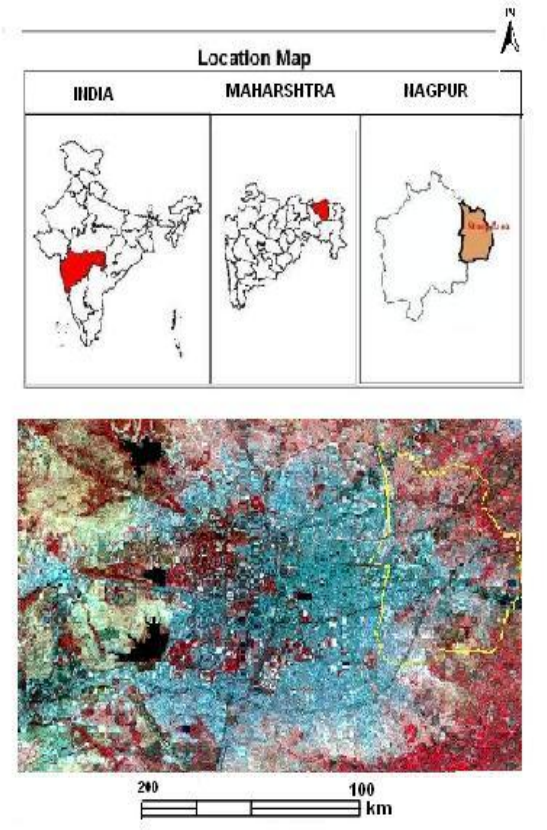


***Figure 1:*** *Location Map of the Study Area*

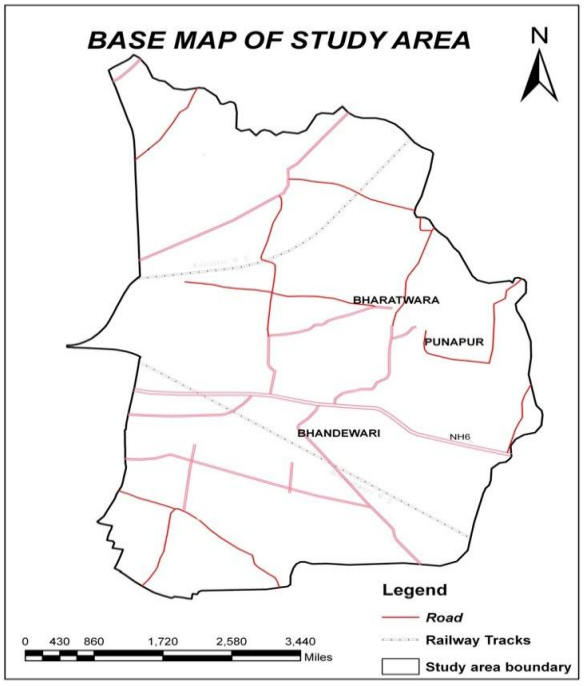


***Figure 2:*** *Base Map of the Study Area*

## 4. Landuse/Landcover

### 4.1. Land Cover / Land Use Changes

For mapping the supervised classification were used and made classes such as crop land, dense forest, open forest, barren land etc. (NRSA, 1989). The study area is situated in Bhandewadi, Punapur and Bharatwada which is covering the East part of the Nagpur city. The total geographical extension of the study area is 30.72 sq.km. From the of analysis the study areas has been classified into Nine classes such as agricultural land, built up, dumping area, industrial and lake, plantation, river, sewage water plant wasteland. In some part of the study area remarkable changes in the landuse/landcover have been observed which is supposed to be the outcome of human interference in the natural environment. According to the above studies of the landuse/landcover of Bhandewadi, Punapur, and Bharatwada villages of East part of Nagpur city showing the study area of 30.72 sq.km. The comparison of two assessment figure shows the statistically changes in the following classes year of 2002 and 2005 (Figure 3, Table 3).

***Table 3:*** *Inventory of LULC in the Study Area 2000-2006*

| LU/LC Classes | 2002 year | 2005 year | Change Detection 2002-2005 |
|---|---|---|---|
| Agricultural Land | 27.98% | 27.29% | 0.69% |
| Built up | 57.44% | 58.26% | 0.82% |
| Plantation | 00.97% | 00.94% | 0.03% |
| Wasteland | 09.36% | 09.25% | 0.11% |
| Other Class (Industrial-land, dumping area etc.) | 4.25 | 4.25 | No changed |

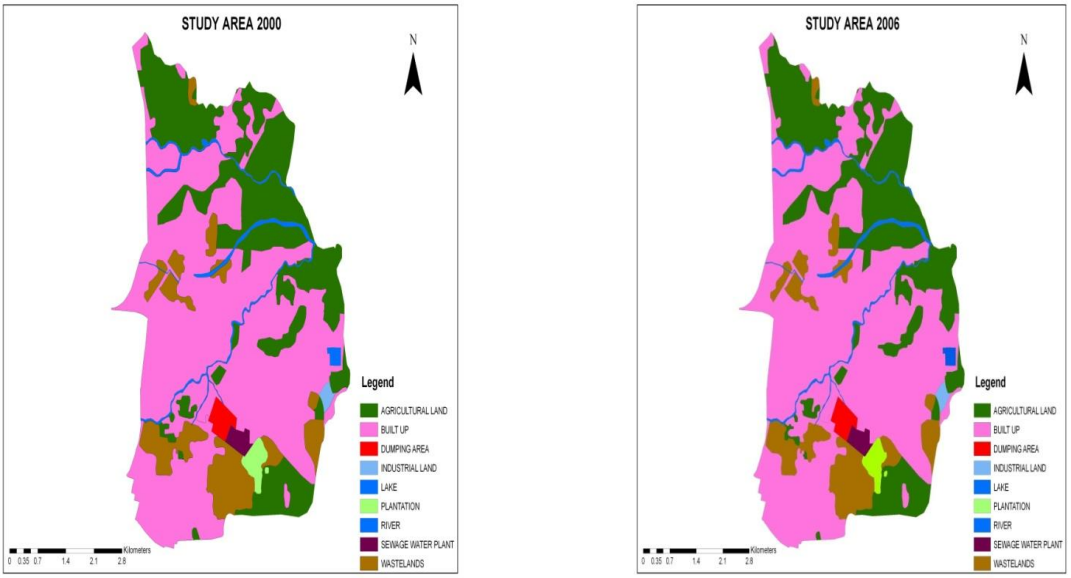


**(a)** **(b)**

***Figure 3:*** *Landuse and Landcover Map of the Study Area (a-2002 & b-2005)*

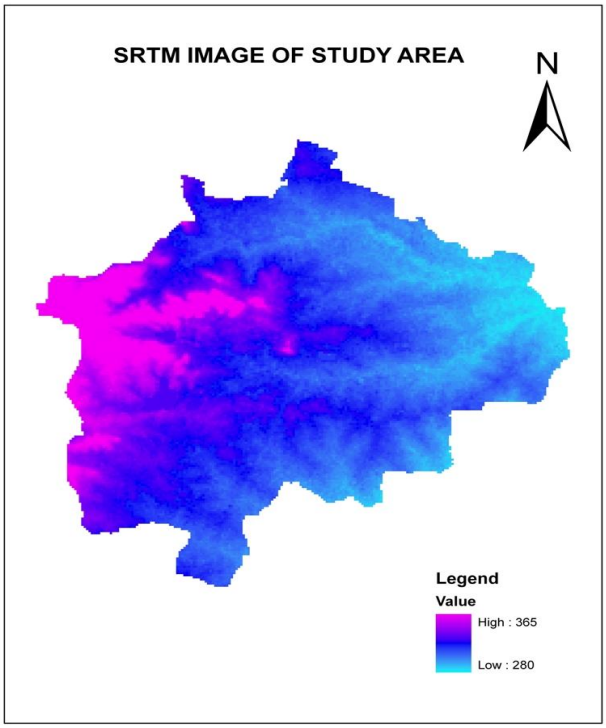


***Figure 4:*** DEM Map Nagpur City (Including Study Area)

## 5. Water Analysis

The quality of water depends upon the water quality parameter like physical, inorganic and heavy metal parameters, the total quantity of dissolved solid represented by milligram per liter, the pH value or the relation of acidity with alkalinity and the nature of the dissolve element in any water development, it is essential to conduct chemical analysis of representative sample of wastewater and treated water to determine their properties. Sample of water are collected from treated wastewater at

Bhandewadi Sewerage Treatment Plant, wastewater sample at Bhandewadi, Bharatwada and Punapur in polythene bottle of one liter capacities (Table 4, 5 & 6).

***Table 4:*** *Water Quality – Physical Parameter*

| Sr. No. | Sampling Location | pH | Turbidity (NTU) | Total Suspended Solids (mg/l) | Total Dissolved Solids (mg/l) | Conductivity (µS/cm) |
|---|---|---|---|---|---|---|
| 1. | Wastewater sample (Bharatwadi area) | 7.92 | 114 | 87.75 | 470 | 680 |
| 2. | Treated Water (Bhandewadi) | 8.42 | 3 | 162.8 | 390 | 560 |
| 3. | Wastewater before treated (Bhandewadi) | 8.56 | 30 | 84.32 | 405 | 710 |
| 4. | Wastewater (Punapur) | 8.76 | 52 | 120.45 | 394 | 720 |

***Table 5:*** *Water Quality – Inorganic Parameter*

| Sr. No. | Sampling Location | Total Alkalinity | Total Hardness | Calcium Hardness | Chloride | Sulphate | Sodium | Potassium | Oil & Grease |
|---|---|---|---|---|---|---|---|---|---|
| | | As $CaCO_3$ | | | | | | | |
| | | mg/l | | | | | | | |
| 1. | Wastewater sample (Bharatwada) | 229.6 | 205 | 138 | 52.40 | 16.30 | 60.32 | 12.34 | 30.65 |
| 2. | Treated Water (Bhandewadi) | 174 | 164 | 110 | 37.90 | 23.58 | 47.02 | 11.82 | 86.01 |
| 3. | Wastewater before treated (Bhandewadi) | 234.4 | 209 | 120 | 36.97 | 19.88 | 52.50 | 10.63 | 14.95 |
| 4. | Wastewater (Punapur) | 233.2 | 182 | 121 | 38.64 | 20.37 | 54.25 | 11.87 | 21.4 |

***Table 6:*** *Water Quality – Heavy Metals*

| Sr. No. | Sampling Location | Ni | Cd | Cr | Cu | Pb | Fe | Mn | Zn | Co |
|---|---|---|---|---|---|---|---|---|---|---|
| 1. | Wastewater sample (Bharatwada) | 0.025 | ND | ND | 2.098 | 0.580 | 8.969 | 0.299 | 0.224 | 0.005 |
| 2. | Treated Water (Bhandewadi) | ND | ND | ND | 0.019 | ND | 0.183 | 0.015 | ND | ND |
| 3. | Wastewater before treated (Bhandewadi) | ND | ND | ND | 0.012 | ND | 1.547 | 0.096 | 0.002 | ND |
| 4. | Wastewater (Punapur) | ND | ND | ND | 0.020 | ND | 2.331 | 0.173 | 0.086 | ND |

ND – Not detectable

### 5.1. Chloride

Water containing less than 250 ppm chloride is satisfactory for water supply, agricultural or industrial use. 500 ppm of chloride water gets a disagreeably salty use. However animal can use water containing as much as 4000 ppm of chlorine. The limit of Cl concentration for drinking water is specified 600 mg/L (WHO, 1993).

### 5.2. Potassium

Relatively high levels of potassium are utilized by growing plant. It is also essentially for the same carbohydrates transformation crop yield are generally great reduced in potassium deficient soils the higher the productivity of the crop. The potassium is varying from 12.34 to 10.63 mg/l.

### 5.3. Sulphate

The sulphate values ranges from 16.30 to 23.58 mg/l. the limit of drinking water is 250 mg/l. The sulphate ions are one of the major anions occurring in natural water. Sulphate is important in both public and industrial water supplies. Its cathartic effect upon human when it is presented in excessive amount.

### 5.4. Temperature

The parameter of temperature is basically important parameter for its effects on the chemistry and biological reactions in the organisms in water; the temperature was measured by the thermometer on the spot.

### 5.5. Turbidity

Turbidity in water is due to colloidal and extremely fine dispersion. Suspended matter such as clay, silt finely divided organic and inorganic matter; phytoplankton and other micro-organisms also contribute to turbidity. Turbidity measurement is helpful to follow the course of self-purification of rivers and streams. The values ranges in the study area are 3 to 114.

### 5.6. Total Dissolved Solids

Total dissolved solids in any sample can be represented by dissolved and particulate organic and inorganic matter. The TDS values in the study area ranges from 390 to 470 mg/l. Higher the TDS shows the longer residence period of water. (Davis & De Wiest, 1966).

### 5.7. Electric Conductivity

Conductivity of a water sample is measure of the ability of the sample to carry electric current. The presence of salt and contamination waste water increase the conductivity of water consequently a sudden shine in conductivity in water will indicate addition of some pollutant to it. The electric conductivity values ranges from 560 to 720 μS/cm. The maximum limit of EC in drinking water is prescribed as 1500 μS/cm (WHO, 1993). The high conduction observed can be attributed high chloride concentration in groundwater (Davis & De Wiest, 1966).

### 5.8. pH

pH is a scale to measure intensity of acidity and alkalinity of hydrogen ions concentration. pH of fresh water varies considerably and mainly depends on concentration of carbonates, bicarbonate and free

$CO_2$ etc. The pH is an important indication of its quality and provides important information in many types of geochemical equilibrium. The pH values ranges from 7.96 to 8.76. The values of Punapur area is 8.76 which is higher than the WHO values.

### 5.9. Total Hardness

The soap consuming capacity of water is known as Hardness. In other word Hardness is the properly of water which prevent lather formation with soap and increased the boiling point of water. Principal cat ions imparting hardness are calcium and magnesium; however other cations such as strontium, ferrous ions, manganese ions, etc. can also contribute to hardness. The values of the Total Hardness in the study are ranges 182 to 209 mg/L. The union responsible for hardness may carbonates, sulphates, chlorides, nitrates and silicates, etc. The water attains hardness largely from their contact with soil.

### 5.10. Total Alkalinity

Alkalinity is a measure of the concentration of such ions in water that would reacts to neutralize hydrogen ions or Alkalinity is that a measure ability of the water to neutralize or “assimilate” acids. Alkalinity indicated the capacity of sample to maintain this equilibrium in the wake of additions of acids. Alkalinity imparts bitter taste to water and makes it unpotable. The values ranges in the study area are 174 to 234.4 mg/L.

## 6. Conclusion

The satellite data and GIS techniques provides an integrative platform for urban planning and sewerage system planning exercise, thus an attempt has been made to apply the technology of GIS, SRTM DEM and Remote Sensing in the planning of sewerage infrastructure. The development and maintenance of a comprehensive sewer system inventory should be regarded as an essential undertaking for all sewerage authorities. Estimate wastewater flow of the year 2020 is calculated by using statistical method of simple regression for projected population of the year 2020 is 28, 56, 068 lakhs. By using pollution load formula – 47, 28, 96, 021 ltrs, wastewater generates. According to this study the city has immediate demand of 300 MLD (wastewater) sewerage treatment plant over 300 MLD sewerage water that unnecessarily goes into Nag River. At the Bhandewadi, the Bharatwada and the Punapur villages are using water of the Nag River for agricultural irrigation and domestic purposes ultimately polluted water threatens crops, soil quality, and public health. Poorly managed water supply and sewerage services threatens public health and environmental harm to ensure that these services managed a significant legislative and regulatory framework must be complied with by those responsible for the provision and management of these services; it is important that planners are aware of the legislative and regulatory framework relating to sewerage services.

## Acknowledgement

Author thanks to the NEERI, Nagpur for the all facility throughout this research work.

## References

Burrough, P.A., 1986: *Principles of Geographic Information System for Land Resource Assessment*. Clarendon Press, Oxford.

Davis, S.N., and De, Wiest, 1966: *Hydrology*. John Welly and Sons Inc., New York.

Lo, C.P. 1981. *Land Use Mapping of Hong Kong from Landsat Images: An Evaluation.* International Journal of Remote Sensing. 2 (3) 231-251.

Mukherjee, S. 1987 *Landuse Maps for Conservation of Ecosystems.* Geographical Review of India. XLIX (3) 23-28.

NRSA, 1989: *Manual of Nationwide Land Use / Land Cover Mapping Using Satellite Imagery.* National Remote Sensing Agency, Hyderabad.

Quarmby, N.A., and Cushine, J.L. 1989. *Monitoring Urban Land Cover Changes at the Urban Fringe from SPOT HRV Imagery in South East England.* International Journal of Remote Sensing. 10 (6) 231-251.

WHO, 1993: *Guidelines for Drinking Water Quality.* World Health Organization, Geneva.

**Cloud Publications**
International Journal of Advanced Remote Sensing and GIS
2014, Volume 3, Issue 1, pp. 532-543, Article ID Tech-248
ISSN 2320 - 0243

Research Article | Open Access

# Estimation of Evapotranspiration using MODIS Sensor Data in Udupi District of Karnataka, India

**G. Dinesh Kumar, B.M. Purushothaman, M.S. Vinaya, and S. Suresh Babu**

Department of Civil Engineering, Adhiyamaan College of Engineering, Hosur, Tamil Nadu, India

Correspondence should be addressed to G. Dinesh Kumar, dineshkumaran10@gmail.com

Publication Date: 30 April 2014

Article Link: http://technical.cloud-journals.com/index.php/IJARSG/article/view/Tech-248



**Abstract** The paper focuses on the estimation of evapotranspiration in the Udupi district, Karnataka using MODIS sensor images. Surface Energy Based Algorithm for Land was utilized for the purpose. Satellite measurements were compared with the concurrent measurements made from meteorological data. Good fit ($r^2$ = 0.96) between 2 data sets with significant positive correlation (r = 0.97) is observed. The evapotranspiration values range between 85 mm and 1230 mm in the study area. Lower values are reported in December & higher values in June with vegetated plains in the foot belt of Western Ghats showing maximum evapotranspiration.
**Keywords** *Evapotranspiration; NDVI; Remote Sensing; SEBAL*

## 1. Introduction

Evapotranspiration (ET) is a combined process of evaporation of liquid water from various surfaces, transpiration from the leaves of plants and trees, and sublimation from ice and snow surfaces. It is a major part of water cycle and is an important factor in understanding the complex feedback mechanisms between the earth's surface and the surrounding atmosphere. Approximately 62% of the precipitation over continents is evapotranspired on an annual scale (Shiklomanov and Sokolov, 1983; Dingman, 1994).

A number of models for ET estimation have been developed which include empirical, semi-empirical and physical models. These models have increased the precision of ET estimation (Brutsert, 1979). There are many methods available to estimate reference ET using meteorological data such as FAO-24 (Doorenbos and Pruitt, 1977), FAO-56 (Allen et al., 1998). Reference ET can be defined as the ET rate of a reference crop expressed in inches or millimeters. Most of these methods are based on point data, which do not provide a good estimation of ET for large areas. The problem of actual ET estimation over a large area can be solved using remote sensing methods that provide ET on pixel by pixel basis. Many researchers (Vidal and Perrier, 1989; Bastiaanssen, 1995; Granger, 1997; Allen et

al., 2007) have worked on developing models by integrating satellite images and weather data on regional scale.

Factors that affect evapotranspiration include the plant's growth stage or level of maturity, percentage of soil cover, solar radiation, humidity, temperature and wind. Isotope measurements indicate transpiration is the larger component of evapotranspiration (Williams et al., 2004).Sensible heat flux is estimated from wind speed and surface temperature using a unique internal calibration of the near surface-to-air temperature difference as described by (Bastiaanssen et al., 1998a). The objective of the present study is to estimate the evapotranspiration in the Udupi district of Karnataka by integrating Remote Sensing and SEBAL Algorithm.

## 2. Study Area

Udupi district is bound by Arabian Sea in west and Western Ghats in the east. Land bordering Western Ghats in the east is covered with forests and hilly terrain. The district is harboring rare species of flora and fauna. The area geographically lies between 13˚26´N & 13˚80´ N latitudes and 74˚63´ E & 75˚41´ E longitudes. The area enjoys a heavy rainfall of 3000–4000 mm per annum. The temperature varies from 18–38$^{o}$C.

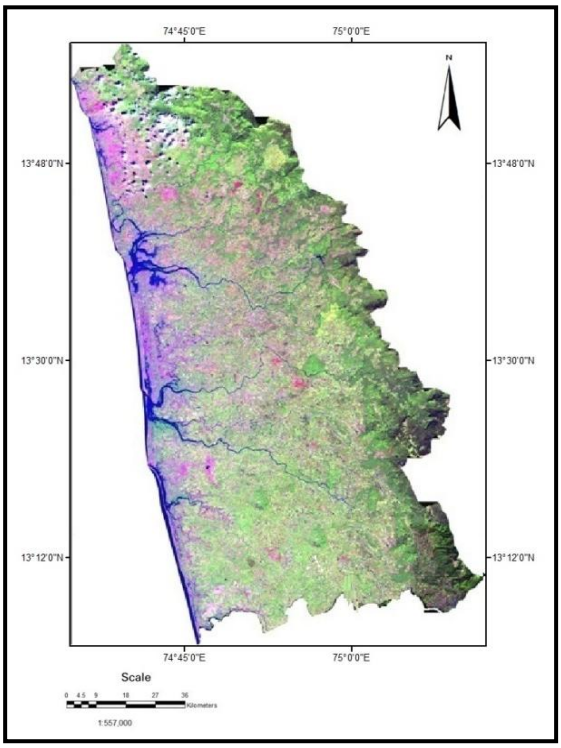


***Figure 1:*** *Study Area as Viewed by IRS P6 – LISS IV*

## 3. Materials and Methods

### 3.1. Meteorological Data

Rainfall, temperature, pressure and relative humidity data for the year 2013 were collected from three meteorological stations of the study area namely Udupi, Karkala and Kundapura. Wind and Solar radiation data were collected from NCDC, USGS.

### 3.2. Satellite Data

Monthly Satellite data of MODIS sensor of Terra/Aqua Satellites were utilized for the estimation of evapotranspiration. The use of MODIS sensor data for agricultural and hydrological applications has been well recognized (Vidal and Perrier, 1989; Cristina et al., 2007). The MODIS Terra sensor data (Table 1) is acquired originally in 36 narrow wavebands. MODIS provides different sets of land products, including different levels of surface reflectance and surface temperature products. Two products namely MOD09 and MOD11A1 were acquired and re-projected using MODIS Re-projection Tool (MRT). Then, the digital numbers were converted into percent reflectance and surface temperature (LST) values using the scale factor provided with the product.

The split window technique was used to estimate surface temperature from the MODIS image. Split window algorithms calculate differential absorption in two close infrared bands to account for the effects of absorption by atmospheric gases when multiple thermal bands are available (band 31and 32).

***Table 1:*** *MODIS Wavelength Bands and its Applications*

| Band | Wavelength Range (nm) | Data Final Format | Potential Applications |
|---|---|---|---|
| 1 | 620 – 670 | Reflectance | Absolute Land cover Transformation, Vegetation Chlorophyll |
| 2 | 841 – 876 | Reflectance | Cloud Amount, Vegetation, Land- cover Transformation |
| 31 | 10780 – 11280 | Brightness Temperature | Cloud Temperature, Forest Fires & Volcanoes, Surface Temperature |
| 32 | 11770 – 12270 | Brightness Temperature | Cloud Height, Forest Fires & Volcanoes, Surface Temperature |

### 3.3. Surface Energy Balance Algorithm for Land (SEBAL)

The SEBAL algorithm uses the surface energy balance to estimate aspects of the hydrological cycle. SEBAL maps evapotranspiration, biomass growth, water deficit and soil moisture.

$$LE = R_n - G - H \qquad (1)$$

Where, LE is the energy needed to change the phase of water from liquid to gas, $R_n$ is the net radiation, G is the soil heat flux and H is the sensible heat flux. Using instruments like a scintillometer, soil heat flux plates or radiation meters, the components of the energy balance can be calculated and the energy available for actual evapotranspiration can be solved.

Surface albedo ($\alpha_s$) was estimated using MODIS daily surface reflectance [2] while surface emissivity ($\varepsilon_s$) was estimated using MODIS NDVI composition [3].

$$\alpha_s = \sum_{b=1}^{7} [\rho_{s,b}\omega_b] \qquad (2)$$

$$\varepsilon_s = 1.009 + 0.047\, ln(\text{NDVI}) \qquad (3)$$

in which $\rho_{s,b}$ is the at-surface reflectance for band "n" and $\omega_b$ is the weighting coefficient representing the fraction of at-surface solar radiation occurring within the spectral range represented by a specific band [2].

From the residual in the instantaneous energy-balance equation and the evaporative fraction (EF) the average ET ($ET_{avg}$: mm·year−1) were estimated. EF has an important characteristic which is its regularity and constancy in cloud-free days [4]. Thus, its instantaneous value can be taken as the daily mean value, so that the spatial variability in average ET can be predicted over large scales.

$$EF = \frac{\mathrm{LE}}{\mathrm{R_n - G}} \qquad (4)$$

$$ET_{avg} = \frac{86400\mathrm{EFR_{n,avg}}}{\lambda} \qquad (5)$$

in which λ is the latent heat of evaporation (J·kg−1) and $R_{n,avg}$ (W·m−2) is the average net radiation balance estimated using a sinusoidal function [5], assuming that during the night Rn and the average G is zero [5,6].

$$R_{n,avg} = \frac{2\mathrm{R_n}}{\pi \sin\left[\left(\frac{\mathrm{t_{overpass} - t_{rise}}}{\mathrm{t_{set} - t_{rise}}}\right)\pi\right]} \qquad (6)$$

Where, $t_{overpass}$ (h) is the time at which the image was acquired and $t_{set}$ (h) and $t_{rise}$ (h) are the times of sunset and sunrise, respectively. The daytime hours were calculated based on latitude and the day of the year.

### 3.4. Data Integration in GIS

Satellite products and the thematic maps were integrated in GIS domain for analyzing the evapotranspiration pattern in the study area. Schematic representation of the methodology is shown in Figure 2.

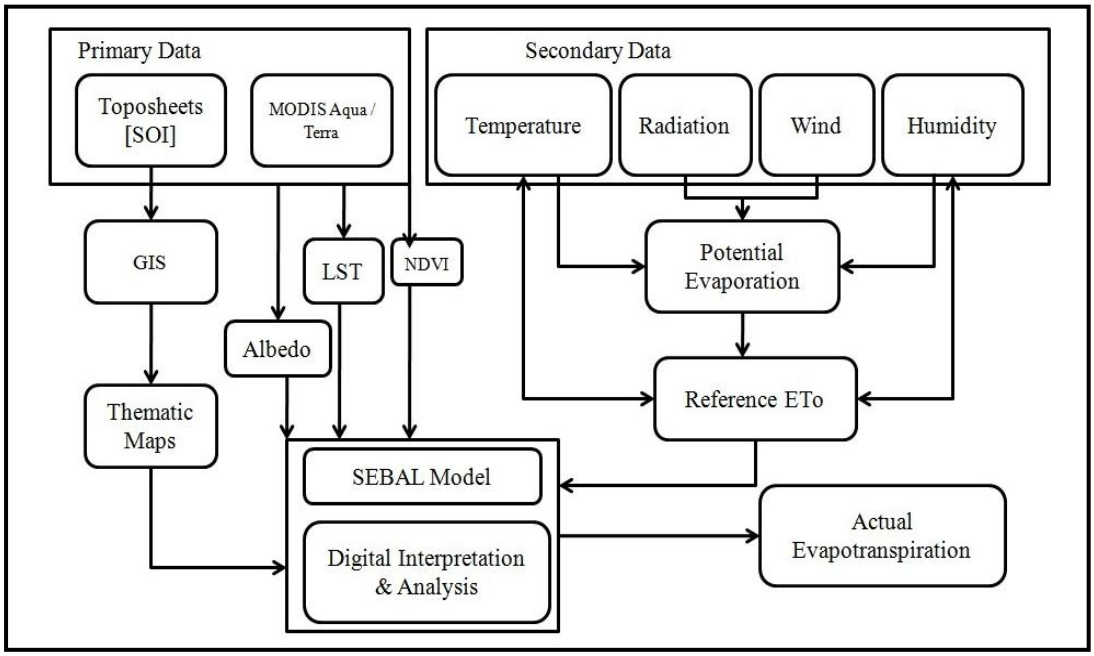


***Figure 2:*** *Flow of Work*

## 4. Results and Discussion

Evapotranspiration was estimated using the SEBAL Algorithm from MODIS Satellite images and concurrent meteorological data for the year 2013 separately. The linear regression shows a good fit between 2 datasets with $r^2$ value of 0.9578 (Figures 14 & 15). Pearson correlation analysis yielded a correlation coefficient (t) value 0.97. Since t > 0.283 (table value) for 36 measurements at p< 0.05, the correlation is positively significant. From the study, it is clear that MODIS retrieved evapotranspiration can be directly used for the study area without modification of the retrieval algorithm. Comparison of temporal variation trend lines of two datasets confirms the above observation.

The evapotranspiration values range between 85 mm and 1230 mm for the year 2013 in the study area. The average annual evapotranspiration is shown in the Figure 11. Lower values are recorded in the month of December (Figure 13) whereas higher values are found in June (Figure 12).

Evapotranspiration is mainly dependent on vegetation cover, wind, temperature, relative humidity and elevation parameters. NDVI analysis gives indirect information on canopy cover, vegetation primary productions and phenology of vegetation classes (Amanda et al., 2013; Barbagallo et al., 2008; Yang et al., 2011). The NDVI products for the months of June and December are shown in Figures 3a & 3b respectively.

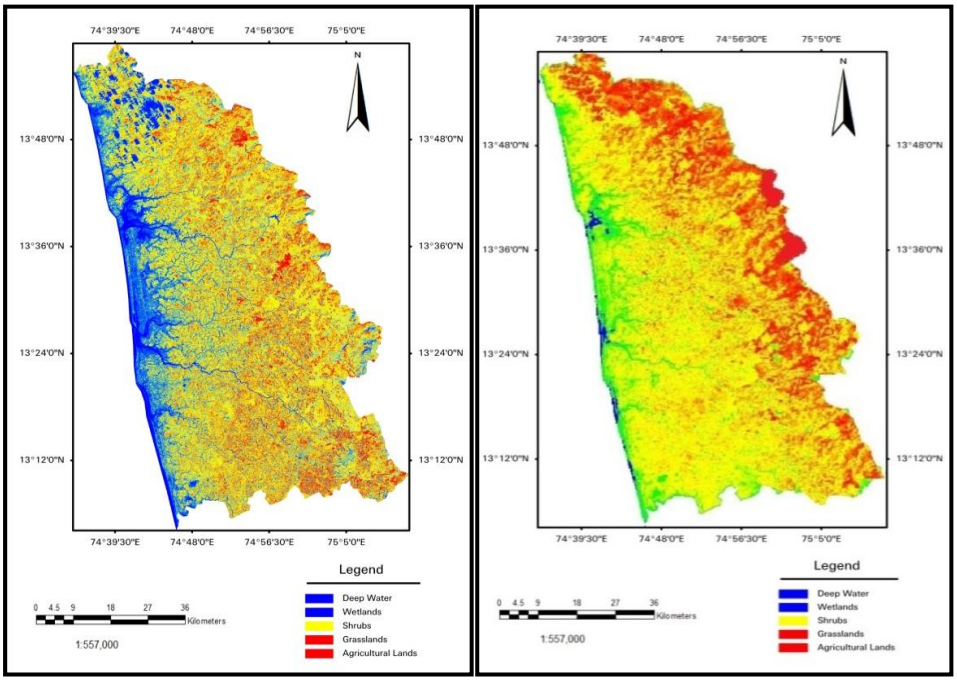


***Figure 3a:*** *NDVI Map for the Month of June* ***Figure 3b:*** *NDVI Map for the Month of December*

Along with meteorological parameters, slope and aspect also play key role in evapotranspiration as they determine the effectiveness solar insolation. The slope map (Figure 4) and the aspect map (Figure 5) give an idea on the higher solar radiation receiving regions in the study area.

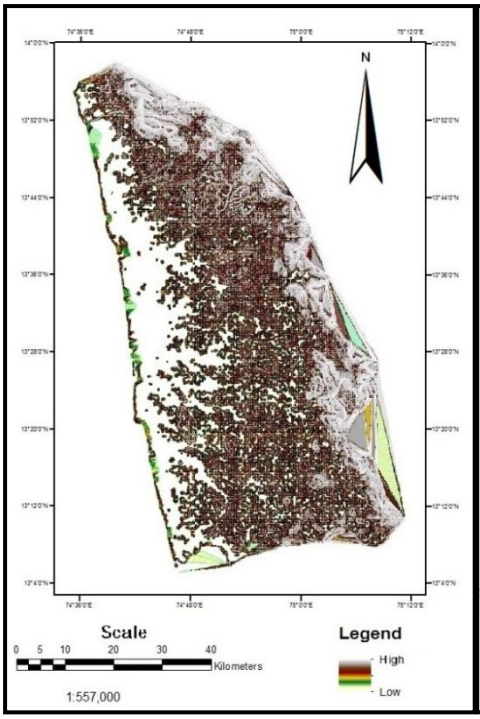


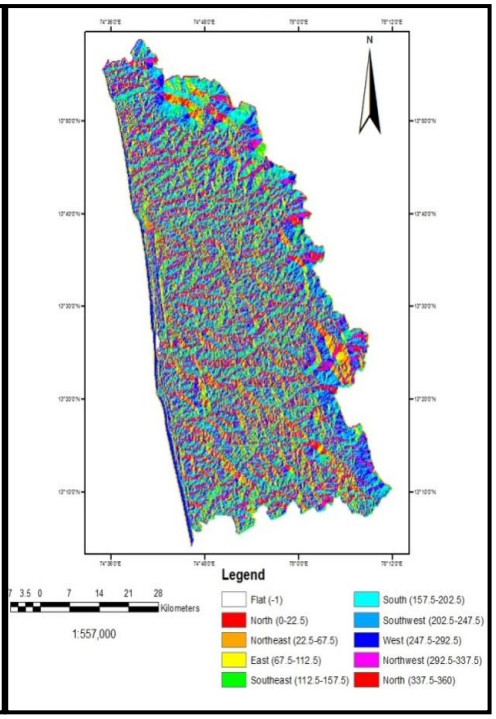


***Figure 4:*** *Slope Map*

***Figure 5:*** *Aspect Map*

Direct relationship between Landuse/landcover classes and evapotranspiration is observed in study (Ayoub and Ibrahim, 2008; Yong et al., 2011). Evapotranspiration is poor in coastal tract as settlements and built-up classes dominating over vegetation cover in this region. Evergreen forest, deciduous forest and grasslands are contributing for higher evapotranspiration in the study area. The landuse/landcover details are presented in Table 2.

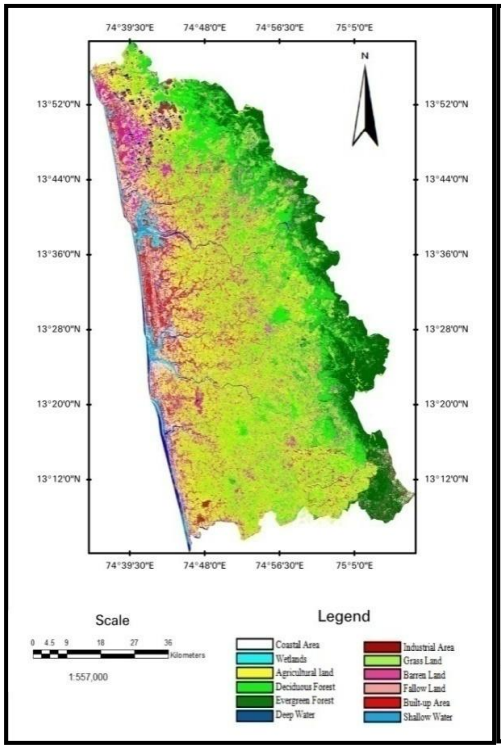


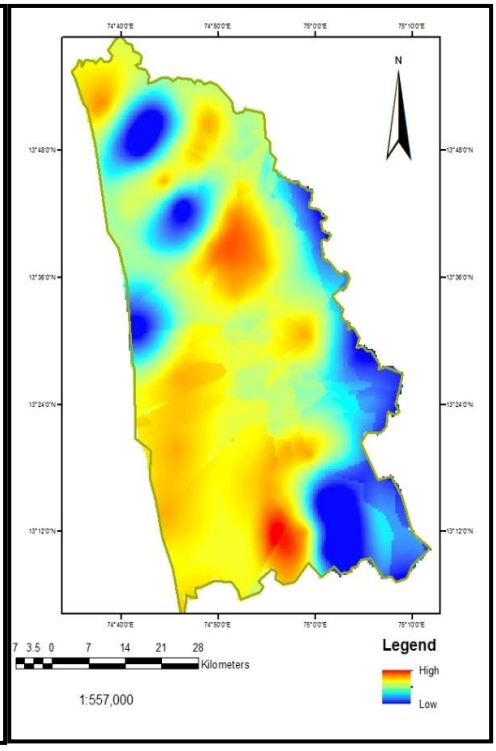


***Figure 6:*** *Landuse / Landcover Map*

***Figure 7:*** *Relative Humidity Map*

Integrating the landuse/landcover map (Figure 6), the evapotranspiration is classified as poor in the built-up areas moderate in the agricultural lands and plantations, good to very good in foot belt of Western Ghats. The shola forests of the study area show higher evapotranspiration.

***Table 2:*** *Landuse/Landcover Area coverage*

| S. No. | Class | Area in Sq. Km |
|---|---|---|
| 1 | Fallow Land | 1383.3275 |
| 2 | Shallow Water | 101.91245 |
| 3 | Built-up Area | 758.66695 |
| 4 | Coastal Area | 430.9242 |
| 5 | Wetlands | 129.75055 |
| 6 | Agricultural Land | 1766.13545 |
| 7 | Evergreen Forest | 1456.35845 |
| 8 | Deciduous Forest | 2268.57485 |
| 9 | Deep Water | 260.63615 |
| 10 | Industrial Area | 222.74945 |
| 11 | Barren Land | 975.13955 |
| 12 | Grass Land | 4125.1477 |

The lower values of evapotranspiration reported in December (Figure 8) is attributed to lower temperature and sunshine conditions whereas the higher values reported in June (Figure 9) could be due to prevailing monsoon winds and associated high rainfall (Immerzeel and Peter, 2008; Chen et al., 2013). Northern vegetated plains of the study area show lower values through the year compared to other similar plains, which may be due to the proximity of the region to the Arabian Sea. Humidity increases towards sea (Figure 7) this in turn reduces the evapotranspiration.

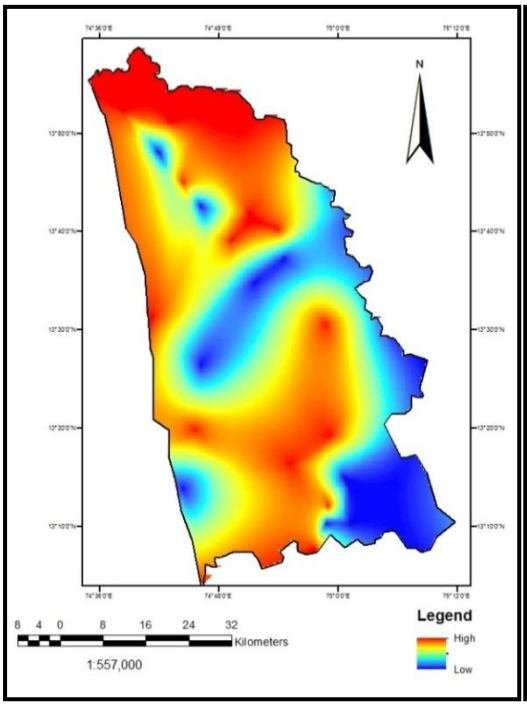


***Figure 8:*** *Temperature Map*

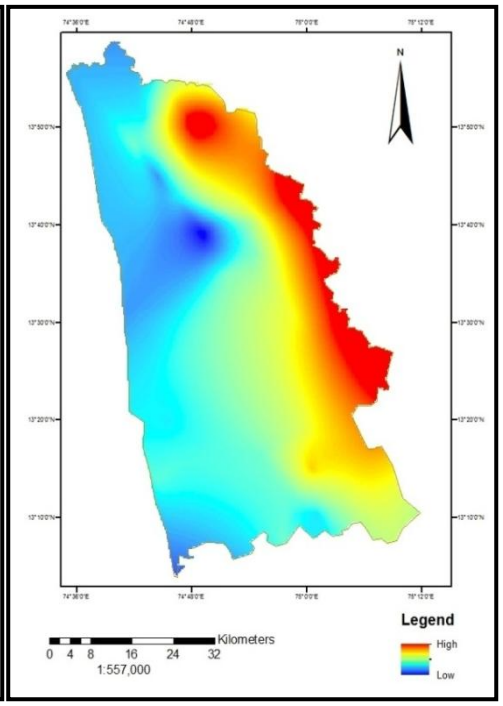


***Figure 9:*** *Rainfall Distribution Map*

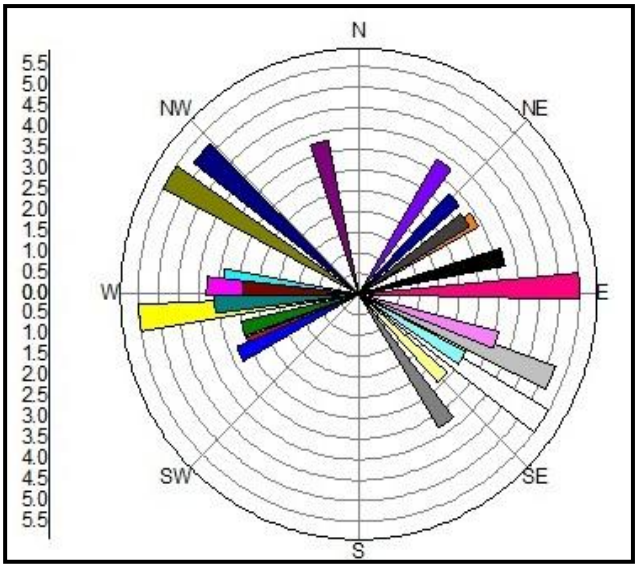


***Figure 10:*** *Wind Rose Plot*

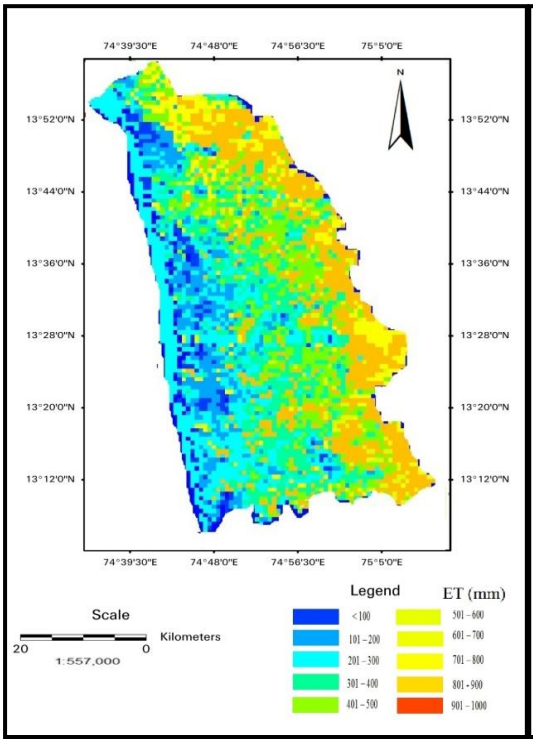


***Figure 11:*** *Average Annual Evapotranspiration Map*

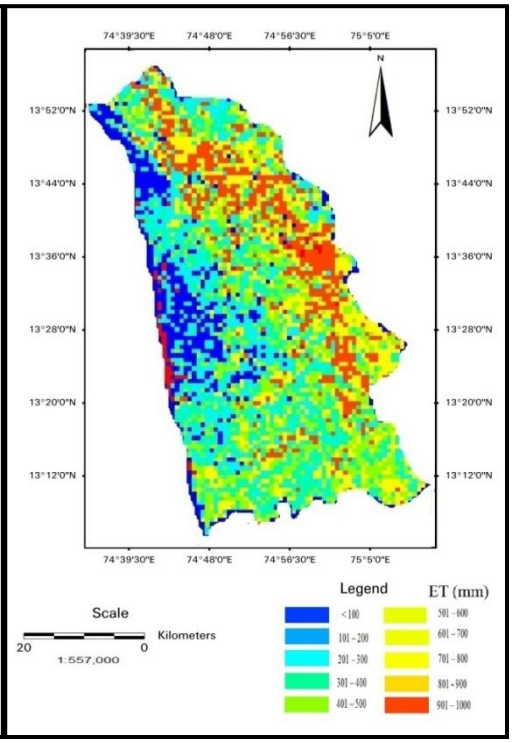


***Figure 12:*** *Evapotranspiration Map for the Month of June*

The variations in wind direction and speed in the study area are shown in Figure 10. The wind measurements were made at a height of 10 m from ground level.

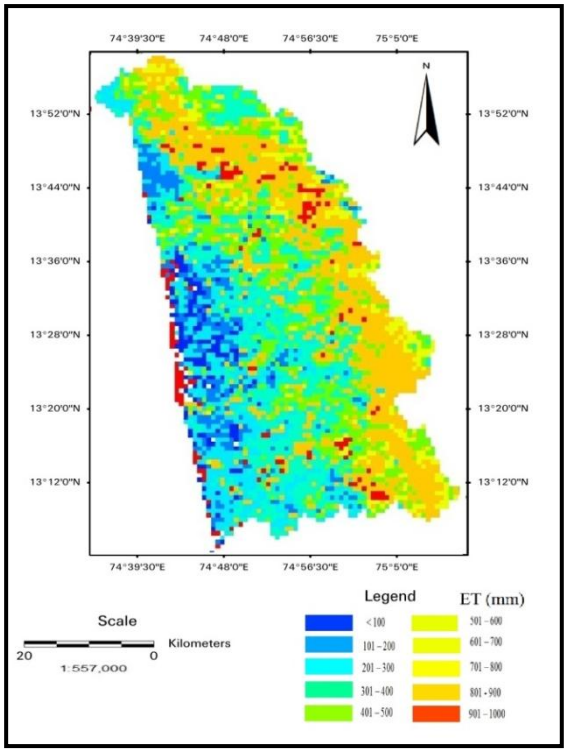


***Figure 13:*** *Evapotranspiration Map for the Month of December*

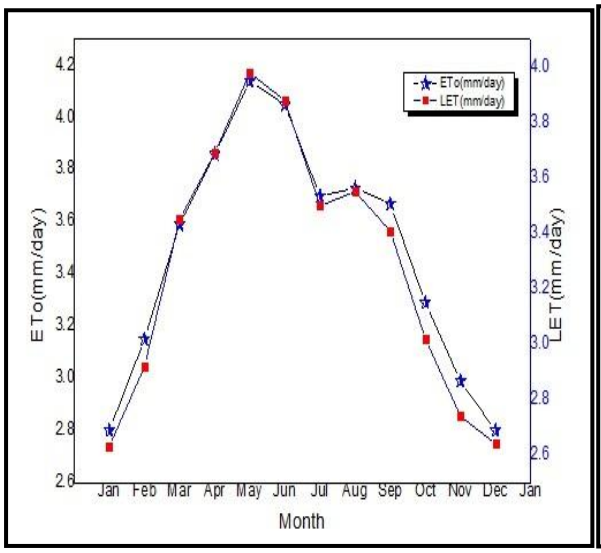


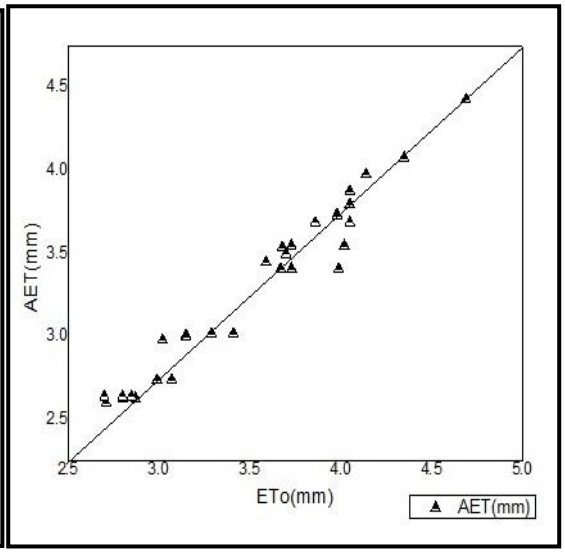


***Figure 14:*** *Comparison of Potential ET and Actual ET* ***Figure 15:*** *Scatter plot for Actual ET and Reference ET*

A Digital Elevation Model (DEM) of the study area was prepared (Figure 16) and integrated in the study to understand the variations in evapotranspiration in relation to topography.

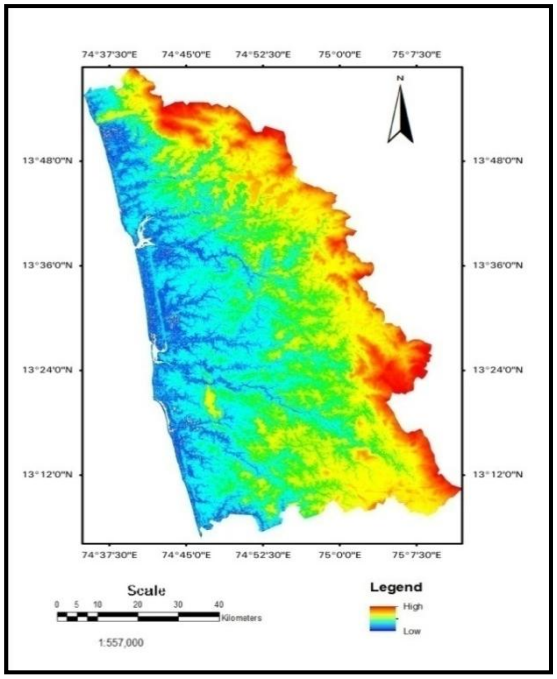


***Figure 16:*** *DEM Map*

Lower values are found in the coastal tract especially in the areas having dense settlements followed by steep slopes of Western Ghats. The higher values are recorded along the foot belt of Western Ghats with thickly vegetated plains recording the maximum evapotranspiration.

## 5. Conclusion

Integration of MODIS satellite products with SEBAL algorithm is proved to be very useful in estimating evapotranspiration. Evapotranspiration is higher in the foot belt of Western Ghats and lower in the vicinity of coast. The direct relationship between landuse/landcover classes and evapotranspiration is well noticed in the study. Integration of satellite products & thematic maps in GIS domain greatly helps in understanding the spatial and temporal variations of evapotranspiration.

## Acknowledgement

The authors are thankful to the Meteorological Department, Udupi district for providing the meteorological data and National Climatic Data Centre and LPDAAC, USGS for providing the MODIS sensor products.

## References

Allen, R.G., Tasumi, M., and Trezza, R. *Satellite-Based Energy Balance for Mapping Evapotranspiration with Internalized Calibration (METRIC) Model*. Journal of Irrigation and Drainage Engineering. 2007. 133 (4) 380-394.

Allen, R.G., Tasumi, M., Morse, A., and Trezza, R. *A Landsat-Based Energy Balance and Evapo-Transpiration Model in Western US Water Rights Regulation and Planning.* Irrig. Drain. Syst. 2005. 19; 251-268.

Amanda Veloso, Valérie Demarez, Eric Ceschia, and Martin Claverie. *Crop Biomass and Evapotranspiration Estimation using SPOT and Formosat-2 Data.* Geophysical Research Abstracts, EGU General Assembly. 2013. 15.

Ayoub Almhab and Ibrahim Busu, 2008: *Estimation of Evapotranspiration Using Fused RS and M-SEBAL Model for Improving Water Management in Arid Mountainous Area*. 3rd International Conference on Water Resources and Arid Environments.

Barbagallo, S., Consoli, S., and Russo, A. *Estimate of Evapotranspiration using Surface Energy Fluxes from Landsat TM.* Options Méditerranéennes. 2008. 84; 105-114.

Bastiaanssen, W.G.M., 1995: *Regionalization of Surface Flux Densities and Moisture Indicators in Composite Terrain: A Remote Sensing Approach under Clear Skies in Mediterranean Climates.* Ph.D. Dissertation. Wageningen Agricultural University, Wageningen.

Bastiaanssen, W.G.M., Menenti, M., Feddes, R.A., and Holtslag, A.A.M. *A Remote Sensing Surface Energy Balance Algorithm for Land (SEBAL) Formulation.* Journal of Hydrology. 1998. 212-213; 198-212.

Brutsert, W. *Heat and Mass Transfer to and from Surface with Complete Vegetation or Similar Permeable Roughness.* Boundary Layer Meteorology. 1979. 16; 365-388.

Cristina Serban (Gherghina), Carmen Maftei, and Alina Barbulescu. *Estimation of Evapotranspiration Using Remote Sensing Data and Grid Computing: A Case Study in Dobrogea, Romania.* Latest Trends on Computers. 2007. II; 596-601.

Dawen Yang, He Chen, and Huimin Lei. *Estimation of Evapotranspiration using a Remote Sensing Model over Agricultural Land in the North China Plain*. International Journal of Remote Sensing. 2010. 31 (14) 3783-3798.

Doorenbos, J., and Pruitt, W.O. *Crop Water Requirements*. FAO Irrigation and Drainage. 1977. 24; 156.

Granger, R.J., 1997: *Comparison of Surface and Satellite-Derived Estimates of Evapotranspiration using a Feedback Algorithm*. Kite, G.W., Pietroniro, A., and Schultz T.J., (Eds). In: Applications of Remote Sensing in Hydrology. Proceedings of the 3rd International Workshop NHRI Symposium. NASA Goddard Space Flight Center, Greenbelt, MD.

Hamid Reza Matinfar. *Evapotranspiration Estimation Base upon SEBAL Model and Fieldwork*. Scholars Research Library. 2012. 3 (5) 2459-2463.

Jackson, R.J., 1967: *The Effect of Slope, Aspect and Albedo on Potential Evapotranspiration from Hill Slopes and Catchments*. Soil Bureau, D.S.I.R. 60-69.

Shiklovmanov, I.A., and Sokolov, A.A., 1983: *Methodological Basis of World Water Balance Investigation and Computation. New Approaches in Water Balance Computations*, International Association for Hydrological Sciences Publication No. 148. Proceedings of a Workshop during XVIIIth General Assembly of the International Union of Geodesy and Geophysics at Hamburg, FR Germany.

Vidal, A., and Perrier, A. *Analysis of a Simplified Relation used to Estimate Daily Evapotranspiration from Satellite Thermal IR data*. International Journal of Remote Sensing. 1989. 10 (8) 1327-1337.

Walter Immerzeel and Peter Droogers. *Calibration of a Distributed Hydrological Model Based on Satellite Evapotranspiration*. Journal of Hydrology. 2008. 394; 411-424.

Williams, D.G., Cable, W., Hultine, K., Hoedjes, J.C.B., Yepez, E.A., Simonneaux, V., Er-Raki, S., Boulet, G., de Bruin, H.A.R., and Chehbouni A. *Evapotranspiration Components Determined by Stable Isotope, Sap Flow and Eddy Covariance Techniques.* Agricultural and Forest Meteorology. 2004. 125; 241-258.

Xiao-chun Zhang, Jing-wei, W.U., Hua-yi, W.U., and Yong, L.I. *Simplified SEBAL Method for Estimating Vast Areal Evapotranspiration with MODIS Data*. Water Science and Engineering. 2011. 4 (1) 24-35.

Zhuoqi Chen, Runhe Shi, Shupeng Zhang. *An Artificial Neural Network Approach to Estimate Evapotranspiration from Remote Sensing and Ameri Flux Data.* Front. Earth Sciences. 2013. 7 (1) 103-111.

**Cloud Publications**
International Journal of Advanced Remote Sensing and GIS
2014, Volume 3, Issue 1, pp. 525-531, Article ID Tech-249
ISSN 2320 - 0243

Research Article | Open Access

# Machine Learning Technique Approaches Versus Statistical Methods in Classification of Multispectral Remote Sensing Data using Maximum Likelihood Classification: Koluru Hobli, Bellary Taluk, District, Karnataka, India

**S.S. Patil[1], Sachidananda[1], U.B. Angadi[2], and D.K. Prabhuraj[3]**

[1]Department of Computer Science, University of Agricultural Sciences, Bangalore, Karnataka, India
[2]CABin, ISRI, New Delhi, India
[3]KSRSAC, Bangalore, Karnataka, India

Correspondence should be addressed to S.S. Patil, spatilsuasb@gmail.com

Publication Date: 28 April 2014

Article Link: http://technical.cloud-journals.com/index.php/IJARSG/article/view/Tech-249



**Abstract** Classification is challenging task on complex features of Remote sensing satellite imageries color pixels variability of patterns. Machine learning techniques have delivered the improved in accuracy of classification of patterns of features. Remote sensing color based imageries having hard to cluster color pixels with variability in intensity of colors. Challenges in estimation of various features viz, crop fields, fallow land, buildings, roads, rivers, water bodies, forest, and other trivial items. Urge in estimation of crop yield predictions through satellite imageries. We are attempted to converging accuracy of estimation of vegetation crop yield of fields. Kappa coefficient to achieve high degree accuracy estimation of crop wise with suitable thresh hold to ground truth data.
**Keywords** *Machine Learning Techniques; Supervised Classification; Maximum Likelihood Classification; Kappa Coefficient; Classification Accuracy; f-measure*

## 1. Introduction

Remote sensing is the science and art of obtaining information about an object, geographic area or phenomenon through the analysis of data acquired by a device that is not in contact with the object, area, or phenomenon under investigation. This study deals with remote sensing data acquired through earth observation satellites. Remote sensing image analysis is done to extract useful information about the earth surfaces. An important step in the analysis of such data is the process of land cover classification. In this the image pixels are assigned to different land cover classes based on the spectral measurements of each pixel. Pattern recognition technique such as Maximum likelihood classification is followed in this process. Machine learning techniques can be applied in a supervised and unsupervised manner. Supervised Classification is a procedure for identifying spectrally similar areas on an image by identifying 'training' sites of known targets and then extrapolating those spectral

signatures to other areas of unknown targets. Classification of images based remote sensing have thrust research area on of the remote sensing community on feasibility study on environmental and socioeconomic applications are based on the classification results (Lu and Weng, 2007). The efficient evaluation of amount of changes in land use land cover through remote sensing satellite digital data analysis make decision support to develop effective plans for the management of land (Gordon, 1980). The assessment of technology of remote sensing has instigated it to develop one of the most regularly used methods in the earth. Supervised classification has been used in this study. Supervised classification of multispectral remote sensing imagery is commonly used for land use land cover determination (Duda and Canty, 2002). There is a consistent logic to all of the supervised classification routines in almost all image processing softwares. In addition, there is a basic sequence of operations that must be followed no matter which of the supervised classifiers is used. In this study the following sequence of operations were used. In thematic mapping from remotely sensed data, the term accuracy is used typically to express the degree of 'correctness' of a map or classification (Foody, 2002). The overall accuracy is expressed as a percentage of the test pixels successfully assigned to the correct classes. Maximum Likelihood produced the highest accuracy with overall accuracy of 87%. Then followed by Mahalanobis gave the overall classification accuracy of 77% and Minimum distance showed the overall classification accuracy of 71%.

## 2. Materials and Methods

### 2.1. Description of the Study Area

Study area consists of Koluru Hobli of Bellary Taluk and District of Karnataka, which lies between $15^0 9'$ to $15^0 15'$N latitude and $76^0 55'$ to $76^0 92'$E longitudes.

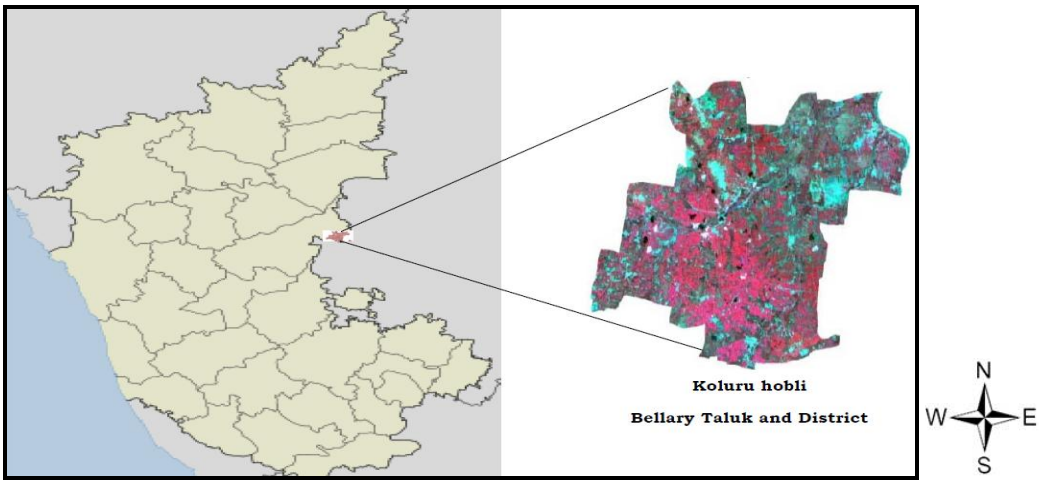


***Figure 1:*** *Sattillite Imagieries of Koluru Hobli of Bellary Taluk and District of Karnataka State*

### 2.2. Details of Image Data

IRS (Indian Remote Sensing Satellite)-P6 LISS-III (Linear Imaging Self Scanner) imageries of 21st November, 2010 is used for the study. The geometrically corrected imageries are obtained from National Remote Sensing Agency, Department of Space, Government of India, Hyderabad. The topographical map of the study area is over laid on this image to extract the digital image of the study area (Plate–2). The spatial resolution of the images is 23.5 mt. The imageries were recorded in three spectral bands. Among these only the first two namely Green, Red are in the small range of electromagnetic spectrum and third one namely blue band is useful in identification of green vegetation like crop. Ground truth data collected during field visits in the study area and the toposheets are used to accomplish the task of selection of training sites for each category for training the classifier in

supervised classification. A part of the data was used as test sites for assessing classification accuracy.

### 2.3. Details of Land Cover Classes Considered

The categories of interest were carefully selected and defined to successfully perform digital image classification. In the present study a broad land use/land cover classification system is adopted with six categories for each study area as follows.

Land use/Land cover categories of Koluru Hobli, Bellary Taluk.

1) Paddy
2) Cotton
3) Jowar
4) Chilly
5) Fallow land
6) Water bodies

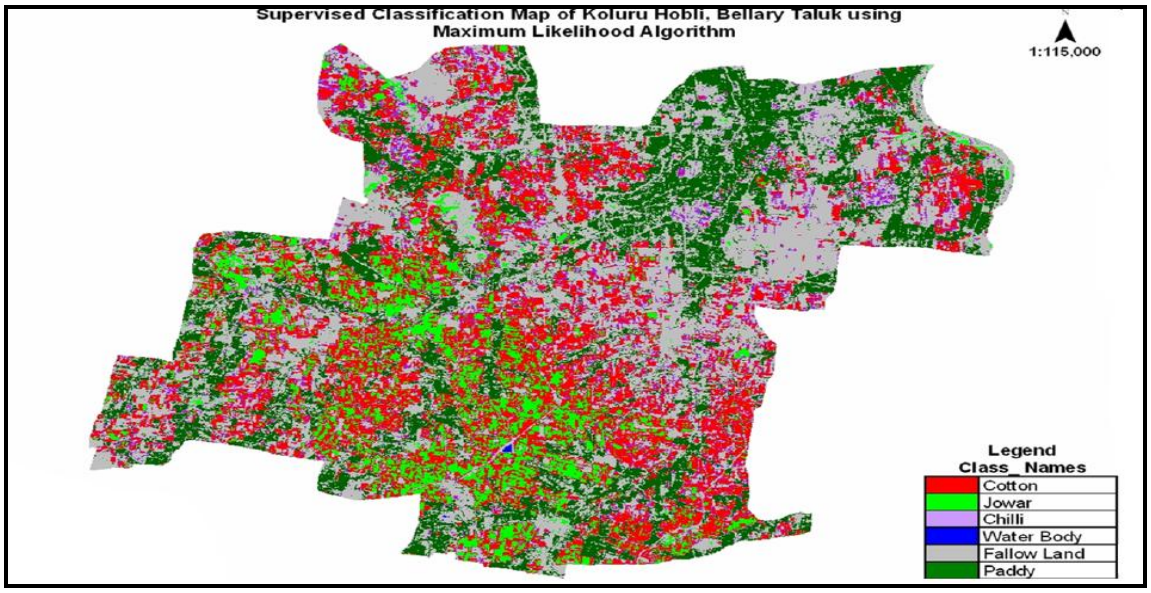


***Figure 2:*** Supervised *Classification Map of Koluru Hobli, Bellary Taluk and District, Karnataka State*

### 2.4. Methods of Image Classification

Image classification is the process of dividing the image into different regions with some similarly and labeling the regions using supplementary ground truth information. In the present study both supervised and unsupervised methods are used for image classification. All classification are done using ERDAS imagine 9.1 software at the Karnataka State Remote Sensing Application Center, Department of IT and BT, Government of Karnataka, M.S. Building, Dr. Ambedkar Veedhi, Bangalore - 01. Mahalanobis distance classifier is similar to Minimum Distance, except that the covariance matrix is used in the equation. This algorithm assumes that the histograms of the bands have normal distributions (Perumal and Bhaskaran, 2010). Var. and Covariance are figured in so that clusters that are highly varied lead to similarly varied classes and vice versa. The Minimum distance classifier is based on training site data. This classifier characterizes each class by its mean position on each band. Minimum distance classifier is highly recommended in all image classification applications (Richards, 1995). The classification is performed by placing a pixel in the class of the nearest mean. The

minimum distance algorithm is also more attractive since it is a faster technique than the maximum likelihood classification.

### 2.5. Maximum Likelihood Classification Algorithm

Maximum Likelihood Classifier (Gaussian): A statistical decision rule that examines the probability function of a pixel for each of the classes, and assigns the pixel to the class with the highest probability. In this algorithm each pixel is modeled to have multivariate normal distribution. Let $\mu_1, \mu_2, \ldots, \mu_m$ and $\Sigma_1, \Sigma_2, \ldots, \Sigma_m$ denote the population mean vectors and population variance – covariance matrices for m classes respectively. The observation vector $\mathbf{X}_r$ at pixel r when it belongs to class c a multivariate normal distribution with mean $\mu_c$ and covariance matrix $\Sigma_C$.

Then,

$$P_{rc} = \left[\frac{1}{2\pi}\right]^{p/2} |\Sigma|^{-1/2} \exp\left\{-\frac{1}{2}(X_r - \mu_c)\,\Sigma_c^{-1}(X_r - \mu_c)\right\}$$

Gives the likelihood of pixel r belonging to class c

Taking logarithm,

$$\ln P_{rc} = \frac{p}{2} ln\left[\frac{1}{2\pi}\right] - \frac{1}{2}\ln|\Sigma| - \frac{1}{2}(X_r - \mu_c)\,\Sigma_c^{-1}(X_r - \mu_c)$$

Ignoring $\frac{p}{2} ln\left[\frac{1}{2\pi}\right]$ which is a constant, the maximum likelihood algorithm assigns pixel r to class c if and only if

$\ln P_{rc} \geq P_{rq}$, for all q= 1, 2, ---, m classes, q≠c.

Since the class mean vectors $\mu_c$ and covariance matrix $\Sigma_C$ are unknown, the sample estimates are obtained from the training set.

Let $\bar{X}_1, \bar{X}_2, \ldots, \bar{X}_m$ be the sample mean vectors and $V_1, V_2 \ldots V_m$, be the sample variance – covariance matrices estimated from the training data for m classes respectively.

The pixel assignment is made based on the estimated value of $p_{rc}$

$$\widehat{p_{rc}} = [-0.5\ln[\det(V_c)] - [0.5(X_r - \bar{X}_c)^T (V_c)^{-1}(X_r - \bar{X}_c)$$

Where, $X_r$ is the observation vector for unclassified pixel r.

The pixel is assigned to that class for which it has the highest similarity if being a member. The decision rule is given as, assign pixel r to the class c if, and only if,

$\widehat{p_{rc}} \geq \widehat{p_{rq}}$ for all q= 1, 2, ---, m classes, q≠c.

The classification of the whole image is performed on a pixel by pixel basis. Every pixel is assigned to one of the mutuality exclusive classes based on the likelihood as described above and no pixel remains unclassified.

### 2.6. Classification Accuracy

The extent to which a manual or automatic processing system correctly identifies selected classes.

**Kappa Coefficient**

A statistical measure of the agreement, beyond chance, between two maps (e.g. output map of classification and ground-truth map). It is represented by the symbol kappa hat or k hat.

**Error Matrix**

An error matrix is a square array of numbers set out in rows and columns which express the number of sample units (pixels) assigned to a particular category relative to the actual category as verified by test data set.

## 3. Results and Discussion

In the classification phase, supervised classification technique was chosen to classify the images. The technique Maximum Likelihood was performed to the images. Accuracy assessment was approved out to compute the probability of error for the classified map. An overall randomly sample points were chosen for accuracy assessment. The measures of accuracy were tested in this study viz overall accuracy, confusion or error matrix and kappa coefficient. Several measures of classification accuracy may be derived from a confusion matrix. Kappa coefficient was generated to portray the amount of agreement between the classification effect and the validation sites after random agreements by possibility are detached from consideration these data.

***Table 1:*** *Producers and Users Accuracy*

| Classified Category | Producer's Accuracy (Percent) | User's Accuracy (Percent) |
|---|---|---|
| Jowar | 93.33 | 82.35 |
| Cotton | 88.00 | 91.66 |
| Chilly | 95.00 | 90.47 |
| Fallow Land | 90.00 | 93.10 |
| Paddy | 90.00 | 95.74 |
| Water body | 93.33 | 90.32 |

Kappa coefficient and overall accuracy results of the measures of accuracy are shown in the Table 1. The overall accuracy is expressed as a percentage of the test pixels successfully assigned to the correct classes. Maximum Likelihood produced the highest accuracy with overall accuracy achieved 91%. The user's accuracy and producer's accuracy for individual classes ranged between 88.00 to 95.00 percent and 82.35 to 95.74 percent for different categories using maximum likelihood algorithm. Producers and users accuracy obtained and presented in the Table 1 for all the classes under study.

### 3.1. Test of Significance of Kappa Coefficients for Koluru Hobli, Bellary Taluk

The kappa coefficient is found to be 0.8321 and the variance of kappa is found to be 0.000675. The Kappa coefficient for Maximum likelihood classification was highly significant, implying that classifier produced classification significantly different from a random assignment.

### 3.2. Area Estimates for Koluru, Hobli, Bellary Taluk (Hectares) using Maximum Likelihood Classification

The estimated area for all the classes under study using Maximum likelihood classification is presented in the Table 2, and which is found to be more nearer to the ground truth observation.

***Table 2:*** *The Estimated Area for all the Classes under Study Using Maximum Likelihood Classification*

| Sl. No. | Classification Categories | Max-Like Classification (ha) |
|---|---|---|
| 1 | Jowar | 2209.32 |
| 2 | Cotton | 6590.27 |
| 3 | Chilly | 2800.49 |
| 4 | Fallow land | 14744.87 |
| 5 | Paddy | 7245.33 |
| 6 | Water body | 65.32 |

The Maximum likelihood classification is achieved the estimation of categories which is found to be more significant on truth observation.

***Table 3:*** *f Measure Table*

| Sl. No. | Classification Categories | Recall | Precision | f-measure |
|---|---|---|---|---|
| 1 | Jowar | 0.93 | 0.95 | 0.94 |
| 2 | Cotton | 0.93 | 0.90 | 0.92 |
| 3 | Chilly | 0.94 | 0.94 | 0.94 |
| 4 | Fallow land | 0.92 | 0.93 | 0.93 |
| 5 | Paddy | 0.97 | 0.93 | 0.95 |
| 6 | Water body | 0.92 | 0.93 | 0.93 |
| | Total f-measure | **0.94** | **0.93** | **0.94** |

The measure of accuracy was tested in this study namely overall accuracy, confusion or error matrix and kappa coefficient. Many measures of classification accuracy may be derived from a confusion matrix. Kappa coefficient was generated to describe the proportion of agreement between the classification result and the validation.

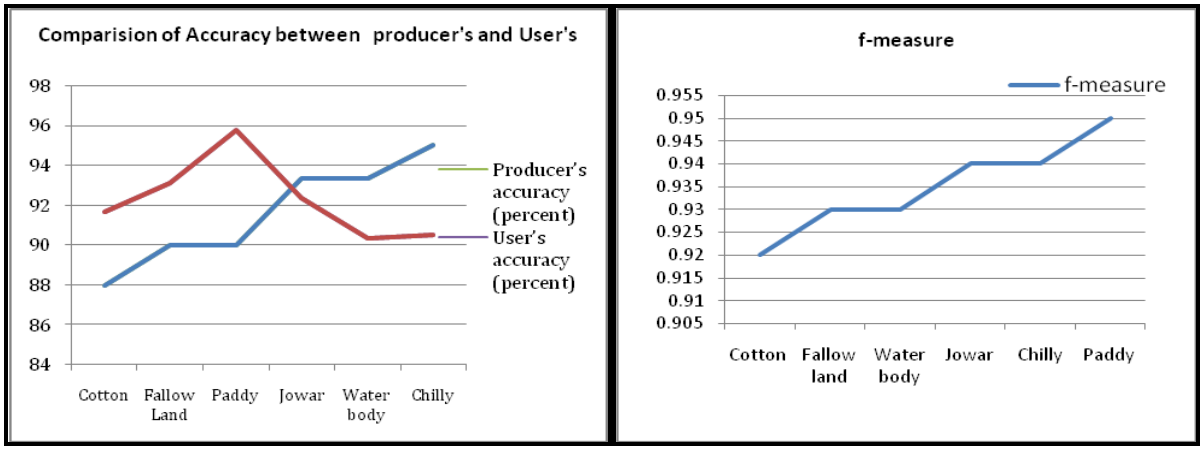


**(a)** **(b)**

***Figure 3:*** *(a) Comparision of Accuracy between producer's and user's (b) Accuracy using f-measure*

## 4. Conclusion

Machine learning technique approach on satellite imageries perform in statistical Maximum likelihood classification is significantly converging to actual classes. Kappa coefficient derives the significantly different from a random assignment. The study achieved more than 95% classification accuracy in agricultural crops. In future accurate estimation can be project with satellite imageries.

## References

Duda, T., and Cantry, M. *Unsupervised Classification of Satellite Imagery: Choosing Good Algorithms.* International Journal of Remote Sensing. 2002. 23 (11) 2193-2212.

Foody, G.M. *Status of Land Cover Classification Accuracy Assessment*. Remote Sensing and Environment. 2002. 80; 185-201.

Gordon, S. *Utilizing Landsat Imagery to Monitor Land Use Change: A Case Study in Ohio*. Remote Sensing of Environment. 1980. 9; 189-196.

Kun Wang, Youchuan Wan, and Shaohng Shen. *Classifications of Remote Sensing Images Using Fuzzy Multi-Classifiers.* IEEE International Conference on Intelligent Computing and Intelligent Systems 2009. (4) 411-414.

Lu, D., and Weng, Q. *A Survey of Image Classification Methods and Techniques for Improving Classification Performanc*e, International Journal of Remote Sensing. 2007. 28 (5) 823-870.

Perumal, K., and Bhaskaran, R. *Supervised Classification Performance of Multispectral Images.* Journal of Computing. 2010. 2 (2) 124-129.

Richards, J.A., 1995: Remote Sensing Digital Image Analysis an Introduction. Springer-Verlag. 265-290.

**Cloud Publications**
International Journal of Advanced Remote Sensing and GIS
2014, Volume 3, Issue 1, pp. 516-524, Article ID Tech-253
ISSN 2320 - 0243

Case Study | Open Access

# Site Suitability Analysis for Urban Development of a Hill Town Using GIS Based Multicriteria Evaluation Technique: A Case Study of Nahan Town, Himachal Pradesh, India

**Santosh Kumar and Ritesh Kumar**

Haryana Space Applications Centre, CCS HAU Campus, Hisar, Haryana, India

Correspondence should be addressed to Santosh Kumar, im2skumar@gmail.com; ritesh.kumar05@gmail.com

Publication Date: 24 April 2014

Article Link: http://technical.cloud-journals.com/index.php/IJARSG/article/view/Tech-253



**Abstract** The study illustrates the use of Geographic Information System (GIS) tools and numerical Multi-Criteria Evaluation (MCE) techniques for selection of suitable sites for urban development of a hill town. This study was conducted to identify suitable sites for urban development of a hill town, Nahan using GIS-based multi-criteria evaluation of slope, road proximity, land use, land values, soil and geomorphology factors. Merged spatial data (Cartosat-1 & LISS-IV) and six thematic information layers were analyzed using ArcGIS 9.3 software to identify suitable areas in Nahan town. It focuses on GIS based Overlay Weight age Average (OWA) Sum and Weighted Linear Combination (WLC). The undulating terrain, steep slope, varied soil depth and high building cost give the impression to find out suitable sites for urban development in the Nahan Town. In this study six factors (slope, road proximity, land use, land values, soil and geomorphology) were identified for criteria evaluation. Different thematic information layers were generated using visual interpretation of satellite data for each variable displaying site suitability measured on an ordinal scale. With the generated criteria, maps were standardized using the pair wise comparison matrix method. Weights for each criterion are generated by comparing with each other according to their importance. Criteria weights and maps were combined using OWA and WLC. Pair wise comparison matrix indicates weights for slope (=0.41), road proximity (=0.26), landuse (=0.15), land values (=0.09), soil (=0.06) and geomorphology (=0.03). Consistency Ratio, (CR =0.0117) <0.10 indicated a reasonable level of consistency in the pair wise comparisons. The final suitability map was obtained from both weighted sum overlay and Spatial Analyst Tools covering an area of 3.6 sq. km. After suitability analysis it was found that from the available area 0.1157 sq km falls under very low suitable, 1.6835 sq km under low suitable, 1.2090 sq. km under moderately suitable, 0.3663 sq. km under high suitable and 0.1248 sq. km under very high suitable. The result shows that highly suitable areas for urban development is either agricultural or forest type.

**Keywords** *Geographic Information System (GIS); Multi-criteria Evaluation (MCE); Overlay Weightage Average (OWA); Weighted Linear Combination (WLC); Analytic Hierarchy Process (AHP); Urban Development; Spatial Analysis*

## 1. Introduction

Identification of suitable sites for urban development in hilly areas is one of the critical issues for planning. To cater the needs of appropriate site in undulating areas, site suitability analysis has become inevitable. Site suitability is the method of understanding existing site qualities and factors that will determine the location for a particular activity. It involves the detailed investigation of the natural resources and processes that characterize a site and include mapping techniques including GIS tools that help in processing the geographical database that display the areas of the site, suitable for various planning objectives and alternatives. Terrain information is used as a major factor used to evaluate the suitability of a hill town for urban development. The topographic characteristics of an area are one of the most important determinants to ascertain the suitability of an area for developmental activities. Severe limitations to subdivision development occur on slopes over 20 percent. For industrial parks and commercial sites, slopes of not more than 5 percent are preferred. Also, hilly terrain increases the building costs, so steep slopes are unfavorable. The soil texture and drainage conditions also affect site suitability. Well-drained, coarse-textured soils present few limitations to development. Poorly drained or very poorly drained, fine-textured soils can present severe limitations. In general, depths to the water table of at least 2 m are preferred. Depths of 1 to 2 m may be satisfactory where public sewage disposal is provided and buildings are constructed without basements (Lillesand M. Thomas, Kiefer W. Ralph, and Chipman W. Jonathan). The number of input factors required in a particular study depends on purpose, location and circumstances surrounding the area under analysis. The various characteristics of a site (e.g. present land use, slope, road proximity, land values, soil, and geomorphology) each influence its suitability for a specific purpose. A scoring and weighting system can be applied to the various aspects of suitability to assess the overall suitability for a specific urban use. Certain characteristics may lead to non-availability of a site for a specific urban land use. A site suitability analysis adds importance to study by helping to identify suitable sites that meet specific criteria. The results of these analyses can greatly reduce the time and effort, which might otherwise be spent manually searching records, processing data or field surveying. Site location is a key factor and initial step in the design of many projects. Acquiring new site for urban development is increasingly more challenging particularly in an increasing real estate market and can be the result of growth of urban areas, and increased environmental standards or regulations. The results of the site suitability analysis produce a detailed display of the most-suitable to least-suitable areas for consideration of placement of a certain facility, while filtering out unusable or less desirable sites. Certain aspects are more important than others in determining the best location for each site, and might include an areas proximity to existing infrastructure, soil types, slope, land values, geomorphology and land use. These site suitability analyses require unlike measurements to be converted to common values that can be summed and compared to ease the final site selection process.

## 2. Study Area

Nahan town is situated on the Shiwalik ridge of Himalayan region in Himachal Pradesh of India functioning as districts headquarter of Sirmour District overlooking emerald fields. It is located at $30^0$33’0” N latitude and $77^0$17’59” E longitudes with an altitude of 932 meters. Its elevation provides good base for making visits to the nearby pilgrim centres including Renuka, Paonta Sahib, Trilokpur temple and the Suketi Fossil Park. The city was founded as a capital in 1621 by Raja Karan Prakash. Nahan is much acclaimed for its clean and spotless streets. A legend says about a saint who lived with Nahar on the site where the Nahan palace now stands. Nahar means a lion and perhaps the city got its name from this saint. The climate of Nahan is pleasant throughout the year. This area of Himachal comprises mainly of lower Shiwaliks of dense forests, lake and rivers. It has an old Municipal Committee, which is the second oldest municipal committee in the country and oldest in Northern India. Revival of Nahan foundry is the oldest foundry of Northern India. The town is watered by man-made lake and decorated with temples and gardens. The town has a bazaar with narrow cobbled streets, which provides all kinds of things. Three gently level walks; Villa Round, Military Round and

Hospital Round are evocative of the city's past. The hub of Nahan's activities is Chaugan, Bikram Bagh and Khadar Ka-Bagh. Gift shops, Rosin & Turpentine factory and local temples are among the other major attractions.

**Location of the Study Area in India**

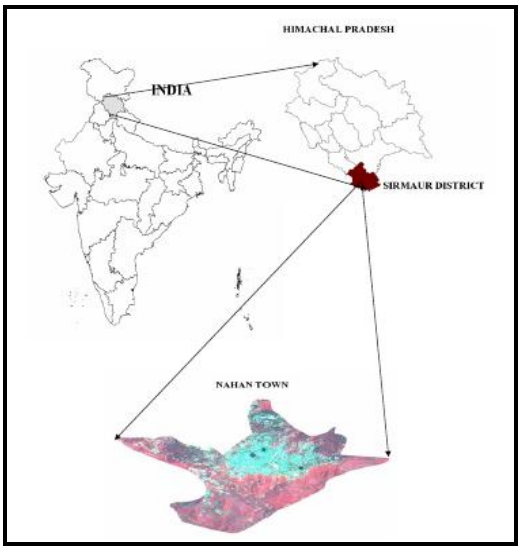


***Figure 1:*** *Location of the Study Area*

## 3. Materials and Methods

The present study attempts to introduce decision support system used for site suitability analysis. Geographic Information System (GIS) and numerical based methodology has been applied to select suitable sites for urban development. For this purpose, various thematic (information) layers such as slope, road proximity, land use/land cover (LU/LC) (Figure 3), land values, soil and geomorphology maps have been generated in ArcGIS 9.3. Internal weights were assigned to each layer with values ranging from 0 to 8 under attribute field weight. Each vector layers were rasterized by taking weight as a feature class. Water bodies, forest, residential, recreational, commercial and industrial were assigned zero weights. Higher weight was given to vacant/ open lands with slopes less than 15 percent and riparian buffer factors for roads are considered. Using these thematic layers as factors, criteria map was generated by applying Spatial Analytic Hierarchy Process (AHP). In this study different scenarios were produced by giving different preference values to decision factors. The optimization of simulated scenarios developed in this study is applied to choose the best suited alternative based on six conflicting criteria. According to evaluation, scenario was defined from least to the most suitable urban development site. Spatial Analytic Hierarchy Process (AHP) is a type of decision support system that combines GIS and AHP to identify and rank areas that are suitable for urban development, through utilization of knowledge-based user preferences. The method is illustrated through a case study for site suitability of a hill town for its urban development using GIS based multi-criteria evaluation technique. The results generated are reviewed in order to derive conclusions with respect to Urban Development Plan that how well they exactly fit into it.

## 4. Site Suitability

High resolution Quick bird Images (0.61m) available on Google Earth was used for image interpretation and field check and merged data (Cartosat-1+LISS-IV) was used for land use classification. Spatial database of various thematic information of the study area was generated by using GIS Software (Arc GIS 9.3). The features like road network, residential, commercial, public and

semi-public, agricultural and forest, recreational and green spaces etc. were derived from satellite images. Spatial Analyst tool available with ArcGIS was used for slope map generation from the DEM (10m) obtained from Cartosat-1(Stereo-pair) data. In this case study of Nahan Town, formation of main factors uses the Saaty's normal AHP technique. The assumption is that the weightings derived from hierarchical comparison in normal AHP would be influenced by the preferences given to a particular criterion factor. Therefore a sensitivity test was carried out on the criterion preferences. It was evaluated based on six preference factors thought to influence weightings. The preferences given to the factors are: (1) slope; (2) road proximity; (3) land use; (4) land values; (5) soil; and (6) geomorphology. Six separate hierarchical pair wise comparisons (Table 1) of main criterion factors were made for each preference to analyze the sensitivity of the weights obtained. The pair wise comparisons of criteria factors were carried out independently and given same judgments for all the preferences. To reflect the preferences towards a certain factor, a definite to very strong preferences was given to that factor in their pair wise comparison (Table 2). The next stage in the analysis is that the consistency must be checked to verify the reliability of the judgment of the decision maker. In this study the CR= 0.0117, and depend on Saaty, if CR ≤ 0.10 the ratio indicates a reasonable level of consistency in the pair wise comparisons (Malczewski, 1999).

This study performs a GIS Spatial analysis in which models are represented as a set of spatial processes, such as buffer, classification, and reclassification and overlay techniques. Each of the input themes is assigned a weight influence based on its importance, then the result is successively multiplied with their factors. This process is often used in site suitability studies where several factors affect the suitability of a site (ESRI, 2000). The result is summed up producing a site suitability map as shown by the formula;

$$\textbf{Site Suitability} = \sum \textbf{[factor map (Cn) x weight (Wn)]}$$

Where, Cn=standardized raster cell,
Wn=weight derived from AHP pair wise comparisons

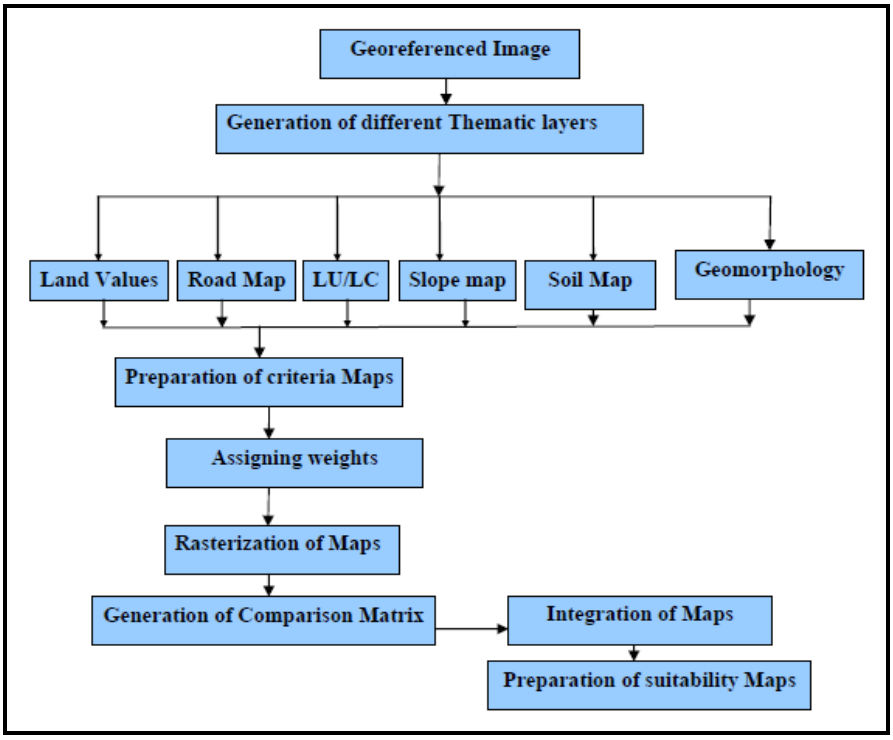


***Figure 2:*** *Flow Chart for Site Suitability Analysis*

### 4.1. Pairwise Comparison Matrix

***Table 1:*** *Showing Pairwise Comparison Matrix*

| | Slope | Road Proximity | Land use | Land values | Soil | Geomorphology | Weight | Lambda Consistency Vector |
|---|---|---|---|---|---|---|---|---|
| **Slope** | 1.00 | 2.00 | 3.00 | 5.00 | 7.00 | 9.00 | 0.41 | 6.15 |
| **Road Proximity** | 0.50 | 1.00 | 2.00 | 3.00 | 5.00 | 7.00 | 0.26 | 5.96 |
| **Land use** | 0.33 | 0.50 | 1.00 | 2.00 | 3.00 | 5.00 | 0.19 | 6.20 |
| **Land values** | 0.20 | 0.33 | 0.50 | 1.00 | 2.00 | 3.00 | 0.09 | 6.03 |
| **Soil** | 0.14 | 0.20 | 0.33 | 0.50 | 1.00 | 2.00 | 0.06 | 5.40 |
| **Geomorphology** | 0.11 | 0.14 | 0.20 | 0.33 | 0.33 | 1.00 | 0.03 | 6.70 |
| **Sum** | 2.29 | 4.17 | 7.03 | 11.83 | 18.50 | 27.00 | 1.00 | 36.44 |

### 4.2. Normalized Pairwise Comparison Matrix

***Table 2:*** *Showing Normalized Matrix for Pairwise Comparison*

| | Slope | Road Proximity | Land Use | Land Values | Soil | Geomorphology | Weight | Priority Vector |
|---|---|---|---|---|---|---|---|---|
| **Slope** | 0.44 | 0.48 | 0.43 | 0.42 | 0.38 | 0.33 | 0.41 | 0.17 |
| **Road Proximity** | 0.22 | 0.24 | 0.28 | 0.25 | 0.27 | 0.26 | 0.26 | 0.16 |
| **Land use** | 0.14 | 0.12 | 0.14 | 0.17 | 0.16 | 0.19 | 0.19 | 0.17 |
| **Land values** | 0.09 | 0.08 | 0.07 | 0.08 | 0.11 | 0.09 | 0.09 | 0.17 |
| **Soil** | 0.06 | 0.05 | 0.05 | 0.04 | 0.05 | 0.07 | 0.06 | 0.15 |
| **Geomorphology** | 0.05 | 0.03 | 0.03 | 0.03 | 0.03 | 0.04 | 0.03 | 0.18 |
| **Sum** | 1.00 | 1.00 | 1.00 | 1.00 | 1.00 | 1.00 | 1.00 | 1.00 |

#### 4.2.1. Calculation

**Suitability = ([Classified Slope] x 0.41) + ([Roadsuit1] x 0.26) + ([Lulcratsuit] x 0.19) + ([Landvaluesli1] x 0.09) + ([Soilrassuit] x 0.06) + ([Geomorrastersuit] x 0.03)**

Slope=(1)(0.41+(2)(0.26+(3)(0.15)+(5)(0.06)+(9)(0.03)=6.15

Land values=(0.50)(0.41)+(1)(0.26)+(2)(0.15)+(3)(0.09)+(5)(0.06)+(7)(0.03)=5.96

Road Proximity=(0.33)(0.41)+(0.50)(0.26)+(1)(0.15)+(2)(0.09)+(3)(0.06)+(5)(0.03)=6.20

Soil=(0.20)(0.41)+(0.33)(0.26)+(0.50)(0.15)+(1)(0.09)+(2)(0.06)+(3)(0.03)=6.03

Geomorphology=(0.14)(0.41)+(0.20)(0.26)+(0.33)(0.15)+(0.50)(0.09)+(1)(0.06)+(2)(0.03)=5.4

**Calculation of lambda (λ)**

λ = (6.15+5.96+6.20+6.03+5.40+6.70)/6=36.44/6=6.073

Consistency Index, CI = (λ-n)/(n-1)=(6.073-6)/(6-1)=0.073/5=0.0146

Consistency Ratio (CR)=CI/RI=0.0146/1.24=0.0117, (RI-1.24 for n=6), (Source: Adopted from Saaty, 1980)

## 5. Results and Discussion

The study area is located in a hilly terrain and covers an area of 3.6 sq. km (approximately). After suitability analysis it was found that from the available area (Figure 7) 0.1157 sq. km falls under very low suitable, 1.6835 sq. km under low suitable, 1.2090 sq. km under moderately suitable, 0.3663 sq. km under high suitable and 0.1248 sq. km under very high suitable. Percentage distribution of site suitability area (Figure 8) shows that 3% of the total study area very low suitable, 48% low suitable, 35% moderately suitable, 10% high suitable and 4% of the total area are very high suitable. Very high suitable means slope is in between (0-15%), Soil is moderately deep (50-100 cm), land use is either a wasteland or open forest or land with scrub or land without scrub, distance to proximity is 100 m, land values distance is 200 m and geomorphology is low dissected structural hill. The result shows that highly suitable areas for urban development is either agricultural or forest type and the low suitable areas is mostly residential. Site suitability map (Figure 6) is fits into the development plan for 2021 (Figure 4). So, after comparing it can be concluded that site suitability map (Figure 6) obtained is exactly in accordance with the development plan prepared for the town.

### 5.1. Identification of Suitable Sites for Urban Development

Effective criteria (factor) used in the identification of suitable sites with their individual importance are:

- Slope (Figure 5): is an important criterion for hilly terrain for finding suitable sites for built-up. Steep slopes are disadvantageous for construction purpose because the slope increases the construction cost.

- Road Proximity (Figure 5): Easy access to road helps in movement and transportation at any place. However, the construction of new road is expensive especially in hilly regions. So effort is made to locate the site nearer to any existing road if possible. Moreover in order to find out better accessibility to the existing road, buffer zones have been created by taking 100 meter distance from the road.

- Land use/cover: Land use/cover map of Nahan town has been categorized as agricultural, commercial, residential and industrial because once a building is constructed, it remains there for minimum 50 to 75 years. River bed is also not suitable for built-up area development. Thus barren land/agricultural land is considered to be the highest suitable for development purpose (Figure 3).

- Land values (Figure 5): Land value means the price of a land at a given point of time based on its location. Land value varies from location to location. Land values are high in the centre of a city whereas low in its periphery. Within a locality, accessibility has an impact on the land value as such values are high for the land nearer to road.

- Soil (Figure 5): Soil type essentially gives a broad idea on the basic soil properties of a location. By knowing a soil type, broad inferences could be drawn on its suitability for its construction. Forest and Hills soils type occur in forest and hill areas. These types of soils are also called as skeleton soils. Soil depth is useful for understanding the depth to foothold and efforts required for making a good foundation during construction. If the depth of soil is very shallow, it requires special type of treatment while making the foundation.

- Geomorphology (Figure 5): The denudational landforms like hills are identified based on stage of denudation, wherein, all the structure gets obliterated. These denudational landforms also can be classified based on dissection. Low dissected structural hills are given higher priority as compared to high dissected structural hills for construction.

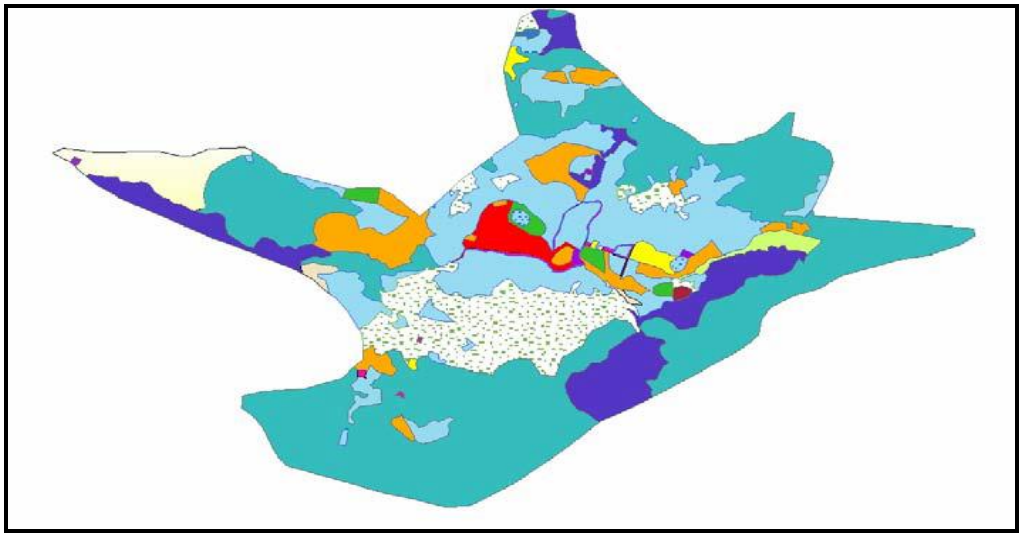

***Figure 3:*** *Land Use and Land Cover of Nahan*

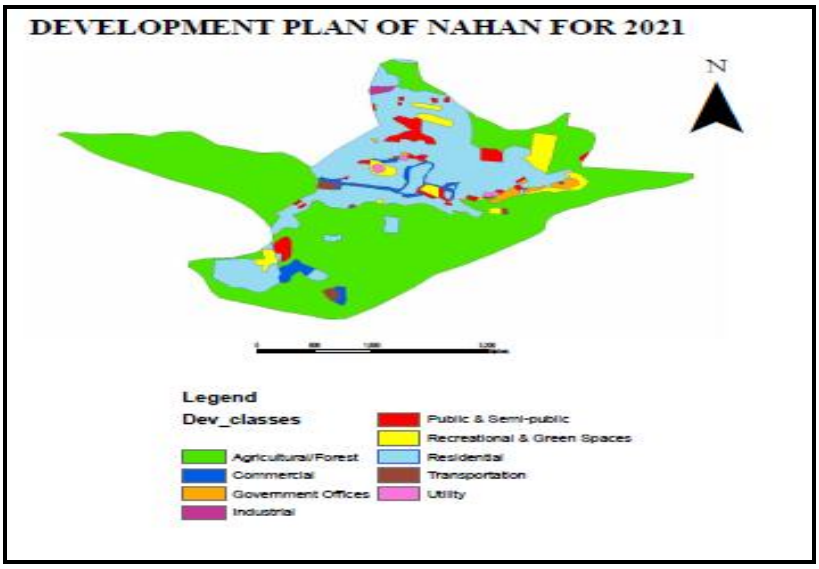


***Figure 4:*** *Development Plan of Nahan for Year 2021*

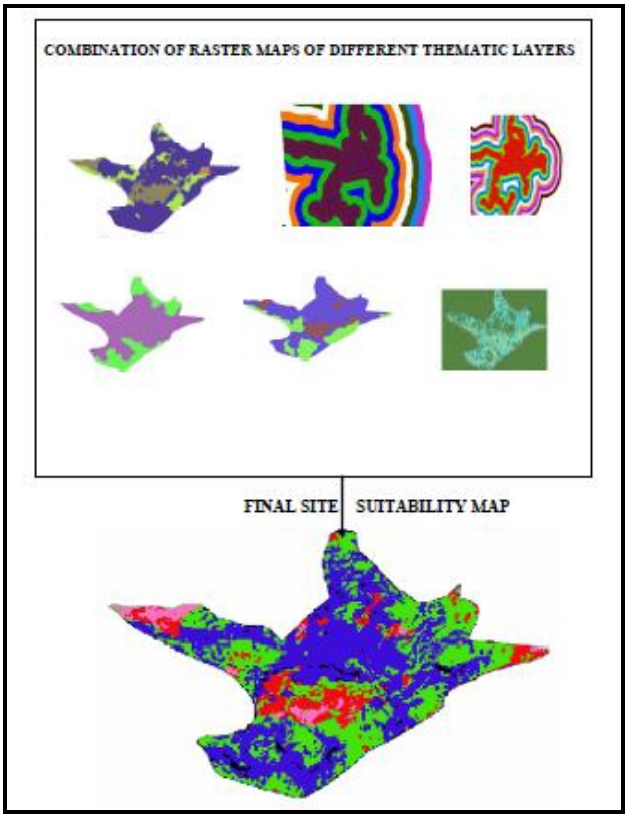


***Figure 5:*** *Combined Raster Thematic Layers*

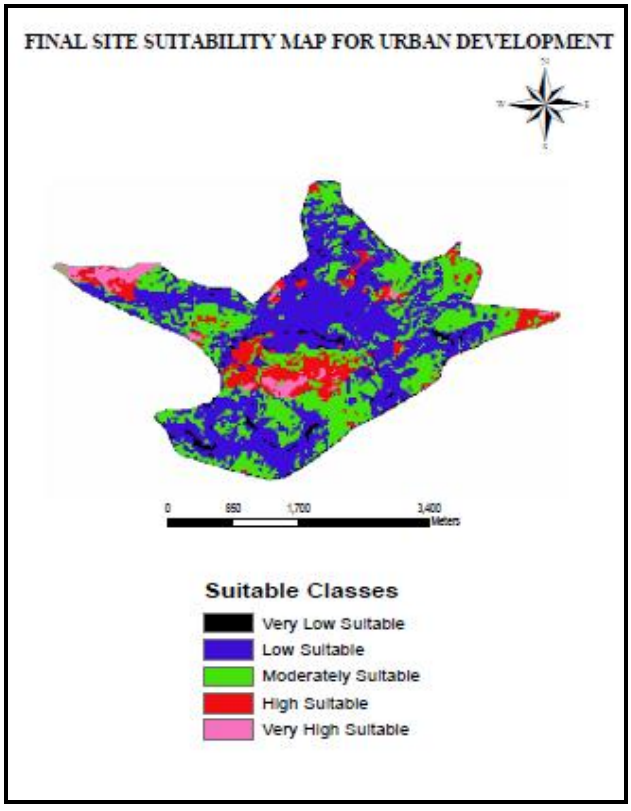


***Figure 6:*** *Proposed Site Suitability for Development of Nahan*

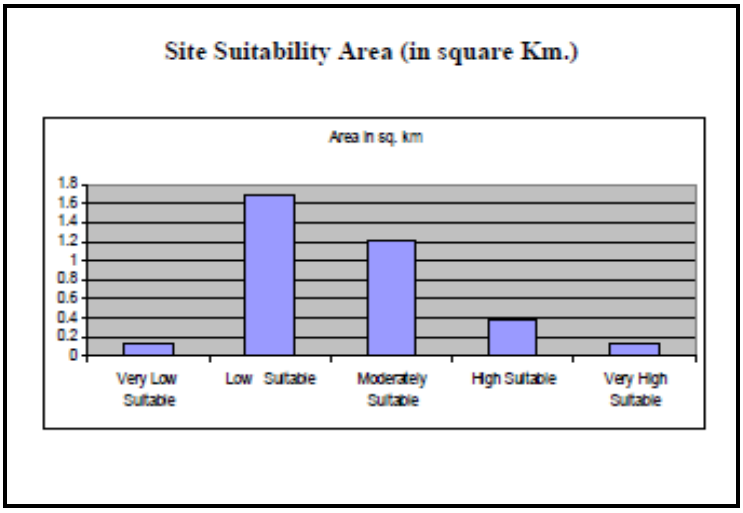


***Figure 7:*** *Area in sq.km for different Suitability Level*

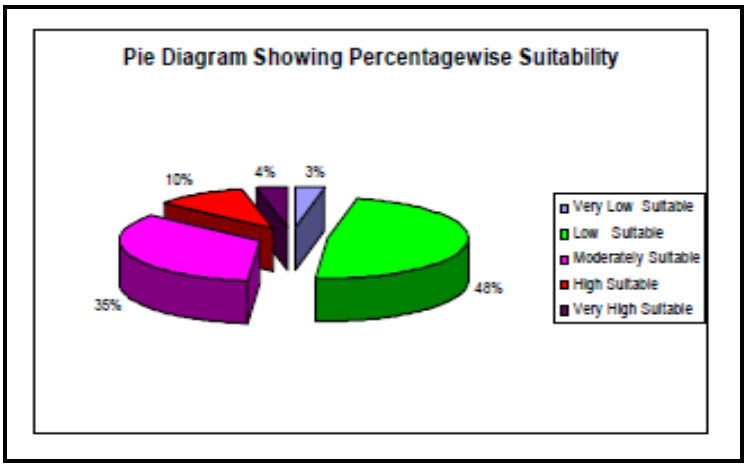


***Figure 8:*** *Area in % Age for Different Suitability Level*

## 6. Conclusion

The GIS based multicriteria evaluation technique is very simple and flexible which can be used to analyze various suitability of a hill town Nahan. It provides a comprehensive and satisfactory database for availability of suitable sites for urban development which in turn will help in solving any specific problem. This case study can encourage general public to use this method in their real time life and assist various planners and authorities to formulate and implement suitable master plan for development of an urban region.

## References

Lillesand Thomas, M., and Kiefer Ralphh, 1993: Remote Sensing Image Interpretation. John Wily and Sons Publication, New York.

Malczewski, G., 1999: GIS and Multicriteria Decision Analysis. John Wily and Sons, Inc., New York.

**Cloud Publications**
International Journal of Advanced Remote Sensing and GIS
2014, Volume 3, Issue 1, pp. 553-568, Article ID Tech-255
ISSN 2320 - 0243

Cloud Publications

**Research Article** **Open Access**

# Assessing the Dynamic of Structural Changes in Cerrado Vegetation of Protected and Non-Protected Areas using NDVI

**Joao Arthur Pompeu Pavanelli and Elza Guimaraes**

Department of Botany, IBB, UNESP, Univ Estadual Paulista, Botucatu, Sao Paulo, Brazil

Correspondence should be addressed to Joao Arthur Pompeu Pavanelli, jpbio@ymail.com

Publication Date: 23 May 2014

Article Link: http://technical.cloud-journals.com/index.php/IJARSG/article/view/Tech-255



**Guest Editor-in-Chief: Dr. Qingmin Meng**
***(This article belongs to the Special Issue "Geospatial Information Sciences: Landscape and Ecosystem Applications")***

**Abstract** The structure of Brazilian savannah, named locally as "*cerrado*", tends to change if the human pressures, such as pasture and intensive fire, are suppressed showing a densification of the physiognomies throughout the time. Vegetation Index acquired from remotely sensed data has been a proper way to study and monitoring large areas, and the Normalized Difference Vegetation Index (NDVI) is one of the most used for this purpose. The aim of this study was to assess the dynamic of structural changes in protected and non-protected areas of *cerrado* vegetation using NDVI. For this purpose, three *cerrado* fragments in the state of São Paulo, Brazil, were evaluated for a 26 year time span from 1985 and 2011, being two of them protected against anthropogenic interference. Landsat 5 –Thematic Mapper images were used and processed in ArcGIS. In the protected areas NDVI indicated that the vegetation followed the expected trend of changes for *cerrado*, with more open physiognomies tending to be denser throughout this period of 26 years, whereas in the non-protected fragment the NDVI evidences human pressure, showing lower phytomass in 2011. NDVI showed to be efficient in detecting and monitoring changes in *cerrado* vegetation structure, and can be useful to study both, the natural dynamics of *cerrado* vegetation and the anthropogenic interference in protected areas.
**Keywords** *Brazilian Savannah; Phytomass; Remote Sensing*

## 1. Introduction

The *Cerrado* (Brazilian savannah) phytogeographic domain occupies more than 20% of Brazilian territory [1], but the intense human pressure during twentieth century led to drastic vegetation suppression, remaining only 34% of original vegetation [2]. Its biodiversity is high expressive, and adding to the fast destruction that it has been submitted, *Cerrado* has been considered a hotspot for global conservation priorities [3].

In São Paulo State, it is estimated that *cerrado* occupied 14% of its territory in the beginning of twentieth century and nowadays the remaining areas occupy minus than 1% of the total state area, and less than half of them are protected in Conservation Units [4]. Furthermore, most of the Guarani Aquifers recharge areas occur under *Cerrado* domain, increasing the importance and necessity of its preservation, recovery and conservation [5].

*Cerrado* presents a complex of physiognomies ranging from grass open vegetation to forest physiognomies [6]. The gradient of density, height and cover of woody species results in different physiognomies presenting an increasing of woody [7] and phytomass content, in this sequence: *campo limpo:* grasslands with no woody component*; campo sujo:* continuous grass vegetation, interspersed by few scrubs and small trees; *campo cerrado:* mid-sized trees, slightly denser than *campo sujo,* but don´t form canopy, because of the distance among the individuals; *cerrado strictu sensu:* a continuous grass layer overlaid by a discontinuous tree and shrub layer; *cerradã*o: an almost closed canopy, forming woodlands [1, 4, 8].

Several studies in Brazil show the structural dynamic of the *cerrado* physiognomies along time, in which denser physiognomies, such as *cerradão* and *cerrado strictu sensu* replace less dense ones [8 9, 10, 11, 12]. These studies associate this structural changes to suppression of human impacts, mainly pasture and fire, assuming that the previous condition would be an ecosystem in which features would remain stable if kept anthropogenic interference, but tending to evolve to a denser physiognomy if protected [9].

In general, density and phytomass of the vegetation are related to the amount of leafs and to the amount and geometry of stems and branches [7]. In the case of *cerrado* vegetation, the amount of leaves is related to the structural gradient of the physiognomies and a rapid and non-destructive way to study and monitoring large-scales phytomass is the use of optical remote sensing [7, 13].

Among several techniques for interpreting qualitatively vegetation cover with optical remotely sensed acquired data, there are the Vegetation Indexes, which are numerical models, having a direct and satisfactory relationship with green leaf biomass [14, 15, 16]. One of the most used Vegetation Indexes is the Normalized Difference Vegetation Index (NDVI). The *cerrado* physiognomies show increasingly cylindrical volume from less dense to more dense vegetation [7], and the NDVI has a direct relationship with the cylindrical volume [14]. A strong relationship between NDVI and biomass has been demonstrated for *cerrado* vegetation [17].

The aim of this study was to assess the dynamic of structural changes of the *cerrado* physiognomies using NDVI, in three *cerrado* fragments of São Paulo state.

## 2. Materials and Methods

### 2.1. Study Areas

Three *cerrado* fragments were studied, placed in São Paulo state in the municipalities of Itirapina, Pratânia and Botucatu (Figure 1). These fragments were chosen due to enable the assessment of changes in vegetation cover in different *cerrado* physiognomies found in the State, under same climatic condition. According to Köppen climate classification, the climate on the region is Cwa, mesothermal with dry winter and the average temperature in the coldest month is below 18°C and the average temperature in the warmest month is above 22°C [18].

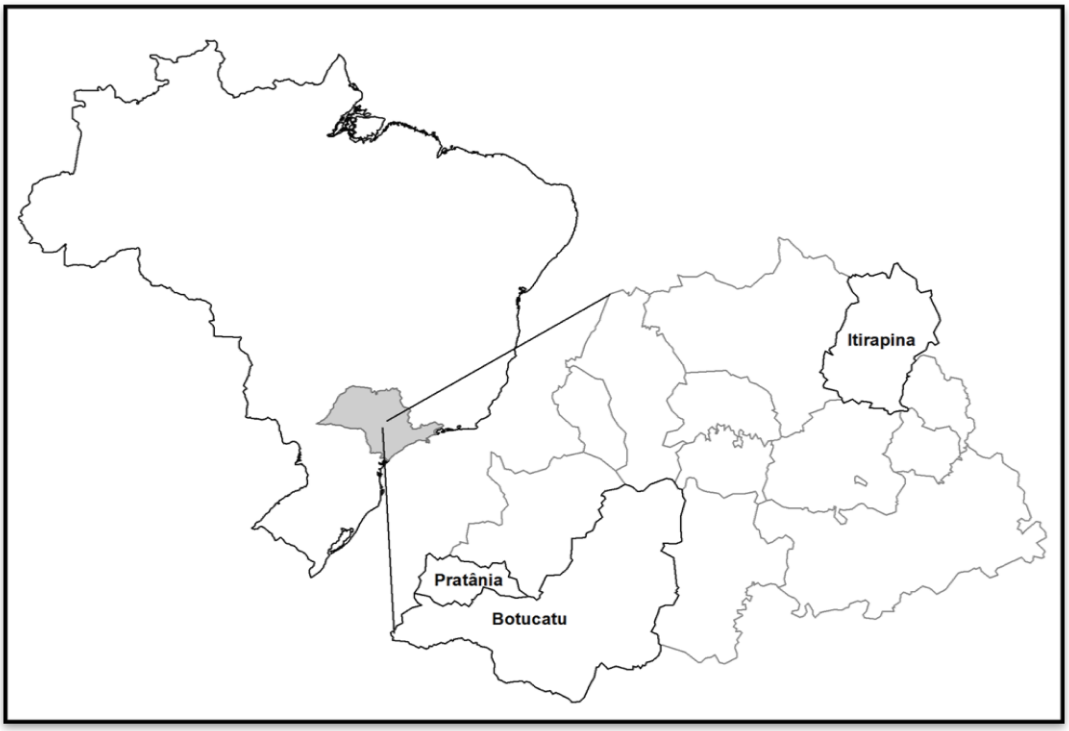


***Figure 1:*** *Location Map of the Municipalities in which the Cerrado Fragments are placed in the State of São Paulo (Gray Colour)*

The *cerrado* fragment placed in Itirapina is part of an integral Conservation Unit, called "*Estação Ecológica de Itirapina* (ESECI), shown in Figure 2. Its total area is 2300 hectares. C*ampo sujo* vegetation predominates with some disrupted patches of *campo cerrado*. The soil is classified as quartzarenic neosol [19].

***Figure 2:*** *Fragment of Cerrado Vegetation at Estação Ecológica de Itirapina (ESECI), Itirapina Municipality, São Paulo State, Brazil*

In Botucatu, the fragment placed in the neighbourhood *Rio Bonito* (Figure 3) is formed by *cerrado sensu strictu* and *cerradão,* and has 31, 5 hectares. The soil is classified as red-yellow latosol [20]. It is

an area on the edge of a highway, surrounded by crops and therefore susceptible to distinct kinds of human impacts.

***Figure 3:*** *Fragment of Cerrado Vegetation at Botucatu Municipality, São Paulo State, Brazil*

The *Cerrado* Reserve *Palmeira da Serra* (CRPS) (Figure 4) is a private reserve in the municipality of Pratânia, with 180 hectares and has areas of *cerrado sensu strictu* and *cerrradão*. Land use around this fragment is characterized by sugar cane and *Eucalyptus* crops. There are two types of soil, red-yellow latosol and red latosol [20].

***Figure 4:*** *Fragment of Cerrado Vegetation at Cerrado Reserve "Palmeira da Serra" (CRPS), Pratânia Municipality, São Paulo state, Brazil (Photo: André Santachiara Fossaluza)*

Polygons were drawn delimiting the perimeter of the fragments based on 2011 Landsat images, and was used the ArcGIS tool "Extract by mask" for processing. From the total area of ESECI we used just 372 hectares for this analysis that characterized the local vegetation.

### 2.2. Satellite Images

Landsat-5 Thematic Mapper images from 1985, March 19th and 2011, March 27th were used. This pre-drought period corresponds to the best season to separate *cerrado* physiognomies. From the spectral point of view, this period has a better contrast between open and dense physiognomies [14]. The study areas are located on the scenes orbit/point 220/75 and 220/76.

### 2.3. Image Processing

The images were registered using a Landsat-7 Enhanced Thematic Mapper orthorectified image, with the software TerraPixel. Other processing steps were made in ArcGIS, 9.3.

The vegetation index is sensitive to atmospheric interference and its necessary to correct this effect [21]. In this study was used the method developed by Chavez [22]. In this method, the atmospheric correction is achieved from the atmospheric interference estimate in each spectral band, and then the digital numbers are converted into radiance values (Equation 1) and following into reflectance (Equation 2).

Radiance values are obtained by the following equation (Equation 1):

$$L\lambda = \left(\frac{Lmax\lambda - Lmin\lambda}{\text{Qcalmax} - \text{Qcalmin}}\right) Qcal - Qcalmin + Lmin\lambda \quad (1)$$

Where, $L\lambda$ is the spectral radiance at the sensor´s aperture (W/m² sr μm); $Lmax\lambda$ is the spectral at-sensor radiance that is scaled to Qcalmax (W/m² sr μm); $Lmin\lambda$ is the spectral at-sensor radiance that is scaled to Qcalmin (W/m² sr μm); Qcalmin is the minimum quantized calibrated pixel value corresponding to $Lmin\lambda$ (Digital Number); Qcalmax is the maximum quantized calibrated pixel value corresponding to $Lmax\lambda$ (Digital Number); Qcal is the quantized calibrated pixel value (Digital Number) [23].

Reflectance in each band is obtained by the following equation (Equation 2):

$$\rho\lambda = \frac{\pi . L\lambda . d^2}{Esun\lambda . Cos\theta} \quad (2)$$

Where, $\rho\lambda$ is the planetary Top-Of-Atmosphere (TOA) reflectance (unitless); π is the mathematical constant equal to ~3,14159 (unitless); $L\lambda$ is the spectral radiance at sensor´s aperture (W/m² sr μm); $d^2$ is the square of Earth-Sun distance (astronomical units); $Esun\lambda$ is the mean exoatmospheric irradiance (W/m² μm); $Cos\theta$ is the solar zenith angle (degrees) [23].

All values to calculate radiance and reflectance were obtained from (Chander e*t al.,* 2009) [23].

### 2.4. NDVI

Green leafs absorb solar radiation in the red spectral region (0, 6 micrometers) and use this radiation as a source of energy in the process of photosynthesis, whereas in the near-infrared spectral region (0, 8 micrometers) the energy is not enough to synthesize organic molecules, moreover the absorption in this wavelength would result in the overheating of the plant and possible damages to the tissues, so the plants reflects the energy in the near-infrared region.

The Normalized Difference Vegetation Index is obtained by calculating the ratio between the difference in reflectance in the red spectral region (TM5 Band 3) and near-infrared (TM5 Band 4), divided by the sum of these wavelengths, according to the equation:

$$NDVI = \left(\frac{NIR - Red}{NIR + Red}\right) \quad (3)$$

Where, NIR is the near-infrared spectral region that corresponds to the TM5 sensor band 4 and Red is the red spectral region that corresponds to the TM5 sensor band 3.

NDVI values vary from -1 to +1, and higher values are related to more dense vegetation (e.g. forest) and lower values are related to less dense vegetation, (e.g. grass fields). Exposed soil values may vary from 0, 2 to negative values, meanwhile water has negative values.

## 3. Results and Discussion

Comparison of the NDVI images and the histograms (Figures 5-6) shows that, over the twenty-six years range, the vegetation in CRPS (Figure 7-9) and in ESECI (Figures 8-10) followed the expected trend of changes in *cerrado* vegetation, observed in protected areas, with more open physiognomies tending to more dense vegetation with higher biomass.

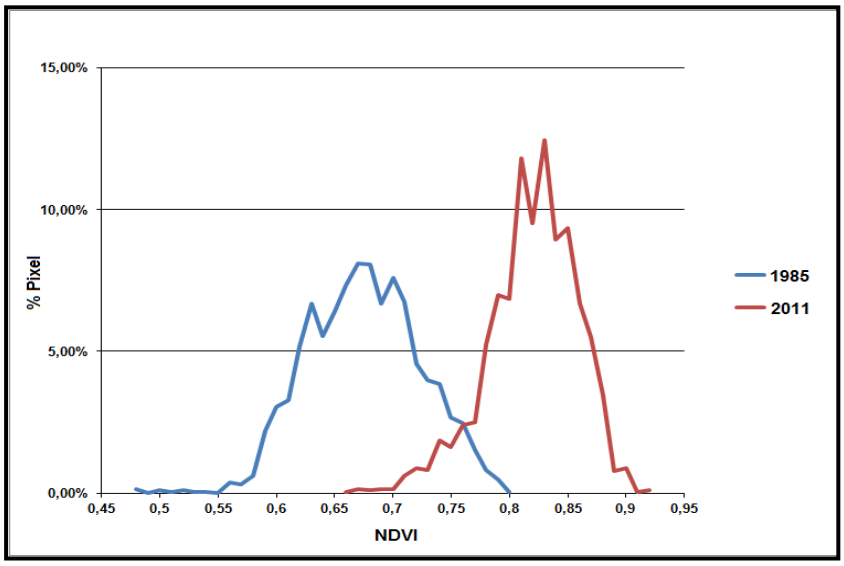


***Figure 5:*** *NDVI Values Histograms for the Fragment of Cerrado Vegetation at Cerrado Reserve "Palmeira da Serra" (CRPS) in 1985 (Blue) and 2011 (Red)*

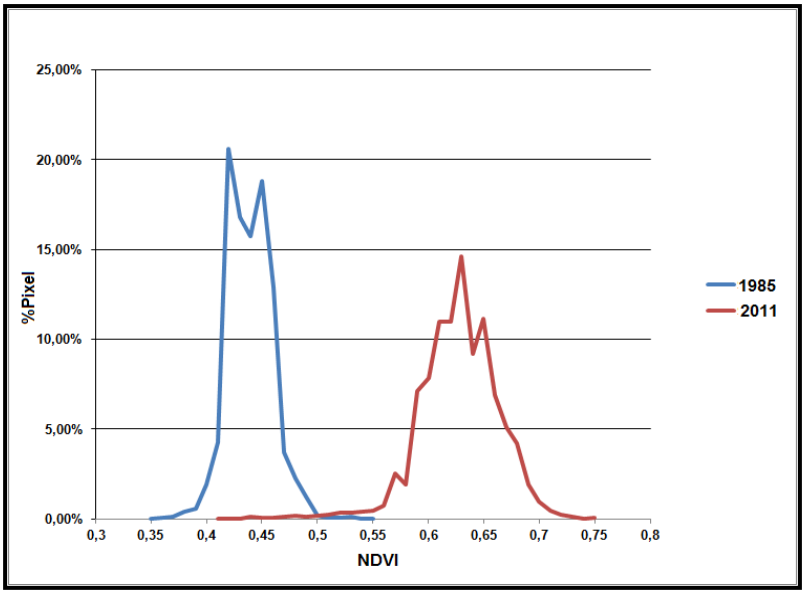


***Figure 6:*** *NDVI Values Histograms for the Fragment of Cerrado Vegetation at "Estação Ecológica de Itirapina" (ESECI) in 1985 (Blue) and 2011 (Red)*

Figure 7 presents the NDVI map of the fragment of cerrado vegetation at Cerrado Reserve "Palmeira da Serra" in 1985. It is possible to find out the heterogeneity of vegetation cover with NDVI varying from the lowest to the highest values possible for vegetation cover. These lower NDVI values verified inside the fragment are associated to less dense physiognomies. In Figure 8, the map of the same fragment shows a more homogeneous vegetation cover with higher NDVI values than in 1985. It means that the denser physiognomies area increasing in area in the fragment, although we can observe some patches of lower NDVI values, indicating areas still covered by opener vegetation. Similar results in interface areas between forest and savannah were found in other studies about vegetation cover dynamics using remote sensing data [8].

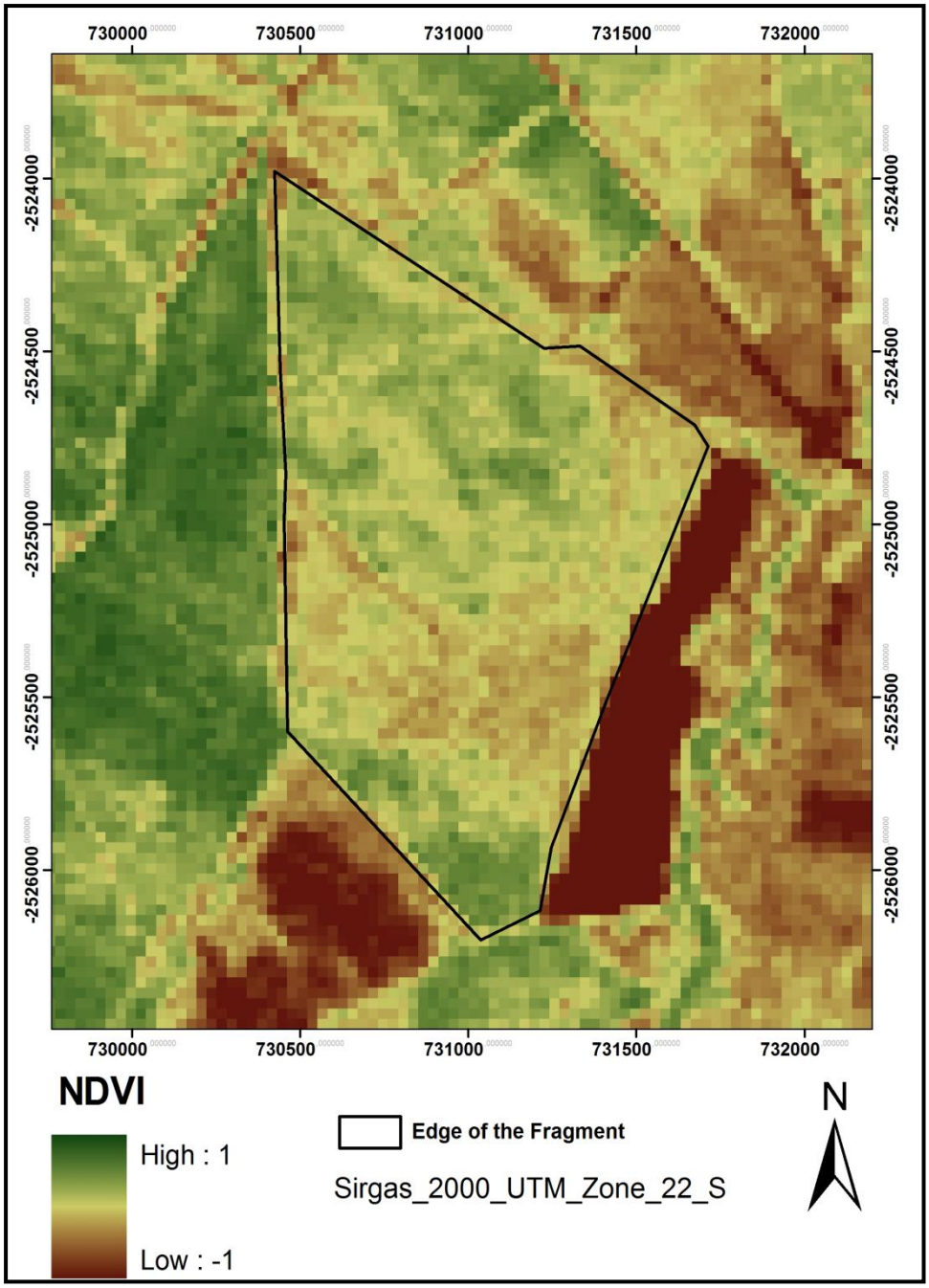


***Figure 7:*** *Fragment of Cerrado Vegetation at Cerrado Reserve "Palmeira da Serra" (CRPS) NDVI image from 1985*

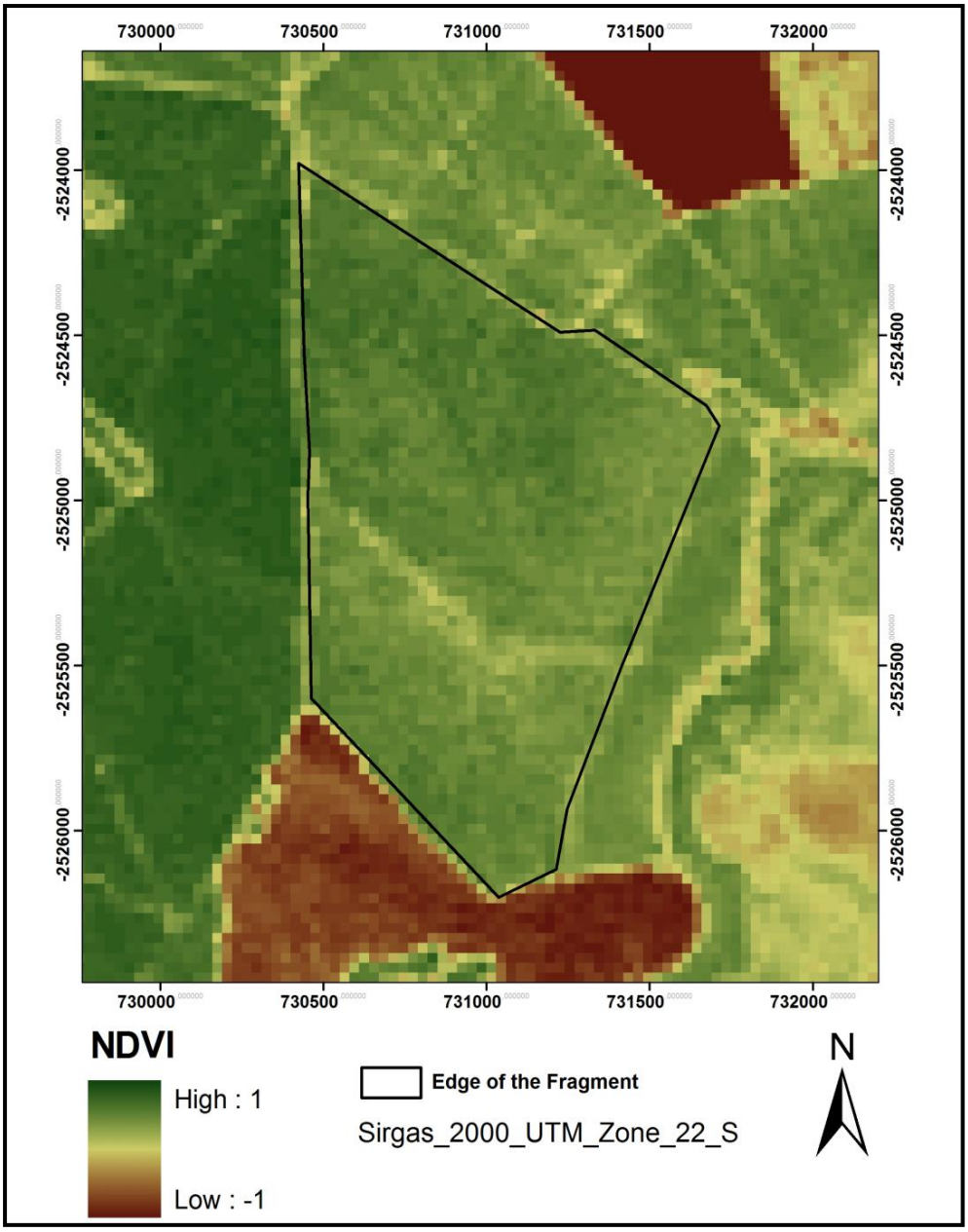


***Figure 8:*** *Fragment of Cerrado Vegetation at Cerrado Reserve "Palmeira da Serra" (CRPS) NDVI Image from 2011*

In this fragment of cerrado there were indicated two main physiognomies [24]. However it is not possible to distinguish accurately these physiognomies using NDVI image.

The *cerrado* fragment at *Estação Ecológica de Itirapina* is nowadays characterized by *campo sujo* interspersed by *campo cerrado* physiognomy, which is less dense than the physiognomies found at CRPS. The NDVI map of 1985 for this fragment (Figure 9) shows very low homogeneous NDVI values with some small patches of slightly denser vegetation, indicating the predominance of grass vegetation with some shrub layer that changed in the period of twenty six years. It evolved to the vegetation cover described above and illustrated in Figure 10. Other studies have found the same trend of structural changes in grass physiognomies in USA, Israel and Australian savannah [25, 26, 27]; all of them in protected areas against pasture and fire. This tendency, found in both protected fragments in our study, could be specially related to the warm temperate climate that presents moderate temperature and moisture [28] favouring forest vegetation. So, when one area in this region is protected from

pasture and fire, we expect an expansion and development of shrub and tree layer towards a denser and forest physiognomies [8]. The increase of the frequency of fire in woody vegetation results in the establishment of opener physiognomies because of high woody mortality rates, which favours grass vegetation development [29, 30]. The pasture impact is more associated to the trampling damage over seedlings by the cattle, hindering growth of shrub and arboreal specimens.

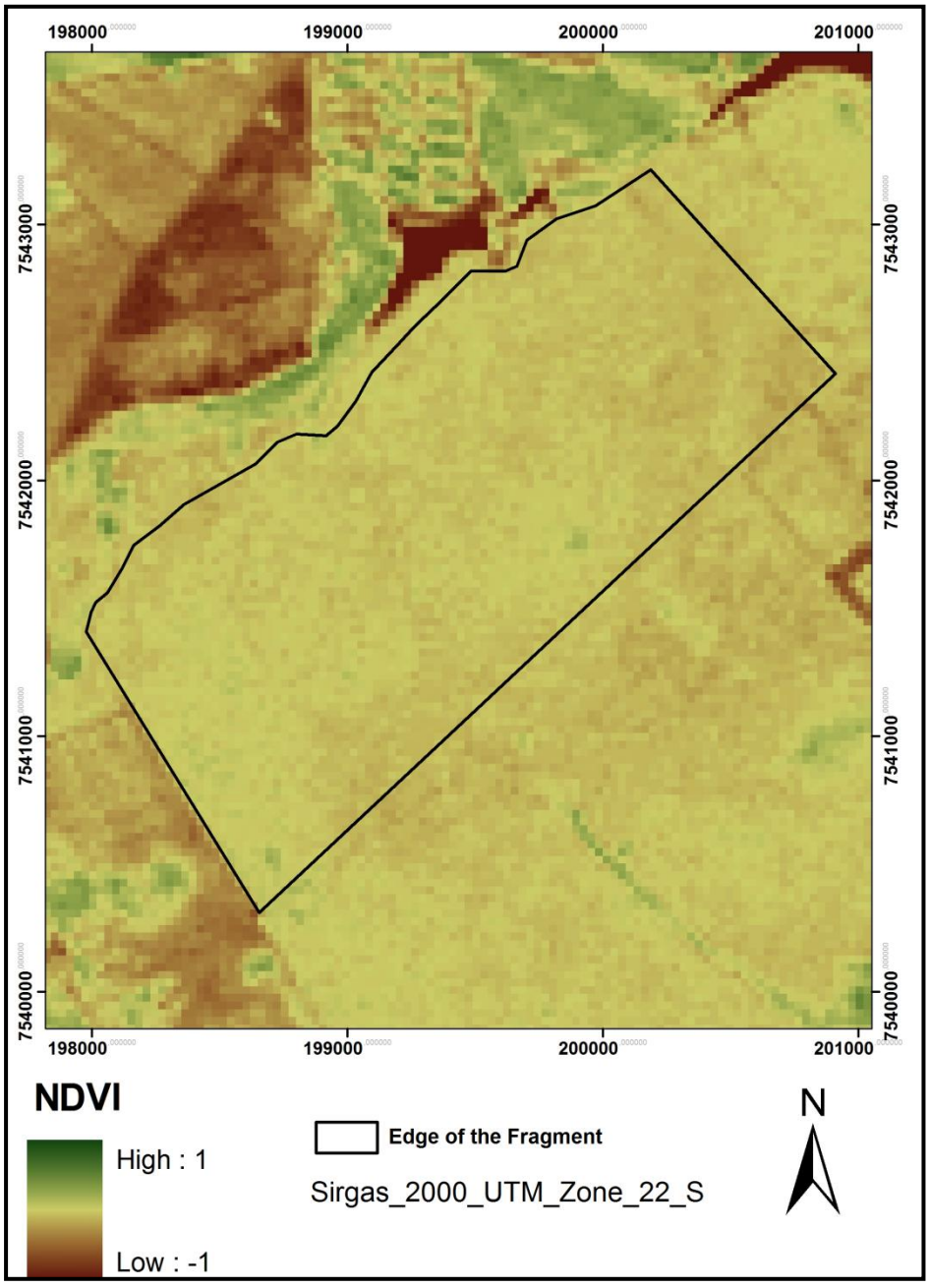


***Figure 9:*** *Fragment of Cerrado Vegetation at "Estação Ecológica de Itirapina" (ESECI) NDVI image from 1985*

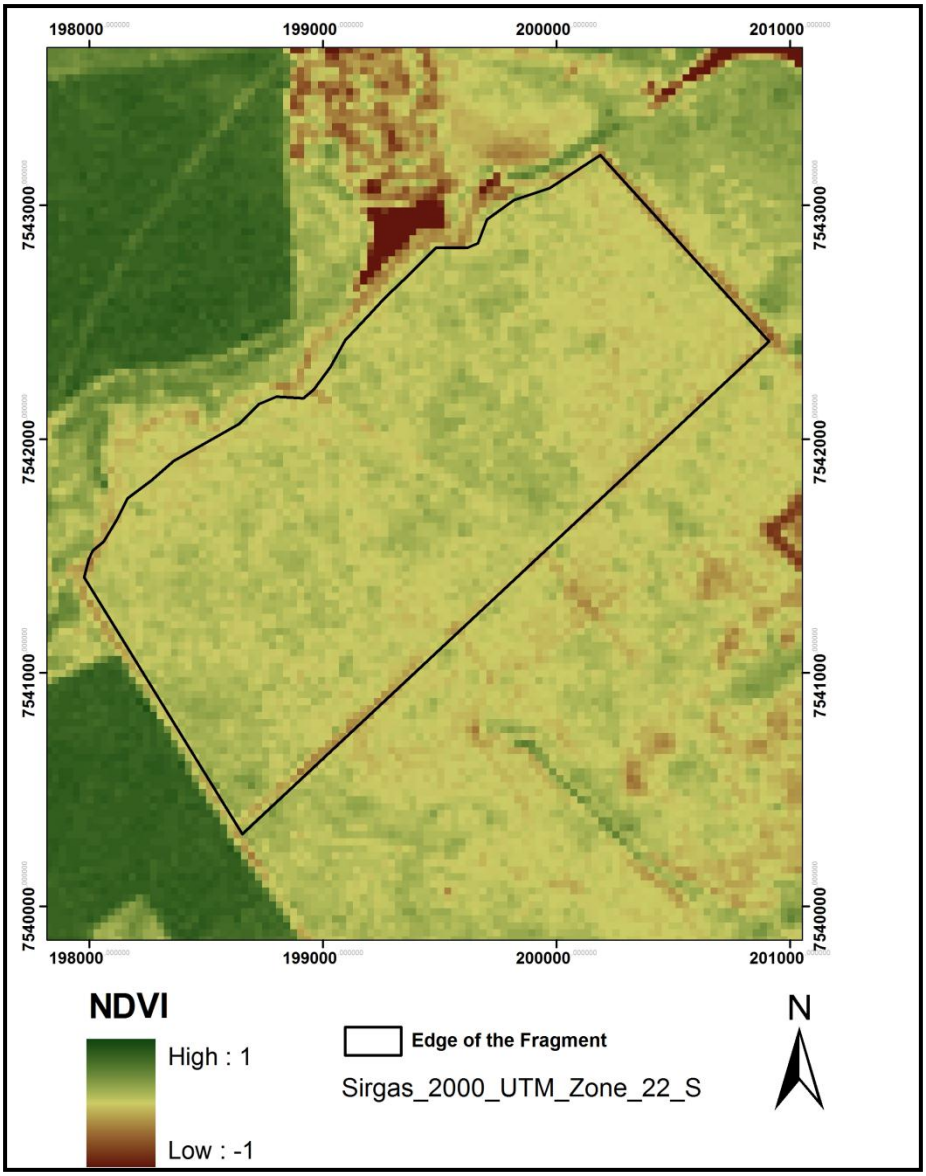


***Figure 10:*** *Fragment of Cerrado Vegetation at "Estação Ecológica de Itirapina" (ESECI) NDVI Image from 2011*

Figure 11 shows the region with lower NDVI values in CRPS that is related to the *cerrado sensu strictu* that when compared with other areas inside this fragment presents lower species richness [24]. The lower NDVI values and species richness may be related to invasion of cattle from adjacent pastures in the past, although this area is currently under environmental recovery process it still presents a mosaic of different physiognomies with distinct floristic composition [24].

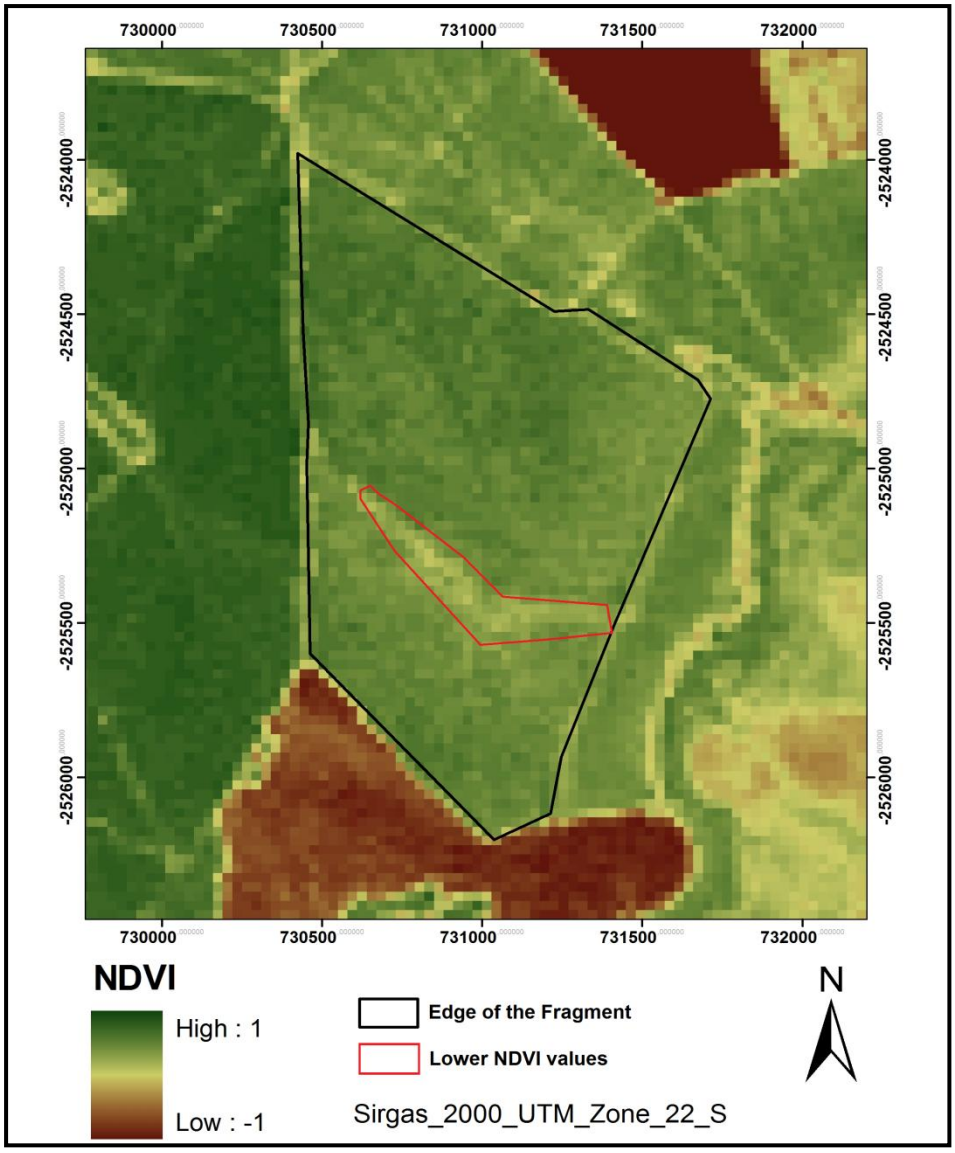


***Figure 11:*** *Fragment of Cerrado Vegetation at Cerrado Reserve "Palmeira da Serra" (CRPS) Map showing a Region with Lower NDVI Values, Evidenced by the Red Polygon in 2011 Map*

In *cerrado* there is a tendency of substitution of physiognomies towards a vegetation type called *cerradão*, a dense forest forming a canopy [9]. So, the result expected for *Botucatu* fragment, if there was no interference in the vegetation dynamics, was similar histograms of the years 1985 and 2011 indicating the maintenance of the dense vegetation, registered in the former analysis. In this scenario NDVI could also be higher in 2011 by the replacement of *cerrado sensu strictu* by *cerradão*, however it was registered lower NDVI values in 2011 (Figure 12). These lower NDVI values may be related to the human interference in this fragment. Similar results were found in African savannah where degraded areas also had lower NDVI values than non-degraded areas across all growth seasons [31, 32]. As a strong correlation has been established between NDVI and vegetation cover, changes in this vegetation cover can be measured using remote sensing data.

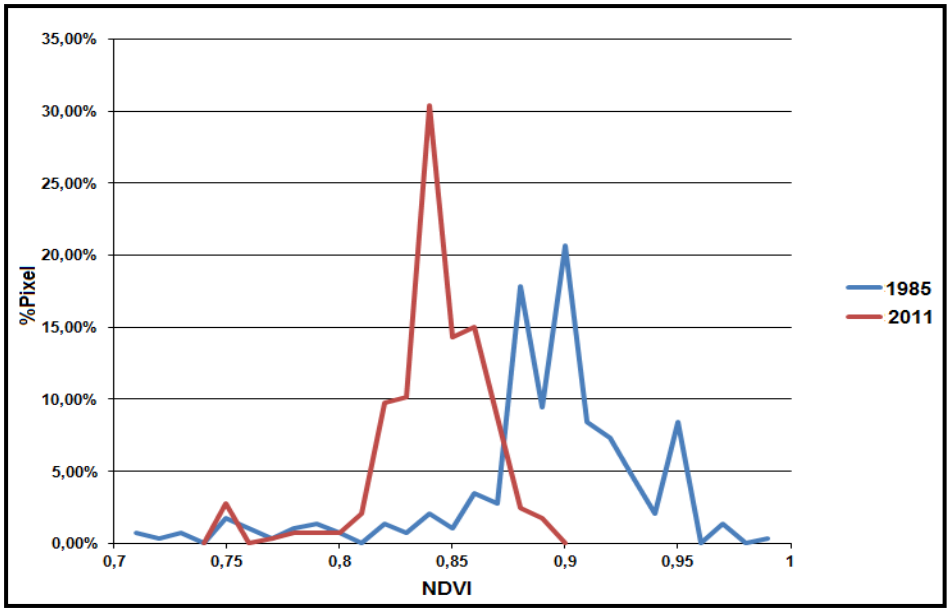


***Figure 12:*** *NDVI Values Histograms for the Fragment of Cerrado Vegetation at Botucatu in 1985 (Blue) e 2011 (Red).*

Although fire is a factor of savannah degradation it does not means that it will always influence NDVI with lower values, once the fire is also important for maintenance of more open physiognomies, leading to maintenance of NDVI in these less dense physiognomies [32]. In the case of *Botucatu* fragment, the fire is a negative impact factor, because of its forest structure, evidenced in both 1985 and 2011 NDVI images (Figure 12-13). Moreover, evidences of fire and gaps opened to install honeybee colonies for apiculture were observed inside the fragment (Figure 14), besides the historical selective logging in the region, which may have contributed to the lower NDVI values in 2011 than in 1985.

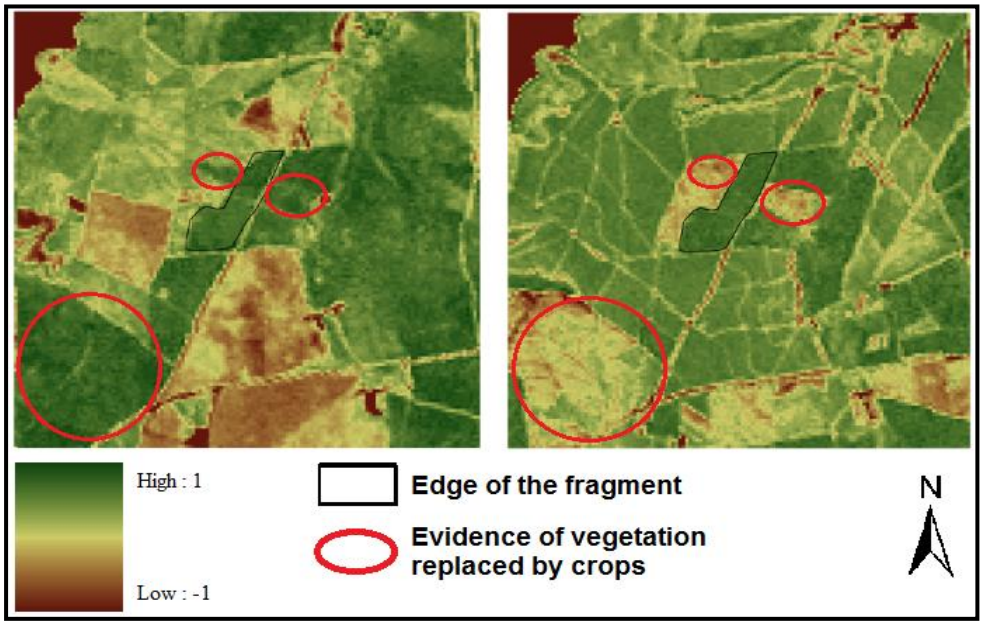


***Figure 13:*** *Fragment of Cerrado Vegetation at Botucatu. NDVI Images from 1985 (Left) and 2011 (Right). The Vegetation around the Fragment in 1985 was replaced by Crops and Pasture during the 26 Years Period, Evidenced with Red Polygons in Both Images*

***Figure 14:*** *Evidences of Fire and Apiculture for the Fragment of Cerrado Vegetation at Botucatu Municipality, São Paulo State, Brazil*

Furthermore, changes in the land use around the fragment can be observed between 1985 and 2011 (Figure 13), with the replacement of the original vegetation by agricultural crops and pasture, confirming that this fragment was under human pressures and several types of impact along the twenty six years period of study.

## 4. Conclusion

In both protected *cerrado* fragments studied, the vegetation showed the same tendency of other protected areas of *cerrado* in Brazil [8, 9]. This tendency means that physiognomies with lower biomass and more open vegetation is being replaced by denser physiognomies with higher biomass, which may continue if maintained protection condition, until reaching the *cerradão* physiognomy.

In the *cerrado* fragment more vulnerable to human impacts, in Botucatu, the NDVI was efficient to detect disturbances in vegetation around the fragment, such as changes in land use, evidencing the replacement of natural vegetation by crops. So the NDVI showed to be useful to verify anthropogenic impacts on vegetation, especially in the Brazilian savannah, which has suffered intensive pressures in the last decades [2, 4, 33].

Additionally, NDVI seems to be efficient to study and assess the dynamics of *cerrado* vegetation, allowing to identify structural changes throughout the period in which the area has been protected.

However, it is not possible to distinguish accurately among different physiognomies of *cerrado*, especially the denser ones just using NDVI images, without field check. It stills remains as a limitation of this method, but efforts should be directed aiming to improve its accuracy.

## References

[1] Sano, E.E., Rosa, R., Brito, J.L.S., and Ferreira, L.G. *Land Cover Mapping of the Tropical Savanna Region in Brazil.* Environmental Monitoring and Assessment. 2010. 166; 113-124

[2] Mantovani, J.E., and Pereira, A., 1998: *Estimativa da integridade da cobertura vegetal do cerrado/pantanal através de dados TM/Landsat*. Extended Abstracts, Simpósio Brasileiro de Sensoriamento Remoto, 9, São José dos Campos/São Paulo.

[3] Myers, N., Mittermeier, R.A., Mittermeier, C.G., Fonseca, G.A.B., and Kent, J. *Biodiversity Hotspots for Conservation Priorities.* Nature. 2000. 403; 853-858.

[4] Durigan, G., Franco, D.C., and Siqueira, M.F., 2004: O que é cerrado? *Viabilidade de Conservação dos Remanescentes de Cerrado no Estado de São Paulo.* Anablume, 28-32.

[5] Bitencourt, M.D., and Mendonça, R.R., 2004: *Viabilidade de conservação dos remanescentes de cerrado no estado de São Paulo.* 1st Ed. Anablume. 170.

[6] Mesquita Júnior, H.N., Malthus, T.J., Bitencourt, M.D., and Furley, P.A., 2004: Structural-Functional Model to Remote Sensing of Vegetation Physiognomies Seasonal Variation based on Life Form. Extended Abstracts, 4th International Workshop on Functional-Structural Plant Models, Montpellier, France.

[7] Bitencourt, M.D., Mesquita Júnior, H.N., Kuntschik, G., Rocha, H.R., and Furley, P. *Cerrado Vegetation Study Using Optical and Radar Remote Sensing: Two Brazilian Case Studies.* Canadian Journal of Remote Sensing. 2007. 33; 468-480.

[8] Pinheiro, E.S., and Durigan, G. *Spatial and Temporal Dynamics (1962-2006) of Cerrado Vegetation Types in a Protected Area, Southeastern Brazil.* Revista Brasileira de Botânca. 2009. 32; 441-454.

[9] Goodland, R., and Ferri, M.G., 1979: *Ecologia do cerrado.* EDUSP, 193.

[10] Ratter, J.A., Leitão Filho, H.F., Agent, G., Gibbs, P.E., Semir, J., Shepherd, G.J., and Tamashiro, J. *Floristic Composition and Community Structure of a Southern Cerrado Area in Brazil.* Notes of the Royal Botanic Garden Edinburgh. 1988. 45; 137-151.

[11] Ratter, J.A., 1992: Transitions between Cerrado and Forest Vegetation in Brazil. *Nature and dynamics of Forest-Savanna boundaries.* Chapman & Hall. 417-430.

[12] Durigan, G. and Ratter, J.A. *Successional Changes in Cerradão and Cerrado/Forest Ecotonal Vegetation in Western São Paulo State, Brazil, 1962-2000.* Edinburgh Journal of Botany. 2006. 63; 119-130.

[13] Pinheiro, E.S., Durigan, G., and Santos, J.R. *Evaluation of QuickBird Data to Estimate Aboveground Cerrado Phytomass.* Ambiência. 2008. 4; 69-83.

[14] Mesquita Júnior, H.N., 1998: Análise temporal com sensor orbital de unidades fisionômicas de cerrado na Gleba Pé-de-Gigante (Parque Estadual de Vassununga – SP). Dissertation, IB, USP, 112.

[15] Tucker, C.J. *Red and Photographic Infrares Linear Combinations for Monitoring Vegetation.* Remote Sensing of Environment. 1979. 8; 127-150.

[16] Gamon, J.A., Field, C.B., Goulden, M.L., Griffin, K.L., Hartley, A.E., Joel, G., Peñuelas, J., and Valentini, R. *Relationships between NDVI, Canopy Structure, and Photosynthesis in Three Californian Vegetation Types.* Ecological Applications. 1995. 5; 28-41.

[17] Mesquita Júnior, H.N. *NDVI Measurements of Neotropical Savanna Physiognomies a Gradiente of: Biomass, Structure and Phenology Changes.* International Archives of Photogrammetry and Remote Sensing. 2000. 33; 93-100.

[18] CEPAGRI, 2010: Centro de Pesquisas Meteorológicas e Climáticas Aplicadas à Agricultura. Clima dos Municípios Paulistas, 85.

[19] Instituto Florestal, 2006: Plano de Manejo Integrado das Unidades de Itirapina. 318.

[20] Oliveira, J.B., Camargo, M.N., Rossi, M., and Calderano Filho, B. *Mapa pedológico do Estado de São Paulo: legenda expandida.* Instituto Agronômico/EMBRAPA-Solos. 1999. 1; 64.

[21] Cabacinha, C.D., and Castro, S.S. *Relationships between Floristic Diversity and Vegetation Indices, Forest Structure and Landscape Metrics of Fragments in Brazilian Cerrado.* Forest Ecology and Management. 2009. 257; 2157-2165.

[22] Chavez, Jr., P.S. *An Improved Dark-Object Subtraction Technique for Atmospheric Scattering Correction of Multispectral Data*. Remote Sensing of Environment. 1988. 24; 459-479.

[23] Chander, G., Markham, B.L. and Helder, D.L. *Summary of Current Radiometric Calibration Coefficients for Landsat MSS, TM, ETM +, an EO-1 ALI Sensors*. Remote Sensing of Environment. 2009. 113; 893-903.

[24] Ishara, K.L., and Maimoni-Rodella, R.C.S. *Richness and Similarity of the Cerrado Vascular Flora in the Central West Region of São Paulo state, Brazil.* Check List. 2012. 8; 32-42.

[25] Archer, S., Scifres, C., and Basshan, C.R. *Autogenic Succession in a Subtropical Savanna: Conversion of Grassland to Thorn Woodland*. Ecological Monographs.1988. 58; 111-127.

[26] Carmel, Y., and Kadmon, R. *Effects of Grazing and Topography on Long-Term Vegetation Changes in a Mediterranean Ecosystem in Israel*. Plant Ecology. 1999. 145; 243-254.

[27] Bowman, D.M.J.S., Walsh, A., and Milne, D.J. *Forest Expansion and Grassland Contraction Within a Eucalyptus Savanna Matrix between 1941 and 1994 at Litchfi eld National Park in the Australian Monsoon Tropics.* Global Ecology & Biogeography. 2001. 10; 535-548.

[28] Archibold, O.W., 1995: *Ecology of World Vegetation*. 1st Ed. Chapman and Hall Press. 510.

[29] Miranda, H.S., Sato, M.N., Neto, W.N., and Aires, F.S., 2009: Fires in the Cerrado, the Brazilian Savanna. *Tropical Fire Ecology*. Springer Berlin Heidelberg. 427-450.

[30] Lehmann, C.E.R., Anderson, T.M., Sankaran, M., Higgins, S.I., Archibald, S., Hoffmann, W.A., Hanan, N.P., Williams, R.J., Fensham, R.J., Felfili, J., Hutley, L.B., Ratnam, J., Jose, J.S., Montes, R., Franklin, D., Russell-Smith, J., Ryan, C.M., Durigan, G., Hiernaux, P., Haidar, R., Bowman, D.M.J.S., and Bond, W.J. *Savanna Vegetation-Fire-Climate Relationships Differ Among Continents*. Science. 2014. 343; 548-552.

[31] Wessels, K.J., Prince, S.D., Frost, P.E., and Van Zyl, D. *Assessing the Effects of Human-Induced Land Degradation in the Former Homelands of Northern South Africa with a 1 km AVHRR NDVI Time-Series*. Remote Sensing of Environment. 2004. 91; 47-67.

[32] Jacquin, A., Sheeren, D., and Lacombe, J.P. *Vegetation Cover Degradation Assessment in Madagascar Savanna based on Trend Analysis of MODIS NDVI Time Series*. International Journal of Applied Earth Observation and Geoinformation. 2010. 12; 3-10.

[33] Brannstrom, C., Jepson, W., Fillipi, A.M., Redo, D., Xu, Z., and Ganesh, S. *Land Change in the Brazilian Savanna (Cerrado), 1986-2002: Comparative Analysis and Implications for Land Use Policy.* Land Use Policy. 2008. 25; 579-595.

**Cloud Publications**
International Journal of Advanced Remote Sensing and GIS
2014, Volume 3, Issue 1, pp. 606-615, Article ID Tech-265
ISSN 2320 - 0243

Research Article | Open Access

# Regression Kriging versus Geographically Weighted Regression for Spatial Interpolation

**Qingmin Meng**

Department of Geosciences, Mississippi State University, MS, USA

Correspondence should be addressed to Qingmin Meng, qmeng@geosci.msstate.edu

Publication Date: 8 July 2014

Article Link: http://technical.cloud-journals.com/index.php/IJARSG/article/view/Tech-265



**Guest Editor-in-Chief: Dr. Qingmin Meng, Department of Geosciences, Mississippi State University, Mississippi, USA**
***(This article belongs to the Special Issue "Geospatial Information Sciences: Landscape and Ecosystem Applications")***

**Abstract** If spatial dependence and/or spatial heterogeneity are taken into account in the process of spatial interpolation, the prediction process can be named local-spatial prediction. Geographically weighted regression is a type of local-spatial prediction models since methodologically it incorporates spatial heterogeneity into a regression model. From the standpoint of spatial interpolation, regression kriging is presented as another local-spatial prediction model that incorporates local-spatial dependence, association between response and auxiliary variables, and the unbiased estimation with minimized variance into an interpolation process. The methodologies of regression kriging and geographically weighted regression are summarized to indicate how local-spatial correlation, spatial heterogeneity, and non-spatial correlation and are incorporated into interpolation process. This paper points out regression kriging applies the local variation of spatial dependence to regression parameter estimation and combines the estimated regression model with residual kriging considering spatial autocorrelation in residuals as a hybrid local-spatial interpolator. Using a raster data with two types of sampling approaches, this study examines and compares the performance of regression kriging and geographically weighted regression. The empirical examples indicate that both regression kriging and geographically weighted regression are powerful local-spatial prediction models, but regression kriging can be better in capturing the spatial structure of the original data.
**Keywords** *Regression Kriging; Geographically Weighted Regression; Local-Spatial Prediction; Spatial Dependence; Spatial Non-Stationarity*

## 1. Introduction

A primary difference between geographic information science (GIScience) and other science disciplines is the description and modeling of spatial differences and similarities. In GIScience, an important research trend has been changed to the focus of differences instead of similarity across

space (Fotheringham and Brunsdon, 1999). It is difficult to use global models to describe the differences across space because a hidden assumption of global models is that variation is the same everywhere for a given study area, while spatial dependence generally varies across space. The first law of geography i.e., “Everything is related to everything else, but near things are more related than distant things (Tobler, 1970)” is a typical description of spatial dependence that forms the primarily foundation of geospatial modeling. It is convenient to use local models to model differences across space. For example, the local indicator of spatial autocorrelation (LISA) is an efficient function for modeling spatial dependence across space (Anselin, 1995). However, it is difficult to have all the measurements of interesting variables across a whole study area and predictions based on sample locations are usually the dominant way in practice. An efficient way is to use spatial prediction models to estimate the values at unsampled locations given both values at sampled locations and values of auxiliary variables across the whole study area for which remotely sensed images have been widely used as auxiliary variables. Incorporating the spatial characteristics of spatial autocorrelation or spatial heterogeneity into prediction, the spatial prediction models can be appropriate. Therefore, the spatial prediction models taking account of local-spatial characteristics (e.g., local dependence or spatial non-stationarity) can be called local-spatial prediction models (LSPM).

Spatial dependence and spatial heterogeneity determine the necessity of using LSPM to estimate values of a geographical property. Unwin and Unwin (1998) emphasized the spatially varying characteristics because of three important properties: (1) spatial dependence exists in most spatial data analysis, (2) many geographic analyses depend on the modifiable areal unit problem (MAUP), and (3) the assumption of spatial stationarity is difficult to build in the observed geographical processes over space. These properties are all determined by the nature of geographical objects while for the MAUP subjective judgments may play important roles in practice. From the standpoint of methodology, Fotheringham (1997) summarized three reasons why a global model may not be appropriate: (1) random sampling variations result in spatial variations in observed relationships; (2) certain relationships intrinsically vary across space; and (3) a global model used to measure relationships is a gross misspecification of reality. For example, a geographical property like temperature, precipitation, pollution, and elevation varies from place to place and a LSPM can be better than a global model to estimate the values of this property at unsampled locations based on the values at locally sampled locations and known values of auxiliary variables (e.g., one typical auxiliary data are remote sensing data).

However, the development of prediction models taking account local-spatial correlation and heterogeneity still has received little attention in the fields of GISystems and GIScience. Geographically weighted regression (GWR) is a type of LSPM that incorporates spatial heterogeneity into a regression process. Regression kriging (RK) that emphasizes spatial correlation and its local variation in interpolation process is another type of LSPM. Regression kriging takes account of local-spatial correlation into both regression parameter estimation and residual kriging.

To clarify regression kriging and emphasize how the two local-spatial interpolators RK and GWR incorporate spatial correlation, spatial heterogeneity, and non-spatial association into a local-spatial interpolation process, this study states the methodological characteristics of regression kriging and geographically weighted regression in section 2. Using raster data as an example and two types of sample schemes, this study examines and compares the performance of the two local-spatial prediction models in section 3. This study closes with a concise conclusion that suggest both regression kriging and geographically weighted regression are powerful in local-spatial prediction and in the process of interpolation regression kriging can be better to capture spatial structure of the original data.

## 2. Methodology

A local-spatial prediction model can be defined as the process to interpolate a real valued function of z(s) given the set of values $z(s_1), z(s_2),..., z(s_n)$ at the neighboring locations {s1, s2… sn}. It is necessary to allow for uncertainty in our descriptions of the predicted results for the insufficient knowledge of a given geographic property. From the standpoint of local-spatial prediction, a concise methodological summarization of the RK and GWR is presented below.

### 2.1. Regression Kriging

Odeh et al., (1994, 1995) originally suggested using the term regression kriging to employ correlation between a response variable and auxiliary variables and spatial autocorrelation within the response variable, while kriging with external drift (KED) is often used when external drift is described through some auxiliary variables (Chiles and Delfiner, 1999; Wackernagel, 1998). Goovaerts (1999) used the term of kriging after detrending to define this kriging process. One advantage of RK is that it does not suffer from instability in practice (Goovaerts, 1997) and RK can be easily integrated with statistical computation like general additive modeling or regression tree (McBratney et al., 2000). The RK is used in this study since it indicates that regression is combined with kriging.

In a local-spatial prediction process, let the values to be predicted for the given locations indicate as $z(s_1)$, $z(s_2)$, $z(s_3)$, …, $z(s_n)$, where, for example, $s_i = (x_{latitude}, y_{longitude})$ is a location with the coordinates of $x_{latitude}$ and $y_{longitude}$ , and location $i$ = 1, 2, 3,…, n. The value to be predicted at a new and unsampled location ($s_0$) can be predicted using RK by adding the spatial trend and random components (i.e., residuals) (Odeh et al., 1994; Meng et al., 2006; Meng et al., 2009) using the equation below.

$$\hat{z}(s_0) = \hat{m}(s_0) + \hat{e}(s_0) \tag{1}$$

Where the residuals $\hat{e}$ are interpolated using ordinary kriging and the trend is modeled using a linear regression as follows:

Where $\hat{\beta}_k$ are the $k$th estimated drift model coefficient, $q_k$ is the $k$th external auxiliary variable or

$$\hat{z}(s_0) = \sum_{k=0}^{p} \hat{\beta}_k \cdot q_k(s_0) + \sum_{i}^{n} w_i(s_0) \cdot e(s_i) \tag{2}$$

Predictor at location $s_0$ (while, $q_0(s_0) = 1$), p is the number of auxiliary variables, $w_i(s_0)$ are the weights determined by the covariance function and $e(s_i)$ are the regression residuals.

Rewrite the RK model in a matrix notation using the following equations:

$$z = q^T \cdot \beta + \varepsilon \tag{3}$$

$$\hat{z}(s_0) = q_0^T \cdot \hat{\beta} + \lambda_0^T \cdot e \tag{4}$$

where $\varepsilon$ is the regression residuals, $q_0$ is the vector of $p$ auxiliary variables at $s_0$, $\hat{\beta}$ is the vector of $p$ +1 estimated drift model coefficients, $\lambda_0$ is the vector of $n$ kriging weights and $e$ is the vector of $n$ residuals. Taking into account the spatial correlation of residuals the model coefficients is solved by a generalized least squares estimation below (Cressie, 1993).

$$\hat{\beta} = (q^T \cdot C^{-1} \cdot q)^{-1} \cdot q^T \cdot C^{-1} \cdot z \tag{5}$$

Where *q* is the matrix of auxiliary variables at all the observed locations, *z* is the vector of sampled response observations, and *C* is the n × n covariance matrix of residuals below.

$$C = \begin{bmatrix} C(s_1, s_2) \cdots C(s_1, s_n) \\ \vdots \quad \ddots \quad \vdots \\ C(s_n, s_2) \cdots C(s_n, s_n) \end{bmatrix} \tag{6}$$

The covariance matrix between sampled pairs $C(s_i, s_j)$ can be estimated using a semivariogram model, which incorporates spatial correlation and its local variations of residuals into the parameter estimations of regression models. At the same process, in order to minimize the spatial autocorrelation in residua and potentially increase the prediction accuracy, the predicted results from the estimated model are added to residual kriging considering local-spatial autocorrelation of residuals. In other words, spatial estimation of regression parameters and local kriging of residuals are incorporated into regression kriging.

In summary, if we would like to illustrate the regression kriging process using simple numerical examples, we need to conduct a simple or multiple-linear regression, select an optimal semivariogram model to explore the residuals, compute the regression coefficients, process the weight matrix, and at last conduct the regression kriging model and obtain the predictions at all unsampled points. Regession kriging is a hybrid interpolator that incorporates spatial correlation and its local variation into the combination of either a simple or multiple-linear regression model with residual kriging. In the process of RK, kriging with uncertainty introduces the regression residuals (i.e., the model uncertainty) into the kriging system, which is then applied directly to predict the response variable. The predictions are combined from two parts: one is the estimation obtained from regression considering spatial correlation, and the second part is the residual estimated from the ordinary kriging. Therefore, a general format of RK can be rewrite in a matrix notation below as Christensen (1990).

$$\hat{z}(s_0) = q_0^T \cdot \hat{\beta} + \lambda_0^T \cdot (z - q \cdot \hat{\beta}) \tag{7}$$

### 2.2. Geographically Weighted Regression

Geographically weighted regression was first explored by (Fotheringham, 1997; Brunsdon et al., 1998; Fotheringham and Brunsdon, 1999 and Fotheringham, 2000). Fotheringham et al., (2002) discussed in detail of geographically weighted regression.

### 2.3. Evaluation Methods

The GWR could provide better fits in terms of the residual because of the flexible estimations of the GWR coefficients at a given location. Regression kriging is another powerful model for local predictions because it takes into account the local dependence of the response variable into both regression parameter estimation and residual kriging. It is necessary to compare the performance of the two local spatial prediction models.

Visual comparisons are necessary to indicate the quality of local predictions of interpolations although the visual analysis is subjective. Statistical methods are performed to objectively quantify the differences between the original image and the predicted images using RK or GWR. (1) Basic statistics including mean, median, range, minimum, maximum, standard deviation (SD), kurtosis, skewness, and histogram are used to describe the basic distribution of the predicted imagery data and the original image data and compare their differences. (2) Root mean square error (RMSE) is used to compare the differences between the original and the predicted imagery across the whole study area; while mean absolute error (MAE) is used to compare the differences at per-pixel level. (3) Pearson

correlation coefficient is applied to check the similarity of the distributions between the original and predicted images. (4) Using a raster data Ikonos images, the original images and the interpolated images are processed using two morphological functions of dilate and erode in order to compare performance of RK and GWR. Assessment of spatial structure is then conducted using Pearson correlation index.

Morphological processing typically is used to understand the structure of an image and identify boundaries or objects within an image. Morphological techniques here are used to indicate the potential spatial structure of spectral values within an image. To evaluate spatial effects of these local predictions, morphological processes with 3x3, 5x5, and 7x7 neighborhoods and the two morphological functions are applied to the predicted images and the original band 2. Dilate is used as a maximum operator to select the greatest values in the neighborhood, while erode is used as a minimum operator to select the smallest values in the neighborhood. Then, Person correlation coefficient is used to measure the agreement between the processed predictions and the original data.

## 3. A Case Study

An Ikonos image with spatial resolution of 4 meter (i.e., band 2 is used as the response variable, and band 3 is used as an auxiliary variable) is used as an example. The GWR models are applied first according to (Fotheringham et al., 2002). Regression kriging is applied to model the images based on the Gstat software package (Pebesma and Wesseling, 1998). The prediction models of RK and GWR are applied to interpolate pixel values of band 2 using band 3 as the predictor. Because all the locations in imagery have recorded values, it is relatively easy to conduct sampling techniques and use the sample data to build local-spatial prediction models. It also is relatively convenient to assess the performance of regression kriging and geographically weighted regression using the predicted values of the unsampled locations in the imagery.

### 3.1. The Data

The coastal area located in Camp Lejeune (34.57° N latitude, 77.28° W longitude, Figure 1), southeastern North Carolina, is used as the study area. Camp Lejeune is a coastal plain that changes in elevation from sea level to 19.2 m (63 feet) (Rootsweb, 2007). Different landscapes including hardwoods, mixed softwoods, vegetated wetlands, and roads cover this region (Figure 1).

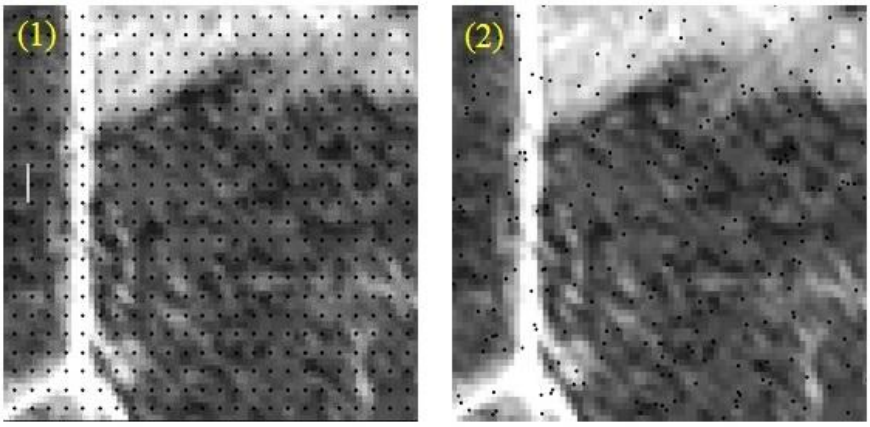


***Figure 1:*** *Study Area is Located in North Carolina, US, Center Coordinates of 34.57º N / 77.28º W. 528 Regularly Distributed Pixels (1) And 264 Pixels Obtained using a Simple Random Sampling (2) are Portrayed Using Iknons Band 2. Solid Dark Points are for Sampled Pixels*

Two popular sample techniques are applied to assess the local predictions using RK and GWR. 528 regularly distributed points are sampled and a simple random sampling is conducted to generate 264 points (Figure 1).

### 3.2. Results

Based on the simple random sample of 264 pixels and the regularly sampled 528 pixels, GWR and RK are applied to predict the values of band 2 at the unsampled locations. The predicted pixels using GWR are depicted in Figure 2, and RK predictions are portrayed in Figure 3. It seems that there is little visual difference between the original band 2 and the predicted bands obtained using GWR and RK. Contrast is a little strong in the predicted band 2 using GWR and the 528 sampled pixels (Figure 2). The band 2 obtained using RK and the 528 sampled pixels also results in a little strong contrast (Figure 3).

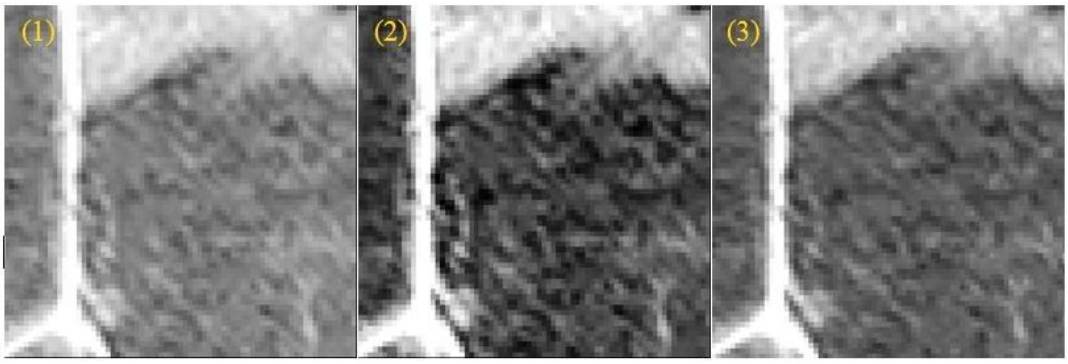


***Figure 2:*** *Visual Comparison of Spatial Prediction using Geographically Weighted Regression (GWR). (1) Predicted Band 2 Using GWR and 264 Sample Pixels; (2) Predicted Band 2 Using GWR and 528 Sample Pixels; (3) The Ikonos Band 2.*

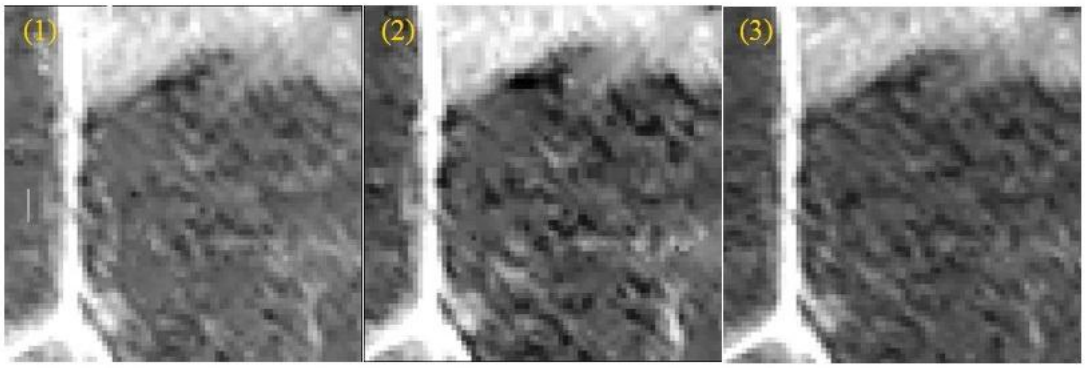


***Figure 3:*** *Visual Comparison of Spatial Predictions using Regression Kriging (RK).*
*(1) Predicted Band 2 Using RK and 264 Sample Pixels; (2) Predicted Band 2 Using RK and 528 Sample Pixels; (3) The Ikonos Band 2.*

The GWR and RK have almost similar values of the basic statistics of mean, median, range, minimum, maximum, SD, kurtosis, and skewness as the original band 2 (Table 1). The predictions using both the sampled 264 and 528 pixels also have the similar values in these statistics. The prediction using RK and 528 sampled pixels has closer values of kurtosis and skewness to the original band 2 while relatively large differences in mean, minimum, and maximum between this prediction and the original band 2. The comparisons of histogram are consistent with the basic statistics, and there is not big difference of distribution between these predictions and the original band 2 (Figure 4).

***Table 1:*** *Descriptive Comparisons of GWR and RK for Local-Spatial Prediction*

| | Mean | Median | Range | Minimum | Maximum | SD | K | S |
|---|---|---|---|---|---|---|---|---|
| Band2 | 272 | 250 | 372 | 191 | 563 | 60 | 3.33 | 1.84 |
| GWR-264 | 274 | 249 | 376 | 187 | 563 | 59 | 3.05 | 1.78 |
| GWR-528 | 274 | 249 | 378 | 185 | 563 | 60 | 3.11 | 1.80 |
| RK-264 | 274 | 248 | 376 | 187 | 573 | 60 | 3.02 | 1.79 |
| RK-528 | 271 | 248 | 364 | 164 | 528 | 57 | 3.22 | 1.81 |

SD, standard deviation; K, kurtosis; S, skewness;
GWR-264 (or 528), geographically weighted regression using 264 (or 528) sampled pixels; RK-264 (or 528), regression kriging using 264 (or 528) sampled pixels

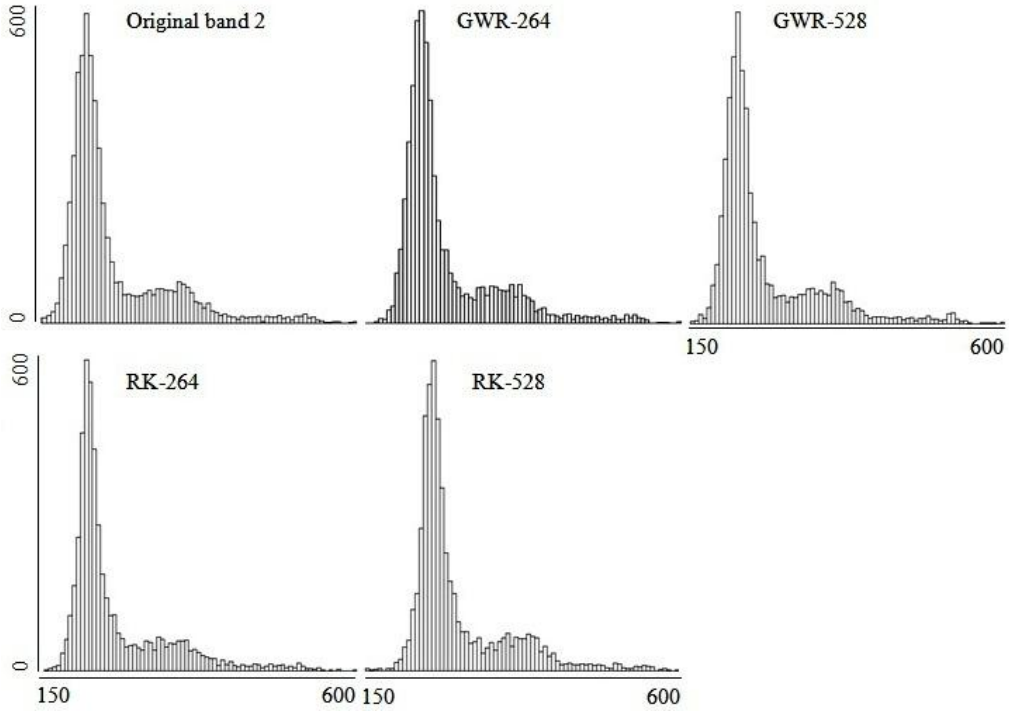


***Figure 4:*** *Histogram of the Original Band 2 and Its Prediction using Geographically Weighted Regression (GWR) and Regression Kriging (RK). GWR-264 (or 528), Prediction using GWR and 264 (or 528) Sampled Pixels; RK-264 (or 528), Prediction using RK and 264 (or 528) Sampled Pixels*

The diagnostic check of the GWR and RK using mean absolute error, relative mean absolute error, root mean square error, and Pearson correlation coefficient is consistent with the above descriptive comparisons. These diagnostics indicate there is not any significant difference between the prediction of GWR and that of RK (Table 2). There is not any significant difference between the prediction using the simple random sample of 264 pixels and the regularly sampled 528 pixels. There are very strong positive associations between all the predictions and the original band 2 (i.e., correlation coefficients are from 0.979 to 0.994). The higher the correlation coefficients, the better is the consistency between the predictions and the original data (e.g., the higher the correlation coefficients, the better the spectral similarity between the predicted imagery and the original imagery). Furthermore, the absolute errors are very small (i.e., from 4.97 to 8.62) and the values of the relative mean absolute error are only between 1.8 % and 3.2%.

***Table 2:*** *Diagnostic Check of GWR and RK*

| | MAE | RMSE | *r* |
|---|---|---|---|
| GWR-264 | 5.81 | 2.236 | 0.992 |
| GWR-528 | 4.97 | 2.000 | 0.994 |
| RK-264 | 7.70 | 2.000 | 0.983 |
| RK-528 | 8.62 | 3.162 | 0.979 |

MAE, mean absolute error; RMAE, relative MAE; RMSE, root mean square error; r, Pearson correlation coefficient between the predicted and original band 2. Other notes as Table 1.

Both the basic statistics and the diagnostics indicate that satisfied predictions are achieved using both the GWR and RK models. Also, the simple random sample (i.e., the 264 pixels) results in almost the same predictions as the much dense sample (i.e., the regularly distributed 528 pixels).

We may wonder whether the GWR and RK models perform similar in characterizing the spatial structure in their predictions. Are there some differences in spatial structures between the predicted values and the original values? Morphological analysis of the predicted pixel values and the original band 2 can help answer the two questions. We use two morphological functions of dilate and erode to process the predicted and the original band 2, and then for the processed bands Pearson correlation coefficients are calculated. The higher the correlation coefficient, the better is the spatial consistence between the predictions and the original band data. Given a window size, the dilate function is used to select the maximum values while the erode function is used to select the minimum values within the given neighborhood. In order to have a relative comprehensive analysis on spatial structure, window sizes of 3x3, 5x5, and 7x7 are applied for the morphologically processed bands. The correlation coefficients are then calculated and summarized in Table 3.

***Table 3****: Correlation between the Original Band and the Predicted Bands after Morphological Processes*

| | | GWR-264 | RK-264 | GWR-528 | RK-528 |
|---|---|---|---|---|---|
| 3x3 window | Dilate | 0.8717 | 0.9765 | 0.7318 | 0.9752 |
| | Erode | 0.9588 | 0.9707 | 0.9766 | 0.9633 |
| 5x5 window | Dilate | 0.8783 | 0.9775 | 0.7471 | 0.9756 |
| | Erode | 0.9488 | 0.9653 | 0.9846 | 0.9462 |
| 7x7 window | Dilate | 0.8829 | 0.9785 | 0.7580 | 0.9758 |
| | Erode | 0.9373 | 0.9575 | 0.7775 | 0.9287 |

Notes as Table 1.

The very high correlation coefficients show that the RK model can be better than the GWR model in characterizing spatial structure in the original data (Table 3). The relatively lower values of correlation coefficients between the GWR prediction and the original band 2 indicate that GWR performs relatively poor in maintaining local maximum values (i.e., after dilate functions are processed, the GWR predicted bands and the original band 2 have relatively lower correlation values. The simple random sample (i.e., 264 pixels) and the much dense 528 sampled pixels (i.e., the regularly distributed sample) result in similar values in correlation coefficients, and these similar correlation coefficients indicate that the much dense sample of 528 pixels cannot have apparent advantages to maintain the spatial structure in prediction.

## 4. Discussions and Conclusions

Regression kriging and geographical weighted regression model the quantitative association between the dependent variable and the predictor variables, therefore, the performance of local-spatial prediction also depends on the correlation represented among response and predictor variables. The

higher the correlation between response and predictor variables, the better is the spatial prediction. The selection of auxiliary variables that are highly correlated with the variable of interest is important for local-spatial prediction of environmental or social-economic variables for which the measurement is time consuming and expensive. Remotely sensed images are typically the first choice of auxiliary variables that are relatively cheap of acquiring up-to-date information over a large area.

Both geographically weighted regression and regression kriging are powerful local-spatial prediction models. The descriptive comparisons between the original data and the predicted data and the diagnostic check of GWR and RK indicate both the LSPM of GWR and RK perform very well in spatial interpolation. Based on the sampled locations and the spatial non-stationarity, GWR provides flexible estimations of parameters and then uses these spatially varying regression parameters to interpolate values at unsampled locations but does not directly consider spatial dependence in the process of model development. The regression kriging model predicts values at unsampled locations by building a spatial regression model (i.e., incorporating spatial autocorrelation and its local variation into parameter estimation) combined with residual kriging (i.e., taking account of local-spatial autocorrelation in residuals). Additionally, regression kriging does not suffer from spatial non-stationarity in practice (Goovaerts, 1997).

The mophorlogical analysis and Pearson correlation coefficients show that regression kriging has a little superiority to geographically weighted regression in predicting spatial structure. Geographically weighted regression emphasizes the spatial non-stationarity but methodologically takes no-account of spatial correlation when model is developed. A distance-decreased function (e.g., Gaussin function is tested as an optimal one in this study) typically is used to calculate the weight matrix used in geographically weighted regression. In the process of prediction using regression kriging, the weight matrix for residual kriging and the spatial semivariogram for regression parameter estimation are determined by a relatively optimal semivariogram function that quantitatively models the spatial dependence and structure.

## References

Anselin, L. *Local Indicators of Spatial Association-LISA*. Geographical Analysis 1995. 27; 93-115.

Brunsdon, C., Fotheringham, A.S., Charlton, M. *Geographically Weighted Regression-Modeling Spatial Non-Stationarity*. The Statistician. 1998. 47; 431-443.

Chiles, J., and Delfiner, P., 1999: *Geostatistics: Modeling Spatial Uncertainty*. Wiley, New York.

Christensen, R. The *Equivalence of Predictions from Universal Kriging and Intrinsic Random Function Kriging*. Mathematical Geology. 1990. 22; 655-664.

Cressie, N., 1993: Statistics for Spatial Data Revised Ed. Wiley, New York.

Fotheringham, A.S. *Trends in Quantitative Methods I: Stressing the Local*. Progress in Human Geography. 1997. 21; 88-96.

Fotheringham, A.S. *Context-dependent Spatial Analysis: A Role for GIS*. Journal of Geographical Systems. 2000. 2; 71-76.

Fotheringham, A.S., and Brunsdon, C. *Local Forms of Spatial Analysis*. Geographical Analysis. 1999. 31; 340-358.

Fotheringham, A.S., Brunsdon, C., and Charlton, M., 2002: *Geographically Weighted Regression: The Analysis of Spatially Varying Relationships*. John Wiely & Sons, Chichester.

Goovaerts, P., 1997: *Geostatistics for Natural Resources Evaluation*. Oxford University Press, New York.

Goovaerts, P. Using Elevation to Aid the Geostatistical Mapping of Rainfall Erosivity. Catena. 1999. 34; 27-242.

Meng, Q., and Cieszewski, C.J., 2006. Using *Geo-Spatial Methods for Derivation of Fine Resolution Forest Inventory in Georgia from Ground Inventory Data and Landsat Ima*gery. Proceedings of SOFOR GIS, 5th Southern Forestry and Natural Resources GIS Conference. 51-62.

Meng, Q., Cieszewski, C.J., and Madden, M. *Large Area Forest Inventory Using Landsat ETM+: A Geostatistical Approach.* ISPRS Journal of Photogrammetery and Remote Sensing. 2009. 64 (1) 27-36.

McBratney, A., Odeh, I., Bishop, T., Dunbar, M., and Shatar, T. An Overview of Pedometric Techniques of Use in Soil Survey. 2000. Geoderma 97; 293-327.

Odeh, I., McBratney, A., and Chittleborough, D., *Spatial Prediction of Soil Properties from Landform Attributes Derived from A Digital Elevation M*odel. Geoderma. 1994. 63; 197-214.

Odeh I., McBratney A., and Chittleborough, D. Further *Results On Prediction of Soil Properties from Terrain Attributes: Heterotopic Cokriging and Regression-Krig*ing. Geoderma. 1995. 67; 215-226.

Pebesma, E.J., and Wesseling, C.G. Gstat: A Program for Geostatistical Modeling, Prediction and Simulation. Computers & Geosciences. 1998. 24; 17-31.

Tobler, W.R. *A Computer Model Simulation of Urban Growth in the Detroit Region*. Economic Geography. 1970. 46; 234-240.

Unwin, W., and Unwin, D. *Exploratory Spatial Data Analysis With Local Statistics*. The Statistician. 1998. 47; 415-421.

Wackernagel, H., 1998: *Multivariate Geostatistics: An Introduction With Applications*, 2nd Ed. Springer, Berlin.

**Cloud Publications**
International Journal of Advanced Remote Sensing and GIS
2014, Volume 3, Issue 1, pp. 616-626, Article ID Tech-266
ISSN 2320 - 0243

Cloud Publications

**Research Article** **Open Access**

# Sediment Yield Estimation for Watershed Management in Lolab Watershed of Jammu & Kashmir State Using Geospatial Tools

**Pervez Ahmed and Abaas Ahmad Mir**

Department of Geography and Regional Development, University of Kashmir, Srinagar, Jammu and Kashmir, India

Correspondence should be addressed to Abaas Ahmad Mir, Geoabaas@gmail.com

Publication Date: 8 July 2014

Article Link: http://technical.cloud-journals.com/index.php/IJARSG/article/view/Tech-266



**Guest Editor-in-Chief: Dr. Qingmin Meng, Department of Geosciences, Mississippi State University, Mississippi, USA**
***(This article belongs to the Special Issue "Geospatial Information Sciences: Landscape and Ecosystem Applications")***

**Abstract** Sediment Yield estimation on the basis of texture, slope, land use and soil erosion has become inevitable component for effective watershed management in terms of conserving soil and water resources. To assess the sediment yield, it is necessary to prepare a land use / land cover map, to characterize the erosion processes and estimate the total yield on the basis of above mentioned defined parameters. This paper aims to prioritize the micro-watersheds by estimating Sediment Yield Index (SYI) for identification of the critical areas which need immediate remedial measures in Lolab watershed of Jammu and Kashmir State. In the present study, the satellite data from IRS P6 (Resourcesat-1) LISS III sensor with spatial resolution of 23.5 meters, Arc GIS 9.3 and Erdas Imagine 9.2 GIS software were used. Land use/ Land cover map with a total of seven categories was prepared. Agriculture was the major class with 38.98 percent followed by sparse forests with 31.85 percent area. Besides this, Slope, Soil texture and Soil erosion maps were also prepared. The soil erosion map revealed that about 30 percent of the total area was in the moderate to severe class of erosion while as about 49 percent area was in the slight to moderate erosion class. Sediment Yield Index (SYI) was estimated for forty three micro-watersheds individually with the help of delivery ratio and weightage value using an empirical formula. The prioritization of micro-watersheds was done on the basis of the estimated SYI value and conservation measures were suggested accordingly.
**Keywords** *Remote Sensing; Micro-Watershed; Sediment Yield Index; Prioritization; Conservation*

## 1. Introduction

Land and water are two basic natural resources for the survival of living systems. These two resources have been interacting with each other in various phases of their respective cycles. The future of the nation depends largely on the effective utilization, management and development of resources in an

integrated and comprehensive manner. Watersheds have long been identified as planning units for conservation of these precious resources [3]; and the basic objectives of any conservation and management strategy are to find out the problems and accordingly adopt a judicious approach for optimum utilization of all natural resources. The total amount of erosional debris exported from a watershed is its Sediment Yield. The sediment yield process can be divided into upland and lowland phases. The sediment detachment process predominates in the upland phase whereas sediment transport and deposition are the main processes in the low land phase [1]. During recent times, Sediment Yield modeling approach is being used to estimate sediment yield from different hydrological units. The specific needs of sediment yield modeling are varied and no single model can meet the requirements fully. Sediment prediction requirements for each of the available models are determined largely by the duration of the event to be simulated; size, shape, the morphometry of the area and the sources of the sediment. The major factors influencing the sediment yield are the land use, soil texture, soil erosion, and slope [6]. Eroded soil in the form of sediment gets deposited in the reservoirs, eventually reducing designed storage capacity [11]. The information on sources of sediment yield within a watershed can be used as perspective on the rate of soil erosion, occurring within that watershed [5]. As such, a holistic approach for land and water management in a watershed is an ideal strategy for effective conservation of the resources. The identification and demarcation of watersheds that are prone to yielding higher sediment yield should be the primary task for soil resource management [7]. In order to opt for such measures, the proper approach is to identify the problematic areas at the micro level and then initiate soil and water conservation measures. So, prioritization at the micro-watershed level assumes much significance as the areas with higher priority are taken first for conservation measures and areas with lower priority are taken subsequently. This helps in conserving the less priority areas and at the same time proves beneficial for the areas where the problem is more severe.

It is in this context, the present study was carried out in order to analyse the land use/ land cover pattern of the Lolab watershed, to estimate the Sediment Yield Index (SYI) for each individual micro-watershed and to prioritize the micro-watersheds for soil conservation measures.

### 1.1. Study Area

The Lolab Watershed of the Kashmir valley with an area of about 28,162 hectares has been taken up as the study area. The watershed lies between $34^0$ 41' to $34^0$ 24' N Latitude and $74^0$ 09' to $74^0$ 23' E Longitude. It has been divided into forty three micro-watersheds in accordance to the guidelines of the Watershed Atlas of India (WAI).

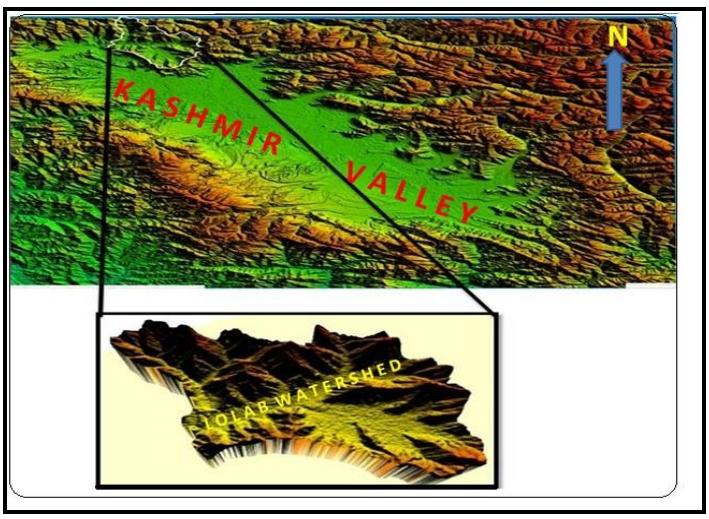


***Figure 1:*** *Location Map of the Study Area*

The watershed can be divided into three distinct physiographic units i.e. the Mountains, the Karewas and the Flood plains. The Lolab Valley is the most fascinating and picturesque of the Himalayan Valleys in Kashmir. The Lolab kol has its source in the Nandmarg, the Kimsar and the Bagalsar heights, north of the Wular Lake. The main stream of the Lolab has a length of about 30 kilometers and flows in a westerly direction. One of its lateral tributaries is the Kalaruch nala which originates below the peak of Nalgat 3645 meters and joins the Lolab below Khumarial. A little before its junction with the Kahmil, the Lolab kol receives the Haheom kol which flows from the north.

## 2. Materials and Methods

The satellite data of Indian Remote Sensing Satellite IRS-P6 (Resourcesat-1) FCC with a resolution of 23.5 meters of June, 2011, Arc GIS 9.3 and Erdas Imagine 9.2 GIS software were used for this study. The methodology for this study included supervised classification approach. A tentative legend with Erosion Intensity Mapping Units was prepared with the help of scheme devised by All India Soil & Landuse Survey (Ministry of Agriculture). The Erosion Intensity Mapping Units (EIMU) implies a set of relevant parameters which are responsible for the detachment of soil (soil erosion) and also exert combined and reciprocal influence on soil detachment. The factors considered include physiography and slope, which control amount and velocity of runoff; soil characteristics, that decide potentiality for erosion; vegetation cover conditions that afford protection to soil; land use that indicates interference by human and biotic factors; present erosion status and existing soil conservation measures that modify the influence of other factors. This was followed by selection of sample strips with observation points for ground truthing exercise. While selecting the observation points, all the EIMUs were given due representation. After the field visit, the legend was finalized and accuracy estimation procedure was performed.

Land use/Land cover map, Slope map, Soil Texture map, and Soil Erosion map were prepared. The Weightage value and Delivery ratio for each mapping unit was included which had been estimated by AIS & LUS using their INGRESS customized software. These Weightage values and Delivery ratios were actually estimated by considering the EIMU parameters and their relevant values. Different mapping units had different Weightage values and Delivery ratios. Besides these two, the area of the each Individual Erosion Intensity Mapping Unit and area of each micro watershed were together used in an empirical formula to estimate the Sediment Yield Index [4]. These SYI values for each micro watershed were then categorized into three priority categories, High, Medium and Low depending upon the intensity of the problem. The individual ranking was also given to all the micro-watersheds and a prioritization map was prepared. Accordingly, conservation measures for each micro-watershed were then suggested.

## 3. Results and Discussion

### 3.1. Land use / Land cover of Lolab watershed (2011)

Agriculture was the dominant land use category (Figure 2) in the Lolab watershed in 2011 with 38.98 percent followed by the sparse forest cover with 31.85 percent. The percentage distribution under different land use / land cover categories is given in Figure 3.

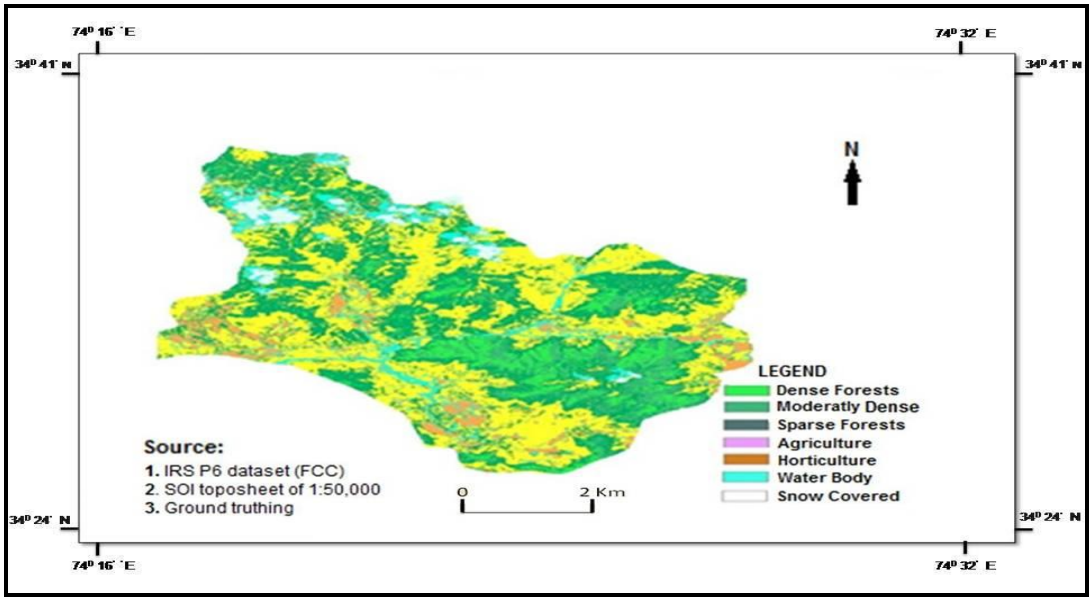


***Figure 2:*** *Land Use / Land Cover Map (2011) of Lolab Watershed*

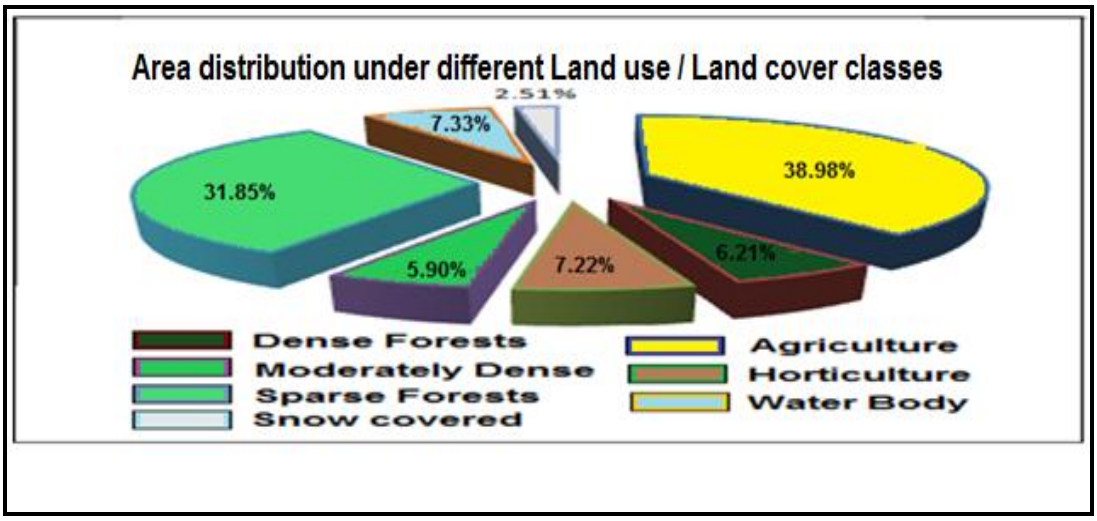


***Figure 3:*** *Area Distribution Under Different Land Use / Land Cover Classes*

### 3.2. Slope

Importance of slope factor in prioritization of watersheds has been recognised at various levels by different researchers [2, 8, 9, 10]. Thus, a slope map (Figure 4) was prepared which is one of the important parameters for estimating Sediment Yield Index. The various categories of slope were, very gentle to gentle, gently to moderately sloping, moderately to steep and steep to very steep. Being a mountainous area, the major slope category was steep to very steep sloping land.

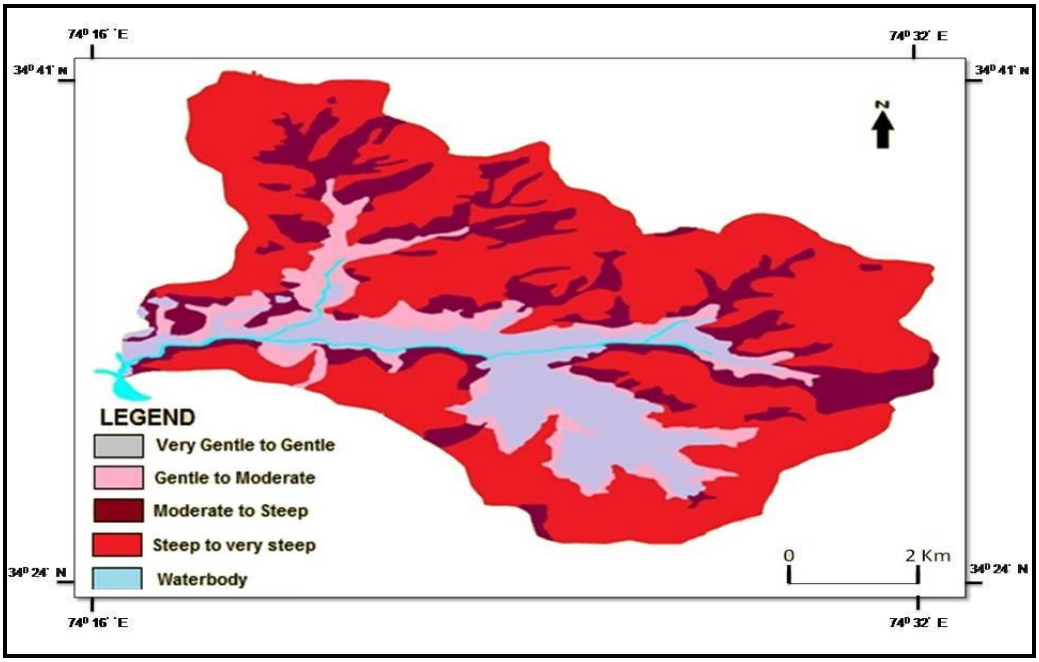


***Figure 4:*** *Slope Map of the Lolab Watershed*

### 3.3. Soil Texture

Soil texture map was prepared to comprehend erodibility characteristics of the soil in the study area, which plays a significant role in influencing the Sediment Yield for a particular mapping unit. A total of three soil texture classes were delineated, out of which the fine loamy soil was the major class which accounted for 79.58 percent of the total area of the watershed and was followed by fine silty soil with 16.53 percent of the total area. The percentage wise description is shown in Table 1.

***Table 1:*** *Soil Texture Classes and Their Percentage*

| S. No. | Classes | Percentage |
|---|---|---|
| 1 | Fine Loamy soils | 79.58 |
| 2 | Fine Silty Soils | 16.53 |
| 3 | Fine Silty to Fine Soils | 3.89 |

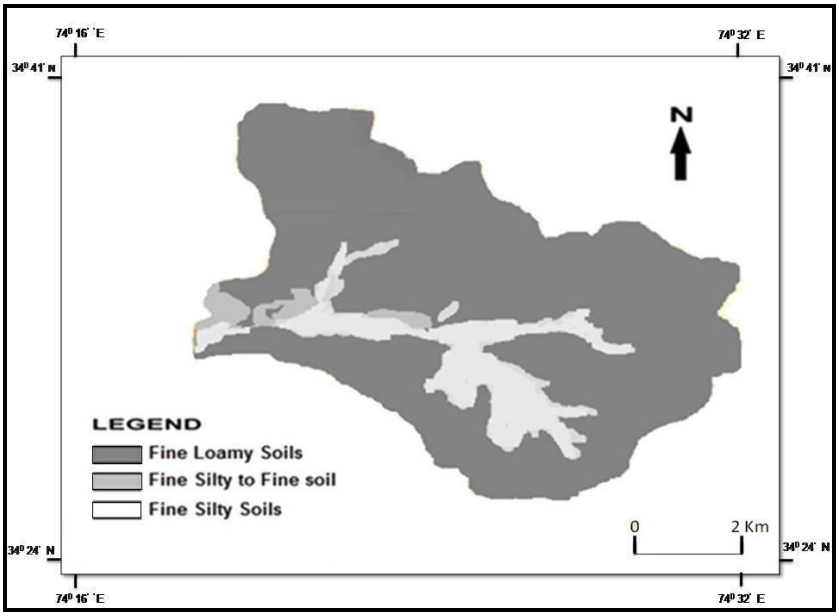


***Figure 5:*** *Soil Texture Map of the Study Area*

### 3.4. Soil Erosion Status

Degradation of agricultural land by soil erosion is worldwide phenomenon leading to loss of nutrient rich surface soil, increased runoff from more impermeable sub soil and decreased water availability to plants. Thus, estimation of soil loss and identification of critical areas for implementation of best management practice is central to the success of all soil conservation programmes. A soil erosion map (Figure 6) was prepared with four soil erosion classes. The major class of erosion was Slight to Moderate erosion with 49 percent followed by Moderate to Severe class with 30 percent area. The percentage wise break up of erosion classes is given in Table 2.

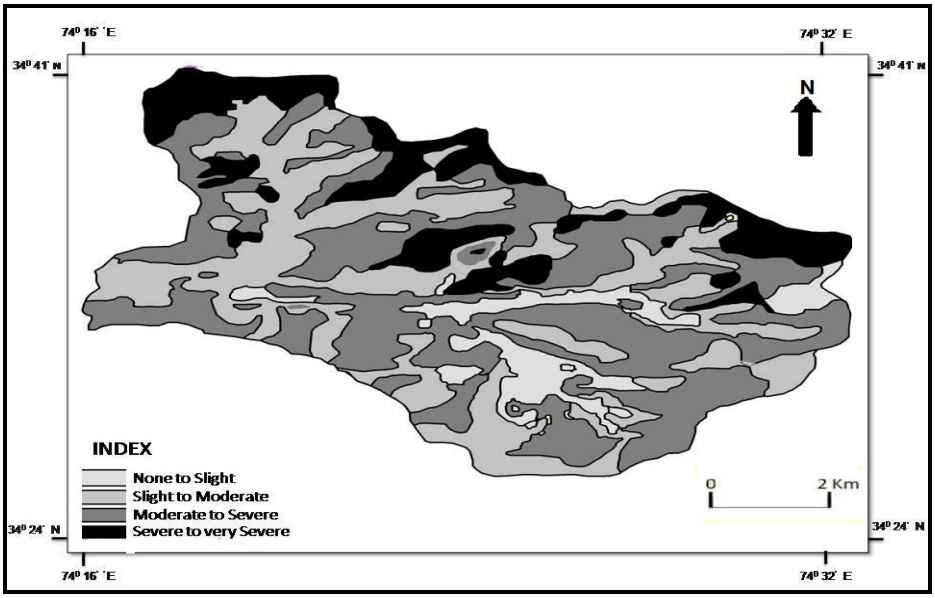


***Figure 6:*** *Soil Erosion Map of the Study Area*

***Table 2:*** *Soil Erosion Classes and their Percentage*

| S. No. | Soil Erosion classes | Percentage |
|---|---|---|
| 1 | None to Slight | 7 |
| 2 | Slight to Moderate | 49 |
| 3 | Moderate to Severe | 30 |
| 4 | Severe to very Severe | 14 |

### 3.5. Prioritization of Micro-Watersheds in Lolab Watershed

Considering the massive investment in the watershed development programmes, it is important to plan the activities on priority basis for achieving fruitful results, which also facilitates, in addressing the problematic areas to arrive at suitable solutions. The resource based approach is found to be realistic for watershed prioritization since it involves an integrated approach. Sediment Yield Index model (SYI) has been used in the present study area to prioritize the micro-watershed of Lolab Watershed. The Erosion Intensity Mapping Units (EIMU) were assigned with their respective weightage values and delivery ratios on the basis of methodology devised by AIS & LUS which takes into account the different characteristics of each mapping unit such as physiography, slope, soil texture, erosion class, management status, soil colour, surface condition, land use / land cover etc.

The Sediment Yield Index was calculated by using the empirical formula:

$$SYI = \frac{\sum_{i=1}^{i=n} (Ae1 \times We1 \times De1) \times 100}{AMW}$$

Where,
SYI= Sediment Yield Index
Ae1= Area (ha) of ith Erosion Intensity Mapping Units
We1= Weight age value of the Erosion Intensity Mapping Unit
De1= Delivery Ratio of ith Erosion Intensity Mapping Unit
AMW= Total area of the micro-watershed

The Sediment Yield Index of forty three micro watersheds along with their relative priority is given in the Table 3.

***Table 3:*** *Sediment Yield Index (SYI) of Micro-Watersheds in Lolab Watershed*

| S. No. | Hydrologic unit | Area in ha. | Sediment Yield Index (SYI) | Relative Priority |
|---|---|---|---|---|
| 1. | 1EIB6m1 | 1474 | 4397.78 | 1 |
| 2 | 1EIB6m2 | 1660 | 1471.27 | 3 |
| 3 | 1EIB6m3 | 1548 | 1163.06 | 16 |
| 4 | 1EIB6n1 | 676 | 2090.442 | 2 |
| 5 | 1EIB6n2 | 1115 | 1129.63 | 20 |
| 6 | 1EIB6n3 | 865 | 1296.34 | 6 |
| 7 | 1EIB6n4 | 1081 | 1190.10 | 14 |
| 8 | 1EIB6n5 | 1105 | 1242.61 | 9 |
| 9 | 1EIB6n6 | 824 | 1240.83 | 11 |
| 10 | 1EIB6n7 | 1406 | 1254.66 | 7 |
| 11 | 1EIB6p1 | 904 | 857.04 | 40 |
| 12 | 1EIB6p2 | 1331 | 884.28 | 39 |
| 13 | 1EIB6p3 | 979 | 977.591 | 34 |
| 14 | 1EIB6q1 | 1441 | 985.15 | 33 |
| 15 | 1EIB6q2 | 950 | 1123.90 | 21 |

| | | | | |
|---|---|---|---|---|
| 16 | 1EIB6q3 | 1429 | 1438.62 | 4 |
| 17 | 1EIB6r1 | 665 | 1170.23 | 15 |
| 18 | 1EIB6r2 | 678 | 805.46 | 41 |
| 19 | 1EIB6r3 | 579 | 1137.24 | 18 |
| 20 | 1EIB6s1 | 1507 | 1146.365 | 17 |
| 21 | 1EIB6s2 | 644 | 1086.56 | 25 |
| 22 | 1EIB6s3 | 1038 | 1230.06 | 12 |
| 23 | 1EIB6s4 | 4032 | 268.49 | 43 |
| 24 | 1EIB6t1 | 908 | 1133.65 | 19 |
| 25 | 1EIB6t2 | 1015 | 1048.67 | 28 |
| 26 | 1EIB6t3 | 892 | 1102.20 | 23 |
| 27 | 1EIB6t4 | 675 | 1223.41 | 13 |
| 28 | 1EIB6t5 | 710 | 957.08 | 35 |
| 29 | 1EIB6t6 | 1270 | 1319.60 | 5 |
| 30 | 1EIB6u1 | 1153 | 913.85 | 36 |
| 31 | 1EIB6u2 | 1415 | 891.50 | 38 |
| 32 | 1EIB6u3 | 1083 | 1057.98 | 27 |
| 33 | 1EIB6u4 | 801 | 1242.21 | 10 |
| 34 | 1EIB6u5 | 1042 | 896.84 | 37 |
| 35 | 1EIB6v1 | 781 | 770.89 | 42 |
| 36 | 1EIB6v2 | 1547 | 1021.43 | 29 |
| 37 | 1EIB6v3 | 939 | 1245.62 | 8 |
| 38 | 1EIB6v4 | 1374 | 1021.23 | 30 |
| 39 | 1EIB6v5 | 1543 | 1098.96 | 24 |
| 40 | 1EIB6k1 | 726 | 1016.46 | 31 |
| 41 | 1EIB6k2 | 932 | 1081.82 | 26 |
| 42 | 1EIB6k3 | 1157 | 1112.06 | 22 |
| 43 | 1EIB6k4 | 660 | 986.01 | 32 |

The Sediment Yield Index (SYI) pertaining to all 43 micro-watersheds of Lolab watershed were estimated. The micro-watersheds were arranged with respect to the decreasing order of their SYI and graded into three categories as high, medium and low on the basis of SYI range as given in Table 4.

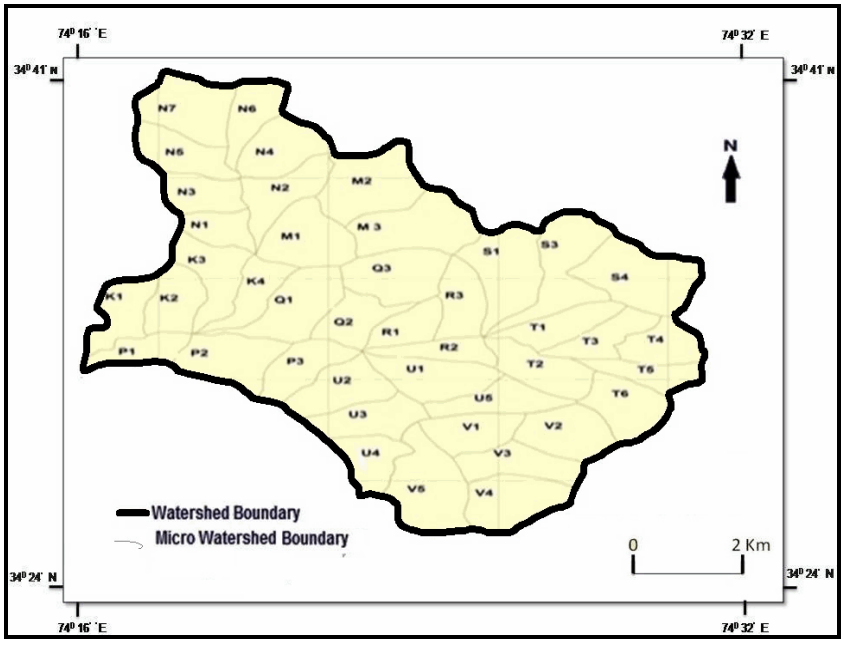


***Figure 7**: Micro-Watershed Index Map of the Study Area*

***Table 4**: Weightage Values and Delivery Ratios of Erosion Intensity Mapping Units (EIMU) considered for calculating Sediment Yield Index (SYI) of Lolab Micro-watersheds*

| S. No. | Erosion Intensity Mapping Unit | Weightage Value | Delivery Ratio |
|---|---|---|---|
| 1 | A1 | 12 | 0.56 |
| 2 | A2 | 14 | 0.60 |
| 3 | A3 | 15 | 0.63 |
| 4 | A4 | 12 | 0.57 |
| 5 | A5 | 17 | 0.70 |
| 6 | K2 | 18 | 0.70 |
| 7 | K3 | 15 | 0.64 |
| 8 | K4 | 19 | 0.77 |
| 9 | K5 | 13 | 0.60 |
| 10 | M1 | 20 | 0.85 |
| 11 | M2 | 13 | 0.67 |
| 12 | M3 | 17 | 0.69 |
| 13 | M4 | 20 | 0.81 |
| 14 | M5 | 14 | 0.70 |
| 15 | M6 | 18 | 0.82 |
| 16 | M7 | 17 | 0.74 |
| 17 | M8 | 13 | 0.64 |
| 18 | M9 | 19 | 0.78 |
| 19 | M10 | 13 | 0.60 |
| 20 | River | | |

**Source:** AIS & LUS; 2002

| S. No. | Priority Category | No. of Watersheds |
|---|---|---|
| **1.** | High | 13 |
| **2.** | Medium | 18 |
| **3.** | Low | 12 |
| **Total No. of Watersheds** | | 43 |

***Table 5**: Micro-Watersheds under Different Priority Categories with their SYI*

| High(1200 & above) | Medium(1000 to 1199) | Low(<1000) |
|---|---|---|
| M1(4397.78) | M3(1163.06) | P1(857.04) |
| M2(1471.27) | N2(1129.63) | P2(884.28) |
| N1(2090.44) | N4(1190.10) | P3(977.59) |
| N3(1296.34) | Q2(1133.90) | Q1(985.15) |
| N5(1242.61) | R1(1170.23) | R2(805.46) |
| N6(1240.83) | R3(1137.24) | S4(268.49) |
| N7(1254.66) | S1(1146.36) | T5(957.08) |
| Q3(1438.62) | S2(1086.56) | U1(913.85) |
| S3(1230.06) | T1(1133.65) | U2(891.50) |
| T4(1223.41) | T2(1046.67) | U5(896.84) |
| T6(1319.60) | T3(1102.20) | V1(770.89) |
| U4(1242.21) | U3(1057.98) | K4(986.01) |
| V3(1245.62) | V2(1021.43) | |
| | V4(1021.23) | |
| | V5(1098.96) | |
| | K1(1016.46) | |
| | K2(1081.82) | |
| | K3(1112.06) | |

Sediment Yield Index calculated reveals the state of erosion problems in the, Lolab watershed. Out of the total 43 micro-watersheds in the watershed, 13 are placed in the high priority category, 18 in medium category and 12 micro-watersheds are placed in the low category (Figure 8).

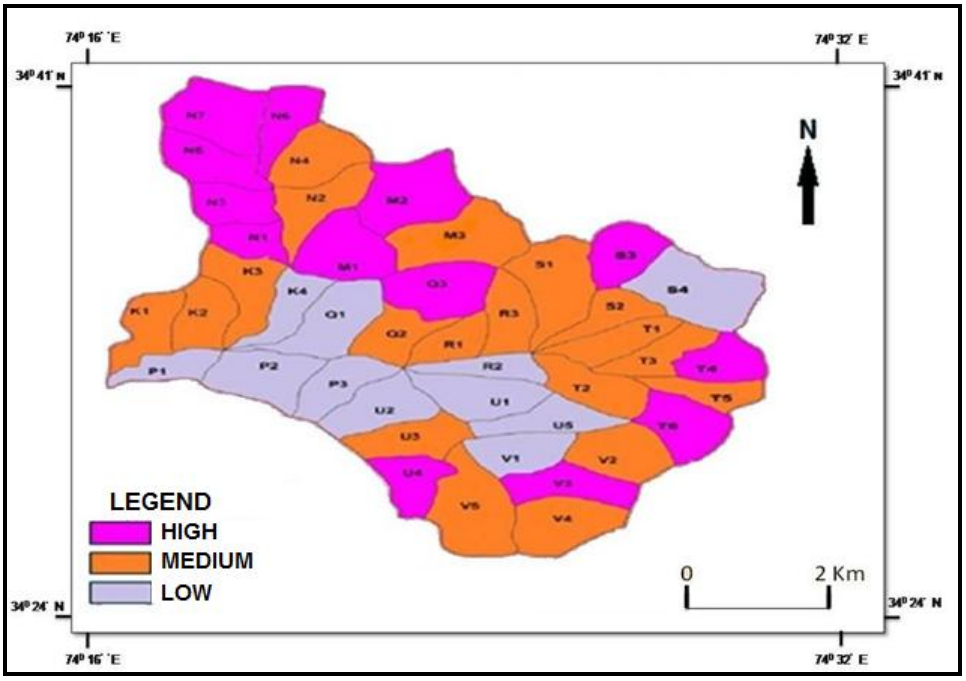


***Figure 8:*** *Micro-Watershed Prioritization Map of the Study Area*

## 4. Conclusion

Watershed prioritization plays a key role in planning and management for sustainable development programmes. The Lolab watershed of Kashmir valley comprising of fourty three micro-watersheds is facing severe soil erosion problems. In some of the micro-watersheds, the severity of the problem is more while as in some, moderate and slight but overall the situation is alarming. The micro-watersheds i.e. M1, M2, N1, N3, N5, N6, N7, Q3, S3, T4, T6, U4, and V3 fall in the high category where the slope is very steep of southern aspects, forests moderately dense and poorly managed, and the micro-watersheds i.e. M3, N2, N4, Q2, R1, R3, S1, S2, T1, T2, T3, T5, U3, V2, V4, V5, K1, K2, K3 fall in the medium priority categories, where slope is very steep of southern aspects, forests moderately dense, slight to moderate erosion, poorly managed, whereas, the P1, P2, P3, Q1, R2, S4, U1, U2, U5, V1 and K4 micro watersheds fall under the category of low priority where the slope is very gently to gently sloping flood plains, slight erosion and comparatively well managed. The prioritization of micro-watersheds for soil and water conservation measures would prove to be a very fruitful exercise for initiating remedial measures in accordance to the intensity and magnitude of the problem. It is one of the basic approaches for effective management of natural resources at the watershed level.

This priority determines the type of measures to be adopted for better management of natural resources. Both Engineering and Biological measures should be adopted to arrest this soil erosion within the watershed. In terms of engineering measures, Crate Wire Mashes should be resorted in nallas having wide cross section up to an extent of 8 meters, stream bank protection by constructing wire crates opposite to direction of flow and strike against stream banks. Besides these measures, construction of Landslide/slip control, Gunny bag check dams, Bench terracing, Silt traps, construction of Bypass Channels and Settling basins should also be initiated depending upon the intensity of erosion. In biological measures, conservation measures like Direct Sowing, Afforestation, Patch

Sowing, Rotational Grazing, and Vegetative Barriers in contour furrows etc. should be initiated in accordance to the severity of the problem.

## References


[1] Anonymous. *Report on Demarcation of Priority Watersheds in Pohru River Valley Project Catchment 2002*. AIS & LUS. Ministry of Agriculture, Report No. 1249. 5-6.

[2] Bayramin, I., Dengiz, O., Baskan, O., and Parlak, M. *Soil Erosion Risk Assessment with ICONA Model: Case Study Beypazari Area*. 2003. http://journals.tubitak.gov.tr/Agriculture/issues/tar-03-27- 2/tar-27-2-7-0211-3.pdf.

[3] Food and Agriculture Organization (FAO). *Soil and Water Conservation in Semi-Arid Areas*. 1987.

[4] Gupta, P., and Uniyal, S. *Watershed Prioritization of Himalayan Terrain, Using SYI Model*. International Journal of Advancement in Remote Sensing, GIS and Geography. 2013. 1 (1) 42-48.

[5] Jain Manoj, K., Mishra Surendra, K., and Shah, R.B. *Estimation of Sediment Yield and Areas Vulnerable to Soil Erosion and Deposition in Himalayan Watershed using GIS*. Current Science. 2010. 98 (2) 25.

[6] Khan, M.A., Gupta, V.P., and Moharana, P.C. *Watershed Prioritization using Remote Sensing and Geographical Information System: A Case Study from Guhiya*. Ind.J.Ari. Environ. 2001. (49) 456-475.

[7] Kothyari, U.C., and Jain Sanjay, A.J. *Sediment Yield Estimation using GIS.* Hydro. Sci. J. Sci. Hydrologique. 1997. 42 (6) 833-844.

[8] Lufafa, A., Tenywa, M.M., and Isabirye, M. *Prediction of Soil Erosion in a Lake Victoria basin Catchment using a GIS-based Universal Soil Loss model*. Agric Syst. 2003. 76; 883-894.

[9] Suresh, M., Sudhakar, S., Tiwari, K.N., and Chowdhary, V.M. *Prioritisation of Watersheds using Morphometric Parameters and Assessment of Surface Water Potential using Remote Sensing*. Journal of Indian Society of Remote Sensing. 2004. 31 (1) 25-35.

[10] Singh, R.K, Saha, S.K and Kumar, S. *Soil Conservation Prioritization of Watershed based on Erosional Soil Loss and Morphometric Analysis using Satellite Remote Sensing & GIS-A Case Study*. Indian Institute of Remote Sensing (NRSA), Dehradun: Map India, 2005.

[11] Vito A.V. *ASCE-Manuals and Reports on Engineering Practice*. 54. Sedimentation Engineering. 1975. 745.

**Cloud Publications**
International Journal of Advanced Remote Sensing and GIS
2014, Volume 3, Issue 1, pp. 660-668, Article ID Tech-267
ISSN 2320 - 0243

Cloud Publications

**Research Article** **Open Access**

# Specialized Mapping using Climatic Zones for Habitat Conservation

**Suneet Naithani and V.B. Mathur**

Wildlife Institute of India, Dehradun, Uttarakhand, India

Correspondence should be addressed to Suneet Naithani, suneetnaithani@gmail.com

Publication Date: 25 July 2014

Article Link: http://technical.cloud-journals.com/index.php/IJARSG/article/view/Tech-267



**Abstract** Mapping of vegetation strata in Great Himalayan National Park Conservation Area (GHNPCA) was conducted using Remote Sensing and GIS. Mapping of major vegetation communities was done by using satellite imageries (FCC of IRS 1-B LISS II Sept/Oct 1993, scale 1:50,000). Ground truthing was carried out for preparation of interpretation key and classification scheme. Mainly the 11 Forest and 11 Non-Forest classes have been delineated in two density classes, viz., close forest (> 40% Canopy cover) and open forest (< 40-10% Canopy cover) for the entire study area. The total area of GHNPCA is estimated to be 1171 $km^2$. On the basis of Climate zoning using contours as climate separators, finally the 14 vegetation classes and 11 non-forest classes were generated including Temperate, Sub-Alpine and Alpine forests and grasslands, while slope grasses around habitation occupy 28.13 $km^2$. Escarpments including exposed rocks with slope grasses and Alpine Exposed Rocks with Slope Grasses are 211.12 $km^2$. The area under glaciers and snow is estimated to be 18.68 $km^2$ and 183.87 $km^2$ respectively. Grasslands form the highest cover in the GHNPCA and cover about 18.9% of the total area. Temperate Mixed Forests occupy majority of the forests is about 17.01% of the total area. The conservation area is also dominated by Alpine Grassland i.e. about 193, 89 $Km^2$. The main upper storey species in conifers are *Pinus wallichiana, Abies pindrow, Picea smithiana, Cedrus deodara, while broad leaved species Asculus indica, Quercus semecarpifolia, Quercus dietata, Betula utilis* are dominant in the study area. The information generated through vegetation mapping valuable for park authorities and can be correlated with the distribution of fauna and avifauna in different habitats. The specialized vegetation mapping on the basis of climatic zoning is seems to be useful for monitoring, assessing and as database will assist the wildlife managers in conservation of endangered species.

**Keywords** *Conservation; GHNPCA; Habitat; RS & GIS; Vegetation Mapping and Wildlife*

## 1. Introduction

Vegetation maps are precious as they are used as habitat maps for the characterization of ecosystem. The forest vegetation map is one of the parameter for assessing biodiversity. Therefore, qualitative and quantitative analysis of vegetation is required future monitoring. These plant community status maps also indicate the unique habitats in terms of disturbances and wealth. These maps have various

other applications in manmade and natural ecosystems for biodiversity characterization. The maps are of great importance for forest managers (stock mapping) and biomass estimation, wildlifers (Faunal studies) for long term monitoring. Monitoring is most crucial to evaluate the success of the management measures. For Great Himalayan National Park Conservation Area (GHNPCA) mapping of communities or habitats has been done to help Park Management to arrive at critical conservation strategies, specially seen in the context of biotic pressure from adjacent settlements for MFP collection, cattle grazing, illegal felling, poaching, and encroachment etc. in fast developing tourism and orchard in the valley of Kullu. The Conservation area represents unique biodiversity of cold region, a typical of Western Himalayas.

Conventionally the flora and vegetation has also been surveyed by (Bharti *et al*., 2011 & 2012; Singh and Rawat, 2000; Rawat and Singh, 2006). The significant works i.e. classification of forest formation by Champion and Seth (1968). In western Himalaya Polunin and Stainton (1984) dealt with the floristic and phytogeographical aspects. Recent studies on the flora and vegetation of high altitude areas of western Himalaya includes Behera *et al.,* (2000), Chandrashekhar *et al.,* (2003), Singh and Rawat (1999) and Kala *et al.,* (1997). With the emergence of technology and its capacities; repetitive coverage, mapping of inaccessible and large area within short time, the true picture of forest cover map emerges with reliable accuracy in mapping (Roy *et al*., 1992; Roy and Ravan, 1994). Mead *et al.,* (1981) and Roy (1996) has used satellite data habitat mapping. In this study to obtain the maximum contrast and phenological differences; vegetation mapping has been done using remotely sensed images.

## 2. Materials and Methods

### 2.1. Study Area

The GHNPCA encompasses nearly 1171 $km^2$ area including Sainj and Tirthan sanctuaries and the Eco-development Zone (EZ) lies between $31^0$33'00" N to $31^0$56'56" N lat., and $77^0$17"15" E to $77^0$52'05" E long., and altitude varies from 1344 to 6248 m. The GHNPCA typically exhibits temperate, sub alpine and alpine climate. Most of the area (approx 64%) falls above subalpine zone which remains snow covered during winter months. Broadly, three season can be recognised for the park area *viz*. summer (April to June), Rainy (July to September) and winter (October to March). The mean annual precipitation in western Himalaya at middle elevations ranges between 1000-2000 mm and more than half of it falls during rainy season and temperature of the area varies from minus 10°C to 35°C (Gaston *et al*., 1981).

The vegetation in the area is mainly temperate, sub-alpine and alpine. Based on the physiognomy and dominance, (Champion and Seth, 1968; Naithani, 2001) had also classified the area in 9 forest classes. The park is also known for its faunal diversity; 31 species of mammals (Vinod and Sathyakumar, 1999), 183 species of birds (Gaston *et al*., 1993; Ramesh *et al.,* 1999), and more than 125 species of invertebrates (Uniyal & Mathur, 1999).

### 2.2. Methodology

The forest type mapping has been done through visual interpretation of satellite data but hilly areas have shadow effect; hence many times it does not offer any clue except for ground truth collection. And realizing this fact intensity of the ground verification has been increased and information in shadow areas has been collected in the field and incorporated in mapping.

Reconnaissance survey was lead by preparation of base map. The study area is covered in 6 scenes and SOI toposheets etc. False Color Composites (FCC) of IRS –1B LISS II sensor, Geocoded data on 1:50,000 scales of September/October of 1993 have been used. During this process interpretation was tested and rectified where ever necessary along with maximum ground truth and the ground information like elevation. Interpretation key was finalized on the basis of tone, texture Physiographic,

altitude, type and vegetation association and with agreed classification; all thematic details have then been transferred to base map.

To meet the study objectives the classification scheme was designed. In higher Himalayas (GHNPCA), elevation has impact on the vegetation. The upper and lower temperate broadleaf forests have been merged together while temperate and alpine grasslands have been put together. However, with the help of contours these were separated in GIS domain. > 40% canopy cover has been delineated as closed forests and < 40% as open forest. Keeping in mind the requirement of wildlife habitats for future planning non-forest land cover has also been delineated. As per the classification scheme interpretation of satellite was finalized with the help of image elements like, tone, texture, association, location etc., and the ground features whereas the shadow areas were checked with ground verifications and appropriate rectification was performed accordingly. The final vegetation map was prepared on 1:50,000 scale. Overall 11 non-forest and 11 forest types were delineated.

## 3. Results and Discussion

Broad forest classes have been mapped in *e.g.* broadleaved forests of temperate zone, subtropical and temperate riverine forest were mapped together. Using elevation as the criteria these types can be broadly separated in GIS domain, consideration of elevation as important parameter as the vegetation changes with change in altitude. Grasslands are the most important as far as wildlife conservation and management is concern. They have also been treated as part of forest as these and are locally known as 'Thatch' or forest blanks. Total estimated area using GIS is about 1171 km$^2$. Northern aspects with higher moisture contents resulting rich unique flora. The general Landuse/cover map of the GHNP conservation is shown in Figure 1 with aerial estimation given in Table 1.

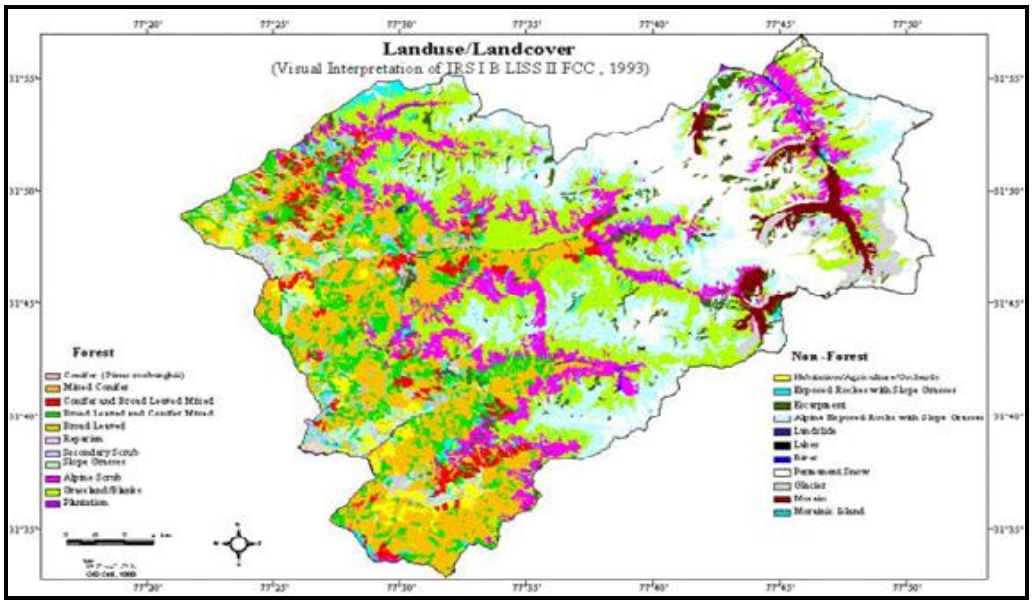


***Figure 1:*** *Landuse/Cover Map, Great Himalayan National Park Conservation Area*

***Table 1:*** *Aerial Estimation of Landuse/cover Categories in Great Himalayan National Park Conservation Area*

| S.N. | Type | Area in $Km^2$ |
|---|---|---|
| | **Forest** | |
| 1 | Conifer ( *Pinus roxburghii* ) | 2.08 |
| 2 | Mixed conifer | 127.98 |
| 3 | Conifer and Broad Leaved Mixed | 33.16 |
| 4 | Broad Leaved | 66.62 |
| 5 | Broad Leaved and Conifer Mixed | 83.36 |
| 6 | Riperian | 0.14 |
| 7 | Slope Grasses | 25.92 |
| 8 | Grasslands/ Blanks (Temp. sub Alpine & Alpine) | 221.80 |
| 9 | Secondary Scrub | 22.28 |
| 10 | Alpine Scrub | 117.62 |
| 11 | Plantation | 0.16 |
| | **Non Forest** | |
| 1 | Habitation/Agriculture/Orchards | 25.55 |
| 2 | Exp. Rocks with Slope Grasses | 27.60 |
| 3 | Alpine Exp. Rocks with Slope Grasses | 149.73 |
| 4 | River | 4.35 |
| 5 | Lakes | 0.87 |
| 6 | Escarpments | 33.82 |
| 7 | Landslide | 0.41 |
| 8 | Snow | 184.01 |
| 9 | Morian | 24.24 |
| 10 | Morainic Islands | 0.48 |
| 11 | Glaciers | 18.82 |
| | **Total** | 1171.00 |

Basically the data has been visually interpreted with 11 forest and 11 non forest classes but as per the species preferences (*Western Tragopan* and Himalayan *Musk Deer*), the specific forest types and grasslands have also been extracted. The logical knowledge based approach has been applied in grid module with the help of climatic zoning through GIS domain using ARC/INFO software. The basis of extraction was on altitudinal variations as shown in Figure 2.

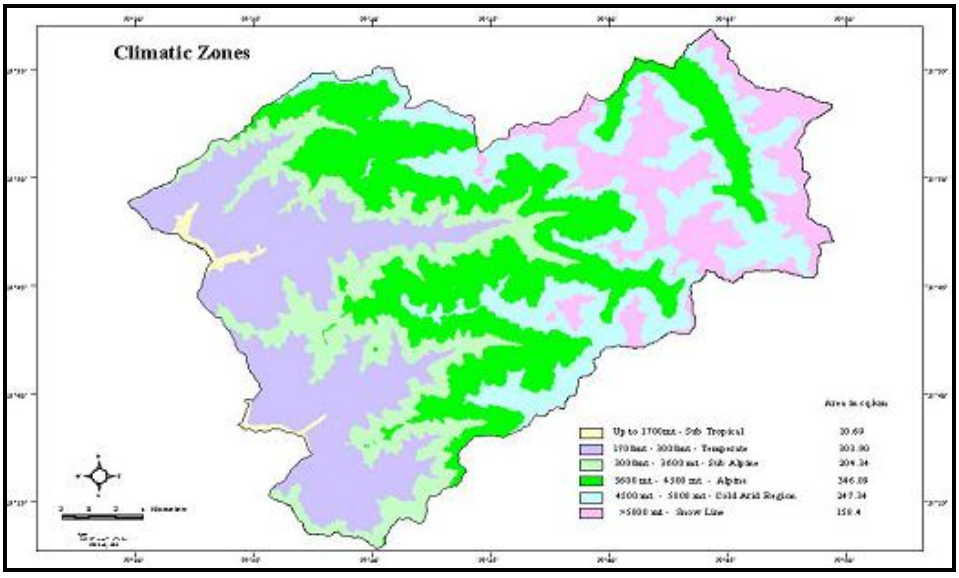


***Figure 2:*** *Climatic Zones on the Basis of Elevations (Champion and Seth, 1968)*

The general types of Broad-leaved forest and Grasslands have been extracted into sub-tropical to sub-alpine broad-leaved forest and sub-tropical to alpine grassland respectively. On the basis of users choice this approach can be applied for extracting the different categories as per the different objectives (14 forest and 11 non-forest classes). The landuse/cover map along with extracted classes through GIS can be seen through Figure 3 and Table 2.

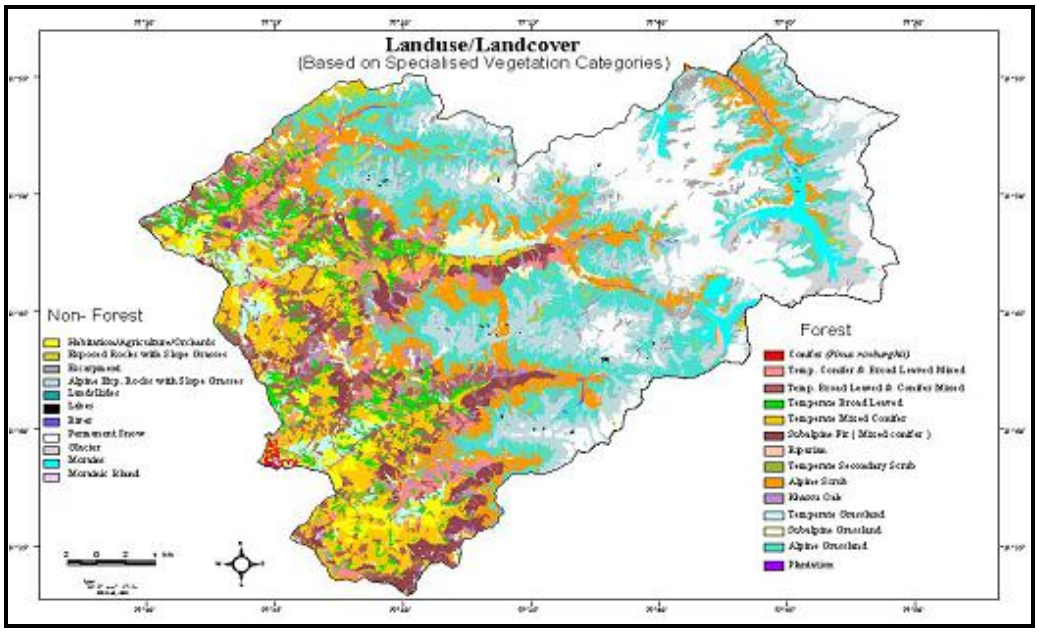


***Figure 3:*** *Specialized vegetation Categories, Great Himalayan National Park Conservation Area*

***Table 2:*** *Aerial Estimation of Vegetation Map Defining Additional Classes on the basis of Climatic Zoning*

| S.N. | Class | Area in km$^2$ | Percentage |
|---|---|---|---|
| 1 | Pinus Roxburghi | 2.1 | 0.18 |
| 2 | Temperate Mixed Conifer | 82.39 | 7.04 |
| 3 | Subalpine Fir | 39.11 | 3.34 |
| 4 | Temp. Conifer and Broad Leaved Mix | 33.21 | 2.84 |
| 5 | Temp. Broad Leaved and Conifer Mixed | 83.44 | 7.13 |
| 6 | Temp. Broad Leaved Forest | 42.95 | 3.67 |
| 7 | Kharsu Forest | 23.7 | 2.02 |
| 8 | Temp Grassland | 31.7 | 2.71 |
| 9 | Subalpine Grassland | 22.25 | 1.90 |
| 10 | Alpine Grassland | 193.89 | 16.56 |
| 11 | Riparian | 0.14 | 0.01 |
| 12 | Temp. Secondary Scrub | 22.26 | 1.90 |
| 13 | Alpine Scrub | 117.71 | 10.05 |
| 14 | Plantation | 0.16 | 0.01 |
| | **Non Forest** | | |
| 1 | Habitation/Orchard Agriculture | 25.53 | 2.18 |
| 2 | Escarpments | 33.69 | 2.88 |
| 3 | Exposed Rocks with Slope Grasses | 27.54 | 2.36 |
| 4 | Alpine Exposed Rocks with Slope Grasses | 149.89 | 12.80 |
| 5 | Land Slides | 0.42 | 0.04 |
| 6 | River | 10.78 | 0.92 |
| 7 | Morrain | 24.25 | 2.07 |
| 8 | Lakes | 0.86 | 0.07 |

| | | | |
|---|---|---|---|
| 9 | Moranic Island | 0.48 | 0.04 |
| 10 | Glacier | 18.68 | 1.58 |
| 11 | Snow | 183.87 | 15.70 |
| | **Total Area** | 1171.00 | 100.00 |

The delineation of specialized category with the help of contours particularly relevant in the spatial delimitation of subalpine forests, which is an ecotone between alpine grasslands and temperate forests. It also reveals the trends of climatic changes; this ecotone is valued as a unique habitat for representative, specialized, and sensitive elements, including distinct biological assemblages, native and endemic floral and faunal species, and richness of economically important species (Rawal and Dhar, 1997; Dhar, 2000). Subedi (2009) studied that under continuing climate change, tree species in these forests will be affected in different ways, and ranges will adjust at different rates and by different processes. Species have limited scope to move further in transition zones between the subalpine and alpine zones and are especially vulnerable to climate change (ICIMOD 2010).

Subtropical forests of Chir Pine (*Pinus roxburghii*) cover about 0.18% in Eco-development zone of the total area. Understory flora is less and is subjected to frequent fires and biotic pressure. Chir Pine forest occurs around Rolla, Sainj and Nevli villages. Temperate Mixed Conifer, Temperate Conifer Mixed with Broad Leaved and Temperate Broadleaf Mixed with Conifer Forests occupy majority of the forested land about 17.01% of the total area. Oaks are predominant species of these forests along with *Acer* sp. *Juglens regia, Rhododendron* sp. etc. Very good high density forests grow in the moist slopes (northern aspects) with rich understory and herbaceous plants with scattered *Taxus wallichiana*.

In complex terrain between subtropical and alpine areas the mixing of broadleaf and coniferous forests has been observed. Because of high moisture contents narrow gorges and valleys are supporting broadleaf forests whereas in drier regions coniferous forests are confined. 7% of the total forested areas are of this kind of forests. Broadleaf species like *Juglens regia, Prunus cornuta, Quercus semicarpifolia, Acer* sp., *Aesculus indica,* etc. and coniferous species like *Abies pindrew, Cedrus deodara, Picea smithiana, Pinus wallichii,* etc.

Alpine Grassland i.e. about 193.89 $Km^2$ is also dominating followed by Temperate Broad Leaved and Conifer Mixed is 83.44 $Km^2$ and Temperate Mixed Conifer is 82.39 $Km^2$; high biotic pressures (grazing). Scattered trees of *Picea smithiana* and *Pinus wallichii* with pure patches of *Cedrus deodara* were also near the area. These mixed forests have other species also like; *Taxus wallichiana* along with varying inter-mixing of broadleaf species as well. The pure patches of *Cedrus deoadara* and *Pinus wallichii* were also observed in Rolla-Shilt area with scattered *Taxus wallichiana.* Between Shilt to Rukhundi villages the patches of bamboo species with rich ground flora along with Lichens were also observed. Varying degree of species like, *Abies pindrew, taxus buccata, Quercus semecarpifolia, Acer acuinatum, Betula alnoides, Celtis sp.* are also observed.

In the subtropical and lower-temperate zones along with valleys covering an area about 1.90% dominated by secondary scrub and is associated with human activities. Between Nevli to Tung village the extensive scrub of *Berberis aristata* is spread on the southern slope. The villages like; Chipni, Galiyar, Bathad and Mashiyar were full of *Lonicera* sp. and *Indigofera* sp. (scrub vegetation) on the bunds and abandoned agricultural fields.

Between temperate forest and alpine vegetation the Alpine scrub (10.05%) was observed as transition. The dominant species are *Rhododendron companulatum and Betula utilis* as pure scrucb patches of *Betula utilis* around Rukhundi top and on northern aspects near Basleo pass. Dhela Thatch and Gumtarao area were observed with extensive growth of *Rhododendron companulatum* and *Betula-Rhododendron* scrub respectively.

Slope grasses mainly on the southern slope aspects have been observed around Baha in Sainj Valley and in Palachan Gad above Chipni village. In association with non-graminaceous plants, tall grasses like *Themeda triandra, Vitiveria ziznoides* etc. grow in the slopes and resting sites for shepherds are grasslands ('thatch'); mainly associated with ridges and peaks with a mixture of herbaceous plants and grasses like *Agrostis pilosila, Chrysopogon echinulatus, Themeda triandra, Andropogon* sp., *Oplismensus compositius and Paspalum* etc.

Subtropical and temperate zone villages and riverbeds were witnessed with Riverine forest in and around Rupa nala, Palachan gad, Dhela khad. Because of the shadow and very narrow belts along streams the mapping of these areas found difficult. The dominant subtropical Riverine species were observed; *Alnus nepalensis* and *Alnus nitida* as along with *Prunus* sp., *Pyrus* sp., *Girardinia* sp. and *Berberis* sp. *Hippophae;* the Temperate Riverine scrub were found before and after Shakti village. These grow along streams gregariously on raised riverbeds. The main species are *Rosa webbiana, Hippophae salicifolia and Sorberia tomentosa*. Viburnum sp. scrub was also marked during mapping between Shakti and Maror village.

Plantation forms only 0.01% of the area. Old plantation of *Pinus wallichiana* is in Jiva nala in Eco-development zone. About 40% of the total area is having less vegetation i.e. Exposed rocks (about 2.5%), Escarpments (2.88%), Alpine exposed rocks with slope grasses (12.80%), Moraine islands (0.04%), Glaciers (1.6%), Moraine (2%), Permanent Snow (15.7%) and Lakes (0.074%) etc., are important habitats for wildlife for fodder, shelter and breeding grounds.

## 4. Conclusion

Baseline information for vegetation cover i.e. 60% areas is under forests whereas non-forest area cover about 40% are equally important; a habitat of many species including endangered species whereas lakes are also the best sites for many wildlife including migratory avifauna. The information generated through vegetation mapping is valuable for park authorities and seems to be useful for monitoring, decision making and management and will also assist the wildlife managers in conservation of protected areas and their habitats.

## Acknowledgement

The corresponding author is working as an Assistant Professor, School of Environmental Studies and Natural Resources (SENR), Doon University whereas the second author is presently The Director, Wildlife Life Institute of India. We express our gratitude to the Director, Wildlife Institute of India (WII) for initiating this project under Forestry Research Education and Extension Project (FREEP) funded by World Bank, was initiated by Himachal Pradesh Department of Forest Farming and Conservation (HPDFFC). We are also thankful to Director and Dr. Sarnam Singh, Scientist, Indian Institute of Remote Sensing (IIRS), Dehradun for providing logistic support and guidance respectively.

## References

Behera, M.D., Srivastava, S., Kushwaha, S.P.S., and Roy, P.S. *Stratification and Mapping of Taxus baccata L. Bearing Forests in Talle Valley Using Remote Sensing and GIS*. Current Science. 2000. 78; 1008-13.

Bharti, R.R., Adhikari, B.S., and Rawat, G.S. *Assessing Vegetation Changes in Timberline Ecotone of Nanda Devi National Park, Uttarakhand*. International Journal of Applied Earth Observation and Geoinformation. 2012. 18; 472-9.

Bharti, R.R., Rai, I.D., Adhikari, B.S., and Rawat, G.S. *Timberline Change Detection Using Topographic Map and Satellite Imagery*: A Critique. Tropical Ecology. 2011. 52; 133-7.

Champion, H.G., and Seth, S.K., 1968: *A Revised Survey of Forest Types of India*. Manager of Publications, Government of India, New Delhi. 404.

Chandrasekhar, M.B., Singh, S., and Roy, P.S. *Geospatial Modeling Techniques for Rapid Assessment of Phytodiversity at Landscape Level in Western Himalayas, Himachal Pradesh*. Current Science. 2003. 84; 663-70.

Dhar, U., 2000: *Prioritization of Conservation Sites in the Timberline Zone of West Himalaya. I*n: Setting Biodiversity Conservation Priorities for India. S., Singh, A.R.K., Sastry, R., Mehta, and V., Uppal (Eds). New Delhi: BCPP Process Document WWF India. 193-211.

Gaston, A.J., Hunter, M.L., and Garson, P.J., 1981: *The Wildlife of Himachal Pradesh, Western Himalayas*. Report of the Himachal Wildlife Project. The Notes No. 82, School of Forest Resources. University of Maine, Orono. 159.

Gaston, A.J., Garson, P.J., and Pandey, S. *Birds Recorded from Great Himalayan National Park, Himachal Pradesh, India*. Forktail. 1993. 9; 45-57.

ICIMOD, 2011: *Climate Change Impact and Vulnerability in the Eastern Himalayas-Synthesis Report.* Kathmandu, Nepal. Accessed December' 29. http://books.icimod.org/index.php/search/publication/696.

Kala, C.P. Rawat, G.S. and Uniyal, V.K., 1997: *Ecology and Conservation of Valley of Flowers National Park, Garhwal Himalaya*. WII Report, Dehra Dun. 761.

Mead, R.A., Sharik, T.L., Prisely, S.P., and Heinen, J.T. *A Computerized Spatial Analysis System for Assessing Wildlife Habitat from Vegetation Maps*. Canadian Journal of Remote Sensing. 1981. 7; 395-400.

Naithani, S., 2001: *Habitat Characterization in Great Himalayan National Park Using Remote Sensing and Geographical Information System (GIS) Technologies with Special Emphasis on Geobotanical Aspects.* Ph.D. Thesis. Wildlife Institute of India, Dehradun. 150.

Polunin, O., and Stainton, 1984: *Flowers of Himalaya*. Oxford University Press, New Delhi. 580.

Ramesh, K., Sathayakumar, S., and Rawat, G.S., 1999: *Ecology and Conservation Status of Pheasants of the Great Himalayan National Park, Western Himalayas.* Report Submitted to Wildlife Institute of India. 85.

Rawal, R.S., and Dhar, U. *Sensitivity of Timberline Flora in Kumaun Himalaya, India: Conservation Implications*. Arctic and Alpine Research. 1997. 29; 112-21.

Rawat, G.S., and Singh, S.K. *Structure and Composition of Woody Vegetation along the Altitudinal and Human Use Gradients in Great Himalayan National Park, North-western Himalaya.* Proc. Natl. Acad. Sci., India, Sect. B. 2006. 76; 194-201.

Roy, P.S., 1996: *Geographic Information System.* Lecture Notes on Application of GIS and Remote Sensing Workshop in Wildlife Management, WII, Dehradun. 23-33.

Roy, P.S., Porwal, M.C., Singh, S., Negi, D.S., and Kumar, K., 1992: *Grassland Mapping Using Satellite Remote Sensing in Alpine Zone.* Pilot Project in Kinnaur District (H.P.). IIRS Project Report, Dehradun. 1-29.

Roy, P.S., and Ravan, S.A. *Habitat Management for Biodiversity Maintenance using Aerospace Remote Sensing*. Tropical Ecology. 1994. 309-345.

Singh, S.K., and Rawat, G.S., 2000: *Flora of Great Himalayan National Park*, Bishen Singh Mahendra Pal Singh, Dehradun.

Singh, S.K., and Rawat, G.S., 1999: *Floral Diversity and Vegetation Structure in Great Himalayan National Park, Western Himalayan*. Final Report. Wildlife Institute of India, Dehradun. 131.

Subedi, M.R. *Climate Change and Its Potential Effects on Tree Line Position: An Introduction and Analysis*. The Greenery–A Journal of Environment and Biodiversity. 2009. 7; 17-21.

Uniyal, V.P., and Mathur, P.K., 1999: *A Study on the Species Diversity among Selected Insect Groups*. Final Technical Report. Wildlife Institute of India, Dehradun. 63.

Vinod, T.R., and Sathayakumar, S., 1999: *Ecology and Conservation of Mountain Ungulates in Great Himalayan National Park, Western Himalaya.* Final Report. Wildlife Institute of India, Dehradun. 92.

**Cloud Publications**
International Journal of Advanced Remote Sensing and GIS
2014, Volume 3, Issue 1, pp. 592-597, Article ID Tech-273
ISSN 2320 - 0243

Cloud Publications

Case Study | Open Access

# Utilization of Resourcesat LISS IV Data for Infrastructure Updation and Land Use/Land Cover Mapping - A Case Study from Simlipal Block, Bankura District, W. Bengal

**V.S.S. Kiran[1], Y.K. Srivastava[2] and M. Jagannadha Rao[3]**

[1]IIC Academy, IIC Technologies Ltd., Visakhapatnam, Andhra Pradesh, India
[2]Scientist-SE, ISRO, RRSC- East, Kolkata, West Bengal, India
[3]Delta Studies Institute, Andhra University, Visakhapatnam, Andhra Pradesh, India

Correspondence should be addressed to V.S.S. Kiran, vsskiran_rsgis@rediffmail.com

Publication Date: 26 May 2014

Article Link: http://technical.cloud-journals.com/index.php/IJARSG/article/view/Tech-273



**Abstract** Rapid population growth and anthropogenic activities on earth is effecting the natural environment profoundly. Hence, an attempt has been made in this paper; a case study has been taken up for Simlipal block of Bankura District of W. Bengal. This is to understand changes in Land use/Land cover and infrastructure development particularly in plain and community development area. For this purpose the infrastructure, Land use/Land cover, drainage, slope, aspect and contour maps have been prepared using SRTM (54/08) data of the study area. Besides this an attempt has been made to prepare LU/LC maps from multispectral remote sensing digital data sets of IRS-1C LISS-III & IRS-P6 LISS-IV, applying DIP techniques and Alarm masking technique for MAXLIK & MINPAR supervised classification as well as to prepare Infrastructure map applying to raster based vector classification and spatial data extraction method. NDVI method was used for the classification of water and forest classes. It is established that the Infrastructure output map and Land use/Land cover output maps can be used for systematic urban development of the study area.
**Keywords** *Alarm Masking; LU/LC Classification; Arc GIS; ERDAS*

## 1. Introduction

Land is one of the most important natural resources and hence all developmental activities are based on it. Landuse refers to the type of utilization to which man has used the land for his daily activities like socio economic activity, urban and agricultural activity and this evaluation of land with respect to various natural characteristics. But the Landcover refers to the type of land which is covered by the physical material at the surface of the earth. Landcover includes grass, asphalt, trees, forest, built up area, bare ground, water, lake etc. Landuse/Landcover and infrastructure are essential for planners, decision makers and those concerned with land resource management also this valuable information is very much helpful for monitoring and sustainable management of the urban environment (Jensen,

J.R, 1999). Rapid population growth and anthropogenic activities have significant impact on our ecosystems and its present conditions. Accurate and updated information on the status and trends of ecosystems is required to develop strategies for sustainable development and to improve the livelihood. The ability to monitor land-cover/land-use & infrastructure is highly desirable by local communities and by policy decision makers. With increased availability and improved quality of multi-spatial remote sensing data as well as ground details and new analytical techniques, it is now possible to monitor changes in Landuse/Landcover and infrastructural developmental data.

## 2. Study Area

Simlapal is a community development block is in Khatra subdivision of Bankura district in West Bengal state, and it is bounded by the Khatra block in west, Taldangra block in north, Sarenga block is south and also covered west Midnapur district in east. The block consists of rural areas with seven gram punchayats (Bikrampur, Dubrajpur, Lakshmisagar, Machatora, Mondalgram, Parsola and Simlapal) covered 203 villages, two police stations and three headquarters. Area of this block is 309.20 sq. kms (119 sq. mile or 1144.04 hectares). Location Map of study area is presented in Figure 1.

### 2.1. Geographic Location

This block is geographically extended from 22˚59'38.84" North to 22˚50'34.42" North latitude and 86˚55'20.15" to 87˚13'06.10" East longitudes. It has an average elevation 57 mts (187 feet). This block is covered by 73J/13 & 73N/1 Survey of India reference maps on 1:50,000 scale. Bankura district is lies on the western part of West Bengal having 7.75% of state's geographical area and 3.98% of states demographic profile.

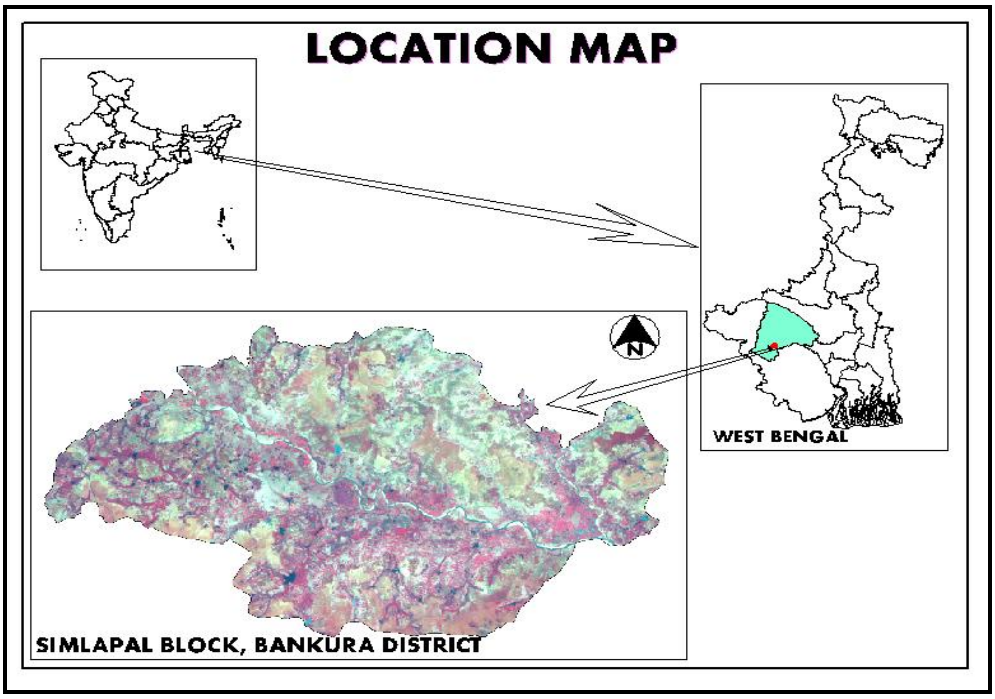


***Figure 1:*** *Location Map of the Study Area*

### 2.2. Demography

As per 2001 census Simlapal community development block has a total population of 1,27,429 of which 65,328 males and 62,101 females. The population density is 310.15 per sq. kms area and its growth rate is 14.48% from the period of 1991-2001. Simlapal has also the population of total schedule

caste and schedule tribe. The population of schedule caste 33,461 and schedule tribe is 18,821. As the sex ratio of 952 females per 1000 males in 2001 census and 953 females per 1000 males in 1991 census. Literacy level of the block is 71% in 2001 census. The male literacy is 58% of total male population of Simlapal and female literacy is 76% of total female population of Simlapal.

### 2.3. Climate

Climate condition of the Simlapal block is tropical as situated in the southeastern part of Bankura district. Seasonal climatic conditions are; winter from November to February, summer from March to May and Rainy season from June to October. The average rainfall is about 1750 mm out of which 1025 mm during June to September. The wind speed of this block varies from time to time and it is atmospheric depended which plays very vital role to contribute in environmental activities. The maximum wind speed is 3.42 km/hr in the month of July and minimum 0.03 km/hr in the month of January. The maximum average wind speed is 1.38 km/hr in the month of July. The maximum temperature of area is 44.6˚c and minimum temperature of the area 6.7˚c.

## 3. Methodology

Remote Sensing and GIS tools have been used for the processing of digital images and preparing of thematic maps. GIS was used as added tool for preparation of many vector layers. Using all thematic maps and GIS information. IRS LISS-IV Data geometrically corrected with reference to already geo-corrected IRS LISS-III Data keeping RMS Error within the range of sub-pixel and output image was resample using nearest neighborhood resampling method (Congalton, K., and Green, A., 1999). The Lambert Conformal Conic projection was used with Everest coordinate system. An AOI (Area of interest) layer of the study area was prepared and applied to IRS LISS-IV data for extraction of the study area. Few enhancement techniques were applied to visually enhance the quality of the image. It was found that linear enhancement algorithms were best suited to identify various features of the study area as well as tonal boundaries of look-alike features. The methodology can be divided into two parts one is rasterization and other one is vectorization. The vectorization process created vector coverages like; administrative boundaries (i.e. block and village boundaries), drainage layers, infrastructure layer (i.e. metal & un-metal roads, water bodies, settlement, canal, sluice, river) and also forest boundaries etc. The rasterization involves creation of sub-setting of image, mosaicking, image enhancement, NDVI techniques, image classification, recoding and reclassification etc., (Lunetta, R., 2006). The calculation parameters were derived from the generated raster and vector layers. For infrastructure layer extraction purpose proper enhancement techniques were applied to enhance the details of drainage with shuffling of different band combination like 4, 1, 2 and 2, 1, 3 and 4, 1, 4. This improves visualization of drainage. LISS–IV data was classified using supervised classification techniques with maximum likelihood algorithm for the preparation of land use/ land cover map. The classification of the imageries was performed by using supervised classification. In this particular type of classification signature extraction are first, based solely on the DN information in the data, and are then matched by the analyst to overall image using Alarm masking technique. Supervised classifiers is utilize training sets basis for classification. Rather it involve algorithms called Maximum likelihood or Minimum Parallelepiped algorithms, that examine the known pixels in an image and aggregate them into a related classes based on the user selection in the image values (Kumar, P., 2010). Thus supervised classification, it starts with a pre-determined set of classes, and it is done completely with human intervention. The entire methodology which has been adopted in this study is explained in the flow chart (Figure 2). Source data details are presented in table (Table 1). The study area is covered by 73J/13 & 73N/1 Survey of India Toposheets on 1:50,000 scales and IRS LISS III & IV satellite imagery with 23.5 and 5 meter resolutions, which was acquired on 17th February 2003 and 21st January 2007 with path and row of 107/56 & 102/56 were used as source data.

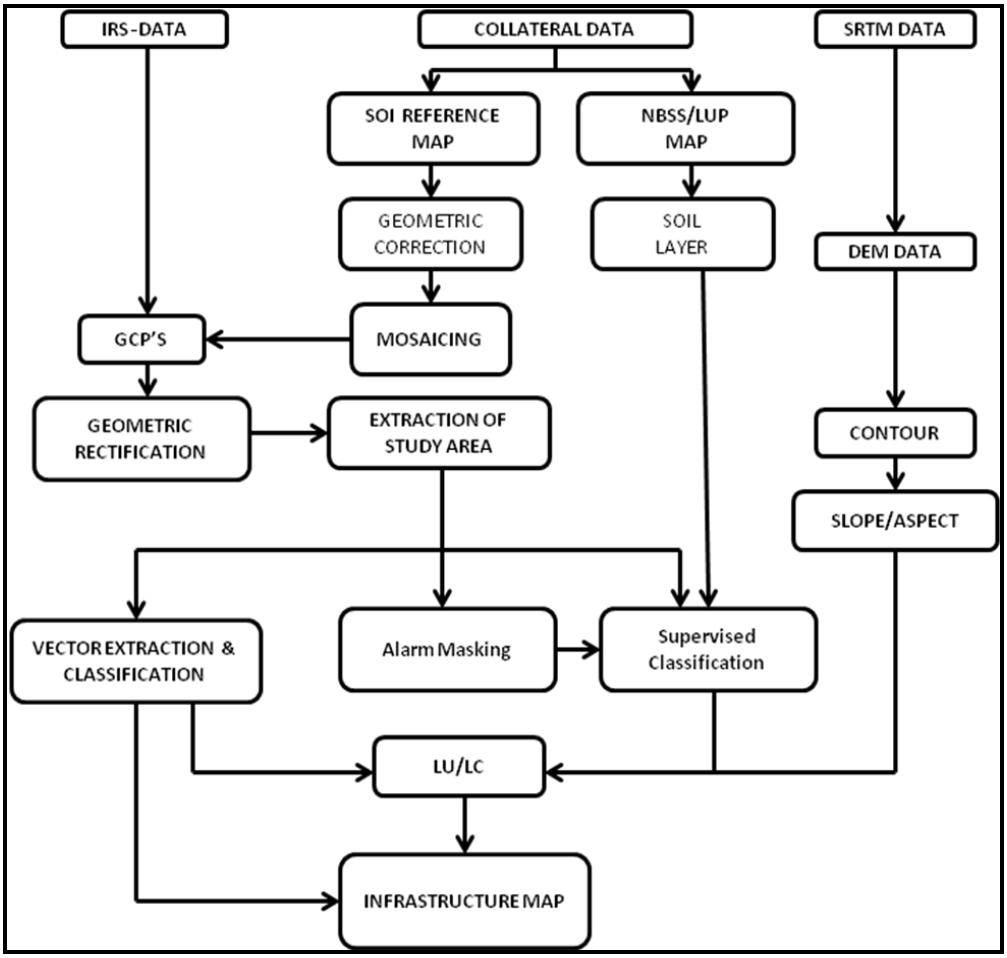


***Figure 2:*** *Methodology of Study*

***Table 1:*** *Land Use-Land Cover Classification Scheme*

| Type of Data | Details of Data | | | | Source of Data |
|---|---|---|---|---|---|
| SOI Reference Maps | 73 J/13, 73 N/1, (scale 1:50,000) | | | | SOI, RRSC-East |
| Thematic maps: Soil Map | (Scale 1:5,00,000) | | | | NBSS/LUP,RRSC-E |
| DEM DATA(SRTM) | 90mtr Resolution, Path/row - 54/08 | | | | SRTM Website |
| Remote Sensing digital data sets of IRS-1C-LISS-III & IRS-P6-RESOURCESAT – LISS-IV | **LISS-III** | | **LISS-IV** | | Regional Remote Sensing Service Center (RRSC-E), |
| | Scene | Date | Scene | Date | |
| | 107/55 | 04/03/2002 | 101/79 | 23/12/2006 | |
| | 107/56 | 17/02/2003 | 101/80 | 23/12/2006 | |
| | | | 102/56 | 21/01/2007 | |

## 3. Results, Discussion and Conclusion

A NDVI (Normalized Difference Vegetation Index) indices was performed to derive the class in the forest area and water-bodies. As all the LISS–IV scenes were acquired in the different time interval hence, each was separately used for NDVI and then desired classes were sliced while clubbing other classes. Final NDVI map was overlaid on the classified image to represent the classes which were not considered during the supervised classification. A supervised classification technique was adopted with maximum likelihood algorithm. Due care was taken in generating the signature sets for the

desired classes and where validated with the error of omission and error of commission. Wherever, overlapping of signatures was found, new sets of signatures were generated to improve the classification of LISS-IV image. Basic visual and digital interpretation parameters were followed like; tone, texture, shape, size, pattern, location and association for the recognition of objects and their tonal boundaries. Further refinement was carried out in the classified image with filtering and recoding of few classes. The final classified output image was assigned 13 classes (Table 2). Validation was performed with respect to SOI reference maps and other collateral data. Overall good accuracy of 90-95% was achieved (Figure 3). Also using resource sat data, we have extracted the infrastructure layer like i.e., metal & un-metal roads, water bodies, settlement, canal, sluice, river etc., and these all layer overlaid into the village boundary map and generated infrastructure layer (Figure 4). The current Land use and land cover data and infrastructure data can be used by State government and local agencies for effective water-resources inventory, flood control, water-supply planning, and waste-water treatment and irrigation planning and other agricultural activities.

***Table 2:*** *Land Use- Land Cover Classification Scheme*

| Code | Land Use/Land Cover Categories | Code | Land Use/Land Cover Categories |
|---|---|---|---|
| 1 | Agriculture | 8 | Forests Blank |
| 2 | Plantation | 9 | Degraded Forest |
| 3 | Fallow | 10 | Dense Forest |
| 4 | Scrub land | 11 | River |
| 5 | Wasteland | 12 | Sand Deposition |
| 6 | Water bodies | 13 | Settlement's |
| 7 | Open Forest | | |

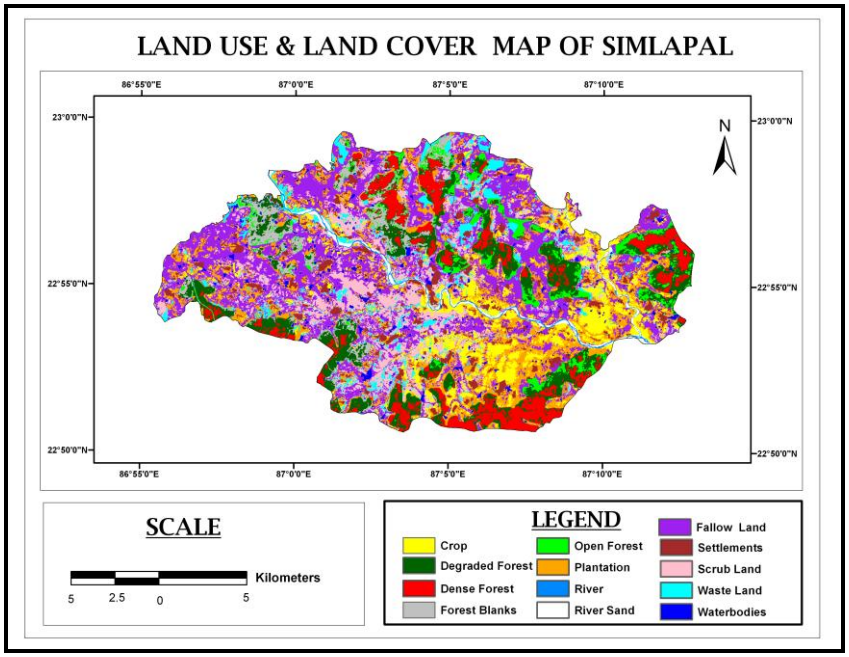


***Figure 3:*** *LU/LC Map of Study*

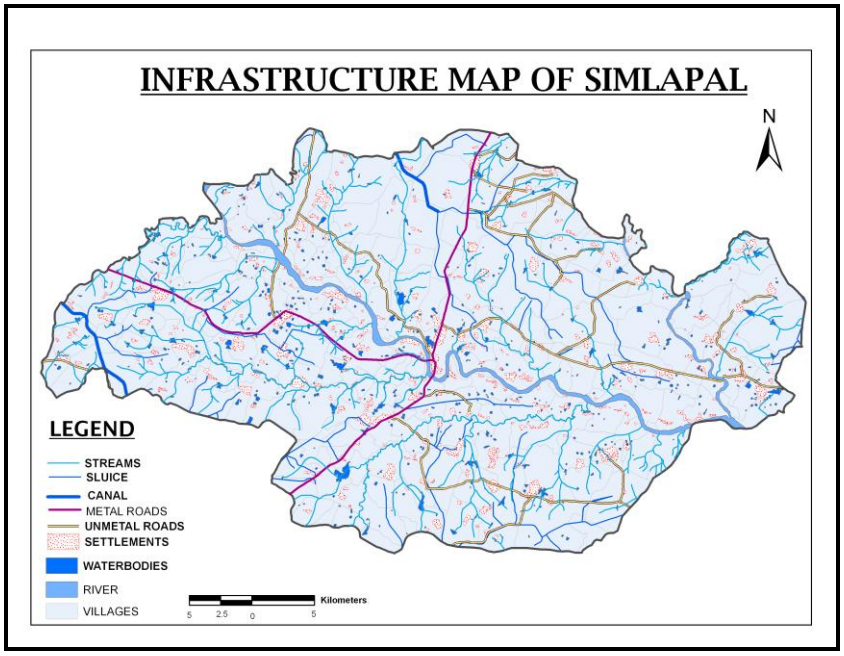


***Figure 4:*** *Infrastructure Map*

## Acknowledgement

The author is thankful to the Region Remote Sensing Centre - East, Kolkata, India for providing the satellite and collateral data and thankful to the IIC Technologies Ltd for providing financial support. Dr. V.M. Chowdhury, Scientist, RRSC-E, Dr. A. Jayaram Ex. GM, RRSC - East and Shri. Shekhar Murthy, President, IIC Academy, Shri. Rajesh Alla, MD, IIC Technologies ltd and overall IIC team for extending all the necessary facilities to complete this work.

## References

Aggarwal, S., 2003: *Principles of Remote Sensing.* Satellite Remote Sensing and GIS Applications in Agricultural Meteorology. Proceedings of a Training Workshop, 7-11 July, Dehra Dun, India, 23-38.

Congalton, K., and Green, A. 1999: *Assessing the Accuracy of Remotely Sensed Data: Principles and Practices, New York.* Lewis Publisher.

Kumar, P. *Monitoring of Deforestation and Forest Degradation Using Remote Sensing and GIS: A Case Study of Ranchi in Jharkhand (India).* Report and Opinion, 2010. 2 (4).

Lunetta, R. *Land-Cover Change Detection Using Multi-Temporal Modis NDVI data*. Remote Sensing of Environment. 2006. 105; 142-154.

Lillesand, T.M., and Kiefer, R.W., 2001: *Remote Sensing and Image Interpretation*. John Wiley and Sons, Hoboken, NJ.

Jensen, J.R., and D.C., Cowen. *Remote Sensing of Urban/Suburban Infrastructure and Socio-Economic Attributes.* Photogrammetric Engineering & Remote Sensing. 1999. 65; 611-622.

**Cloud Publications**
International Journal of Advanced Remote Sensing and GIS
2014, Volume 3, Issue 1, pp. 669-680, Article ID Tech-274
ISSN 2320 - 0243

Research Article | Open Access

# Study on Potential Application of Geographic Information Systems (GIS) to find out Suitable Aquaculture Site in Pune - Maharashtra, India

**Raushan Kumar Raman[1, 2] and Nikunj B. Gajera[2]**

[1]Symbiosis Institute of Geoinformatics, Pune, Maharashtra, India
[1, 2]Gujarat Institute of Desert Ecology, Bhuj, Gujarat, India

Correspondence should be addressed to Raushan Kumar Raman, ramankt@gmail.com; gajeranikunj@gmail.com

Publication Date: 4 August 2014

Article Link: http://technical.cloud-journals.com/index.php/IJARSG/article/view/Tech-274



**Abstract** GIS and remote-sensing provides better options for managing resources and enhancing the productivity. This study is carried out to access the optimum Aqua farming or Aquaculture sites in Pune area. Using the different essential parameters for selecting sites provides the optimum sites in the project area that will help Aqua farmers and results in overall progress in Business. The present study has predicted that about 0.25% (64.22453 ha) of the total land area of Pune city are optimum aqua sites with availability of market and better network connections. Pune has fresh water sources that leads to huge production of fishes and will also contribute profits for aqua farmers. The implementation of GIS technologies in finding suitable site for aquaculture will give a great result in the market productions and profits. Rivers channels and Road networks analysis is the two important factors for selecting the Aqua sites. The analysis is done using LISS-III satellite imagery and aster image. The methodology adopted is based on standard scientific processes. Weighted overlay technique is used in order to frame the exact model surface buildup criteria for the optimum sites throughout the project area.
**Keywords** *Aquaculture; Weighted Overlay; GIS; Model; LISS-III; Aster*

## 1. Introduction

GIS and Remote-Sensing is such a technology that caters the solutions systematically and gives optimum solution scientifically considering time, quality and risk factors. The increasing population requires much food today to sustain. Hence Aquaculture will provide add on to the increasing food demand.

Aquaculture means the farming of aquatic organisms like fish, aquatic plants etc. It includes cultivation of fresh and salt water populations under controlled conditions [1]. Mostly the aquaculture producers also farms ornamental fish for the aquarium trade, and growing plant species used in a range of food,

pharmaceutical, nutritional, and biotechnology products. Aqua farming or Aquaculture has a potential to create huge job opportunities, and food.

There are mainly two types of aquaculture i.e. Marine aquaculture and Fresh water aquaculture. Marine aquaculture includes farming of species especially lives in the ocean while Fresh water aquaculture includes farming of species which is found in rivers, channels, lakes especially on land water bodies or man-made aquaculture structures.

GIS and Remote-Sensing technology will give the proper solution for the site suitability for aquaculture. It includes the parameters containing road network, rivers, channels, streams etc. Aquaculture depends upon the market availability for selling fish and other essential conditions for survival of aquatic organisms. The analysis of the proper site will result in better productivity and also good for business.

India is a large producer of inland fish, ranking next only to Japan. Pune city is the seventh largest metropolis in India, the second largest in the state of Maharashtra.

For, the city like Pune there is big demand of food in the market and aqua farming will provide better options for food.

Fish culture in ponds and reservoirs were contributing above 60% of the overall inland fish production i.e. over 3.6 million metric tons per year [2]. There are two types of ponds i.e. seasonal and perennial. Seasonal ponds can retain water for at least four to five months and used for short term fish culture and also easy to harvest fish while perennial ponds can be used since water dries up and that are suited for fish culture on a larger scale. Therefore, finding suitable sites through GIS and remote-sensing provides the overall analysis for finding suitable aquaculture sites in the study area.

### 1.1. Standards for this Project

For identifying suitable sites for the aquaculture we consider certain standard parameters i.e. Pond shape and size, water resources nearby aquaculture site, best suited road networking from aquaculture site to market, good soil (Clay soil) and suitable water quality that more appropriate to sustain and better yields [3].

### 1.2. Objectives

- Demarcation of important zones in Pune
- Suitable Aquaculture site selection

### 1.3. Study Area

**Pune City** Coordinates: 18°28′25″N 73°47′52″E

Pune City is located in Pune district of the State Maharashtra, India. It is having urban Population of 6,226,959 as per census 2011. It is one of the greenest urban areas in India. The climate of Pune is temperate and it is mainly having summer, monsoon and winter season. It is also one of the greenest urban areas in the country. The city is surrounded by hills. The availability of water sources like small ponds and river streams of Bhima River adds on different landscapes throughout the city. Further, details about location and selected study area are given in Figure 1 and Table 1.

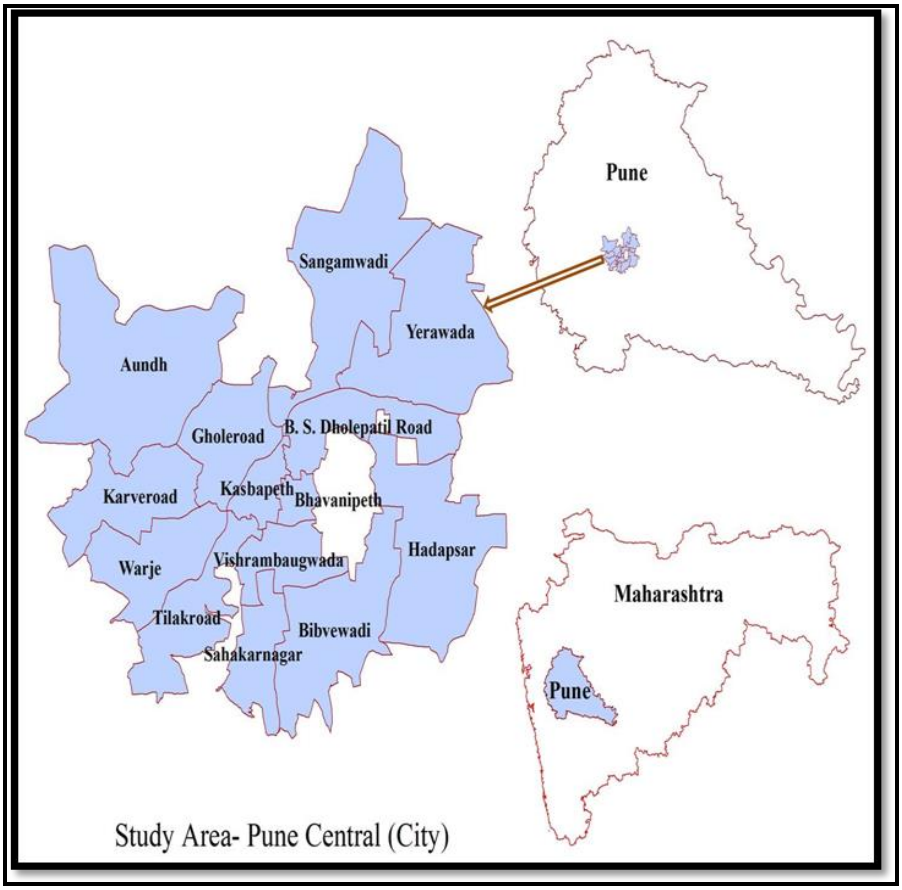


***Figure 1:*** *Study Area Map*

***Table 1:*** *Selected Wards for Suitable Aquaculture Site Selection in the Study Area*

| Ward_Name | Area (Ha.) |
|---|---|
| Karveroad | 1555.557462 |
| Hadapsar | 2690.746743 |
| Gholeroad | 1370.463265 |
| B. S. Dholepatil Road | 1323.417779 |
| Bibvewadi | 2279.945151 |
| Bhavanipeth | 281.079216 |
| Aundh | 4096.801666 |
| Yerawada | 2916.341831 |
| Warje | 1488.54416 |
| Vishrambaugwada | 861.35269 |
| Tilakroad | 1425.49164 |
| Sangamwadi | 3107.406085 |
| Sahakarnagar | 926.059662 |
| Kasbapeth | 459.559352 |
| Total Area (Ha.) | 24782.7667 |

### 1.4. Materials

Data: Linear Imaging Self Scanning System (LISS-III), No. of Spectral bands = 4, Spatial Resolution = 23.5 m, Roads Shapefile, River Shapefile, Hillshade and Slope data, Pune Aster Image.
Software's used for Analysis: ArcGIS 9.3.1, Erdas Imagine 9.1.

### 1.5. Methodology

The main theme for this project is to find the optimum sites in the Pune city for developing aquaculture in the area. The GIS concepts are applied for the basic of projects and the remote-sensing techniques are used for better calibration of data and result generation [3, 4].

## 2. Satellite Data Processing

First the layer stacking is done using Erdas and then atmospheric correction is made using actor extension of Erdas. After that the classification is performed using supervised technique by taking areas of interest based on signature files for making classes out of pixel values. For classifying different features the NDVI (Normalized Differential Vegetative Index) is used for vegetation mapping of the study area [5, 6, 7, 8].

$$NDVI = (NIR — Red) / (NIR + Red) \quad (i)$$

Where NIR stands for Near Infrared Region

Calculations of NDVI for a particular pixel always result in a number that ranges between one (-1 to +1) where the zero means no vegetation and close to (+1) indicates the highest possible density of green leaves.

The validation is done using ground control points and accuracy assessment is performed for final supervised classified imagery.

## 3. Data Merging Interpretation and Model Making

Non-spatial Data and Spatial Data is calibrated and based on the model parameters the data in used for further Process [9, 10, 11]. The methodology for making model is on satellite process using GIS and remote-sensing software's and finding suitable site for aquaculture depends upon weighted overlay. In weighted overlay, the maximum value is given to water and wasteland (Figures A & B).

### 3.1. Detailed Methodology Flow Chart

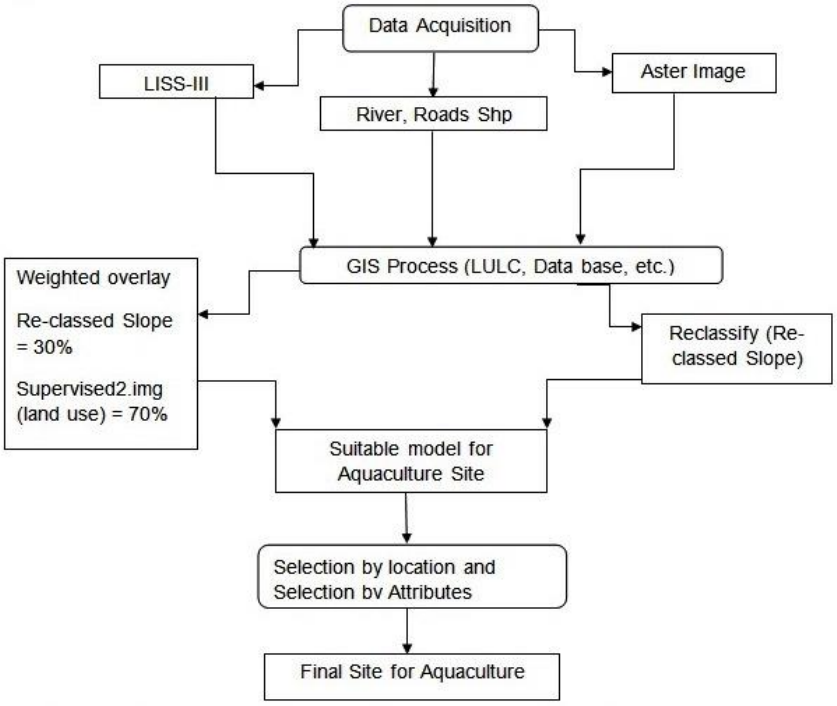


***Figure A:*** *Methodology Flow Chart*

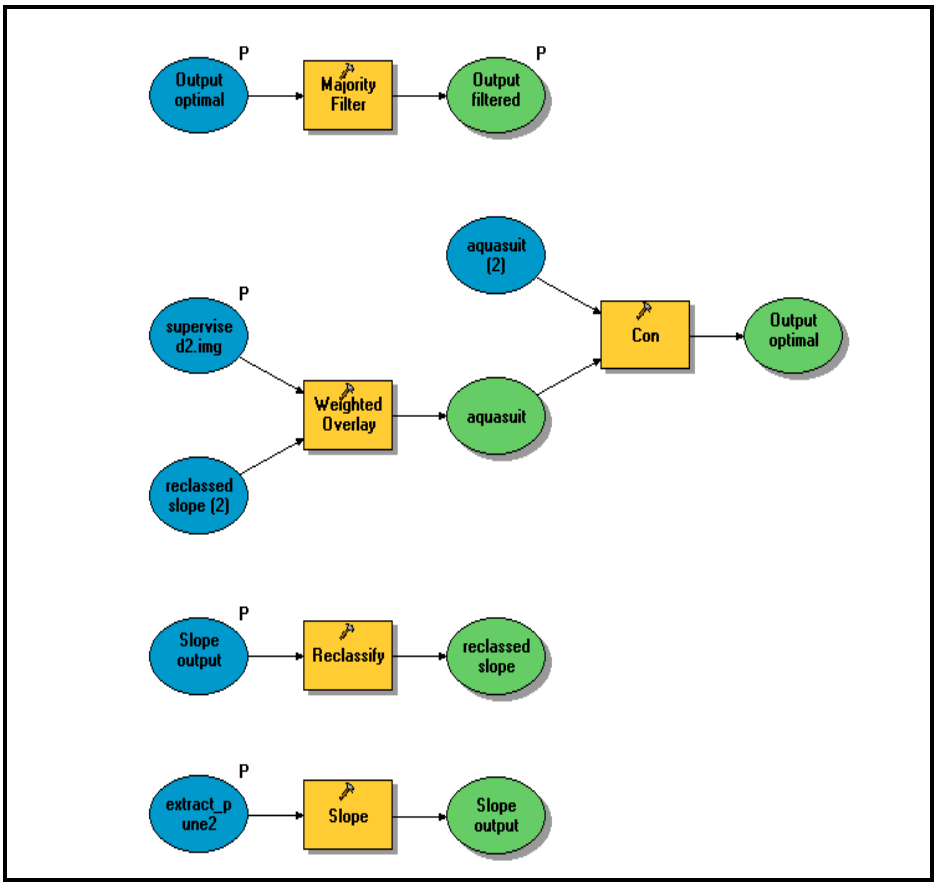


***Figure B:*** *Aquaculture Site Model Process*

This is the final model for Aquaculture Site with different model parameters developed during study. The P stands for model parameter. The model making system involves the majority filter technique, weighted overlay and conditional probability for finding potential sites.

## 4. Results and Discussion

Scientifically, the study carried out using GIS and Remote-Sensing technique. The different parameters like water for site buildup, proper road network for market availability, river streams for fresh water etc., is considered for the model making and finding suitable site for the project [12, 13, 14] (Figures 2 & 3).

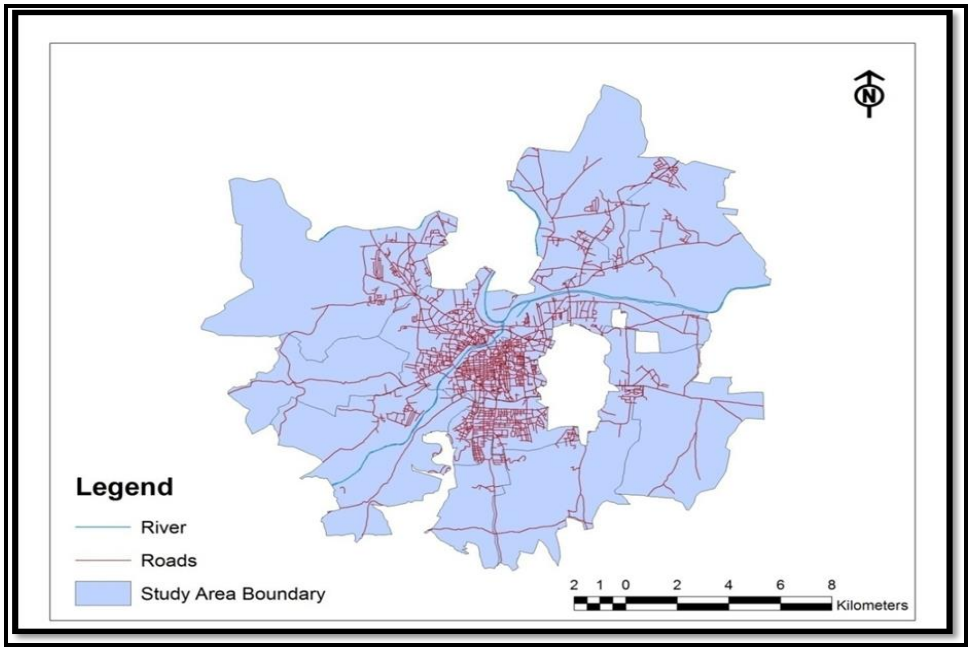


***Figure 2:*** *Shape File Integrated Study Area Map*

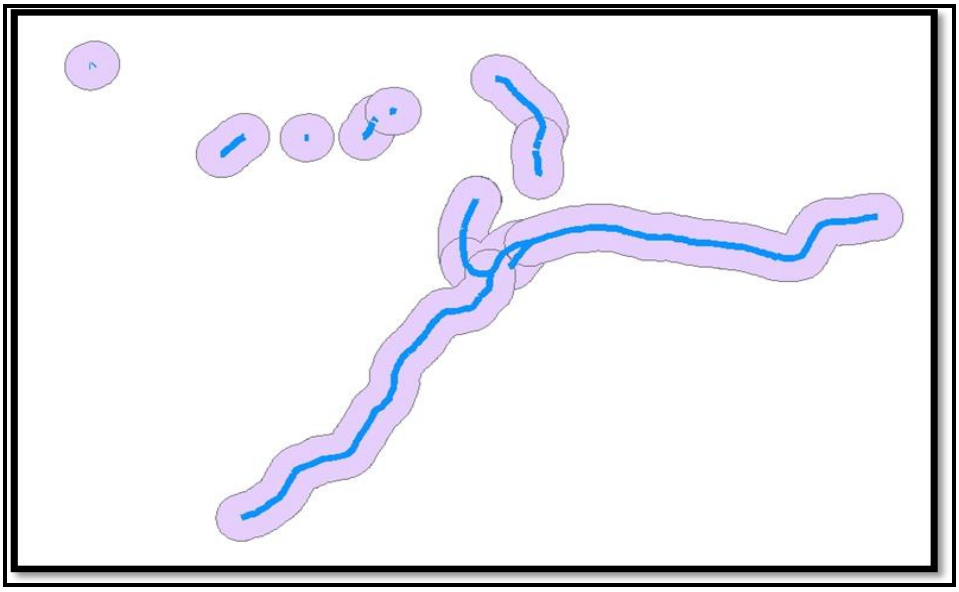

***Figure 3****: River Buffer Shape File*

Integration of data: the satellite imagery of Pune (LISS-III), Aster Images, shape files into geo-database resulted in baseline of the study. Supervised classification is performed based on the priori knowledge and the process is carried out in Erdas Imagine software by taking different pixel values for classes like Agriculture, Vegetation, Plantation, Water, Urban, Shrub and Wasteland [15, 16, 17]. (Figure 4).

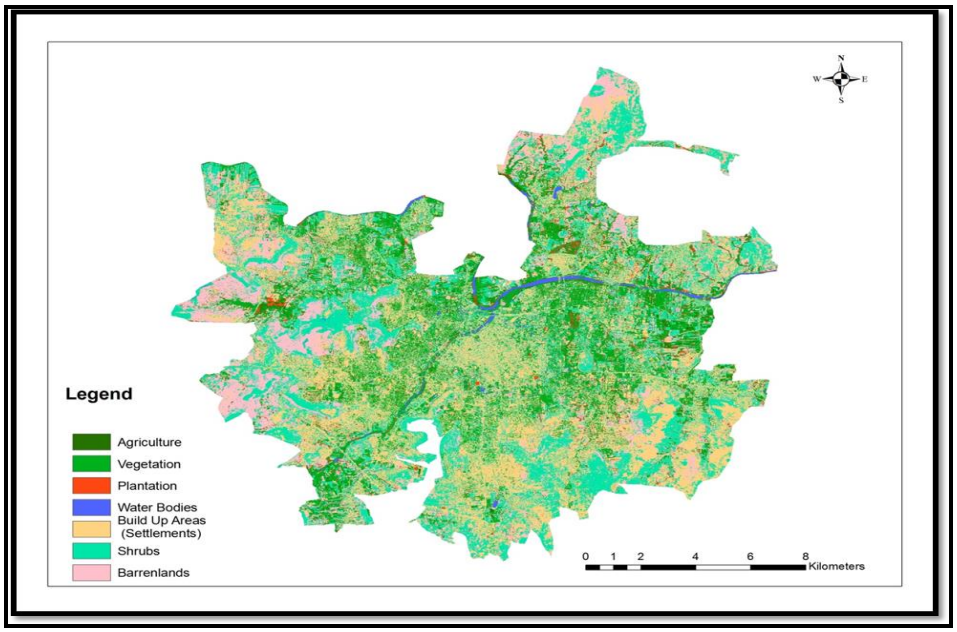


***Figure 4**: Supervised Map*

The use of overlay method includes the weighted mechanism where the individual classes are having different weightage. Further the model is framed based on the weighted overlay method, where Water is given maximum weightage for aquaculture site selection. As the water is the necessity for setting the Aqua- farming.

The River Buffer created for the water availability and the analysis is done during the study for the essential conditions for Fresh water Fish breeding and other aquatic organisms (Figure 5 (a & b), 6, 7, 8).

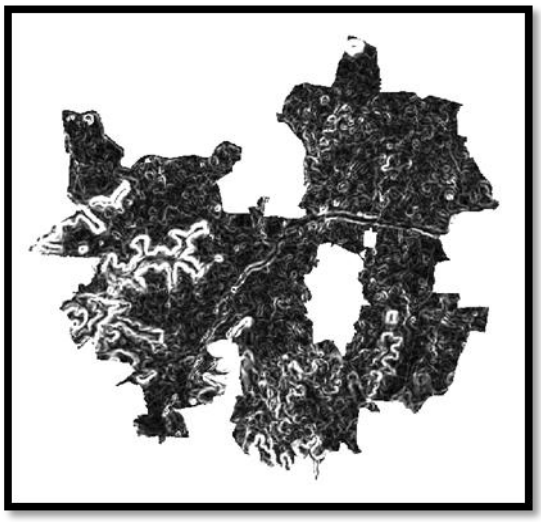

***Figure 5 (a):** Aster Slope of the Study Area*

***Figure 5 (b):** Reclassed Slope*

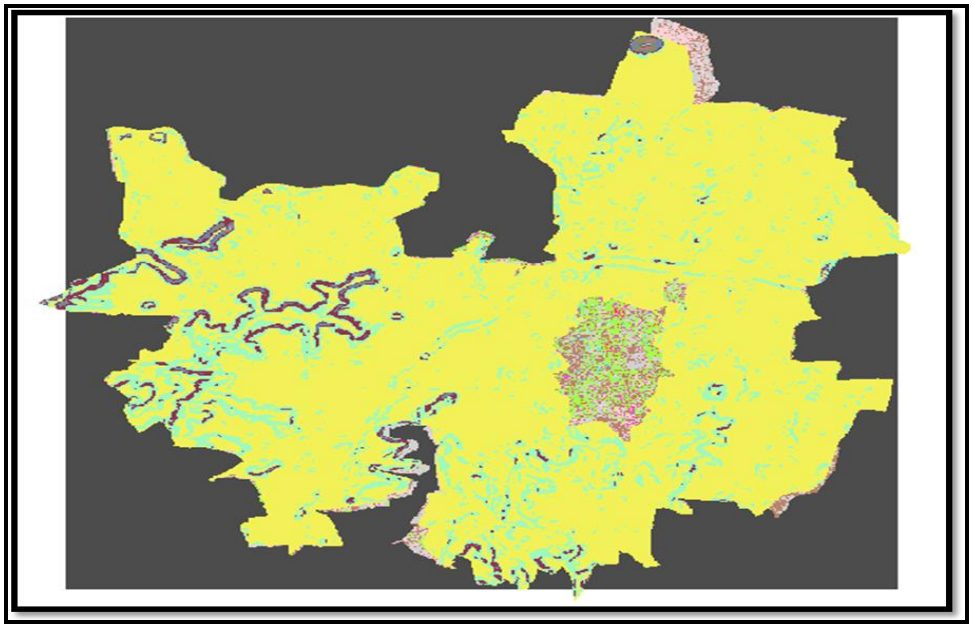

***Figure 6:*** *Re-Classed Slope Pattern*

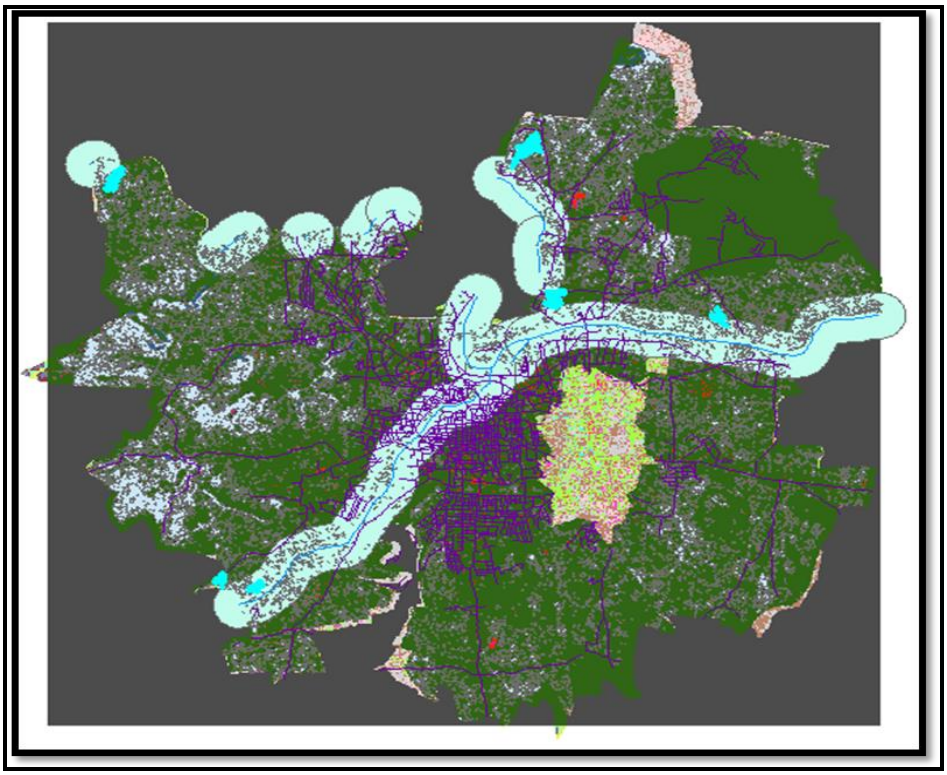

***Figure 7****: Final Site for Aquaculture Cyan Spot Including Buffer Area around Rivers*

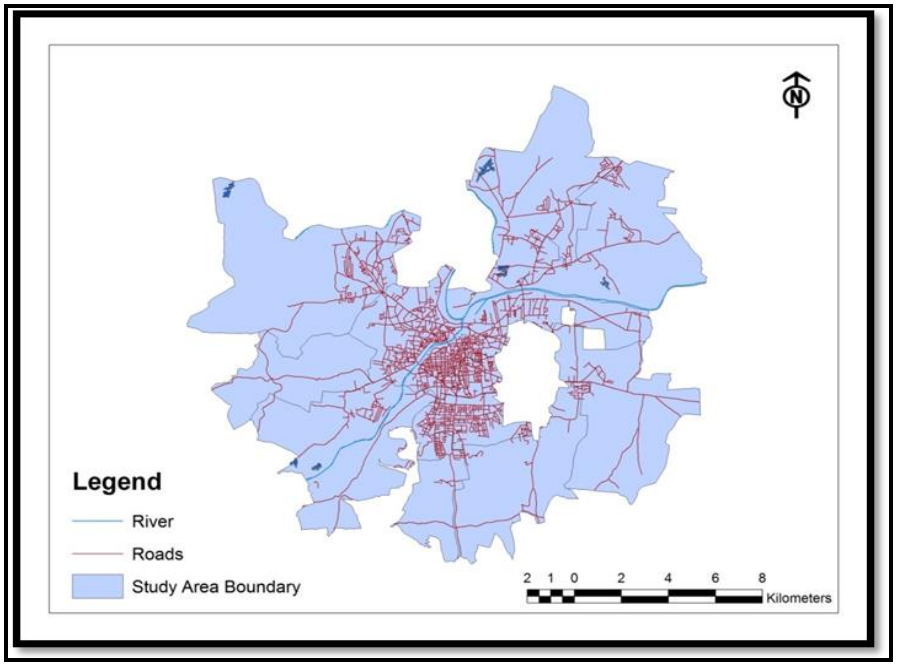


***Figure 8:*** *Suitable Aqua Farming Site with Roads and Rivers*

The final suitable site for aquaculture in Pune city area is shown in the developed model. Basically the model gives us the exact place with site specific area where aqua farming will be highly suitable and yields maximum output [18, 19] (Table 2) (Figure 9 (a & b), 10). Since the model helps finds the optimum locations throughout the area for setting the aqua farming sites. It will improve the productivity as well as options for future.

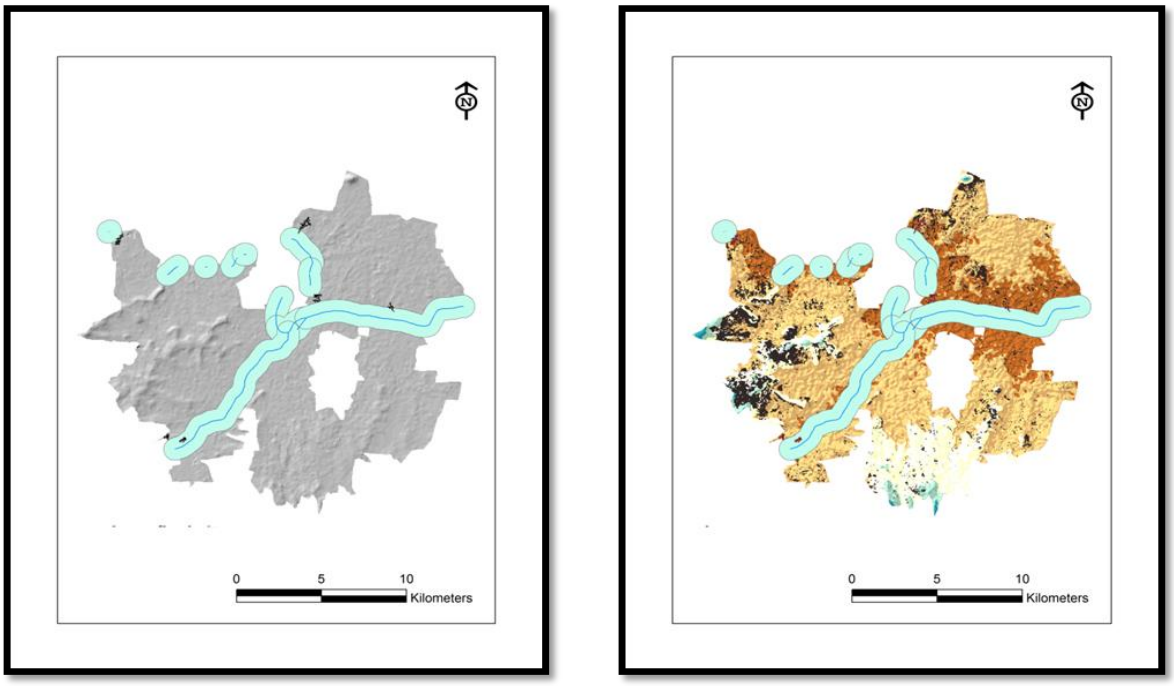


**(a)** **(b)**

***Figure 9 (a):*** *Potential Aqua Sites with River Buffer Shapefile on Hill shade Image*
***Figure 9 (b):*** *Potential Aqua Sites with River Buffer Shapefile on Reclassed Slope Image*

Land use/Land Cover (LULC) defines landscape patterns. Land use is typically defined as human modifications land as agriculture land, infrastructural development etc [20, 21]. While land cover is natural like forest, hills etc. Land use is constrained by environmental factors like climate, topography, soil characteristics etc. Supervised classification is used in the study based on prior knowledge.

***Table 2:*** *Final Aquaculture Site with Area*

| Aqua Site_ FID with Ward Name | Area in Hectares |
|---|---|
| P - Sangamwadi | 19.95246792 |
| Q - Aundh | 12.30836041 |
| R - Sangamwadi | 13.02339584 |
| S - Yerawada | 6.471747332 |
| T - Warje | 6.123757878 |
| U - Warje | 6.34479615 |

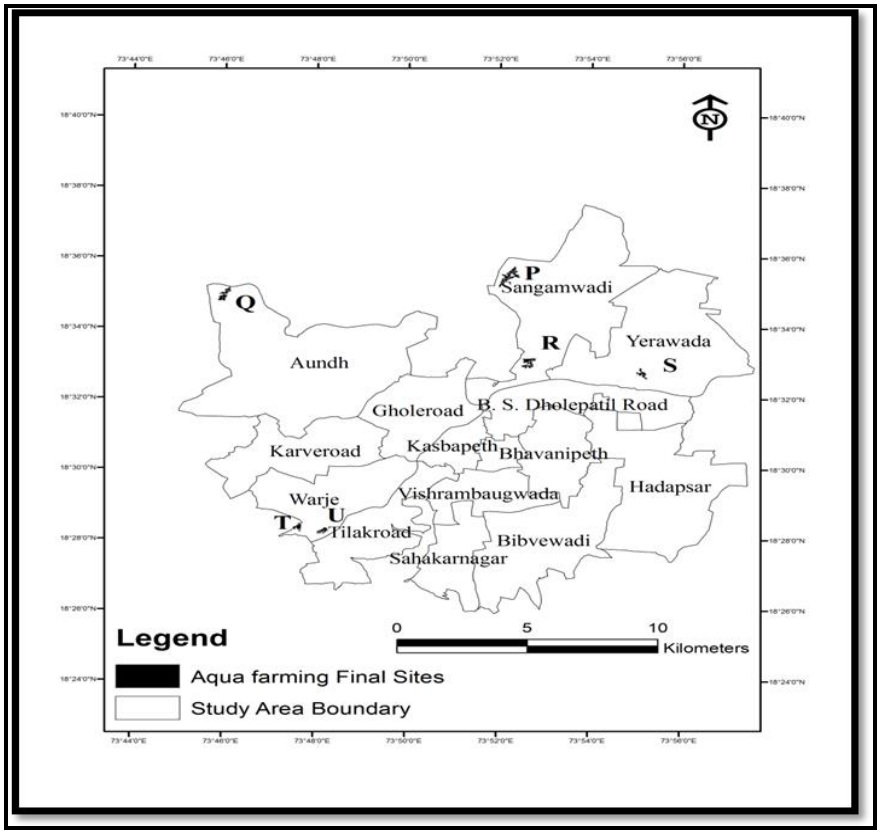


***Figure 10:*** *Suitable Aqua Farming Site*

## 5. Conclusion

Latest GIS and remote sensing technique allows users to integrate spatial as well as non-spatial information to model the current scenario of the study concerned. So, it is expected that during the aquaculture development process the near water body area is much suitable for the aquaculture result to optimum production in fish marked which helps farmers for net benefits. The present study also focuses on the different parameters for a suitable aquaculture site with the ease of routing patterns based on network analysis. If model will be implemented than it is sure that one can achieve good result in terms of production and market.

## Acknowledgement

The authors acknowledge special thanks to Director and Add. Director (Gujarat Institute of Desert Ecology). We also expresses thanks to Director Symbiosis Institute of Geoinformatics, Pune and also thankful to friends and staffs of Symbiosis Institute of Geoinformatics. We are also expresses thanks to entire Scientists and Scholars of Gujarat Institute of Desert Ecology, Bhuj for their support.

## References

[1] Raj Chandar and Karuppasamy. *Marine Fishery Information System and Aquaculture Site Selection Using Remote Sensing and GIS*. International Journal of Advanced Remote Sensing and GIS. 2012. 1 (1) 20-33.

[2] Pounraj and T., Rathakrishnan. *Adoption Behaviour of Fish Farmers in Critical Inland Fish Culture Technologies in Tamil Nadu.* Madras Agric. J. 2011. 98 (7-9) 286-290.

[3] R., Ramesh and R., Rajkumar. *Coastal Aquaculture Site Selection and Planning in Tamilnadu Using Remote-Sensing and GIS*. Asian Pacific Remote Sensing and GIS Journal. 1996. 9; 39-49.

[4] Peter C., Longdill, Terry, R., Healy and Kerry, P., Black. *An Integrated GIS Approach for Sustainable Aquaculture Management Area Site Selection. Ocean & Coastal Management*. 2008. 51; 612-624.

[5] Zainul Hidayah. *Application of GIS for Assessing Prawn Farm Development in Tully-Cardwell, North Queensland.* Jurnal Kelautan. 4 (2) 62-67.

[6] Nyoman Radiarta, Sei-Ichi Saitoh and Akira Miyazono. GIS-Based Multi-Criteria Evaluation Models for Identifying Suitable Sites for Japanese Scallop (Mizuhopecten Yessoensis) Aquaculture in Funka Bay, Southwestern Hokkaido, Japan. Aquaculture. 2008. 284; 127-135.

[7] C., Silva, J.G., Ferreira, S.B., Bricker, T.A., DelValls, M.L., Martín-Díaz and E., Yáñez. *Site Selection for Shellfish Aquaculture by Means of GIS and Farm-Scale Models, with an Emphasis on Data-Poor Environments*. Aquaculture. 2011. 1-14.

[8] W., Brian Szuster and Hatim Albasri. *Site Selection for Grouper Mariculture in Indonesia*. International Journal of Fisheries and Aquaculture. 2010. 2 (3) 87-92.

[9] Reyahi Khoram, Shariat, Moharamnejad, Azar and Mahjub. *Ecological Capability Evaluation for Aquaculture Activities by GIS.* Iran. J. Environ. Health. Sci. Eng. 2005. 2 (3) 183-188.

[10] Brian W., Szuster and Hatim Albasri. *Mariculture and Marine Spatial Planning: Integrating Local Ecological Knowledge at Kaledupa Island, Indonesia*. Island Studies Journal. 2010. 5 (2) 237-250.

[11] M., Abdus Salama, Lindsay G., Ross and C.M., Malcolm Beveridge. *A Comparison of Development Opportunities for Crab and Shrimp Aquaculture in Southwestern Bangladesh, Using GIS Modeling*. Aquaculture. 2003. 220; 477-494.

[12] P., Mahalakshmi, N., Kalaimani, M., Krishnan and T., Ravisankar. *Use of Information Technology in Aquaculture Research and Management*. Fishing chimes. 2004. 24 (9) 50-53.

[13] R., Sivakumar, Mrs. A.M., Kiruthika and S., Suresh Babu. *Remote Sensing and GIS Application in Brackish Aquaculture in Northern Part of Andhra Pradesh from Srikakulam to West Godavari.* International Journal of P2P Network Trends and Technology. 2012. 2 (2) 42-49.

[14] K., Nageswara Rao, G., Murali Krishna, D., Ramprasad Naik and B., Hema Malini. *Remote Sensing and GIS Applications in the Identification of Aquaculture Hotspots at Village Level*. Journal of the Indian Society of Remote Sensing. 2003. 31 (2) 71-80.

[15] P., Mynar Babu, G., Jai Sankar and V., Sreenivasulu. Impacts of Aquaculture on Water Resources Utilization and Land Resources of Krishna District Using With Remote Sensing and GIS Techniques. International Journal of Engineering Trends and Technology (IJETT). 2013. 4 (7) 3201-3206.

[16] I., Nyoman Radiarta, Sei-Ichi Saitoh and Hajime Yasui. *Aquaculture Site Selection for Japanese Kelp (Laminaria Japonica) in Southern Hokkaido, Japan, Using Satellite Remote Sensing and GIS-Based Models*. ICES Journal of Marine Science. 68 (4) 773-780.

[17] R., Filgueira, J., Grant, R., Stuart and M.S., Brown. Ecosystem *Modeling for Ecosystem-Based Management of Bivalve Aquaculture Sites in Data-Poor Environments.* Aquaculture Environ Interact 2013. 4; 117-133.

[18] M., Shadat Hossain, Nani Gopal Das. *GIS-Based Multi-Criteria Evaluation to Land Suitability Modelling for Giant Prawn (Macrobrachium Rosenbergii) Farming in Companigonj Upazila of Noakhali, Bangladesh*. Journal Computers and Electronics in Agriculture. 2010. 70 (1) 172-186.

[19] Claudio Silva, Maria A., Barbieri, Eleuterio Yanez, Juan C., and Tomas Angel DelValls. *Using Indicators and Models for an Ecosystem Approach to Fisheries and Aquaculture Management: The Anchovy Fishery and Pacific Oyster Culture In Chile: Case Studies.* Lat. Am. J. Aquat. Res. 2012. 40 (4) 12 955-969.

[20] Rumana Yasmin, Mehady Islam and Md. Jobaer Alam. *A Study on Potential Application of Geographic Information Systems (GIS) in Fisheries and Aquaculture of Bangladesh*. World Journal of Fish and Marine Sciences. 2012. 4 (6) 609-619.

[21] Abdulaziz Guneroglu, Ercan Kose, Coskun Eruz, Ersan Basar, Sebnem Erkebay and Fevzi Karsli. *Use of Geographic Information System to Select Fish Cage Farming Sites in Surmene Bay, Black Sea*. The Israeli Journal of Aquaculture–Bamidgeh. 2005. 57 (2) 81-89.

**Cloud Publications**
International Journal of Advanced Remote Sensing and GIS
2014, Volume 3, Issue 1, pp. 642-659, Article ID Tech-286
ISSN 2320 - 0243

Case Study | Open Access

# Climate Change Impact on Agricultural Productivity and Environment Influence based on Simulation Model

**Thanh Van Hoang[1], Tien Yin Chou[2], Bruno Basso[3], Mei Ling Yeh[2] and Chih Yuan Chien[2]**

[1]Civil and Hydraulic Engineering Program, College of Construction and Development, Feng Chia University, Taiwan
[2]GIS Research Center, Feng Chia University, 100 Wenhwa Rd, Situn Taichung, Taiwan R.O.C
[3]Departments of Geosciences, Michigan State University, US

Correspondence should be addressed to Thanh Van Hoang, st_van@gis.tw

Publication Date: 24 July 2014

Article Link: http://technical.cloud-journals.com/index.php/IJARSG/article/view/Tech-286



**Abstract** In this paper a physical simulation model SALUS is used to explore crop productivity responses to a range of management strategies over multiple years. This research firstly set up a spatial database of experimental site rice production area polygon identified from satellite images, and collected detail daily weather data from meteorology stations for the past 30 years, with soil profile information and management strategy and genetic coefficient. Secondly, Salus model simulation was applied to accurate reflect real observed yield information to compare with simulated result. The residual mean square of the comparison proved around 90 percent of confidence that the model can successful simulated yield output changes for each year. By running model simulation under different predicted weather regime conditions arising from climate change, the effect on rice crop productivity and the output of carbon emission, nitrate leaching, and irrigation demand in the Red River Delta area of Northern Vietnam are spatially compared. The simulation results showed increased rice productivity in this field due to predicted temperature rise. However, there are high costs associated with environmental effects emanating from carbon emissions, greater nitrate leaching and water resources and fertilizer demand etc. to sustain the rice productivity. This paper examined these critical issues by integrating SALUS model and GIS function to demonstrate the possible output both economically and environmentally affect for better agricultural decision on experimental area.
**Keywords** *Climate Change; Vietnam Agriculture; Geography Information System; SALUS Model; Web-GIS*

## 1. Introduction

The environmental and socio-economic effects of climate change are major and diverse, including food production and security, water demand, health, energy, tourism, industry and ecosystem functioning (Phan D.B., et al., 2011). Through improving understanding of each of these aspects,

policy-maker may make better informed decisions to facilitate sustainable development (Cowie J., 2007).

Climate change manifests as global warming and sea level rise, changes in rainfall, hurricane frequency and intensity. According to the IPCC (Inter-governmental Panel on Climate Change) Fourth Assessment Report in 2007, the 5$^{th}$ Assessment Report in 2013, the global average temperature has risen about 0.74$^{0}$C for the period 1906-2005 and the warming trend over the last 50 years is nearly twice that for the previous years. The observed sea level data of 1961-2003 showed an increasing rate of the average global sea level of about 1.8±0.5 mm/year. The satellite data from TOPEX/POSEIDON in the period of 1993-2003 showed an increasing rate of the average global sea level of about 3.1±0.7 mm/year, considerably faster than that of 1961-2003.

Vietnam is a long narrow country consisting of an extensive coastline, two major river deltas, and mountainous areas on its eastern and northeastern borders and is very much exposed to the risks of climate variability and climate change. Its vulnerability to climate risk has given rise to the need for the country to design and implement measures to mitigate the effects of droughts, flooding, storms, and similar events on agriculture and other sectors of the economy. Assessing the potential impacts of climate change and determining how best to adapt represents a new and significant challenge, for which past experience may be a guide, but which, given large uncertainties, requires constant reassessment.

Crop models have the capability to predict crop development and dry-weight grain as affected by the climatic conditions, soil characteristics, nitrate leaching. Crop modeling is becoming an increasingly essential tool in environment management since they can potentially provide quantitative estimates of yield under various environmental conditions and simulate the impact of climate change on yield, water balance and nutrient balance.

There are indeed numerous crop models in the literature, usually designed for particular crops, for example for wheat, ARCWHEAT (R.A.C., Mitchell et al.) and CERES-Wheat (Ritchie, J.T., et al., 1985) while still others are more generic in nature. In this paper, the SALUS model was employed in an experiment for the Red River Delta, the second largest delta in Vietnam. The Red River Delta is chosen for this analysis due to its being representative of other regions in North Vietnam in terms of climate and crop diversity (Singh, 2009). The experimental site covers a total area of 21050, 9 km$^2$ and with a population density which is the second highest in the country at 961 person/km$^2$, second only to the Mekong River Delta in southern Vietnam. Pressure on its natural resources is mounting and this issue poses considerable challenges for food security, raising concerns about the possible impact of climate change at local, regional and national levels. Effective strategies are clearly needed given the diverse threats of future climate change.

The object of this research was thus to test the performance of SALUS-web GIS in Red River Delta by comparison with the true data, for a range of climate change and food crops carried out under different management strategies. Validation of this platform will offer the opportunity to evaluate the effect climate change on crop yield which are the most important for Red River Delta, the second biggest delta in Vietnam, based on the effect of climate variability which can be applied to this model for other regions on whole country.

## 2. Materials and Methods

### 2.1. Study Area

The Red River Delta covers ten provinces (Figure 1), and cities including Hanoi, Bac Ninh, Vinh Phuc, Ha Nam, Hai Duong, Hai Phong, Hung Yen, Nam Dinh, Ninh Binh, and Thai Binh. The delta region is known to be subject to increasing population pressure.

*Climate Change in Vietnam:*

According to the most recent Ministry of Natural Resources and Environment report (MoNRE 2009), and based on the results of studies made by IPCC 2013, data on daily temperature variability, rainfall of seven climatic zones of Vietnam and sea level rise have been collated. This indicates a predicted mean annual temperature rise in Vietnam by 2.3$^0$C by the end of 21st century in relation to the average of 1980-1999; both total annual and wet season rainfall are expected to increase. For the entire country, annual rainfall is predicted to increase 5% by the end of 21st century compared to that of the period 1980-1999. Sea level rise is predicted to increase by about 30cm by mid of 21st century and by 75cm by the end of 21st century compared to the period 1980-1999.

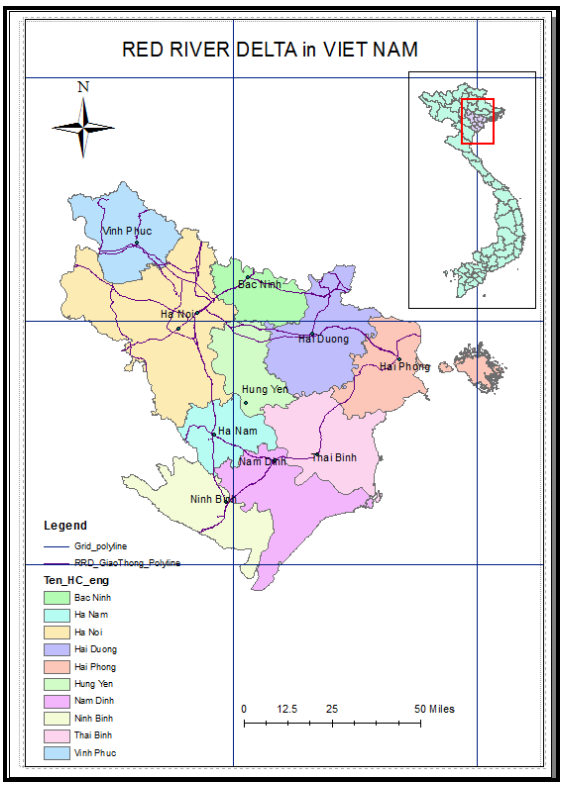


***Figure 1:*** *Map of Red River Delta in Vietnam*

### 2.2. Impact of Climate Change on Agriculture in Vietnam, and its Implication for Red River Delta

The MoNRE scenario falls in the middle of a range of alternative climate change scenarios for Vietnam when these are ordered according to climate moisture indices. The impact of the various climate scenarios on crop production has been explored using projections of runoff, as this influences the availability of irrigation water, as well as agronomic models that consider temperature and rainfall patterns, water availability for rainfed and irrigated crops, and other factors to estimate the impact of climate change on crop yields.

While the country had a rapid rate of industrialization in the last two decades, agriculture remains a major economic sector in Vietnam. Climate change is expected to affect the sector significantly and in a number of different ways.

Table 1 shows that much attention has been focused on the potential impact changes in temperature on rice yield, due to salinization and flooding. The impact of, and adaptation to, climate change on agriculture must also take account of changes in land use driven by other processes, including market prices and globalization. Higher temperature and changes in precipitation amount and seasonality may permit the cultivation of some crops in areas that were previously unsuitable for crop production. The impacts are, therefore, not necessarily all negative but appropriate planning and policy making requires accurate modelling of such potential changes.

***Table 1:*** *Possible Impact of Climate Change on Agriculture*

| Climate Change | Possible Impact |
|---|---|
| Increasing temperature | Decreased crop yields due to heat stress and increased rate of evapotranspiration |
| | Increased livestock deaths due to heat stress |
| | Increased outbreak of insect pests and diseases |
| Changes in rainfall | Increased frequency of drought and floods causing damages to crops |
| | Changes in crop growing season |
| | Increase soil erosion resulting from more intense rainfall and floods |

Climate change, together with sea level rise, affects both rice yields and production. The impacts explored in this study rely upon projections generated by a series of models, from climate models to crop-growth models. The impacts estimated in the analysis are based upon projected changes in climate variables and sea level, so they assume that all other variables. Rice yield declines by 7.2 percent to 32.6 percent, yields of other crops decline by 4.1 percent to 32.9 percent. The largest yield reduction can be with either the Dry or Wet scenarios, depending on crops. MoNRE scenario has the least yield reduction.

The Red River Delta floods frequently and in certain localities flood levels may exceed 14m above the surrounding countryside. Flood control has therefore been vital to the economy of the delta region for many centuries contain the river while at the same time providing irrigation water for rice. This ancient system has sustained a high population density and made double-cropping wet-rice cultivation possible across half the region (Zhenli et al., 2006). The delta has a tropical monsoon climate, and the climate varies among ten provinces with the mean annual temperatures ranges from 18-29°C. The dry season from November to April and the warm rainy season from May to September. The mean annual rainfall: 600-5,000mm, about 80-90% is concentrated in the short rainy season. Vietnam is clearly vulnerable to tropical storms and typhoons, since large populations live in the low-lying Mekong and Red River delta areas. Present day climate extremes and potential changes in the typhoon regime as a result of increased inter-annual climate variability in the future are obvious threats. However, an analysis of the climate regime by itself can not predict the extent to which the population – may become more vulnerable to the impacts of climate extremes so that the analysis presented here focuses on the complex interplay of processes influencing agricultural productivity in the context of climate change and using Red River Delta region as a case study.

### 2.3. Crop Model

Brief overview of SALUS model (Figure 2)

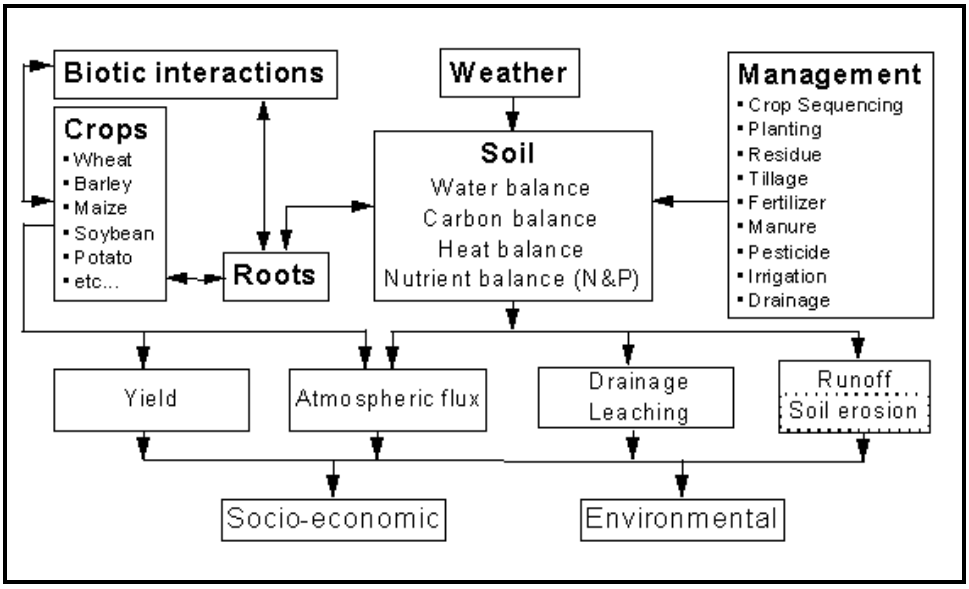


***Figure 2:*** *The Components of SALUS*

The SALUS (System Approach to Land Use Sustainability) program is designed to model continuous crop, soil, water and nutrient conditions under different management strategies for multiple years (Figure 2). These management strategies have various crop rotations, planting dates, plant populations, irrigation and fertilizer applications, and tillage regimes. The program simulates plant growth and soil conditions on a daily basis (during both the growing season and fallow periods) for any time period given known or simulated weather conditions on the days in question. The model allows several different management strategies to be applied simultaneously in a simulation run, in so allowing comparison of the effects of different management interventions on crops and soil under the same weather conditions. This also provides a framework of different areas managed under contrasting management practices that can be easily compared.

Every day, and for each management strategy being run, all major components of the crop-soil-water model are executed. These components are as follows: management practices, water balance, soil organic matter, nitrogen and phosphorous dynamics, heat balance, plant growth and plant development (T.Y. Chou et al., 2011). The water balance component includes surface runoff, infiltration, surface evaporation, saturated and unsaturated soil water flow, drainage, root water uptake, soil, evaporation and transpiration. The soil organic matter and nutrient sub-model simulates organic matter decomposition, nitrogen mineralization and formation of ammonium and nitrate, nitrogen immobilization, gaseous nitrogen losses and three pools of phosphorous. The development and growth of plants incorporates the environmental conditions (especially temperature and light) to calculate potential plant growth rates which are then adjusted to account for water and nitrogen limitation (T.Y. Chou et al., 2011).

The biophysical sub-model is composed of three main structural components: i) a set of crop growth modules; ii) a soil organic matter and nutrient cycling module and; iii) a soil water balance and temperature module.

The crop growth modules are derived from the CERES model (Ritchie et al., 1985) and IBSNAT (Ritchie et al., 1989) family of crop production models that were originally developed for single year,

monoculture simulations (Chunzhao Liu et al., 2010). The crop growth algorithms were extracted and restructured into crop growth modules that are linked to the soil water, nutrient and management sub-models. The "C" language was set up in SALUS Model to make the memory allocation more dynamic and program code more platform independent. Maize, wheat, barley, sorghum and millet were shown in the current operational crop growth modules. Carbon consumption and dry matter production are a function of potential rates (controlled by light interception and parameters defining the different-specific growth potential) which are then reduced according to water and/or N limitations. The inputs required for the crop growth routines are the genetic (variety-specific) coefficients and day by day solar radiation as a driving variable (T.Y. Chou et al., 2011).

The soil organic matter (SOM) and nitrogen module is derived from the Century model (Parton W.J., 1996), and a number of modifications incorporated. The SALUS model simulates organic matter and Nitrogen mineralization/immobilization from three SOM pools (active, slow and passive) which vary in their turnover rates and characteristic C: N ratios (T.Y. Chou et al., 2011). There is SALUS model can be downloaded at website http://www.salusmodel.net (Bruno Basso, 2013).

### 2.4. Integrating SALUS Model – webGIS

Integrating SALUS model and webGIS

SALUS-WEBGIS is an integrated system which follows a tight coupling strategy, integrating SALUS model (Karimi et al., 1996) with EasyMap object into a web application (T.Y. Chou et al., 2011). SALUS model is converted into a dynamic link library that can be called from the new application and linked to it at runtime. This allows a smooth integration between Geographic Information System (GIS) and the simulation models (Chang K.T., 2004).

SALUS-WEBGIS was deployed in a Windows environment, and is built around IIS and the Microsoft SQL Server relational database management system, which was chosen due to its ability to efficiently store, search, and retrieve data in large databases. The user interface was built by using ASP.NET and AJAX technology. The web server receives the requests from the client side and retrieves data from SQL server and maps from EasyMap (designed by GIS.FCU) object according to the requests (T.Y. Chou et al., 2011). The server also provides the KML service that follows OGC standards in generation a KML file compatible with Google Earth to facilitate visualization of the outputs.

SALUS-WEBGIS adopts ESRI shapefile as source of spatial data with geometry type limited to polygons. Polygon features were used to display the spatial variability of simulations. A management practice is called an experiment in SALUS-WEBGIS. Experiments record weather data, soil data and the strategies of cultivation including planting, irrigation, tillage, residues, fertilizer and harvest. Each polygon was linked to a unique experiment. Similarly, the simulation results of experiments were appended to the attributes of polygons (T.Y. Chou et al., 2011).

SALUS-WEBGIS has essentially an identical model kernel as SALUS model, although with some differences. In order to reduce complexity, input data were either reduced in number or set to default values. Output data were reduced because only a few simulation results proved suitable for mapping (T.Y. Chou et al., 2011).

SALUS-WEBGIS is designed to be used by advisors of farmers or agricultural officers and is intended to operate as a tool for precision agriculture. The three main components are a crop growth simulation module, ii) data management module and iii) thematic map module (T.Y. Chou et al., 2011).

The crop growth simulation module is the central controller of SALUS model and receives requests from the client (Figure 3). Subsequently, it lists all features that are selected and then starts to simulate all experiments corresponding to those features.

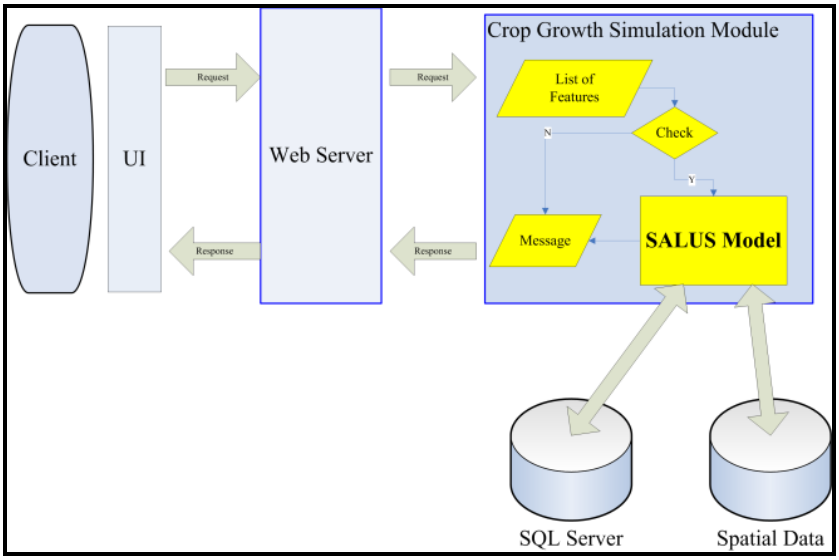


***Figure 3:*** *The Workflow of Crop Growth Simulation Module*

The thematic map module creates thematic maps from the spatial data which were linked to the simulation results (Figure 4). In SALUS-WEBGIS, the simulation results may represent multiple years. The thematic map module can therefore create Time-Series maps of a particular simulation result. After retrieving all simulation results of features, the module appends all results to the attributes. Jenks' natural breaks classification was used to classify the values of all features in a map in order to create a choropleth map. The choropleth map is published to the web server using Easymap object. Besides the web server, this module also has a KML service that can convert time-series choropleth maps into KML files which are compatable with Google Earth.

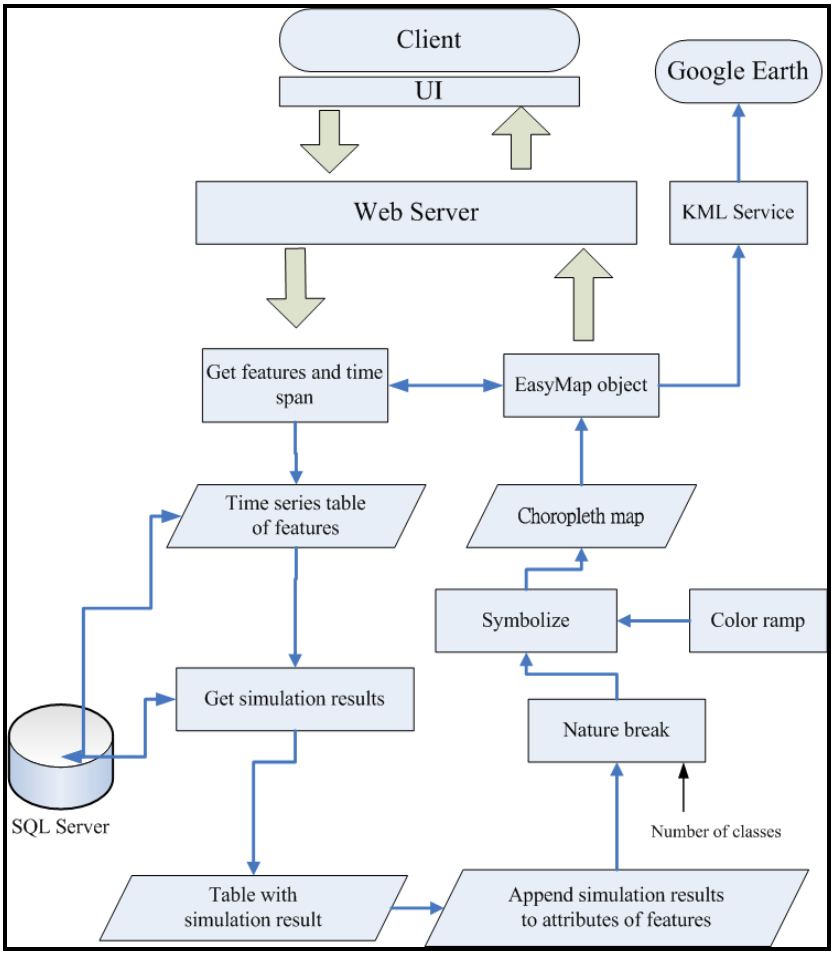


***Figure 4:*** *The Workflow of Thematic Map Module*

## 2.5. The Real Time Input Data

*The System Implementation*

The main page of SALUS-WebGIS is shown as Figure 5 below. There are three services, viz. Project, Map, and Experiment that users can access and utilise. In SALUS-WebGIS, it is not possible for users to run any simulations without maps and experiments. In the Map element, users can upload their own shapefile or digitize the area of interest on Google maps. In experiment element, users (farmers, policy-makers or other stakeholders) can create, edit or the delete an experiment. Soil data and weather data were obtained from the Vietnam Ministry of Natural Resources and Environment, and Vietnam National Centre for Hydro-Meteorological Forecasting with format data (sol or wth) or SALUS format (.sdb or .wdb). After simulating, results can be displayed in a time series choropleth map or chart.

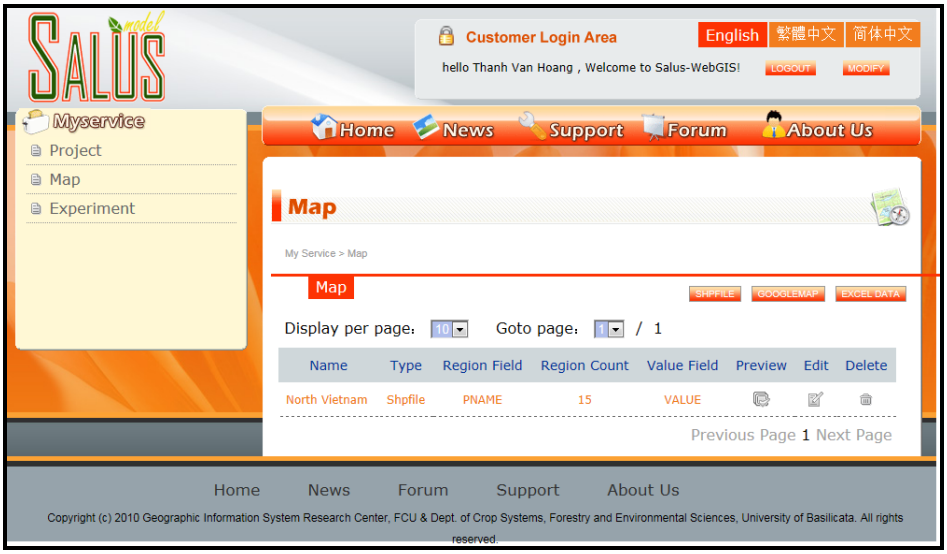


***Figure 5:*** *SALUS-WebGIS User Interface*

## 2.6. Meteorological Data

The soil data, daily weather, including daily temperature, precipitation, sunshine hour data used in this study are sourced from the Vietnam National Centre for Hydro-Meteorological Forecasting over 30 years from 1982–2011. Those data were obtained for seven major meteorology stations in the Red River Delta (Table 2).

***Table 2:*** *Seven Meteorology Stations in Red River Delta*

| | Provinces | Meteorology Station | ID Station | Latitude | Longitude |
|---|---|---|---|---|---|
| 1 | Ha nam | Ha Nam | Hnam | 20.5 | 105.9 |
| 2 | Hung Yen | Hung Yen | Hyen | 20.7 | 106.1 |
| 3 | Ha Noi | Lang | Lang | 21 | 105.8 |
| 4 | Nam Dinh | Nam Dinh | NamD | 20.4 | 106.2 |
| 5 | Ninh Binh | Ninh Binh | Nbin | 20.3 | 106 |
| 6 | Hai Phong | Phu Lien | PhuL | 20.8 | 106.6 |
| 7 | Thai Binh | Thai Binh | ThBi | 20.4 | 106.4 |
| 8 | Bac Ninh | Lang | Lang | 21 | 105.8 |
| 9 | Vinh Phuc | Lang | Lang | 21 | 105.8 |
| 10 | Hai Duong | Phu Lien | PhuL | 20.8 | 106.6 |

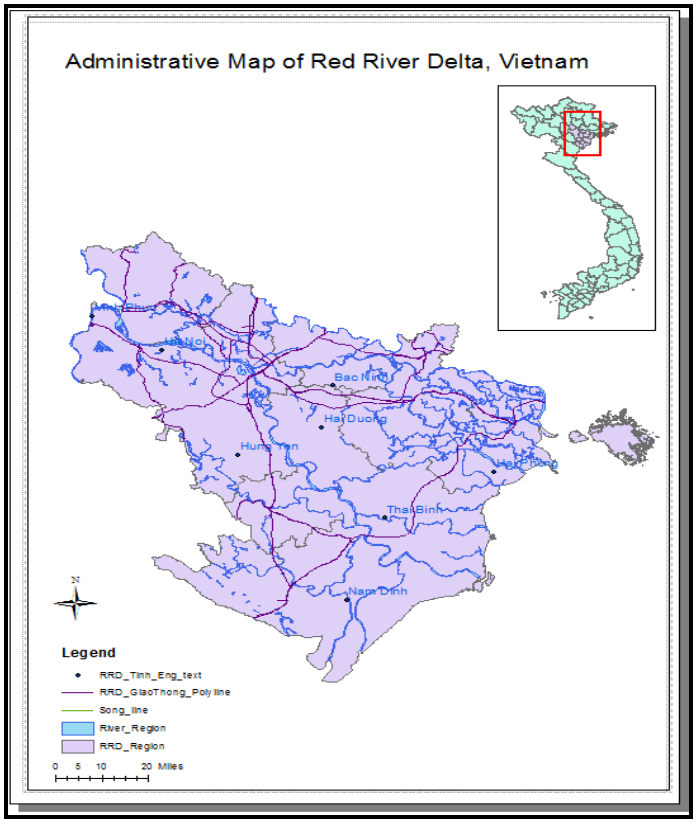


***Figure 6:*** *Location Map*

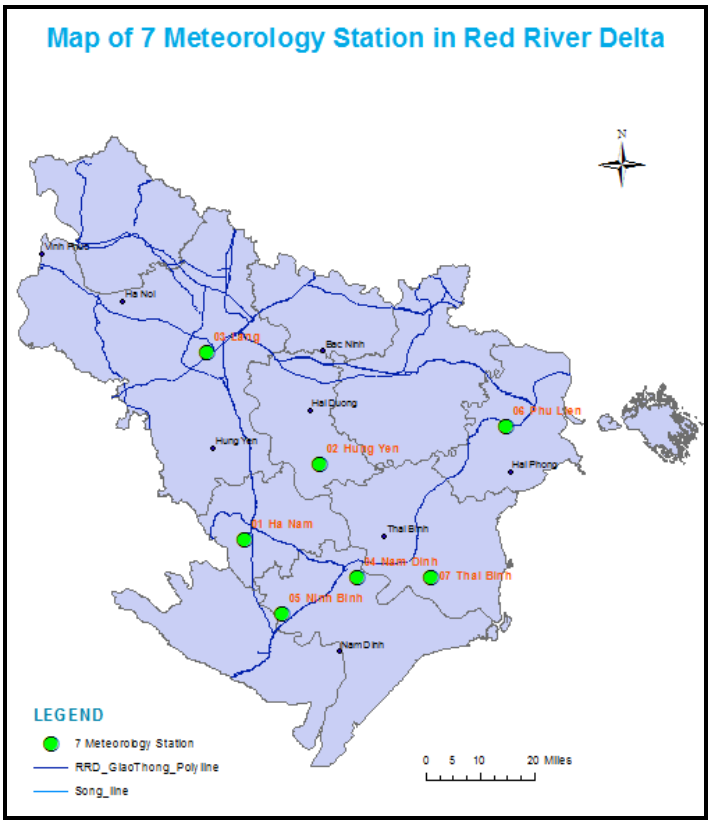


***Figure 7:*** *Location of Seven Meteorological Stations for Red River Delta*

## 3. Results and Discussion

### 3.1. Comparison of Model Simulations with Observation

Ha Nam station: Simulated and observed for Rice Productivity from 1982 to 2011.

The SALUS model was used to simulate rice productivity for the past 30 years from 1982 to 2011. A validation model was used to adjust some parameter co-efficient inside the model such as soil, genetic, management, and real daily weather data. We tried to adjust simulation parameters to fit with observed results (Figure 8: Ha Nam station). The outcome shows that simulated results are quite fit with observed one. Hence the model can predict rice yield very well. It illustrates almost the same pattern observed ones. The model can predict for true conditions under different climates and as the simulated rice yield line fits closely to the observed one (Figure 8).

At Ha Nam station, the actual rice yield in 1982 is 2900 kg/ha, after adjusting data the simulated yield is 3436.4 kg/ha. In 2010: the observed yield is 5940 (kg/ha), after adjusting data in model, the simulated yield is 5838 (kg/ha). In 2011: the observed yield is 6080 (kg/ha), after adjusting data in model the simulated yield is 6243 (kg/ha). This process shows that rice productivity has increased during the last three decades, a good trend for the Red River Delta, the second biggest delta in Vietnam.

The reason rice yield increased is due to delta soil. Soil profiles were station specific and represented typical regional soil for rice cultivation. Soil profile data for each station were extracted from the Vietnam Ministry of Agriculture and Rural Development. Red River Delta has high soil quality. Ha Nam station have soil depth with 5 layers, the lower limit of soil water is 0.17 (it means even it is in dry weather, still have 17% of water inside this layer).

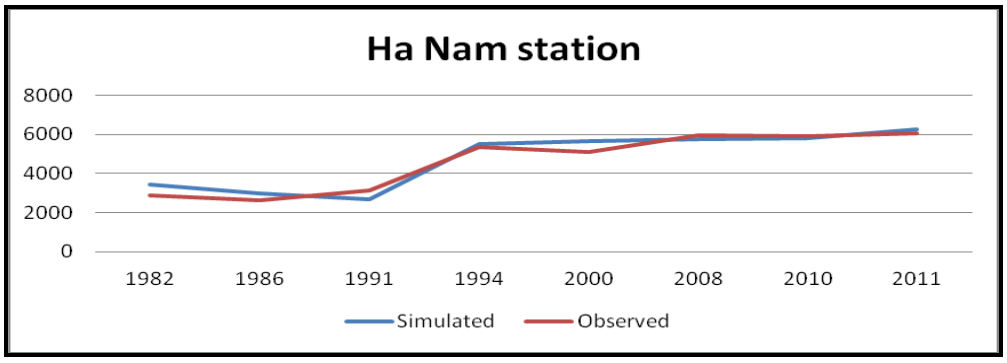


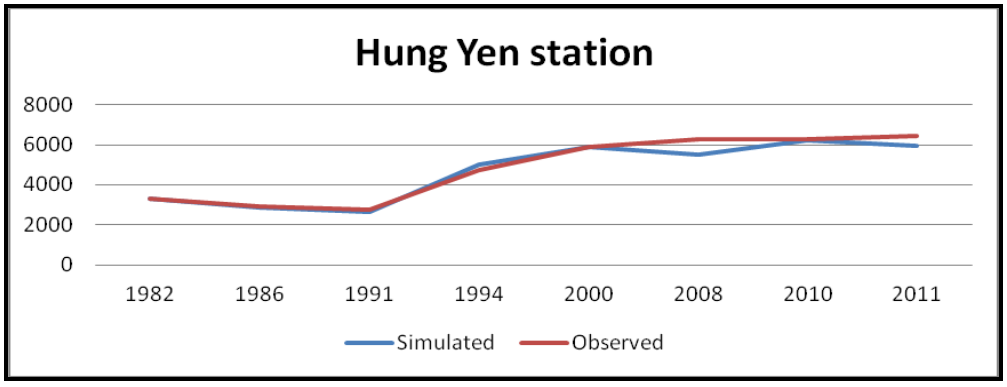

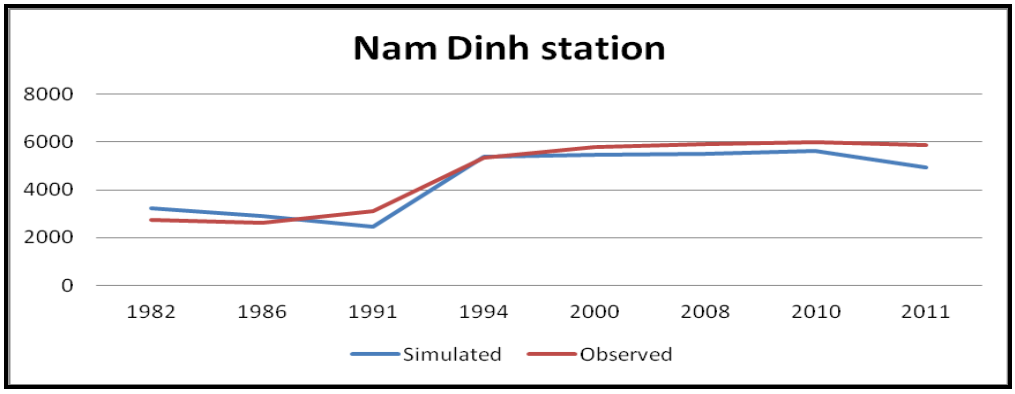


***Figure 8:*** *Observed and Simulated Rice yield from 1982-2011*

### 3.2. Validation of SALUS Model

Rice is the most important staple food crop of the world's population. For each station and rice growing season we used experiment records from one year for model parameters calibration, and the records of several other years for model validation. The experiment records included detailed information on crop phenology, management practices such as irrigation, fertilization, tillage) and crop yield and yield component. Each crop has two crop growing seasons including winter crop, and spring crop. Automatic planting was defined as planting once soil temperature and moisture conditions.

Soil profiles were station specific and represented typical regional soils for rice cultivation. Soil profile data for each station were extracted from Vietnam Ministry of Agriculture and Rural development. We evaluate the accuracy of models by calculating the root mean square error (RMSE) between the observed and simulated value:

$$RMSE = \sqrt{\frac{1}{m}\sum_{k=1}^{m}(t_k - y_k)^2}$$

Where, $t_k$ is the actual value, $y_k$ is the predicted value produced by the model, and m is the total 31 observed years. In the two validation studies with the CROPSYST model, RMSE was between 383 and 560 kg ha-1 (Bellochi et al., 2002). In the study with the APSIM model, RMSE was obtained from simulated and observed above ground biomas at 1200 kg ha-1. In our study RMSE range from (-1000) to 294. The measure weather data were provided by Vietnam National Centre for Hydro-meteorological Forecasting and from each local meteorological station located about 10-20 km away from the study area. Soil input data (sand, silt and clay content, bulk density, organic carbon and water limits) were determined, to minimize the RMSE values for the complete field and obtain an average percentage difference between simulated and measured values of yield within the stable zone (T.Y. Chou et al., 2011).

The simulation accuracy regarding the soil water contents shows two different patterns. The simulation quality was evaluated using also RMSE obtained from simulated and observed rice yield. RMSE obtained from the comparison of observed yield with those simulated by SALUS model. The grain yield was obtained in the model from a conversion that R2 = 0.8715 the model (Figure 9) shows that the observed data fits closely to the simulated data.

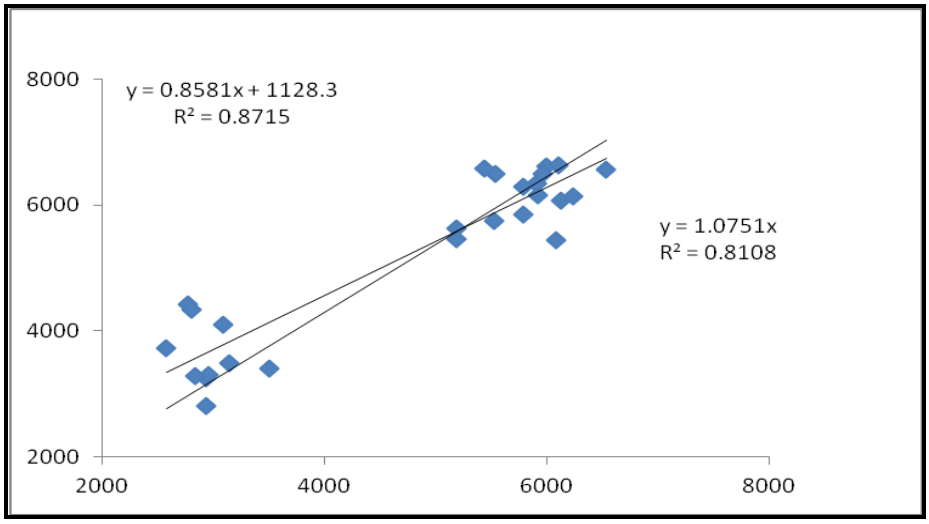


***Figure 9:*** *Simulated with Observed Rice Yield for 30 years*

Using the data in the past 30 years was shown that SALUS model is a very good model to simulate the impact of climate change on grain yield (Figure 8).

SALUS generates precipitation, daily maximum and minimum temperatures, and solar radiation. For each station, we first parameterized SALUS by using daily precipitation data from 1982-2011 as well as daily maximum (Tmax) and minimum (Tmin) temperature and solar radiation data. SALUS helps the users prepare and analyze weather data for parameterization and generation. SALUS model was used to generate 30 years (1982-2011) of daily weather data of maximum and minimum temperature, precipitation, and solar radiation for each station to represent the baseline climate conditions. To evaluate the performance of SALUS, we extracted 30 years of daily weather data, and compared these values with actual daily weather data.

### 3.3. Climate Change Projection in Study Areas

According to International Food Policy Research Institute (IFPRI) 2010, a brief overview of climate change in temperature and rainfall in the Red River Delta, and their projection features on the study stations are presented in Table 3, and Table 4. Those illustrate substantial differences in projected $CO_2$ concentration trajectories. Based on IFPRI 2010 the time series of global warming as projected, changes in temperature in the Red River Delta range from 1-2 degree Celsius, and changes in rainfall range from (-14)–10%, hence we created climate change scenarios for the Red River Delta in this research.

***Table 3:*** *Average Annual Temperature (in degrees) Increase Compare Red River Delta among Agro-Ecological Zone*

| Agroecological Zone | IPSL-2030 | IPSL-2050 | GISS-2030 | GISS-2050 | MONRE-2030 | MONRE-2050 |
|---|---|---|---|---|---|---|
| North West | 1.18 | 2.22 | 0.91 | 1.39 | 0.80 | 1.33 |
| North East | 1.18 | 2.22 | 0.89 | 1.41 | 0.73 | 1.28 |
| Red River Delta | 1.19 | 2.21 | 0.87 | 1.42 | 0.70 | 1.28 |
| North Central Coast | 1.14 | 2.02 | 0.85 | 1.41 | 0.85 | 1.55 |
| South Central Coast | 0.86 | 1.61 | 0.99 | 1.62 | 0.53 | 0.93 |
| Central Highlands | 0.84 | 1.57 | 0.94 | 1.55 | 0.50 | 0.85 |
| South East | 0.81 | 1.49 | 0.78 | 1.30 | 0.63 | 1.03 |
| Mekong River Delta | 0.84 | 1.54 | 0.78 | 1.31 | 0.62 | 1.02 |

Source: Authors' calculations.

***Table 4:*** *Average Percentage Changes in Annual Precipitation Compare Red River Delta among Agroecological Zone*

| Agroecological Zone | IPSL-2030 | IPSL-2050 | GISS-2030 | GISS-2050 | MONRE-2030 | MONRE-2050 |
|---|---|---|---|---|---|---|
| North West | -16.5 | -12.7 | 9.8 | 19.4 | 1.7 | 2.8 |
| North East | -16.5 | -11.8 | 10.5 | 13.5 | 1.8 | 3.0 |
| Red River Delta | -14.2 | -9.2 | 8.6 | 10.1 | 2.1 | 3.5 |
| North Central Coast | -11.9 | -7.0 | 7.6 | 10.0 | 2.2 | 3.6 |
| South Central Coast | -7.8 | -9.7 | 5.2 | 5.7 | 1.6 | 2.8 |
| Central Highlands | -11.0 | -5.6 | 4.3 | 6.0 | 0.1 | 0.0 |
| South East | -10.7 | -5.0 | 5.1 | 6.3 | 0.7 | 1.3 |
| Mekong River Delta | -10.5 | -6.3 | 5.2 | 6.3 | 0.9 | 1.5 |

Source: Authors' calculations.

The scenarios for Red River Delta catchment used in this study are based on two strong changing forces based on temperature and/or precipitation. Scenario from the past 30 years from 1982-2011 follow:

Scenario A: For temperature – plus, minus 1 degree, Rainfall – plus, minus 10%; $CO_2$: 550ppm

Scenario B: For temperature – plus, minus 2 degree, Rainfall – plus, minus 14%; $CO_2$: 550ppm

After adjusting all parameters, we run the model again the outcome from those figures follows:

Comparison of Dry-weight grain among 3 scenarios:

At Ha Nam station:

The outcome of Dry-weight grain is always uncertain as it depends on climate variables. A correlation between achieved Dry-weight grain during the 30 year study period and cumulative irrigation totals during the growing season is evident. The results of Dry-weight grain are compared with observed yield for the years 1982-2011 are presented in Figure 10. The figure shows that every year was 2 crop rotations, and most Dry-weight grain yields are increased. Out of three scenarios, grain yield in scenario B dramatically increased under climate change. Especially in 1984, grain yield in scenario B is increased double than the past 30 years scenario, from 3343 to 6503 kg/ha.

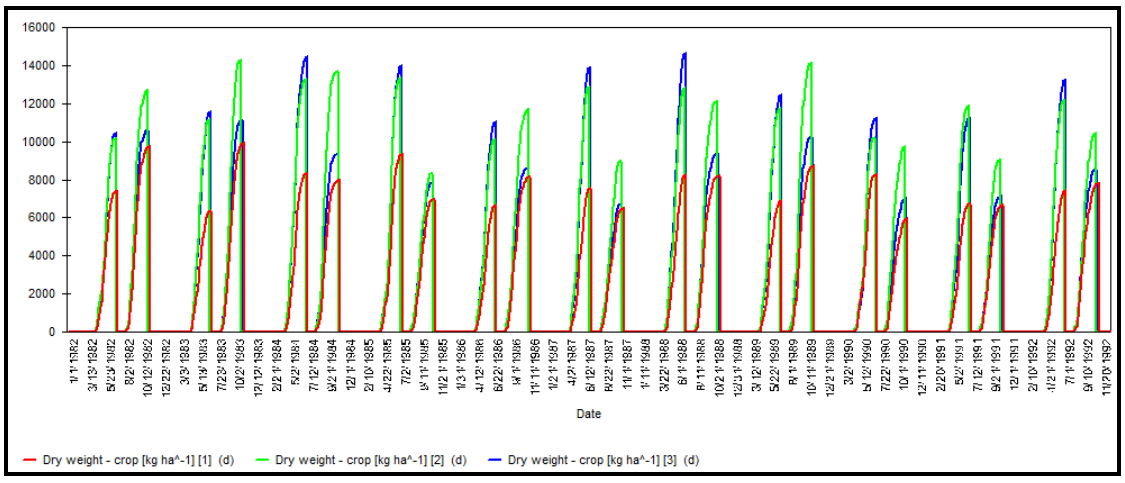


***Figure 10:*** *Dry Weight-Crop in Ha Nam Station from 1982-1992*

Ha Nam station: The figure shows that cumulative irrigation.

The simulation results of the SALUS model estimating the effect of the conventional tillage, minimum tillage and no tillage on carbon loss from the soil surface as carbon dioxide ($CO_2$) are presented in the figure below (Bruno Basso et al., 2006). The no tillage clearly showed a reduction in C losses through $CO_2$ as expected due to lower soil mineralization and higher accumulation of organic matter. The Figure 11 shows that the no tillage treatment sequestered in the soil about 20000 kg ha-1 of carbon compared to the minimum and conventional tillage treatment in the simulated period of 30 years. There were no significant differences. Tillage practices were observed between the two tilled treatments. Tillage practices disturb soil structure lead to fracturing which increases the movement of $CO_2$ out of the soil and oxygen into it (Reicosky et al., 1995; Lal, 1997; Lal, 2004a). In this study, the reduction of $CO_2$ emission in the no tillage systems converts into an increase in carbon storage which builds organic matter and long term productivity.

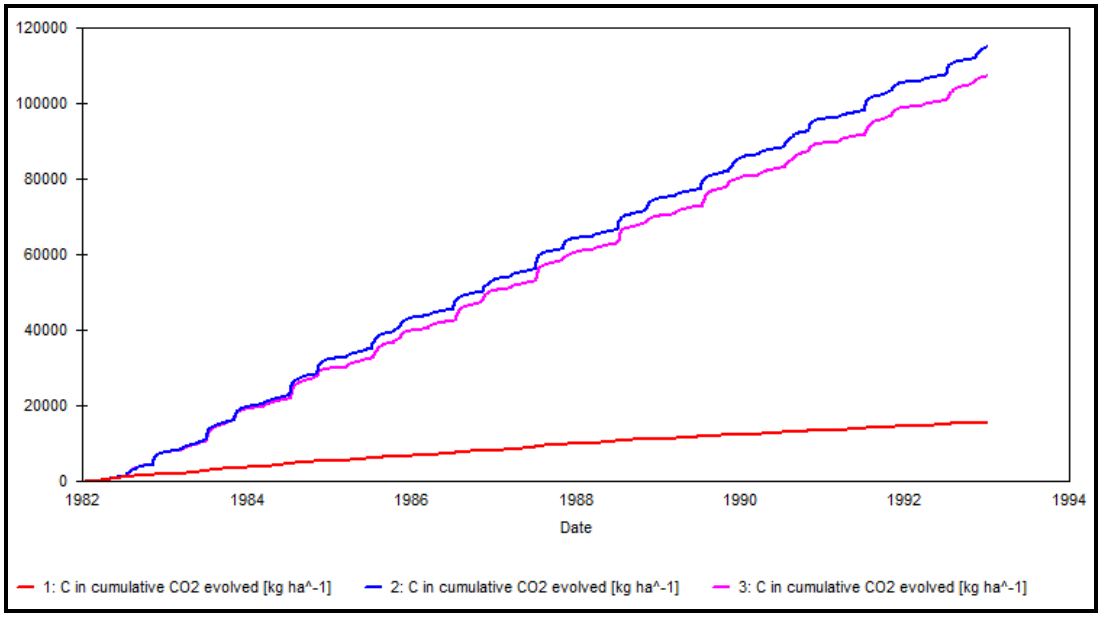


***Figure 11:*** *Simulated Carbon in Cumulative $CO_2$ Evolved from a Loamy Soil under Different Tillage Systems (Ha Nam Station, Red River Delta, Vietnam)*

### 3.4. Water Use

In this context water resources will play a key role as crops and livestock need a lot of water to grow (WWAP, 2012). Irrigation plays an important role, but in the past, irrigation areas have varied across the different countries. Climate change will have a particularly strong impact on water resources. The most direct impact of higher temperatures and drier periods is the decrease of soil moisture and thus a decrease of the water availability for plants. An increasing demand of irrigation water might consequently contribute to increased competition for scarce water resources. The outcome shows rice yield in Red River Delta, and carbon in cumulative $CO_2$ evolved are also increased, it is good for agriculture productivity but it means pressure on future water demand and availability in Red River Delta may increase.

In Vietnam, Red River Delta is the second biggest delta, and there is an urgent need to understand the dynamics of the local climate and make predictions to respond to climate variability and change. Climate change is a serious problem in Vietnam, and a serious challenge to social and economic development in developing countries such as Vietnam.

## 4. Conclusion

The results from the study suggested that the effect of predicted future climate change on rice productivity can be determined using the SALUS model together with GIS platform. Climate changes pose severe challenges to the adaptive capacity of rural households and communities and, given that - Vietnam is one of the country's most vulnerable to climate change. It is important to try and understand how these ways vary from region to region according to the type of agriculture. The SALUS model proves quite successful in quantifying climate change impacts on agriculture farmland in the Red River Delta of northern Vietnam. Results of the experiment establish that such maps can show the spatial variations in the impact of climate change and $CO_2$ emission on rice production in an agricultural context. With sufficient data, the SALUS model can be used to simulate these elements for entire countries.

Based on the results of this study, yield changes vary widely across crops and agro-ecological zones under climate change impact. $CO_2$ emission should theoretically tend to increase yields and can play a positive role in plant growth. Recognizing potential impacts of climate change, the government of Vietnam recognizes the potential impact of climate change on its agricultural economy and has developed a legal framework for sustainable development and climate change that includes policy instruments and energy efficient strategies for agriculture. The SALUS-WebGIS tool can assist decision makers in understanding the applicability of various management practices to relevant regions.

## Acknowledgement

The authors acknowledge the supporting by Vietnam Ministry of Natural Resource and Environment, Vietnam National Centre for Hydro-Meteorological Forecasting, and Vietnam General Statistics Office. We thank Professor Mike Meadows from the Department of Environment and Geographical Science at the University of Cape Town for his helpful comments. All support is gratefully acknowledged.

## References

Bruno Basso, J.T., Ritchie, P.R., Grace and Luigi Sartori. *Simulation of Tillage Systems Impact on Soil Biophysical Properties using the SALUS Model*. Italian Journal of Agronomy. 2006. 4; 677-688.

Bruno Basso, 2013: *SALUS Software.* System Approach for Land Use Sustainability. http://salusmodel.net.

Bellochi, G., Silvestri, N., Mazzoncini, M. and Menini, S. *Using the CROPSYST Model in Continuous Rainfed Maize (Zea mais L.) using Alternative Management Options*. Italian Journal Agronomy. 2002. 6 (1) 43-56.

Chang, K.T., 2004: *Introduction to Geographic Information Systems*, McGraw Hill.

Chunzhao Liu, Dan Ma, Xianlei Shan, Jianfei Yang, 2010: *Eco-simulation and Modeling of Monoculture and Polyculture Milkfish Farming in the Bolinao Area and Its Economic Analysis*. Proceeding CESCE '10 Proceedings of the 2010 International Conference on Challenges in Environmental Science and Computer Engineering. Vol. 1. 222-226.

Phan, D.B., Wu, C.C., and Hsieh, S.C. *Impact of Climate Change on Stream Discharge and Sediment Yield in Northern Vietnam*. Water Resources. 2011. 827-836.

IPCC Intergovernmental Panel on Climate Change, 2007: *IPCC Climate Change 2007: Impacts, Adaptation, Vulnerability*. 145-148.

IPCC Intergovernmental Panel on Climate Change, 2013: *IPCC Climate Change 2013: The Physical Science Basis*. The 5th Assessment Report. Cambridge University Press.159-254.

IPONRE, Vietnam, 2009: *Vietnam Assessment Report on Climate Change (VARCC)*, Van hoa-Thong tin Publishing House. 25-71.

Cowie, J., 2007: *Climate Change, Biological and Human Aspects*. Cambridge University Press, America. 1-65.

Karimi, H.A., and Houston, B.H. *Evaluating Strategies for Integrating Environmental Models with GIS: Current Trends and Future Needs, Computers, Environment and Urban Systems*. 1996. 20 (6) 413-425.

Kyoto Protocol/United Nations, 1998: *Framework Convention on Climate Change*. http://www.unccc.org.

Lal, R. *Residue Management, Conservation Tillage and Soil Restoration for Mitigating Greenhouse Effect by $CO_2$ Enrichment*. Soil & Tillage Research. 1997. 43 (1-2) 81-107.

Lal, R. *Managing Soil Carbon*. Science. 2004. 304; 393.

Ministry of Natural Resources and Environment MONRE, 2009: *Climate Change, Sea Level Rise Scenarios for Vietnam*. 6-16.

Ministry of Natural Resources and Environment MONRE, 2010: *Vietnam Agriculture Development Strategies in Period 2011-2020* (Vietnamese language). 35-40.

Parton, W.J., 1996: *The Century Model*. NATO ASI Series I. Springer-Verlag, Berlin, Germany, 759. 283-295.

Mitchell, R.A.C., Lawlor, D.W., and Porter J.A. *Interaction of CO2 and Temperature in the Growth and Yield of Winter Wheat: Test of ARCWHEAT Model.* Journal Plant Ecology. 1993. 104-105 (1) 460-461.

Reicosky, D.C., 1995: *Impact of Tillage on Soil as a Carbon Sinkin*: *Farming for a Better Environment. A White Paper.* Soil and Water Conservation Society, Ankeny, Iowa, USA. 50-53.

Ritchie, J.T., Godwin, D.C., Otter-Nacke, S., 1985: *CERES-Wheat: A Simulation Model of Wheat Growth and Development*. Texas A&M University Press, College Station, TX.

Ritchie, J.T., Singh U., Godwin, D.C., and Hunt, L., 1989: *A User's Guide to CERES Maize-V.2.10*. Muscle Shoals, AL. International Fertilizer Development Center.

Singh, S.N., 2009: *Climate Change and Crop*. J. Environment Science and Engineering.

The Vietnam Water Partnership, 2010: *Report on Climate Change Activities in Vietnam*.

Chou, T.Y., Chih, Y.C., Lung, S.Y., Bruno Basso and Yeh, M.L., 2011: *The Study of Integrating Web-GIS with Sustainable Land-use Model*. Conference ISPRS Workshop on Dynamic and Multi-dimensional GIS, Shanghai.

United Nation, 2009: *Vietnam and Climate Change: A Discussion Paper on Policies for Sustainable Human Development*. 5-14.

Vietnam General Statistic Office, 2000, 2005, 2012: *Vietnam Statistic Year Book.*

WWAP, 2012: *The United Nations World Water Development.* Report 4. WWAP, Paris, France.

Zhen Li, Yoshiki Saito, Eiji Matsumoto, Yongji Wang, Shigeko Haruyama, Kazuaki Hori and Le Quoc Doanh, 2006: *Palynological Record of Climate Change during the Last Deglaciation from the Song Hong (Red River) Delta, Vietnam, PALAEO*. 235, 406, 430.

**Cloud Publications**
International Journal of Advanced Remote Sensing and GIS
2014, Volume 3, Issue 1, pp. 598-605, Article ID Tech-287
ISSN 2320 – 0243

Research Article | Open Access

# Assessment of Glacier Health in Alknanada, Sub Basin of Ganga Using Remote Sensing and GIS Techniques

**Swati Tak[1], A.K. Sharma[2], A.S. Rajawat[2], Ajai[2] and S. Palria[1]**

[1]Department of Remote Sensing & Geoinformatics, Maharshi Dayanand Saraswati University, Ajmer, Rajasthan, India
[2]Space Applications Centre (ISRO), Ahmedabad, Gujarat, India

Correspondence should be addressed to Swati Tak, takswati7@gmail.com

Publication Date: 3 July 2014

Article Link: http://technical.cloud-journals.com/index.php/IJARSG/article/view/Tech-287



**Abstract** Glacier is a key component and plays an important role in the hydrological system. The melt water from glacier is an important source in the Himalayan regions as millions of people rely on it. The source of melt water depends on the distribution of glaciers and its mass balance. Monitoring of glaciers and assessment of its health is thus important to assess the availability of water in Indian Himalaya. In Himalaya and Trans Himalaya regions, the distribution of glaciers varies widely and depends mainly on the topography and monsoon characteristics. Around 32,392 glaciers are spread over in the Indus, Ganga and Brahmaputra Basins covering the Himalaya and Trans Himalaya regions, and it is difficult to monitor these via field due to rugged terrain. Therefore, in this study remote sensing and GIS techniques have been used to study the glaciers and its health in Alaknanda, sub-basin of Ganga, India.
**Keywords** *Glacier Health; Composite Health Index; Alaknanda; Ganga Basin*

## 1. Introduction

The glacier regions of Indus, Ganga and Brahmaputra basins encompass about 0.94 million $km^2$ areas respectively. Almost 71,182 $km^2$ are covered by glaciers and spread over the karakoram to North eastern Himalayan region (Sharma et al., 2011; Kulkarni and Buch, 1991; Kulkarni et al., 1999; 2005; WIHG & HPRS, 1992-93). Besides the annual mass balance, other technique for classification of glacier into healthy or fragile glaciers is the assessment of the health status which is very much needed to estimate the effect of climate on the glacial environment (Benn, 1998; Flint, 1971; Paterson, 1994; Sugden, 1976). Therefore, in this study, the glacier health is assessed based on Remote Sensing and GIS technique along with ancillary data. Further, Composite Health Index (CHI) method is used for the classification and to understand the present health condition of glaciers in Alaknanda, Sub-basin of Ganga.

## 2. Study Area

The Alaknanda River Basin is one of the major basins of Ganga. The Alaknanda basin lies between 30°0' N to 31°0' N and 78°45' E to 80°0' E and represents the eastern part of the Garhwal Himalaya (Figure 1). Alaknanda covers an area of 10882 km$^2$. Out of the total area, 433 km$^2$ is covered by glaciers (Figure 2). The altitude of the glaciers varies between 3500 to 6000 meters (Figure 5).

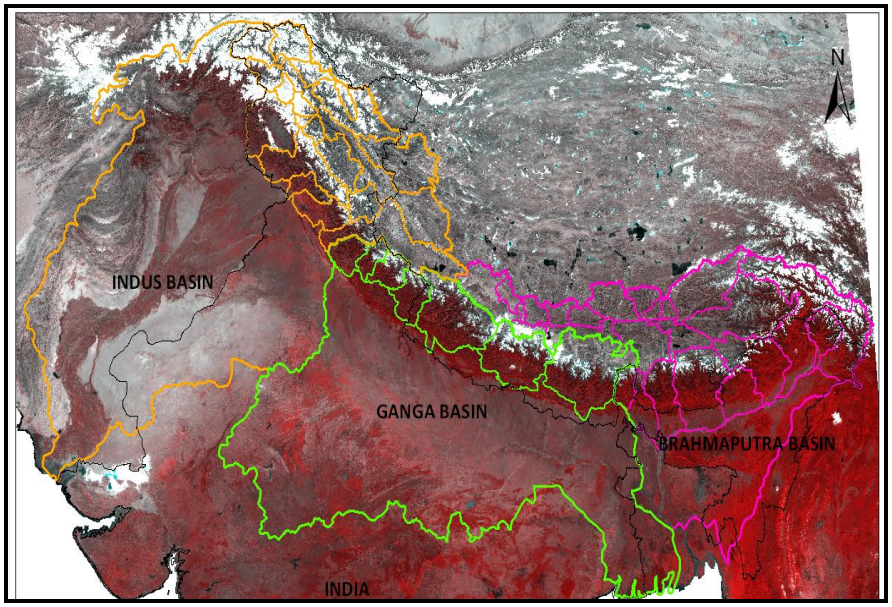


***Figure 1:*** *Index of Alaknanda, Sub Basin of Ganga River Basin*

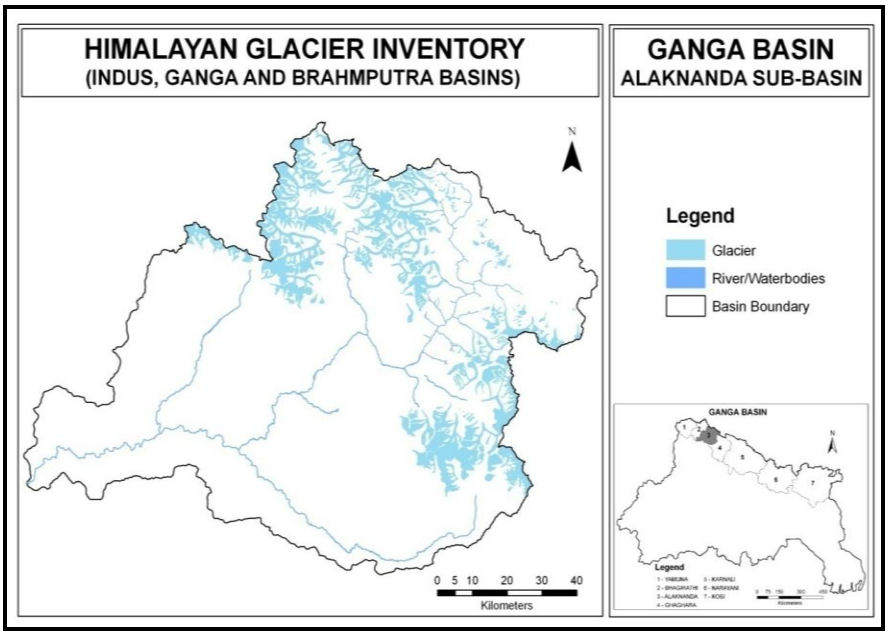


***Figure 2:*** *Glaciers and Watershed of Alaknanda Basin*

## 3. Data used and Methodology

The data used are IRS AWiFS and SRTM DEM (Table 1). Advanced Wide Field Sensor (AWiFS) includes four spectral bands with 56m spatial resolution covering a swath of 740 km. The band combinations are green (0.52-0.59 μm), red (0.62-0.68 μm), NIR (0.77-0.86 μm) and SWIR (1.55-1.70 μm). AWiFS data is obtained from National Data Centre of National Remote Sensing Center (NRSC) Hyderabad and DEM from Shuttle Radar Topography Mission (SRTM). The glacier morphology map and data sheet for glacier inventory are prepared using IRS-P6 AWiFS data from 2005 to 2007. The morphological parameters like Area of glacier, Length, Elevation, Orientation and Ice exposed area are taken from the inventory datasheet and with these parameters, the secondary parameters such as Accumulation area ratio, Percent debris cover, Percent slope are obtained. Further, they are grouped into 5 classes and rank is assigned as per the significance.

***Table 1:*** *Primary Data Set Used for Analysis*

| Theme | Feature Type | Main Source | Remarks |
|---|---|---|---|
| 1. Base Map | | | |
| Topographic map | Polygon | SOI open series maps | 15’ 15’ latitude-longitude grid and SOI reference no. |
| Country Boundary | Polygon | SOI and admin. Maps | Country |
| Digital Elevation Model | Grid | SRTM data | Image grid |
| 2. Hydrology | | | |
| Drainage lines | Line | Irrigation Atlas & Satellite Data | Streams – nomenclature |
| Drainage poly | Polygon | - DO - | Water body, river boundary |
| Watershed Boundary | Polygon | Watershed Atlas, Satellite data | Watershed boundary and alpha numeric codes |
| 3. Glacier | | | |
| Glacier boundary | Polygon | Satellite data | Ablation, accumulation, snow cover areas, etc |
| Glacier lines - Snow Line / Ice divide | Line | Satellite data | Line divide between accumulation and ablation area |
| Glacier point - Snout location | Point | Satellite data | Glacier terminus point and glacier coordinate point |
| Glacier elevation locations | Point | Satellite data & DEM | Glacier elevation location points like highest or lowest elevation of glacier, etc. |

Based on Saaty's (Saaty, 2008) method, the parameters are assigned and the comparison matrix is prepared. The matrix is solved by Eigen vector method and the consistency index including Eigen weights and consistency ratio are derived. The consistency ratio less than or equal to 0.1 is acceptable (Saaty, 2008). Larger values require the decision maker to reduce the inconsistencies by revising judgments. Weighted ranks are obtained by multiplying the Eigen weights and rank assigned. For a given glacier, the composite weights are obtained by summation of all weighted ranks, known as Composite Health Index (CHI) values. They are categorized into five health status classes to identify the relative fragile or healthy glaciers in the Alaknanda basin (Figure 3).

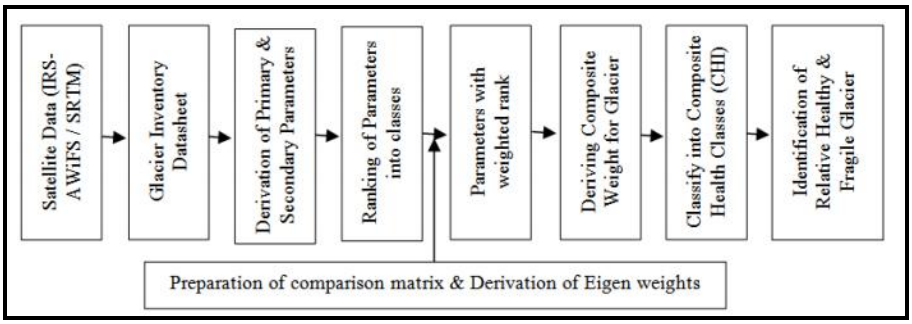


***Figure 3:*** *Development of Comparison Matrix & Derivation of Eigen Weights*

## 4. Results

The Alaknanda sub-basin spread over in 10882 km$^2$ area and it has 253 glaciers, covering 39 percent as the glaciated area. The aerial distribution varies from 3500 to 6000 m.a.s.l. The accumulation area is 787.07 km$^2$, debris covered ablation area debris is 349.79 km$^2$, ice exposed ablation area is 193.07 km$^2$. The total volume of glacier ice as estimated in Alaknanda sub-basin is 183.85 km$^3$. For all the 253 glaciers in Alaknanda, the weighted analysis has been carried based on the eight parameters in GIS and CHI values lies between 241 and 544. Each of the eight parameters is ranked as per its significance for the glacier health. Thereafter, they are categorized in to five relative glacier health categories (Figure 4, Table 9). Based on the CHI values, it is estimated that out of 253 glaciers in Alaknanda basin, there are 35 fragile glaciers having CHI values less than 290, which cover area of 73.9 km$^2$ and 11 healthy glaciers having CHI values greater than 440, which cover area of 26 km$^2$. The mean size of fragile glaciers (CHI category I and II) is 3.4 km$^2$ healthy glacier (CHI category IV and V) is 5.8 km$^2$. The glaciers in this basin are with less albedo, because of higher percentage of debris covered ablation area. The Glaciers having AAR greater than 0.6 are 122, which covers 10.75%, area and less than 0.6 are 131, which cover 85.29% area.

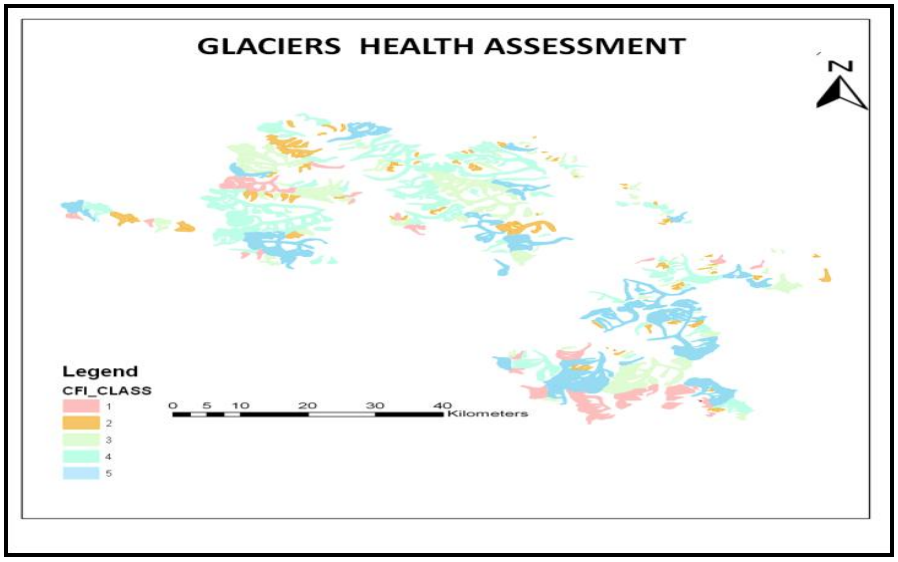


***Figure 4:*** *Assessment of Glaciers Health in Alaknanda Sub-basin*

There glaciers with around 21% are oriented in northeast direction but cover only 9% area. The 19% southeast direction glaciers cover almost 31% area. The southwest direction has 20% glaciers covering 21% area. The south facing glaciers are very few in number about 9% glaciers, which cover 16% area. The west facing glaciers are the least in number and area i.e. 5% with an area of 1%. The ranks of the eight parameters are given in Tables 2 to 8. Higher rank has been assigned to the higher values of AAR, Area, Length, elevation, percentage debris cover and vice versa in the case of ice exposed area and percentage slope. The lower CHI values represent the relatively fragile glacier and the higher values represent the relatively healthy glaciers.

***Table 2:*** *Glaciers Length*

| Class | Class-Interval (Km) | No_of_Counts | Rank |
|---|---|---|---|
| 1 | <1.0 | 25 | I |
| 2 | =>1.0 TO <2.0 | 71 | II |
| 3 | =>2.0 TO <5.0 | 114 | III |
| 4 | =>5.0 TO<10.0 | 26 | IV |
| 5 | >10.0 | 17 | V |

***Table 3:*** *Glaciers Area*

| Class | Class-Interval (Km) | No_of_Counts | Rank |
|---|---|---|---|
| 1 | <1.0 | 199 | I |
| 2 | =>1.0 TO <2.0 | 103 | II |
| 3 | =>2.0 TO <5.0 | 98 | III |
| 4 | =>5.0 TO<10.0 | 35 | IV |
| 5 | >10.0 | 49 | V |

***Table 4:*** *Percent Debris Cover*

| Class | Class-Interval (Km) | No_of_Counts | Rank |
|---|---|---|---|
| 1 | <1.0 | 26 | I |
| 2 | =>1.0 TO <2.0 | 44 | II |
| 3 | =>2.0 TO <5.0 | 52 | III |
| 4 | =>5.0 TO<10.0 | 22 | IV |
| 5 | >10.0 | 17 | V |

***Table 5:*** *Percent Slope*

| Class | Class-Interval | No_of_Counts | Rank |
|---|---|---|---|
| 1 | <1.0 | 77 | I |
| 2 | =>1.0 TO <2.0 | 78 | II |
| 3 | =>2.0 TO <5.0 | 81 | III |
| 4 | =>5.0 TO<10.0 | 14 | IV |
| 5 | >10.0 | 3 | V |

***Table 6:*** *Area Accumulation Ratio (AAR)*

| Class | Class-Interval | No_of_Counts | Rank |
|---|---|---|---|
| 1 | <1.0 | 215 | I |
| 2 | =>1.0 TO <2.0 | 8 | II |
| 3 | =>2.0 TO <5.0 | 3 | III |
| 4 | =>5.0 TO<10.0 | 1 | IV |
| 5 | >10.0 | 1 | V |

***Table 7:*** *Ice Exposed Area*

| Class | Class-Interval | No_of_Counts | Rank |
|---|---|---|---|
| 1 | <1.0 | 38 | I |
| 2 | =>1.0 TO <2.0 | 42 | II |
| 3 | =>2.0 TO <5.0 | 107 | III |
| 4 | =>5.0 TO<10.0 | 67 | IV |
| 5 | >10.0 | 53 | V |

***Table 8:*** *Orientation of Ablation & Accumulation Areas*

| Direction | No. of Glaciers |
|---|---|
| E | 18 |
| N | 20 |
| NE | 52 |
| NW | 27 |
| S | 23 |
| SE | 48 |
| SW | 50 |
| W | 15 |
| Total | 253 |

***Table 9:*** *Weightage Classes of Glaciers in Alaknanda Sub-Basin*

| Health Class | Class Weight | No Of Glaciers |
|---|---|---|
| I | <205 | 35 |
| II | 205 - 235 | 82 |
| III | 235 - 265 | 66 |
| IV | 265 - 295 | 46 |
| V | >295 | 24 |

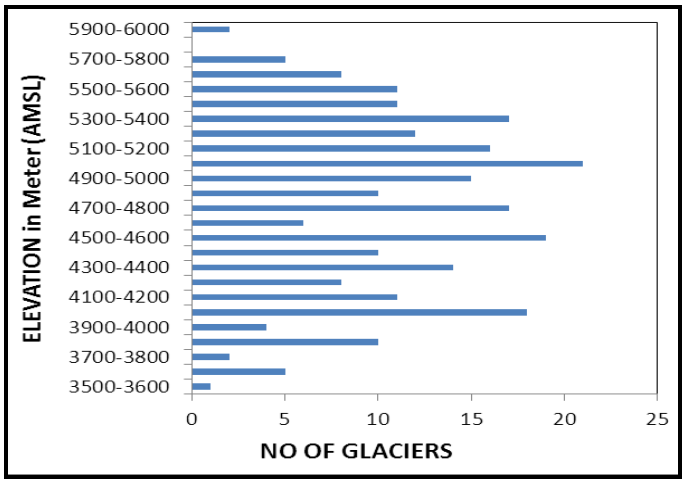


***Figure 5:*** *Area Altitude distribution of Glaciers in Alaknanda Basin*

## 5. Discussion

The glaciers oriented in northeast direction may retreat partly than the glaciers located in the southwest direction. This depends upon the availability of solar energy on the glacier surface. Among the eight parameters considered for the study, the AAR and altitude plays a major role, as these indicate the health of the glaciers and the status of mass balance. The CHI values represent the health condition of the glaciers, i.e., the lower value represents the fragile glaciers and vice versa in case of healthy glaciers.

## 6. Conclusion

The weighted analysis method based on multi parameter is very useful for deriving the Composite Health Index (CHI). Thus, the different health classes can be derived using remote sensing and GIS techniques at Sub-basin or Basin level. Thereafter, the derived parameters can be validated upon the availability of retreat values.

## Acknowledgement

Authors would like to thank the authorities at Maharshi Dayanand Saraswati University, Ajmer, and Space Applications Centre for the infrastructure provided and continuous support.

## References

A.K., Sharma, S.K., Singh, A.V., Kulkarni and Ajai et al., 2011: *Snow and Glaciers of the Himalayas.* Space Applications Centre, Ahmedabad.

Glacier Atlas of Satluj, Beas and Spiti Region at 1: 50k Scale Using IRS 1A / 1B (1992-93) Data - By SAC, Ahmedabad, Wadia Institute of Himalayan Geology, Dehradun and HP Remote Sensing Cell, Shimla.

Benn, D.I., 1998: Glaciers and Glaciation. Oxford University Press Census, 2001, Primary Census abstract, Census of India, 2001.

Flint, R.F., 1971: Glacial and Quaternary Geology. Wiley, 892.

Kulkarni, A.V., and Buch, A.M., 1991: *Glacier Atlas of Indian Himalaya*. SAC/RSAG-MWRD/SN/05/91, 62.

Kulkarni, A.V., Philip, G., Thakur, V.C., Sood, R.K., Randhawa, S.S., and Ram Chandra. *Glacier Inventory of Satluj Basin using Remote Sensing Technique*. Himalayan Geology. 1999. 20 (2) 45-52.

Kulkarni, A.V., Rathore, B.P., Randhawa, S.S., Sood, R.K., and Kaul Manoj, 2005: Glacier Atlas of Chenab basin.

Patterson, W.S.B., 1994: The Physics of Glaciers, Third Edition. Pergamon, 480.

Sugden, D.E., and John, B.S., 1976: Glaciers and Landscape. Arnold, 376.

**Cloud Publications**
International Journal of Advanced Remote Sensing and GIS
2014, Volume 3, Issue 1, pp. 627-641, Article ID Tech-288
ISSN 2320 - 0243

Research Article | Open Access

# Pixel-Wise Surface Water Balance Computation: Lower Yamuna Basin

**Ritu Ahlawat**

Department of Geography, Miranda House, University of Delhi, Delhi, India

Correspondence should be addressed to Ritu Ahlawat, ritu.ahlawat@gmail.com

Publication Date: 11 July 2014

Article Link: http://technical.cloud-journals.com/index.php/IJARSG/article/view/Tech-288



**Abstract** Traditional techniques in surface water balance computations revolve around point-based observed results of climatic variables. Basin-wide areal estimates derived from point interpolations may not reflect true character of sub-regional variations. Hence, pixel-wise water balance computation in the case of lower Yamuna river basin falling under Himalayan river system of India, is attempted in this paper using remote sensing and Geographical Information System based approach. A comparison of point and area-based estimates has been done based on both Thornthwaite and Penman methods. Water balance computations, aridity, humidity and moisture indices, surplus and deficit values at given data points have been used in map-based calculations by developing a script in GIS software – ILWIS (Integrated Land Water Information System). It was found that water balance computations, using point-based rainfall and other climatological data, result into broad generalization of deficit and surplus zones around meteorological stations. But, when zonal landuse and soil maps are crossed in GIS environment, then pixel-wise calculations of available water capacity can be used along with isohyetal maps to produce better areal estimates of hydrological regions. The results of pixel-wise computations have clearly brought out meso-level variations in hydrological categories. In addition, indirect energy balance estimates obtained from satellite images at different spatial scales can provide significant clues for better planning of water resources especially in design stage.
**Keywords** *Hydrological Regionalization; Map Calculations; Areal Estimation*

## 1. Introduction

Long-term yield estimates based on normal standards can differ significantly in terms of their areal extent especially in the case of extreme events and thus may affect developmental designs of irrigation/multipurpose projects in the region. It is the extension of point-based hydrological data record to areal estimates that decides the practical utility of potential yield. Various predictive models are nowadays being used to estimate frequency and intensity of rainfall and other climatic variables. The areal estimation of rainfall, however, could not be given due importance in many countries of the world. Present day hydrological capabilities, however, demand high level of accuracy in the statistics

obtained from collected data. Therefore, based on estimates of time-averaged areal mean of precipitation, configurations of spatial network were analysed particularly with respect to their location, duration of observation and measurement of error (Bras and Colon, 1978).

More important than precipitation is the water need because it defines the utilizable quantity of water. To determine water need the concept of potential evapotranspiration (PET), introduced by Thornthwaite (1948) still remains the most useful parameter. A book-keeping procedure presented in the form of water balance table formed the important basis of his climatic classification. At the same time, another significant attempt towards estimation of evapotranspiration was made by Penman (1948) who tried to combine aerodynamic and energy budget approach in his experiments. Several scholars worked on this principle as exemplified by the works of Tanner (1968) and Chidley & Pike (1970). Although there exist many a number of computer programmes to solve Penman equation but most of these are particular in data input, form of equation and data output. The options in estimation of evapotranspiration as discussed by Penman earlier and later on modified by Monteith (1981) are quite useful and these have incorporated in CROPWAT software of Food and Agriculture Organisation (FAO, 1992). A regional application of PET in different environmental conditions has also been discussed (Bruin, 1988). Another conceptual model of a catchment's annual water balance has also been developed that can be used to separate annual precipitation into three major components: surface runoff, base flow and vaporization. The model parameters can be estimated from past experience or can be calibrated using measured data (Ponce and Shetly, 1995).

In India, the most significant and leading contribution in the field of water balance studies were made by Subrahmanyam (1956) of Andhra University. He prepared maps covering whole of sub-continent to show spatial pattern of average annual water surplus and deficit computed after Thornthwaite method. Penman method was followed by Rao et al., (1971) to compute PET at all the climatological stations in India. Extent of water surplus and deficit based on these estimates of PET is seldom reliable as flood and droughts are unpredictable. In order to present water problem of an area in its perspective, variability in water balance obtained by averaging the results of 18 individual years showed greater fluctuations in water surplus. Hydrological regions have also been delineated in associations with combinations of surplus and deficit (Pandeya and Prasad, 1983). But, the hydrological region formed on the basis of Penman-based PET pose severe constraints due to limited stations in India recording all climatic parameters (Ahlawat, 1999). Therefore, the applicability of water balance method in the case of a small watershed and for a shorter time-period has been rendered useless.

Implications of water balance can be understood properly if basin-wise water budget is computed. Water resource development becomes more prominent in an area of both least and maximum rainfall like that of the Upper Vagai basin (Vishwanath and Ganesh, 1985). Popularity of applied studies of water balance became more important in the field of agriculture in India. Crop water requirements, irrigation scheduling methods (Doorrenbos and Pruitt, 1977), estimation of Hargreaves's reference crop evapotranspiration (Mandal and Challa, 1991), moisture adequacy index-based classification of agro-climatic zonation, influence on crop yield (Hema Malini, 1986), identification of drought prone areas (Dwivedi, 1993) and problems of water balance (Dwivedi and Bhar, 2003) - are few examples of such studies. However, the regional estimates of PET are interpolations made on the basis of point-based calculations of PET, and average soil and landuse conditions of the area as demonstrated at catchment level in Bundelkhand region (Ahlawat, 2000).

Of late, the search for theories and models has enhanced the need for precision in observation and analysis. Utility of Geographical Information System (GIS) in large-scale rainfall-runoff modeling, watershed modeling, soil erosion etc. is being demonstrated and applied by many scholars (Singh and Fiorentino, 1996). With the availability of remotely sensed data, regional estimates of evaporation and evapotranspiration have been made using surface temperature, surface *albedo*, vegetative cover and incoming solar radiation (Mallick et al., 2007; Minacapilli et al., 2009). As the reliability of hydrological

yield estimates depends upon spatial network of observational points therefore, an attempt has been made here to assess the network of hydrological data stations and their implications in hydrological regionalization. The components of water balance have to be computed in accordance with the corresponding soil and landuse for the smallest spatial unit of pixel chosen in GIS environment at basin scale.

## 2. Study Area

The river Yamuna, originating from Yamunotri glacier in the Mussorie range of the lower Himalayas at an elevation of about 6320 m above mean sea level traverses a journey of 1376 km before joining river Ganga at Allahabad at an elevation of just 94 m. The major input of flow in lower Yamuna is through Chambal near Etawah and, subsequently, through Sindh, Betwa and Ken rivers (Figure 1a). The lower Yamuna basin, being a transitional area of climate and geology with most of its coverage in central India, is selected for the present study. All right and left bank tributaries, downstream of Agra-Etawah ridge till its confluence with the river Ganga at Allahabad, are included in lower Yamuna basin. It drains about 76% of the total area under Yamuna basin falling in three states of Rajasthan, Uttar Pradesh and Madhya Pradesh (Figure 1b). The lower Yamuna basin, covering the catchments of Chambal, Sind, Betwa and Ken rivers on right bank; Rind and Senegar on left bank, extends from 22°30′ North to 27°20′ North latitudes and 72°10′ East to 82°0′ East longitudes. It is bounded by the Yamuna-Ganga *doab* in the north, Panna-Ajaigarh hills in the east, Vindhyan range in the south and Aravalli range in the west. Their catchments cover an area of about 260 thousand km$^2$ of which, 20 thousand km$^2$ (24%) lies in southwestern and southern Uttar Pradesh districts in Bundelkhand region, parts of districts along Yamuna left bank; 79 thousand km$^2$ in Eastern Rajasthan, parts of districts in Aravalli belt, districts in Mewar region; and remaining 140 thousand km$^2$ (76%) lies in northern Madhya Pradesh, M.P. Bundelkhand, Malwa plateau region, Sagar, Damoh and parts of districts in Central M.P.

The main problem of the region rests with the improvement of agriculture, which ultimately depends upon development of water resources. Although the region is drained by the Yamuna system, its higher southern bank and increasing gradient of land towards south do not permit the diversion of its flow southwards. Thus, water can be considered as a pivot of the whole regional economy particularly, in the ravinous and underdeveloped tract of the region. The severity of droughts and famines can be reduced if the potential of small ephemeral stream is estimated scientifically. Hence, regional water balance of the basin is presented in the present study.

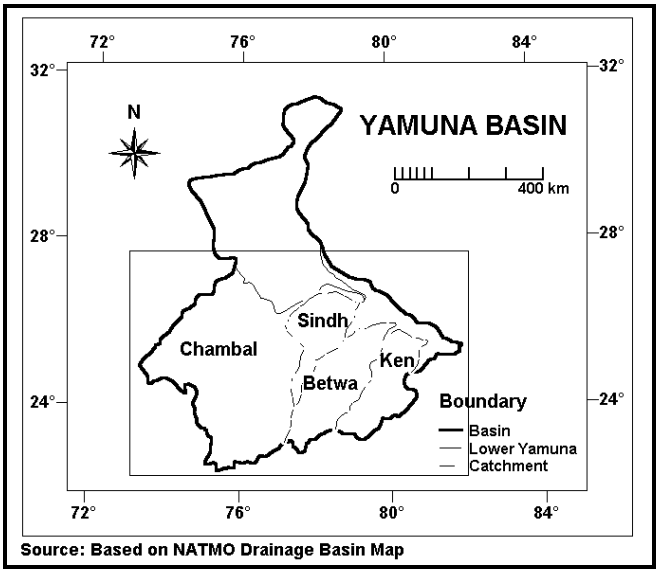


*(a)*

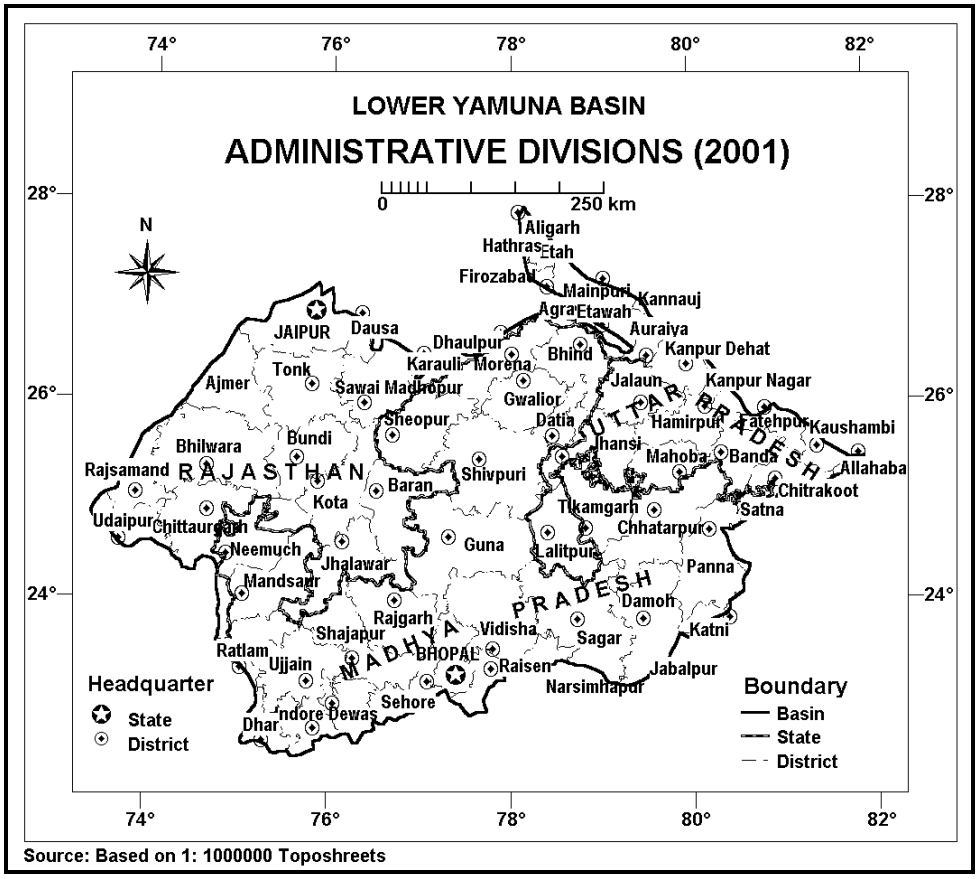


*(b)*

***Figure 1 (a & b):*** *Location of Study Area (Lower Yamuna Basin)*

## 3. Materials and Methods

The analysis is based mainly on data collected from secondary sources. Data on station-wise normal climatic tables covering 30-year period for meteorological stations was obtained from Indian Meteorological Department (IMD) report (1999) *Climatological Tables of the Observatories, 1951-80*. Base maps are drawn using toposheets of Survey of India at 1:250,000 scale and plates of drainage and water resources series of National Atlas Thematic Mapping Organisation (NATMO) at 1:1,000,000 scale. Further, primary data regarding the nature and functioning of data stations, maintenance, communication and publication of data, and the economic or other managerial problems, has also been collected at some of the selected sites.

Realising the data constraints, the boundaries of the lower Yamuna basin were drawn and it was, first, divided into 5 sub-catchments according to relief and drainage characteristics according to Watershed Atlas of India. Then, hydro-meteorological stations were located on base map. According to published records of meteorological observatories, stations having more than 30 years of record (1951-80) were included to get estimates of mean values of various hydrological parameters. For estimation of their areal means, Thiessen polygons and isohyetal maps based on moving average pixel-wise computations were drawn in a GIS system ILWIS (Integrated Land and Water Information System) 3.6 version.

For Penman-based PET determination, CROPWAT software of FAO was used. Point estimates were obtained in MS EXCEL using water balance equations. Now with the possibility of pixel-wise map-based computations in GIS for all equations of water balance based on both the methods of PET, an improvement was made by writing a script in ILWIS. Pixel-size of 1000 m in case of lower Yamuna

basin was used in order to get a better spatial picture. It was run successfully after many trials of 156 map-based calculations and comparison of values was also made at given points for verification. Depending upon the range of water surplus and deficit, a general picture of regional water balance was obtained by interpolating between their values. Thereafter, a comparison of surface water runoff pattern was also done with remote sensing data for the next 30 year period (1981-2010) GLDA (global land data assimilation system) time-averaged data. Analyses and visualizations used in this study were produced with the Giovanni online data system, developed and maintained by the NASA GES DISC.

## 4. Results and Discussions

As the description of rainfall characteristics and resultant water balance depends upon distribution of meteorological stations, accuracy and precision of their record, therefore, quantitative analysis of data becomes essential to determine its suitability and optimality. Hence, an assessment of the hydro-meteorological data network was considered in detail here first for explaining the relationship between number of stations and spatial variations in average annual values.

### 4.1. Status of Hydro-Meteorological Data Network

There are about 38 meteorological stations having long-term data published record in the study region, 6 covering area of main lower Yamuna tract, 18 in Chambal, 3 in Sindh, 6 in Betwa and 4 in Ken river catchment (Figure 2). Out of these, only 10 stations belong to class I observatories that record data on climatic variables. The average density of meteorological stations network in the study region works out to be 6842 $Km^2$ for the stations having sufficient long-term record. According to modern WMO standards, minimum density of 1000-2500 $Km^2$ per station is required in the interior plains and undulating regions like lower Yamuna basin. Hence, adequacy of stations required for arriving at better areal estimates will have impact at sub-catchment level.

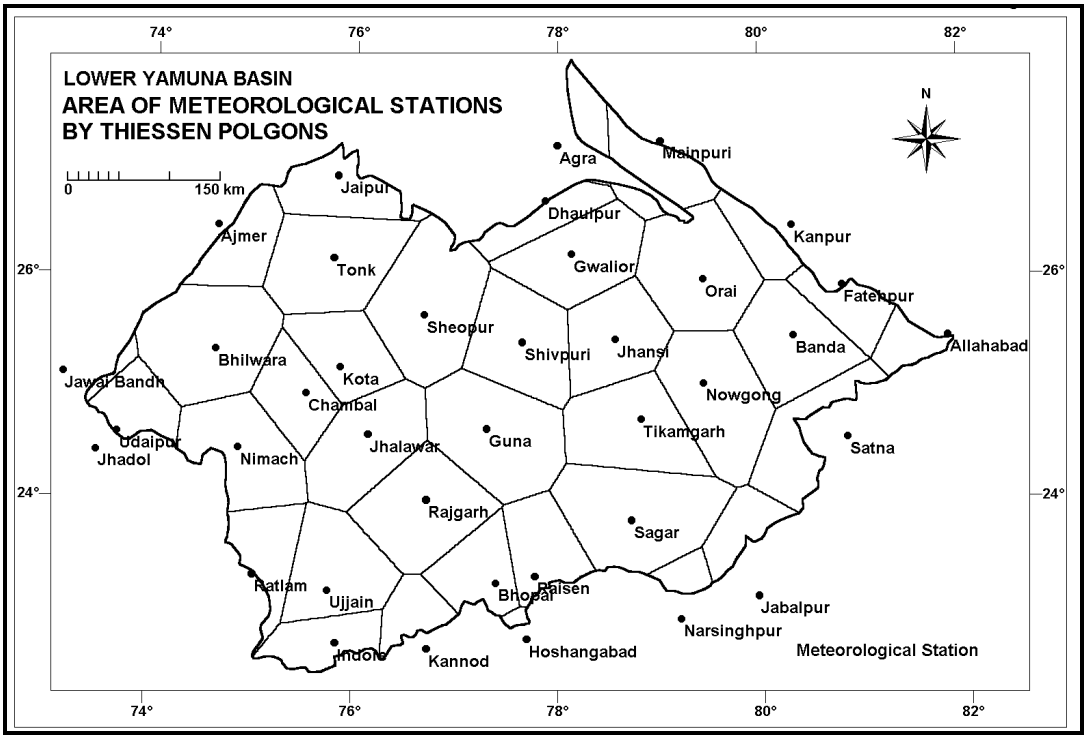


*(a)*

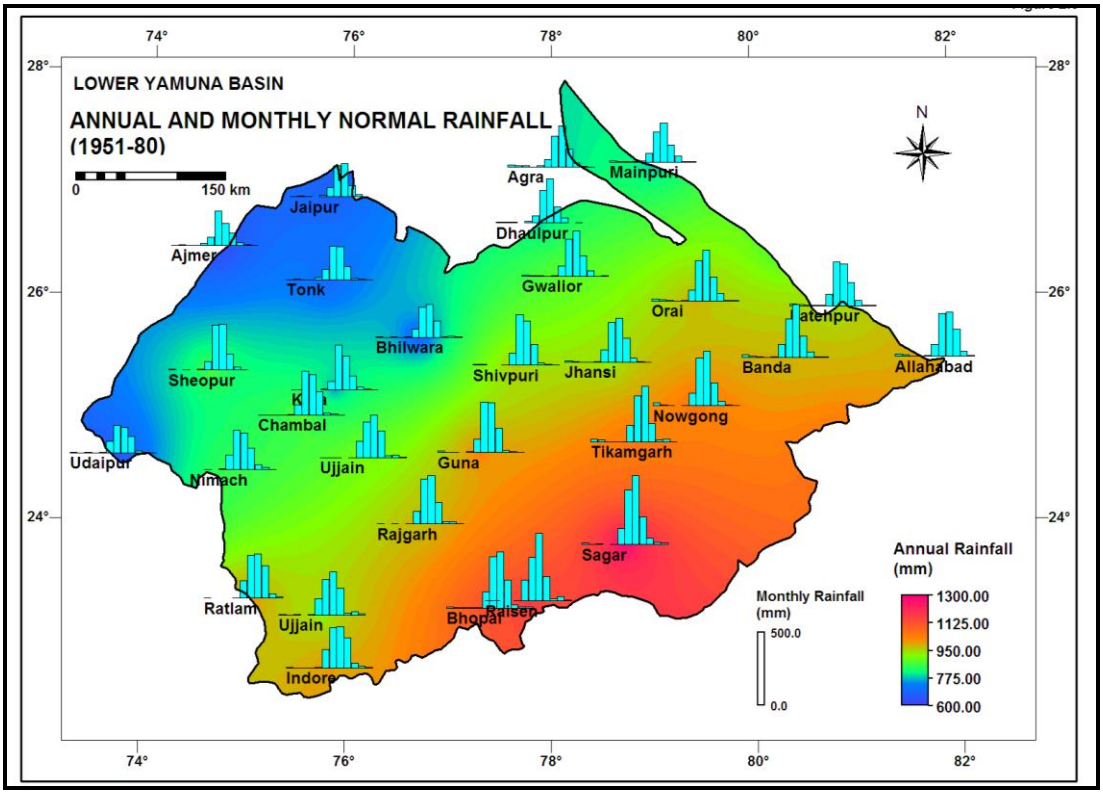


***(b)***

***Figure 2 (a & b):*** *Meteorological Stations and Rainfall*
(**Source:** Author Based on IMD Data)

### 4.2. Mean Estimates of Basin Rainfall

The arithmetic average, the most commonly used method puts the mean annual rainfall in the lower Yamuna basin as 918.29 mm. But, this approach provides a reasonable estimate if, the gauges are distributed uniformly and the topography is flat which, except for the northern region, is not found in abundance in the study area. Areal mean rainfall estimate based on Thiessen polygon method, calculated in GIS, works out to be 931.57 mm with large variations found in the size of polygons (Figure 2a). Isohyetal average, obtained here by interpolating precipitation values using moving average method results into mean rainfall at 928.32 mm (Figure 2b). Both the methods compute higher mean rainfall than the one by arithmetic method. Hence, for all regional water balance computations weighted isohyetal average values were used.

### 4.3. Surface Water Balance

Water balance based on climatological approach is one of the most common methods of hydrological regionalization. However, the spatial extent of hydrological regions and magnitude of surplus and deficit values was found to vary according to the method used, *i.e*. Thornthwaite/Penman for determination of PET needs and available water capacity (AWC). Average regional value of AWC varies from 131.3 mm in north to 300 mm in southeast (Figure 3).

It was clear from all water balance tables that all stations in the region are dry, with annual summation of positive P-PET values always lesser than that of negative P-PET values. Annual rainfall in the region remains short of annual potential evapotranspirative demands. It is not sufficient even to recharge soil up to its field capacity at most of the places. Accumulative potential water loss at these stations is therefore adjusted for its balance amount from wet season.

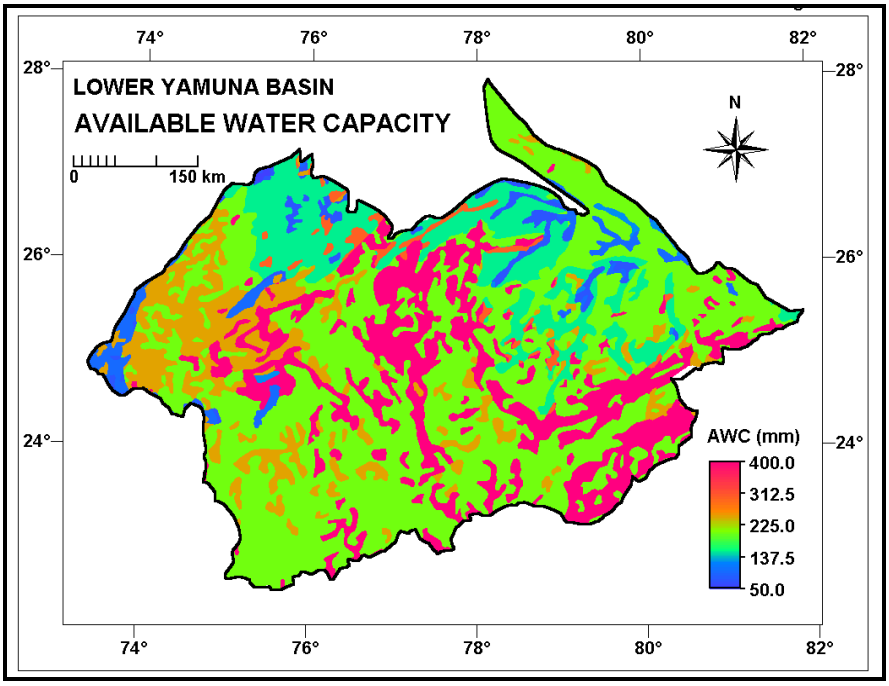


***Figure 3:*** *Spatial Variability in Available Water Capacity of Fields*
(**Source**: Author using ILWIS based on NATMO Soil and Landuse Plates)

### 4.4. Aridity, Humidity and Moisture Indices

Moisture index was found to be negative everywhere except at Jabalpur, thus, defining the limit between dry and wet climate. According to Thornthwaite scheme of climatic classification, climatic condition in the region varies form semi-arid conditions (D) in the west to dry subhumid ($C_1$) type in the central part. Towards the southeastern section, it graduates towards moist subhumid ($C_2$) conditions. The slight increase of surplus over deficit (Figure 4 and Figure 5) here results in positive moisture index. In rest of the region, moisture index values show close correspondence with the rainfall pattern. Thus, leaving aside the differences in magnitude of moisture indices following both the methods of computation, the spatial pattern of moisture condition reveals that there exists an overall deficiency in the region particularly in the northern plains.

Seasonality of moisture condition becomes clearer by comparing aridity and humidity index separately. Aridity index in the region shows large winter deficiency of more than 50% at most of the places. This deficit cannot be made up even by soil moisture storage. Humidity index, on the other hand, is not even one-fourth of the annual PET demand computed after Penman method. Further, it shows larger spatial variation as compared to aridity index. Moisture adequacy index also shows the varying proportion of the ratio of AET to PET. It varies from 33 to 60%, thereby reflecting the suitability of crops, which can grow even if half or one-third of their evapotranspiration demands are met by rainfall and the rest can be supplemented by irrigation, if necessary.

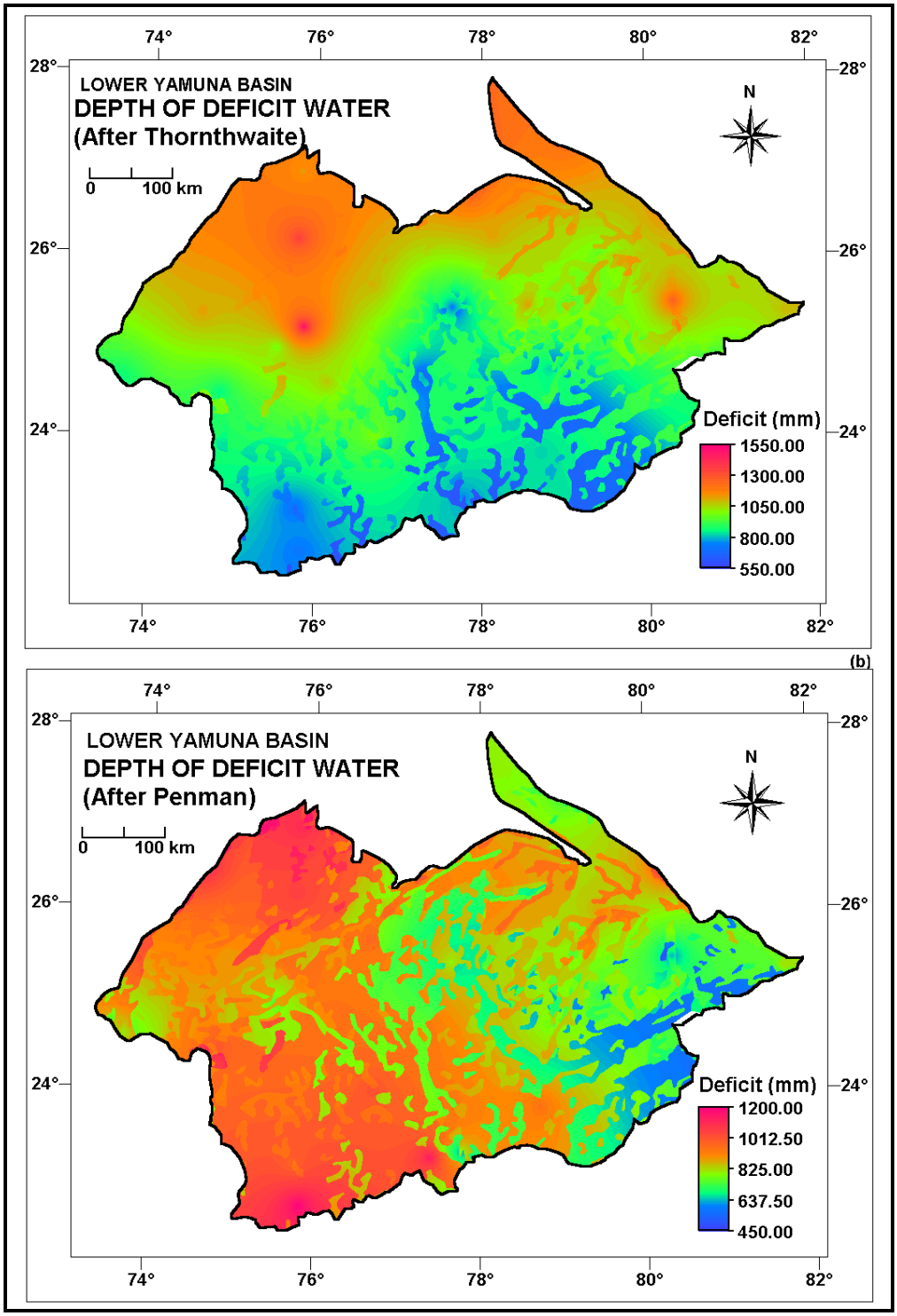


***Figure 4 (a & b):*** *Spatial Pattern of Water Deficit*
(**Source**: Author using ILWIS Based on Pixel-wise computations of Water Balance Components)

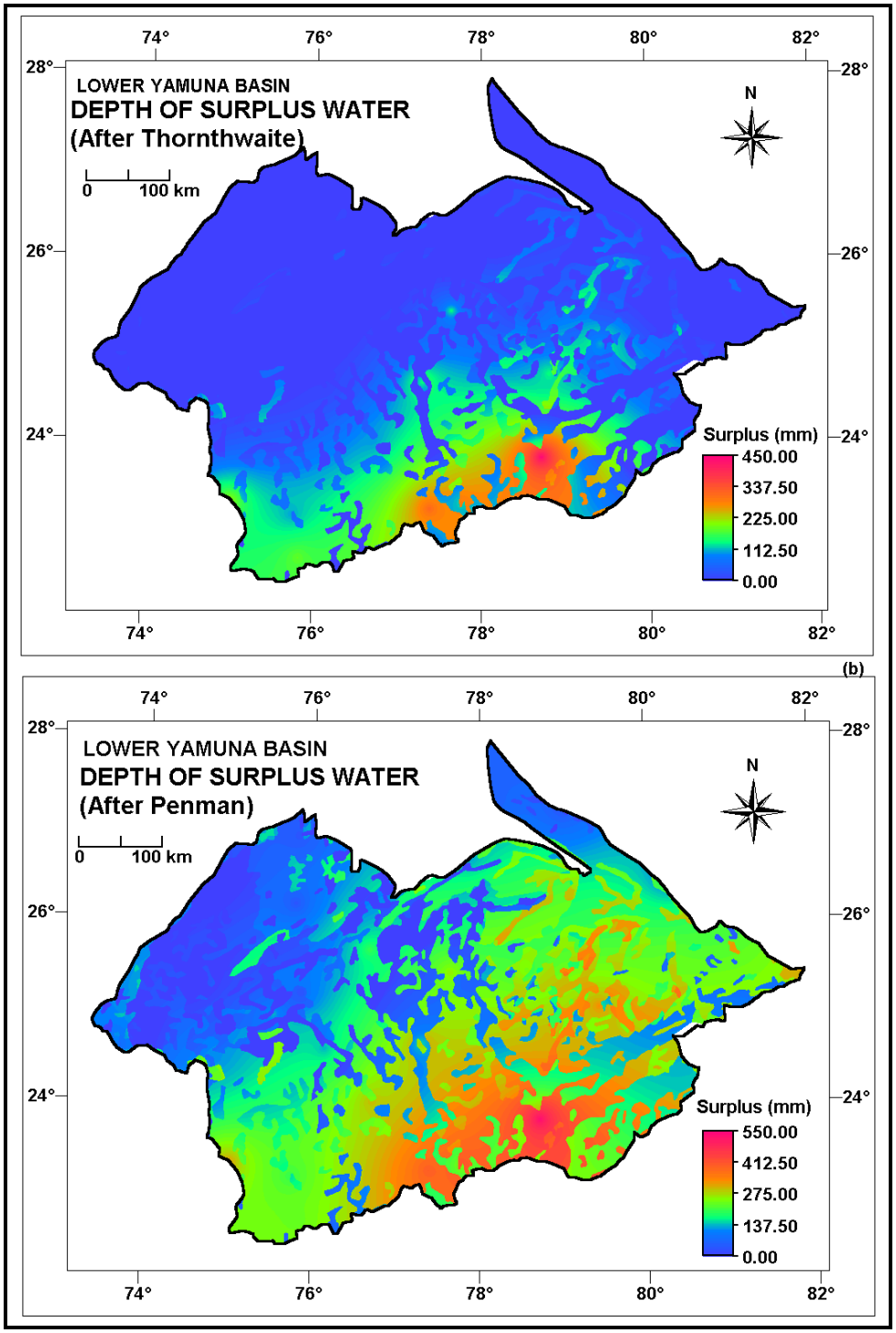


***Figure 5 (a & b):*** *Spatial Pattern of Water Surplus*
(**Source:** Author using ILWIS Based on Pixel-wise computations of Water Balance Components)

### 4.5. Hydrological Regions and Spatial Network of Data Stations

In case of hydrological regions, five categories, each of annual surplus and deficit values of water have been identified (Figure 6 and Table 1). Ten hydrological regions were formed based on Thornthwaite's PET estimates, whereas Penman-based PET results into twelve hydrological regions. In both the methods, the predominant combination is that of low surplus and high deficit. However, the magnitude of surplus is underestimated and deficit is overestimated by Thornthwaite method. Interestingly, high surplus region towards southeast also witnessed high deficit in the lean season.

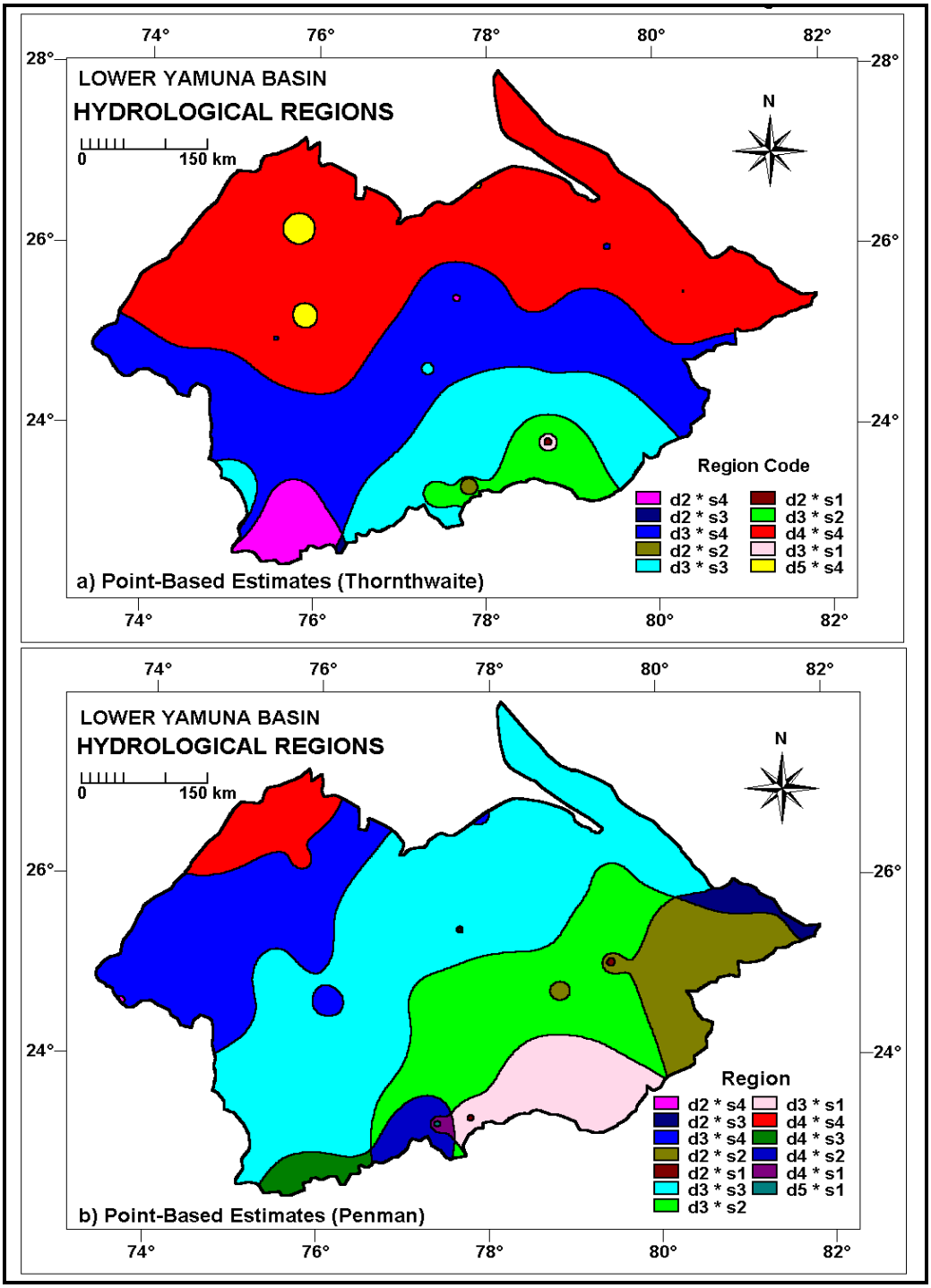


***Figure 6 (a & b):*** *A Comparative View of Point-Based Hydrological Regionalization*
(**Source:** Author using ILWIS Based on Water Balance Tables computations in MS-EXCEL)

***Table 1:*** *Hydrological Regions*

| Hydro-logical Region | Surplus Regions | Deficit Regions | Area ( $km^2$) | | | |
|---|---|---|---|---|---|---|
| | | | Thornthwaite | | Penman | |
| | | | (1) | (2) | (1) | (2) |
| s5 * d4 | No surplus | Very high deficit | -- | 1.05 | -- | -- |
| s4 * d2 | Very low surplus | Moderate deficit | 3,969.02 | 14.63 | -- | -- |
| s4 * d3 | Very low surplus | High deficit | 65,729.73 | 44,101.36 | 45,671.40 | 44,082.54 |
| s4 * d4 | Very low surplus | Very high deficit | 133,403.73 | 153,564.49 | 15,439.13 | 12,142.25 |
| s4 * d5 | Very low surplus | Very very high deficit | 2,160.64 | 745.30 | -- | -- |
| s3 * d2 | Low surplus | Moderate deficit | 1,341.12 | 988.86 | 4,259.61 | 3,680.51 |
| s3 * d3 | Low surplus | High deficit | 42,586.71 | 49,302.79 | 100,478.76 | 105,663.46 |
| s3 * d4 | Low surplus | Very high deficit | -- | -- | 1,010.81 | 2,094.79 |
| s2 * d2 | Moderate | Moderate Deficit | 145.30 | -- | 21,685.87 | 17,826.61 |
| s2 * d3 | Moderate | High Deficit | 12,684.76 | 13,171.87 | 46,443.88 | 47,526.82 |
| s2 * d4 | Moderate | Very High Deficit | -- | -- | 237.28 | 1,489.56 |
| s1 * d2 | High surplus | Moderate deficit | 36.59 | 18.82 | 10,731.09 | 9,491.36 |
| s1 * d3 | High surplus | High deficit | 187.11 | 335.54 | 15,246.80 | 16,483.39 |
| s1 * d4 | High surplus | Very high deficit | -- | -- | 1,019.17 | 1,720.57 |
| s1 * d5 | High surplus | Very very high deficit | -- | -- | 20.91 | 42.86 |
| | | | 262,244.70 | 262,244.70 | 262,244.70 | 262,244.70 |

**Source:** Computed in ILWIS from Figure 6 a & b. Note: (1) Computations based on 37 stations; (2) 32 stations

The macro-hydrological regions carved out in Figure 6 (a & b) do not reflect meso-level variations due to lower density of meteorological data stations. The fact can be ascertained by excluding five stations that have less number of years of record from the analysis (Table 1; Column (2) under both the methods). Boundaries of each zone get shifted and the respective areas change depending upon location and number of stations included in spatial analysis. A significant difference in sub-zonal boundaries can be seen when pixel-wise calculations are done in GIS (Figure 7 a & b).

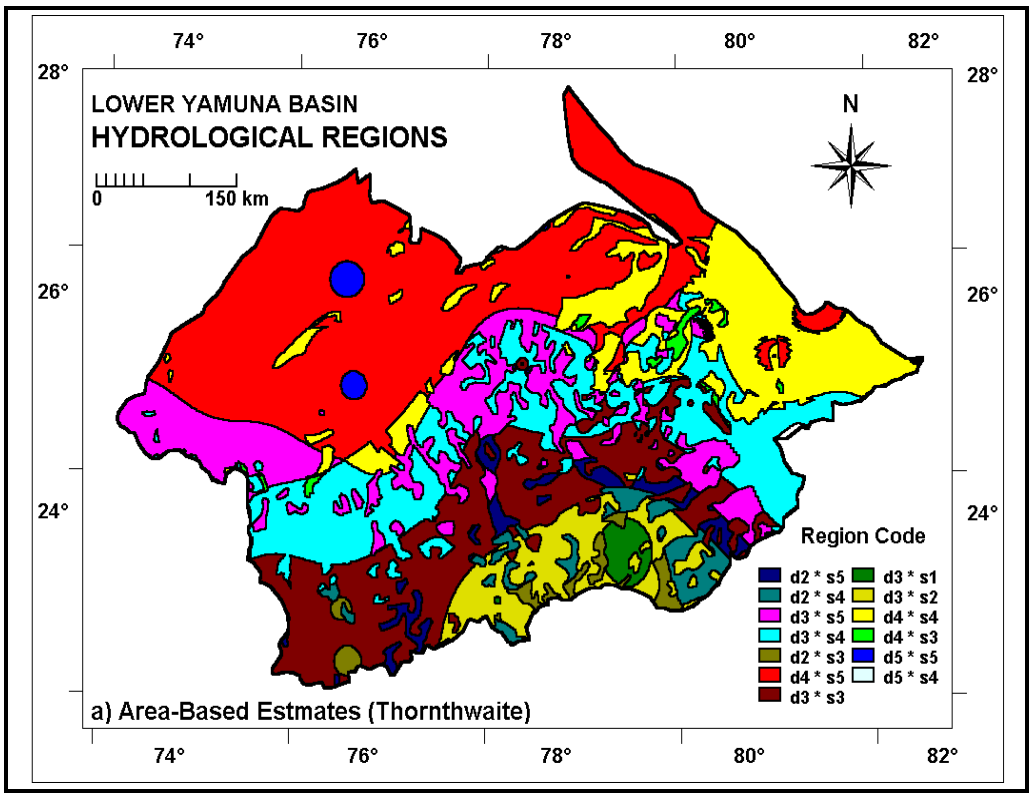

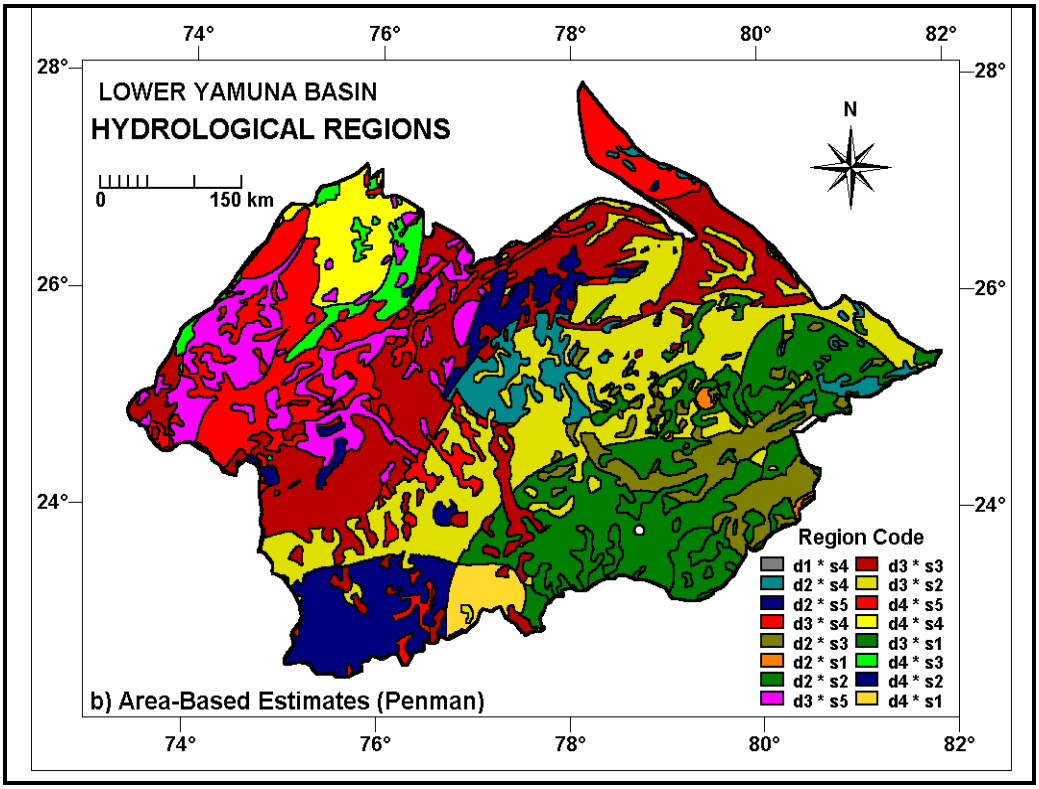


***Figure 7 (a & b):*** *A Comparative View of Area-Based Hydrological Regionalization*
(**Source:** Author using ILWIS Based on Pixel-wise computations from Figure 4 & 5)

Further, a comparison of surface runoff pattern obtained from online remotely sensed recent data shows the similar trend of south-eastward increase (Figure 8 a & b). Here again, broad zones change when different simulation models like community land model (CLM) 1 degree and NOAH 0.25 degree subsets are used. Thus, area based calculations have been demonstrated here to represent their role in water resource planning at macro-level. It can be further broken down to medium scale and small scale catchments with the availability of high resolution remote sensing data.

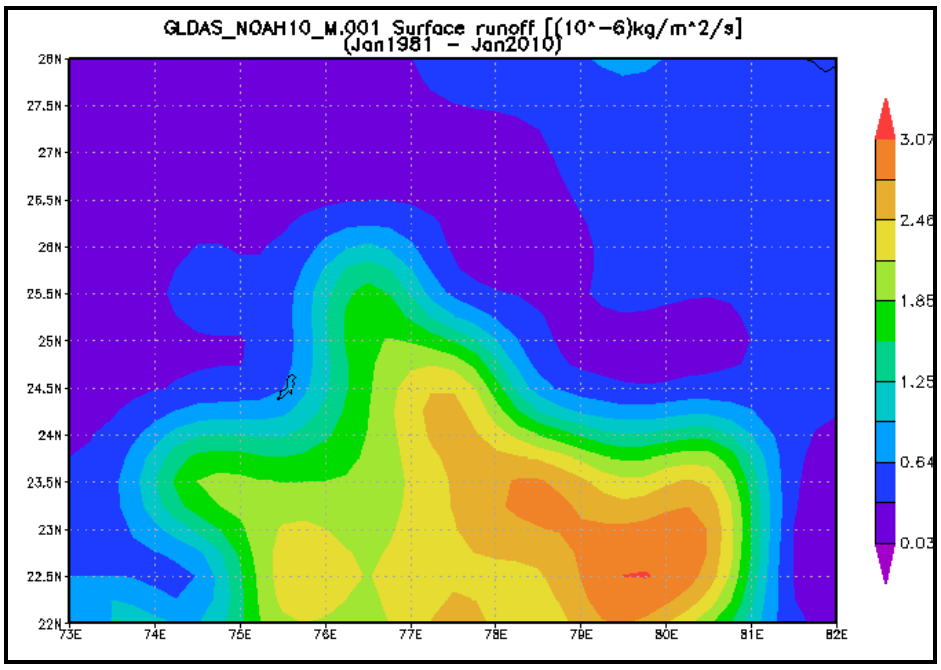


***(a)***

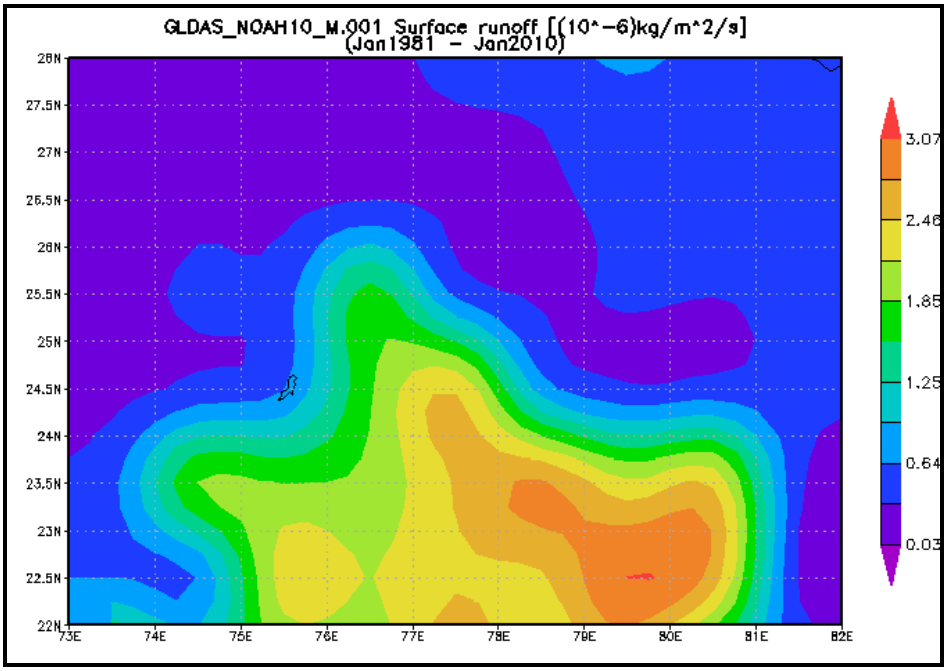


***(b)***

***Figure 8 (a & b):*** *A Comparison of Grid-wise Surface Runoff Computation based on Remote Sensing Data*
(**Source:** Giovani Online Visualization Plot, NASA, http://daac.gsfc.nasa.gov/)

## 5. Conclusion

The method used for spatial estimates also affects the results as can be seen from differing results of mean basin rainfall and water balance. Corresponding zone of influence of each station would also vary if area based computations are used. The choice of method used and the number of stations included in optimum analysis is a question yet to be satisfactorily answered.

The choice of available water capacity is another important issue in these water balance computations based on crossed map of landuse and soil cover. This change of value for a given pixel-size and discretionary choice of putting several categories under similar available water capacity zone can significantly alter results. Same could be observed in case of remotely sensed grid plot based on different resolutions. An exclusively detailed study utilizing more stations is required to prove conclusively that the results shown here are not a function of the stations chosen for spatiotemporal study.

## Acknowledgement

The author sincerely thanks Prof. B. Thakur (Retd.), supervisor of Ph.D, from Department of Geography, University of Delhi to write this research paper. Prof. S.K. Pal (Retd.) also motivated the author initially in understanding of basic concept, solution of problem and in conducting further research in the area. Training rendered by Scientists of Indian Institute of Remote Sensing, Dehradun assisted in making better use of GIS software and in analysis of mapping work. Financial assistance provided by University Grants Commission in the form of minor research project for the research work is duly acknowledged. Support of officials of Indian Meteorological Department both at headquarter and field level who provided gainful insight into the process of data handling was of immense help in completion of the work.

## References

Ahlawat, R., 1999: *Water Resource Potential and Utilisation in the Bundelkhand Region.* Unpublished M. Phil Dissertation. University of Delhi: Department of Geography.

Ahlawat, R. *Hydrological Regions in the Budelkhand: The Catchments of Betwa and Ken Rivers*. Annals of the National Association of Geographers, India. 2000. 20 (1) 27-50.

Bras, R.L., and Colon, R. *Time-Averaged Areal Mean of Precipitation Estimation and Network Design.* Water Resource Research. 1978. 14 (5) 878-88.

Bruin, H.A.R., 1988: *Evaporation in Arid and Semi-Arid Regions.* In: Estimation of Natural Groundwater Recharge; I., Simmers (Ed.). Dordrecht, Holland: Reidel Pub. Co. 73-88.

Chidley, T.R.E., and Pike, J.G. *A Generalized Computer Program for the Solution of the Penman Equation for Evapotranspiration*. Journal of Hydrology. 1970. 10; 75-89.

Dunne, T., and Leopold, L.B., 1978: *Water in Environmental Planning*. San Francisco: W.H. Freeman and Company.

Doorrenbos, J., and Pruitt, W.O., 1977: *Guidelines for Predicting Crop Water Requirements*. FAO Irrigation and Drainage; Paper 24. Rome: FAO, UN.

Dwivedi, D.K. *Water Balance Technique for the Identification of Drought Prone Areas in Bihar*. Geographical Review of India. 1993. 55 (2) 53-62.

Dwivedi, V.K., and Bhar, A.K., 2003: *Problems of Water Balance and Trend in the Water Level of Upper Bhopal Lake, M.P., India*. In: B., Venkateswara Rao, K.R., Reddy, C., Sarada and K., Raju (Eds.) Proceedings of the International Conference on Hydrology and Watershed Management. Vol. I & II. Hyderabad: BSP Pub. 237-243.

Food and Agricultural Organisation, 1992: *Expert Consultation on Revision of FAO Methodologies for Crop Water Requirements*. Rome: FAO, UN. 1-60.

Hema Malini, B. *Water Budgeting and Crop Yield: A Case Study of Groundnut Yields in Anantapur District, Andhra Pradesh*. National Geographer. 1986. 21 (2) 179-186.

Mallick, K., et al. *Evapotranspiration using MODIS Data and Limited Ground Observations over Selected Agroecosystems in India*. International Journal of Remote Sensing. 2007. 28 (10) 2091-2110.

Mandal, V.S.C., and Challa, V.S. *Comparison of Hargreaves ETO under Different Climatic Conditions in India*. Geographical Review of India. 1991. 53 (4) 1-7.

Minacapilli, M., et al. *Estimation of Actual Evapotranspiration of Mediterranean Perennial Crops by Means of Remote-Sensing Based Surface Energy Balance Models.* Hydrology & Earth System Sciences. 2009. 13 (7) 1061-1074.

Monteith, J.L. *Evaporation and Surface Temperature*. Quarterly Journal of the Royal Meteorological Society. 1981. 107 (451) 1-27.

Pandeya, B., and Prasad, N. *Hydrological Regions of Bihar.* Transactions of the Institute of Indian Geographers. 1983. 5 (1) 170-178.

Penman, H.L., 1948: *Natural Evaporation from Open Water, Bare Soil and Grass.* Proceedings of the Royal Society of London. 193 (Series A); 120-145.

Ponce, V.M., and Shetly, A.V. *A Conceptual Model of Catchment Water Balance*. Journal of Hydrology. 1995. 173; 27-50.

Rao, K.N., et al., 1971: *Potential Evapotranspiration over India*. Scientific Report No. 136. New Delhi: IMD.

Singh, V.P., and Fiorentino, M., 1996: *Geographical Information Systems in Hydrology*. Dordrecht, Netherlands: Kluwer Academic Pub.

Subrahmanyam, V.P. *The Water Balance of India According to Thornthwaite Concept of PET.* Annals of the Association of American Geographers of India. 1956. 46 (3) 300-311.

Tanner, C.B., 1968: *Evaporation of Water from Plants and Soil*. In: T.T., Kozeowski (Ed.) Water Deficits and Plant Growth. Vol. I. Academic Press, 75-105.

Thornthwaite, C.W. *An Approach toward a Rational Classification of Climate*. Geographical Review. 1948. 38; 55-94.

Vishwanath, V., and Ganesh, A. *Hydrometeorological Characteristics and Water Balance of the Upper Vagai Basin, South India*. Transactions of the Institute of Indian Geographer. 1985. 7 (2) 163-9.

World Meteorological Organisation, 1994: *Guide to Hydrological Practices*. 5th Edition. WMO Pub. No. 168.

**Cloud Publications**
International Journal of Advanced Remote Sensing and GIS
2014, Volume 3, Issue 1, pp. 681-698, Article ID Tech-297
ISSN 2320 - 0243

Case Study | Open Access

# Potential of Geospatial Techniques to Facilitate the Tourist & Administration: A Case Study of Shimla Hill Station, Himachal Pradesh, India

**Shruti Kanga[1], Krishan Thakur[2], Santosh Kumar[1] and Hemant Gupta[3]**

[1]Centre for Land Resource Management, Central University of Jharkhand, India
[2]Aryabhatta Geo-informatics & Space Application Centre (AGiSAC), Shimla, Himachal Pradesh, India
[3]State Council for Science Technology & Environment, Shimla, Himachal Pradesh, India

Correspondence should be addressed to Shruti Kanga, shruti.mgi@gmail.com

Publication Date: 8 September 2014

Article Link: http://technical.cloud-journals.com/index.php/IJARSG/article/view/Tech-297



**Abstract** Tourism is an important sector in terms of source of income for any country. The success of any tourism business is determined by tourism planning, development and marketing. Thus, success of tourism industry is determined by the effective planning. The main objective of this research work is to review the potential of geospatial techniques to facilitate the tourism and administration in the Shimla city of Himachal Pradesh. Geospatial technologies offer great opportunities for the development of modern tourism applications using maps. This technology integrates with spatial and non-spatial database and provides the facility of query, analysis and to visualization through digital maps to the end users. GIS database for the present study has been generated through extensive field survey. Global Position System (GPS) is used to collect the spatial information. Base map for the study area is developed by using IRS Cartosat-1 satellite data. Various thematic layers on basic tourist facilities such as hotel, home stay, guest house, transportation, food hubs, heritage sites, bank, ATM, post office, police help, health facilities and all the tourist attraction sites etc., has been developed. Present study deals on to develop a GIS based information system for the tourist and as well as for the tourist administrators or planners which will also help in management and department of tourism for enhancement and beautification of site.
**Keywords** *Geospatial; Tourism; GPS Survey; Spatial Planning*

## 1. Introduction

Tourism is the act of travel for the purpose of recreation, and the provision of services for this act (Encyclopedia of Tourism 2005). "Tourism is a composite of activities, facilities, services and industries that deliver a travel experience, i.e. transportation, accommodation, eating and drinking establishments, entertainment, recreation, historical and cultural experiences, destination attractions, shopping and other services available to travelers away from home" (Kushwaha, 2012). In this

connection it is further defined tourism as a service industry that takes care of visitors when they are away from home. Also, tourism is defined as sum of the phenomenon and relationships arising from the interaction of tourist and host communities in the process of attracting and hosting these tourists, and other visitors (Macintosh and Goeldner, 1986 and Fadahunsi, 2003). Tourists are people who are travelling and staying in places outside their usual environment for not more than one consecutive year for leisure, business and other purposes not related to the exercise of an activity remunerated form within the place visited (Encyclopaedia of Tourism 2005). Geospatial approach was used for allocation of potential tourism gradient sites in a part of Shimla district in Himachal Pradesh, India. Shimla is most popular hill station among North India as it has several attractions, healthy climatic conditions and easy accessibility. Shimla is full of tourists throughout the year due to its splendid views of the snow-clad ranges of the Himalayas. All these make Shimla an attractive destination throughout the year Kanga et al., (2011). Fung and Marafa (2002) suggested that Geographical Information System (GIS) can have great potential for tourism development using Ikonos satellite images and both spectral and textural data. Fung and Marafa have investigated the cultural heritage for its tourism potential in 2002. GIS application for tourism planning in Zimbabwe was taken into consideration by Dondo et al., 2003. Armstrong (1994) used Remote Sensing (RS), GIS and Multi Criteria Decision Making (MCDM) for the identification of the nature-based tourism potential sites based on the socio-economic and environmental indicators. GIS and MCDA framework has been used by Bukenya (2002) for developing special multi objective, rankings, prioritizing in national park of Uganda. The park was divided in to 3 sub-groups with rankings which show the importance of subjects, potentials and different abilities of tourism in the regions. Andrera et al., in 2009 shows the use of multi-temporal satellite imagery for rate and range of land changes throughout Angkor basin from 1989-2005. The same corollary can be applied for tourism planning in a given area. A large number of spatial and non-spatial data associated with the diverse resources and activities in the park were used by Andrew and Shaw in 2007, which demonstrated that GIS is logically used for storage, managing, analyzing and visualizing the data.

## 2. Study Area

The study area constitutes Shimla City which is the capital of Himachal Pradesh state. The spatial extent is 31.61°N 77.10°E with an average altitude of 2397 meters above mean sea level. The highest point of Shimla city is the top of Jakhu hill which is 2454 meters shown in Figure 1. Extend of the city is on a ridge and its seven spurs and stretches nearly 9.2 kms from east to west. There are no water bodies near the main city and the closest river is Sutlej River which is about 21 km away. The green belt in Shimla planning area is spread over 414 hectares (1023 acres). The main forests in and around the city is that of pine, deodar, oak and rhododendron (Batra, 2001). The climate in Shimla is predominantly cool during winters and moderately warm during summer. Major seasons are the winter season (Oct.-Feb.), summer season (March-June), followed by the monsoon period (July-September). Average annual rainfall in the district is about 1253 mm. Snowfall usually takes place in the month of December to February every year.

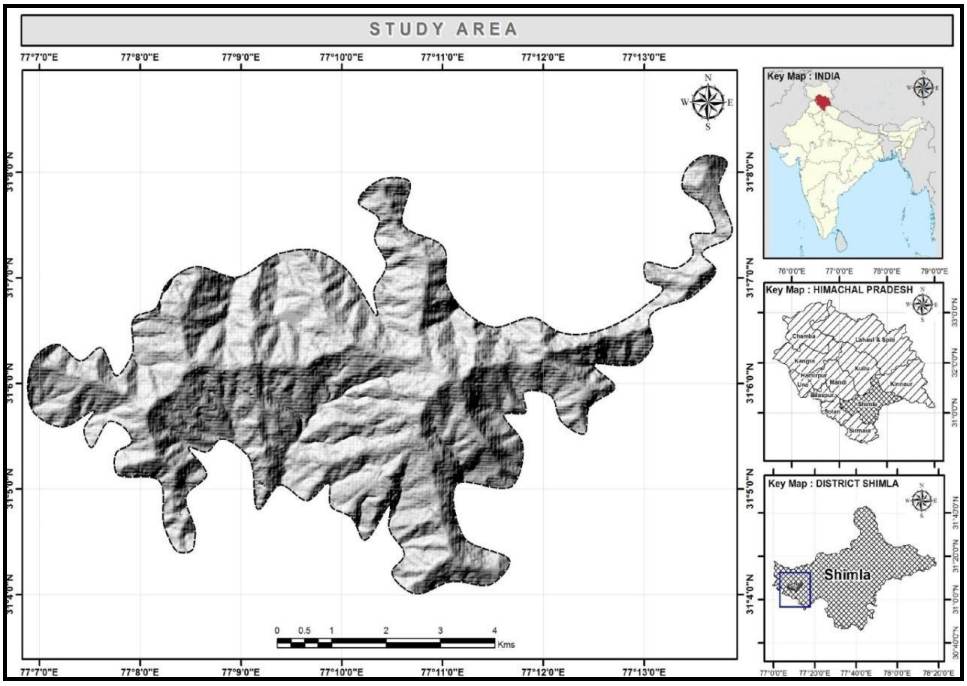


***Figure 1:*** *Study Area*

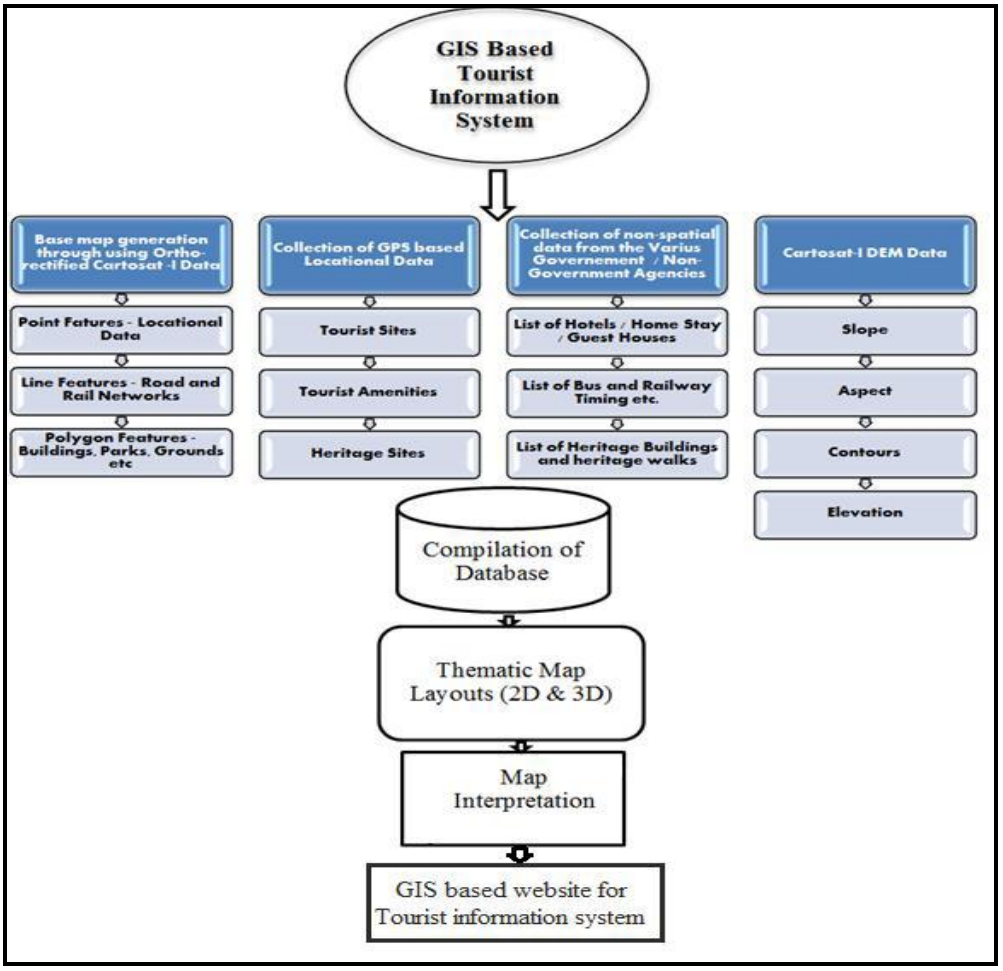


***Figure 2:*** *Flow Diagram*

## 3. Data and Methodology

The present study makes use of both primary as well as secondary data. The primary data is collected through intensive field work by visiting various destinations in the study region using a hand held Global Positioning System (GPS) to obtain coordinates. At the same time, attribute data such as type, owner, tourist name location and specific attraction of each of the tourist centers are obtained through secondary data. The secondary data has been collected from published as well as unpublished sources. The published data includes information from various publications of central and state governments, books, journals and newspapers etc. The unpublished data has been collected from Shimla municipal corporation, Shimla development authority, Directorate of transport, Himachal Pradesh state pollution control board (PCB), Department of tourism and civil aviation and other non-government agencies. Since the study is concerned with the use of GIS and Remote Sensing to generate a geo-spatial database for end users and in order to give a picture of the identified information related with tourist in the study area, a hand held Global Positioning System (GPS) receiver was used to obtain coordinates of all the newly and verify identified Tourist information places. In present study ESRI (Environmental Systems Research Institute) Arc GIS 10.2, and ERDAS Imagine-2013 software has been used for data processing, analysis and map layout preparation. The steps of the procedure followed in the development of the spatial database are as follows. Firstly primary data is collected using GPS and Secondary Data from Govt. & Private Organisation (hotels, parking place Information office, Tourist places etc.). Secondly the collected information is digitized in Arc GIS software e.g. tourist spot, hotel, etc., roads, railway line, built-up area etc. Thereafter attributes are added to make the data more informative. Field checking is done to determine the reliability of the map using GPS and editing is done to remove errors. Cartographic presentation e.g. thematic map layout in 2D & 3D with legend, scale, grid etc., are prepared. The GIS database for Shimla consisted of road network, tourist spots, important places, aspect, slope and contour line etc. Finally, GIS based website for tourist information system has also been developed by team AGiSAC (Aryabhatta Geo-informatics & Space Application Centre) i.e. www.agisac.gov.in/tourgis and hosted on live web server.

## 4. Results and Discussion

### 4.1. Physical Feature

Shimla city is built over several hills and connecting Ridges. Jakhu hill, Prospect hill, Observatory hill, Elysium hill and summer hill were mapped as shown in Figure 9. ArcGIS 3D analyst extension of ArcGIS 10.2 has been used for contour mapping using Cartosat-1 DEM of 10 meter interval (Figure 3). Shimla is lying between 1500 meters to 2400 meters elevation from the mean sea level shown in Figure 4. Slope map was also prepared for the Shimla town as shown in Figure 5. Colour coded aspect map of the study area has been generated and from 0-360 degrees categorized into 8 directions shown in Figure 6.

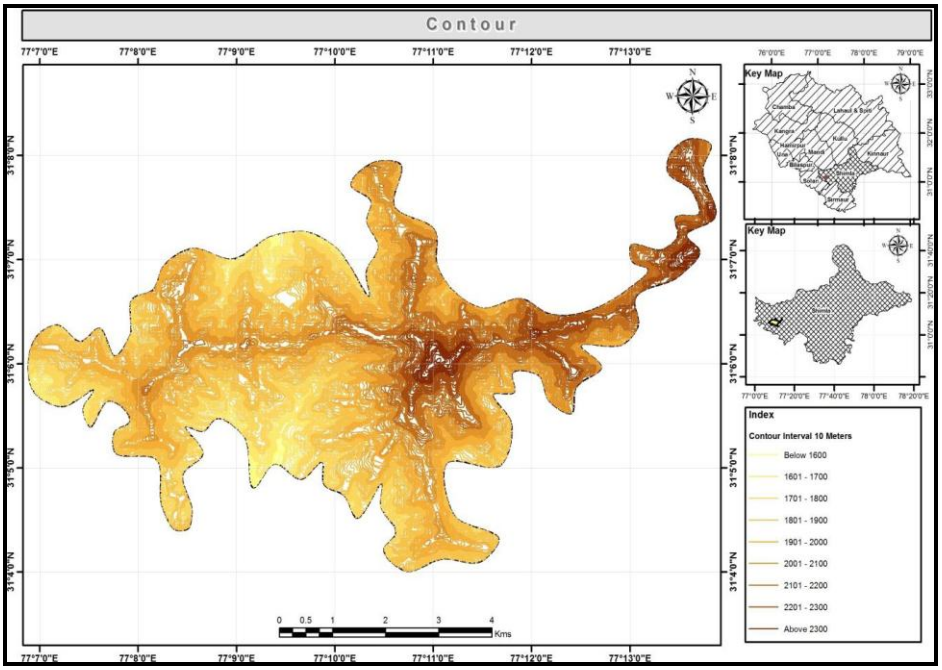


***Figure 3:*** *Contour Map*

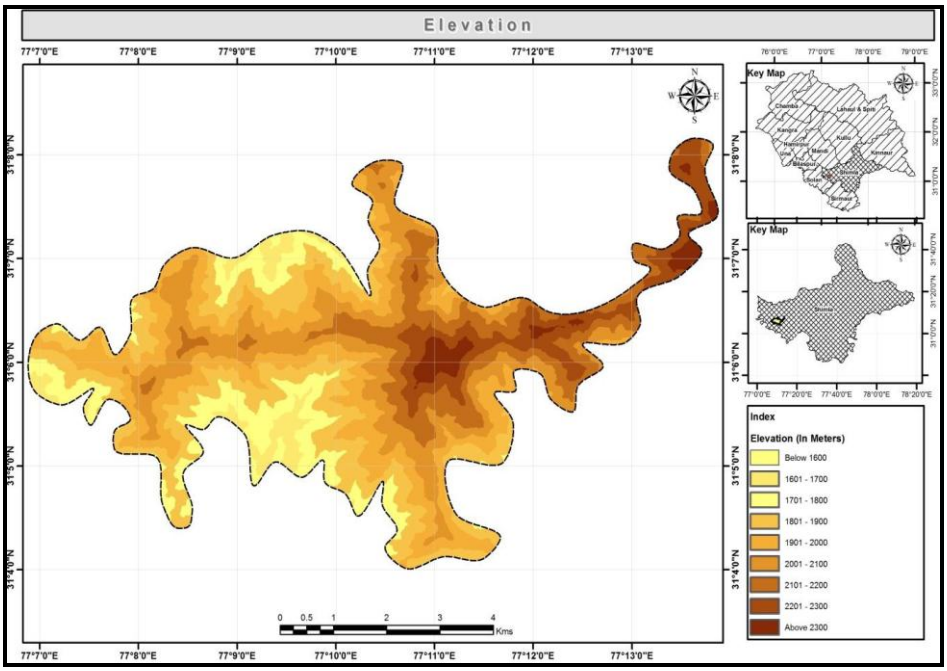


***Figure 4:*** *Elevation Map*

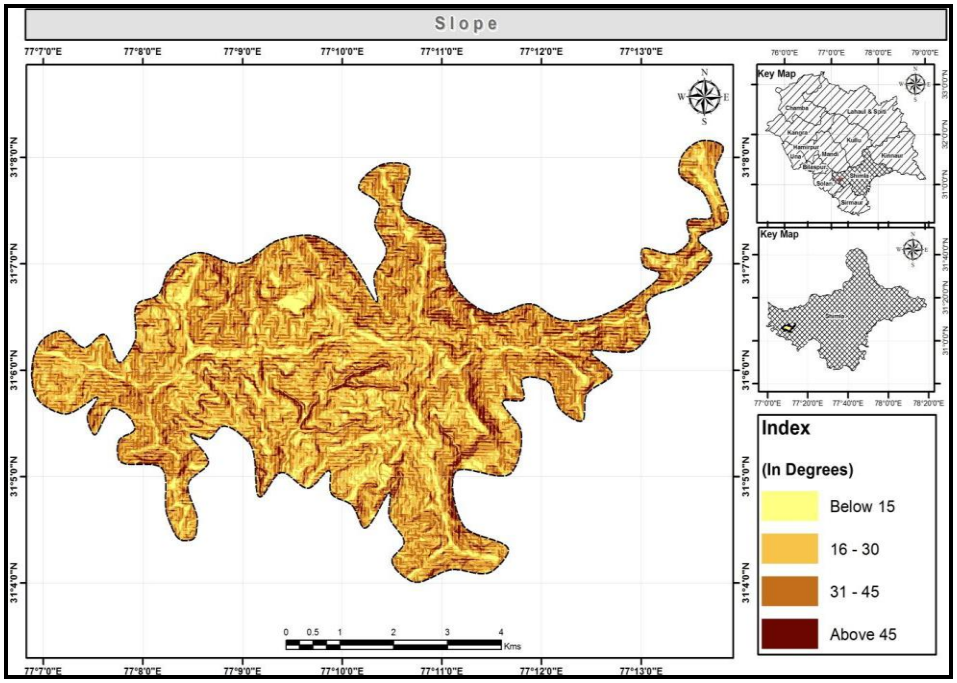


***Figure 5:*** *Slope Map*

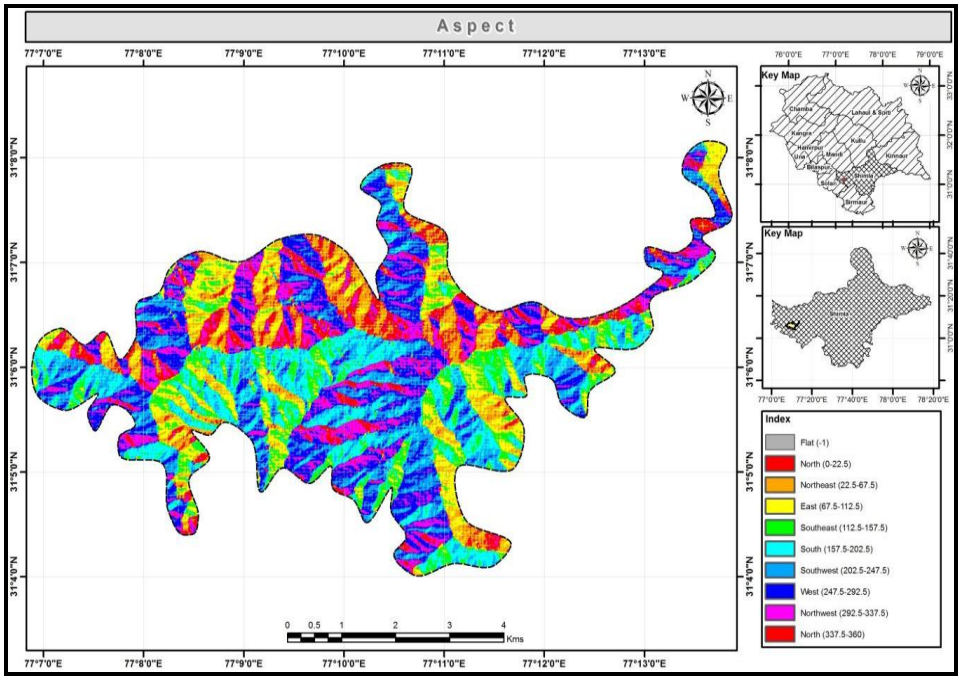


***Figure 6:*** *Aspect Map*

### 4.2. Built-up Area

Shimla is one of the very famous tourist places and capital of Himachal Pradesh state having high population density in the city area. During the field survey and interaction with local people, few areas like New Shimla, BCS, Kasumpti, Vikas Nagar, Sanjauli and Fingask estate etc., have developed in and around the Shimla city. These places are growing rapidly in term of built area including buildings, parks, and shops, residential, industrial, commercial areas etc., were mapped and shown in the map in red colour. Along with built-up area road network of the city was also mapped i.e. NH (National

highway), SH (State highway) and other road shown as dark grey colour in the map and black colour line is depicting railway line in Shimla city. Out of total geographical area i.e. around 35 square kilometer, 6.781 square kilometer area falls under the built up area (Figure 7).

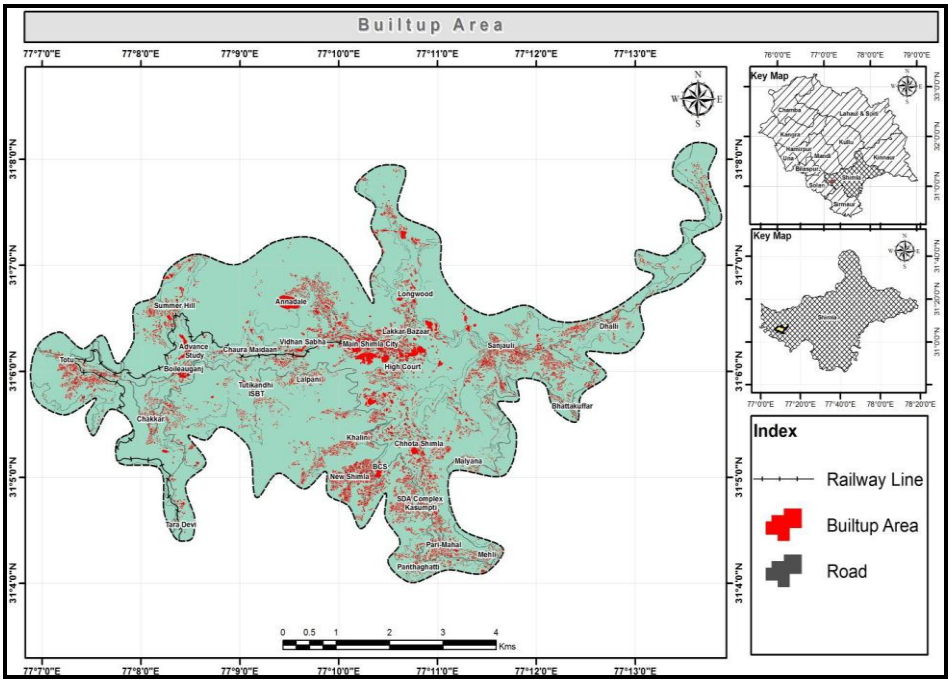


***Figure 7:*** *Built-up Areas*

### 4.3. Prime Tourist Attractions

Shimla is bestowed with many heritage sites and walks which include The Scandal Point in Shimla, The Mall Road, The Ridge, Viceregal Lodge & Indian Institute of Advanced Studies, Heritage Museum, Shimla Heritage Museum, Glenn, The General Post Office in Shimla, Gaiety Theatre in Shimla, Annandale, Gorton Castle, Yarrows, The Railway Board Building, Loreto School, Wood Ville, Bhalku and Kalka-Shimla Railway, Town Hall in Shimla, and Ellerslie. There are around 36 heritages Figure 8. The city is also having four major heritage walks listed Figure 8. Shimla has seven hills and also called as the City of Seven Hills. These hills are Bantony/Museum Hill (2201m), Elysium Hill, Inverarm/Potter Hill, Jakhu Hills, Observatory Hills, Prospect Hill, and Summer Hill which are being mapped and shown in Figure 9.

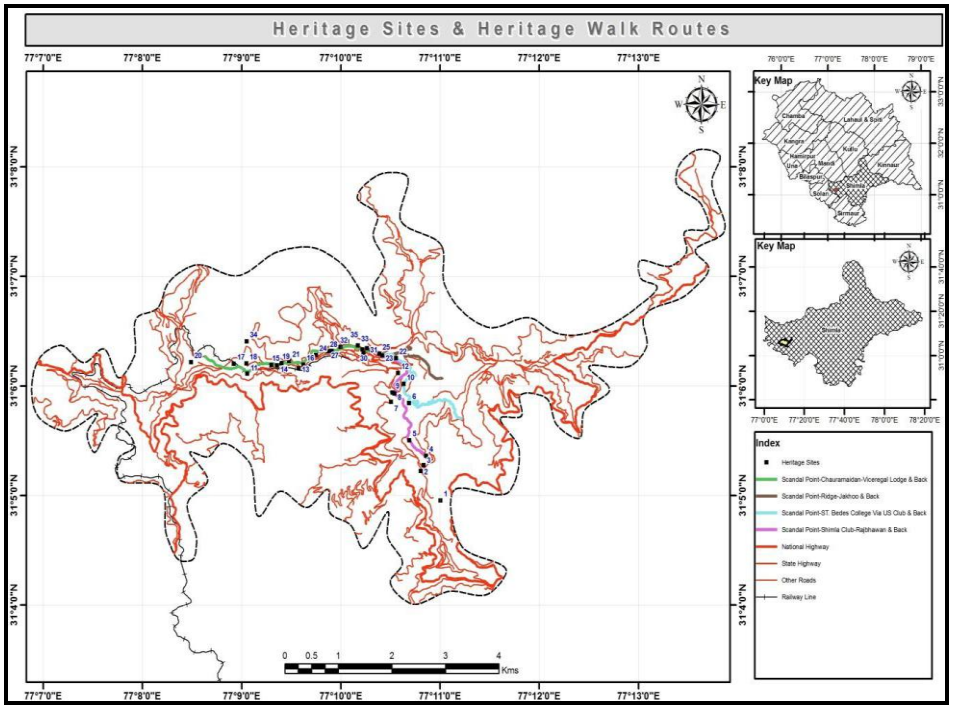


***Figure 8:*** *Heritage Sites & Heritage Walk Routes*

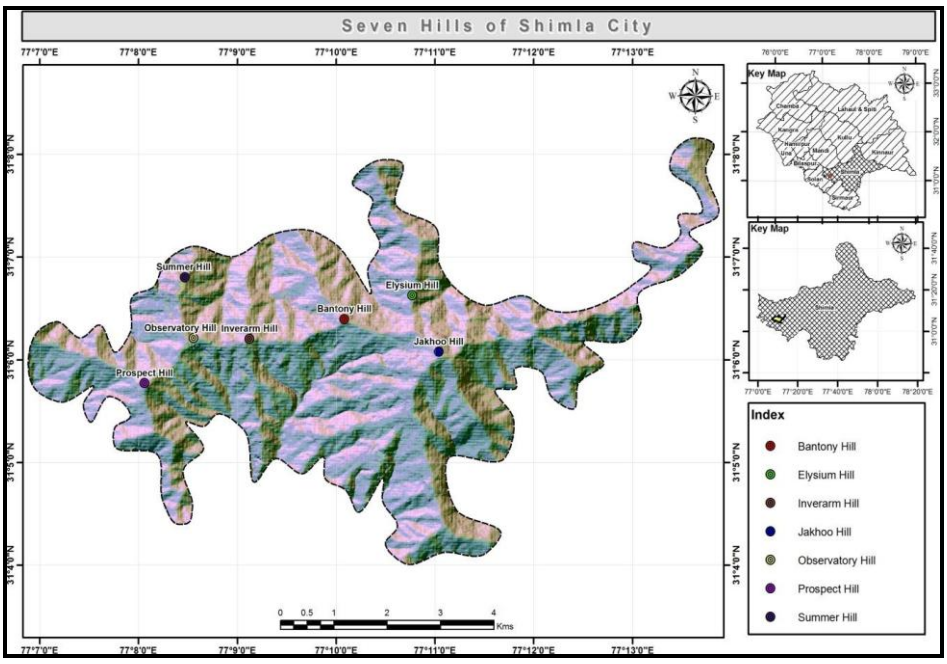


***Figure 9:*** *Seven Hills*

In the study two trekking routes have been mapped i.e. Taradevi bus stop to Taradevi temple and Ridge to Jakhu Temple shown in Figure 10. Taradevi bus stop to Taradevi temple has total 3.3 kilometers distance and elevation starts from 1850 meters - 2100 meters from mean sea level. Distance of the second trekking route i.e. Ridge to Jakhu Temple is 1.35 kilometers and the elevation from the mean sea level is from 2200 meters - 2450 meters.

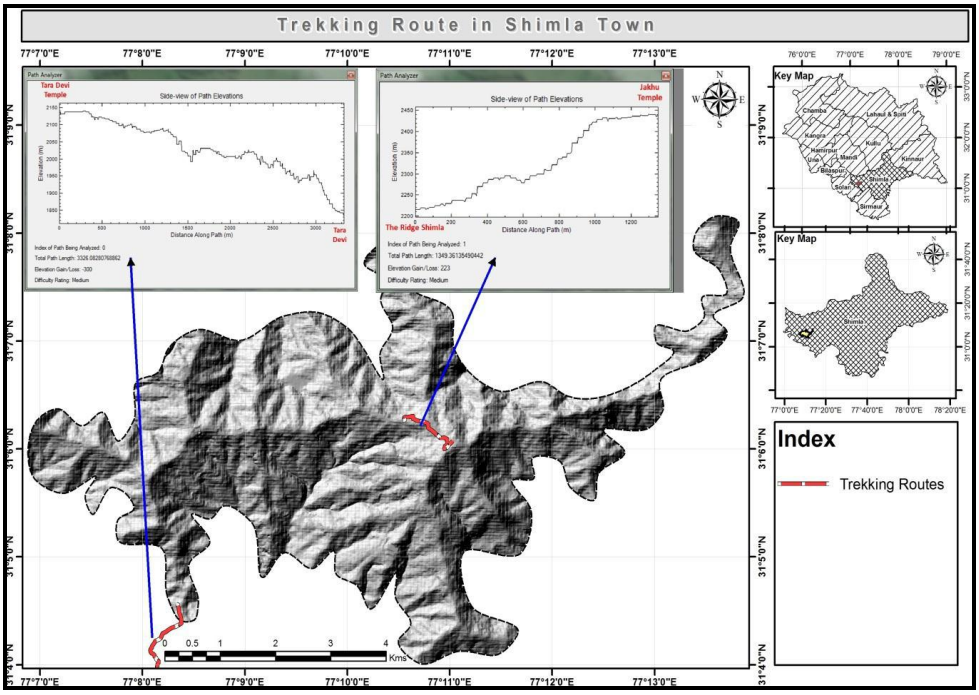


***Figure 10:*** *Trekking Routes in Shimla City*

There are many important local places in Shimla city where government offices, hotels, guest houses etc., are established e.g. Mashobra, Kasumpti, Chhota Shimla, Fingask estate, Mall road, Panthaghati, BCS, Khalini, Summer Hill etc. The best shopping area in Shimla is The Mall, Lower Bazaar, Tibetan Market and Lakkar Bazaar etc., as shown in Figure 11. There are many recreational places and religious places in Shimla city which includes cinema, theaters, sports complexes and stadiums, halls (Roller Skating) etc. These recreational places and places of religious interests were mapped and shown in Figure 12 and Figure 13.

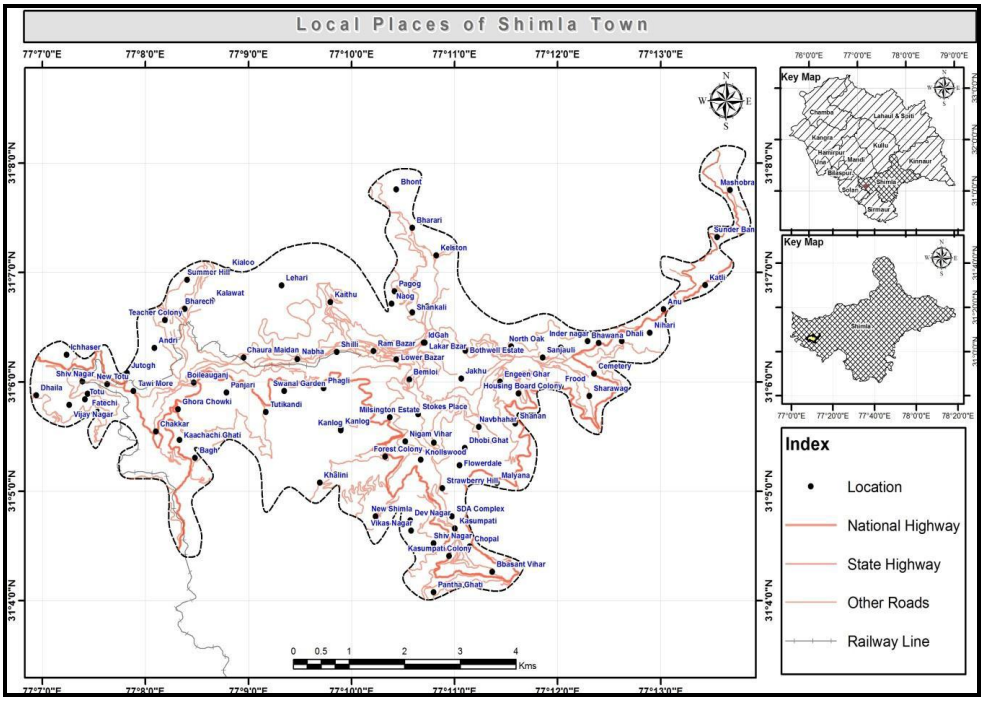


***Figure 11:*** *Local Places*

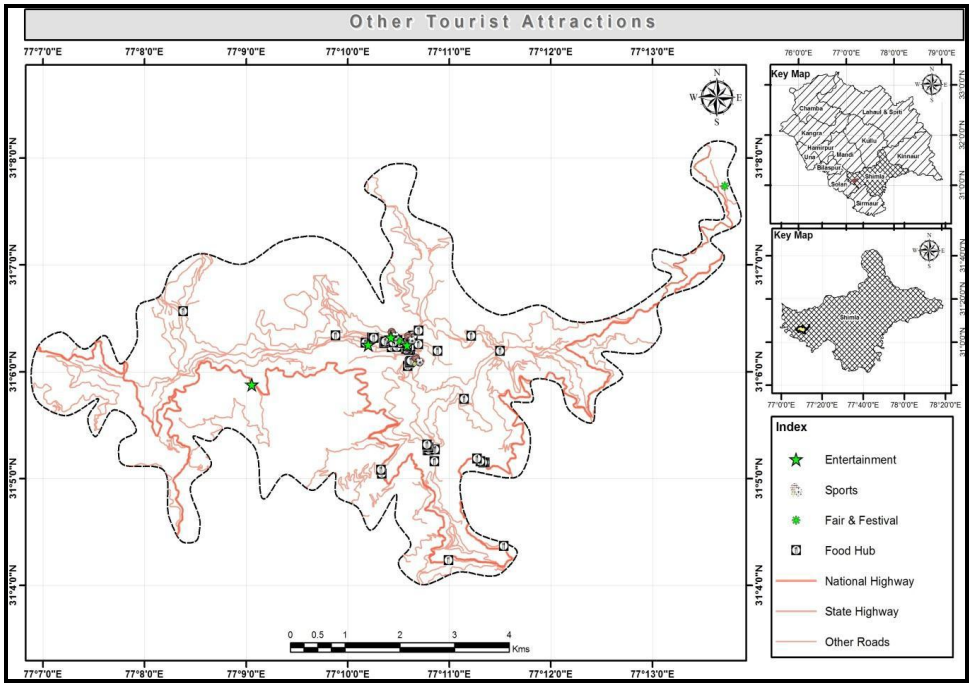


***Figure 12:*** *Tourist Attraction Site Map*

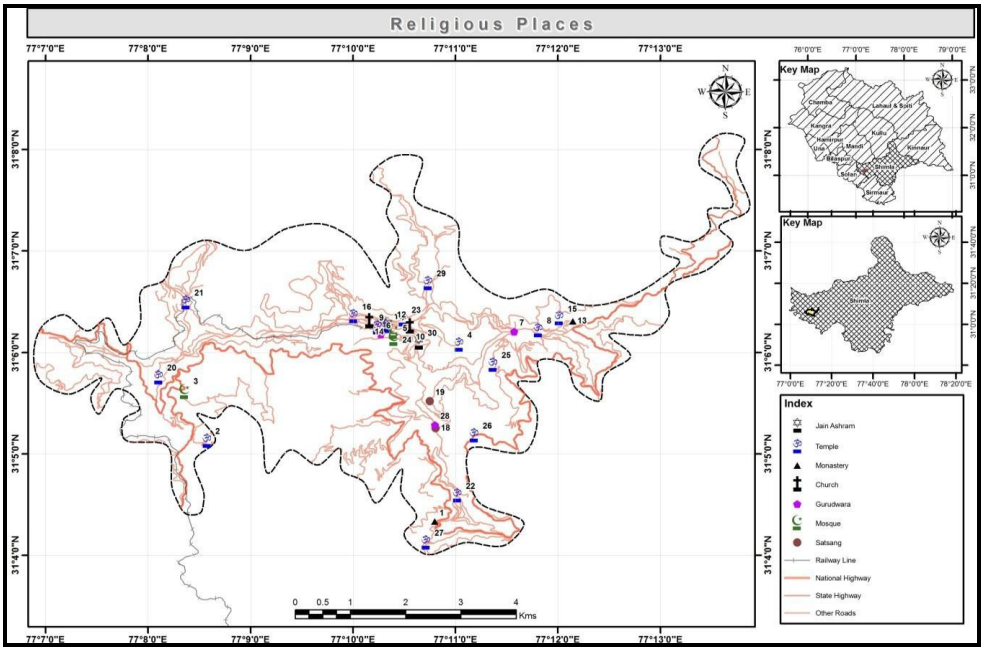


***Figure 13:*** *Religious Places*

In Shimla there are many types of economic services and we have mapped all the ATM and Post offices in and around the Shimla city and shown in Figure 14. They help in providing services to the local people as well as the tourists who visit Shimla for their vacation from all over the world. The postal services of Shimla have a great historical heritage. People and tourist use for economical purposes e.g. deposited money, money order, money transfer etc. There are many sub post office and one head post office in Shimla city (Figure 14).

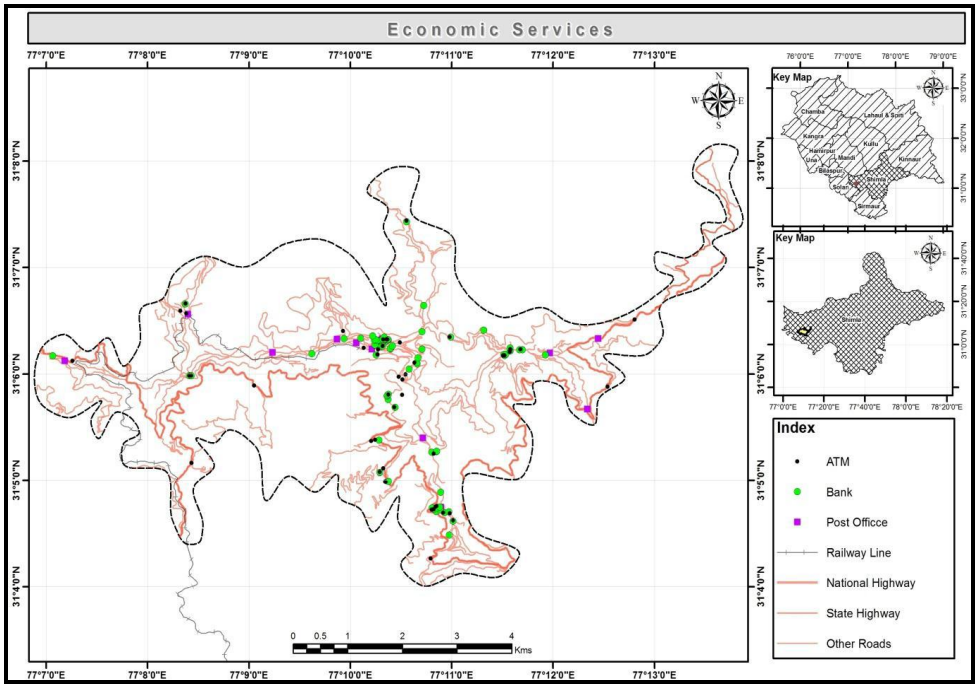


***Figure 14:*** *Economic Services*

There are many 5, 4, 3 star hotels and resorts situated in and around the Shimla city. These hotels provide the luxurious accommodation for the elite class of the society and the foreign visitors, who want to enjoy their visit to Shimla. Shimla is full of Hotels and Restaurants and there are around 240 hotels in and around Shimla, which includes premier hotels, e.g. Peterhof Hotel, The Oberoi Cecil, Hotel Holiday Home, Radisson Hotel, Wildflower-Hall and The Grand Hotel etc. There are two HPTDC hotels, 211 registered private Hotels, 19 home stays and 10 guest houses in Shimla town. So accommodation is no problem in Shimla (Figure 15).

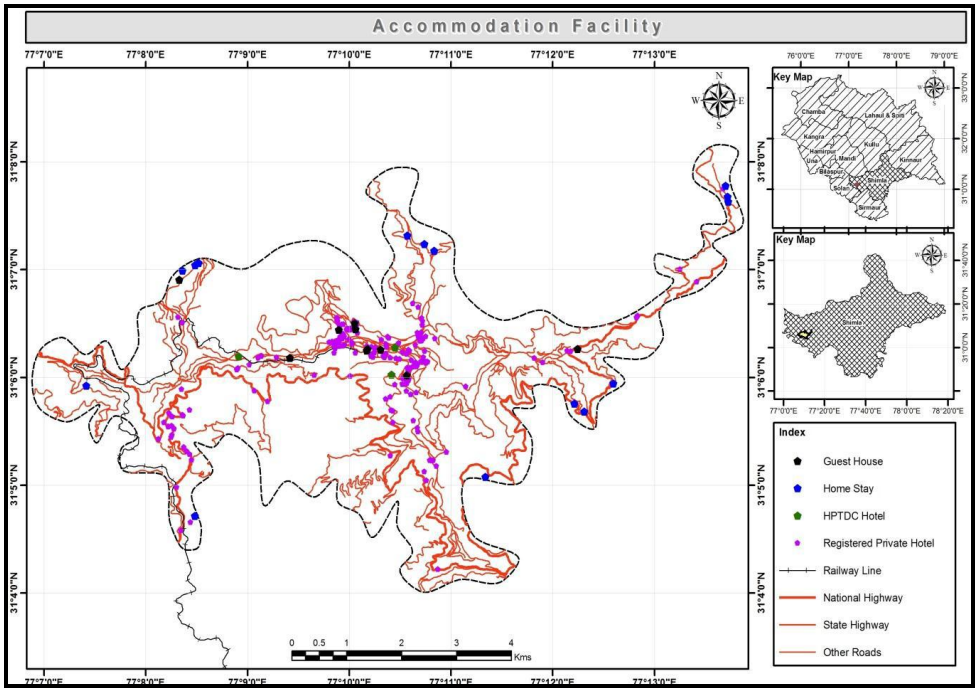


***Figure 15:*** *Accommodation Facilities*

### 4.4. Tourist Information Centre

Shimla is serene tourist spots and unbeatable natural beauty. On just entering Shimla one will find the Tourist Information Centre recently built in Himachali Architecture Style. The centre will provide proper guidance to the tourists visiting Shimla. The other Tourist Information Centre is located adjacent to the Scandal Point on the mall and other areas (Figure 16).

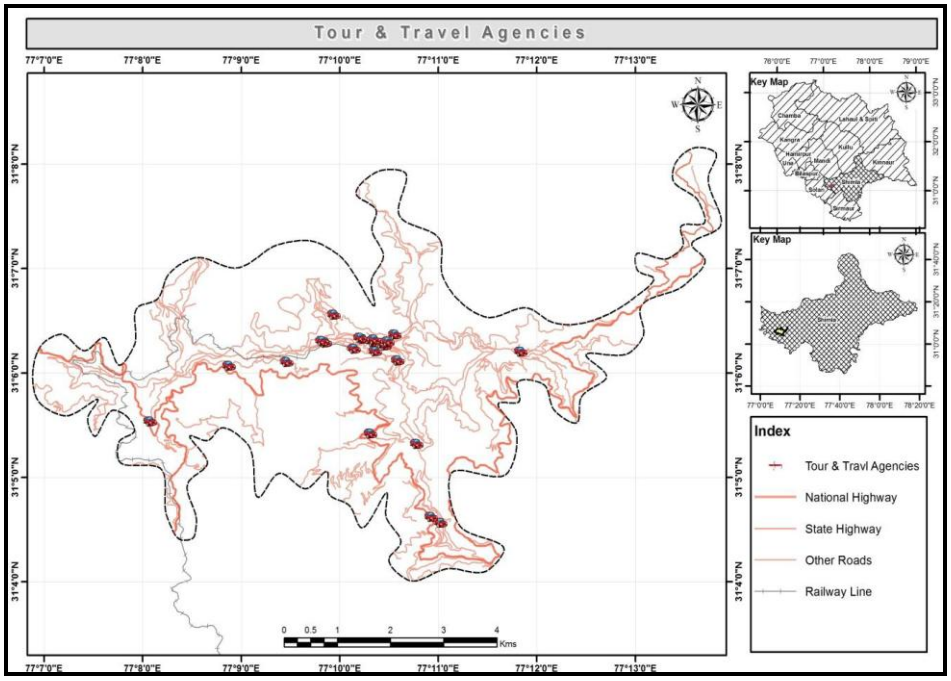


***Figure 16:*** *Tour & Travel Agencies*

### 4.5. Traffic Management and Services

Taxis as well as private cabs can be hired to roam around various places within the city. Throughout the day, taxis and cabs are found and they can be hired from anywhere in Shimla. HPTDC also has taxi services for within the city for local tours, for surrounding areas of Shimla and also interstate services. Taxi services for local sightseeing can be booked from the local stands, car/taxi rental offices and also through online sites. Local tours for half or full day are available as per the requirement of the tourists at these private taxi/car rental services. List of Notified Taxi Stands in Shimla is given below in Figure 17.

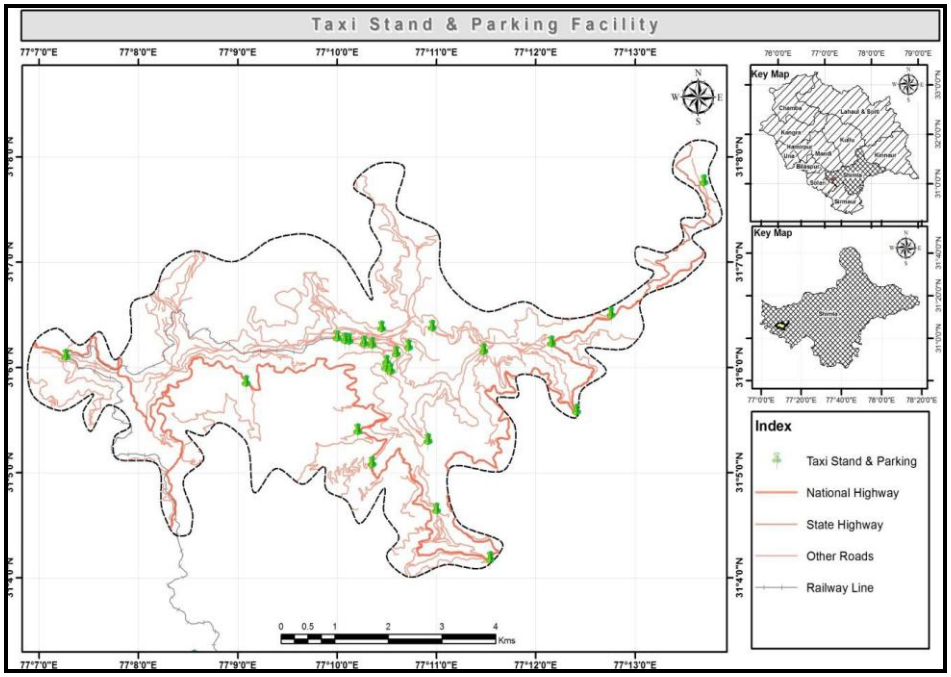


***Figure 17:*** *Taxi Stand & Parking Facility*

### 4.6. Parking Facility

Shimla is congested town and one can face parking problem if coming by own vehicle. There are many parking places operated by private parties. One should take special care of Sealed and Restricted roads in Shimla, all the roads leading from cart road to mall side are sealed and restricted roads. Parking on the sides of Cart Road is also prohibited. There is heavy fine on violation of any of the rules (Figure 18).

### 4.7. Fuel Station

Without the service of the Petrol Pump, it would be difficult for the tourist to continue their work and the pleasure. Shimla is natural that the city has a fair number of the petrol pumps which are spread all over the area. In Shimla city, there are eight petrol pumps. Here we provide the details of the some petrol pumps which are established in different part of Shimla e.g. Anup Service Station Kaithu, DD Mehta Sanjauli, Indian Oil Malyana, KDF petrol pump Dhali, HP Auto care Vikas nagar, Indian oil Taradevi etc., (Figure 18).

### 4.8. Services and Repair Facility

The transport that we use becomes a part and parcel of our life. If anything wrong happens to our transport we feel helpless. Thus it is very important to keep a note of the automobile repairing centres nearby roads. In Shimla you can find quality automobile repairing centre for transport. It is repairing any kind of car, cab, bus, truck etc. There are some example of services & Repair centre: Munsi Ji Tyre, SMC Isuzu Automobile, Pal & Ashok Car Washing, Auto Centre etc. (Figure 18).

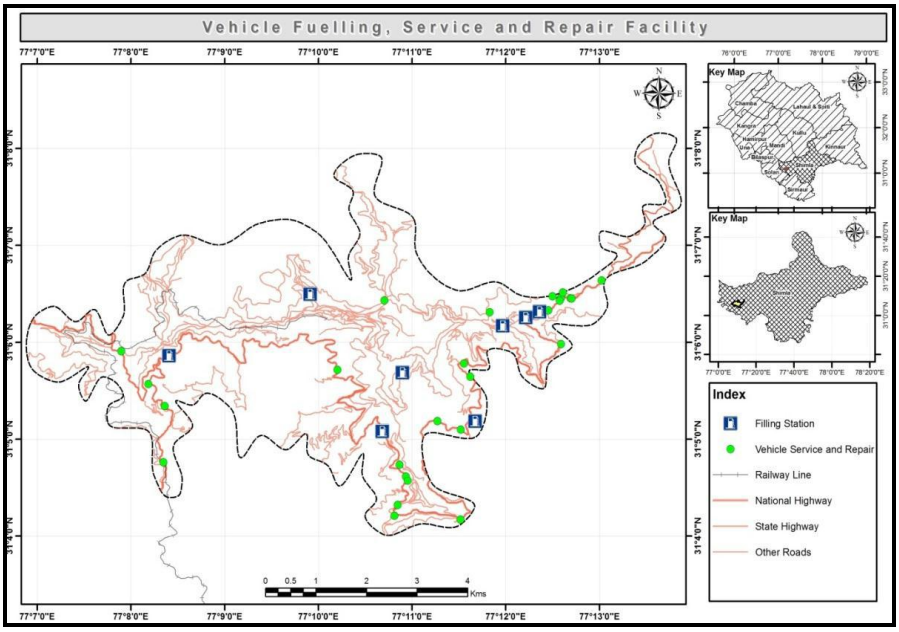


***Figure 18:*** *Vehicle Fueling, Service and Repair Facility*

### 4.9. Transportation Accessibility in Shimla

In transportation, accessibility refers to the ease of reaching destinations in Shimla. A measure that is often used is to measure accessibility in a traffic analysis zone is where: For a non-motorized mode of transport, such as walking or cycling, the generalized travel cost may include additional factors such as safety or gradient. Abundant transport accessibility connecting Shimla to other neighboring areas like Chail, Kufri, Manali etc. within Himachal Pradesh as well as to other states and cities like Delhi, Chandigarh, and Amritsar, makes Shimla one of the most visited tourist spots. Though buses are the most common way to move around within Shimla but taxis are available in ample numbers within the city. Shimla and Kalka are connected through narrow gauge railway line (Figure 19).

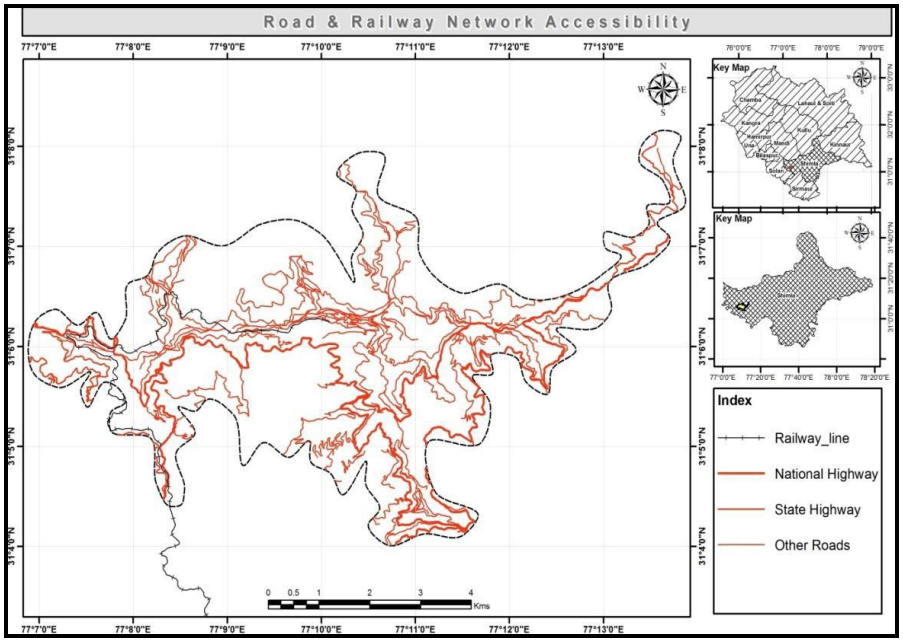


***Figure 19:*** *Road & Railway Network Accessibility*

### 4.10. Himachal Pradesh Tourism Development Corporation (HPTDC)

HPTDC organizes daily sightseeing tour as well as specialized tours. Customized tourism packages are also available so that tourists get sightseeing tours as per their choice. Seats for these sightseeing tours can be booked at the tourist information centres located at the Mall and the Railway Station (Figure 20).

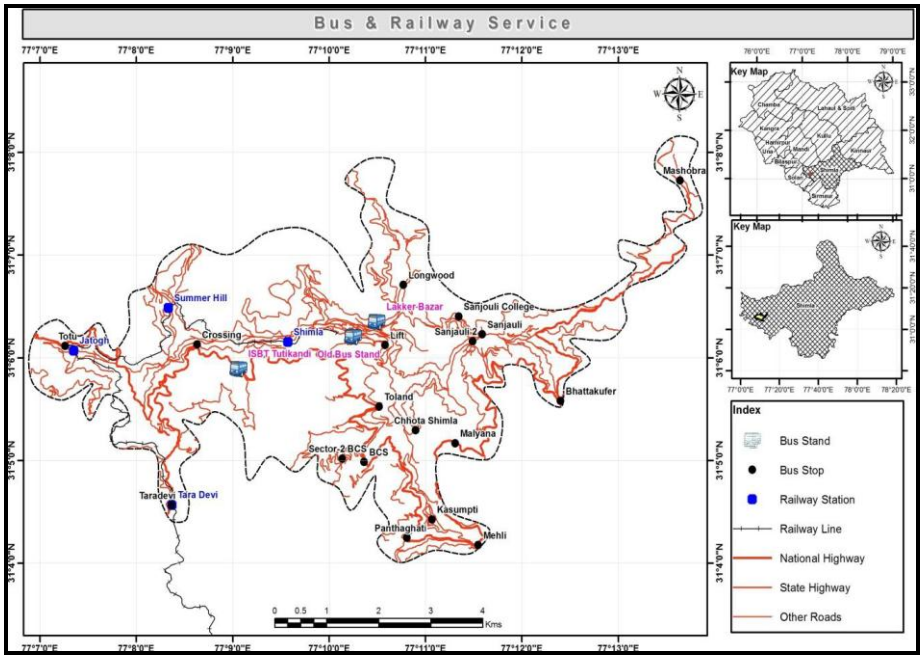


***Figure 20:*** *Bus & Railway Service Map*

### 4.11. Emergency Services

The tragedies or the disasters, whether it is due to the natural causes or man-made can strike anywhere such as the homes, roads or workplaces at any time. These tragedies and the man-made disaster create an emergency situation. Shimla has also emergency services e.g.: Health Service around 30 Health facilities in Shimla city (Figure 21). Police and fire Stations have also been mapped (Figure 21).

### 4.12. Government Offices and Educational Hubs

The city has approximately 82 anganwaris and 63 primary schools. Some of the popular schools in the city are Bishop Cotton School, Auckland House School, St. Edwards School, Tara Hall School, Chelsea School, DAV Public School (Lakkar Bazaar), and Chapslee School. The medical institutes in Shimla are Indira Gandhi Medical College and Dental College, St. Bede's College Shimla and Rajkiya Kanya Maha Vidayaliya (RKMV) are girls-only colleges.

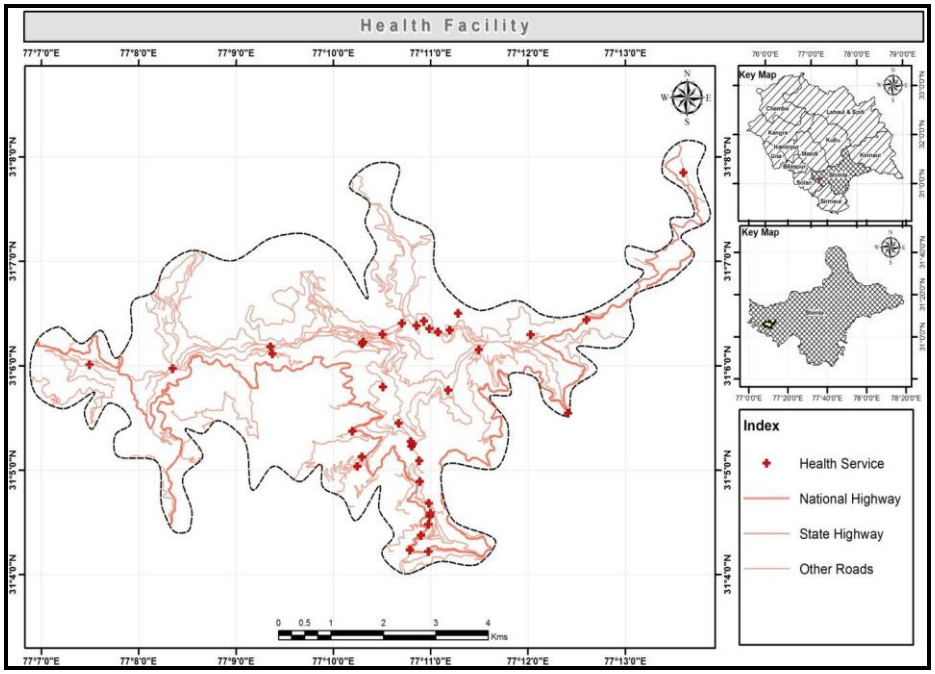


Government College, Sanjauli, and Rajiv Gandhi Government College, Chaura Maidan is also located in the city. The Indian Institute of Advanced Study, housed in the Viceregal lodge, is a residential Centre for research in Humanities, Indian culture, religion, and social and natural sciences. The Himachal Pradesh University is also based in summer hill, Shimla (Figure 22, 23).

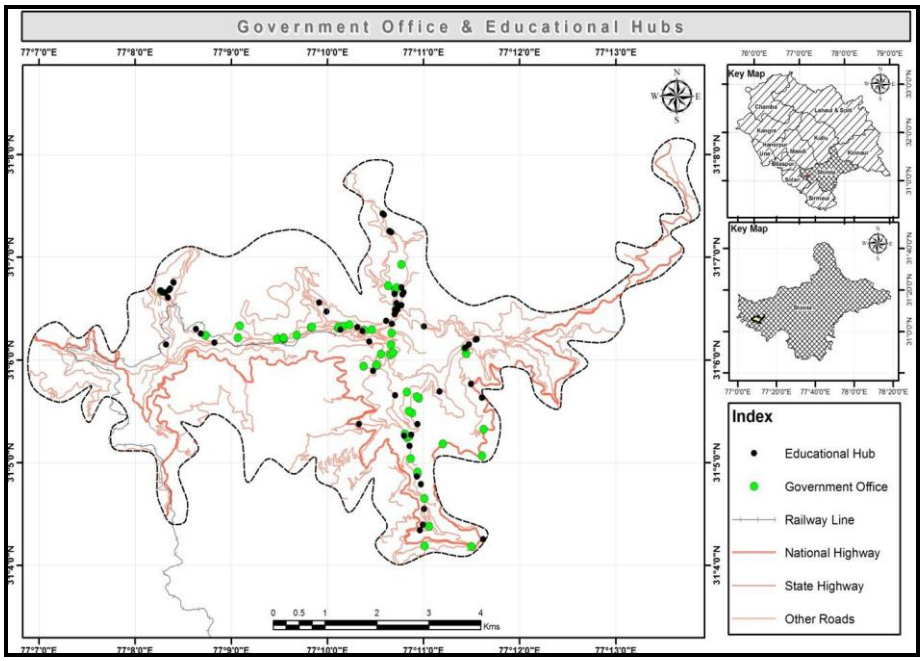


***Figure 22:*** *Government Offices & Educational Hubs*

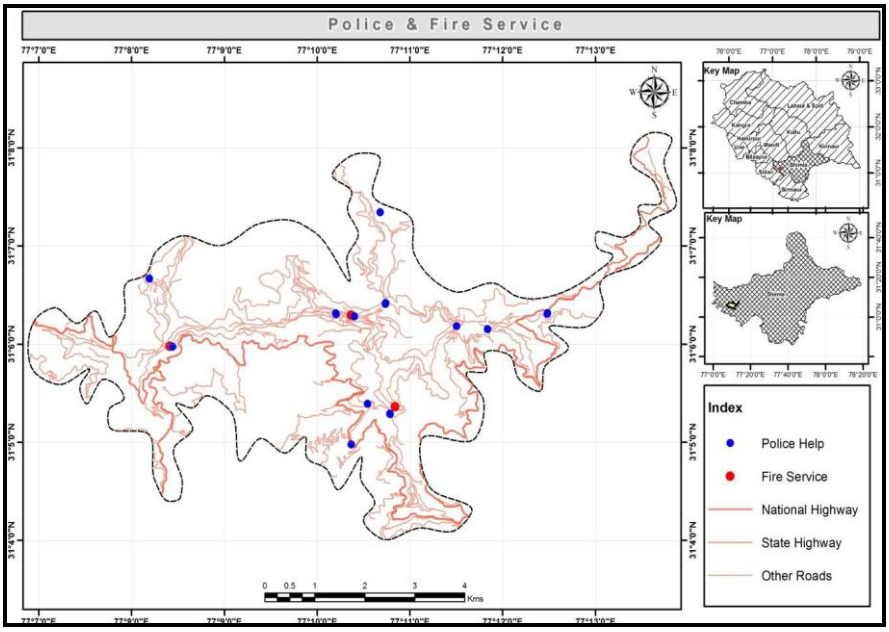


***Figure 23:*** *Police & Fire Service*

## 5. Conclusions

The present study was done to equip tourism and administration with the awareness of the historical development of geographical data with the help of GIS technology and also to discuss and examine the basic data (primary and secondary) so as to develop a basic database and perform critical spatial analysis. Several types of spatial information has been developed for present study such as map coordinates expressed in longitude and latitude of various places; hotels, heritage site and walk, emergency services, economic services, tourist spots, religious places, recreations transportation routes etc. The geospatial technology make it easier for tourists to find their way around their destinations such how to find the best route, how to set up locations to visit, what are the closest facility, how to customize directions, and how to evaluate accessibility across destinations. In addition, using the Geospatial technology the tourist identifies where he is, where are the tourist attractions, where are the trade areas of tourism/retailing stores, where are the best hotels, what are their characteristics, the distances between various tourist locations with an approximate time duration to travel that area can be calculated in real time.

## References

Kushwaha, A., Chatterjee, D., and Mandal, P., 2011: *Potentials of GIS in Heritage & Tourism.* Geospatial World Forum, Hyderabad. Paper Reference No.: Pn-71.

McIntosh, R.W., and Goeldner, C.R., 1986: *Tourism: Principles, Practices and Philosophies.* 5th Ed. John Wiley & Sons, New York.

Fadahunsi, J.T., 2003: *Tourism Management through Geographical Information Systems: A Case Study of Osun State*. Unpublished PGD Project Report. GIS Unit, RECTAS OAU Campus: Ile-Ife, Nigeria.

Kanga, S., Sharma, L.K., Pandey, P.C., Nathawat, M.S., and Sinha, S. *Eco-tourism of Taradevi Range of Shimla Forest Division in Himachal Pradesh (India)*. Journal of GIS Trends. 2011. 2 (1) 1-6.

Fung, T., and Marafa, L.M. *Landscape Ecology of Feng Shui Woodlands and the Potential for Ecotourism using IKONOS Images and GIS*. Int. Geoscience Remote Sensing Symposium. 2002. 6; 3246-3248.

Armstrong, M. *Requirements for the Development of GIS-Based Group Decision-Support Systems.* American Society for Information Science. 1994. 45 (9) 669-677.

Bukenya, J.O., 2012: *Application of GIS in Ecotourism Developments: Evidence from the Pearl of Africa.* Research Paper. http://www.rri.wvu.edu/wp-content/uploads/2011/03/bukenya2012.pdf.

Andrera, E.G., Michael, W.B., and Jane, S. *Tourism, Forest Conversion and Land Transformations in the Angkor Basin. Cambodia*. Applied Geography. 2009. 29; 212-223.

Andrew, S.D., and Shaw, S.L. *A GIS-based Spatial Decision Support System for Tourists of Great Smoky Mountains National Park*. J. Retailing Consumer Services. 2007. 14; 269-278.

Batra, A. *Himalayan Eco-tourism in Shimla*. ABAC Journal. 2001. 21 (3) 49-61.

Dondo, C.H., Bhudu, S.T., and Rivett, U. *GIS in Tourism- A Zimbabwean Perspective.* Int. Arch. Photogramtry Remote Sensing Spatial Inform. Sci. 2003. 34; 197-200.

**Cloud Publications**
International Journal of Advanced Remote Sensing and GIS
2014, Volume 3, Issue 1, pp. 723-733, Article ID Tech-303
ISSN 2320 - 0243

Methodology Article | Open Access

# GIS Technology for Agricultural Management of Tank Irrigation Systems in South India

**Krishnaveni M. and Rajeswari A.**

Centre for Water Resources, CEG Anna University, Chennai, Tamil Nadu, India

Correspondence should be addressed to Rajeswari A., raje_kesavan@yahoo.co.in; mkveni@annauniv.edu

Publication Date: 31 October 2014

Article Link: http://technical.cloud-journals.com/index.php/IJARSG/article/view/Tech-303



**Abstract** For many centuries village tanks have been the backbone of the village economy in South Asia. Tank storage structures are the prime water source to store rainwater and help farmers during crop growing period and provide stability to agricultural production. This resource has to be utilized properly by carrying out the On Farm Developmental works in its command area. The objective of the present study is to develop a GIS based Agricultural management of tank irrigation information system to facilitate the planning, operation and management of tank system. The study area selected was the Maragathapuram tank in Villupuram district served by the Ponnaiyar River. Developing agricultural tank information system involves the collection of various information of the command area. This information can be recorded and stored as different layers in GIS in the form of spatial and non-spatial data and GIS has the capability of integrating and analyzing spatial, non-spatial and multi-layered information available in different formats in framing various strategies for agricultural management and for socio-economic development. GIS based information system is also capable of generating outputs in the form of maps, tables and graphs that will help the irrigation engineers, agriculturalists, farmers and Government officials to monitor their performance of the tank at any place and time and take necessary steps to manage the resources effectively.

**Keywords** *Tank Irrigation; Agriculture; Information System; GIS; Framing Strategies; Managing Resources*

## 1. Introduction

Water is the primary resource for agriculture. The major source of irrigation in Tamil Nadu is mostly by tank water [1]. Tanks are low earthen bund which is constructed along slope of a valley or terrain to store the rain water. In Tamilnadu there are 39,202 tanks spread all over the state. A tank system comprises of catchment area, feeder channel, tank bund, water spread area, sluice outlets, command area, field distributaries and surplus weir. In recent years many of these tanks have started showing signs of big damage to their potential utility because of heavy siltation,

excessive pollution and encroachments. The potential returns from tank irrigation system was evaluated and concluded that tank irrigation is a profitable technology in economic, environmental and social terms but under present conditions of management it is rapidly deteriorating [2]. The tank irrigation system performance was evaluated in terms of economic output and revenue generation for irrigation and other uses [5]. The results indicate that irrigation and other productive uses put together raised the total value of output at tank level by 12% in 1996-97 and just 6% in 2009-10. Hence it is necessary to formulate agricultural management works of tank command area in a systematic, scientific and technical manner synchronously to achieve the sustained development by efficient utilization of the tank water [10].

Information plays a crucial role in the management and efficient utilization of resources. So, it is necessary to develop an information system for carrying out sustainable development [3]. A well-designed and comprehensive tank information system will result in substantial improvement in the efficiency of the agricultural sector and will also lead to better planning [6]. An interactive information system will facilitate the operation and management of resources effectively [7]. GIS with its capability of integration and analysis of spatial, a spatial, multi–layered information obtained in wide variety of formats has proved to be an effective tool in planning and managing the agricultural activity in the command area [8]. GIS is now being utilized not only as a system to monitor the rehabilitation process but also to measure changes in agricultural patterns and its management [11]. GIS and GPS technology are the most effective in examining the problems associated with the tank irrigation systems and to analyze rehabilitation works [4]. The significant benefit of GIS technology is its ability to visualize spatial data, to interpret information visually and to improve intuitive understanding of the distribution of and interrelationships among phenomena. GIS will be capable of delivering accurate, useful and timely information to various applications [9].

## 2. Materials and Methods

### 2.1. Study Area and Database

The study area taken is Maragathapuram village tank of Villupuram district in Tamil Nadu, India served by the Ponnaiyar river. It is located at the head reach of Ellis Choultry Anicut System. There are four sluices in Maragathapuram tank. The registered ayacut (command area) of this tank is 265.87 ha which is spread over the two revenue villages, Maragathapuram (whole) and Kandiyamadai (a part). In this study, all the required spatial and non-spatial data about the command area were collected for Maragathapuram tank and a digital database has been created in GIS environment. The secondary data collected are Command area map, rainfall data, ground water level data of the observation well, soil information and hydraulic particulars of Maragathapuram tank. In primary data collection, farmer's response survey directly from the beneficiaries had been carried out. For this a well-designed questionnaire had been prepared. Questionnaire was focused mainly on three aspects namely irrigation, agricultural and socio-economic aspects. Land parcel boundary was used as the primary database for the command area. The database consists of two components (i) Spatial data representing the distribution of features in the command area and (ii) attribute database representing agricultural, irrigation and social data of each of the land holdings. The spatial database was created using ArcGIS.

### 2.2. GIS Technology for Agricultural Management

GIS got a major role in developing the information system that is being adapted to the kind of decision and management functions that lie at the heart of the planning process of any development activities. Handling and analyzing data that are referenced to a geographic location are key capabilities of a GIS, the power of the system is most apparent when the quantity of data involved is too large to be handled manually. There may be hundreds of factors or thousands of

features to be considered, or there may be hundreds of factors associated with each feature or location. These data may exist as maps, tables or even as lists of names and addresses. Such large volumes of data are efficiently handled using GIS. Spatial analysis, the study of geographic features, and the relationships that exist between them can be applied to many areas of the agriculture sector. By better understanding how features within the landscape interact, decision makers can optimize operational efficiency and improve economic returns. GIS is becoming fully integrated and widely accepted for assisting government agencies to manage programs that support farmers and protect the environment.

As the Agricultural management of tank command area involves with spatial data, the database created (spatial and non-spatial) can be linked effectively only with the GIS concepts. The ability to manipulate, integrate and analyses the spatial data and its corresponding attributes at high speed is unmatched by any manual methods. Development of Agricultural Management Information System provides tools to handle, store, process, distribute and interpret the command area related data for assessment. The GIS based Agricultural management information system consists of menu driven modules for accessing, organizing, analyzing and displaying the tank command area information. The structure of the information system is shown in the Figure 1. Visual Basic was used as front end, MS access as back end for handling the attribute data and Arc GIS for maps. Object linking technique was used to link the ArcGIS maps and Access table and graphs with Visual Basic. Agricultural Management system is compiled with the Land System database integrated with all possible data available on the Agricultural tank command area. The database developed can be analyzed to identify a set of parameters together. Spatial analysis can be carried out to identify land unity matching with parameters. The Agricultural Management information system comprises of the following modules and shown in Figure 1. Each module has menus and submenus to access the relevant information of that particular module.

A. Water Resource module;
B. Agricultural module;
C. Irrigation module; and
D. Socio-economic module

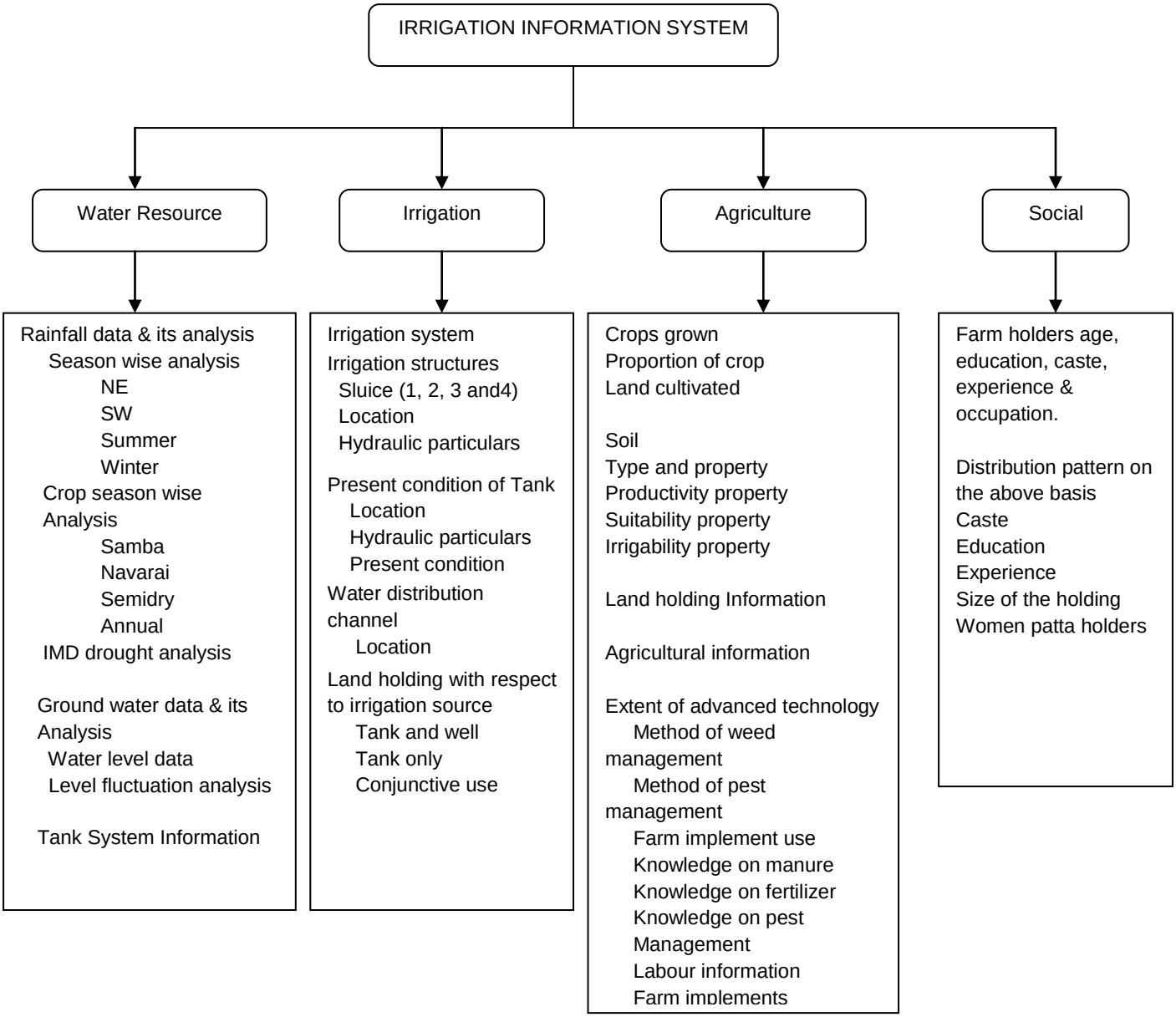


***Figure 1:*** *Structure of GIS based Agricultural Management of Tank Irrigation Information System*

### A. Water Resources Module

The water resource database module has the menus to display the water resource related information in the form of tables and analysis graphs. Mean monthly, monsoon seasonal and crop seasonal temporal rainfall pattern were determined for the study area, which are presented in the form of tables and graphs. The water resource database has information on rainfall, groundwater and specification of the tank details respectively. Rainfall menu consists of four submenus namely rainfall data, season wise rainfall distribution, crop season wise rainfall distribution, meteorological drought analysis and classification for the study area. The season wise rainfall analysis distribution consists of submenus of Northeast, Southwest, Summer and Winter. The graph showing the rainfall distribution over the years in the command area for that particular season can be obtained as shown in Figure 2. Similarly crop season wise rainfall analysis has submenus of Samba, Navarai, Summer (semi dry) and Annual respectively based on the crop season adopting in that command area. Each of this crop season will show the rainfall distribution pattern over years for

that particular crop season. The submenu of IMD drought analysis will provide information on the drought condition of the command area.

Groundwater menu consists of submenu of ground water level data and level fluctuation analysis of the observation well in the command area. This method of computation of ground water level fluctuation is a true reflection of the input and output from the ground water regime and is utilized in computation of ground water resources assessment. A geology and hydrogeology submenu gives the general information about the geology and hydrogeology information of the tank command area as a whole. Tank menu provides the general information about the tank system. The information in this module will help the water resource organization of public works department for carrying out the planning and implementation of irrigation structures and rehabilitation measures depending upon the requirement. It will also help the agricultural officers to know the availability of water resource potential of both surface and ground water and according to which they can suggest the cropping pattern.

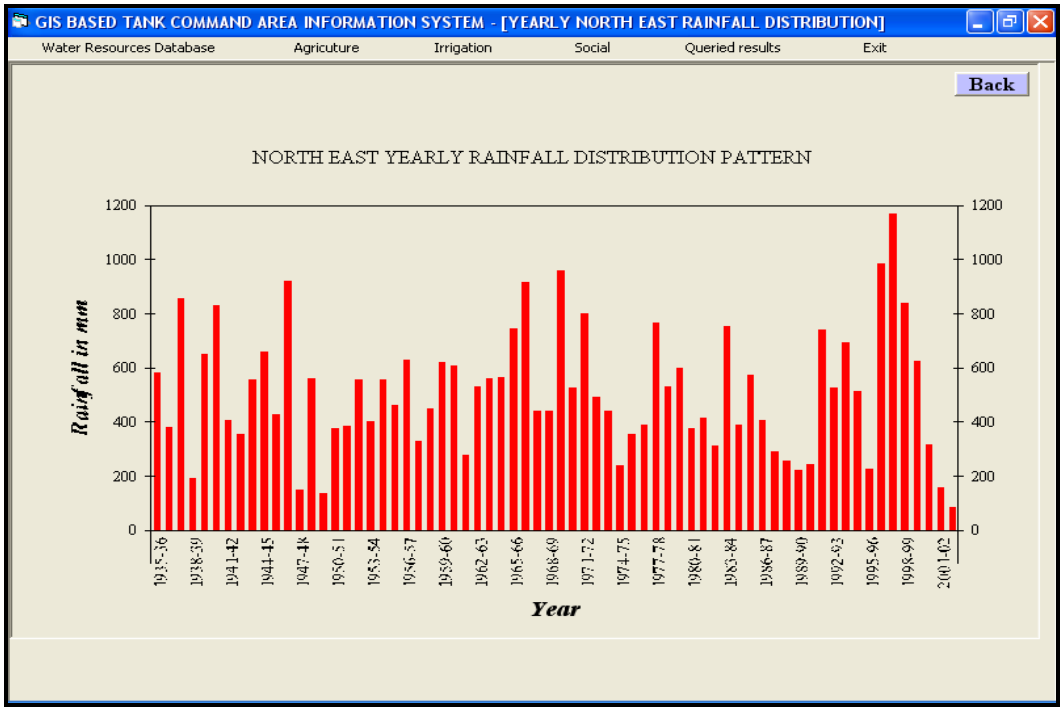


***Figure 2:*** *Graph of Northeast Rainfall Distribution in the Tank Command Area*

**B. Agriculture Module**

This module consists of five menus for information about the crops grown, soil information, land holding information, agricultural information and extent of the transfer of advance technology respectively. First menu gives the information about the crops grown in the command area, which have land cultivated submenu, shows the land holdings that are cultivated in various seasons and the lands that were not under cultivation and proportion of the area under each crop submenu gives the information about the crops grown in the land holdings in that season as shown in Figure 3. Crop water requirement for different crops information along with data of water availability during entire year, crop calendar, soil suitability also can be accessed. Paddy is cultivated in the entire command area in the first season and is followed by a second crop of paddy if adequate water is available in the tank. Whenever the tank water supply is not sufficient enough, well owning farmers prefer to grow groundnut, ragi, pulses and also vegetables to a certain extent. Sugarcane cultivation is confined to farms having wells with sufficient water supplies. This menu provides land

use information, land suitability maps based on natural and social factors and information on the distribution of transmigration villagers. The information system developed led them to the evaluation of potential agricultural land and compilation of the possible agricultural development maps.

Soil forms the most important non-renewable natural resource determining the success of agriculture. Second menu is incorporated with Soil information containing information for researchers, planners, and scientist. It consists of information about the type of soil in the command area and its properties related with land capability, irrigability, productivity and crop suitability details. The third menu has the information on land holdings, which tells about the type, patta number and owner of each land holding and also gives the land holding map. Parcel level information can be the had in this menu by clicking the relevant land parcel or owner and the information is displayed in the forms designed for the specific table of information. The agricultural information menu gives the information of agricultural related activities of each of the land holding. Agricultural information such as crops grown, cultural practices the landholders adopt and the farm implements they use can be obtained from this menu by clicking the relevant land parcel or owner. Extent of transfer of advanced farming technology menu gives information on various aspects such as levels of inputs used, mechanization the farmer adopt in their fields, method of crop culture adopting in each of the land holdings can be obtained, for example Information regarding source of seed for the land holding as shown in Figure 4. Information in the module will help the Survey and land Record department for referring. Agricultural and Agricultural Engineering department can be better benefited by the information of this module to carry out any agricultural related developmental and management activities in the command area.

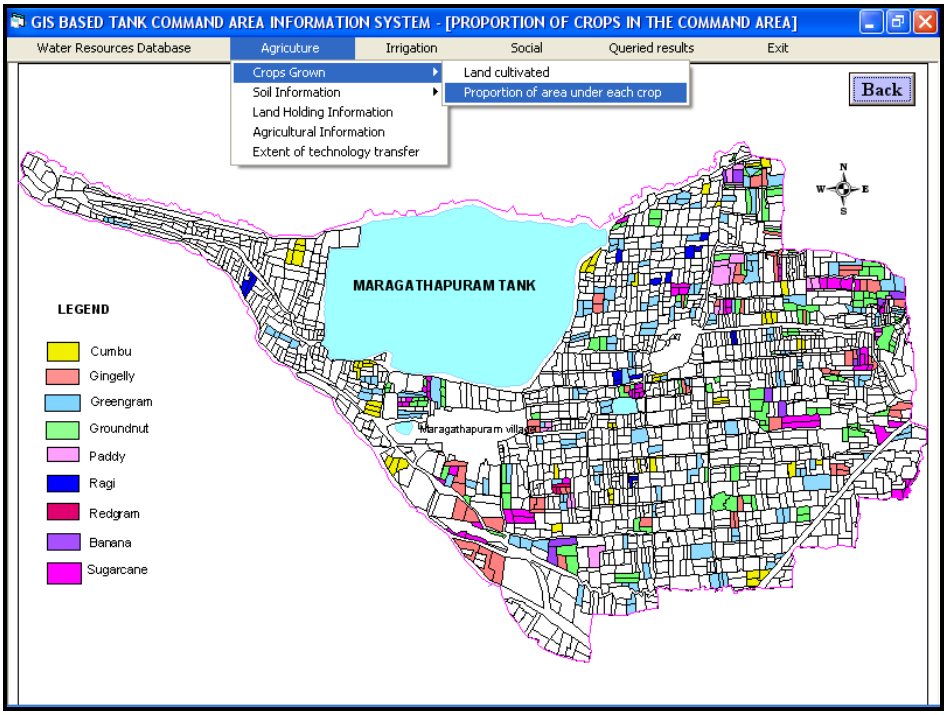


***Figure 3:*** *Information on Proportion of Area under Each Crop in the Tank Command Area*

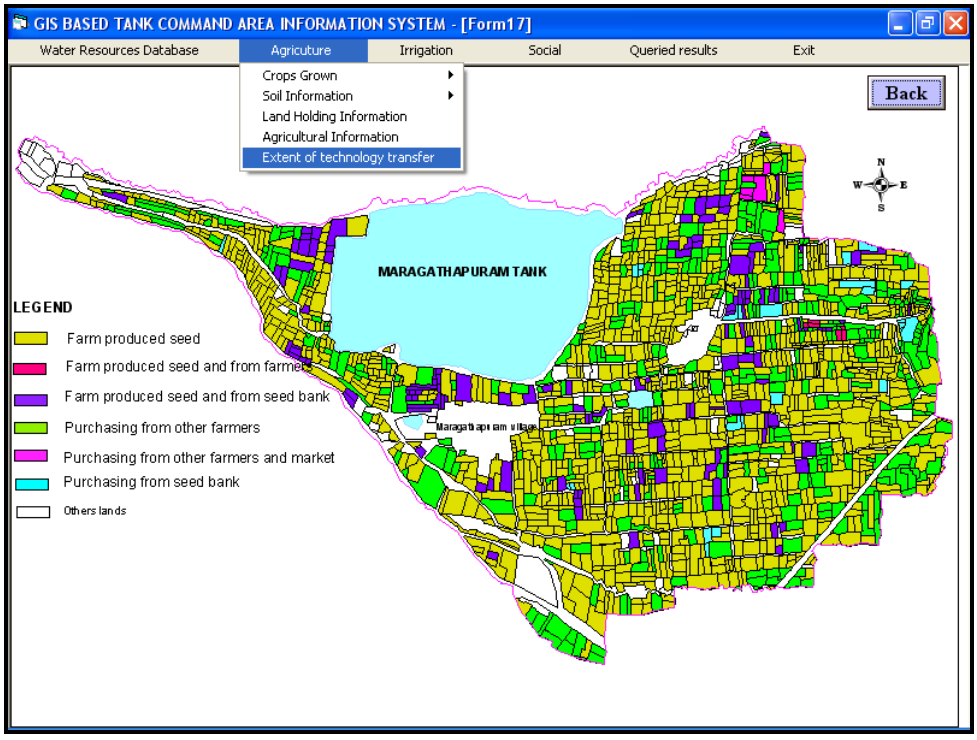


***Figure 4:*** *Information on the Source of Seed for Each of the Land Holdings*

### C. Irrigation Information Module

This module consists of three menus for information on irrigation related activities in each of the land holding, the irrigation structures, irrigation source wise area distribution respectively. General information on irrigated related activities menu gives the information about the source of irrigation, if well means Hp of motor, type of well, depth of well, reach of the land holding from the tank, method of irrigation practices as given in Figure 5. Irrigation structure menu provides access for information about the structures such as location of irrigation structures like tank, sluices, water distribution channels and wells in the command area. It also describes about the particulars of each structure such as hydraulic particulars of the tank, sill level and the area served under each sluices. This menu also provides information about the present condition of each of these structures. The condition of Sluice 2 can be obtained as shown in Figure 6. Information on land holding classification based on its irrigation source such as areas that are irrigated by tank water, well water and both tank and well water can be obtained. This menu also gives the information of the land holdings that are making conjunctive use of surface and ground water. There are four sluices in the tank for serving the command area. Information about the landholding covered under each of the sluices also made accessible from this menu. This module will help the water resource organization to plan, operate and maintenance of the irrigation systems.

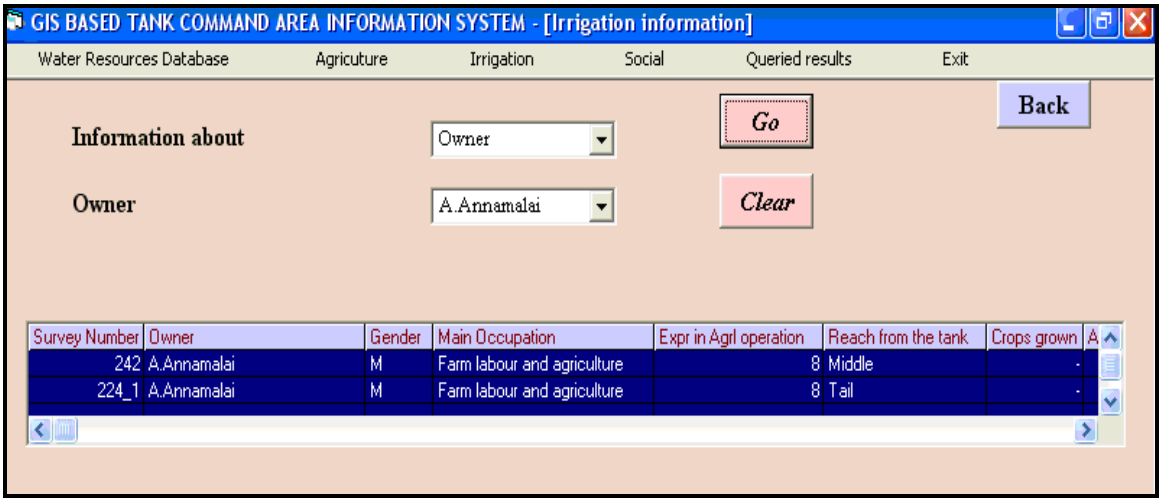


***Figure 5:*** *Menu Showing the Irrigation Information of the Landholder*


***Figure 6:*** *Menu Shows the Condition of Inlet and Outlet of Sluice 2*

### D. Socio-economic Module

This module consists of information about the social aspects of land holding farmers such as caste, literacy level, age, occupation and their experience in agricultural operation which is available in tabular format and classification of land holding with respect to caste, education as shown in Figure 7, experience in agricultural operation, size of holding and women patta holders as shown in Figure 8 can be obtained respectively. Agricultural officers can get the information about the experience of the farming farmers with which they can conduct training programs. This module will also provide information to the Administrative officers to carry out any activities related with the upliftment of farming community based on their literacy level and their occupation.

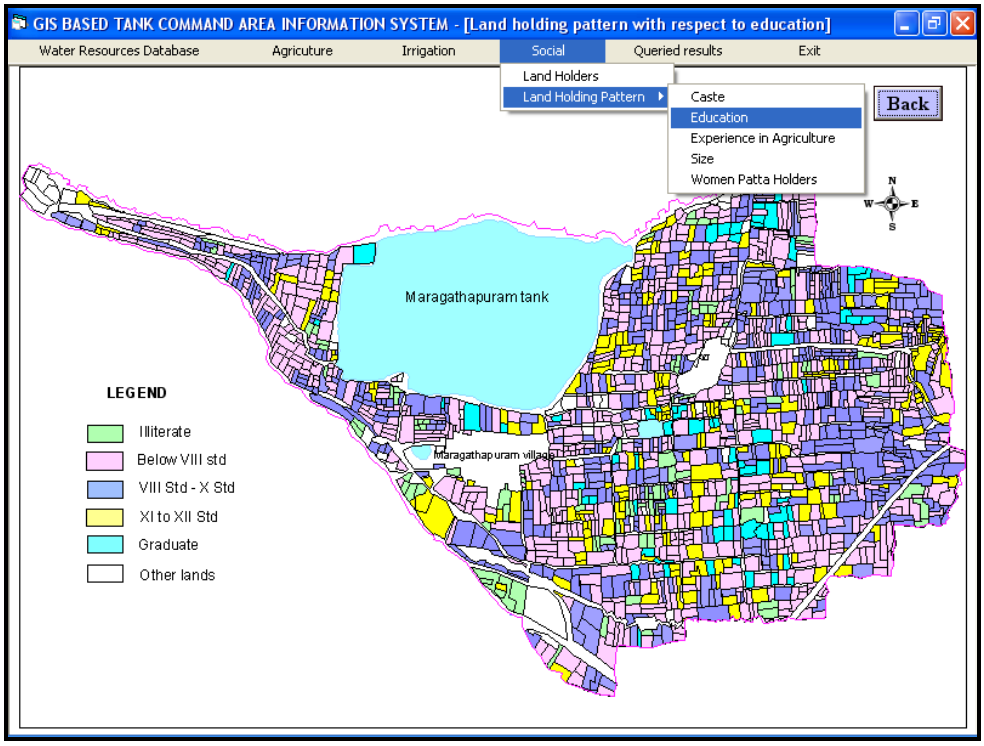


***Figure 7:*** *Land Holding Pattern with Respect to Education of Land Holders*

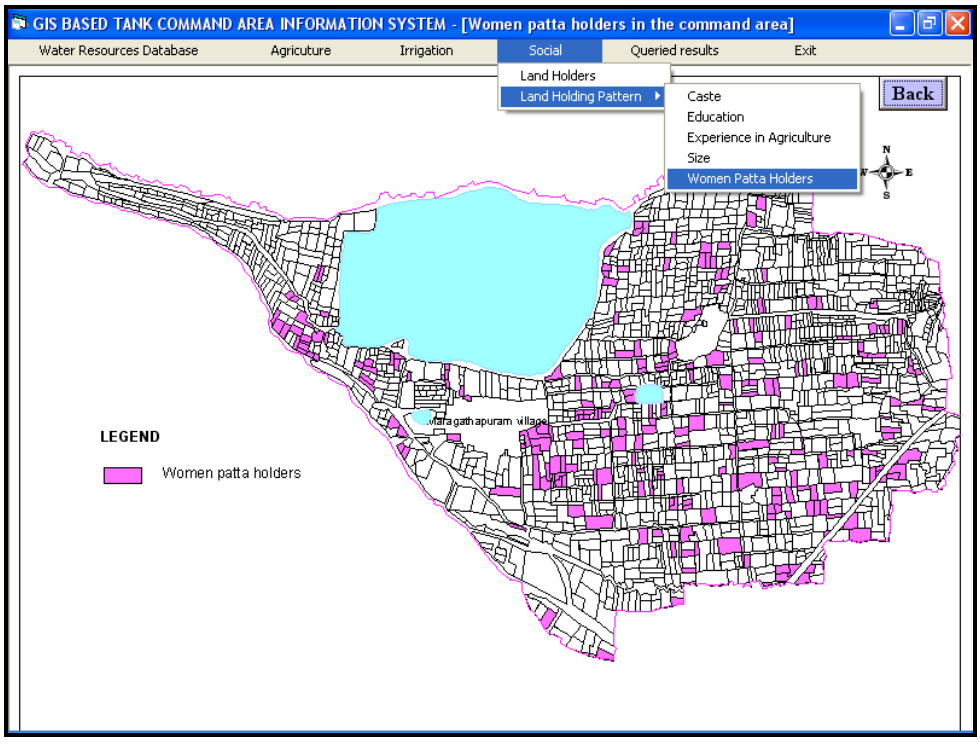


***Figure 8:*** *Distribution of Land under Women Patta Holders in the Command Area*

## 3. Results and Discussion

A flexible and user friendly information system developed will assist planners for village level planning with reference to managing the resource of Maragathapuram tank command area. Furthermore the spatial analysis tool of the system is a handy option for the planners to correlate

spatial information. Agricultural management information system needs only the maintenance and updates of spatial as well as attributes data if changes occur in existing cropping patterns and management practices, it has become a valuable and cost-saving tool for decision-making. In natural resource management, there is a great need for timely and accurate information about what is on the ground. The task of optimal resources management and sustainable development has been greatly synergized by the enhanced speed and reliability with which spatial and temporal information is generated. Designing the GUI and data layer presentation help the landowners to use the data and information more easily. The information system gives access to data for agricultural resource management and to foster a better understanding of the local agricultural resource base.

## 4. Conclusion

Development of the agricultural management information system will help in effective use of the resources available for agricultural development. It also serves as a powerful media to create awareness about the various agricultural and command area related developmental activities visually to the farmers. This helps the engineers, agriculturalists and irrigation managers to understand the water needs and to develop schedules, operating procedures and maintenance requirement to maximize the benefit from the farm land. Also help them to develop and conduct training programs for the farmers by combining multimedia with the information system. Provide Information to various users such as Public Works Department for operation and maintenance of the irrigation systems, Revenue Department for the tax collection and Electricity Board for electric charges. It is important, for an agricultural country like India, that the classification of agricultural land, its measurement, the assessment of its produce and maintenance of land records are properly maintained and updated. It can be better used to channelize the existing manpower, resources and infrastructure right from the village level in a proper manner. The methodology thus developed for Agricultural management of tank command information system with the GIS concepts is found to be effective in utilizing the resources and for sustainable agricultural development

## References

[1] Ambler, John, 1994: *Basic Elements of an Innovative Tank Rehabilitation Programme for Sustained Productivity.* Workshop on Regeneration of Farmers' Management of Tank Irrigation System, Madurai, India.

[2] Anbumozhi, V., Matsumots, K., and Yamaji, E. *Towards Improved Performance of Irrigation Tanks in Semi-Arid Regions of India: Modernization Opportunities and Challenges*. Irrigation and Drainage Systems. 2001. 15; 293-309.

[3] Chowdhary, H., Jain, S.K., and Ogink, H.J.M., 2000: *Emerging Information Technology for Sustainable Water Resources Development in India*. Proceedings of International Conference on Integrated Water Resources Management for Sustainable Development, 19-21 Dec., New Delhi, India.

[4] Krishnaveni, M., Siva Sankari and Rajeswari, A. *Rehabilitation of Irrigation Tank Cascade System using Remote Sensing, GIS & GPS*. International Journal of Engineering Science & Technology. 2011. 3; 1464-1469.

[5] Palanisami, K., Ruth Meinzen Dick., Mark Giordano., Barbara Van Koppen and Ranganathan, C.R. *Tank Performance and Multiple Uses in Tamil Nadu, South-India, Comparison of 2 Periods (1997-98) (2009-10)*. Irrigation and Drainage Systems. 2011. 25; 121-134.

[6] Rajeswari, A., 2004: GIS Based Tank Command Information *Syste'*, M.E. Thesis Center for Water Resources, Anna University, Chennai. 75.

[7] Shanthi, C. and Pundarikanthan, N.V. *Application of Management Information System in Improving Irrigation System Performance in a Developing Country.* Water International. 1999. 24 (3) 229-239.

[8] Sharma, A.K., Naval Gund, R.R., Pandey, A.K., and Rao, K.K., 2001: *Micro–Watershed Development Plans Using Remote Sensing and GIS for a Part of Shetrunji River Basin, Bhavnagar District, Gujarat*. www.gisdevelopment.net/application.

[9] Sharma, S.D, Randhir Singh and Anil Rai, 2002: *Integrated National Agricultural Resources Information System (INARIS)*.
http://www.gisdevelopment.net/application/agriculture/overview/agrio0007.htm

[10] Sinha, M.K., 2001: *Constraints in Implementation of CAD Programme in N.E. States and Its Remedial Measures*. National Seminar on Water and Land Management Including CAD for Socio Economic Upliftment of North East Region.

[11] Steve Stone, Emil J. Dzuray, Deborah Meisegeier, Anna Sara Dahlborg and Manuel la., 2000: *Decision-Support Tools for Predicting the Performance of Water Distribution and Wastewater Collection System*. U.S. Environmental Protection Agency, Cincinnati, U.S.A.

**Cloud Publications**
International Journal of Advanced Remote Sensing and GIS
2014, Volume 3, Issue 1, pp. 784-789, Article ID Tech-304
ISSN 2320 - 0243

Review Article | Open Access

# Location Privacy, Its Significance and Methods to Achieve It

**Purnima Dasgupta**

Institute for Geoinformatics, University of Münster, Germany

Correspondence should be addressed to Purnima Dasgupta, purnima.dasgupta27@gmail.com

Publication Date: 17 December 2014

Article Link: http://technical.cloud-journals.com/index.php/IJARSG/article/view/Tech-304



**Abstract** The advancement in location based services has also lead to the increase in concerns of location privacy. Revealing personal location information can be risky but also advantageous. The consequences of leaked personal location data can be quite adverse. The effects of location privacy invasion and ways to achieve location privacy are a less explored field. This paper presents a concise report of some the ways to overcome privacy issues and threats, and also sheds light upon what drives Location Based Service users to share their personal location information. The paper reviews studies about behavior and attitude of Location Based Service users towards sharing location information which depends upon the nature of the requester, the reason for requirement of location information and also the apt level of detail of location information required. The paper will discuss about methods or schemes for protecting privacy such as anonymity, mix zones and obfuscations. The main focus will be on computational location privacy concerns.
**Keywords** *Location Based Service; Location Privacy; Threats; Identity*

## 1. Introduction

Location tracking of mobile phones enables Location Bases Services to spread outside closed environments [6]. With the increase in the prevalent nature of Location Based Services, also increases the temptation of users to give away their personal location information. This is the main factor that gives rise to privacy concerns.

Barkhuus, Louise, and Anind K. Dey [6] categorized Location Based Services into two types. Position - aware services wherein the device has knowledge of its own location and location - tracking services wherein the other parties track the user's location. It was realized that location - tracking services give rise to more number of privacy concerns as compared to position - aware services. Therefore position - aware services are more preferable. At this point we ask ourselves, what is location privacy? The essence of location privacy lies in the word "identity" which is also the core of all privacy issues. A user whose location is being measured should be able to control the viewing audience of his or her location information in order to protect his or her identity. Krumm, John discussed about the factors that influence location privacy. They are "When", "How" and "Extent" [1]. Often people are more concerned

about their present or future location information being disclosed as compared to the concern for disclosing past location information. But it should also be considered that real time location could enable attackers to find a person, but past data could help them discover who the person is, where he or she lives, and what he or she does. People are more comfortable with their friends and acquaintances manually requesting for location information rather than automatic alerts being sent when he or she enters a food joint or movie theatre. More preference is given to reveal less specific location information in the form of an ambiguous region than a specific point is order to pertain location privacy.

Need of the hour was formulating methods or schemes to deal with privacy concerns. One way to do so is the anonymization method. Anonymization is a way of blurring location information appropriately in order to prevent access to higher fidelity information. Another way to define data anonymization would be “Data anonymization is the process of destroying tracks, or the electronic trail, on the data that would lead an eavesdropper to its origins” [12]. Gedik, Bugra, and Ling Liu [7] described the personalized k-anonymity model for protecting location privacy against various privacy threats through location information sharing. Another method is to use pseudonyms instead of actual identifiers. This gives rise to the concept of Mix Zones [5]. Mix Zones are developed to enhance a user’s privacy while using Location Based Services. The Mix Zone model restricts the location information about where a user can be present and therefore anonymizes his or her identity. Spatial and temporal degradation is another way of achieving location privacy. Introducing obfuscation is the process of deliberately degrading the quality of spatial and temporal information by formalizing the concepts of inaccuracy and imprecision [1].

Many studies about the attitudes of people in case of location privacy have revealed that Location Based Service users actually don’t mind and don’t care much about location privacy. This may be because they are unaware of the negative consequences of a location leak such as stalking or even physical harassment. Maybe they will become much more sensitive about location privacy and realize its need if there is a major news story about the negative consequences of a location data leak [1]. Location Based Service users generally disclose information that they think would be useful to the requester. They disclose specific or generic information because they think that it would be useful to the requester in their respective forms [2].

The structure of the paper is as follows. Section 2 gives brief background information regarding the need for location privacy protection models. Section 3 discusses about and explains the major methods to overcome location privacy concerns in Location Based Services. Section 4 talks about the attitudes and perspectives of Location Based Service users towards location privacy, its invasion and consequences location leak. The paper concludes with section 5, followed by the references used in the paper in listed in the last section.

## 2. Background

Location Based Services are of two types, location – tracking services and position-aware services. The outcome and usefulness of both the methods are similar, but location – tracking services give rise to more number of privacy concerns than location - aware services and therefore the latter is more preferable. Research within location – tracking in indoor environments have been conducted over decades but outdoor Location Based Services (using GSM and GPS) generate a different set of privacy issues [6]. Failure to protect and maintain location privacy has negative consequences or effects in broadly three areas. Location Based spam, wherein location information can be used by businesses to attack a person with unsolicited marketing of products related to his or her location. While public disclosure of location information enables a variety of useful services such as improved emergency assistance, it also exhibits significant potential for misuse [8]. Access to information about a person’s location could potentially lead to harmful encounters, for example stalking or physical

harassment jeopardizing his or her personal wellbeing and safety. Location information can aid an attacker to infer other personal information about a person [11].

## 3. Methods to Achieve Location Privacy

There are two kinds of privacy threats, communication privacy threats and location privacy threats [7; 10]. During the past decades, various methods have been formulated to protect location privacy and overcome its threats. Some of them will be discussed during the course of this paper.

### 3.1. Mix Zone Model

A simple approach to prevent location information from being misused is assigning pseudonyms to individuals using the Location Based Services instead of the actual identifiers. But using long term pseudonyms for each user does not provide much privacy because applications could identify users by following the "footsteps" of a pseudonym [9]. Therefore constantly changing pseudonyms can be used to ensure higher privacy. This is the basis behind the concept of Mix Zone model. Beresford, Alastair R., and Frank Stajano [5] talk about the Mix Zone model. The Mix Zone model anonymizes a user's identity by restricting the positions where he or she can be located. This model comprises of mainly two elements. The first is a trusted middleware system that provides anonymized location information to third party applications i.e. it is positioned between the underlying location system and untrusted third party application. The second element is a quantitative estimate of the level of anonymity provided by the middleware with particular set of applications. All third party applications are treated as a global hostile observer [5; 9].

The Mix Zone model, as shown in Figure 1, consists of two zones, application zone and mix zone. Application zone is the area where a user has registered with a Location Based Service for a callback. For example restaurants, airports, hospitals, university campus etc. Mix Zone is the area where no applications can trace the movements and positions of the user [9]. It is assumed that users will only report their location regions, application zones. In the mix zones outside the application zones a mobile user is given a new pseudonym to help mix him or her with other users in the same zone. This helps prevent an attacker from linking pseudonyms, because the new pseudonym could have been assigned to anyone else in the mix zone [1]. The user carries different pseudonyms while entering the Mix Zone as well as while exiting. The drawback is that user movement patterns are not time invariant, but tend to be self-similar over a period of time. An attacker can link pseudonyms and therefore track long term user movements with the aid of historical data. It is also possible to infer likely user movements within Mix Zones for example in the case of corridors or walls [5].

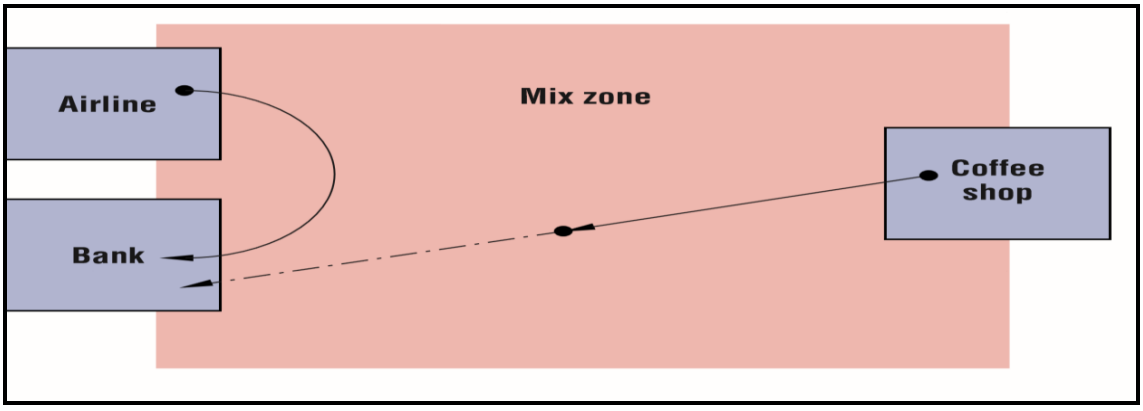


***Figure 1:*** *Showing an Image of Application Zone and Mix Zone, from [9]*

### 3.2. Anonymization Method

Anonymization is a way of blurring location information appropriately in order to prevent access to higher fidelity information. Anonymity is the state of being not identifiable within a set of subjects, the anonymity set [7; 10]. Samarati, Pierangela, and Latanya Sweeney [3] presented a methodology for anonymizing through generalization (i.e. to generalize relationships in between domains and in between values that attributes in a database can assume) and suppression (i.e. to remove data from tables so that they are not released) techniques for data privacy in a public database. Their objective was to design a methodology that is able to release information freely but does so in such a way that the identity of an individual contained in the data cannot be recognized [3]. Most people do not realize the significance and outcomes of shared information even at a lower level such as a local grocer keeping track of what people purchase and when do they purchase those items. This kind of user data put together can be a very intrusive catalogue of data [5; 3].

Taking inspiration and ideology from Sweeney's method, Gruteser, Marco, and Dirk Grunwald introduced the k-anonymity for location information. They considered a subject as k-anonymous with respect to location information, if and only if the location information presented is indistinguishable from the location information of at least k−1 other subjects [10; 1]. Gedik, Bugra, and Ling Liu [7] explained about the personalized k-anonymity model for protecting location privacy. They introduced a personalized anonymization model, wherein users can specify the minimum level of anonymity preferred by them, which uses an algorithm for identity removal and spatio temporal cloaking of location information called the "CliqueCloak Algorithm". The draw backs specified by them are, deterioration of quality of service due to providing more coarse grained location information to users, communication processing overhead and extra delay introduced through temporal cloaking of location information which may decrease perceived service quality.

### 3.3. Obfuscation Techniques

Obfuscation can be defined as the practice of deliberately degrading the quality of information in some way, so as to protect the privacy of the individual to whom that information refers [8]. Obfuscation can be achieved in many ways, such as, adding additional noise to the location data or reporting regions instead of points. The key is to strike a balance between privacy and usefulness of the Location Based Service in order to receive high quality information services by using lo quality positional information. Spatial and temporal degradation of location information for introducing obfuscations formalizes the concepts of inaccuracy, imprecision and vagueness. Inaccuracy corresponds to a lack of correspondence between information and reality, imprecision corresponds to a lack of specificity in information and vagueness corresponds to the existence of boundary cases in information [11; 4].

Ardagna, Claudio Agostino, et al., [4] mentioned three basic obfuscation techniques assuming that the area returned by a location measurement is planar and circular in nature. Obfuscation by enlarging the radius, obfuscation by shifting the center and obfuscation by reducing the radius. All these cases it can be inferred that the accuracy of position is inversely proportional to location privacy. The goal was to enable users to express their privacy preferences in an intuitive and straight forward way. A user can specify 140 meters as his or her privacy preference meaning that he or she wishes to be located with accuracy not better than 140 meters. Applying only one obfuscation technique did not yield very high location privacy. Therefore a combination of obfuscation techniques is discussed (see Figure 2). Such as applying the combination of, enlarging the radius of circular area with shifting the center of circle. Also, applying the combination of, reducing the radius of circular area with shifting the center of circle. Theoretically it is possible to combine all three techniques but practically it is inconvenient to combine more than two techniques at a time.

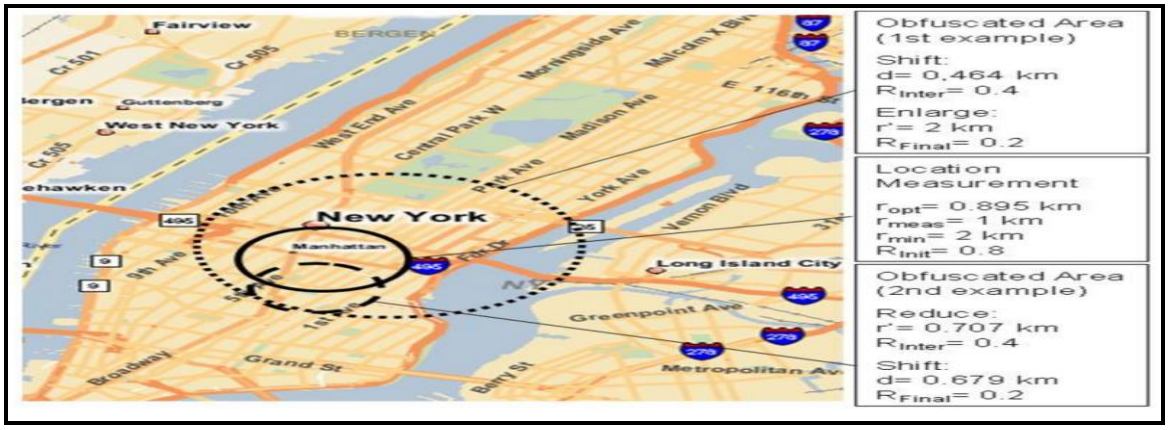


***Figure 2:*** *Showing the Combination of Enlarge with Shift and Reduce with Shift Obfuscations from [4]*

## 4. User's Perspective

Many studies about the attitudes of people in case of location privacy have revealed that Location Based Service users actually don't care much about location privacy. This may be because they are unaware of the negative consequences of a location leak such as stalking or even physical harassment. There are applications and architectures that prompt users to reveal their location information to third parties. These Location Based Services are comparatively thriving. This shows that users are comfortable with sharing their location data with third parties [1]. In case of social act of rendezvousing, users become overly positive about giving up their location information. They are less concerned about their location being tracked as long as they find the service useful [6]. A three phased formative study conducted by Consolvo, Sunny, et al., [2] concluded that users disclose information that they think will be useful to the requester. They disclose less specific information because they think it would be more useful in that form to the requester. Often the relationship of the requester with respect to the user also influences the user's response. Another influencing factor is the distance if the user with respect to the requester. The location, activity performed and mood of the user at the time of request also play an important role in the nature of response. Often users reject requests of location disclosure when they feel it is not useful to the requester or they are afraid of their location information being misused.

## 5. Conclusion

This paper discussed significance of location privacy. The main methods of enhancing location privacy are presented in the paper. They are the methods of using pseudonyms in Mix Zone model, anonymizing using k-anonymity model and obfuscating location information using various obfuscation techniques are mentioned in the paper. The drawbacks of these methods are also mentioned. Furthermore the perspectives of a user of Location Based Services are explained in brief.

## References

[1] Krumm John. *A Survey of Computational Location Privacy.* Personal and Ubiquitous Computing. 2009. 13 (6) 391-399.

[2] Consolvo Sunny, et al., 2005: *Location Disclosure to Social Relations: Why, When, & What People Want to Share.* Proceedings of the SIGCHI Conference on Human Factors in Computing Systems. ACM.

[3] Samarati, Pierangela and Latanya Sweeney, 1998: *Protecting Privacy When Disclosing Information: K-Anonymity and Its Enforcement Through Generalization and Suppression*. Technical Report, SRI International.

[4] Ardagna, Claudio Agostino, et al. *Location Privacy Protection through Obfuscation-Based Techniques.* Data and Applications Security XXI. Springer Berlin Heidelberg. 2007. 47-60.

[5] Beresford, Alastair R., and Frank Stajano. 2004: "Mix Zones: User Privacy in Location-Aware Services." *Pervasive Computing and Communications Workshops, 2004. Proceedings of the Second IEEE Annual Conference on*. IEEE.

[6] Barkhuus, Louise and Anind K. Dey. *Location-Based Services for Mobile Telephony: A Study of Users' Privacy Concerns*. INTERACT. 2003. 3.

[7] Gedik, Bugra and Ling Liu, 2005: *Location Privacy in Mobile Systems: A Personalized Anonymization Model.* Distributed Computing Systems, 2005. ICDCS 2005. Proceedings 25th IEEE International Conference on. IEEE.

[8] Gruteser, Marco and Dirk Grunwald. *Enhancing Location Privacy in Wireless LAN through Disposable Interface Identifiers: A Quantitative Analysis*. Mobile Networks and Applications. 2005. 10 (3) 315-325.

[9] Beresford, Alastair, R., and Frank Stajano. *Location Privacy in Pervasive Computing.* Pervasive Computing, IEEE. 2003. 2 (1) 46-55.

[10] Gruteser, Marco and Dirk, Grunwald, 2003: *Anonymous Usage of Location-Based Services through Spatial and Temporal Cloaking.* Proceedings of the 1st International Conference on Mobile systems, Applications and Services. ACM.

[11] Duckham, Matt and Lars, Kulik. *A Formal Model of Obfuscation and Negotiation for Location Privac*y. Pervasive Computing. Springer Berlin Heidelberg. 2005. 152-170.

[12] Janssen, Cory. "What is Anonymization?" *Techopedias*. N.p., n.d. Web. 16 Aug. 2013. http://www.techopedia.com/definition/28007/anonymization-data.

**Cloud Publications**
International Journal of Advanced Remote Sensing and GIS
2014, Volume 3, Issue 1, pp. 699-712, Article ID Tech-308
ISSN 2320 - 0243

Cloud Publications

Research Article | Open Access

# GIS and Remote Sensing Technologies for the Assessment of Soil Erosion Hazard in the Mediterranean Island Landscapes

**Filippo Catani, Minja Kukavicic and Caterina Paoli**

Department of Earth Sciences, University of Firenze, Firenze, Italy

Correspondence should be addressed to Filippo Catani, filippo.catani@unifi.it

Publication Date: 22 September 2014

Article Link: http://technical.cloud-journals.com/index.php/IJARSG/article/view/Tech-308



**Abstract** The islands of the Mediterranean Sea are widely subjected to desertification problems due to the concurrent impact of deforestation and climate change leading to soil losses. The Cyclades islands represent a typical example of such a situation and in particular the island of Naxos is a very suitable prototype site for studying the evolution, the characteristics and the possible methods to mitigate soil erosion and soil loss risks. Here we develop an RS and GIS-based method to evaluate a multi-temporal model for soil loss prediction and management in Naxos. The model, a modified distributed version of the USLE equation, is based on a set of variables depending on land cover, soil characteristics, hydrology and morphometry. Remote sensing techniques and field surveys and measurements, applied to different periods of time from 1987 to 2006, have been used to produce GIS based soil, land cover, topographic and geological maps. Such data has been used to assess the soil loss potential through the distributed cell-based application of the modified USLE equation using GIS tools. The results show that there has been a notable increase in soil losses from 1987 to recent times and that future scenario forecast a possible complete loss of soil in the Naxos Island in the next century, unless countermeasures are taken. We demonstrate that soil conservation practices have degraded in the last 30 years mainly due to the widespread change of land use and to the progressive abandon of agriculture from rural communities that have shifted their main activity towards tourism development and exploitation. Possible countermeasures are represented by the restoration of terracing systems throughout the island and by the construction of micro-dams acting as sediment repository and water storage system within steep sloping channels.
**Keywords** *Soil Erosion; Naxos Island; USLE; Landsat; ASTER; Soil Depth*

## 1. Introduction

Mediterranean islands are characterized by a widespread scarcity of forest coverage. This trait is a known heritage of centuries of man overexploitation with respect to the environment. It is known, in fact, that most of the islands in the entire Mediterranean Sea were completely vegetated by dense forests at the beginning of historic times. Main clearances started around 8000 yrs BP (Ruddiman,

2003) and were probably concentrated in the period between 8000 and 2000 yrs BP in the Mediterranean area (Zohary and Hopf, 1993).

After the starting of the main civilizations facing the challenge of navigation for exploration and commerce, the forests which were typical of such environments were quickly depleted so that just after the tenth century A.D. most of the main islands were already bare lands. Nowadays, only a few of them have been partly reforested (for example the Elba island in Italy) whilst the great majority still show a landscape typical of semi-arid climates. Some authors have recently verified that this trend will be further increased by climate change, with a general shift from humid to semi-arid conditions in all the Mediterranean (Nunes et al., 2008).

In such conditions the probability for accelerated soil erosion is high, also owing to the rainfall regimes typical in the Mediterranean, characterized by very dry summers, mild winters and high frequency of severe, intense rainstorms which strongly contribute to the annual total rainfall.

The status of soil in most of the islands is thus critical and it has even worsened in the last twenty years by the increase of meteorological extremes probably connected to climate change.

The soil is a non-renewable resource that is crucial for the ecosystems equilibrium and existence. At the same time, it is also of paramount importance for agriculture, a very important component of socio-economic welfare for the Mediterranean populations, and for cultural heritage protection (Canuti et al., 2000). The rate of soil depletion by accelerated erosion is therefore a fundamental indicator of sustainability (Pimentel et al., 1995; Bianchi and Catani, 2002; Montgomery, 2007), especially in insular ecosystems which are by definition closed, fragile and vulnerable to rapid changes. Despite the wide diffusion and perfection level of hydrological-erosive models able to predict losses, one of the main challenges in fighting soil erosion is the lack of up-to-date information on the fundamental parameters and on the rate and spatial extent at which depletion processes operates (Bianchi et al., 2001, Rossi et al., 2013). An important research issue is thus the development, implementation and proposal of methods able to gather and summarize distributed continuous environmental information related to the assessment of soil erosion over large areas with the purpose of building future scenarios and designing possible countermeasures. The European Union, through the establishment of the Joint Research Center (JRC) Soil Portal and the funding of specific projects on soil protection (such as the ENVASSO http://eusoils.jrc.ec.europa.eu/projects/envasso/) has defined the main key points for soil conservation and proposed a process-based spatially distributed soil erosion assessment model (the Pan-European Soil Erosion Risk Assessment PESERA model, Kirkby et al., 2008) which gives an estimate of soil losses for the entire EU territory. This estimate, even though derived from a specific and modern soil erosion model, is carried out at a scale (grid map at spatial resolution 500 m) which is not suitable for assessing the local distribution of hazardous areas within Mediterranean complex landscapes such as islands or coasts. Therefore, a simple soil erosion mapping method able to make use of easily available local data in a GIS environment to produce high resolution estimates of soil losses at the basin scale is still needed.

In this work we explore these issues with the help of a test site represented by the island of Naxos (Cyclades, Greece) and we show how a simple combination of field techniques and remote sensing GIS applications can be used to map the spatial extension and intensity of potential soil losses over time. After a brief explanation of the environmental settings we will then describe the methods and materials used for the study and thence focus on the results which compare the situation in 1987 and 2006.

## 2. The Island of Naxos

The island of Naxos is located in the middle of the Cyclades archipelago (Greece) in the eastern part of the Mediterranean Sea (Figure 1) and is the largest, with an area of about 430 $km^2$ and a coastal perimeter of 148 km. The topography of the island is varied with flat coastal margins to the west and steep rocky cliffs to the north-eastern part. The main elevation (1001 m.a.s.l.) is reached at the top of mount Zas but most of the interior is characterized by high relief energy, rugged terrain and mountain ecosystems. By contrast, on the coasts, especially to west and south-west, gentle hills, dunes and alluvial plains are dominant. There, the main agricultural settlements were located since ancient times. One of the peculiar features of Naxos, with respect to the other Cyclades, is, however, the presence of important villages in the interior mountain part of the island. The principal activities carried out in such areas are pasture and mining. It is clear that pasture in particular has exerted a strong impact on soils which were already endangered by clear cutting.

As to the climate, Naxos shows again something very specific. The rainfall regime is typical of Mediterranean islands, with a very dry summer (average monthly rainfall of June, July and August near zero) and precipitation concentrated in autumn and spring. However, the spatial distribution of the cumulated rainfall is quite uneven. If we look at the mean annual precipitation at the three main rain gauge stations on the island, we easily see that the mountains (Kinidaros rain gauge: 400 m.a.s.l. with 730 mm/year and Apirathos rain gauge: 600 m.a.s.l. with 750 mm/year) experience a much higher rainfall amount than the coasts (Naxos rain gauge: 10 m.a.s.l. with 350 mm/year).

Everywhere on the island, the strongest impact is exerted by the short but intense storms that are typical of the end of summer and winter (see e.g. the storms of October 1994, February 2003 and October 2006). According to the Koppen classification Naxos has a climate of Csa type.

From a geological point of view, Naxos is part of the Attic-Cycladic massif, mainly constituted by magmatic and metamorphic rocks of Alpine age an connected to the Hellenic trench, locus of the subduction of the African plate beneath the Apulian-Anatolian. The main feature at the center of the island is an anticline with a migmatite core and a variegated sequence of overlaying marbles, schists and metavolcanites of Mesozoic age (Durr, 1987). These terrains are in turn overlaid, at least partially, by sedimentary units of Mio-Pliocene age among which the Upper Pliocene conglomerates that probably represent the remains of the erosive processes on the flanks of the dome during unroofing. Nowadays, the outcropping formations are mainly represented by the gneiss of the migmatite in the central mountain part of the island, the very large Mesozoic complex of interbedded marble and schist formations and, mainly to the west, by the Pliocene Upper Unit (conglomerates, sandstones and sands) and an intrusive granodiorite.

The soils of the island have a quite strong dependence on geology but they have also experienced a long influence of human activities. They are represented by three main typologies: soils on marbles (mainly syrosem, rendzina and red rotlehme soils), soils typical of schist outcrops (mainly ranker and dark-brown Mediterranean soils) and terraced soils, typical of agricultural areas at low or medium slope steepness (terraced colluvial soils, gley soils, pararendzina and alluvial soils).

The development of soil horizons already slowed down and limited by the water deficit typical of Naxos climate, is further hampered by the wind (during the summer *meltemi*-wind season) and water erosion (in autumn and winter). The most developed soils are those of terraced type, which are preserved by agricultural practices such as terracing, nowadays at risk given the steady trend of decrease in land utilization by farmers.

Vegetation, as already seen, is scarce and of typical arid Mediterranean variety. Only a few areas in the interior (e.g. Chalki community) exhibit a small wood with prevalence of oaks (*Quercus ilex* and

*Quercus coccifera*). The dominant vegetation (Paoli, 2004) is bush with a typical association (*Pistacia lentiscus, Erica manupuliflora, Rhamnus alaternus, Phillyrea latifolia, Calycotome villosa, Sarcopterium spinosum, Euphorbia acanthothamnos, Thymus capitatus, Cistus creticus, Genista acanthoclada*). The presence of vegetation cover is, however, extremely discontinuous, mainly due to grazing activity on pasture lands. In the very few humid areas along the temporary streams the most common species is the oleander (*Nerium oleander*).

This leaves a lot of space to accelerated erosion processes acting on the fragile soils of the island.

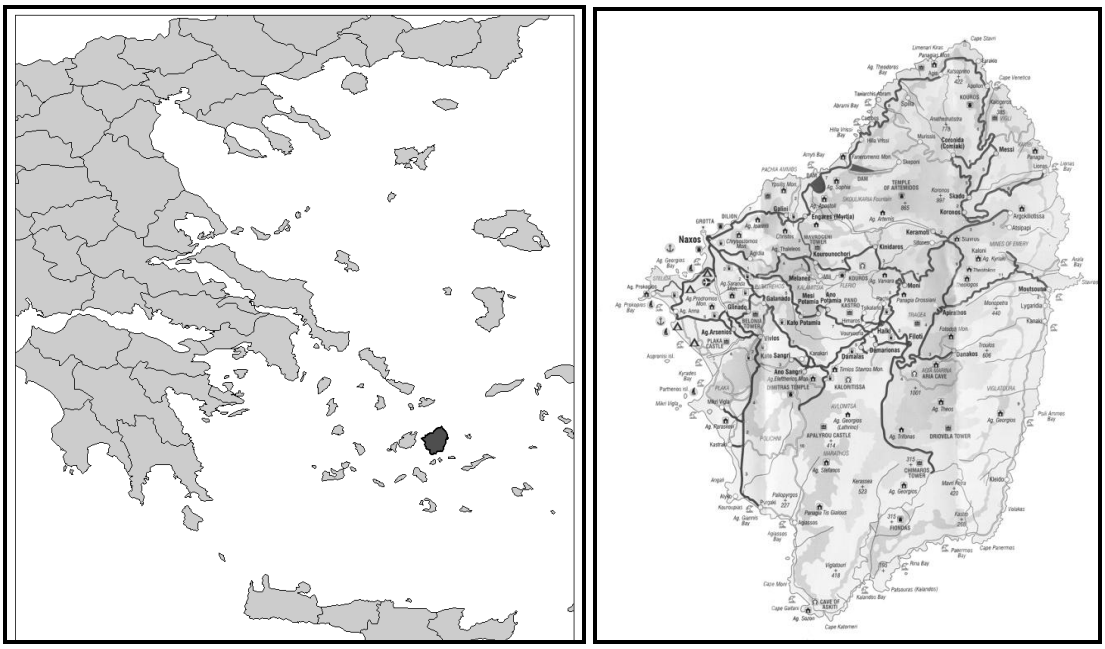


***Figure 1:*** *The Cyclades Islands (Greece). Naxos (in Darker Tone in the Left Image) is the Largest Island and has a Central Position. Its Complexity and Variability make it an Ideal Test Site Representative of the Entire Central and Eastern Mediterranean*

## 3. Materials and Methods

The attempt carried out in this research work is the application of a simple yet spatially distributed and multitemporal approach to the definition of soil erosion hazard for the whole island using a combination of field and remotely sensed data. This would lead to the definition of maps of potential soil losses for the studied area which will be useful for the definition of land sustainability policies and planning.

The model that has been applied is a modified version of the widely used USLE (Universal Soil Loss Equation, Wischmeier and Smith, 1958, 1965, 1978). The USLE model has been preferred here over the PESERA specific-point application (or other similar process-based methods) because of the unavailability of the input data at the required resolution in the studied environments. For example, the PESERA model application requires data on cultivation practice (planting month, planting marker, dominant arable crop and so on) that have to be derived from low-resolution EU databases such as the Farm Structure Survey (FSS, Eurostat) or the Planting Dates Database (Van Orshoven, 1999) or data on soil properties (crust storage, effective soil water storage capacity, soil water available to plants and so on) that are reported for all Europe in the European Soils Data Base (ESDB, http:eusoils.jrc.it) at regional scale (usually at scales smaller than 1:250,000). The application of PESERA-like models at higher resolutions (around 1:25,000 to 1:10,000) would require a huge effort to directly measure or derive such parameters, an effort that cannot be done widely over large areas due to time and economic constrains, especially in Mediterranean island environments. Therefore, we

attempted the application of a specific modification of the traditional USLE approach (Wischmeier and Smith, 1958, 1965, 1978), whose needed parameters are often available or that can be easily derived from simple field campaign and basemap data. To adapt the USLE approach, defined and calibrated at the land parcel scale, we used a spatially distributed definition of the main parameters in which variation in both space and time can be embedded.

Remote sensing and GIS mapping techniques can be of great help in such applications for at least three reasons: i) in the application of hydrological-erosive models at the basin or regional scale it is very crucial to work on homogeneous terrain data having the same scale of survey and the same level of accuracy; ii) it is also very important to collect the data over the entire investigated surface, avoiding parameter interpolation typical of spot-like or gridded field surveys (this is even more true when dealing with areas with problems in the availability of geographic information); iii) finally, the dynamical analysis of surface processes must be inherently multitemporal and hence the parameter estimation procedure should rely on remote sensing methods at least for those more subjected to change.

The material needed and the subsequent relevant operational steps are clearly dictated by the form of the USLE equation translated towards a spatially distributed concept. In particular, the original equation A=RKLSCP can be expressed in a spatially distributed form, where A is the annual soil loss per hectare (Mg/ha y), R is rainfall erosivity (MJ mm $ha^{-1}$ $h^{-1}$ $y^{-1}$), K is soil erodibility (ton h $MJ^{-1}$ $mm^{-1}$), L is a quantity proportional to the slope length, S is a parameter proportional to slope gradient, C is an adimensional parameter (values from 0 to 1) reflecting the soil protection by vegetation cover (and including crop seasonal variability) and P is a second adimensional quantity (values from 0 to 1) expressing the effect of soil conservation practices, where present.

The contribution of remote sensing and GIS to this computation can be very comprehensive and can cover the whole set of parameters. In the following, the spatial definition of each USLE variable will be considered as well as the contribution of remote sensing and GIS to its estimation.

### 3.1. Rainfall Erosivity

The R factor, expressed as in the original formulation of the authors (Wischmeier and Smith, 1958, 1965, 1978), represents the energy of rainfall at ground level. The correct profile-scale procedure for its estimation would be through direct measurement of the product of the average kinetic energy of rainfall (mainly dependent upon raindrops mass since velocity at ground is practically constant) times the average maximum rainfall intensity over 30 minutes time intervals. Such method, quite easy to apply to single slope profiles in selected experimental plots, is very expensive and impractical to use for large areas. A simplified approach has been used in this study in substitution for the energy computation technique, based on the widely accepted assumption that rainfall erosivity is proportional to average annual rainfall H. In particular, we used the expression proposed by Wischmeier and Smith (1978) and Roose et al. (2006) for Mediterranean-type areas, where:

(1) $R = 0.5H$

The value of H, however, must be computed according to local variations in annual rainfall quantities. As already seen, Naxos has a rather variable rainfall pattern with a strong difference between the coasts and the interior. For this reason, we studied the distribution of average rainfall data over a 20 years period for the four main rainfall gauge stations and found a logarithmic relationship (correlation coefficient: 0.98) between H and elevation z above sea level of the form:

(2) $H = 95.38\mathrm{Ln}(z) + 147.48$

The spatial mapping of R values on the studied area was thus obtained substituting equation (2) into (1) and applying a distributed computation scheme in a GIS environment at 20 m spatial resolution.

### 3.2. Soil Erodibility

The potential erodibility of a bare soil is dependent upon specific quantities that can be estimated by field surveys and laboratory analysis and then generalized in space with the help of soil maps and remote sensing techniques giving information on bare soil spectral properties.

In the classical application for single profiles the suggested expression for K is:

(3) 100 K = 2, 1 M 2, 14 (10 –4) (12-a)+3.25 (b-2)+2,5 (c-3)

Where M is dependent on soil texture, *a* on organic content, *b* on soil structure and *c* on permeability. The main supporting data for the determination of spatial distribution of K was a soil map produced during the research by means of the integration of field surveys, laboratory analyses, geological mapping and remote sensing. The soil survey showed the presence of 6 different types of coverages in connection with source rocks (schists soils, marble soils, terraced soils, colluvial soils, sand dunes and rocky outcrops). For each one (with the obvious exception of rocky outcrops where erosion is clearly zero in absence of soils) a series of samples were taken and analyzed whose average properties are summarized in Table 1.

***Table 1:*** *Soil Properties Used for the Computation of K Factors. Parameters are not defined for Rock Outcrops since they Lack a Soil Coverage*

| Soil Class | %Silt + %Very Fine Sand | %Sand | %Clay | %Org.Cont. | Structure | Permeability | K |
|---|---|---|---|---|---|---|---|
| Terraced | 37.46 | 46.30 | 7.60 | 3.55 | 3 | 2 | 0.027 |
| Schists | 26.13 | 49.64 | 5.80 | 1.84 | 4 | 3 | 0.028 |
| Marble | 36.68 | 39.25 | 10.73 | 4.12 | 2 | 3 | 0.021 |
| Colluvial | 30.92 | 48.27 | 7.46 | 4.35 | 3 | 2 | 0.019 |
| Sand dunes | 7.40 | 92.00 | 0.60 | 0.50 | 2 | 1 | 0.020 |
| Rocky Outcrops | - | - | - | - | - | - | - |

### 3.3. Morphometric Factor LS

The two morphometric factors, proportional respectively to slope length and slope gradient, are usually directly measured on single slope applications and taken constant for small experimental plots of a few tens of meters in length. In the case of basin scale applications, though, this is clearly not feasible and oversimplified.

For this reason, we adopted a distributed approach proposed by Moore et al. (1993) that relies on the fact that the contribution of topography to soil erosion is reflected by the relative stream power exerted by running (or overland flow) water on land. In turn, this stream power can be computed by a series of suitable elaborations of a DEM. The final form of LS factor is therefore:

(4) $LS= (As/22.13)^n (\sin\beta/0.0896)^m$

Where As is the specific contributing area ($m^2/m$) of the selected land parcel (a DEM cell in our case), $\beta$ is the slope gradient (m/m) for the same cell and n and m are two adimensional empirical constants that in our case were selected to be n=0.4 and m=1.3 by direct calibration in test areas.

The computation of contributing area and slope gradient is carried out by standard DEM analysis codes in a GIS environment (Tucker et al., 2001) starting from a 20 m DEM derived by the combination of topographic maps at the 1:25.000 scale with an ASTER derived DEM. Two ASTER images were

acquired and the best one, selected for absence of cloud cover and quality, used to generate a 25 m resolution DEM using NASA-USGS specifications. The interpolation technique contained in the *topogrid* code (Hutchinson, 1989) was used on contour line derived information and the resulting preliminary DEM was afterwards completed by grid matrix integration with ASTER data. A geostatistical autocorrelation analysis was carried out to locally weight the two different contributions and to compute the optimal values for elevation. The final resulting DEM was validated by GPS direct measurement over about 50 target locations scattered within the studied area. Average errors and accuracies are compatible with a 1:20.000 scale and with a cell resolution of 20 m.

### 3.4. Cultivation Practices and Conservation Measures

The two parameters C and P are non-dimensional quantities that reduce soil erosion in presence of a vegetation cover and measures of soil protection. In the case of Naxos island, and in general for all the Mediterranean island environments, the correct estimation of both C and P is of critical importance due to the high vulnerability of soils and to the intensity of human impacts. Whilst the definition of C is complex due to the differences in land cover existing in the study area and to the dynamic nature of vegetation presence (both on short and long term), the assessment of P is easier. This is mainly due to the fact that in Naxos the sole conservation practice which is widely used is the construction of terraces by local farmers, a practice broadly adopted in the entire Mediterranean area. A simple approach in the spatial estimation of P is thus based on the mapping (mainly through satellite imagery interpretation backed by field control) of terracing over the hillslopes. Where terracing is present, the P factor can be assumed as being lower than 1 whilst where absent equal to 1. In particular, in this research we also tried to evaluate the state of conservation of terraces, nowadays endangered by the lack of maintenance in several parts of the island, a common problem in the Cyclades islands (Figure 2). For damaged terraces we selected a value P=0.5 whilst for well-preserved terraces we adopted a value of P=0.1 (Lehman, 1993).

***Figure 2:*** *Naxos Terracing Systems in Different State of Conservation. From Left to Right, Clockwise: a Completely Disrupted Terracing; a Poorly Maintained One Which Still Retains Some Protection Efficiency; a Well Maintained System Newly Restored in the Apirathos Area*

The assessment of C values was strongly connected with the multitemporal mapping of land cover. Using two satellite images of May 1987 (Landsat 5 TM) and April 2003 (Landsat 7 ETM), the CORINE land cover map (updated 1989) and field surveys carried out by the authors in the spring of 2003, we performed an accurate analysis of land uses that resulted in the production of two maps (relative to the years 1987 and 2003). First of all we compare the CORINE land cover classification (European Commission, European Environment Agency, 1997) with the multispectral TM data set, through several basic analyses such as different color composites (457, 432, 321) and NDVI. Afterwards we proceed to update the third level of CORINE database with two different approaches: on the one side we compare the land use classes with the newer status offered by ETM Landsat image and on the other side we use a field survey carried out in 2003, same period of the satellite acquisition date. The adopted methodology for the updating of 19 different classes present on the Naxos Island was based on the methodological guide by Perdigao and Annoni (1997). The field survey provided the basis for supervised Maximum Likelihood classification of ETM image. Finally, both products were integrated in a GIS system in order to generate an updated land cover.

The comparison of the land cover of 1987 and 2003 shows a series of changes mainly linked to urbanization (e.g. the construction of the new airport and of two artificial water reservoirs) and agriculture. According to literature data and to an empirical relationship linking the C factor and the Landsat-based NDVI, that we hypothesized valid for most of the vegetated parts of the island (land cover classes 333 and 323), we assigned C values for each land cover class for both 1987 and 2003.

## 4. Results and Discussion

The final computation of soil erosion potential according to the spatially distributed USLE model is a matter of a few simple mathematical grid overlay operations in a GIS environment. We repeated the procedure for three different values of P (0.1, 0.5 and 1) for both analyzed years so that we ended up with two sets of 3 maps, giving an estimation of erosion in Mg/ha y.

The most relevant information that can be deduced by a first look at the general results is that soil losses have increased from 1987 to 2003 of about 7%. The Figure 3 shows the spatial distribution of expected soil losses for the six scenarios whilst Figure 4 presents a quantitative comparison between the worst case scenarios (P=0) in 1987 and 2003. The latter reveals that only limited areas experiences a decreasing erosion trend while for the most part we register increments in soil losses. Such losses seem to be mainly connected with land use changes.

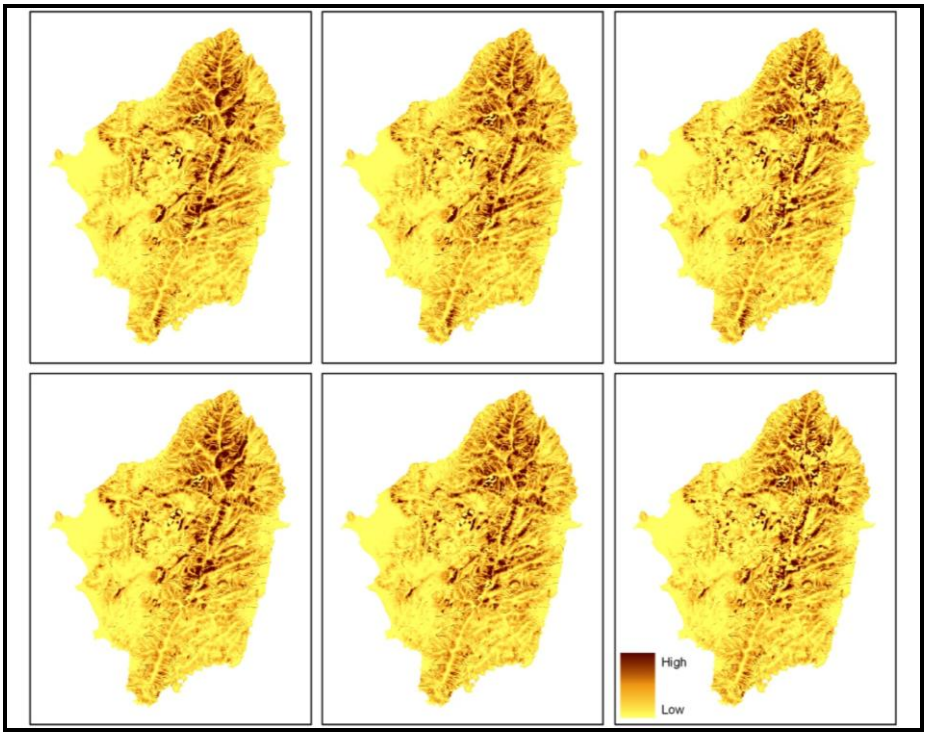


***Figure 3:*** *Soil Erosion Maps for the Year 1987 (Top Row) and 2003 (Bottom Row). For Each Year the Three Different Scenarios for Terracing Maintenance are Shown (P=1 Left, P=0.5 Center, P=0.1 Right)*

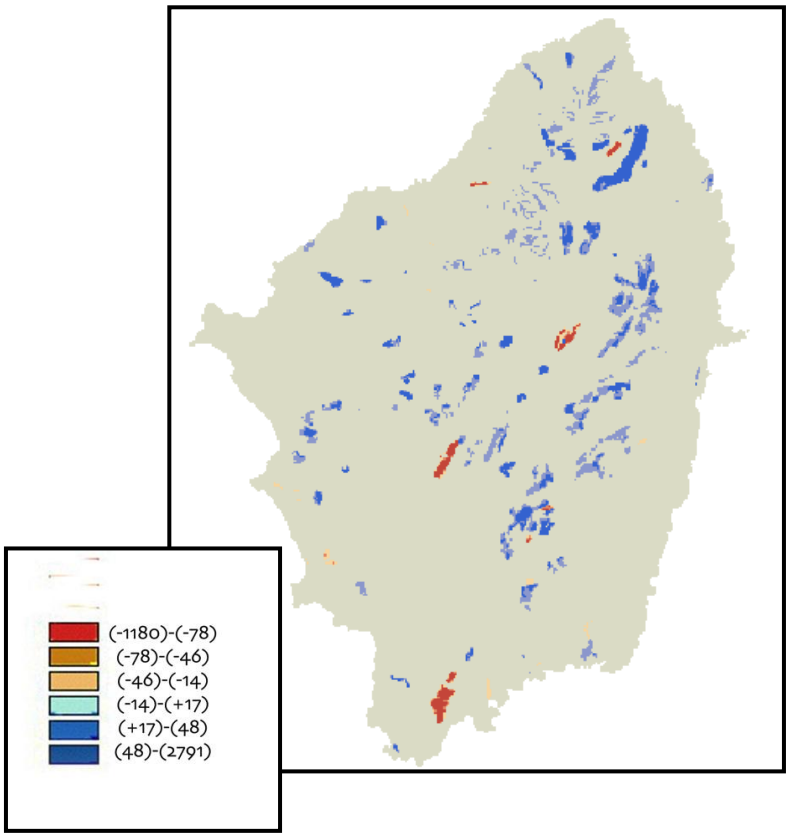


***Figure 4:*** *Differences in Erosion Potential (in Absence of Protection Measures) between 1987 and 2003. Negative Values (Red) Shows Locations in Which Erosion Exhibits a Decreasing Trend Whilst Positive Values (Blue) Shows Location Where Soil Losses Have Increased Mainly Owing to Land Use Changes*

However, the quantitative results provided by USLE-based models are very sensitive to local variations. Furthermore, the adoption of empirical estimation for parameters which were adapted for areas with similar but not identical climates imposes caution on the use of the values of soil losses generated by the model. For this reasons, it is usually advisable to rely on classes or ranges of values rather than on exact figures. This is even more true in cases in which no field validation data are available concerning long term soil losses. The results of the analysis carried out in Naxos must thus be regarded as a multitemporal mapping of the soil erosion proneness over the island territory and of the impact of land use practices on it.

Another problem that is not considered in the spatially distributed application of USLE-like models is that there is no explicit accounting for soil transport and deposition after erosion. A realistic distributed model for the prediction of sediment budgets at the regional scale should consider this aspect. The definition and application of such models, requiring a large number of field and laboratory parameters, was not within the scope of this research. Furthermore, at present, dynamic hydrological-erosive rainfall-runoff sediment transport models are difficult and very expensive to apply over extensions larger than a few squared kilometers.

However, an average measure of soil loss for the whole island can be obtained using a constant sediment delivery ratio (SDR). An acceptable general value for Mediterranean areas that accounts for the typically convex topography of the islands is proposed by Giordani and Zanchi (1995) as equal to SDR=0.22. If we apply this correction the total erosion in the 6 different scenarios computed is as depicted in Table 2.

***Table 2:*** *Final Figures for Soil Losses for the Three Different Conservation Status of Terraces after the Application of SDR=0.22. Units are in Mg/y*

| | | | |
|---|---|---|---|
| 1987 P=1 | 721,425 | 2003 P=1 | 769,695 |
| 1987 P=0.5 | 638,400 | 2003 P=0.5 | 678,286 |
| 1987 P=0.1 | 592,660 | 2003 P=0.1 | 625,114 |

The impact of the potential soil losses computed by the model can be quantified more precisely if we compare the results with the local depth of the soil itself. It is obvious, in fact, that erosion rates unsustainable for a thin layer of rendzina on marbles can be perfectly compatible with the rate of soil formation in an alluvial area. For this reason, a soil depth map was elaborated for Naxos using a recently developed methodology based on topography and basic field sample measurements (Catani et al., 2010). The final result shows that the thickness of the regolith over the island has an average value of about 0.8 m. Maximum values of about 3 m can be found on the alluvial plains in the western part of the island whilst several areas in the mountains have no soil at all and expose bare rock. If we assume an average bulk density of about 2.0 $Mg/m^3$ for the regolith terrains, we have that an erosion of 1 (Mg/ha y) will detach 0.05 mm of soil each year. We recomputed the erosion maps and evaluated the time needed for completely eroding the soil layer in each scenario (Figure 5). According to our computations, at the present stage 9.9% of the island (42.3 $km^2$) will be bare rock in less than 200 years and 1.6% (6.8 $km^2$) in less than 100 years (Figure 6). Soils are considered a non-renewable resource since their development rate from source rocks is very slow and incomparable to accelerated erosion processes such as those revealed by the analysis. Usually, a depletion time smaller than 100-200 years can be considered catastrophic and in need of urgent mitigation measures. For this reason, and also because the most endangered areas are in locations where very thin soils support grazing as the second important local income source after tourism, this results are not encouraging and should draw the attention of local administrators towards erosion protection systems such as micro-damming and terracing. One such experimentation was carried out successfully in the Apirathos area from 1992 to 1994 but remained a confined exception so far (Lehman, 1993).

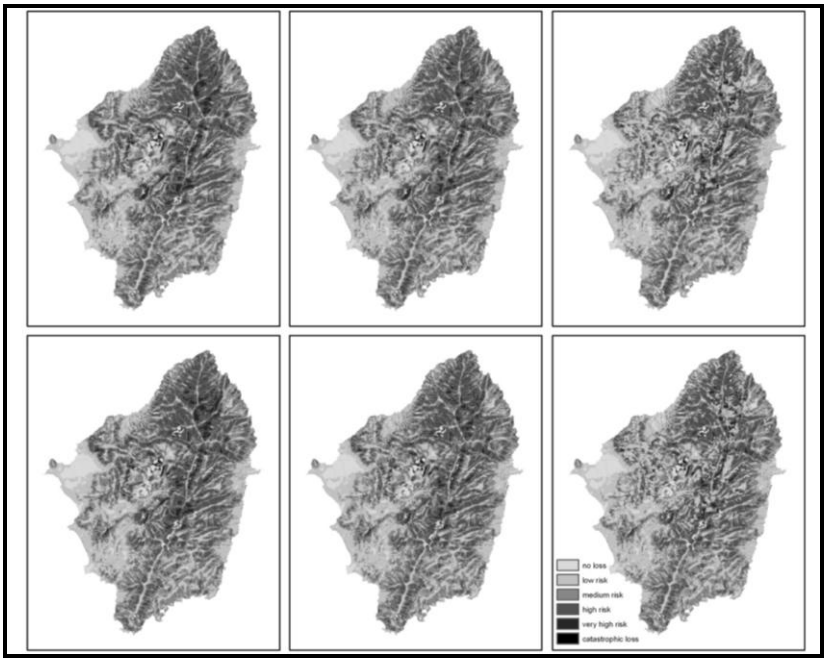


***Figure 5:*** *Soil Erosion FAO Classes after SDR Correction for the Year 1987 (Top Row) and 2003 (Bottom Row). Again, Three Different Scenarios for Terracing Maintenance are Shown (P=1 Left, P=0.5 Center, P=0.1 Right)*

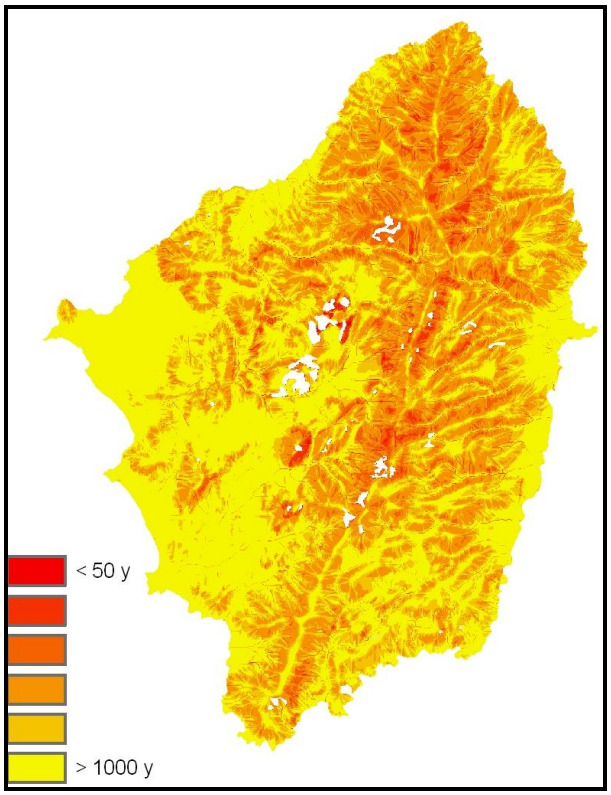


***Figure 6:*** *Expected Time to Attain Complete Soil Depletion in the Hypothesis of Lack of Protection Measures on Hillslopes. Soil Erosion Rates have been assessed with the Approach Described in the Text, Using an Average Bulk Density of 2.0Mg/m$^3$. This Value has been Slightly Overestimated to Indirectly Take into Account the Possible Positive Contribution of Soil Forming Processes*

A partial confirmation of the spatially distributed results obtained by the application of USLE model comes from the study of the effects of the recent storm that affected the entire Aegean Sea in October-

November 2006. We acquired two ASTER images from July and November 2006 and we analyzed the differences through change detection. The impact of the storm is wide and clearly visible. Its impact on sediment erosion and transport can be appreciated if we look at the two main artificial water reservoirs in the north-western Naxos. The water of both looks clear in the July image whilst suspended sediments are visible in the November image. Furthermore, as a partial validation of the soil loss mapping, the northernmost reservoir, draining a basin for which we predicted above 40% of land under severe erosion risk, presents a much higher amount of suspended load than the other, which is located at the closing section of a less steep valley in which we forecasted no more than 15% of soils under severe threat.

## 5. Conclusions

The research has concerned the processes relative to, and the quantification of, the soil erosion within the territory of the island of Naxos. In summary, we collected the necessary parameters with a combination of field surveys and remote sensing techniques, we applied a spatially distributed modification of the USLE equation and we analyzed the significance of the results under the assumption that in the Mediterranean environments soil losses are an irreversible process.

We found that, according to the FAO classification, in 1987 about 27% of the island (115 $km^2$) was subjected to erosion greater than 30 (Mg/ha y) whilst in 2003 the situation had worsened, despite some conservation attempt carried out in the nineties, with 29% of land (123 $km^2$) over the 30 (Mg/ha y) limit (Figure 3). Following a simple approach that makes use of a soil depth map and the estimated rates of erosion, we also obtained a forecast of probable depletion time for soils. This information tells us that in short times a large proportion of Naxos pedologic environment will be lost forever. This figure could be even worsened by the possibly increasing trend of extreme hydrological events due to climate change (Nunes et al., 2008).

At present, only about 10% of the island territory is protected by terraces and most of them are in a poor maintenance status. If this protection system could be extended over another 10% of land, precisely the one which is under the strongest risk of erosion today, we will have a reduction of soil loss rates of about 90% locally, with an increase of depletion time well over security levels.

Further studies are needed in order to: i) properly validate the model using a combination of field measurements (possibly combined to the setup of experimental parcels) and remote sensing, such as the one proposed in this paper; ii) understand the still poorly documented relationship between short intense rainfalls and soil losses; and, iii) devise possible countermeasures among which the construction of micro-dams on steep channels and the construction/maintenance of terraces over all the endangered areas.

## References

Bianchi, F., and Catani, F. *Landscape Dynamics Risk Management in Northern Apennines (Italy).* Environmental Studies. 2002. 2; 319-328.

Bianchi, F., Catani, F., and Moretti, S. *Environmental Accounting of Hillslope Processes in Central Tuscany (Italy).* Advances in Ecological Sciences. 2001. 10; 229-238.

Canuti P., Casagli N., Catani F., and Fanti, R. *Hydrogeological Hazard and Risk in Archaeological Sites: Some Case Studies in Italy.* Journal of Cultural Heritage. 2000. 1 (2) 117-125.

Catani, F., Segoni, S., and Falorni, G. *An Empirical Geomorphology-Based Approach to the Spatial Prediction of Soil Thickness at Catchment Scale.* Water Resources Research. 2010. 46; W05508.

Durr, S. *Evolution of Continental Crust; the Central Aegean as an Example*. Terra Cognita. 1987. 7; 56.

Giordani, C., and Zanchi, C., 1995: *Fundamentals of Soil Conservation*. Bologna, Patron. 220 (In Italian).

Hutchinson, M.F. *A New Procedure for Gridding Elevation and Stream Line Data with Automatic Removal of Spurious Pits.* Journal of Hydrology. 1989. 10; 211-232.

Kirkby, M.J., Irvine, B.J., Jones, R.J.A., and Govers, G. *The PESERA Team*. *The PESERA Coarse Scale Erosion Model for Europe I- Model Rationale and Implementation.* European Journal of Soil Sciences. 2008. 59; 1293-1306.

Lehman, R., 1993: *Terrace Degradation and Soil Erosion in Naxos island, Greece.* In: Farm Land Erosion in Temperate Plains Environments and Hills. Wicherek S. (Ed.). Amsterdam: Elsevier. 429-450.

Montgomery, D.R. *Soil Erosion and Agricultural Sustainability.* Proc. Nat. Acad. Sciences. 2007. 104 (33) 13268-13272.

Moore, I.D., Keith Turner, A., Wilson, J.P., Jenson, S.K., Band, L.E. 1993: *GIS and Land-Surface-Subsurface Process Modeling (Chapter 19).* Environmental Modeling with GIS. Goodchild, M.F., Parks, B.O., and Steyaert, L.T. (Eds.). Oxford University Press: Oxford. 196-230.

Nunes, J.P., Seixas, J., and Pacheco, N.R. *Vulnerability of Water Resources, Vegetation Productivity and Soil Erosion to Climate Change in Mediterranean Watersheds.* Hydrological Processes. 2008. 22; 3115-3134.

Paoli, C., 2004: *Evolution of Soil Erosion Processes in the Naxos Island (Greece).* Unpublished MSc Thesis. University of Firenze (In Italian).

Perdigão, V., and Annoni, A., 1997: *Technical and Methodological Guide for Updating CORINE Land Cover Data Base*. JRC/EEA.

Pimentel, D., Harvey, C., Resosudarmo, P., Sinclair, K., Kurz, D., McNair, M., Crist, S., Shpritz, L., Fitton, L., Saffouri, R., and Blair, R. *Environmental and Economic Costs of Soil Erosion and Conservation Benefits.* Science. 1995. 267 (5201) 1117-1123.

Roose, E.J., Lal, R., Feller, C., Barthès, B., and Stewart, B.A., 2006: Soil Erosion and Carbon Dynamics. Advances in Soil Science. CRC Press, Boca Raton, Florida. 55-72.

Rossi, G., Catani, F., Leoni, L., Segoni, S., and Tofani, V. HIRESSS A physically based slope stability simulator for HPC applications. Natural Hazards and Earth System Science. 2013. 13(1); 151-166.

Ruddiman, W.F. *The Anthropogenic Greenhouse Era Began Thousands of Years Ago.* Climatic Change. 2003. 61; 261-293.

Tucker, G.E., Catani, F., Rinaldo, A., and Bras, R. *Statistical Analysis of Drainage Density from Digital Terrain Data.* Geomorphology. 2001. 36; 187-202.

Van Orshoven, J., Terres, J.-M., Willekens, A., and Feyen, J. *Transfer Procedures for Model-Based Agricultural Monitoring.* In: Proceedings of 1st International Symposium on Modelling Cropping Systems. M. Donatelli, C. Stockle, F. Villalobos & J.M. Villar Mir (Eds.). Lleida, Spain. 1999. 21-23.

Wischmeier, W.H., and Smith, D.D. *Rainfall Energy and Its Relationship to Soil Loss.* Transactions of the American Geophysical Union. 1958. 39; 285-291.

Wischmeier, W.H., and Smith, D.D. *Predicting Rainfall Erosion Losses from Cropland East of the Rocky Mountains.* Agric Handbook U.S. Dept. Agric. 1965. 282; IV-47.

Wischmeier, W.H., and Smith, D.D., 1978: Predicting Rainfall Erosion Losses–A Guide for Conservation Planning. Agriculture Handbook 537. U.S. Department of Agriculture, Washington DC.

Zohary, D., and Hopf, M., 1993: *Domestication of Plants in the Old World.* Oxford University Press, Oxford.

**Cloud Publications**
International Journal of Advanced Remote Sensing and GIS
2014, Volume 3, Issue 1, pp. 713-722, Article ID Tech-313
ISSN 2320 - 0243

Research Article | Open Access

# Identification and Mapping of Wasteland in Birbhum District, West Bengal

**Sahina Khatun and Gopal Chandra Debnath**

Department of Geography, Visva Bharati, Santiniketan, Bolpur, West Bengal, India

Correspondence should be addressed to Sahina Khatun, sahin.geo@gmail.com

Publication Date: 31 October 2014

Article Link: http://technical.cloud-journals.com/index.php/IJARSG/article/view/Tech-313



**Abstract** The objective of this paper is to the identification and mapping of the wastelands using satellite data and GIS techniques of Birbhum District. The wastelands of the district are identified and categorized through the successive stages of visual interpretation of satellite data on 1:50,000 scale, field checking and final interpretation. The wasteland boundaries as well as area coverage are processed and finalized category-wise and block-wise. The study has shown that six different types of wastelands are present in the district with total coverage 14854 hectares i.e. 3.31% of total geographical area of the district. Out of these total wastelands, land with/without scrub is the most dominant type (67.44% of total wasteland of the district) followed by degraded forest (26.52%), barren hill/rocky/stony wastes (2.31%), sand riverine (2.15%), mining (1.15%) and gullied and or ravenous (0.41%). The first two categories of wastelands combinedly form majority (93.96%) while others constitute very low or negligible share in wasteland area of the district. Such type of information base is very useful in plan formulation and implementation at various levels.
**Keywords** *Degraded Notified Forest; GIS Technique; Land With/Without Scrub; Satellite Data; Visual Interpretation*

## 1. Introduction

In India, to mitigate the increasing demand of food, fodder, fuel and fibers from limited land, any conversion of agriculturally productive land into wastelands has to be avoided and area which has already turned into wasteland must be reclaimed. Ecologically its value is so precious that cannot be measured by any monetary price. Desired one third of geographical area under forest, climate & soil protection, secure and economically and ecologically viable energy supply, biological diversity, increasing biomass can be achieved by reclaiming wastelands. It will also help in creation of rural employment, strengthening of rural infrastructure and social development & equity. It is very necessary to bring all the wastelands under productive and sustainable use through the programme of afforestation, pasture development, cropping pattern and other economic use. For this purpose reliable database on type, extent, location, morphogenesis, ownership of wastelands are required and it is also

necessary to categorize the wastelands in accordance with their intrinsic characteristics and causative factors. The estimate of wastelands is a controversial issue as there is no structurized opinion about what constitutes wastelands. So, the estimates of wastelands differ widely depending on how the word 'waste' is interpreted or played upon and what potential uses are visualized for the wasteland as such or offer it is reclaimed and soon (Farmer, 1974; Miglani et al., 1988; IFPRI, 1995; G.K. Chadha, 1982; Govt. of India, 1993, 1995). In its far-stretching interpretation, the term wasteland can be taken to mean all rural land unoccupied or unutilized by human beings. On the other extreme only the 'cultivable wasteland' which can possible be brought under plough after some land reclamation operation is gone through, is taken as the estimates of wasteland. In between these two extremes, there are many other estimates regarding different points of assessment. Society for Promotion of Wasteland Development (SPWD, 1984) suggested some characteristics for wastelands – lands which are (a) ecologically unstable (b) whose top soil has been nearly completely lost and (c) which have developed toxicity in the root zones for growth of most plants, both annual crops and trees. National Wasteland Development Board (NWDB, 1986) defined wasteland as "that land which is degraded and is lying unutilized (except as current fallow) due to different constraints". Integrated Wasteland Development Programme (IWDP, 1987) has adopted following definition "Wastelands mean degraded land which can be brought under vegetative cover, with reasonable effort, and which is currently underutilized and land which is deteriorating for lack of appropriate water and management or on account of natural causes. Wasteland can result from inherent/imposed disabilities such as by location, environment, chemical and physical properties of the soil or financial or management constraints". On the basis of above criteria two tier classification system i.e. culturable and unculturable wastelands was used. These two classes were further classified into 14 different types in the Level-II. However, later on a simplified 13 fold classification system has been adopted for mapping work of wastelands.

## 2. Materials and Methods

In the present study toposheets (72P and 73M series) of Survey of India and NATMO, Satellite imageries LISS-III, Geological map of Geological Survey of India, Climatic data of Meteorological Department District planning map of Birbhum from NATMO, Satellite imageries and numerous data regarding soil, ground water, irrigation etc. and related books and articles (Fitzpatrick, Lins, K. and Chambers, M.J., 1977; Kalwar, S.C., 1990; Khan, S. and Qureshi, M.A., 1997; Yadav, H.R., 1987) are collected from different departments and websites in pre-field session and Primary data are collected from intensive field work. After gathering these information different morphometric, hydrologic, climatic and pedogenic maps are prepared and wasteland of different types is identified on the basis of integrated approach through GIS application.

### 2.1. Wastelands Mapping through Remote Sensing and GIS Application

Identification and delineation of wasteland on satellite imagery can be grouped under three phases of activities, viz. - preliminary analysis, ground truth and final interpretation (Figure 1).

Preliminary Analysis: Visual analysis of IRS, LISS-III geocoded data on 1:50,000 scale is accepted as the mapping techniques for the present work. The first step to this is that base maps of the selected area have been prepared from topographical sheet on 1:50,000 scale taking roads, forest boundaries, rivers, prominent water bodies, district, state and international boundaries, Block boundaries are taken from district census handbook and super imposed on the base maps. All the base maps and block boundary have been scanned and digitized in arc info software. All these maps are projected in polyconic projection on 1:50,000 scale. Satellite images of IRS-LISS-III have been loaded on computer for visual interpretation. Based on image interpretation keys like tone, texture, site, and situation, association of known field objects wasteland is delineated and classified according to the classification system. In present study certain category of wastelands like degraded forest, sand riverine are easily

delineated by virtue of their spectral separability, pattern and location whereas gullied or ravenous land, mining waste etc. are delineated with moderate success. However the category of land with/ without scrub, which is widely prevalent throughout the district, could not be easily delineated due to its merging with fallow land.

Ground Truth: Interpretation details have been verified on the ground in selected areas, particularly where confusion arose in case of preliminary interpretation.

Final Interpretation: Through ground check the image interpretation key has also been further developed. With the help of these final interpretation is carried out. The wasteland boundaries as well as the area coverage under particular type are finalized through this exercise. Maps, thus prepared were made ready for cartographic work.

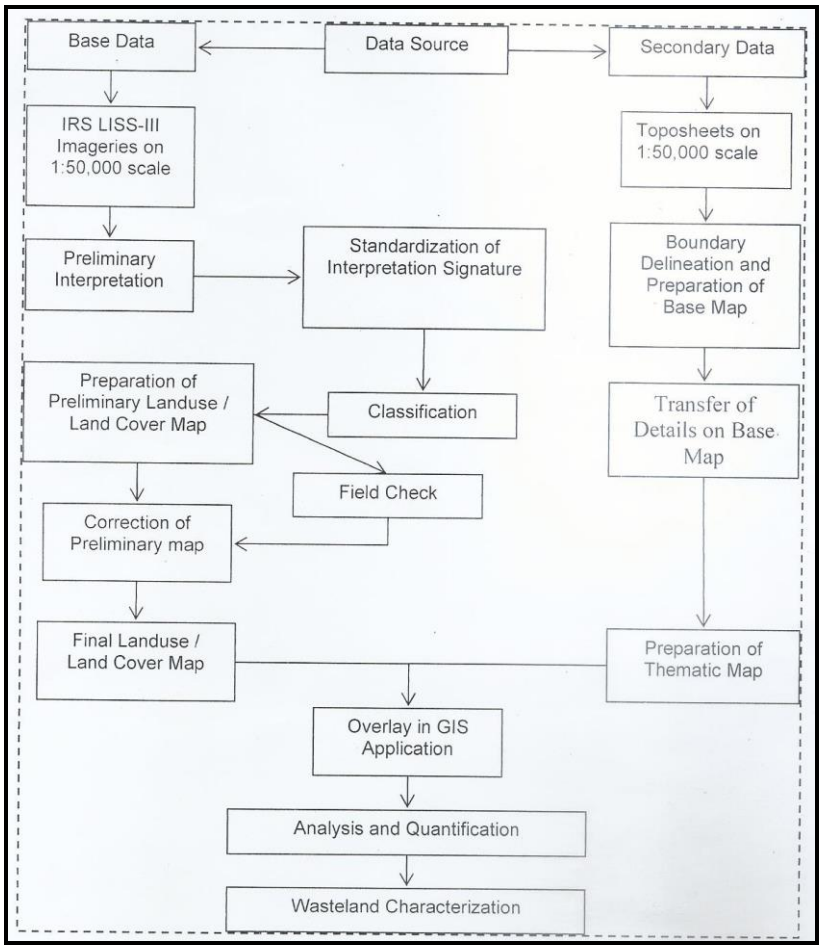


***Figure 1:*** *Flow Chart Showing Methodology of Wasteland Mapping*

## 3. Study Area

The absolute location of the study area is from $23^0$32'30"N to $24^0$35'00"N latitude and from $87^0$05'25"E to $88^0$01'40"E longitude. From relative point of view the district is bounded by Santal Parganas on north and west, by the districts of Murshidabad and Barddhaman on east and on the south by Barddhaman (Figure 2). From administrative point of view Birbhum covering 4545 sq.km area includes 19 blocks and 6 municipalities. From more micro level the district consists of 167 gram panchayet and 2473 mouzas.

As the region belongs to Rarh region, it possesses some exclusive physical features and climatic conditions. Among these the important physical conditions are as follows:

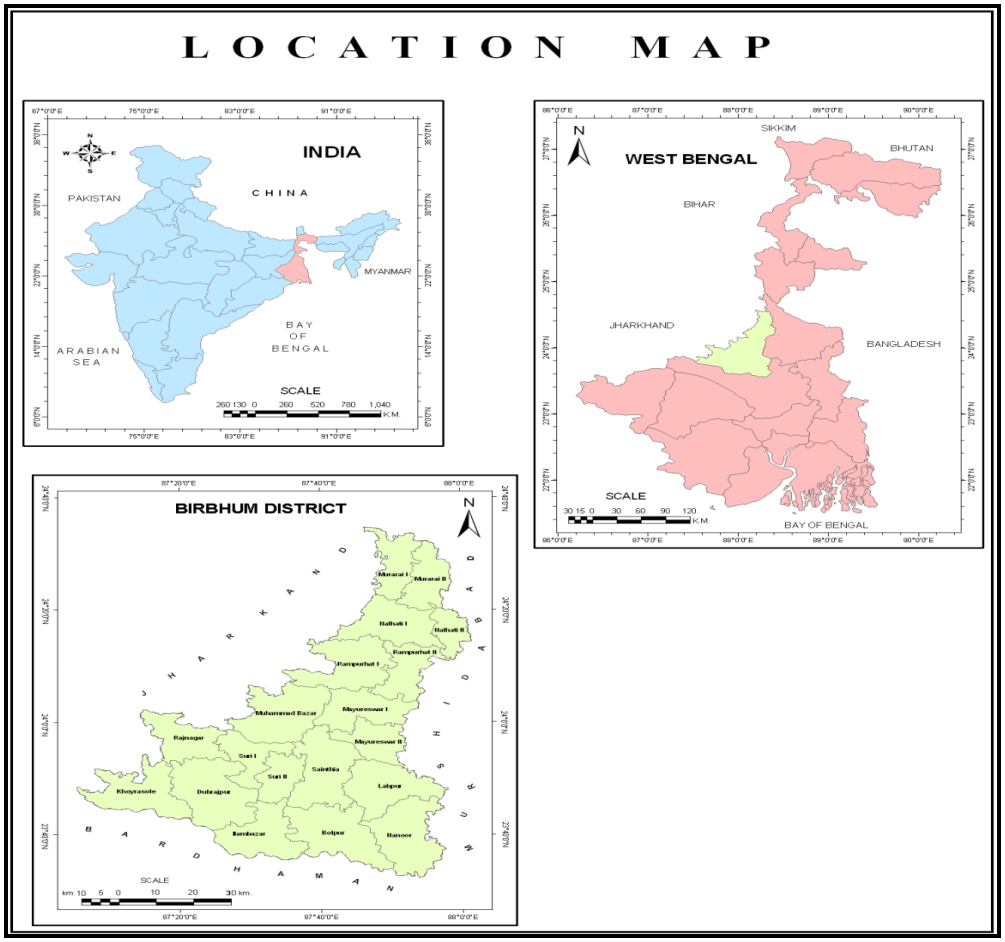


***Figure 2*: *Study Area***

1) The study area is covered with Archeanian granite-gneisses, Gondwana system, Rajmahal basalt, laterite and old and young alluvium (Oldest to Youngest). Archean gneiss is mainly found in Suri, Dubrajpur block, has big blocks of granite and gneiss, the Gondwanas of Carboniferous-Permian age cover a small area along Ajay river in the western part, the basalt of early Cretaceous age occur in western part of Rampurhat and Nalhati blocks, the laterite of Cenozoic age occurs largely in western and southwestern parts, particularly in Bolpur, Dubrajpur, Suri, Rampurhat Rajnagar etc. (Geological Survey of India, 2001).

2) The climate of the study area has wet dry, Subhumid and subtropical climate with rainfall generally varies from <1100 mm to >1400 mm. However, spatial pattern of rainfall indicates that rainfall is maximum in northern and western part (>1400 mm) while it decreases with eastern and south-eastern move. Mean summer air temperature (April, May and June) is 37.3°C and mean winter air temperature (December, January and February) is 26.4°C.

3) The average elevation of the district is about 80 m above Mean sea level. The western and south-western margin is characterized by upland, ridge with frequently dissected riverine network and this upland gradually faded out towards east and north-east.

4) According to Pascoe (1973) laterites of Birbhum is marked as low level laterite which was broken off from the high level laterites of Rajmahal hills (Eastern parts) and then carried to the

eastern lower level by the action of streams, rain wash, surface runoff and then redeposited in this area. In this wet and dry type of monsoonal climate and due to ground water fluctuations those materials become cemented again through segregative action of hydrated oxides.

5) The important types of the soil found in the area are: entel, metel, bangha entel, pali, bandi, doanas, bele, kankar and bastu. There is 'kankara' soil which is literally uricru and it is reddish, loose and friable lateritic soil (low fertility) containing ferruginous concretion (Duricrustmorum bed) usually covers the soils of the south-western blocks.

6) We have found that in pre-monsoon the average water level is above 10 meter depth (April, 2006) and in post monsoon the average water level is near about 3 meter depth (November, 2005).

7) The vegetations of the study area belong to the tropical dry type deciduous with few evergreens occurring here and there. Though once upon a time, the whole study area was covered with forest of Sal but due to encroachment of Stone crushers and agriculture there is only few glimpse of forest. In the drier parts of highland the characteristics shrubs and grass field are found.

## 4. Results and Discussion

### 4.1. Identified Categories of Wastelands

Wasteland is a type of land cover/landuse is not suitable for either cultivation or any other beneficial use under the existing conditions of land management (V.C. Jha, 1987). In the study area the wastelands are largely inherent (natural cause) but some are the result of imposed factors (misuse or overexploitation of land resources). Some cases both are overlapping. Out of 13-fold categories of wastelands, only 6 types are identified in the district (Table 1). These are Land with/without scrub, degraded notified forest, Gullied/Ravenous, Sand riverine, Barren hill/Rocky/Stony waste and Mining wasteland. In some parts of the study area, there is overlapping of two or more wastelands. In this case the area is included into one category. The area under different wastelands of the district is the Birbhum District has its 14854 hectares (i.e. 3.31% to total geographical area) area under various categories of wastelands. Out of total wasteland, land with/without alone covers 67.44% followed by degraded forest (26.52%), barren hill /rocky/stony wastes (2.31%), sand riverine (2.15%), mining (1.15%) and gullied and or ravenous (0.41%). The first two categories of wastelands combinedly form majority (93.96%) in wasteland area of the district (Table 1).

***Table 1:*** *Identified Categories of Wasteland in Birbhum District*

| Wasteland Category | Wasteland Area (Ha.) | % to Total Wastelands | % to Total Geographical Area |
|---|---|---|---|
| **Land with/without Scrub** | 10018.6 | 67.45 | 2.20 |
| **Degraded Notified Area** | 3939.73 | 26.52 | 0.87 |
| **Gullied/ Ravine** | 61.43 | 0.41 | 0.01 |
| **sand Riverine** | 320.07 | 2.15 | 0.07 |
| **Barren hill/Rocky/Stony Waste** | 343.65 | 2.31 | 0.08 |
| **Mining Waste** | 170.54 | 1.15 | 0.04 |
| **Total** | 14854.02 | 100 | 3.31 |

Source: Satellite imageries, Topographical Map and other corresponding Maps and Field checking

### 4.2. Spatial Distribution

In respect to total geographical area, the maximum concentration of the wasteland is found in Rajnagar block which is 14.55 percent to total geographical area and it is followed by Khoyrashole (8.34%), Suri-I (8.17%), Md. Bazar (6.72%), Dubrajpur (4.46%), Illambazar (3.9%) and Bolpur-Sriniketan (2.61%) (Table 2). Table 2 reveals that four blocks constitute approximately 2/3$^{rd}$ of the total wasteland of the district. These blocks are Rajnagar, Khoyrashole, Md. Bazar and Dubrajpur. More than half of the wasteland of the district is concentrated in three blocks i.e. Rajnagar (21.69%), Khoyrashole (15.28%) and Md. Bazar (14.27%). Other blocks having significant percentage-sharing of wasteland are Suri-I (8.5%), Illambazar (6.91%), Bolpur-Sriniketan (5.85%), Rampurhat–I (4.35%), Nalhati-I (3.35%) and Murarai (2.83%). The Table 3 shows the five categories of percentage of wasteland to total geographical area. These categories are assigned as very low (<1%), low (1-3%), medium (3-5%), high (5-7%) and Very high (>7%).

***Table 2:*** *Spatial Pattern of Wasteland of Birbhum District*

| S.l No. | C.D. Block | Total Area | Total Wastelands | % to TGA | Block-Wise Share |
|---|---|---|---|---|---|
| 1 | Murarai-I | 17551.1 | 420.04 | 2.39 | 2.83 |
| 2 | Murarai-II | 18533 | 85.52 | 0.46 | 0.57 |
| 3 | Nalhati-I | 24970.9 | 497.53 | 1.99 | 3.35 |
| 4 | Nalhati-II | 10915.3 | 54.3 | 0.51 | 0.36 |
| 5 | Rampurhat-I | 28762.6 | 646.36 | 2.25 | 4.35 |
| 6 | Rampurhat-II | 18154.6 | 95.02 | 0.52 | 0.64 |
| 7 | Mayureswar-I | 22483.3 | 84 | 0.37 | 0.56 |
| 8 | Mayureswar-II | 15657 | 65.5 | 0.42 | 0.44 |
| 9 | Md. Bazar | 31564.1 | 2120.16 | 6.72 | 14.27 |
| 10 | Rajnagar | 22146.6 | 3222.75 | 14.55 | 21.69 |
| 11 | Suri-I | 15465 | 1263.22 | 8.17 | 8.5 |
| 12 | Suri-II | 13580.6 | 125.89 | 0.93 | 0.85 |
| 13 | Saithia | 30278.1 | 263.33 | 0.87 | 1.77 |
| 14 | Labhpur | 26798.4 | 99.92 | 0.38 | 0.67 |
| 15 | Nanoor | 31182.7 | 105.71 | 0.34 | 0.71 |
| 16 | Bolpur-Sriniketan | 33458.3 | 869.46 | 2.61 | 5.85 |
| 17 | Illambazar | 26154.3 | 1026.16 | 3.9 | 6.91 |
| 18 | Dubrajpur | 34488.3 | 1538.97 | 4.46 | 10.36 |
| 19 | Khoyrashole | 27219 | 2270.18 | 8.34 | 15.28 |
| 20 | Total | 449363.2 | 14854.02 | 3.31 | 100 |

Source: Satellite imageries, Topographical Map and other corresponding Maps and Field checking
N.B. – TGA = Total Geographical Area

The very high category is constituted by 5.26% blocks, high category by 15.79%, moderate by 31.58 % and low by 47.37% blocks. It is observed from the Figure 3, 4, 5, 6, 7 that the blocks situated in the eastern part of the district reveals the low percentage of wasteland while high and very high percentage is found in western and southern part of the district. This variation initially roots to their geographical location and natural environment.

***Table 3*****:** *Wasteland Intensity Categorization*

| Range of Wasteland (% to Total area) | Category | No. of Blocks | % of Blocks | Name of the Blocks |
|---|---|---|---|---|
| Below 2 | Low | 9 | 47.37 | Murarai-II, Nalhati-II, Rampurhat-II, Mayureswar-I, Mayureswar-II, Suri-II, Labhpur, Nanoor, Saithia |
| 2-6 | Moderate | 6 | 31.58 | Dubrajpur, Illambazar Bolpur-Sriniketan, Rampurhat-I, Nalhati-I, Murarai-I |

| | | | | |
|---|---|---|---|---|
| 6-10 | High | 3 | 15.79 | Khoyrashole, Md. Bazar, Suri-I |
| Above 10 | Very High | 1 | 5.26 | Rajnagar |
| Total | | 19 | 100 | |

### 4.3. Category-Wise Details

The distribution of wasteland according to the categories indicates that land with/without scrub is found to be maximum concentration in Rajnagar block i.e. 9.75% to the total geographical area due to higher elevation, poor ground water resource and poor soil. This is followed by Khoyrashole (6.83%), Suri-I (6.43%), Md. Bazar (3.44%), Dubrajpur (3.04%) blocks situated adjoining to Rajnagar block and also has similar characteristics as Rajnagar to some extent. Other blocks having more wasteland under this category are Murarai-I (2.17%), Rampurhat-I (1.65%), Nalhati-I (1.57%), Bolpur-Sriniketan (1.56%), Illambazar (1.36%). These blocks are situated in hilly tract of south western part of the district. The rest of the blocks possess a minimum percentage of this wasteland to their total geographical area. In regard to degraded notified land more than 4 percentage areas to total geographical area in Rajnagar block and it is the highest percentage. Others blocks having more geographical area under degraded forest are Md. Bazar (2.76%), Illambazar (2.39%), Suri–I (1.58%), Khoyrashole (1.24%) and Dubrajpur (1.12%). Rest of the blocks have either negligible percentage or does not have this category of wasteland. In case of barren hill/rocky/stony wasteland Rajnagar again tops among all the blocks followed by Md. Bazar. Their percentage to total area is 0.39% and 0.33% respectively. Other blocks having more area under this wasteland are Khoyrashole (0.17%), Dubrajpur (0.18%) and Rampurhat–I (0.11%). Rest of the blocks either has negligible percentage or nil wasteland of this category. The sand riverine land is observed to be high in Sainthia (50.4 ha.) followed by Illambazar (38.76 ha.), Bolpur (35.33 ha.), Suri-II (33.8 ha.) and so on. On the basis of percentage of sand riverine land to total geographical area Suri-II tops among all the blocks of the study area as this block covers 0.248% sand riverine wasteland to total geographical area. Sainthia, Illambazar also have significant percentage of this wasteland and these percentages are 0.17% and 0.115% respectively. In respect of percentage of mining wasteland to total geographical area, this category covers only 170.54 hectares i.e. equivalent to 0.04% to total geographical area. The maximum area under this category is found in Rampurhat-I (60.5 ha. or 0.21% to total area) and it is followed by Md. Bazar and Rajnagar. Md. Bazar possesses 43.32 ha. and Rajnagar occupy 30.22 ha. and both are 0.14% to their total geographical area. Other blocks having wasteland of that category are Murarai-I, Nalhati-I and Khoyrashole. These three blocks holds very little percentage to their area. Rest of the blocks has no mining wasteland. It is very interesting to note that like other wasteland gullied and/ or ravenous land also concentrated in south western part of the district while north eastern part devoid of this type of wasteland. Maximum concentration (above 0.04%) is found in two blocks viz. Md. Bazar and Rampurhat-I, moderate concentration in five blocks and low concentration in two blocks.

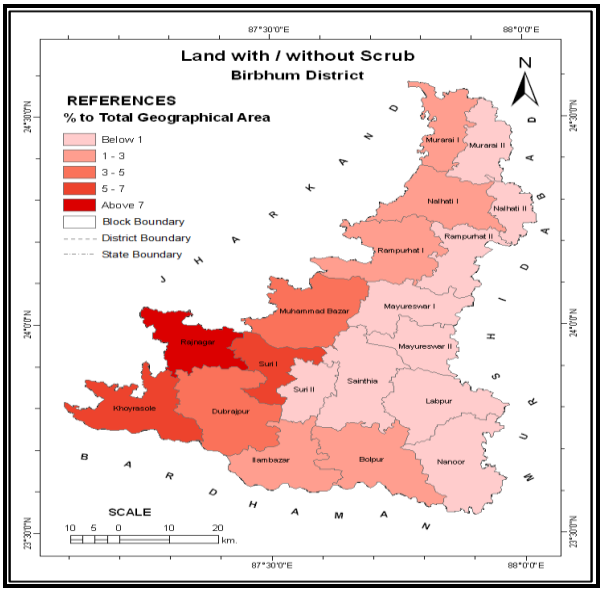


***Figure 3:*** *Land With/Without Scrub*

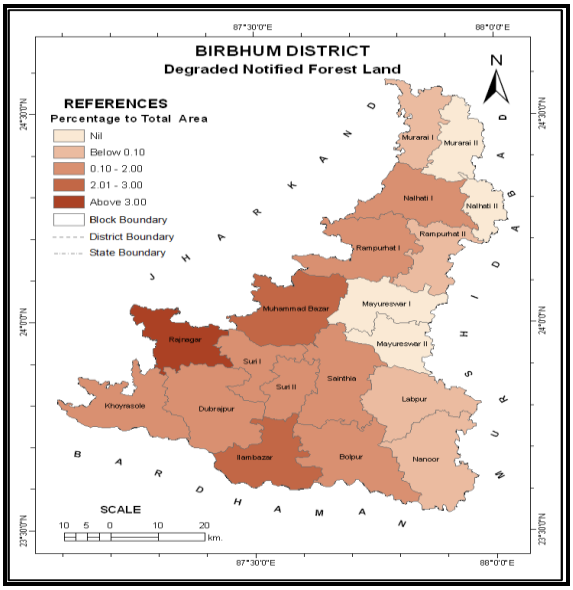


***Figure 4:*** *Degraded Notified Forest*

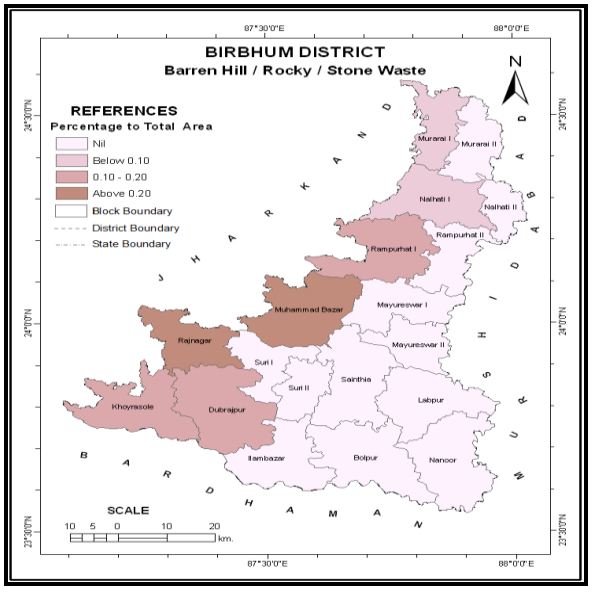


***Figure 5***: *Barren Hill/Rocky/Stony Wasteland*

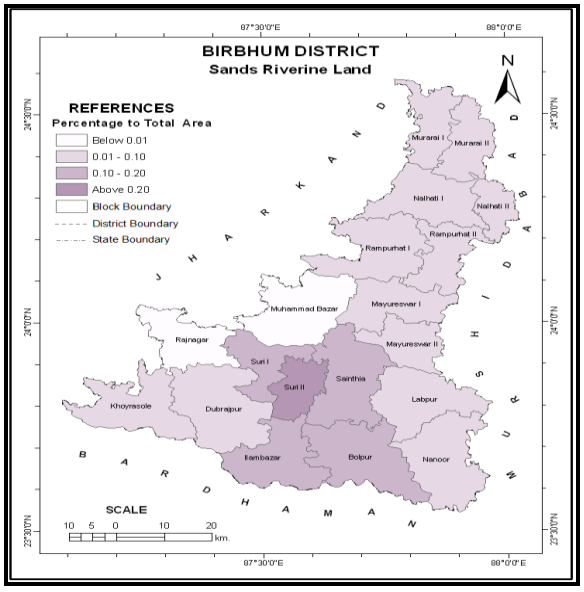


***Figure 6:*** *Sand Riverine Land*

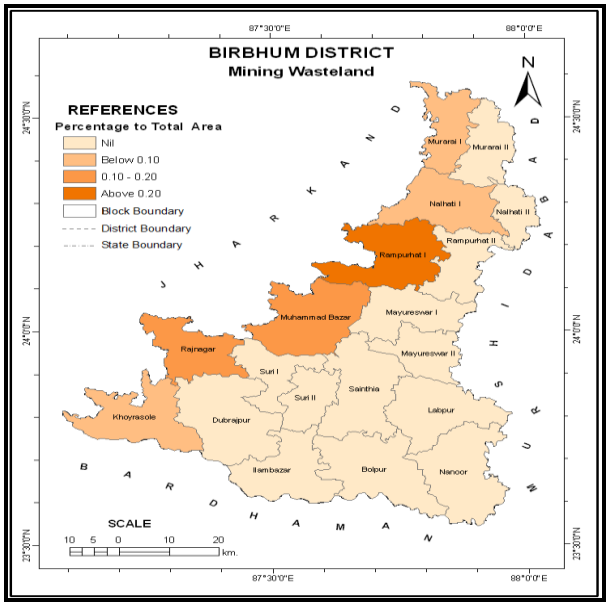


***Figure 7:*** *Mining Wasteland*

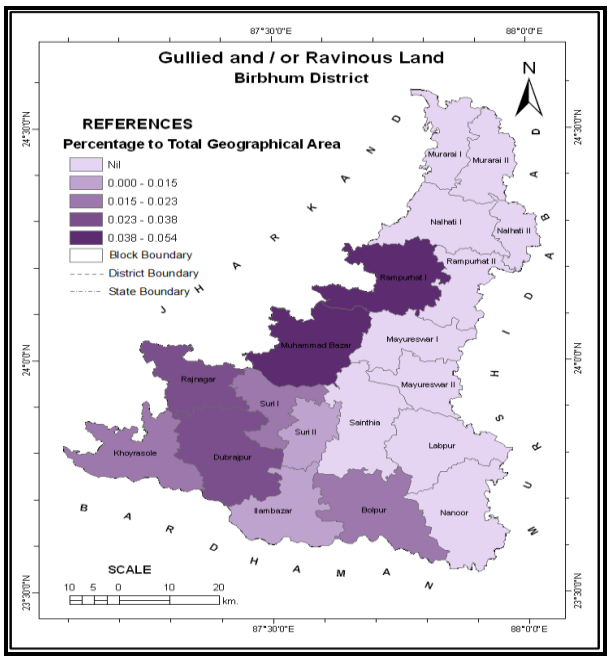


***Figure 8:*** *Gullied and / or Ravenous Land*

## 5. Conclusion

This study demonstrates that the data from satellite imageries and processing of the data can be used to map and monitor wastelands. This type of task makes a sound, healthy and accurate database with details of wasteland at various level i.e. country level, state level, tehsil level, village level or watershed level. These spatial, temporal and attribute in formations on wasteland at village level can be utilized for various reclamation measures and subsequent use under crop cultivation, social forestry, agro-forestry, fuel and fodder farm forestry and afforestation programmes.

## Acknowledgements

The authors wish to express sincere thanks to those officials and personnel like NRSA; Survey of India, NATMO, Kolkata; NRDMS, Suri, Birbhum etc. who have extended their helping hand by providing information, data, maps etc.

## References

Anonymous, 1986: *Wasteland Definitions and Classifications, National Wasteland Development Board.* Technical Task Group Report, Ministry of Environment and Forest, Govt. of India.

Anonymous, 1998: *Wasteland Manual 15 Steps for Preparation of Digital Database*. NRSA, India.

Chadha, G.K., 1982: *Future of Landuse Pattern in India Golden Harvests: A Survey of Agriculture*, Patriot, New Delhi. 31.

Farmer, B.H., 1974: *Agricultural Colonization in India since Independence*. Oxford University Press.

Fitzpatrick, Lins, K. and Chambers, M.J. *Determination of Accuracy and Information Contents of Landuse and Land Cover Maps at Different Scales*. J Rem. Sens, Electromagnetic Spectrum. 1977. 4; 41.

Government of India, 1993: *Wasteland Atlas of India.* Vol. I. NRSA, Hyderabad.

Government of India, 1995: Annual Report of the Department of Wastelands Development. Ministry of Rural Development. 1-2.

IFPRI, 1995*:* IFPRI Report. International Food Policy Research Institute, Washington DC. 1.

Jha, V.C. *Wasteland Types and their Effective Utilization in Birbhum District.* The Deccan Geographer. Secunderabad. 1987. Xxv (2 & 3) 231-242.

Kalwar, S.C. *Forest Cover Monitoring and Management in Jaipur District Using Remote Sensing Data.* Annals of the Association of Rajasthan Geographers. 1990. VIII; 59-65.

Khan, S. and Qureshi, M.A., 1997: *Changing Detection in Wasteland using Geographic Information System and Remote Sensing.* NISTADS, India.

Miglani, M.K., 1988: *Landuse in Haryana- Some Basic Issues*. In: Singh, Mahendra et al., (Eds.). Land Use in Haryana, Land Use Board, Govt. of Haryana. 4-9.

Yadav, H.R., 1987: *Genesis and Utilisation of Wastelands.* Concept Publishing Company. New Delhi. 32-79.

**Cloud Publications**
International Journal of Advanced Remote Sensing and GIS
2014, Volume 3, Issue 1, pp. 769-783, Article ID Tech-317
ISSN 2320 - 0243

Cloud Publications

Case Study | Open Access

# Site Suitability for Urban Solid Waste Disposal Using Geoinformatics: A Case Study of Pune Municipal Corporation, Maharashtra, India

**Ravindra Jaybhaye, Nitin Mundhe and Bhalachandra Dorik**

Department of Geography, Savitribai Phule Pune University, Pune, Maharashtra, India

Correspondence should be addressed to Nitin Mundhe, mundhenitin8@gmail.com

Publication Date: 2 December 2014

Article Link: http://technical.cloud-journals.com/index.php/IJARSG/article/view/Tech-317



**Abstract** Urban solid waste disposal is a major problem, faced by majority of cities or towns in the world. Rapidly increasing population growth, urbanization, industrialization and rural to urban migration created acute problem of solid waste management. Solid waste per capita generation rate in India has increased from 0.44 kg per day in 2001 to 0.5 kg per day in 2011. These increasing rates of waste generation stress on all infrastructural, natural and budgetary resources with adverse impacts on human health and environment due to the improper and unscientific solid waste dumping. Pune is one of the fastest growing city, it generates total quantity of waste is about 1300 to 1400 metric tons per day. So, there is need suitable solid waste disposal sites for prevention of environment. The present research work to find out the suitable solid waste dumping sites using Geoinformatics approach for Pune Municipal Corporation (PMC). For this purpose topographical maps and medium resolution satellite data were used to generate various thematic layers. Site suitability analysis for urban solid waste disposal consider the nine parameters such as, road network, rivers, lakes, canals, geology, population density, slope, airport and land use/land cover. The generated thematic maps of these criteria were standardized using multi-criteria analysis method. A weight for each criterion was generated by comparing them with each other according to their importance. With the help of these weights and criteria final site suitability map was prepared. This site suitability map presented in four suitability level such as highly suitable, moderate suitable, less suitable and unsuitable. The result shows that around 1.70 % area is under high suitable for solid waste disposal site, 7.86 % is moderate suitable, 80.92 % of study area is less and 9.52 % area is unsuitable for dumping site. There are ten potential site have been determine based on sitting criteria and all sites are identify surrounding part of city area within newly added 34 villages. The suggested potential sites are economically and environmentally suitable for solid waste dumping.

**Keywords** *Geographic Information System (GIS); Multi-Criteria Analysis; Remote Sensing (RS); Urban Solid Waste*

## 1. Introduction

Solid waste comprises unwanted and discarded materials from houses, street sweeping, commercial and industrial operations. Uncontrolled momentum of urbanization, industrialization and modernization lead to the generation of solid waste (Basagaoglu et al., 1997). There has been a significant increase in solid waste generation in India over the years from 100 gm per person per day in small towns to 500 grams per persons per day in large towns. These increasing rates of waste generation stress on all infrastructural, natural and budgetary resources with adverse impacts on human health and environment due to the improper and unscientific solid waste dumping. The unscientific landfill site may reduce the ground water quality, drinking water purity and causes the disease like nausea, jaundice, asthma etc (Bean et al., 1995).

Pune is the second largest fast developing urban agglomerations in Maharashtra and ranks eight at national level. In Pune Municipal Corporation (PMC) primary sources of waste are local households, commercial establishments, vegetable markets, hotels, restaurants and hospitals. Pune Municipal Corporation generates huge amount of solid waste. The quantity of waste generated per day is about 1400 to 1500 metric tons (approximate generation per capita per day is 500 grams). This large amount of waste poorly disposed and untreated. Pune city does not have a scientific landfill site and the capacity of Uruli Devachi dump site cannot provide the future demand of the waste generated (Mundhe et al., 2014).

It is very critical issue to identify the suitable location for disposal of solid waste. Since the land is limited resource, there is a shortage of land as the land prices are raising. Moreover the sight of garbage is not pleasing hence there is a lot of opposition from the masses and a Hercules task for the municipality to decide a place for dumping the garbage. If the land is selected on a scientific basis, there is less likely to have an opposition to the place of dumping.

The present research work focused on to find out suitable dumping sites for urban solid waste generated from Pune Municipal Corporation using Geoinformatics techniques like Geographical Information System (GIS), Remote Sensing (RS) and Global Positioning System (GPS) with the help of multi-criteria analysis to minimize adverse effects on environment, social and economic of solid waste management.

## 2. Study Area

Pune Municipal Corporation lies between latitudes 18°25'N and 18°37'N and longitudes between 73° 44'E and 73°57'E and the geographical area is over 243.84 Sq. Km with a population of 3.1 million (according to Census of India, 2011). Now there are 34 villages added in Pune Municipal Corporation therefore after State Government notification area of Pune Municipal Corporation over 500 Sq. Km. Pune has had traditional old-economy industries, which continue to grow. Pune is the cultural capital of Maharashtra since the after independence. The city is now also known for information technology and educational hub that attract migrants and students from other places.

Pune city situated at an altitude of 560 meters above mean sea level (MSL) on the western margin of the Deccan plateau. The city is bounded by Thane district to the north-west, Raigad district to the west, Satara district to the south, Solapur district to the south-east and Ahmednagar district to the north and north-east (Figure 1).

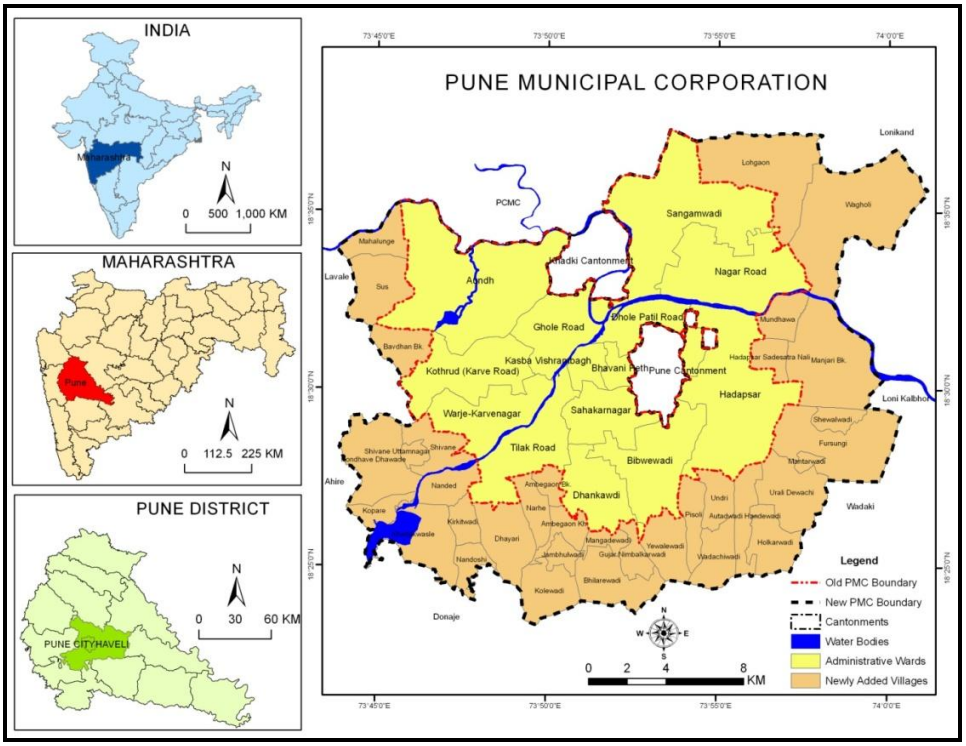


***Figure 1:*** *Location Map of Study Area*

## 3. Objective

The main objective of this present research work is to find out suitable dumping sites for urban solid waste using Geoinformatics technique with the help of multi-criteria analysis.

## 4. Materials and Methods

In the present study primary and secondary data were used. The primary data were collected from field surveys using GPS instrument to measure the coordinates of some location in the study area. Whereas, the secondary data for the study was acquired from governmental institutions, reports, books, journals and internet. The main data used for this study were Landsat 8 OLI/TIRS image with spatial resolution of 30m and topographical maps like 47F/10; 47F/11; 47F/14; 47F/15; 47J/2 and 47J/3 were used. Aster data also used to create the slope map of study area. Geological maps were used to create geology layer of the study area and which is obtained from Geological Survey of India, Pune. Demographic data obtained from Census of India, which is useful for the creation of population density map. Ward maps and administrative boundaries of the study area were collected from Pune Municipal Corporation (PMC). Hence, in the present study various thematic maps are prepared by visual interpretation of the satellite imagery and SOI toposheets.

Pre-processing operations involved scanning, geo-referencing and digitization of Survey of India (SOI) topographical maps, satellite image and other solid waste related base maps. Firstly, Survey of India (SOI) toposheets has been geo-referenced using WGS 1984, Universal Transverse Mercator (UTM) projection system. After geo-referencing the SOI toposheets and other maps are digitized in different features like point, line and polygon such as ward boundaries, road network, contour, drainage network, river and lakes etc.

Landsat 8 image obtained from USGS website, this image already geo-rectified. Initially, standard image processing techniques have been applied for the analysis of satellite image such as

enhancement, band extraction, restoration and classification (Congalton et al., 1999). The hybrid image classification technique was employed with for the image classification using ERDAS software. The classification of land use/land cover was categorized into seven major classes such as agriculture land, vegetation, built-up (residential & commercial), scrub land, fallow land, river and lakes and canal. About seven training sites for each class were used in hybrid image classification approach (Lillesand et al., 1993).

The present research work used multi-criteria analysis technique to identify the most suitable solid waste dumping site (Bilgehan et al., 2010). Multi-criteria approaches have the potential to reduce the costs and time (Kontos et al., 2005). The solid waste disposal site selection mapping was done using multi-criteria analysis and creating layers to yield a single output map or index of evaluation (Wiley and Sons, 2009). The procedure by which the weights were produced follows the logic developed by Saaty (1977) under the analytical hierarchy process (AHP) which is utilized to determine the relative importance of the criteria in a specified decision-making problem.

Classifications were done on various layers and the values were assigned ranging from unsuitable to high suitable. Whereas, reclassification of layers were classified into the 1's, 2's, 3's and 4's ranking system, where first, represented unsuitable, second, less suitable, third, moderate suitable and fourth, highly suitable after distance calculation was done, respectively. These criteria were developed by referring to different sources like Central Pollution Control Board (CPCB), Municipal Solid Waste (Management and Handling rules) 2000 and CPHEEO manual have been used as a guide to determine the best site location. These criteria were then analyzed using multi-criteria analysis to evaluate and to seek potential locations of sanitary landfills. When potential sites were found in several locations, appropriate ranking techniques were applied to decide the best choices produce by Geoinformatics approach (Figure 2). The analysis has been used to find out potential sites for PMC region.

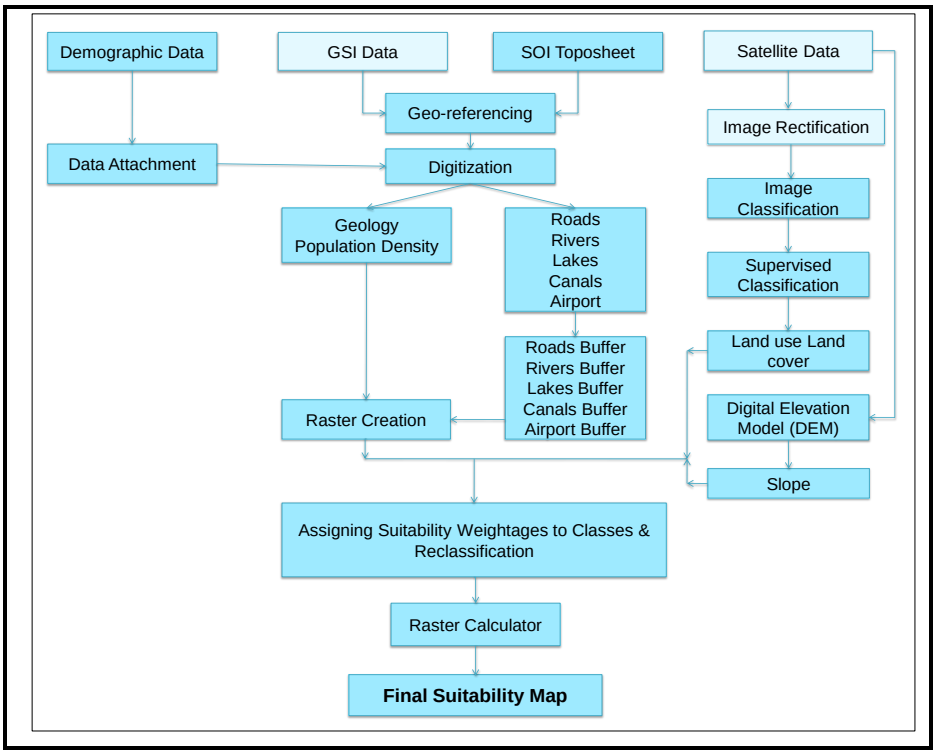


***Figure 2:*** *Flow Chart of Methodology*

## 5. Decision Rules/ Criteria for Selection of Potential Dumping Site

Present study evaluation criteria were determined depend on Central Pollution Control Board (CPCB), Municipal Solid Waste (Management and Handling rules) 2000 and CPHEEO manual. There are nine criteria that were considered when selecting a landfill site in the Pune Municipal Corporation. These are slope, geology, population density, land use/land cover, distance from road network, distance from rivers, distance from lakes, distance from canals and distance from airport. Each criterion was explained below in detailed.

### 5.1. Slope

The slope map was generated from the ASTER DEM data. Slope refers to the measures of the rate of change of elevation of surface location (Chang, 2010). In the study area North, East and middle part of the city mostly flat and southern and western part is covered by hilly area. The lower degree of slope is highly suitable than the higher degree of slope. Different research states that area with high slope will have high risk of pollution, lichet and potentially not good site for dumping (Ebistu et al., 2013). Slope is indicates in degree and divide into four categories with assigning values are given below Figure 3. In the results, most of the study area falls under slope category less than $10^0$ which covered 84% of the total study area. This is highly suitable, slope from $10^0$ to $15^0$ is moderately suitable and slope $15^0$ to $20^0$ and more than $20^0$ are less suitable and unsuitable respectively for solid waste dumping site selection.

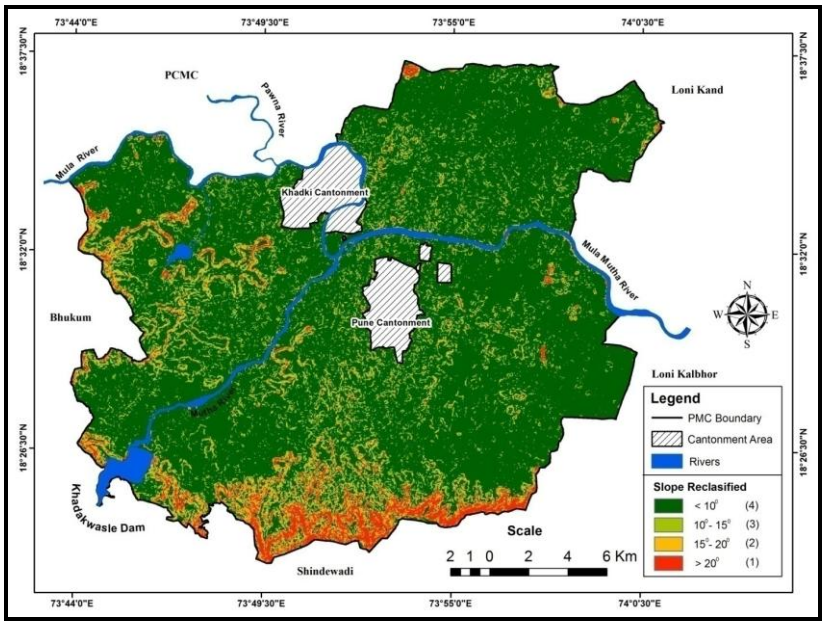


***Figure 3:*** *Reclassified Slope Map*

### 5.2. Geology

Geological layer created from the Geological Survey of India maps. There are five Geological formation type found in study area. Geological formation thickness is considered to analyze suitability. The Purandargarh and Diveghat formation is highly suitable for solid waste dumping site due to their 50m to 350m high thickness and Upper Ratangarh Formation thickness is 50m to 100m so this formation is unsuitable due to the low thickness. Purandargarh and Diveghat formation assigned the value 4s, Indrayani formation 3s, Karla formation 2s and Upper Ratangarh formation assigned 1s based on their thickness for suitability criteria (Figure 4).

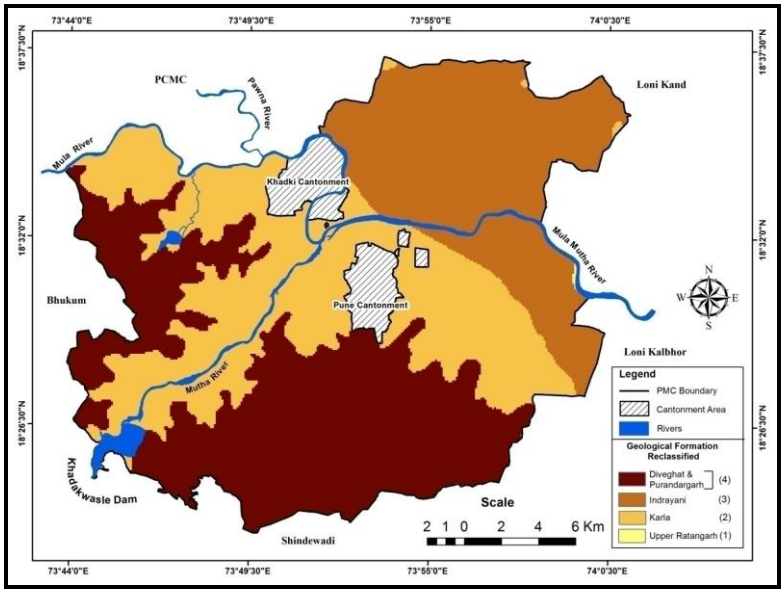


***Figure 4:*** *Reclassified Geology Map*

### 5.3. Population Density

Population density is also important suitability parameter. The population of PMC as per Census of India, 2011 is more than 31 lakhs. Population density of Pune city is 12,777 persons per sq. km in 2011. There are 34 newly added villages in Pune Municipal Corporation in June 2014. Highest population density found in Bhavani Peth and Kasba Vishrambaghwada that is 661 and 445 persons per hectare respectively in city and lowest density recorded in newly added village Kolewadi is 1P/Ha, Wadachiwadi and Nandoshi both are 2P/Ha. Population less than 200 P/Ha persons per hectare is found in all newly added villages highly suitable, population within 200 P/Ha to 400 P/Ha is recorded in Sahakarnagar and Dhankavdi wards moderately suitable, population between 400 P/Ha to 600 P/Ha is found in Kasba Vishrambagh less suitable and more than 600 persons per hectare in Bhavani Peth is unsuitable for waste dumping site (Figure 5).

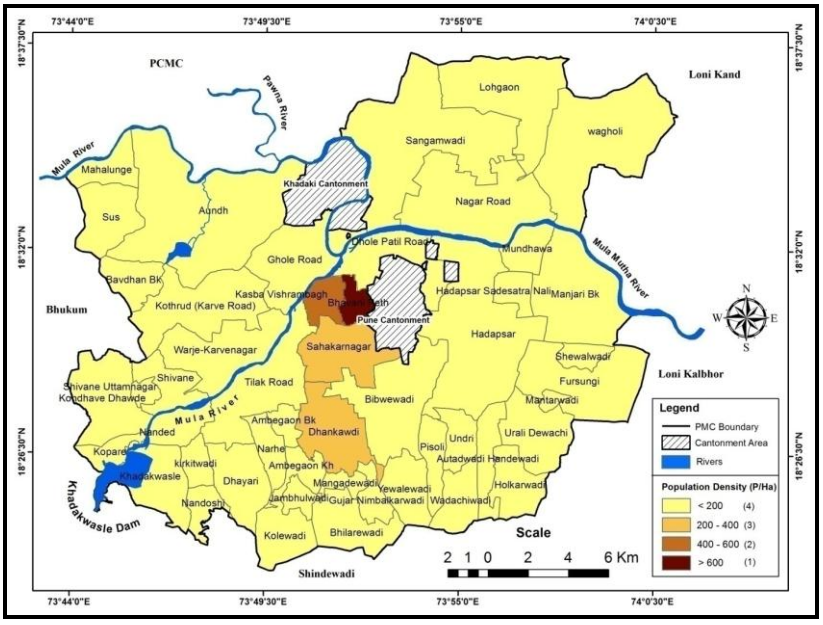


***Figure 5:*** *Reclassified Population Density Map*

### 5.4. Suitability of Land Use/Land Cover

The land use/land cover of the present study area was analyzed from Landsat 8 data for the solid waste dumping site selection. The dumping site should not be selected close to settlement to avoid adversely affecting land value and future development and to protect human being from environmental hazards created from dumping sites (Clark et al., 1974). It should be selected at a suitable distance from the residential area. Scrub land and fallow land both are most suitable for dumping site. Rivers and lakes, canals, built-up, vegetation, agricultural land, scrub land and fallow land are major land use/land cover classes in the present study. Ranking were assigned of each class of land use and land cover. Hence, small value give for unsuitable and highest value give for highly suitable to solid waste disposal site location. Fallow land and scrub land classes covered near about 33% from the total study area which is most suitable for dumping site (Figure 6).

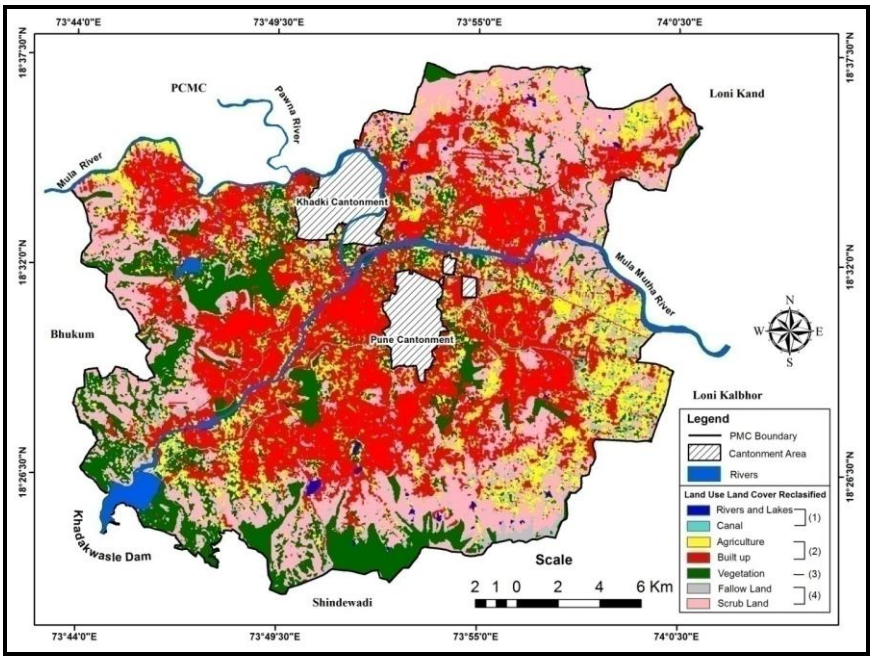


***Figure 6:*** *Reclassified Land Use Land Cover Map*

### 5.5. Distances from Road Network

The waste disposal site should not be located within 250m distance from transportation network (Bhambulkar, 2011). Solid waste landfill site must be located at suitable distance from road network to decrease the cost of transportation. Distance of 250m, 500m, 750m and more than 750m, multiple ring buffer were created around the road network and ranked were assigned of each buffer zone based on siting criteria are shown in (Table 1). Distance less than 250m from road is unsuitable for dumping site, distance from 250m to 500m is less suitable, distance from 500m to 750m is moderately suitable and distance more than 750m is highly suitable for urban solid waste landfill site (Figure 7).

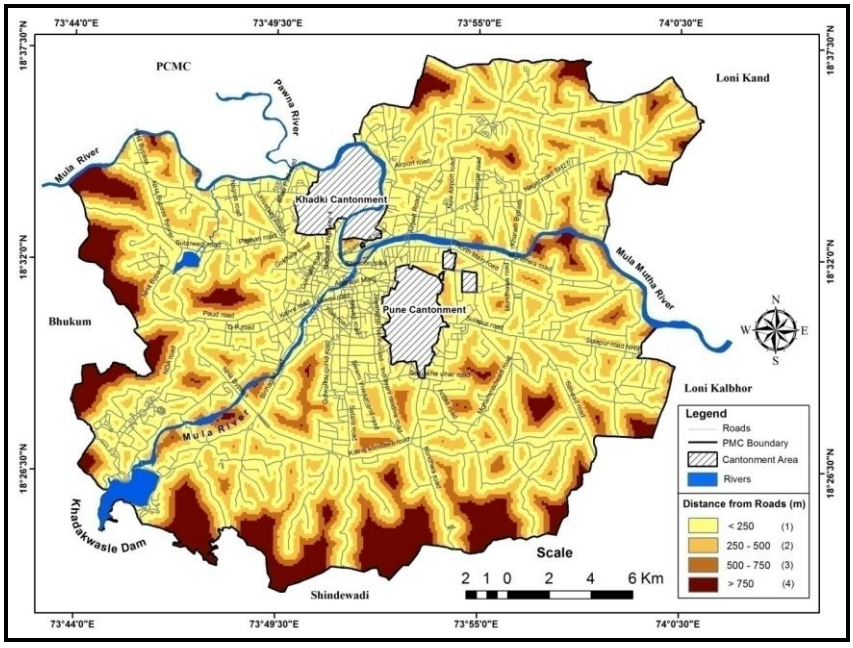


***Figure 7:*** *Reclassified Road Network Map*

### 5.6. Distances from Rivers

As per Central Pollution Control Board, it is clearly states that dumping of solid waste on any water surface be it river or lake is prohibited. Solid waste disposal site must not be located near river, stream and surface water (Paul, 2012). In the study area Mula - Mutha are two main rivers in PMC. Using Arc GIS tool, multiple ring buffer are created for distance of 250m, 500m, 750m and more than 750m from rivers and 1, 2, 3 and 4 ranked were assigned each buffer ring respectively. Distance less than 250m from rivers is unsuitable, distance from 250m to 500m and distance from 500m to 750m are less suitable and moderately suitable respectively and distance more than 750m is highly suitable for disposal site (Figure 8).

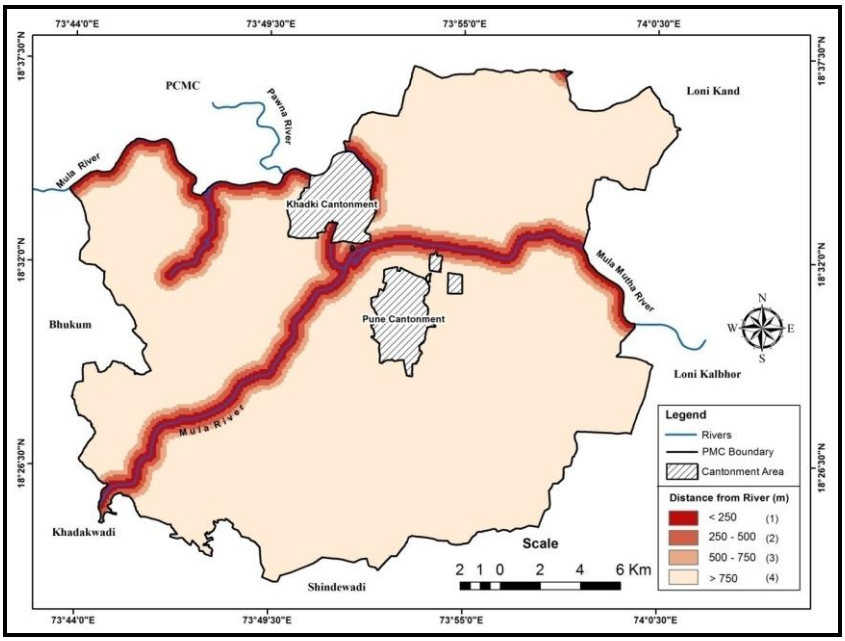


***Figure 8:*** *Reclassified River Map*

### 5.7. Distances from Lakes

Khadakwasla reservoir is main source of water supply to Pune city and cantonment areas, which is constructed on Mutha River approximately 10 km from the city in south western direction and Pashan Lake, Katraj Lake, Lohegaon Lake, Vishrantwadi Lake, Jambhulwadi Lake; these lakes are also within different part of the city. Dumping site near the lakes and rivers also prohibited. Criteria of lakes for dumping site same as rivers and canal layer. Distance from lakes less than 250m is unsuitable and distance more than 750m is highly suitable for solid waste dumping site (Figure 9).

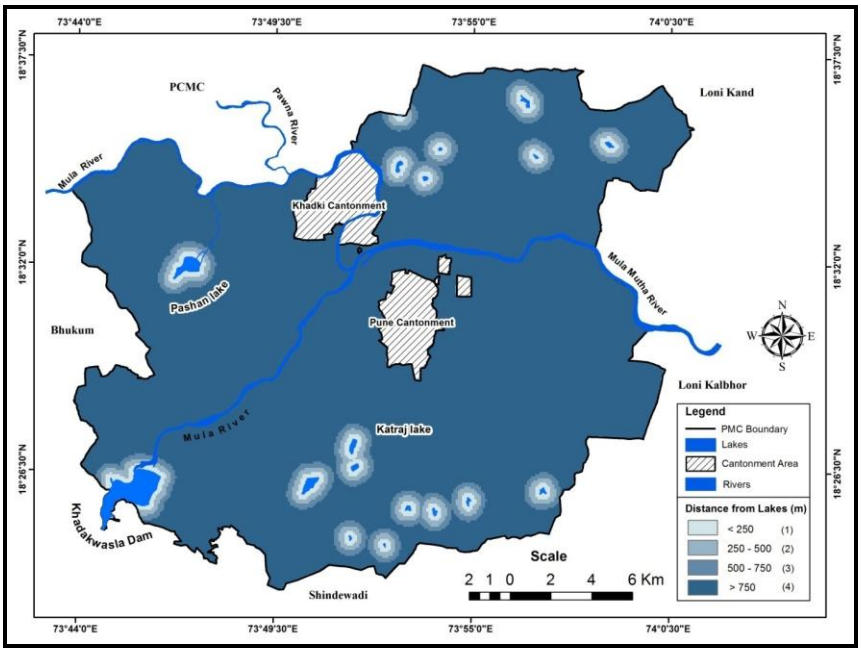


***Figure 9:*** *Reclassified Lakes Map*

### 5.8. Distances from Canals

Canal layer digitized from the Survey of India, topographical maps. Mutha left bank canal and Mutha right bank canal constructed within core part of the study area. Dumping site not located near the canal is environmentally hazardous. It is located suitable distance from canal. Multiple ring buffers were created around the canal. Distance less than 250m is unsuitable and distance more than 750m from canal is highly suitable for urban solid waste dumping site (Figure 10).

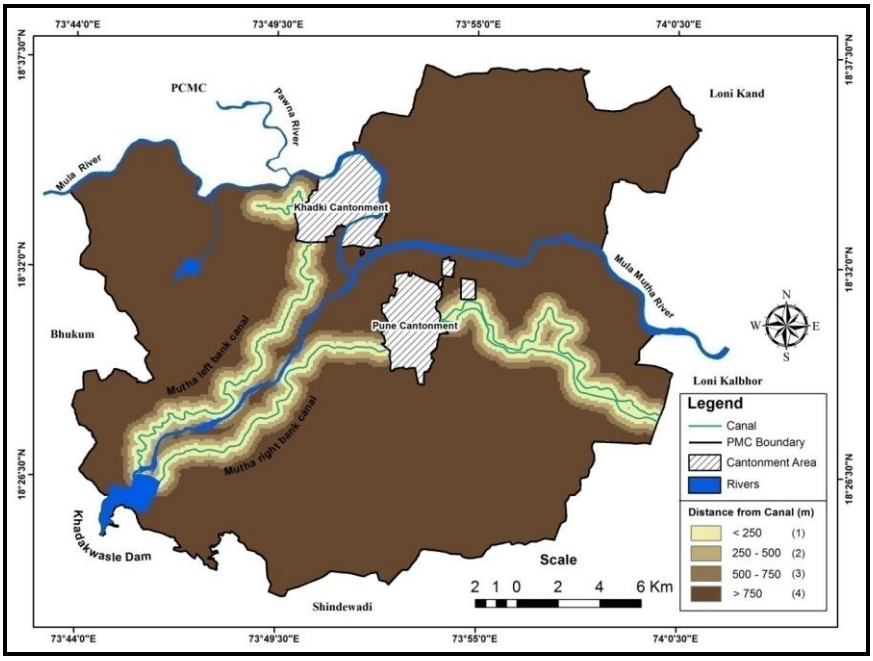


***Figure 10:*** *Reclassified Canals Map*

## 5.9. Distances from Airport

Airport parameter also considers finding the suitable dumping site. International Airport in Pune at Lohegaon. It shared its runways with Indian Air force. Based on siting criteria distance less than 500m, 1000m, 1500m and more than 1500m multiple ring buffer zones was created around the both airport location and ranked were assigned each buffer zone on the base of suitability criteria. Distance less than 500m from airport and ranked assigned value 1s which is unsuitable and distance more than 1500m ranked assigned value 4s, which is highly suitable for dumping site (Figure 11).

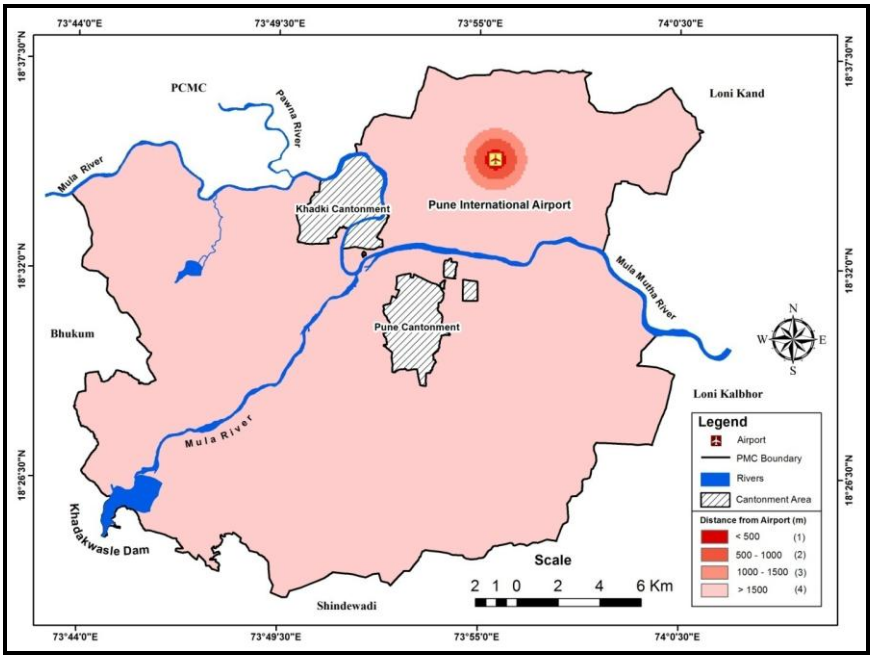


***Figure 11:*** *Reclassified Airport Map*

***Table 1:*** *Summary of Rankings and Suitability Level used in Selection of Dumping Site*

| Criteria | Sub Criteria | Ranking | Level of Suitability |
|---|---|---|---|
| Slope | $>20^0$ | 1 | Unsuitable |
| | $15^0$ - $20^0$ | 2 | Less suitable |
| | $10^0$ - $15^0$ | 3 | Moderate suitable |
| | $< 10^0$ | 4 | Highly suitable |
| Geology | Upper Ratanghar | 1 | Unsuitable |
| | Karla formation | 2 | Less suitable |
| | Indrayani formation | 3 | Moderate suitable |
| | Diveghat/ Purandarghar | 4 | Highly suitable |
| Population Density | > 600ha | 1 | Unsuitable |
| | 400ha - 600ha | 2 | Less suitable |
| | 200ha - 400ha | 3 | Moderate suitable |
| | < 200ha | 4 | Highly suitable |
| Land Use/Land Cover | Rivers, Lakes and Canals | 1 | Unsuitable |
| | Built up and Agriculture | 2 | Less suitable |
| | Vegetation | 3 | Moderate suitable |
| | Scrub and Fallow Land | 4 | Highly suitable |
| Distances From Roads | < 250m | 1 | Unsuitable |
| | 250m -500m | 2 | Less suitable |
| | 500m- 750m | 3 | Moderate suitable |
| | > 750m | 4 | Highly suitable |
| Distances From Rivers | 0m - 250m | 1 | Unsuitable |
| | 250m - 500m | 2 | Less suitable |
| | 500m - 750m | 3 | Moderate suitable |
| | 750m - 1000m | 4 | Highly suitable |
| Distances From Lakes | < 250m | 1 | Unsuitable |
| | 250m -500m | 2 | Less suitable |
| | 500m- 750m | 3 | Moderate suitable |
| | > 750m | 4 | Highly suitable |
| Distances From Canals | 0m - 250m | 1 | Unsuitable |
| | 250m - 500m | 2 | Less suitable |
| | 500m - 750m | 3 | Moderate suitable |
| | 750m - 1000m | 4 | Highly suitable |
| Distances From Airport | < 500m | 1 | Unsuitable |
| | 500m - 1000m | 2 | Less suitable |
| | 1000m - 1500m | 3 | Moderate suitable |
| | > 1500m | 4 | Highly suitable |

## 6. Results and Discussion

To identify the urban solid waste disposal site there are nine parameter, different siting criteria, various referenced materials and sources are used. The overlay analysis of the given factors using raster calculator in Arc GIS software produced the suitable solid waste dumping site (Figure 12). The final solid waste dumping site suitability map was divided into four categories: unsuitable, less suitable, moderate suitable, highly suitable. The result indicate that 9.52 % of the study area is unsuitable, 80.92 % area is less suitable, 7.86 % area is moderate suitable and 1.70 % study area is highly suitable for dumping site (Table 2). Out of total study area 1.70% means 8.52 $km^2$ (2105.04 acres) area is highly suitable for dumping. There are 10 potential site are identify in study area, out of them

Uruli Devachi is the existing waste dumping site. Now Uruli Devachi dumping site is not sufficient to dumped waste. Remaining nine sites are suggested to solid waste dumping (Table 3).

***Table 2:*** *Level of Suitability and Percent Total Area Coverage*

| Sr. No. | Suitability Classes | Area ($km^2$) | Area (acres) | Area (%) |
|---|---|---|---|---|
| 1 | Unsuitable | 47.84 | 11,822.61 | 9.52 |
| 2 | Less Suitable | 406.54 | 1,00,458.47 | 80.92 |
| 3 | Moderate Suitable | 39.48 | 9,756.31 | 7.86 |
| 4 | Highly Suitable | 8.52 | 2,105.04 | 1.70 |
| | **Total** | **502.39** | **1,24,142.43** | **100** |

***Table 3:*** *Potential Sites of PMC*

| Sr. No. | Potential Disposal Sites | Area ($Km^2$) | Area (acres) |
|---|---|---|---|
| 1 | Near Mahalunge | 0.65 | 159.807 |
| 2 | Near Kirkatwadi | 0.7 | 172.91 |
| 3 | Near Yeolewadi | 0.32 | 78.79 |
| 4 | Near Pinjanwasti | 0.58 | 142.48 |
| 5 | Near Authadewadi | 0.75 | 185.25 |
| 6 | Near Wagholi | 0.74 | 184.06 |
| 7 | Near Shindewasti, Lohgaon | 0.68 | 167.8 |
| 8 | Near Dighi | 1.41 | 347.21 |
| 9 | Near NDA, Khadakwasale | 0.6 | 147.92 |

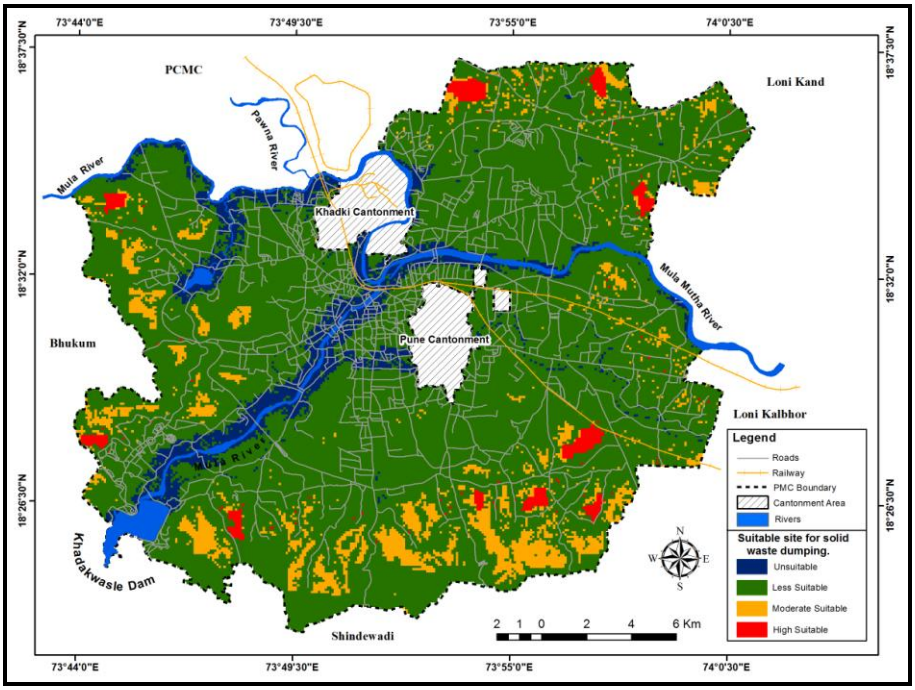


***Figure 12:*** *Final Suitability Map of Solid Waste Dumping Site*

By using the stated criteria, the suitable areas for solid waste dumping site fall on the northwestern, northeastern and southern direction from the city (Figure 12). The areas were highly suitable for solid waste dumping site suggested that selecting the optimum site for solid waste dumping may facilitate transportation and reduce the cost of transport. Moreover, suitability, for slope analyses had shown that slope less than 10 % are more suitable in order to minimize environmental impacts.

The total area of the nine most appropriate sites is 1586.23 acres out of a total area of 502.39 Sq. Km. for the study area. The areas of the potential sites are given as 347.21 acres for Near Dighi being the largest site; 185.25 acres, 184.06 acres and 172.91 acres for Near Authadewadi, Near Wagholi and Near Kirkatwadi respectively.

Near Authadewadi site with an area of 185.25 acres and an indigenous residential area located far away from any resource of economical/ecological value can be described as one of the most appropriate site. Near Kirkatwadi has an area of 172.91 acres and is described as an undeveloped land.

## 7. Conclusion

The analysis has taken land use/land cover, slope, geology, population density, water sources, and settlement and transport facilities as determining factor in order to find appropriate site for solid waste dumping site. The results have shown that nine sites were selected as the highly suitable. The sites are easy to access; manage for disposal of solid wastes. These places are far-away from any water sources and other variables put into analysis.

The study demonstrated the capacity to use GIS and remote sensing technology for the effective identification of suitable solid waste dumping sites will minimize the environmental risk and human health problems. The study is useful in planning for the city in future. It emphasizes on the importance of the requirement of solid waste management system. The use of multi criteria analysis is a new attempt to get the potential site. There is no limit to the scope of the innovations and technology use. With the given time and the limited knowledge with the data constraint this was an attempt to derive the site suitability analysis for urban solid waste disposal.

## Acknowledgements

We thank University Grants Commission (UGC), New Delhi for financial assistance and Department of Geography, Savitribai Phule Pune University, Pune for providing research related facilities. We are grateful to Pune Municipal Corporation, Pune for providing ancillary data.

We thank Mr. Raosaheb Khemnar and Miss Poorva Kale for their active participation in field data collection and in preparation of base layers. We thank anonymous referees for their critical review, comments and suggestions, which helped in improving the research work.

## References

Basagaoglu H. et al. *Selection of Waste Disposal Sites using GIS*. Journal of the American Water Resources Association. 1997. 33 (2) 455-464.

Bean, E.A., Rovers, F.A., and Farquhar, G.J., 1995: *Solid Waste Landfill Engineering and Design.* Prentice Hall, NJ. 380.

Bhambulkar, A.V. *Municipal Solid Waste Collection Routes Optimized with ArcGIS Network Analyst*. International Journal of Advanced Engineering Sciences and Technologies. 2011. 11 (1) 202-207.

Bilgehan, N., Tayfun, C., Fatih, I., and Ali, B. *Selection of MSW Landfill Site for Koyna, Turkey Using GIS and Multi-Criteria Evaluation*. Environ Monit Assess. 2010. 160; 491-500.

Census of India, 2011: Demographic Data of Pune City 2011. http://censusindia.gov.in.

Central Pollution Control Board, 2000: A Support Manual for Municipal Solid Waste (Management and Handling) Rules.

Chang, K.T., 2010: *Introduction to Geographic Information System*, 5th Ed. Mc Graw-Hill International Edition.

Clark, R.M., and Gillean, J. *Systems Analysis and Solid Waste Planning.* Journal of the Environmental Engineering Division. 1974. 7-25.

Congalton, R.G., and Green, K., 1999: *Assessing the Accuracy of Remotely Sensed Data*. 137.

Comprehensive Mobility Plan for Pune city, Pune Municipal Corporation. Chapter 3. 3.1-3.13. http://www.punecorporation.org/Mobility%20Plan.aspx

CPHEEO, 2000: *Manual on Municipal Solid Waste Management.* http://moud.gov.in/swm_manual.

Department of Economic Affairs, 2009: *Ministry of Finance, Government of India. Position Paper on the Solid Waste Management Sector in India.* Public Private Partnerships in India.

Dhere, A.M., Pawar, C.B., Pardeshi, P.B., and Patil, D.A. *Municipal Solid Waste Disposal in Pune City–an Analysis of Air and Groundwater Pollution.* Journal of Current Science. 2008. 95 (6) 773-777.

Ebistu, T.A., and Minale, A.S. *Solid Waste Dumping Site Suitability Analysis Using Geographic Information System (GIS) and Remote Sensing for Bahir Dar Town, North Western Ethiopia.* African Journal of Environmental Sciences and Technology. 2013. 7 (11) 976-989.

Environment Status Report of Pune Municipal Corporation, 2001 to 2012.

Jaybhaye, R.G., and Mundhe, N.N. *Hybrid Image Classification Technique for Spatio-temporal Analysis of Pune City*. Transactions of the Institute of Indian Geographers. 2013. 35 (2) 210-223.

Kontos, T.D., Komilis, D.P., and Halvadakis, C.P. *Siting MSW Landfills with a Spatial Multiple Criteria Analysis Methodology.* Waste Management. 2005. 25; 818-832.

Lillesand, T.M., and Kiefer Ralphh, 1993: *Remote Sensing Image Interpretation.* New York: John Wily and Sons Publication.

Mundhe, N.N., Jaybhaye, R.G., and Dorik, B. *Assessment of Municipal Solid Waste Management of Pune City Using Geospatial Tools*. International Journal of Computer Applications. 2014. 100 (10) 24-34.

Mundhe, N.N., and Jaybhaye, R.G., 2014: *Site Suitability Analysis for Urban Solid Waste Disposal using Remote Sensing & GIS Techniques*. Unpublished Minor Research Project, BCUD, Savitribai Phule Pune University, Pune.

Pune Municipal Corporation. City Sanitation Plan, 2011. http://www.indiaenvironmentportal.org.in/files/DraftCSPPune_CSP.pdf

Paul, S. *Location Allocation for Urban Waste Disposal Site Using Multi-Criteria Analysis: A Study on Nabadwip Municipality, West Bengal, India*. International Journal of Geomatics and Geosciences. 2012. 3 (1) 74-87.

Saaty, T.L. *A Scaling Method for Priorities in Hierarchical Structures*. Journal of Mathematical Psychology. 1977. 15; 231-281.

Saaty, T.L., 1980: *The Analytic Hierarchy Process.* New York: McGraw-Hill. 20-25.

Wiley, J., and Sons, L., 2009: *Essential Image Processing and GIS for Remote Sensing.* Imperial College London, UK.

**Cloud Publications**
International Journal of Advanced Remote Sensing and GIS
2014, Volume 3, Issue 1, pp. 734-738, Article ID Tech-318
ISSN 2320 - 0243

Research Article | Open Access

# Atmospheric Influences on Bleaching and Paling Events Occurred at Lakshadweep Reef System during 2010 and 2011

**R. Ranith, M. Machendiranathan, L. Senthilnathan, A. Saravanakumar and T. Thangaradjou**

Centre of Advanced Studies in Marine Biology, Faculty of Marine Sciences, Annamalai University, Parangipettai, Tamilnadu, India

Correspondence should be addressed to T. Thangaradjou, umaradjou@gmail.com

Publication Date: 6 November 2014

Article Link: http://technical.cloud-journals.com/index.php/IJARSG/article/view/Tech-318



**Abstract** Last few decades were evident with an increase in frequency and intensity of bleaching events at different reef systems around the globe. The present work was carried out to disseminate the importance of atmospheric variables in inducing bleaching and coral reef degradation at Lakshadweep system. SST, UVR, cloud fraction and water vapor content was obtained from MODIS aqua and TOMS and interpreted with stress response to identify their influence in coral bleaching at Kavaratti and Agatti islands during 2010 and 2011. Results indicates that in Lakshadweep reef system water vapor positive feedback do have more influence in causing coral bleaching when compared with previously established cloud shading theory. This study is also an evidence for the integrated influence of stressors in causing bleaching when compared to the influence of single parameter alone.
**Keywords** *Coral Reef; Lakshadweep; Bleaching; Water Vapor Feedback*

## 1. Introduction

Coral reefs are considered as one of the prime victim to the variabilities occurred in the global climate pattern. Increasing frequency and amplitude of disturbances have put the corals in the verge of degradation in few decades ahead (Hoeg-guldberg et al., 2007). Increased frequency of extreme events (bleaching due to elevated sea surface temperature and increasing acidity) in the tropical marine ecosystem would result in the reduction of coral survival. Increased bleaching events and ambiguity in response of reef system to varying level of stress at varying spatial and temporal scales compromised precise reef targeted monitoring and management programs. Indian reef systems with massive bleaching event during 2010 at Andaman and Lakshadweep have hampered the recovery of corals in these regions. Synergetic combination of stressors like SST (Sea Surface Temperature) and UVR (Ultraviolet Radiation) possibly triggers massive bleaching (Munday et al., 2008). Studies from Lakshadweep island also shown that combined influence of SST and UVR can put corals under increased threat and high bleaching possibility. The present work is hence carried out to understand the role of varying atmospheric influences as stressors (SST and UVR) over the Lakshadweep reef

system and its effect on coral reef endurance through a hypothetical investigation on the impact of cloud shading and water vapor positive feedback system.

## 2. Materials and Methods

Benthic surveys to understand the prevalence of stress among coral colonies of Kavaratti and Agatti lagoons (Figure 1) of Lakshadweep archipelago was achieved by establishing belt transects of 50×5 meters and the survey was conducted following the methods of English et al. (1997). A total of 10 permanent survey sites were fixed at each island and observed. Coral colonies were surveyed to identify prominent paling or bleaching which were considered as stressed colonies. Response prevalence or stress prevalence of corals was determined using the following equation,

$$Stress\ prevalence = \frac{Total\ number\ of\ colonies\ under\ stress}{Total\ number\ of\ colonies\ surveyed}$$

Observations on Sea Surface Temperature (SST), Photosynthetically Active Radiation (PAR), cloud fraction and water vapor content were obtained from MODIS aqua 4km satellite data. Ultra Violet Radiation (UVR) observation over the region for the study period was obtained from Total Ozone Mapping Spectrometer (TOMS) of spatial resolution 1º×1.25º and rescaled to 9 km. Pearson correlation analysis were carried out using SPSS ver. 16.0 to understand the influence of climatological variables on coral bleaching.

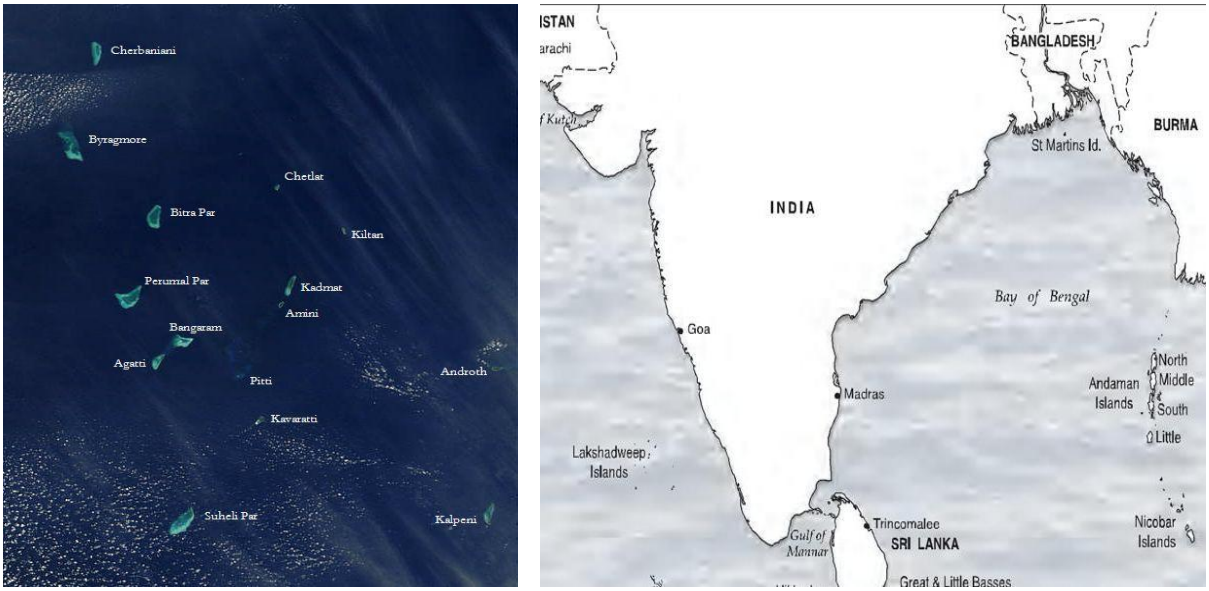


***Figure 1:*** *Map Showing the Study Area Map*

## 3. Results and Discussion

Stress prevalence recorded from Kavaratti and Agatti islands (Figure 2) shows that stress prevalence during 2011 was found lesser than 2010. Stress prevalence at Kavaratti during 2010 was ranged between 37.5% and 80% while it was 8 to 51.5% during 2011. In case of Agatti island, stress prevalence was higher during 2010 when compared with 2011. But the range of stress prevalence at Agatti island illustrated that Agatti was more exposed to stress than Kavaratti island with stress prevalence ranged between 69.2% and 100% during 2010, while it was 38.4% to 71% during 2011.

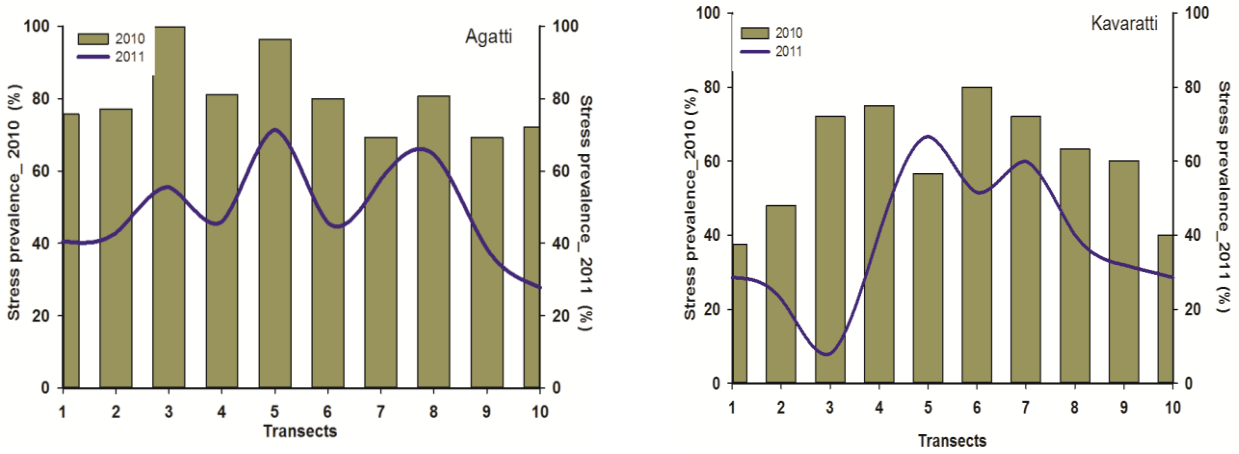


***Figure 2:*** *Stress Response of Corals during 2010 and 2011 at Agatti and Kavaratti Islands*

It is clear from the Figure 3, that impact of these stresses were high in Agatti island when compared to Kavaratti island. SST ranged from 28.7 to 31.5ºC at Kavaratti and 28.7 to 31.6ºC at Agatti.

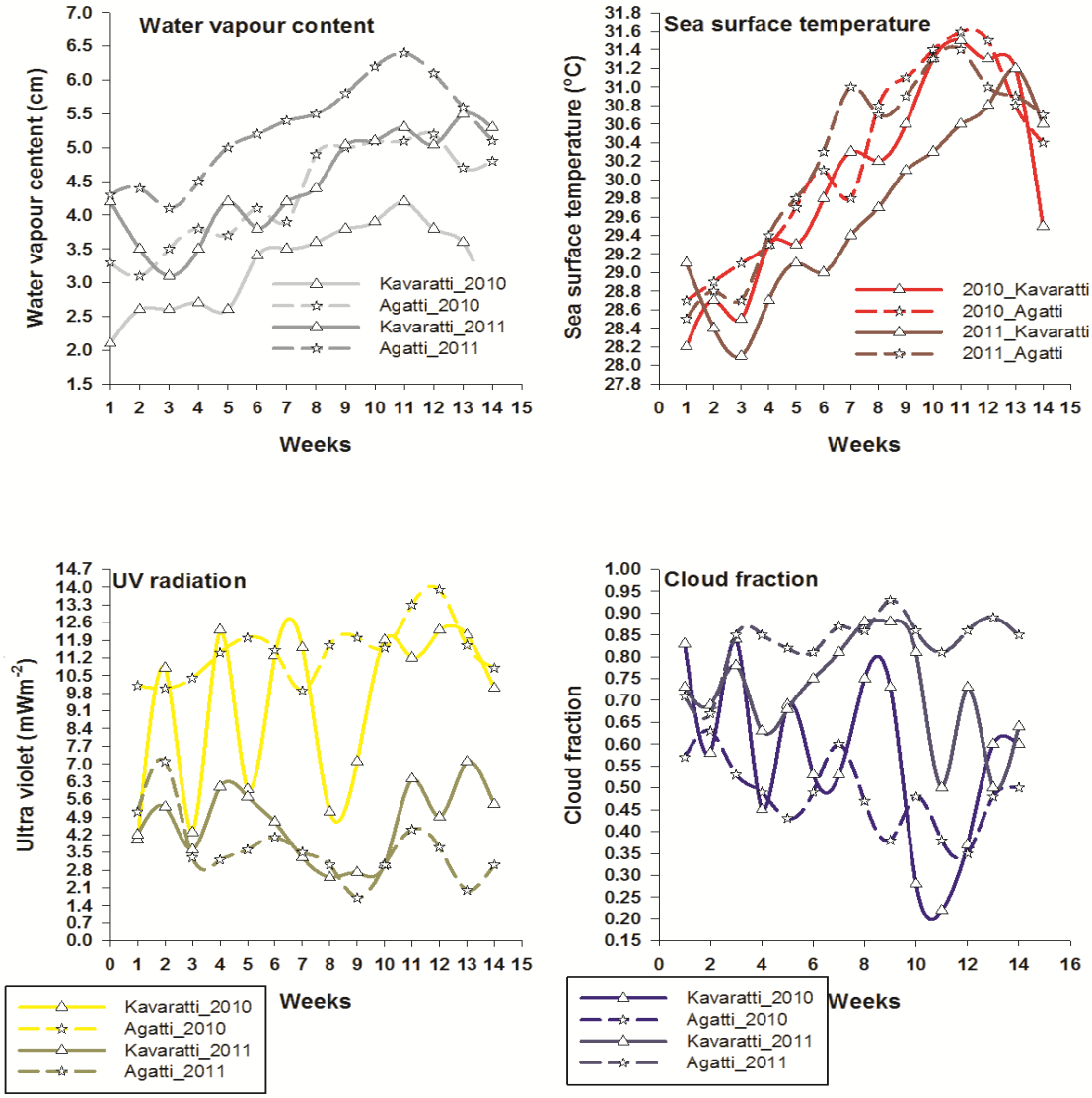


***Figure 3:*** *Pattern of Atmospheric Influences over Lakshadweep Region*

Cloud cover was found higher at Kavaratti (0.2 to 0.8) and lower at Agatti island (0.4 to 0.6). Higher cloud covers increases shading activity and prevents solar radiation to reach the earth's surface and hence results in the reduction of UVR. UVR was found higher in Agatti during the summer weeks ranged from 9.9 to 13.9 $mWm^{-2}$ followed by Kavaratti island (4.3 to 12.3 $mWm^{-2}$). Water vapor content was found higher at Agatti (5.2 to 3.1 cm) followed by Kavaratti island (2.1 to 4.2 cm).

Observations from these climatic variables indicates that corals of Agatti was found to be more threatened with high SST and UVR during 2010 and 2011 when compared with Kavaratti island. This variability in these stressors hence justifies the observed geographical variability in stress prevalence among coral reefs. Highly stressed reef system responds with increasing bleaching and paling rate (Mumby et al., 2008*).* Infinitesimal UVR prevailed over the region during summer 2011 even at high SST pattern might have resulted in the reduced stress prevalence. Integrated impact of stressors in combination has more possibility in triggering bleaching response in coral reefs (Sridhar et al., 2012). Prevalence of UVR was highly reduced by the cloud cover and variability in SST was influenced by water vapor positive feedback than by cloud cover at Lakshadweep. This shows that influence of water vapor feedback over cloud shading theory (Mumby et al., 2001) in the Lakshadweep coral reef system.

Increased water vapor content in atmosphere traps surface reflected and emitted long wave radiations causing a hike in atmospheric temperature and SST at events of low insolation from cloud shading. This observation was highly supported by significant relationship observed between cloud fraction and UVR ($r=-0.936$, $P<0.05$) and water vapor and SST ($r=0.694$, $P<0.05$). However, such significant relationship was not observed between SST and cloud. From the results it is evident that cloud cover and water vapor positive feedback plays a vital role in regulating the environmental stressors of corals in Lakshadweep region. Results have shown that atmospheric influences do have important role in regulating the stresses exerted on corals at spatial and temporal scales. The superior role of water vapor feedback in regulating SST pattern over Lakshadweep region was evident from the present results. This study also endorses the necessity of inclusion of satellite derived atmospheric variables in the art of predicting coral bleaching which can provide more robust predictions.

## 4. Conclusion

Role of water vapor feedback mechanism was recorded as a major control over SST in Lakshadweep when compared to cloud shading. Present work hence validated the importance of satellite derived atmospheric variables in predicting coral bleaching with greater precision.

## Acknowledgement

The authors are grateful to Prof. K. Kathiresan, Director and Dean, and Prof. T. Balasubramanian, former Director and Dean, Centre for Advanced Studies (CAS) in Marine Biology and authorities of Annamalai University for support and encouragement. The authors also thank the National Remote Sensing Centre, Hyderabad, for providing the financial support and DST and DEF of Lakshadweep for logistic support.

## References

Munday, P.L., Jones, G.P., Pratchett, M.S., and Williams, A.J. *Climate Change and the Future for Coral Reef Fishes*. Fish and Fisheries. 2008. 9 (3) 261-285.

Mumby, P.J., Chisholm, J.R.M., Edwards, A.J., Andrefouet, S., and Jaubert, J. *Cloudy Weather May Have Saved Society Islands Reef Corals During the 1998 ENSO Event*. Marine Ecology Progress Series. 2001. 222; 209-216.

Mumby, P.J., Elliott, I.A., Eakin, C.M., Skirving, W., Paris, C.B., Edwards, H.J., Enrıquez, S., Iglesias-Prieto, R., Cherubin, L.M., and Stevens, J.R. *Reserve Design for Uncertain Responses of Coral Reefs to Climate Change*. Ecology Letters. 2011. 14; 132-140.

Hoegh-Guldberg, Mumby, P.J., Hooten, A.J., Steneck, R.S., Greenfield, P., Gomez, E., Harvell, C.D., Sale, P.F., Edwards, A.J., Caldeira, K., Knowlton, N., Eakin, C.M., Iglesias-Prieto, R., Muthiga, N., Bradbury, R.H., Dubi, A., and Hatziolos, M.E. *Coral Reefs Under Rapid Climate Change and Ocean Acidification*. Science. 2007. 318; 1737-1742.

Sridhar, P.N., Ali, M.M., Rao, M.V., and Nagamani, V. *Photosynthetically Active Radiation, a Critical Parameter for Mass Coral Bleaching in the North Indian Ocean*. Current Science. 2012. 102 (1) 114-118.

**Cloud Publications**
International Journal of Advanced Remote Sensing and GIS
2014, Volume 3, Issue 1, pp. 748-768, Article ID Tech-320
ISSN 2320 - 0243

Cloud Publications

**Research Article** **Open Access**

# Diversity and Taxonomic Implication of Angiosperms in Sinai Peninsula as Revealed by Hyperspectral Remote Sensing

**Ghada A. Khdery[1], Usama K. Abdel-Hameed[2], Mohamed A. Aboelghar[1] and Sayed M. Arafat[1]**

[1]Agricultural Applications Department, National Authority for Remote Sensing and Space Sciences, Cairo, Egypt
[2]Botany Department, Ain Shams University, Khalifa El-Maamon St. Cairo, Egypt

Correspondence should be addressed to ghadabotany@yahoo.com

Publication Date: 27 November 2014

Article Link: http://technical.cloud-journals.com/index.php/IJARSG/article/view/Tech-320



**Abstract** Monitoring natural vegetation through remote sensing data in Egypt is just beginning. Only few studies were carried out to monitor Mangrove communities along Red Sea coast. ASD field spectroradiometer was used to measure spectral reflectance in the wavelength ranged from 350 to 2500 nm for 20 species belonging to the following genera *Achillea* (one species), *Aerva* (one species), *Alkanna* (one species), *Asclepias* (one species), *Astragalus* (one species), *Ballota* (one species), *Echinops* (one species), *Fagonia* (one species), *Hyoscyamus* (one species), *Matthiola* (two species), *Origanum* (one species), *Peganum* (one species), *Phlomis* (one species), *Pyrethrum* (one species), *Stachys* (one species), *Teucrium* (one species), *Verbascum* (one species), *Zilla* (one species), *Zygophllum* (one species). Then, hyperspectral reflectance characteristics and Macro/micro-morphological features were investigated. One Way ANOVA (Tukey's HSD Post Hoc Analysis) and Linear Discriminate Analysis were carried out to identify the optimal wavebands and wavelengths to classify the different genera with high pharmaceutical values. It was found that red (550 - 750 nm) and NIR (760 - 1000 nm) spectral zones were the optimal to discriminate the different genera. The specific wavelengths that could be used to isolate each genera were identified. It was found that *Asclepias sinaic*, *Stachys aegyptiaca* and *Verbascum sinaiticum* could be clearly isolated from the rest of the genera with unique spectral characteristics. At the same time, no specific wavelengths were investigated for *Alkanna orientalis* and *Fagonia glutinosa*.
**Keywords** *Hyper Spectral; Natural Vegetation; Anatomy; Sinai Peninsula*

## 1. Introduction

Unique geomorphological formations of south Sinai lead to a wide variation in its climate and vegetation than elsewhere. The most obvious and universal characteristic of desert vegetation is scarcity of plant growth and near lack of trees [1; 2]. The Sinai Peninsula is one of Egypt's most floristically diverse and phytogeographically interesting regions. Many of the plants growing the desert in Sinai are utilized by Bedouin for medicine, food and fodder [3].

The number of species recorded from Sinai was subjected to many changes by various authors *viz* El-Hadidi, [4] who recorded two new species to Egypt, thirty new to Sinai, making a total of 298 species belonging to 53 families; Abdallah *et al*. [5] stated that the flora of the Sinai region preserved in the Flora & Phytotaxonomy & Agriculture Research Center (CAIM) herbarium represented 88 families, 404 genera, 732 species, 16 subspecies and seventy varieties of the native flora of Egypt; A total of 886 species were recorded from Sinai by Danin *et al*. [6]; forty species were recorded for the first time from Sinai in this publication; Danin, [7] stated that there were 28 endemic species in Sinai, of which 25 occurred in the mountainous districts. El-Hadidi, [8] suggested that Sinai has 984 plant species belonging to 465 genera of vascular Cryptogams and flowering plants; he counted 108 species belonging to the Rosales families, with four species new to Sinai: *Astragalus asterias* (Leguminosae), *Lotus halophilus*, *Medicago lupulina* and *Tephrosia purpurea*. Gamal El-Din, [9] collected a total of 114 species of seed plants from Gebel El-Halal in northern Sinai during one season, of which 12 were new records; In his synthesis of the Egyptian flora, Boulos, [10] noted that 1285 taxa had been recorded from Sinai, of which 23 are doubtful records, leaving 1262 including infra specific taxa. There were 33 taxa endemic to Sinai and another four endemic to Sinai and other mainland regions of Egypt; Moustafa & Kamel, [11] listed the species growing in the Saint Katherine Mountains, identifying 221 plant species during their study. Abdou, [12] identified 107 species belonging to 31 families from South Sinai; 12% were considered to be endemic; Aayed *et al.* [13] suggested that Sinai contains approximately 1285 species, with South Sinai supporting 800, including 34 endemics; 62% were estimated as being rare or very rare; Gazara *et al.* [14] recorded 154 species from Sinai representing 32 families, with 48 rare, four endemic and 13 medicinal species contributing about 8.4% of the total recorded from Gebel El-Halal. Sinai Peninsula represents one of the most important centers of medicinal plants in the Arabian deserts [15]. Environmental conditions and human impacts have a significant influence on diversity and distribution of threatened, endemic, and medicinal plants in Sinai [16-18].

Remote sensing is an essential tool in the real-time identification of crops [19-22]. The tools for vegetation remote sensing have developed considerably in the past decades [23]. Developments in hyperspectral remote sensing have provided more accurate information on structural, biochemical and physiological properties of vegetation [24]. Most of the work on hyperspectral remote sensing of biophysical and biochemical parameters has been achieved through the development of new hyperspectral indices [25-28]. Hyperspectral data can provide significant improvements in spectral information content when compared with broad bands for detecting plant stress [27-29]; measuring chlorophyll content of plants [30]; identifying small differences in percent green vegetation cover [31]; extracting biochemical variables such as nitrogen and lignin [32]; discriminating land cover (LC) types [33], crop moisture variations [34-35], and leaf pigment concentrations (30); modeling quantitative biophysical and yield characteristics of agricultural crops [36]; improving detection changes in sparse vegetation [37; 38]; and assessing absolute water content in plant leaves [39]. In recent years, advances have been made in classifying vegetation using optimal spatial resolutions [40], red-edge first derivatives and green peak statistical indices [41]. The spectral signatures of features obtained are used as end members in hyperspectral classifications [42]. Also, it may help to improve the accuracy of supervised classification through machine learning process. [43].

## 2. Study Area

The Sinai lies in the arid belt of North Africa and belongs to the Saharan Mediterranean area with a true desert climate [44; 45]. The Saint Katherine region is situated in the southern Sinai and is part of the upper Sinai massif [45]. It is located between 33°55' to 34°30' East and 28°30' to 28°35' North (Figure 1). Elevation ranges from 1300 to 8530 ft. This region is characterized by outcrops of smooth granite uplifted to form several mountain peaks (e.g.: Gebel Katherine 2642 m and Gebel Musa 2285 m) [48]. The study area includes Wadi Al Arbaeen that is located between 33°56'60" East and 28°33'5" North and Wadi EL Sal that is located between 34°12'0" East and 28°44'0" North (Figure 1).

The Saint Katherine region contains a wide range of habitats and landscapes that are a consequence of varying climatic conditions, a wide range of altitudes, and variable topography. This region is characterized by outcrops of smooth granite uplifted to form several mountain peaks [46]. Because of these different conditions of temperature and humidity, there is a high level of biodiversity, particularly in the high altitude mountain area, which has the highest proportion of endemism in Egypt [47].

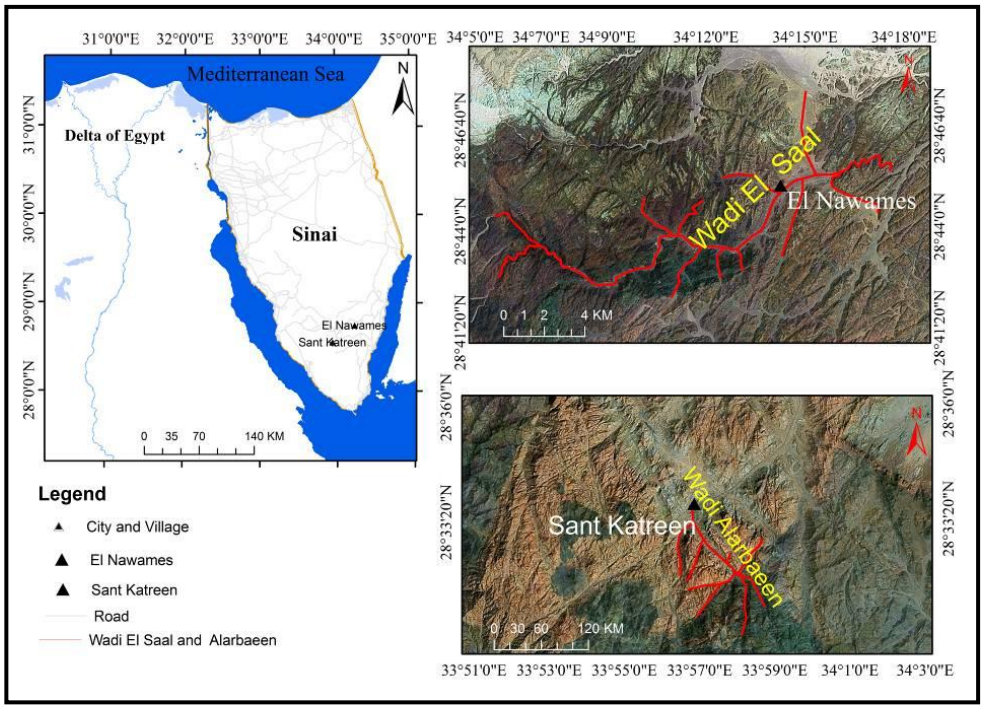


***Figure 1:*** *Location of Study Area*

## 2.1. Material and Methods

The present study comprised 20 taxa grown in South Sinai, Sinai Peninsula, Egypt, representing 20 species belonging to 19 genus. Plant materials were kindly supplied by two wadies of Saint Catherine as indicated in Table 1.

Identification and nomenclature of the wild Egyptian species follows Täckholm, [48] and Boulos, [49], Voucher specimens were kept at (CAIA) Herbarium of Botany Department, Faculty of Science, Ain Shams University, Cairo, Egypt.

***Table 1:*** *The Studied Taxa and Their Sources*

| No. | Taxa | Source | Date of Collection |
|---|---|---|---|
| 1. | *Achillea fragrantissima* Sch.Bip. -- Flora 38: 13. 1855 (IK) | Wadi Al Arbaeen | 16-12-2012 |
| 2. | Aerva tomentosa *Forssk. -- Fl. Aegypt.-Arab. p. cxxii. 170; Lam. Encyc. i. 46. (IK)* = Aerva javanica (Burm. f.) Juss. ex Schult. | Wadi EL Sal | 16-12-2012 |
| 3. | *Alkanna orientalis* Boiss. -- Diagn. Pl. Orient. ser. 1, 4: 46. 1844 [Jun 1844] (IK) ≡*Anchusa orientalis L. (basionym)* | Wadi Al Arbaeen | 20-5-2012<br>16-12-2012<br>10-4-2013 |
| 4. | *Asclepias sinaica* Muschl. -- Man. Fl. Egypt ii. 753 (1912). (IK) = Gomphocarpus *sinaicus Boiss.* | Wadi Al Arbaeen | 20-5-2012<br>16-12-2012 |
| 5. | *Astragalus sieberi* DC. -- Prodr. [A. P. de Candolle] 2: 295. 1825 [mid Nov 1825] (IK) | Wadi EL Sal | 10-4-2013 |

| | | | |
|---|---|---|---|
| 6. | *Ballota kaiseri* V.Tackh. -- Svensk Bot. Tidskr. 1932, xxvi. 378. (IK) | Wadi Al Arbaeen | 16-12-2012<br>10-4-2013 |
| 7. | *Echinops spinosus* L. -- Mant. Pl. 119. 1767 [15-31 Oct 1767] (IK)<br>*= Echinops spinosus Sm. In Sibth. & Sm.,*<br>*= Echinops viscosus DC.,*<br>*= Echinops creticus Boiss. & Heldr. in Boiss.* | Wadi Al Arbaeen | 10-4-2013 |
| 8. | *Fagonia glutinosa* Delile -- Fl. Egypte 230. t. 28. f. 2. (IK)<br>*= Fagonia glutinosa Delile*<br>*var. grandiflora Boiss.*<br>*= =Fagonia glutinosa Delile var. nuda Hadidi* | Wadi EL Sal | 17-12-2012 |
| 9. | *Hyoscyamus muticus* L. -- Mant. Pl. 45. 1767 [15-31 Oct 1767] (IK) | Wadi EL Sal | 17-12-2012 |
| 10. | *Matthiola arabica* Boiss. -- Ann. Sci. Nat., Bot. sér. 2, 17: 49. 1842 (IK)<br>*=Matthiola arabica Velen.* | Wadi Al Arbaeen | 20-5-2012<br>16-12-2012 |
| 11. | *atthiola longipetala* (Vent.) DC. -- Regni Vegetabilis Systema Naturale 2 1821 (APNI)<br>*= Cheiranthus longipetalus Vent. (synonym)*<br>*=Matthiola oxyceras DC.* | Wadi Al Arbaeen | 16-12-2012 |
| 12. | *Origanum syriacum* L. -- Sp. Pl. 2: 590. 1753 [1 May 1753] (IK)<br>*= Origanum maru L.*<br>*= Majorana crassifolia Benth.* | Wadi EL Sal | 17-12-2012<br>10-4-2013 |
| 13. | *Peganum harmala* L. -- Sp. Pl. 1: 444. 1753 [1 May 1753] (IK) | Wadi Al Arbaeen | 20-5-2012<br>10-4-2013 |
| 14. | *Phlomis aurea* Decne. -- Ann. Sci. Nat., Bot. sér. 2, 2: 251. 1834 (IK) | Wadi Al Arbaeen | 16-12-2012<br>10-4-2013 |
| 15. | *Pyrethrum santolinoides* Dc. - Ann. Sci. Nat., Bot. sér. 2, 2: 264. 1834 (IK)<br>*= Tanacetum sinaicum (Fresen.) Delile ex Bremer & Humphries.*<br>*=Santolina sinaica Fresen.* | Wadi Al Arbaeen | 10-4-2013 |
| 16. | *Stachys aegyptiaca* Pers. -- Syn. Pl. [Persoon] 2(1): 124. 1806 [Nov 1806] (IK) | Wadi EL Sal | 17-12-2012 |
| 17. | *Teucrium polium* L. -- Sp. Pl. 2: 566. 1753 [1 May 1753] (IK) | Wadi Al Arbaeen | 20-5-2012<br>16-12-2012<br>10-4-2013 |
| 18. | *Verbascum sinaiticum* Benth. -- Prodr. [A. P. de Candolle] 10: 236. 1846 [8 Apr 1846] (IK) | Wadi Al Arbaeen | 20-5-2012<br>16-12-2012 |
| 19. | *Zilla spinosa* Prantl -- Nat. Pflanzenfam. [Engler & Prantl] iii. 2 (1891) 175. (IK)<br>*=Bunias spinosa L.*<br>*=Zilla microcarpa (DC.) Vis.* | Wadi EL Sal | 17-12-2012<br>10-4-2013 |
| 20. | *Zygophyllum simplex* L. -- Mant. Pl. 68. 1767 [15-31 Oct 1767] (IK)<br>*=Zygophyllum portulacoides Forssk.* | Wadi EL Sal | 10-4-2013 |

### 2.2. Macro & Micromorphlogical Attributes

Morphological description of the whole plant was made from the investigated living specimens or compiled from literature. Stem parts were collected and a portion of the middle lamina; including the midrib was cut from the mid. Cuttings were fixed in FAA and stored in 70% ethanol until use. Stems and lamina sections were prepared using hand microtome at 10-20µm; double stained using safranine and light green; mounted in Canada Balsam [50]; inspected by light microscope; photographed using a Reichert Microstar IV microscope at the Plant Taxonomy Research Laboratory, Botany Department, Faculty of Science, Ain Shams University, Cairo, Egypt. Cumulative plates and tables were prepared

to investigate the collected data. Terminology of Eames, [51] and Koller & Rost, [52] was used to describe the anatomical features.

## 2.3. Statistical Analysis of Hyperspectral Data

### 2.3.1. *One Way ANOVA and Tukey's HSD Post Hoc Analysis*

Spectral zones that represent the atmospheric windows (portions of the electromagnetic reflectance that include data noise because of the relative air humidity) were removed. Spectral pattern of each measured sample was identified. Generally, spectral reflectance could be divided into six different spectral portions as follows: blue (350 - 440 nm), green (450 - 540 nm), red (550 - 750 nm), NIR (760 - 1000 nm), SWIR I (1010 - 1775 nm) and SWIR II (2055 - 2315 nm).

***Table 2:*** *The ASD Field Spec 3 Specifications*

| | |
|---|---|
| **Spectral Range** | 350 - 2500 nm |
| **Spectral Resolution** | 3:700 nm<br>8.5:1400 nm |
| **Sampling Interval** | 6.5:2100 nm<br>1.4:350 - 1050 nm<br>2:1000 - 2500 nm |

### 2.3.2. *Comparing Standard Deviations from Several Populations*

Analysis of variance (ANOVA) methods are presented throughout this text, for comparing means from several populations or processes. While similar methods are occasionally used for comparing several standard deviations, often using the natural logarithm of sample variances as the response variable, they are not a main focal point of this text. There are also a number of alternative procedures that are not based on ANOVA methods that can be used to compare standard deviations. Two of these are described below. Both are highly sensitive to departures from the assumption of normality; consequently, they should be used only after verification that the assumption of normally distributed errors is reasonable. When using ANOVA models with data from designed experiments, a valuable assessment of the assumption of constant standard deviations across k factor-level combinations is given by the F-max test. The F-max test is used to test the hypotheses [53] (Equation (1)).

$$F_{\max} = \left( \frac{\max(s_i)}{\min(s_i)} \right)^2 \qquad (1)$$

### 2.3.3. *Multiple Comparisons*

The F-statistics in an ANOVA table provide the primary source of information on statistically significant factor effects. However, after an F-test in an ANOVA table has shown significance, an experiment usually desires to conduct further analyses to determine which pairs or groups of means are significantly different from one another [53].

### 2.3.4. *Tukey's Significant Difference Procedure*

Tukey's procedure controls the experiment wise error rate for multiple comparisons when all averages are based on the same number of observations. The stated experiment wise error rate is very close to the correct value even when the sample sizes are not equal. The technique is similar to Fisher's LSD procedure. It differs in that the critical value used in the TSD formula is the upper 100$\alpha$% point for the difference between the large stand smallest of $k$ averages. This difference is the range of the $k$

averages, and the critical point is obtained from the distribution of the range statistic, not from the *t*-distribution (Equation (2)).

Two averages $y_i$ and $y_j$, based on $i$ and $n_i$ observations respectively, are significantly different if

$$\left|\overline{y}_i - \overline{y}_j\right| > TSD$$

Where

$$TSD = q(a;k,v)\left(MS_E \frac{n_i^{-1} + n_j^{-1}}{2}\right)^{1/2} \qquad (2)$$

### 2.3.5. *Linear Discriminate Analysis*

Linear Discriminate Analysis (LDA) is a method to discriminate between two or more groups of samples. The groups to be discriminated can be defined either naturally by the problem under investigation, or by some preceding analysis, such as a cluster analysis. The number of groups is not restricted to two, although the discrimination between two groups is the most common approach. Linear Discrimination Analysis (LDA) is a commonly used technique for data classification. LDA approach is explained by [21]. It easily handles the case where the within-class frequencies are unequal and their performance has been examined on randomly generated test data. This method maximizes the ratio of between-class variance to the within-class variance in any particular data set thereby guaranteeing maximal separability. LDA doesn't change the location but only tries to provide more class separability and draw a decision region between the given classes. This method also helps to better understand the distribution of the feature data. In the current study, Class-independent transformation type of LDA was performed. This approach involves maximizing the ratio of overall variance to within class variance. It uses only one optimizing criterion to transform the data sets and hence all data points irrespective of their class identity are transformed using this transform. In this type of LDA, each class is considered as a separate class against other classes. In LDA, within-class and between- class scatter are used to formulate criteria for class separability. Within-class scatter is the expected covariance of each of the classes. The scatter measures are computed using Equations (3) and (4).

$$Sw = \sum_j Pj \times \left(\mathrm{cov}_j\right) \qquad (3)$$

Therefore, for the two-class problem,

$$Sw = 0.5 \times \mathrm{cov}_1 + 0.5 \times \mathrm{cov}_2 \qquad (4)$$

All the covariance matrices are symmetric. Let and be the covariance of set 1 and set 2 respectively. Covariance matrix is computed using the following Equation (5).

$$\mathrm{cov}\, j = \left(x_j - \mu_j\right)\left(x_j - \mu_j\right)^{\mathrm{T}} \qquad (5)$$

Then, the between-class scatters computes using the following Equation (6).

$$Sb = \sum_j \left(\mu_j - \mu_3\right) \times \left(\mu_j - \mu_3\right)^{\mathrm{T}} \qquad (6)$$

Sb can be thought of as the covariance of data set whose members are the mean vectors of each class. As defined earlier, the optimizing criterion in LDA is the ratio of between-class scatter to the within-class scatter. The solution obtained by maximizing this criterion defines the axes of the transformed space. As LDA is a class independent type in this study, the optimizing criterion is computed as Equation (7)

$$\text{criterion} = inv(sw) \times Sb \qquad (7)$$

Finally, transforming the entire data set to one axis provides definite boundaries to classify the data. The decision region in the transformed space is a solid line separating the transformed data sets thus Equation (8)

$$\text{transforme\_set} = \text{transform\_spec}^{T} \times \text{data\_set}^{T} \qquad (8)$$

This analysis was carried out to discriminate between twenty species of plant.

## 3. Results and Discussion

### 3.1. Morphological Characters

In the present part, the different macromorphological characters of the studied taxa are presented in cumulative tables in order to facilitate deducing the most important diagnostic characters. Habit shrub in nine taxa, Sub shrubs in *Ballota kaiseri*, *Origanum syriacum* and *Teucrium polium*, or herb in the remaining studied taxa; Stem branching unbranched in *Hyoscyamus muticus* & *Pyrethrum santolinoides* or branched in eighteen taxa; Leaf arrangement alternate in nine taxa, alternate/ spirally rosette in *Hyoscyamus muticus* & *Verbascum sinaiticum* or opposite in the remainings; Leaf composition simple in thirteen taxa, pinnately compound in *Astragalus sieberi*, *Echinops spinosus*, *Matthiola longipetala* & *Pyrethrum santolinoides* & *Origanum syriacum*, trifoliolate in *Fagonia glutinosa* or dissected twice or more in *Peganum harmala*; shape of blade oblong-lanceolate in *Achillea fragrantissima* & *Alkanna orientalis*, linear to narrow-ovate in *Aerva tomentosa*, linear-lanceolate in *Asclepias sinaica*, *Matthiola longipetala*, *Matthiola arabica & Peganum harmala*, lanceolate in *Astragalus sieberi*, crenate-denate in *Ballota kaiseri*, ovate in *Echinops spinosus*, oblong-ovate to rhombic in *Fagonia glutinosa*, elliptical to ovate *Hyoscyamus muticus*, oblong-ovate in *Origanum syriacum*, linear in *Phlomis aurea*, oblong – elliptic in *Pyrethrum santolinoides*, oblong-lanceolate to elliptic in *Stachys aegyptiaca*, oblong – linear in *Teucrium polium*, elliptic in *Verbascum sinaiticum*, oblanceolate in *Zilla spinosa* or oblong- cylindric in *Zygophllum simplex*; Apex of blade rounded in *Achillea fragrantissima*, acute in eight taxa, acuminate in *Astragalus sieberi*, *Astragalus sieberi*, *Fagonia glutinosa* and *Hyoscyamus muticus*, obtuse in *Matthiola arabica, Origanum syriacum* and *Pyrethrum santolinoides* and *Stachys aegyptiaca*, subacute to obtuse in *Matthiola longipetala*, cuspidate in *Verbascum sinaiticum* or Subacute in *Teucrium polium*; Colour of blade white to greyish-green in *Achillea fragrantissima*, bluish-green to whitish-hairy in *Aerva tomentosa*, grey–green in *Alkanna orientalis*, greenish-yellow in *Asclepias sinaica*, green in six taxa, grayish green in *Astragalus sieberi*, pale green in *Fagonia glutinosa*, greyish-white in *Matthiola arabica* bright green in *peganum harmala*, olive or silver-green in *Phlomis aurea*, Mid-green in *Stachys aegyptiaca*, white in *Teucrium polium*, yellowish-green in *Verbascum sinaiticum*, gray-green in *Zilla spinosa* or yellowish-green in *Zygophyllum simplex*; Margin of blade dentate in *Achillea fragrantissima*, entire in thirteen taxa, undulate in *Alkanna orientalis* & *Matthiola longipetala*, revolute in *Asclepias sinaica*, serrate in *Astragalus sieberi* or scarious in *Matthiola arabica* & *Pyrethrum santolinoides*; Petiole detection petiolate in all taxa. This is in agreement with [54; 55; 44; 56-70].

Inflorescence position terminal in fourteen taxa, solitary axillary in *Fagonia glutinosa*, *Hyoscyamus muticus*, *Pyrethrum santolinoides* & *Teucrium polium* & *Zygophllum simplex* or Solitary in *Zilla spinosa*; Panicle in five taxa, cyme umbellate in *Asclepias sinaica*, raceme in six taxa, spike in *Ballota kaiseri* &

*Stachys aegyptiaca*, cymose in *Fagonia glutinosa*, *Peganum harmala* & *Zygophllum simplex*, paniculate in *Matthiola arabica*, *Matthiola* & *longipetala* or corymbose in *Pyrethrum santolinoides*; Number of flowers / inflorescence few in ten taxa or many in the rest of the studied taxa; Flower unisexual in *Achillea fragrantissima* & *Aerva tomentosa* or bisexual in the remaining studied taxa; Subsessile in *Matthiola longipetala* or sessile in the remaining studied taxa; Zygomorphic in nine taxa or actinomorphic in remaining studied taxa; sepals four in *Matthiola arabica*, *Matthiola longipetala*, *Origanum syriacum*, *Peganum harmala* & *Zilla spinosa* or five in the remaining taxa under investigation; Sepal shape tubular in six taxa, ovate in *Aerva tomentosa* & *Asclepias sinaica*, funnel in *Alkanna orientalis*, ovate–oblong in *Fagonia glutinosa*, tubular-campanulate in *Hyoscyamus muticus*, linear to oblong in *Matthiola arabica*, oblong in *Matthiola longipetala* & *Zilla spinosa*, obovate–oblong in *Peganum harmala*, slender in *Pyrethrum santolinoides*, triangular in *Stachys aegyptiaca*, bell-shaped in *Teucrium polium*, linear-oblong to elliptic in *Verbascum sinaiticum* and elliptic-oblong in *Zygophyllum simplex*; Cohesion of sepals polysepalous in eight taxa or gamosepalous in remaining taxa under investigation; Corolla colour yellow in seven taxa, white in *Aerva tomentosa*, *Origanum syriacu*m, *Stachys aegyptiaca* & *Teucrium polium*, pale yellow in *Astragalus sieberi*, Purple White in *Ballota kaiseri*, purplish-pink in *Fagonia glutinosa* & *Matthiola arabica*, white to pink with dark violet veins or spots in *Hyoscyamus muticus*, Purple to white in *Matthiola longipetala*, yellowish white in *Peganum harmala*, Light violet in *Zilla spinosa* or yellowish in *Zygophyllum simplex*; Petal shape tubular in 6 taxa, oblong-obovate in *Aerva tomentosa* and *Peganum harmala*, funnel in *Alkanna orientalis* & *Hyoscyamus muticus*, valvate in *Asclepias sinaica*, papilionaceous in *Astragalus sieberi*, limb in *Echinops spinosus* & *Phlomis aurea*, spathulate in *Fagonia glutinosa*, linear to oblong-obovate in *Matthiola arabica*, oblong to linear in *Matthiola longipetala*, cylindric in *Pyrethrum santolinoides*, Cupulate in *Verbascum sinaiticum* or elliptic or pathulate in *Zygophyllum simplex*; number of petals are five in all the taxa under investigation except *Aerva tomentosa* (two petals) or *Matthiola longipetala* & *Zilla spinosa* (4 tepals); Cohesion of petals polysepalous in seven taxa or gamosepalous in remaining taxa under investigation; number of stamens five in seven taxa, ten in *Astragalus sieberi*, *Zygophyllum simplex* & *Fagonia glutinosa*, four stamens in six taxa, two stamens in *Echinops spinosus*, six stamens in *Matthiola arabica* & *Zilla spinosa* or fifteen in *Peganum harmala*; Direction of anther absent in *Aerva tomentosa*, introse in nine taxa or extrose in remaining taxa under investigation; Ovary position inferior in seven taxa or superior in remaining taxa under investigation; Ovary setting subsessile in *Achillea fragrantissima*, *Matthiola arabica* & *Matthiola longipetala* or sessile in the rest of the studied taxa; Ovules (no/locule) one ovules in eight taxa, five ovules in *Asclepias sinaica*, *Ballota kaiseri* & *Fagonia glutinosa*, two ovules in seven taxa, three ovules in *Matthiola arabica* or four ovules in *Zygophyllum simplex*; Stigma form capitate in seven taxa, filiform in *Aerva tomentosa* & *Teucrium polium*, Papillate in *Alkanna orientalis*, *Asclepias sinaica*, *Ballota kaiseri*, *Origanum syriacum*, *Phlomis aurea* & *Teucrium polium*, terminal or penicillate in *Astragalus sieberi*, subcapitate in *Hyoscyamus muticus*, obconical in *Pyrethrum santolinoides*, spherical in *Verbascum sinaiticum* or globose in *Zygophyllum simplex*; Fruit type achene in *Achillea fragrantissima*, *Alkanna orientalis, Echinops spinosus* & *Pyrethrum santolinoides*, capsule in eight taxa, berry *Asclepias sinaica*, legume *Astragalus sieberi* or schizocarp in six taxa; colour yellow in six taxa; white in *Aerva tomentosa*, *Echinops spinosus*, bright red in *Alkanna orientalis*, black or brown in *Astragalus sieberi*; viola in *Ballota kaiseri*, brownish in *Hyoscyamus muticus*, purple to pink in *Matthiola arabica*, purple to white in *Matthiola longipetala* Pale green in *Origanum syriacum*, orange-brown in *Peganum harmala*, violet in *Phlomis aurea*, brown to black in *Stachys aegyptiaca*, light-brown to dark brown in *Teucrium polium* or green in *Zilla spinosa*; dehiscence indehiscent in six taxa or dehiscent in remaining taxa under investigation; Shape of fruit oblong to ovoid in *Achillea fragrantissima*, *Ballota kaiseri*, *Origanum syriacum*, *Stachys aegyptiaca* & *Teucrium polium*, subglobose in *Aerva tomentosa* & *Zilla spinosa*, ovoid in *Alkanna orientalis* & *Zygophyllum simplex*, spherical in *Asclepias sinaica*, ovoid-elliptic in *Astragalus sieberi*, elongate in *Echinops spinosus*, *globose* in *Fagonia glutinosa*, *Hyoscyamus muticus* & *Peganum harmala*, glabrous in *Matthiola arabica*, *Matthiola longipetala* & *Phlomis aurea*, elliptic to subglobose in *Verbascum sinaiticum* or subglobose in *Zilla spinosa*. This is in agreement with [70; 44; 61; 58-60, 62-64; 54-55; 65-67; 56].

### 3.2. Anatomical Characters

Stem out-line terete in 10 taxa, quadrangular in *Ballota kaiseri*, angular in *Echinops spinosus*, *Fagonia glutinosa*, *Hyoscyamus muticus*, *Matthiola arabica* & *Matthiola longipetala* or square in *Origanum syriacum*, *Phlomis aurea*, *Pyrethrum santolinoides* & *Stachys aegyptiaca*; Eglandular trichomes unicellular, unbranched in nine taxa, multicellular- branched in *Aerva tomentosa*, *Matthiola longipetala*, *Phlomis aurea*, *Pyrethrum santolinoides* & *Stachys aegyptiaca*, unicellular & multicellular- unbranched in *Astragalus sieberi* & *Zilla spinos*a, unicellular – unbranched & multicellular - branched in *Ballota kaiseri* & *Matthiola arabica* or absent in the *Echinops spinosus* & *Peganum harmala*; Glandular trichomes are unicellular head & unicellular stalk in seven taxa, unicellular head & multicellular stalk in *Matthiola longipetala*, *Phlomis aurea* and *Teucrium polium* or absent in the rest of the studied taxa; Cuticle thick in eight taxa or thin in the rest of the studied taxa; subepidermal periderm present in *Aerva tomentosa* or absent in the rest of the studied taxa; Hypodermis present in *Ballota kaiseri*, *Echinops spinosus* & *Peganum harmala* or absent the rest of the studied taxa; Epidermal cells shape barrel to papillose in *Achillea fragrantissima*, tangentially in *Aerva tomentosa*, *Matthiola longipetala* & *Origanum syriacum*, radially in six taxa, barrel in *Asclepias sinaica*, *Phlomis aurea*, *Pyrethrum santolinoides* & *Verbascum sinaiticum*, tangentially elongated in *Ballota kaiseri*, *Fagonia glutinosa* & *Zygophyllum simplex*, papillose in *Echinops spinosus* and *Stachys aegyptiaca* or rectangular in *Teucrium polium*; Parenchyma rows in ground tissue one row in *Achillea fragrantissima*, two rows in *Aerva tomentosa & Matthiola arabica*, 2-3 rows in *Alkanna orientalis* & *Asclepias sinaica*, 4-5 rows in eight taxa, 1-2 rows in *Ballota kaiseri* & *Matthiola longipetala*, 3-4 rows in *Echinops spinosus*, *Stachys aegyptiaca* & *Zilla spinosa*, 5-6 rows in *Peganum harmala* & *Hyoscyamus muticus*; Chlorenchyma tissue 3-4 rows in *Achillea fragrantissima*, *Stachys aegyptiaca* & *Zilla spinosa*; absent in *Aerva tomentosa*, *Alkanna orientalis* & *Origanum syriacum*, 2-3 rows in six taxa; 4-5 in *Echinops spinosus* & *Matthiola arabica*, 2 rows in *Fagonia glutinosa*, *Pyrethrum santolinoides*, 3 rows in *Hyoscyamus muticus*, 1-2 in *Matthiola longipetala* or 5-6 in *Zygophyllum simplex*; Collechyma tissue angular & Lamellar in *Achillea fragrantissima*, *Phlomis aurea* & *Stachys aegyptiaca*; absent in *Aerva tomentosa*, *Astragalus sieberi*, *Matthiola longipetala*, *Zilla spinosa* & *Zygophllum simplex* or angular in the remaining studied taxa; Sclerenchyma tissue absent in *Matthiola longipetala* & *Origanum syriacum* or present in the remaining studied taxa; Pith width narrow in six taxa and wide in the remaining studied taxa; type of cells in pith lignified in ten taxa or thin in the remaining studied taxa; Aspect in fascicular region are separated strands in *Aerva tomentosa* or continuous strands in the remaining taxa under investigation; Rays in fascicular region, uniseriate in *Asclepias sinaica* or absent in the remaining studied taxa; Xylem contents in inter fascicular region fibers & vessels in fourteen taxa or fibers in six taxa; Rays in inter fascicular region uiseriate in *Achillea fragrantissima*, *Aerva tomentosa*, *Asclepias sinaica*, *Hyoscyamus muticus* & *Zygophllum simplex* or absent in the remaining studied taxa; Cambium absent in *Peganum harmala* or present in the remaining studied taxa; Crystals druces in 12 taxa; Raphides in six taxa, absent in *Matthiola arabica* or raphides & druses in *Origanum syriacum*.

Leaf outline in T.S flattened adaxially in *Achillea fragrantissima*, *Fagonia glutinosa* & *Matthiola longipetala*, raised adaxially in six taxa, depressed adaxially in nine taxa or v shape in *Echinops spinosus*; Eglandular trichomes absent in five taxa, multicellular-unbranched in *Aerva tomentosa*, *Asclepias sinaica* & *Teucrium polium*, uni & multicellular, unbranched in *Alkanna orientalis* & *Astragalus sieberi*, unicellular-unbranched & multicellular-branched in *Ballota kaiseri*, unicellular & unbranched in *Matthiola arabica*, *Fagonia glutinosa, Zygophyllum simplex* & *Origanum syriacum* or multicellular-branched in *Hyoscyamus muticus*, *Phlomis aurea*, *Stachys aegyptiaca* & *Verbascum sinaiticum*; Glandular trichomes absent in ten taxa, unicellular head & multicellular stalk in *Alkanna orientalis*, *Matthiola longipetala*, *Phlomis aurea* & *Teucrium polium*, multicellular head with uni & biseriate stalk in *fagonia glutinosa*, multicellular head & multicellular stalk in *Hyoscyamus muticus* & *Matthiola arabica*, unicellular head & unicellular stalk in *Origanum syriacum* or unicellular head-unicellular stalk & unicellular head, bi cellular stalk in *Stachys aegyptiaca*; Cuticle thin in twelve taxa and thick in seven taxa; Shape of epidermal cells tangentially in *Achillea fragrantissima*, *Origanum*

*syriacum* & *Peganum harmala*, barrel in *Aerva tomentosa*, *Alkanna orientalis*, *Matthiola longipetala* & *Teucrium polium*, tangentially radially in *Asclepias sinaica*, tangentially elongated *Astragalus sieberi* & *Fagonia glutinosa*, papillose in *Ballota kaiseri*, tangentially elongated to papillose in *Echinops spinosus*, radially in *Hyoscyamus muticus*, *Verbascum sinaiticum* & *Zilla spinosa*, oblong-ovoid in *Matthiola Arabica* & *Zygophyllum simplex* or radially elongated in *Phlomis aurea* & *Stachys aegyptiaca*; Type of mesophyll tissue isobilateral in ten taxa or dorsiventral in nine taxa; Palisade rows number two rows in six taxa or one rows in the remaining studied taxa; Palisade extended at mid rib region present in seven taxa or absent in the remaining studied taxa; Collenchyma in ground tissue absent in *Aerva tomentosa*, *Matthiola longipetala*, *Matthiola arabica* & *Fagonia glutinosa*, angular in *Hyoscyamus muticus*, lamellar in *Stachys aegyptiaca* or annular in the remaining studied taxa; parenchyma in ground tissue 4-5 rows in *Achillea fragrantissima*, *Asclepias sinaica*, *Astragalus sieberi*, *Peganum harmala* & *Phlomis aurea*; 3-4 rows in *Aerva tomentosa*, *Alkanna orientalis* & *Ballota kaiseri*, 1-2 rows in *Echinops spinosus*, *Matthiola arabica* & *Matthiola longipetala*, 2 rows in *Origanum syriacum*, 2-3 rows in six taxa, 5-6 rows in *Hyoscyamus muticus*; Aspect shape in vascular tissue centric single in nine taxa or crescent form in ten taxa; Crystal raphides in *Ballota kaiseri*; absent in *Astragalus sieberi* or druces in eighteen taxa; stomata present in lower epidermis in six taxa, stomata absent in *Pyrethrum santolinoides*, *Stachys aegyptiaca* & *Zygophyllum simplex* or present in lower and upper epidermis in ten taxa. This is in accordance with [71-75; 70; 76] (Figure 2a and b).

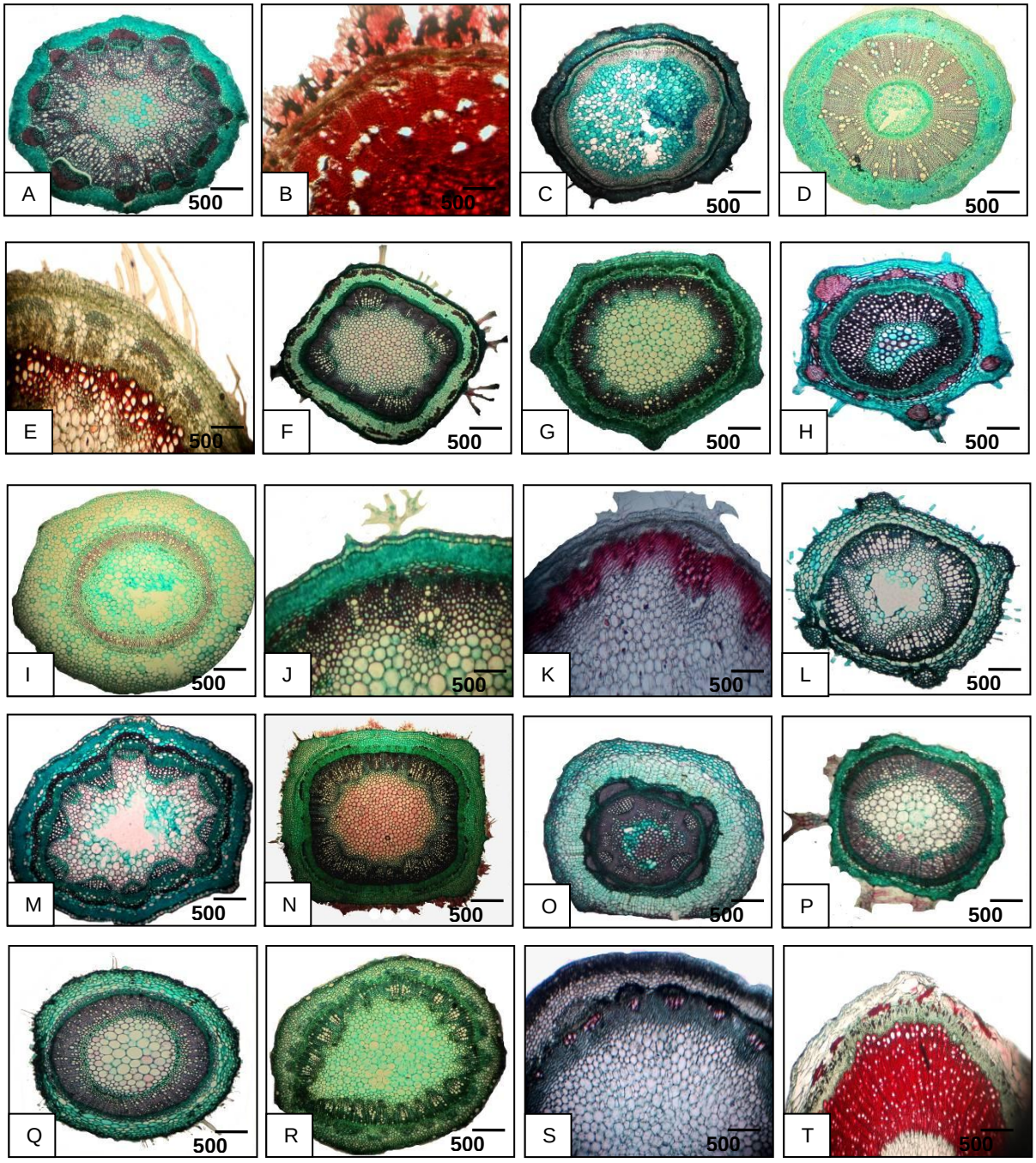


***Figure 2a:*** *Macro and Microphotographs Analysis*
*Stem Anatomy (A) Achillea Fragrantissima (B) Aerva Tomentosa (C) Alkanna Orientalis (D) Asclepias Sinaica (E) Astragalus Sieberi (F) Ballota Kaiseri (F) Echinops Spinosus (G) Fagonia Glutinosa (H) Hyoscyamus Muticus (I) Matthiola Arabica (J) Matthiola Longipetala (K) Origanum Syriacum (L) Peganum Harmala (M) Phlomis Aurea (N) Pyrethrum Santolinoides (O) Pyrethrum Santolinoides (P) Stachys Aegyptiaca (Q) Teucrium Polium (R) Verbascum Sinaiticum (S) Zilla Spinosa (T) Zygophyllum Simplex*

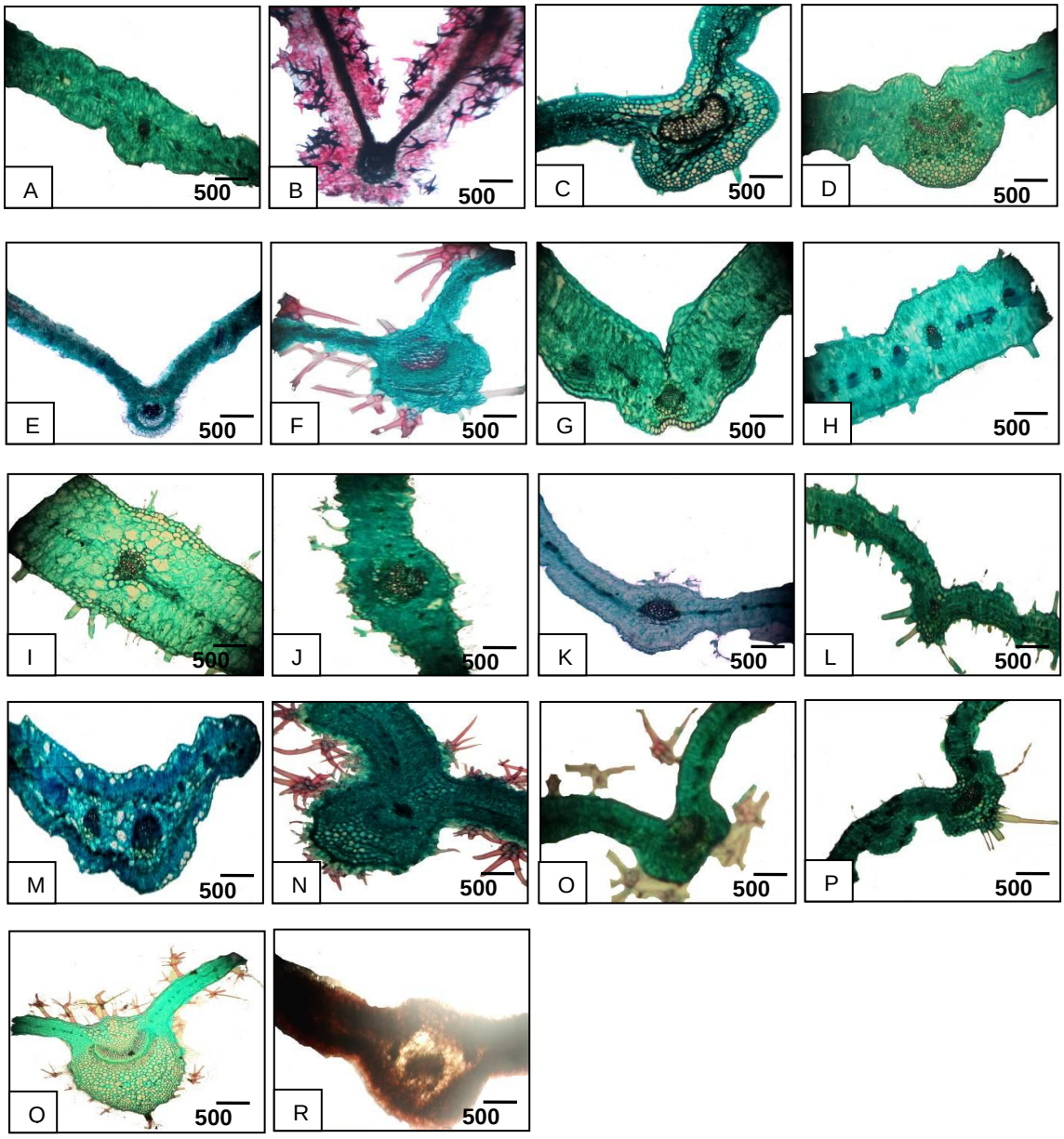


***Figure 2b:*** *Macro and Microphotographs Analysis*
*Lamina Anatomy* (A) *Achillea Fragrantissima* (B) *Aerva Tomentosa* (C) *Alkanna Orientalis* (D) *Asclepias Sinaica* (E) *Astragalus Sieberi* (F) *Ballota Kaiseri* (F) *Echinops Spinosus* (G) *Fagonia Glutinosa* (H) *Hyoscyamus Muticus* (I) *Matthiola Arabica* (J) *Matthiola Longipetala* (K) *Origanum Syriacum* (L) *Peganum Harmala* (M) *Phlomis Aurea* (N) *Pyrethrum Santolinoides* (O) *Stachys Aegyptiaca* (Q) *Teucrium Polium* (R) *Verbascum Sinaiticum* (S) *Zilla Spinosa*

### 3.3. Spectral Reflectance Pattern and Spectral Discrimination

Spectral reflectance of plant leaves could be characterized as absorption centered at about 0.65 µm (visible red) by chlorophyll pigment in green-leaf chloroplasts that reside in the outer of Palisade leaf, and to a similar extent in the blue, removes these colors from white light, leaving the predominant but diminished reflectance for visible wavelengths concentrated in the green. Strong reflectance between 0.7 and 1.0 µm (near IR) in the spongy mesophyll cells located in the interior or back of a leaf, within which light reflects mainly at cell wall/air space interfaces, much of which emerges as strong reflection rays.

It was found that all plants (measured samples) gave the general form of the spectral signature matched to a large extent in different spectral zones in the field of visible light and infrared. It was found that SWIR1 spectral zone was generally similar to the reflectance in the field of visible spectral zone and that was more memorable and less overlap between the various plants. The spectral Reflectance in SWIR1 was higher than the spectral reflectance in SWIRII. It was found that spectral reflectance of *Verbascum sinaiticum*, *Phlomis aurea*; *Stachys aegyptiaca* was higher than the rest of the plants in all spectral zones except the spectral zone SWIR2, where *Achillea fragrantissima* showed close spectral reflectance with *Verbascum sinaiticum*. *Hyoscyamus muticus* showed the lowest reflectance in SWIR2 while *Asclepias sinaica* showed the lowest reflectance in Infrared. In visible zone, reflectance was largely convergent except *Verbascum sinaiticum* and *Stachys aegyptiaca* (Figure 3).

In visible zone, *Achillea fragrantissima* showed relatively different reflectance pattern.

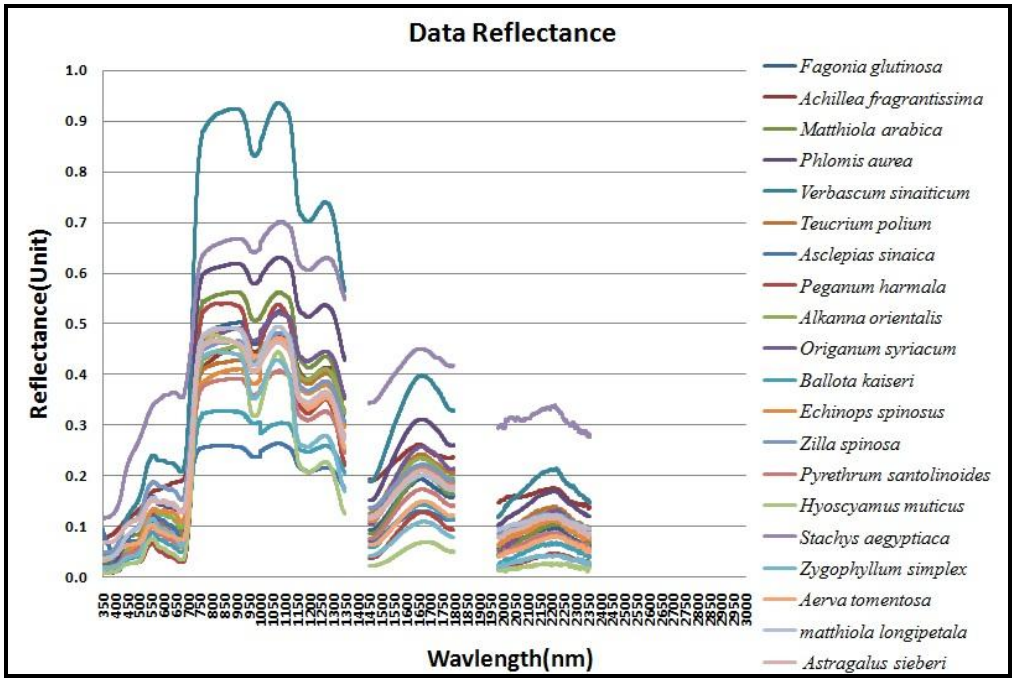


***Figure 3:*** *The Spectral Reflectance Pattern for the Different Species*

Blue spectral zone showed significant reflectance for species *Stachys aegyptiaca*, *Astragalus sieberi* and *Achillea fragrantissima*. Green spectral zone showed significantly different reflectance pattern with *Stachys aegyptiaca* and *Verbascum sinaiticum*. NIR spectral zone showed significantly different reflectance with *Stachys aegyptiaca*, *Verbascum sinaiticum*, *Phlomis aurea*, *Matthiola arabica*, *Ballota kaiseri*, *Asclepias sinaica* and *Pyrethrum santolinoides*. Red spectral zone showed significantly different reflectance with ten samples (*Verbascum sinaiticum*, *Stachys aegyptiaca*, *Achillea fragrantissima*, *Zilla spinosa*, *Hyoscyamus muticus*, *Peganum harmala*, *Ballota kaiseri*, *Echinops spinosus*, *Alkanna orientalis* and *Pyrethrum santolinoides*). SWIR1 spectral zone showed significantly different reflectance with *Phlomis aurea*. SWIRII spectral zone showed significantly different reflectance with *Phlomis aurea*, *Stachys aegyptiaca*, *Ballota kaiseri* and *Hyoscyamus muticus*. Generally, the results of Tukey's HSD showed that Red was the best spectral zone for the discrimination between the most of the samples. Also, it was found that SWIR1 was not sufficient to discriminate the spectral reflectance of the different samples. The other four spectral zones showed acceptable results to for discrimination different samples. The results explained the optimal wavebands that could be used to identify each plant species (Figure 4). It was found that (*Fagonia glutinosa* and *Alkanna orientalis*) did not show any unique spectral zone. The three plants *Verbascum*

*sinaiticum*, *Stachys aegyptiaca* and *Asclepias sinaica* showed relatively wide unique spectral zones as shown in table. It was found that seven of the samples (*Zilla spinosa*, *Astragalus sieberi*, *Echinops cornigerus*, *Matthiola arabica*, *Matthiola longipetala*, *Origanum syriacum*, *Teucrium polium* and *Aerva tomentosa*) have only one unique spectral zone. Following the spectral signature of all samples showed that the three plants *Verbascum sinaiticum*, *Stachys aegyptiaca* and *Asclepias sinaica* are the most vulnerable for discrimination and segregation through different sensors. These samples are characterized by unique and quite separable wavelengths and high values of reflection. This could be the core of future studies to survey, monitor and produce maps for the distribution of these plants in Sinai. It was also found that red spectral zone showed compatible results with morphological and anatomical studies as ten samples were quietly spectrally, anatomically and morphologically separable. Spectral reflectance characteristics of other species were observed to identify the optimal waveband and wavelength *Viz* [77-83].

***Table 3:*** *The Optimal Waveband to Differentiate Between the Different Species*

| Species | Optimal Wavelength Zones (nm) |
|---|---|
| *Achillea fragrantissima* | 719: 725 |
| *Aerva tomentosa* | 718 |
| *Alkanna orientalis* | ------- |
| *Asclepias sinaica* | 350: 705, 1552: 1799, 1981: 2081, 2263: 2359 |
| *Astragalus sieberi* | 713 |
| *Ballota kaiseri* | 715: 716 |
| *Echinops spinosus* | 712 |
| *Fagonia glutinosa* | ------ |
| *Hyoscyamus muticus* | 715:716, 1313:1320 |
| *Matthiola arabica* | 719 |
| *Matthiola longipetala* | 714 |
| *Origanum syriacum* | 716 |
| *Peganum harmala* | 721, 1343: 1349 |
| *Phlomis aurea* | 719: 725 |
| *Pyrethrum santolinoides* | 716:718 |
| *Stachys aegyptiaca* | 702:719, 1562 :1799 |
| *Teucrium polium* | 720 |
| *Verbascum sinaiticum* | 718: 1349 |
| *Zilla spinosa* | 711 |
| *Zygophllum simplex* | 708: 709, 1330:1336 |

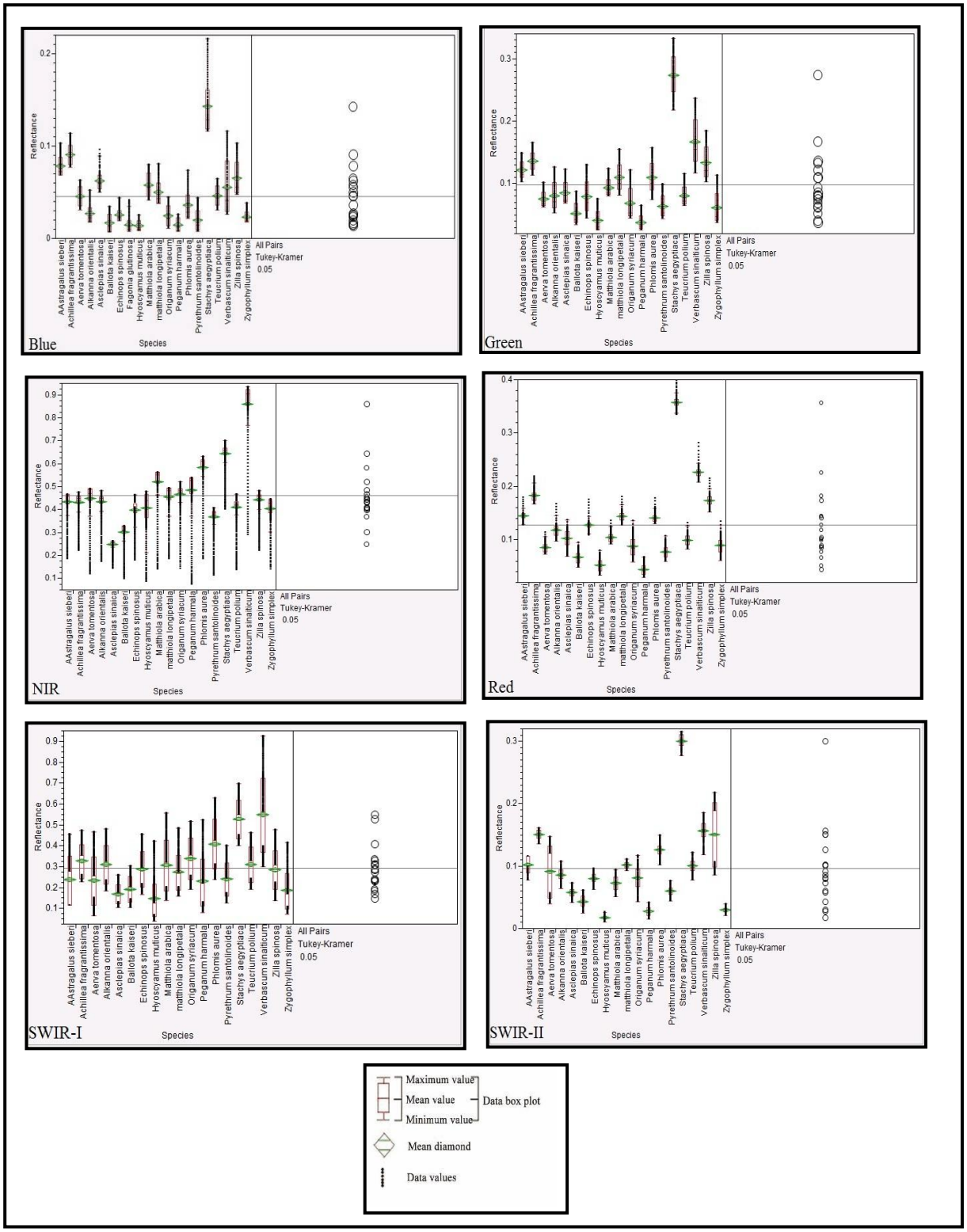


***Figure 4:*** *The Spectral Reflectance Pattern for the Different Plant Species*

## 4. Conclusion

In the current study, ASD field spectroradiometer was used to measure spectral reflectance in the wavelength ranged from 350 to 2500 nm for twenty (20) species belonging to nineteen (19) genera. Hyperspectral reflectance characteristics and Macro/micro-morphological features were investigated.

One Way ANOVA (Tukey's HSD Post Hoc Analysis) showed that red (550-750 nm) and NIR (760-1000 nm) spectral zones were the optimal to discriminate the different genera. These results were consistent with morphological and anatomical studies as ten samples were quietly spectrally, anatomically and morphologically separable. Linear Discriminate Analysis identified the optimal wavebands and wavelengths to classify the different genera with high pharmaceutical values. Three species *(Asclepias sinaic, Stachys aegyptiaca and Verbascum sinaiticum)* could be clearly isolated from the rest of the genera with unique spectral characteristics. No specific wavelengths were investigated for Alkanna orientalis and Fagonia glutinosa. The results of the current study could be the basis for accurate mapping, monitoring and surveying three plant species with highly pharmaceutical value.

## Acknowledgments

The authors are very thankful to Prof. Tantawy M.E. and Abou-El-Enain M.M. for their suggestions, expert advice and support. Authors also thank the research staff of the Agricultural applications department at the Egyptian National Authority for Remote Sensing and Space Sciences.

## References

[1] Moustafa, A.A., 2000a: Impact of Grazing on the Vegetation of South Sinai, Egypt. Conf. Sustainable land use in Desert, Springer, Germany. 218-228.

[2] Moustafa, A.A., and Zaghloul, M.S. *Environment and Vegetation in the Mountain St. Katherine Area, South Sinai, Egypt.* Journal of Arid Environments. 1996. 34; 331-349.

[3] Bailey, C. and Danin, H. *Bedouin Plant Utilization in Sinai and the Negev.* Econ. Bot. 1981. 35 (2) 145-162.

[4] El-Hadidi, M.N. *Observations on the Flora of the Sinai Mountain Region.* Bull. Soc. Geogr. d'Egypt. 1969. 40; 125-155.

[5] Abdalla, M.S., Sa'ad, F.M., Eweida, A.E.A. and Mahmoud, M.A. *Materials from CAIM Herbarium. II. Flora of the Sinai Peninsula.* Notes from ARC Herb. Egypt. 1984. 6; 15-214.

[6] Danin, A., Schmida, A. and Liston, A. *Contribution to the Flora of Sinai. III. Check List of the Species Collected and Recorded by the Jerusalem Team (1967-1982).* Willdenowia. 1985. 15; 255-322.

[7] Danin, A. *Flora and Vegetation of Sinai.* Proceedings of the Royal Society of Edinburgh. 1986. 89B; 159-168.

[8] El-Hadidi, M.N. *Annotated List of the Flora of Sinai (Egypt).* The Taxa of Pteridophyta and Gymnospermae. Taeckholmia. 1989. 12; 1-6.

[9] Gamal El-Din, E.M. *Contributions to the Flora of Gebel Halal, North Sinai, Egypt*. Taeckholmia. 1993. 14; 59-70.

[10] Boulos, L., 1995: *Flora of Egypt Checklist.* Al Hadara Publishing, Cairo, Egypt.

[11] Moustafa, A.A. and Kamel W.M. *Ecological Notes on the Floristic Composition and Endemic Species of St Katherine Area, South Sinai, Egypt.* Egyptian Journal of Botany. 1995. 35 (2) 177-200.

[12] Abdou, M.S.Z., 1997: *Ecological Studies on Some Endemic Plant Species in South Sinai, Egypt.* Botany Department, Suez Canal University, Ismailia, Egypt.

[13] Ayyad, M.A., Fakhry and Moustafa, A.R.A. *Biophysical and Biochemical Sources of Variability in Canopy Reflectance.* Remote Sensing of Environment. 2000. 64; 234-253.

[14] Gazara, M.H., Moustafa, A.A. and Kamel, W.M. *Ecological Notes and Floristic Composition of Gebel El-Halal, North Sinai, Egypt.* Bull. Fac. Sci., Assiut Univ. 2000. 29 (1D) 323-334.

[15] Abd El Wahab, R.H, Zaghloul, M.S. and Moustafa, A.A., 2004: *Conservation of Medicinal Plants in St. Catherine Protectorate, South Sinai. Evaluation of Ecological Status and Human Impact.* Proceedings of first International conference on Strategy of Egyptian Herbaria, Giza, Egypt. 231-235.

[16] Zaghloul, M.S., 1997: *Ecological Studies on Some Endemic Plant Species in South Sinai, Egypt.* M.Sc. Thesis, Faculty of Science, Suez Canal University.

[17] Moustafa, A.A., Zaghloul, M.S., Abd El Wahab, R.H. and Shaker, M. *Evaluation of Plant Diversity and Endemism in Saint Catherine Protectorate, South Sinai, Egypt.* Egyptian J. of Bot. 2001. 41 (1) 123-141.

[18] Abd El Wahab, R.H, Zaghloul, M.S, Moustafa, A.A., 2004: *Conservation of Medicinal Plants in St. Catherine Protectorate, South Sinai. Evaluation of Ecological Status and Human Impact.* Proceedings of First International Conference on Strategy of Egyptian Herbaria, Giza, Egypt. 231-235.

[19] Anderson, J.R., Hardy, E.T., Rocha, J.T. and Witmer, R.E., 1976: *Land Use and Land Cover Classification System for Use with Remote Sensor Data.* US Geological Survey Professional Paper, Government Printing Office, Washington DC.

[20] Kauth, R.J. and Thomas, G.S. *The Tasselled Cap-A Graphic Description of the Spectral Temporal Development of the Agricultural Crops as Seen by Landsat.* In: Proceedings of the Symposium on Machine Processing of Remotely Sensed Data, Purdue University, West Lafayette, 2004. 4B-41-4B-51.

[21] Nirala, M.L. and Venkatachalam, G. *Rotational Transformation of Remotely Sensed Data for Land Use Classification.* International Journal of Remote Sensing. 2000. 21 (11) 2185-2202.

[22] Prakash, H.N.S., Nagabhushan, P. and Chidanada, G.K. *Symbolic Agglomerative Clustering for Quantitative Analysis of Remotely Sensed Data.* International Journal of Remote Sensing. 2000. 21 (17) 3239-3251.

[23] Asner, G.P. *Plant Biodiversity in the St. Katherine Area of the Sinai Peninsula, Egypt.* Biodiversity & Conservation. 1998. 9; 265-281.

[24] Blackburn, G.A. *Spectral Indices for Estimating Photosynthetic Pigment Concentrations: A Test Using Senescent Tree Leaves.* International Journal of Remote Sensing. 1998. 19 (4) 657–675.

[25] Chappelle, E.W., Kim, M.S. and McMurtrey III and J.E. *Ratio Analysis of Reflectance Spectra (RARS): An Algorithm for the Remote Estimation of the Concentrations of Chlorophyll A, Chlorophyll B, and Caroteniods in Soybean Leaves.* Remote Sensing of Environment. 1992. 39 (3) 239-247.

[26] Vogelmann, J.E., Rock, B.N. and Moss, D.M. *Red-Edge Spectral Measurements from Sugar Maple Leaves.* International Journal of Remote Sensing. 1993. 14; 1563-1575.

[27] Carter, G.A. *Ratios of Leaf Reflectances in Narrow Wavebands as Indicators of Plant Stress.* International Journal of Remote Sensing. 1994. 15; 697-703.

[28] Gitelson, A.A. *Wide Dynamic Range Vegetation Index for Remote Quantification of Biophysical Characteristics of Vegetation.* Journal of Plant Physiology. 2004. 161; 165-173.

[29] Carter, G.A. *Reflectance Bands and Indices for Remote Estimation of Photosynthesis and Stomatal Conductance in Pine Canopies.* Remote Sensing of Environment. 1998. 63; 61-72.

[30] Blackburn, G.A. *Towards the Remote Sensing of Matorral Vegetation Physiology: Relationships between Spectral Reflectance, Pigment, and Biophysical Characteristics of Semiarid Bushland Canopies.* Remote Sensing of Environment. 1999. 70; 278-292.

[31] McGwire, K., Minor, T., and Fenstermaker, L. *Hyperspectral Mixture Modeling for Quantifying Sparse Vegetation Cover in Arid Environments.* Remote Sensing of Environment. 1999. 72 (3) 360-374.

[32] Curran, P.J. *Imaging Spectrometry*. Progress in Physical Geography. 1994. 18 (2) 247-266.

[33] Janetos, A.C., and Justice, C.O. *Land Cover and Global Productivity: A Measurement Strategy for the NASA Programme*. International Journal of Remote Sensing. 2000. 21 (6) 1491-1512.

[34] Penuelas, J., Filella, I., Biel, C., Serrano, L., and Save, R. *The Reflectance at the 950-970 Region as an Indicator of Plant Water Status.* International Journal of Remote Sensing. 1993. 14 (10) 1887-1905.

[35] Penuelas, J., Filella, I., Lloret, P., Munoz, F., and Vilajeliu, M. *Reflectance Assessment of Mite Effects on Apple Trees.* International Journal of Remote Sensing. 1995. 16; 2727-2733.

[36] Thenkabail, P.S. *Biophysical and Yield Information for Precision Farming from Near-Real-Time and Historical Landsat TM Images.* International Journal of Remote Sensing. 2003. 24 (14) 839-877.

[37] Elvidge, C.D., Chen, Z. and Groeneveld, D.P. *Detection of Trace Quantities of Green Vegetation in 1990 AVIRIS Data.* Remote Sensing of Environment. 1993. 44; 271-279.

[38] Lyon, J.G., Yuan, D., Lunetta, R.S. and Elvidge, C.D. *A Change Detection Experiment Using Vegetation Indices*. Photogrammetric Engineering and Remote Sensing. 1998. 64; 143-150.

[39] Bauer, M.E., Daughtry, C.S.T., and Vanderbilt, V.C. 1981: Spectral-agronimic Relationships of Corn, Soybean, and Wheat Canopies (17). Report SR-P1-04187. West Lafayette, In: Laboratory for Applications of Remote Sensing, Purdue University.

[40] Marceau, D.J., Gratton, D.J., Fournier, R.A. and Fortin, J.P. *Remote Sensing and the Measurement of Geographical Entities in a Forested Environment. 2. The Optimal Spatial Resolution.* Remote Sensing of Environment. 1994. 49; 105-117.

[41] Portigal, F., Holasek, R., Mooradian, G., Owensby, P., Dicksion, M., Fene, M., Elliot, M., Hall, E. and Driggett, D. *Vegetation Classification Using Red-Edge First Derivative and Green Peak Statistical Moment Indices with the Advanced Airborne Hyperspectral Imaging System (AAHIS).* Third International Airborne Remote Sensing Conference and Exhibition, Copenhagen, Denmark. 7-10 July 1997. II (Ann Arbor, MI: ERIM); 789-797.

[42] Kneubuehler, M., Schaepman, M.E. and Kellenbergerm, T.W. *Comparison of Different Approaches of Selecting Endmembers to Classify Agricultural Land by Means of Hyperspectral Data (DAIS7915).* IEEE International Geoscience and Remote Sensing Symposium Proceedings, Seattle. 6-10 July 1998. 888-890.

[43] Thenkabail, P.S. *Inter-Sensor Relationships between IKONOS and Landsat-7 ETM+ NDVI Data in Three Ecoregions of Africa.* International Journal of Remote Sensing. 2004. 25 (2) 389-408.

[44] Zohary, M., 1973: *Geobotanical Foundations of the Middle East*. Gustav Fischer Verlag, Stuttgart. 739.

[45] Danin A., 1983: *Desert Vegetation of Israel and Sinai.* Cana Publishing House, Jerusalem, 148.

[46] Said, R., 1962: *The Geology of Egypt*. Elsevier, Amsterdam, 348.

[47] El-Alqamy, H.M., 2002: *Developing and Assessing a Population Monitoring Program for Dorcas Gazelle (Gazella dorcas) Using Distance Sampling in Southern Sinai, Egypt.* M.Sc. Thesis, School of Biology, Division of Environmental and Evolutionary Biology, University of St. Andrews, Scotland. 118.

[48] Täckholm, V., 1974: *Students Flora of Egypt*. 2nd Ed., Cairo University, Beirut, 888.

[49] Boulos, L., 2005: *Flora of Egypt*. Vol. 4. Al Hadara Publishing, Cairo, Egypt.

[50] Johansen, D.A., 1940: *Plant microtechnique* (Jodrell Lab.). New York: McGraw-Hill.

[51] Eames, A.J., 1929: *The Role of Floral Anatomy in the Determination of Angiosperm Phylogeny.* Proceedings of the International Congress of Plant Sciences, Ithaca. 1926. 423-427.

[52] Koller, A.L. and Rost, T.L. *Leaf Anatomy in Sansefieria (Agavaceae).* Am. J. Bot. 1988. 75; 615-633.

[53] Mason, R.L., Gunst, R.F. and Hess, J.L., 2003: *Statistical Design and Analysis of Experiments with Applications to Engineering and Science.* 2nd Edition. John Wiley & Sons, Hoboken.

[54] Puech, S. Contribution à l'étude des Teucrium de la section polium (Labiatae) de Tunisie. Bull. Soc. Bot. Fr., 132, Lettres Bot. 1985. (1) 41-50.

[55] Barry, J.C. *Teucrium Pilbaranum (Labiatae), a New Species from the Pilbara, Western Australia Australia*. Telopea. 8 (3) 299-303.

[56] Batanouny, K.H. 1999: *Wild Medicinal Plants in Egypt.* Academy of Scientific Research and Technology, Egypt. The World Conservation Union (IUCN), Switzerland. 60-64.

[57] Farhat, M., Tóth, J., Héthelyi, B.É., Szarka, Sz. and Czigle, Sz. *Analysis of The Essential Oil Compounds of Origanum syriacum L.* Acta Facultatis Pharmaceuticae Universitatis Comenianae. 2012. 59 (2) 6-14.

[58] Khalifa, S.F., 1972: *Morphological and Phytoch Studies on Some Members of Family Solanaceae in Egypt*. Ph.D. Thesis. Dept. of Botany, Ain Shams Univ., Cairo.

[59] Hill, A.F., 1951: Economic Botany. 256, McGraw-Hill Book Co., London.

[60] Boulos, L., 2000: *Flora of Egypt.* Al Hadara Publishing, Cairo, Egypt. 3; 168-170.

[61] Hepper, F.N. and Friis, I., 1994: *The Plants of Pehr Forsskal's "Flora Ageyptiaco-Arabica".* Kew: K.

[62] Pottier Alapetite, G. 1979: *Flore de la Tunisie. Angiospermes- dicotylédones, Apétales - Dialypétales*. Programme flore et vegetation tunisiennes. 655.

[63] Ozenda, P., 1991: Flore et végétation du Sahara. Paris, Ed. du CNRS.

[64] Le Floc'h, E. *Contribution À Une Étude Ethnobotanique De La Flore Tunisienne. Programme Flore Et Végétation Tunisienne.* Min. de l'En. Sup. et de la Rech. Sci. 1983. 387.

[65] Barker, R.M. *Notes on Zygophyllum (Zygophyllaceae) in Australia Including the Descriptions of Five New Species and One New Subspecies, Revised Keys and Typifications.* Journal of the Adelaide Botanic Gardens. 1998. 18; 43-74.

[66] Curtis, W.M. and Morris D.I., 1975: *Zygophyllaceae.* The Student's Flora of Tasmania 1, 2nd Edn, 93.

[67] Bentham, B. *XXVI Zygophylleae*. Flora Australiensis. 1863. 1; 286-294.

[68] Brullo, C., Brullo, S., Giusso del Galdo, G., Minissale, P. and Sciandrello, S. *Astragalus kamarinensis* (Fabaceae), A New Species from Sicily. - *Ann. Bot. Fennici.* 2013. 50; 61-67.

[69] Bedevian, A.K., 1936: *Illustrated Polyglottic Dictionary of Plant Names.* Cairo, Argus D Papazian Presses.

[70] Canan, O. and Yasin, A. *Morphological and Anatomical Investigation of Some Endemic Alkanna Species.* Pak. J. Bot. 2006. 38 (3) 527-537.

[71] Ahmed, K.O*. Comparative Anatomical and Palynological Studies on Genus Ballota (Lamiaceae) From Egypt.* Journal of Medicinal Plants Research. 2012. 6 (47) 5797-5812.

[72] Muhittin D. and Ozturk, M. *Comparative Morphological, Anatomical, and Palynological Studies on the Genus Stachys L. Sect. Ambleia Bentham (Lamiaceae) Species in Turkey.* Turk J Bot. 2008. 32; 113-121.

[73] Dehshiri, M.M. and Azadbakht, M. *Anatomy of Iranian Species Teucrium Polium (Lamiaceae).* Journal of Biology and Today's World. 2012. 1 (2) 93-98.

[74] Mammen, D., Daniel, M. and Sane, R.T. *On The Anatomical Features of The Semi-Arid Plant Aerva lanata.* Universal Journal of Pharmacy. 2013. 2 (3) 94-97.

[75] Mehmet, T., Gülden, Y. and Esra, M. *Morphological, Anatomical and Palynological Studies on Endemic Matthiola Anchoniifolia Hub. -Mor. (Brassicaceae).* Not. Sci Biol. 2013. 5 (2) 163-168.

[76] Onur, K., Dervis, O, Đsmühan, P. and Ayse, K. *Anatomical and Palynological Studies on Economically Important Peganum Harmala L. (Zygophyllaceae).* Biology Diver Conservation BioDiversity. 2008. 20; 108-115.

[77] Somdatta, C. *Application of Hyperspectral Data for Development of Spectral Library of Mangrove Species in the Sunderban Delta.* International Journal of Geomatics and Geosciences. 2013. 4 (2).

[78] Wang, L.E. and Wayne, P.S. *Distinguishing Mangrove Species with Laboratory Measurements of Hyperspectral Leaf Reflectance.* International Journal of Remote Sensing. 2009. 30 (5).

[79] James, H.E., Chenghal, Y., Kenneth, R.S., Leeann, M.G. and Chetta, S.O. *Evaluation of Hyperspectral Reflectance Data for Discriminating Six Aquatic Weeds.* J. Aquat. Plant Manage. 2011. 49; 94-100.

[80] Aschbacher, J., Tiangco, P., Giri, C.P., Ofren, R.S., Paudyal, D.R. and Ang, Y.K., 1995: *Comparison of Different Sensors and Analysis Techniques for Tropical Mangrove Forest Mapping.* In: Proceedings of the International Conference IGARSS. 2109-2111.

[81] Saxena, A., Rawat, J.K. and Singh, S.K., 2004: *Survey and Mapping of Mangrove Cover using Remote Sensing - A Case Study of Sundarbans.* Map Asia.

[82] Vaiphasa, C., 2003: *Innovative Genetic Algorithm for Hyperspectral Image Classification*. In: Proceedings of International Conference Map Asia.
http://www.gisdevelopment.net/technology/ip/ma03071abs.htm

[83] Vaiphasa, C. and Ongsomwang, S., 2004: *Hyperspectral Data for Tropical Mangrove Species Discrimination*. Proceedings of the 25th ACRS Conference. 22-28.

[84] Cochrane, M.A. *Using Vegetation Reflectance Variability for Species Level Classification of Hyperspectral Data.* Int. J. Remote Sensing. 2000. 21 (10).

**Cloud Publications**
International Journal of Advanced Remote Sensing and GIS
2014, Volume 3, Issue 1, pp. 790-806, Article ID Tech-322
ISSN 2320 - 0243

Case Study | Open Access

# Land Cover Transitions and Forest Spatial Patterns within Four Developing Oregon Communities

**Michael G. Wing[1], Kevin Brown[1], Derek C. Godwin[2], Paul D. Ries[3], and Robert Emanuel[4]**

[1]Forest Engineering, Resources, and Management, Oregon State University, Corvallis, Oregon, USA
[2]Outreach and Engagement Regional Administrator, Oregon State University, Corvallis, Oregon, USA
[3]Forest Ecosystems and Society, Oregon State University Corvallis, Oregon, USA
[4]Clean Water Services, 2550 SW Hillsboro Hwy, Oregon, USA

Correspondence should be addressed to Michael G. Wing, michael.wing@oregonstate.edu

Publication Date: 22 December 2014

Article Link: http://technical.cloud-journals.com/index.php/IJARSG/article/view/Tech-322



**Abstract** We examined land cover transitions and forest spatial patterns within four developing communities in Oregon. Our primary objectives were to quantify land cover change and resulting spatial patterns of forested areas during a time of recent rapid development (1994-2005). A secondary objective was to identify the most prevalent land cover categories resulting from transitions with an emphasis on forest cover. We found emergent patterns in land cover transitions. For three communities, the only appreciable gains in land cover area in 2005 were within developed land cover types. Developed low intensity land cover was prevalent, being either the largest or second largest land cover category for 1994 or 2005 in all communities. Developed medium intensity land cover increased in three communities in 2005, with large increases (17.4%) in land area occurring within one of the communities. Developed high intensity also increased within all four communities in 2005. Forest cover decreased in all four communities, with one community having over a third of the forest cover area being replaced by other land cover types. Forest spatial patterns in all four communities changed across time. Three of the communities experienced increases in areas exhibiting patch forest patterns, which represented the most fragmented forest areas. The community that experienced the greatest increase in developed land cover also had the largest increase in patch forest area. Our findings suggest that not only is forest often replaced as developed land cover increases, but that the spatial patterns of forests are also impacted, often by increased fragmentation.
**Keywords** *Land Use; Development; Forest Fragmentation*

## 1. Introduction

Challenges from population growth and urban spread confront many communities throughout the world. Within the United States (US), Oregon's population grew from 2,842,321 to 3,421,399 between 1990 and 2000, an increase of over 20% (USDC Census Bureau, 2010). Oregon's population is projected to reach 4.8 million by 2030, a 41% growth from the 2000 census data and the 10th most

rapid in the US. While population continues to grow, urban growth and infrastructure development follow, leading to landscape transformation. Typically in this transformation, areas that were once natural or used for forestry or agricultural applications are developed for an urban environment and to support infrastructure. Larger contiguous natural areas either disappear or become fragmented into smaller sections that are either entirely separate from one another or share a reduced boundary. Benefits that were once provided by natural and other replaced cover types, such as storm water runoff interception and carbon sequestration, are also replaced by other landscape functions. The trend in land development in the US has been one of at least steady increase; developed land area grew by over 56% between 1982 and 2007. Within Oregon, developed areas increased by 81% during this same time period (USDA NRCS, 2009). We applied freely available remotely sensed imagery to examine land cover transitions and forest spatial patterns within four developing Oregon communities as identified by their urban growth boundaries. Our primary objectives were to quantify land cover change and forest spatial patterns within each of the communities during a time of recent rapid development in order to better understand change dynamics. A secondary objective was to identify the most prevalent land cover categories that resulted from transitions and spatial patterns with an emphasis on forest cover and other rural land transitions.

## 2. Background

A number of techniques and resources have been employed by researchers investigating land cover change where urban development has supplanted more rural land uses such as forests or agriculture. One of the most commonly used databases is the USDA National Resources Inventory (NRI) (USDA NRCS, 2009). The NRI provides land cover change metrics on a national and state basis for several land cover categories for select time periods. These data have been used for a variety of land cover research involving historical and predicted transition patterns (Alig et al., 2003; Alig and White, 2007; Polyakov and Zhang, 2008a). While the NRI data can be linked to states, it is not spatially dynamic and can't readily be associated with individual communities. The US Department of Commerce (USDC) Census Bureau data provide population growth and housing density statistics that are collected on a 10 year basis. These data have been applied to establish development growth patterns and trends (Theobald, 2005; Nowak and Walton, 2007). The USDA Forest Service Forest Inventory and Analysis (FIA) unit uses plot-based statistics to provide estimates of forest land and nonforest land uses such as urban or agriculture (Gray et al., 2005). FIA data are collected periodically and are intended to provide nationwide assessments of non-federal lands. FIA estimates have been used as baseline land cover transition probabilities (Kline and Alig, 1999; Alig and White, 2007).

Land cover change can also be assessed directly through remote sensing techniques such as aerial photo interpretation or satellite imagery. With advancements in data availability and software capabilities, remote sensing has become an economically feasible and potentially reliable means of analyzing land cover change across broad landscapes. A number of previous studies have considered elements of land cover change within U.S. communities through remote sensing techniques (e.g. Yang et al., 2003; Yaun et al., 2005).

Oregon is located within the Pacific Northwest region of the US. Previous studies have quantified elements of land cover transitions within the Pacific Northwest through remote sensing techniques and other approaches. Cohen et al. (1998) applied Landsat Thematic Mapper (TM) imagery to map forest clearcuts in the Pacific Northwest from 1972 to 1993. The study used a combination of image classification approaches. Initially, an unsupervised classification included merging five date-pairs of imagery. A second method involved a single unsupervised classification of the full image data set. Cohen et al. (1998) determined that 14.7% of the 1.2 million hectare study area was harvested between 1972 and 1993.

Alberti et al. (2004) assessed land cover change between 1991 and 1998 in central Puget Sound, Washington. A combination of a supervised classification approach and a spectral un-mixing was used to apply seven different land cover classifications to a landscape. An overall image classification accuracy of 85% was reported. Alberti et al. (2004) found that a paved urban cover category had increased by 6.7% and a mixed urban category had increased by 7.8%. In addition, forest cover had declined by 8.2%, representing a 5% loss of forest cover across the study site. Wimberly and Ohmann (2004) assessed how human and environmental constraints influenced forest land cover change within the Oregon coast range. Using a combination of satellite imagery, historical maps, and other supporting databases, they determined a slight decrease in closed canopy forest area from 68% in 1936 to 65% in 1996. A large decrease was reported for large conifer forest area from 42% in 1936 to 17% in 1996. Gray et al. (2005) applied FIA data to examine changes in the amount of timberland on non-federal lands between 1989 and 2001 in western Washington. Timberland was defined as an area that is capable of producing wood products and not in a protected or reserved state. There was a reduction in timberland of almost 5% with about half of this reduction being due to land use conversions to urban and agricultural cover types. Other factors included right-of-ways and areas being placed in a reserved status. Alig and White (2007) examined land use changes in western Washington with an emphasis on the transitioning of land use types relative to forested land cover. Based on NRI data for western Washington, a 95.5% probability was reported that 1982 forestland would remain forestland in 1997. When forestland transitioned to an alternate land cover, the most common transition types were urban and other developed uses. Croplands were reported to transition into urban areas at a probability of 10.4% over the same time period. The only land cover types that had a probability of transitioning into forest cover included pastureland (2.2%) and cropland (0.4%). Urban and developed lands were reported to have a 100% probability of maintaining their status between 1982 and 1997. A Markov model was used with the NRI probabilities to forecast land cover change. Alig and White (2007) predicted an 8% reduction in forestland within western Washington between 1997 and 2027.

Azuma et al. (2009) examined land use change on non-federal lands in Oregon between 1974 and 2005. A sample of 37,003 points across Oregon was photo-interpreted and assigned to one of eight land use classes so that land use change could be calculated. Azuma et al. (2009) reported that 98% of the non-federal lands that were assigned to a forest, agriculture, or range cover type in 1974 remained in the same cover type in 2005. When land cover transitions occurred, 72% of the transitions involved forest, range, and agriculture land uses converting to a developed cover type. The next largest shift (13%) was reported to be range lands moving to agricultural uses. Low-density residential and urban land cover increased by 53% and 49%, respectively.

Forest patterning and fragmentation has been frequently studied in terms of wildlife habitat in previous studies (Askins et al., 1987; Mladenoff et al., 1995; Gibbs, 1998). Previous studies have also considered the spatial variation of patterns and fragmentation of forests and relationships to land cover change in various locations worldwide (Nagendra et al., 2004; Wickham et al., 2007; Wulder et al., 2011). Little research, however, has expressly examined temporal land cover change and forest pattern relationships in communities within the U.S. Pacific Northwest. Stanfield et al. (2002) examined ownership patterns and forest structure within a set of Oregon coastal range watersheds. Findings indicated that forest cover diversity increased with land ownership diversity and that ownership patch size was related to forest patch size. Butler et al. (2004) developed a fragmentation index for western Oregon and western Washington and examined socio-economic and environmental explanatory variables for the index. Population density, income, percent of agricultural and federal lands, distance to highway, and slope were each significantly correlated with the fragmentation index. Alig et al. (2005) investigated the influence of economic indicators and land quality measures on forest fragmentation within western Oregon. Land quality was based on a ranking of soil characteristics and their relevance for crop production. Results indicated that land quality fragmentation was a significant explanatory variable for land fragmentation.

## 3. Materials and Methods

We selected four communities within western Oregon for analysis. The selection criteria required that communities have less than 50,000 inhabitants, be in a state of perceived rapid development, and be located in several distinct geographical zones within western Oregon. Funding collaboration also required that two of the communities be located near the Portland metropolitan area, Oregon's most populous region. The final study sites included the communities of Damascus, Grants Pass, Newport, and Sherwood (Figure 1). We used the 2009 urban growth boundary (UGB) of each community to delineate the study area for each community.

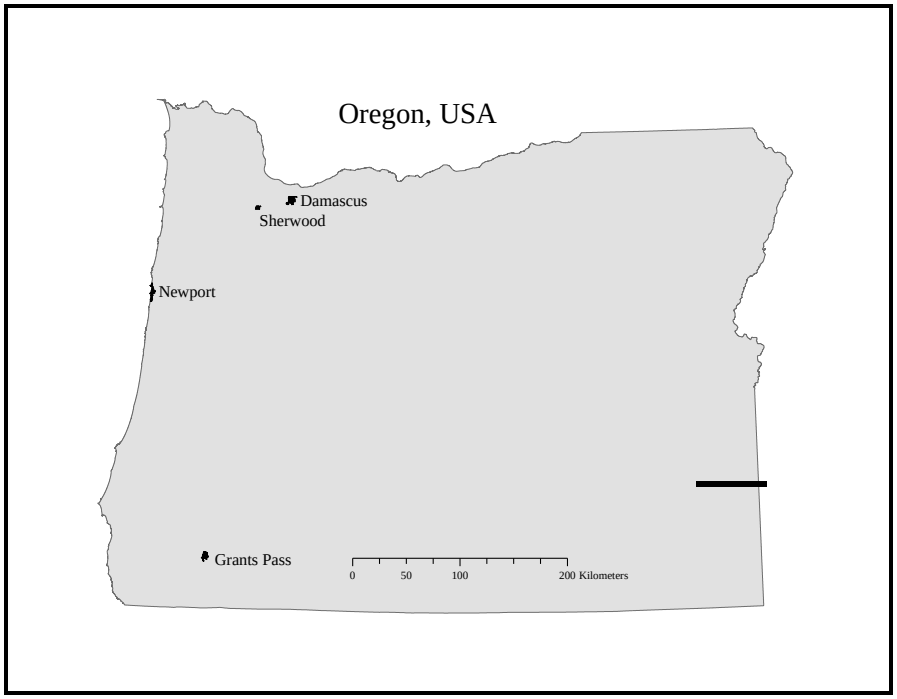


***Figure 1:*** *Four Oregon Communities*

The four communities vary in terms of geography and descriptive characteristics. Damascus became incorporated as a city in 2004 and the population estimate as of 2009 is 9,985 residents (City of Damascus, 2010). The total area of the UGB is 4,163 ha. Grants Pass became incorporated in 1887, had a population estimate in 2007 of 34,237 residents (Grants Pass, 2010), and a total UGB area of 3,461 ha. Newport became incorporated in 1882, had a population of 10,240 residents in 2006 (Newport Oregon, 2010), and an UGB area of 2,570 ha. Sherwood became incorporated as a city in 1893, had a population estimate in 2006 of 16,115 residents (City of Sherwood, 2010), and a UGB area of 1,384 ha.

We chose a remote sensing approach for our analysis so that we could measure land cover change efficiently across the broad landscapes associated with our four study communities. We selected two time periods for our change analysis: 1994 and 2005. We chose these time periods as georeferenced digital aerial photography was available for all study sites during these times. In addition, this was a period of rapid development within western Oregon's populated regions. Georeferenced digital orthophographs were used as a source of ground truth information for the satellite imagery classification process. Black and white digital orthophographs were available at one meter resolution for 1994 through archives at the Oregon State University library. A set of half-meter resolution color orthophotographs was available from the Oregon Imagery Explorer (OSU, 2010). Both data sources were available at no cost.

Landsat TM imagery was downloaded from the USGS Global Visualization Viewer (GLOVIS) (USGS, 2010). GLOVIS makes Landsat products freely available. Images were selected from either July or August of 1994 and 2005. These were the primary months in which the digital aerial photography was flown. While an attempt was made to select satellite imagery from GLOVIS from time periods that were from within the same week for both years, cloud cover in some candidate images made this impractical. Landsat TM imagery from GLOVIS is geo-rectified but can be subject to radiometric variation due to atmospheric influences. This could result in a change being detected between two images even if the cover types were identical. The 1994 images at each site were radiometrically normalized to the 2005 images in order to support classification. The normalization process applies regression to each sensor bandwidth independently to determine normalization amounts. The result of the normalization process is that spectral signatures can be compared between images while reducing image differences that are due to atmospheric and other effects.

### 3.1. Land Cover Classification

ERDAS Imagine and ArcMap geographic information system (GIS) software were used to analyze and classify satellite image land cover types. Our land classification scheme was initially based on categories developed by Anderson et al. (1976) and subsequently used for the National Land Cover Database (NLCD) mapping effort (MRLC, 2010). We modified this initial classification scheme to represent the dominant land cover types common to our four study areas and to support our research objectives. Our final classification included nine cover categories (Table 1).

***Table 1:*** *Land Cover Categories, Abbreviations, and Descriptions*

| | |
|---|---|
| **Developed Open Space (DOS)** | Includes areas with a mixture of some constructed materials, but mostly vegetation in the form of lawn grasses. Impervious surfaces account for less than 20 percent of total cover. These areas most commonly include large-lot single-family housing units, parks, golf courses, and vegetation planted in developed settings for recreation, erosion control, or aesthetic purposes.* |
| **Developed Low Intensity (DLI)** | Includes areas with a mixture of constructed materials and vegetation. Impervious surfaces account for 20-49 percent of total cover. These areas most commonly include single-family housing units.* |
| **Developed Medium Intensity (DMI)** | Includes areas with a mixture of constructed materials and vegetation. Impervious surfaces account for 50-79 percent of the total cover. These areas most commonly include single-family housing units.* |
| **Developed High Intensity (DHI)** | Includes highly developed areas where people reside or work in high numbers. Examples include apartment complexes, row houses and commercial/industrial. Impervious surfaces account for 80 to100 percent of the total cover.* |
| **Forest Cover (FC)** | Deciduous, evergreen, and mixed forests |
| **Forest Transition (FT)** | Clear-cut and partial cut forests including areas that are in early stages of forest regeneration with a prevalence of seedlings and saplings. |
| **Agriculture, Bare Land, Shrub, Scrub (AGL)** | Cultivated crops including grass, pasture, and hay fields. Areas dominated by shrubs less than five meters tall. |
| **Open Water (OW)** | Areas covered by water |
| **Wetlands (WT)** | Woody and herbaceous vegetation where the soils or substrate is inundated or covered by water. |

*Descriptions from MRLC (2010)

We conducted a supervised classification approach to derive land cover types from the satellite imagery. A supervised classification approach involves an analyst delineating areas on the imagery that are associated with a known cover type (ERDAS, 2008). This method is time consuming but has the potential for reliable classification results. Using the digital aerial orthophotographs, we created polygons representing each of the individual land cover types. This collection of individual land cover polygons constitutes a set of training classes for image classification. The training classes are used to capture the associated spectral signatures from the satellite imagery that correspond with each land cover type. To generate signatures that reliably classified the nine land cover types, we strove to create at least five training classes for each cover type when possible. The UGB areas sometimes did not include prevalent examples of some of our cover types, making training class development challenging.

The training classes were imported into ERDAS Imagine and visually compared to the satellite imagery to confirm conformality with the associated land cover types. After successful comparison, the training classes were used to conduct the supervised image classification process. The supervised image classification process uses the spectral signatures of the land cover types to search for similar signatures within the satellite imagery, and to assign a land cover category to each pixel within the imagery based on spectral signature correlations.

### 3.2. Accuracy Assessment

We completed an accuracy assessment of our image classification results in order to verify our classification protocol. An accuracy assessment compares classified imagery to select locations (ground truth locations) where actual ground cover features are known or can be derived with confidence (Congalton and Green, 1999). A stratified random sampling design was chosen to delineate the number of ground truth points to test within each land classification stratum (Ramsey & Schafer, 2002). We selected 240 ground truth locations to test within each study area. The specific number of ground truth locations for each classification stratum was proportional to the size of each stratum's land area but was not less than 20 for any stratum. Ground truth locations were randomly selected and digital aerial orthophotographs were used within ArcMap GIS software to derive a land cover category for each location. The derived land cover category was imported back into ERDAS Imagine where it was compared to the classification results. A report of the producer, user, overall accuracy, and a kappa coefficient is generated from this comparison. We strove to reach an overall classification accuracy of 75%. When this standard was not met, we created additional training classes, re-ran the classification process, and repeated the accuracy assessment.

The accuracy assessment of the classified imagery from the four study areas was evaluated though an error matrix within ERDAS Imagine software, where overall accuracies and kappa coefficients were calculated. Overall accuracies are computed using a simple descriptive statistic technique; the number of cells classified correctly is divided by the total number of classified cells. The kappa coefficient is more complex and includes a multivariate statistical technique (Xiuwan, 2002; Lowell and Jaton, 1999). The kappa coefficient explains the amount of error or agreement generated by the land classification process in contrast to the error of a completely random classification (ERDAS, 2008; Congalton and Green, 1999).

Based on the image classification results, we applied a methodology to consider change in forest spatial patterns based on earlier work (Vogt et al., 2007). Forested lands, water features, and all other land cover types were each segregated into separate categories. We then applied a spatial algorithm that instituted a proximity effect to create four forest sub-categories defined as core, perforated, edge, and patch forests. These forest sub-categories form a gradient leading from core forests, which represent larger contiguous forest areas, to patch forests, which are typically smaller areas that are surrounded by non-forest lands. The proximity effect defined core forest areas as contiguous forested

lands that were separated by at least 100 m from all other land covers. We chose the 100 m proximity effect based on earlier research (Forman, 1999). Perforated forest constitutes areas within core forest that are adjacent to non-forest land cover. Edge forests are areas on the outside perimeter of core forests that fall within 100 m of other land cover. Patch forests are small forest areas that are entirely enclosed by other land cover types.

Once the areas within the four urban growth boundaries were classified for the 1994 and 2005 imagery, the final classified image files were transferred to ArcMap GIS for analysis including the quantification of forest pattern change. Land cover area change, transitions statistics, and spatial forest pattern shifts between the two time periods were generated with ArcMap and Microsoft Excel software.

## 4. Results

We derived an overall image classification accuracy and a kappa coefficient for the remote sensing classification process for all four communities (Table 2). Damascus had the highest overall accuracy of 86.8% and a kappa coefficient of 81.1%. Sherwood had the lowest overall accuracy of 81.9% and a kappa coefficient of 77.8%. All four communities exceeded our overall mapping accuracy standard and kappa coefficient threshold of 75%. These accuracy assessment results provided confidence in using the classification results for land cover analysis.

***Table 2:*** *Land Cover Classification Accuracies*

| Study Area | Overall Accuracy (%) | Kappa Coefficient (%) |
|---|---|---|
| Damascus | 86.8 | 81.1 |
| Grants Pass | 82.4 | 80.0 |
| Newport | 82.0 | 79.2 |
| Sherwood | 81.9 | 77.8 |

We used the image classification results to map the land cover change within all four communities so that results could be visually examined and analyzed through GIS databases. We used the GIS databases to tabulate land cover change and transition percentages. The dominant land cover in Damascus was developed low intensity which increased from 37 to 39% of the total UGB area in 2005 (Table 3, Figure 2). The largest percent increase in area change for Damascus was for developed open space which rose nearly five percent. The largest decreases were with the agricultural and other lands (5.0%) and forest cover (2.1%) categories. Among the four communities, Damascus was perhaps the most stable in terms of land cover change; the maximum change in area was 5.0% and changes were 2.1% or less for seven of the nine land cover categories.

***Table 3:*** *Percent of Land Cover Area and Change for Four Oregon Communities between 1994 and 2005*

| | Damascus | | | Grants Pass | | | Newport | | | Sherwood | | |
|---|---|---|---|---|---|---|---|---|---|---|---|---|
| | 1994 % | 2005 % | Change | 1994 % | 2005 % | Change | 1994 % | 2005 % | Change | 1994 % | 2005 % | Change |
| Developed Open Space | 6.6 | 11.4 | 4.8 | 10.5 | 6.3 | -4.2 | 0.8 | 1.6 | 0.8 | 14.0 | 14.2 | 0.1 |
| Developed Low Intensity | 37.4 | 39.3 | 1.9 | 33.5 | 30.3 | -3.1 | 19.2 | 25.7 | 6.5 | 21.3 | 22.6 | 1.3 |
| Developed Medium Intensity | 4.0 | 5.1 | 1.1 | 21.4 | 30.9 | 9.6 | 17.6 | 11.3 | -6.3 | 5.6 | 23.0 | 17.4 |
| Developed High Intensity | 1.7 | 2.0 | 0.3 | 9.9 | 11.3 | 1.5 | 2.1 | 5.0 | 2.9 | 6.8 | 10.0 | 3.3 |
| Forest Cover | 18.6 | 16.4 | -2.1 | 8.2 | 6.8 | -1.3 | 30.5 | 26.1 | -4.4 | 15.3 | 10.1 | -5.2 |
| Forest Transition | 6.5 | 5.6 | -1.0 | 0.0 | 0.0 | 0.0 | 10.7 | 12.7 | 2.0 | 0.0 | 0.0 | 0.0 |
| Agriculture, Bare Land, Shrub, Scrub | 24.7 | 19.6 | -5.0 | 15.7 | 13.3 | -2.4 | 10.6 | 11.4 | 0.8 | 30.9 | 15.4 | -15.5 |
| Open Water | 0.5 | 0.6 | 0.1 | 1.0 | 1.0 | 0.1 | 0.0 | 0.0 | 0.0 | 0.0 | 0.0 | 0.0 |
| Wetlands | 0.0 | 0.0 | 0.0 | 0.0 | 0.0 | 0.0 | 8.4 | 6.2 | -2.2 | 6.1 | 4.8 | -1.3 |

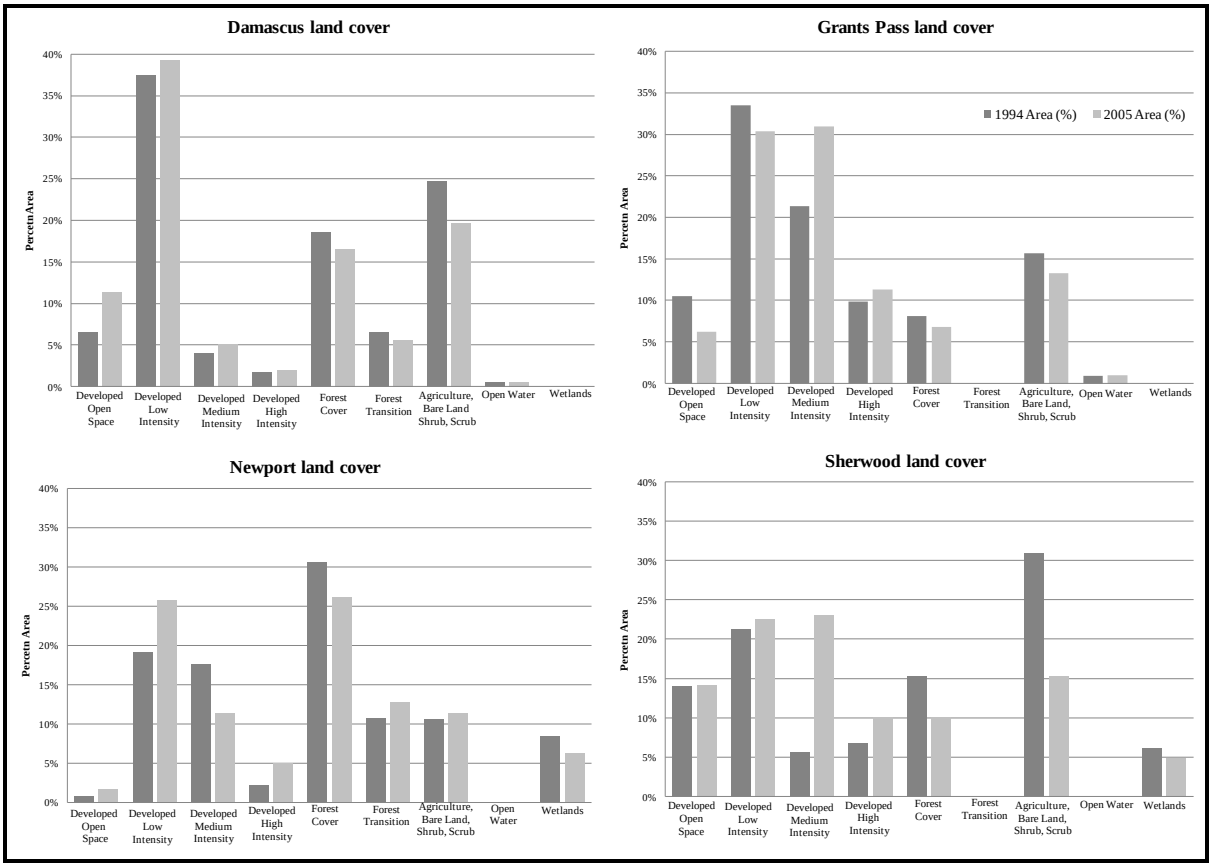


***Figure 2:*** *Land Cover Change Percentage in Four Oregon Communities between 1994 and 2005*

The largest land cover area within the Grants Pass UGB was developed low intensity in 1994 (33.5%). There was slightly more developed medium intensity land in 2005 (30.9%) than developed low intensity (30.3%). The largest increase in land cover area for 2005 was developed medium intensity which increased by nearly ten percent. The strongest decreases in 2005 occurred with the developed open space (4.2%) and developed low intensity (3.1%) categories. Although Grants Pass had 8.2% of the land within the UGB boundary in the forest cover category in 1994, our classification process did not result in any land area within the forest transition category in either 1994 or 2005. The forest cover area decreased to 6.8 percent in 2005. Forest cover was reduced within all of the communities in 2005 but Grant Pass had the lowest decrease of any community.

Newport was the only community in which the developed medium intensity land cover did not increase in 2005. The developed medium intensity cover exhibited a 6.3% drop in land area; the strongest decrease among any category although there were at least modest increases in the other developed categories. Forest cover was the dominant land cover for both time periods covering 30.5% of the UGB area in 1994 and 26.1% in 2005. Forest cover also had the second strongest decline among all land cover categories at 4.4 percent. No other community had such a large percent of area designated within the forest cover category. The decrease in forest cover was the second largest decrease in forest cover among all four communities. The largest increase in land cover occurred in the developed low intensity category at 6.5%; developed low intensity was also the second dominant land cover for both time periods, and was less than one half percent less (25.7%) of the total land area than forest cover in 2005 (26.1%). Developed high intensity increased from 2.1 to 5.0% in 2005, and forest transition increased from 10.7 to 12.7% in 2005. Newport was one of only two communities (Sherwood was the other) in which we were able to remotely sense wetlands. Wetlands decreased from 8.4 to 6.2% in 2005.

Among the four communities, land cover transitions had the greatest variability within Sherwood. Change in 2005 was most pronounced in Sherwood for two land cover categories. Developed medium intensity increased from 5.6 to 23.0%, an increase of 17.4% of the land area that resulted in its becoming the most prevalent land cover in 2005. In addition, this was the largest change in area for any land cover category, positive or negative, within all four communities. Conversely, the agricultural and other lands category declined from 30.9 to 15.4% in 2005 in Sherwood, a 15.5% change in land area. The agricultural and other lands category spanned the largest area in 1994 (30.9%) but was supplanted by gains in developed medium intensity in 2005 (23.0%). The 15.5% decrease in land area associated with agricultural and other lands was the largest decrease for any category within any of the communities. Change in forest cover in Sherwood was the largest among the four communities. Forest cover decreased from 15.3 to 10.1% in 2005, a decrease of over five percent. Wetlands decreased from 6.1 to 4.8% in 2005.

We split the cover types into two broad categories to further investigate change in the four communities. The four developed cover types were combined into a single urban category and the remaining cover types were combined into a non-urban category with the exception of open water, which was excluded from these combinations. Within each of the communities, the urban category increased in total area in 2005 while the non-urban decreased (Figure 3, Table 4). The largest increase was in Sherwood with 22.1% of the land within the UGB being added to the urban category in 2005. The next largest increase in the urban category occurred in Damascus (8.1%).

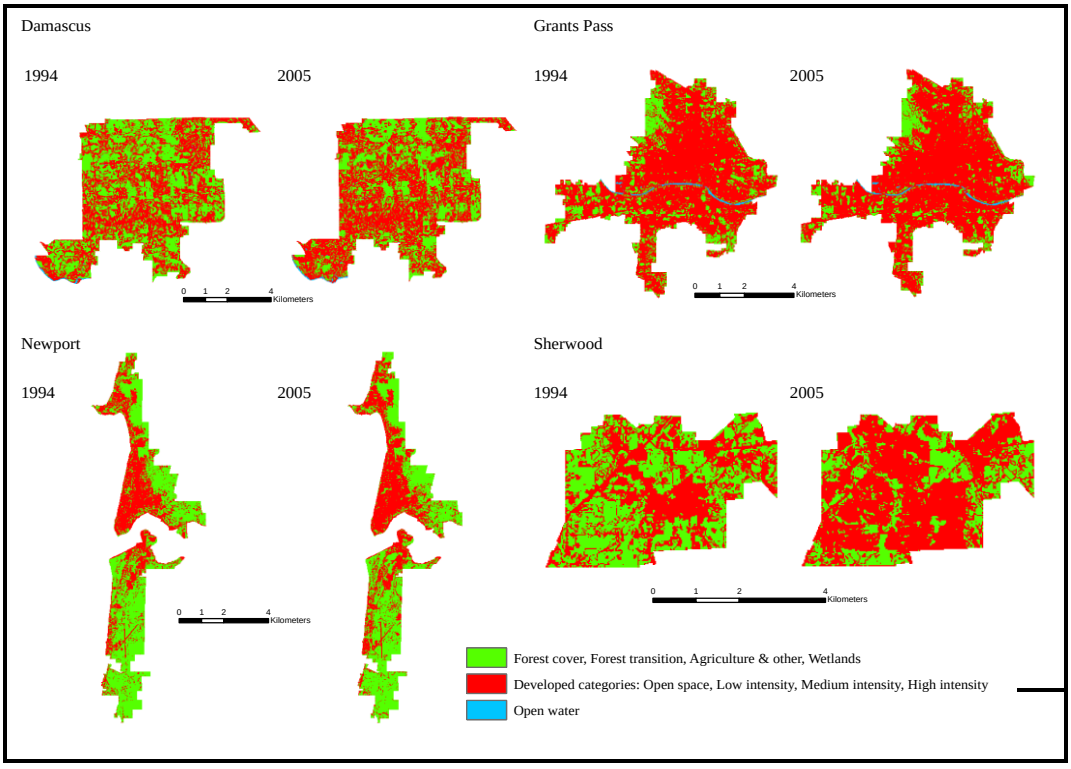


***Figure 3:*** *Urban and Non-Urban Land Cover Change in Four Oregon Communities between 1994 and 2005*

***Table 4:*** *Percentage of Land Area and Change for Urban and Non-Urban Land Cover Types for Four Oregon Communities between 1994 and 2005*

| | **Damascus** | | | **Grants Pass** | | | **Newport** | | | **Sherwood** | | |
|---|---|---|---|---|---|---|---|---|---|---|---|---|
| | 1994 % | 2005 % | Change | 1994 % | 2005 % | Change | 1994 % | 2005 % | Change | 1994 % | 2005 % | Change |
| DOS, DLI, DMI, DHI | 49.7 | 57.7 | 8.1 | 75.2 | 78.9 | 3.6 | 39.8 | 43.6 | 3.8 | 47.7 | 69.8 | 22.1 |
| FC, FT, AGL, WT | 49.8 | 41.7 | -8.2 | 23.8 | 20.1 | -3.7 | 60.2 | 56.4 | -3.8 | 52.3 | 30.2 | -22.1 |

We also tabulated the changes that occurred in each of the land cover categories in 2005 for all four communities (Table 5). These results show the types of land cover transitions that occurred within each of the land cover areas as they were measured in 1994. The two most stable land cover categories in Damascus included the forest cover and developed low intensity categories. Of the forest cover land area in 1994, 68.2% remained in a forest cover classification in 2005, while 63.6% of the developed low intensity area in 1994 remained in 2005. Developed low intensity was the dominant transition to occur within the forest cover, and replaced 22.2% of the forest cover in 2005. The next most dominant transition within the forest cover category was forest transition which replaced 4.3% of forest cover in 2005. The forest transition category was the most prone to change in Damascus with only 17.5% remaining in 2005. Developed low intensity replaced 44.6% of the forest transition area in 2005. Agricultural and other lands were replaced primarily by developed low intensity when change occurred in 2005.

***Table 5:*** *Land Cover Transition Percentage for 2005 Land Cover Categories Based on Initial 1994 Cover Category*

| Damascus | | Percent of 2005 landcover within 1994 land cover | | | | | | | | | |
|---|---|---|---|---|---|---|---|---|---|---|---|
| | Category | DOS | DLI | DMI | DHI | FC | FT | AGL | OW | WT | 1994 area (%) |
| 1994 | DOS | 43.2 | 22.5 | 2.4 | 0.4 | 7.0 | 1.8 | 22.7 | 0.0 | 0.0 | 6.6 |
| | DLI | 8.1 | 63.6 | 4.3 | 1.0 | 8.1 | 6.3 | 8.1 | 0.7 | 0.0 | 37.4 |
| | DMI | 0.5 | 38.1 | 44.2 | 7.6 | 0.0 | 3.2 | 6.5 | 0.0 | 0.0 | 4.0 |
| | DHI | 0.9 | 14.5 | 18.8 | 43.2 | 0.0 | 2.4 | 20.1 | 0.3 | 0.0 | 1.7 |
| | FC | 3.2 | 22.2 | 0.4 | 0.2 | 68.2 | 4.3 | 1.1 | 0.4 | 0.0 | 18.6 |
| | FT | 8.0 | 44.6 | 3.0 | 0.9 | 2.5 | 17.5 | 23.4 | 0.0 | 0.0 | 6.5 |
| | AGL | 17.6 | 20.5 | 4.0 | 1.8 | 0.2 | 4.0 | 51.8 | 0.0 | 0.0 | 24.7 |
| | OW | 0.3 | 29.0 | 1.6 | 1.6 | 14.5 | 2.5 | 0.3 | 50.3 | 0.0 | 0.5 |
| | WT | 0.0 | 0.0 | 0.0 | 0.0 | 0.0 | 0.0 | 0.0 | 0.0 | 0.0 | 0.0 |
| Grants Pass | | Percent of 2005 landcover within 1994 land cover | | | | | | | | | |
| | Category | DOS | DLI | DMI | DHI | FC | FT | AGL | OW | WT | 1994 area (%) |
| 1994 | DOS | 31.1 | 21.2 | 18.4 | 5.4 | 2.4 | 0.0 | 21.6 | 0.0 | 0.0 | 10.5 |
| | DLI | 3.8 | 61.2 | 20.2 | 2.0 | 5.8 | 0.0 | 6.7 | 0.4 | 0.0 | 33.5 |
| | DMI | 1.2 | 13.2 | 72.3 | 10.9 | 0.0 | 0.0 | 2.3 | 0.0 | 0.0 | 21.4 |
| | DHI | 1.1 | 3.8 | 25.9 | 65.1 | 0.0 | 0.0 | 3.6 | 0.5 | 0.0 | 9.9 |
| | FC | 5.2 | 24.9 | 4.8 | 0.5 | 54.1 | 0.0 | 10.5 | 0.0 | 0.0 | 8.2 |
| | FT | 0.0 | 0.0 | 0.0 | 0.0 | 0.0 | 0.0 | 0.0 | 0.0 | 0.0 | 0.0 |
| | AGL | 6.1 | 15.0 | 24.5 | 8.0 | 1.3 | 0.0 | 45.1 | 0.0 | 0.0 | 15.7 |
| | OW | 0.0 | 5.5 | 0.4 | 4.7 | 0.2 | 0.0 | 0.0 | 89.2 | 0.0 | 1.0 |
| | WT | 0.0 | 0.0 | 0.0 | 0.0 | 0.0 | 0.0 | 0.0 | 0.0 | 0.0 | 0.0 |
| Newport | | Percent of 2005 landcover within 1994 land cover | | | | | | | | | |
| | Category | DOS | DLI | DMI | DHI | FC | FT | AGL | OW | WT | 1994 area (%) |
| 1994 | DOS | 69.2 | 0.6 | 0.0 | 0.0 | 10.3 | 14.1 | 5.6 | 0.0 | 0.3 | 0.8 |
| | DLI | 0.3 | 58.8 | 6.1 | 1.0 | 10.4 | 8.4 | 7.4 | 0.0 | 7.5 | 19.2 |
| | DMI | 0.4 | 26.0 | 45.2 | 16.6 | 0.2 | 1.7 | 9.4 | 0.0 | 0.6 | 17.6 |
| | DHI | 0.1 | 7.3 | 19.5 | 66.7 | 0.3 | 0.6 | 4.4 | 0.0 | 1.1 | 2.1 |
| | FC | 0.5 | 9.3 | 0.8 | 0.2 | 67.1 | 15.0 | 2.9 | 0.0 | 4.2 | 30.5 |
| | FT | 3.8 | 10.9 | 3.1 | 0.9 | 23.4 | 34.8 | 15.3 | 0.0 | 7.7 | 10.7 |
| | AGL | 2.8 | 24.4 | 9.2 | 1.5 | 1.5 | 9.6 | 46.0 | 0.0 | 5.0 | 10.6 |
| | OW | 0.0 | 0.0 | 0.0 | 0.0 | 0.0 | 0.0 | 0.0 | 0.0 | 0.0 | 0.0 |
| | WT | 0.5 | 36.7 | 2.2 | 1.6 | 10.4 | 15.5 | 9.1 | 0.0 | 24.0 | 8.4 |
| Sherwood | | Percent of 2005 landcover within 1994 land cover | | | | | | | | | |
| | Category | DOS | DLI | DMI | DHI | FC | FT | AGL | OW | WT | 1994 area (%) |
| 1994 | DOS | 25.6 | 21.4 | 21.1 | 9.2 | 3.0 | 0.0 | 14.1 | 0.0 | 5.5 | 14.0 |
| | DLI | 12.7 | 37.4 | 21.7 | 6.1 | 11.3 | 0.0 | 8.2 | 0.0 | 2.6 | 21.3 |
| | DMI | 5.9 | 34.2 | 52.8 | 5.4 | 0.6 | 0.0 | 0.6 | 0.0 | 0.4 | 5.6 |
| | DHI | 7.2 | 11.6 | 13.3 | 52.0 | 0.1 | 0.0 | 15.3 | 0.0 | 0.4 | 6.8 |
| | FC | 10.1 | 21.5 | 15.7 | 1.0 | 43.8 | 0.0 | 5.1 | 0.0 | 2.7 | 15.3 |
| | FT | 0.0 | 0.0 | 0.0 | 0.0 | 0.0 | 0.0 | 0.0 | 0.0 | 0.0 | 0.0 |
| | AGL | 13.8 | 15.5 | 27.1 | 10.1 | 1.0 | 0.0 | 27.9 | 0.0 | 4.5 | 30.9 |
| | OW | 0.0 | 0.0 | 0.0 | 0.0 | 0.0 | 0.0 | 0.0 | 0.0 | 0.0 | 0.0 |
| | WT | 20.1 | 13.2 | 13.2 | 5.2 | 2.8 | 0.0 | 18.6 | 0.0 | 26.9 | 6.1 |

Besides the open water category, the most resilient cover types in 2005 within Grants Pass included the three primary development categories. In 2005, developed medium intensity retained 72.3% of its original land, developed high intensity retained 65.1%, and developed low intensity retained 61.2%. Among the categories that exhibited the greatest change from the 1994 categories, developed open space maintained only 31.1% of its original area by 2005, and agricultural and other lands kept 45.1%. The primary covers that replaced agricultural and other lands was developed medium intensity (24.5%) and developed low intensity (15.0%). Just over half (54.1%) of the forest cover area exhibited change in 2005. The most common cover type to replace forest cover was developed low intensity (24.9%) followed by agricultural and other lands (10.5%).

The land cover category that remained the most intact in Newport was the developed open space category with 69.2% of the original area remaining in 2005. No other community in our study had a higher percentage of area within the UGB in a forest category than Newport (30.5% in 1994 and 26.1% in 2005). Forest cover was the second most stable land cover in Newport with 67.1% enduring in 2005. The most prevalent land category replacing forest cover was the forest transition category at 15.0% suggesting that forest management activities might have played a role in the transition. Developed low intensity was the next most common category to replace forest cover and replaced 9.3% by 2005. About 66.7% of the developed high intensity lands also remained in 2005, making this category the third most stable in Newport. Newport had the largest percentage of land classified as wetlands in 1994 (8.4%) among the four communities and this category was the most prone to change. Only 24% of the 1994 wetland area remained in 2005, being predominantly replaced by developed low intensity (36.7% of the 1994 area), forest transition (15.5%), and forest cover (10.4%) categories. The forest transition category was the second most prone to change in 2005 (34.8% remaining), being replaced predominantly by forest cover (23.4%) and developed low intensity (10.9%). About 46% of agricultural and other lands remained stable in Newport in 2005, with developed low intensity replacing 24.4% of the 1994 area.

Land cover results among the four communities demonstrated the largest changes within Sherwood. Not surprisingly, specific land cover transitions from 1994 to 2005 also revealed larger changes for Sherwood than other communities. Only the developed medium intensity (52.8%) and developed high intensity (52.0%) retained more than 50% of their 1994 land cover categorization in 2005. The next most stable category was forest cover (43.8%). The most prevalent land categories that supplanted the 1994 forest cover included developed low intensity (21.5%), developed medium intensity (15.7%), and developed open space (10.1%). Agricultural and other lands (27.9%), wetlands (26.9%), and developed open space (25.6%) were the cover categories in Sherwood that were most prone to change in 2005. The most common categories to replace agricultural and other lands included developed medium intensity (27.1%), developed low intensity (15.5%), and developed open space (13.8%).

We used the land cover results for both 1994 and 2005 to quantify and examine changes in forest spatial pattern that occurred during the same time period. We used a spatial algorithm that identified all forest areas in the four communities as either core, perforated, edge, or patch forests (Figure 4). All four communities experienced a decline in the total area that was classified as one of the four forest sub-categories from 1994 to 2005 (Figure 5). Within Damascus, the absolute percent of patch and core forest areas increased while both edge and perforated forest areas decreased in 2005. Absolute percentage change in forest types was greater in Damascus than in any other community. The absolute increase in patch forest type (13%) in 2005 was the largest of any forest type in the four communities. The absolute area of edge forest declined from 41% in 2005 to 30% in 1994, the second largest change among the four communities.

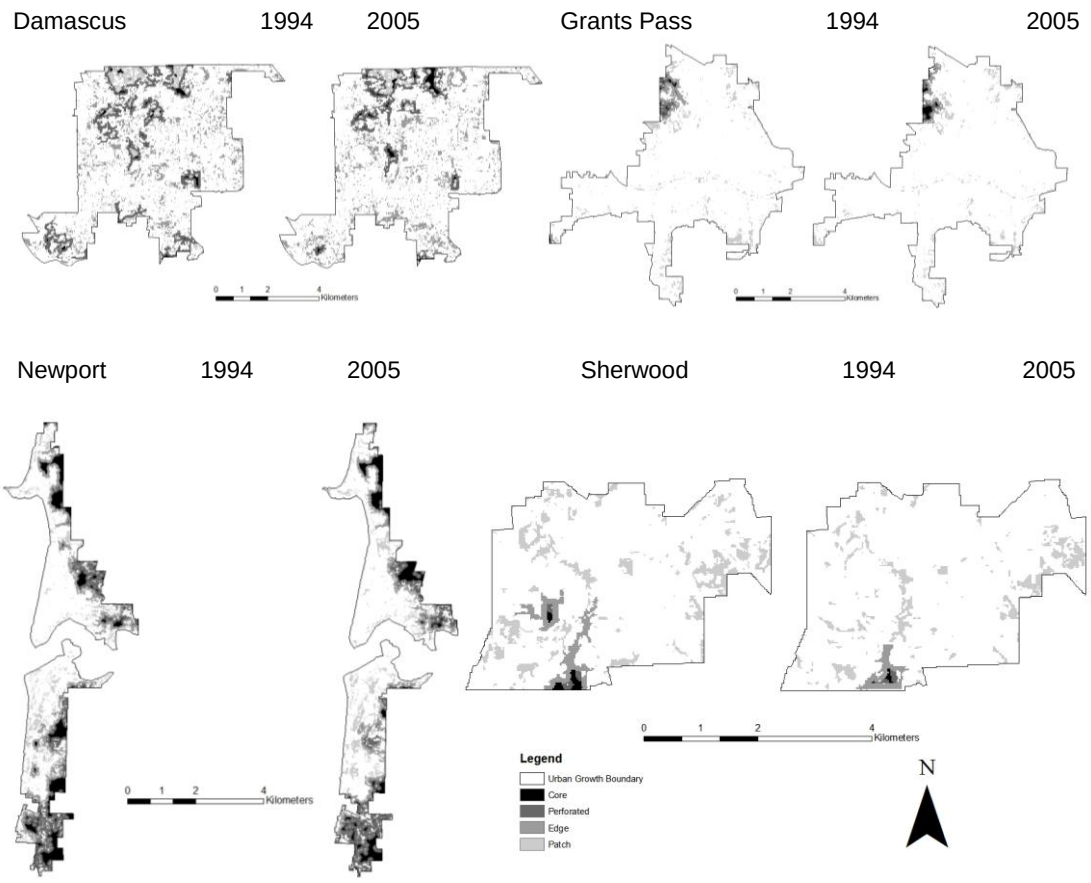


***Figure 4:*** *Spatial Forest Patterns in Four Oregon Communities between 1994 and 2005*

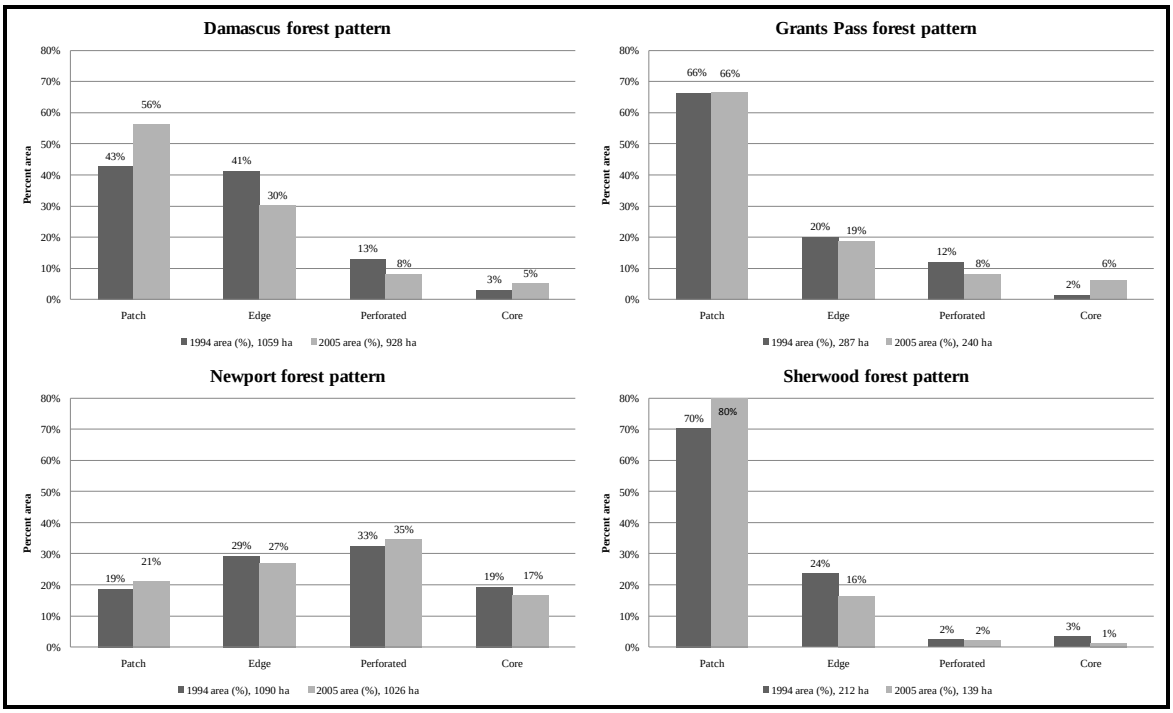


***Figure 5:*** *Forest Spatial Pattern Area Changes in Four Oregon Communities between 1994 and 2005*

In Grants Pass, both patch and edge forest types remained constant or nearly constant between 1994 and 2005. Perforated forest area decreased while core forest areas increased in 2005. Newport was very consistent in that the total amount of forest area did not change greatly between 1994 and 2005, and that absolute percent areas among the forest types remained relatively stable. In terms of absolute percentage change, patch and perforated forest types increased by 2%, while edge and core forest types decreased by 2% in 2005. Sherwood had a relatively small forest area in 1994 and lost a large portion of these lands in 2005. After Damascus, Sherwood also had the greatest change in forest type percentages. The absolute percentage of patch forest types increased by 10% within Sherwood in 2005 while other forest types either decreased or remained constant. Edge forest types experienced the next largest absolute change in Sherwood and decreased by 8% in 2005.

We also considered the forest types in 1994 and determined what the dominant land cover types were within each forest type in 2005 (Figure 6). Developed low intensity was the non-forested land cover type that most often replaced forest types in Damascus, Grants Pass, and Newport in 2005. In all three communities, the greatest change took place within the patch forest type. In Sherwood, developed medium intensity was the dominant land cover to replace both perforated and edge forest types, while developed low intensity was the most frequent land cover to replace core and patch forest types.

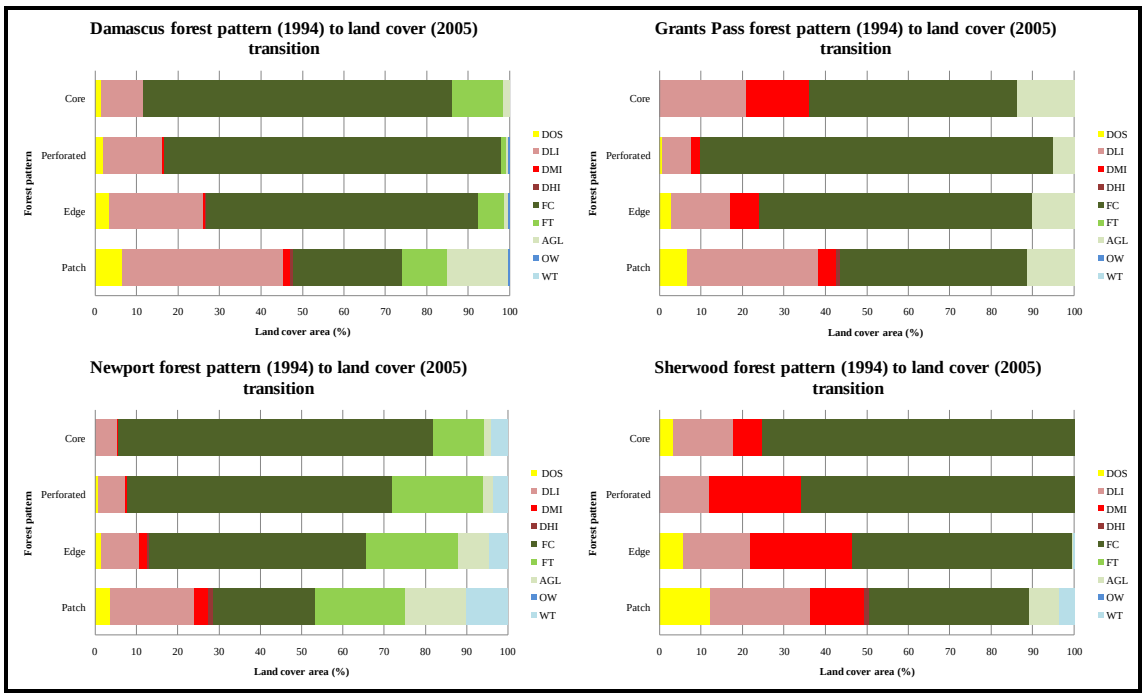


***Figure 6:*** *Forest Pattern (1994) to Land Cover (1995) Transition in Four Oregon Communities*

## 5. Discussion

We applied remotely sensed imagery to quantify land cover change and changes in the spatial pattern of forest areas within four developing communities over an 11 year time period. Significant population growth occurred within Oregon during this time and our results in each community reflect the increasing concentration of urban features that are often associated with population growth.

There were some observable patterns in land cover transitions across the communities. Urban and developed land uses occupied a larger portion of the landscape in all communities in 2005 when compared to 1994. In most cases, forested and rural lands were transitioned into developed land uses although the rates of change varied depending on the community. For three of the communities,

Damascus, Grants Pass, and Sherwood, the only appreciable gains in land cover area in 2005 were for the developed categories. Developed open space area increased in 2005 for all communities except Grants Pass. The developed low intensity land cover was a prevalent cover type in all communities, being either the largest land cover category for 1994 or 2005, or the second largest within all communities. Developed medium intensity land cover increased in three communities in 2005, with large increases in land area occurring within Sherwood (17.4%). Developed high intensity was modest in all communities in that it covered no more than 11.3% within any of the UGB areas in 1994 or 2005, but developed high intensity also increased within all four communities in 2005.

Forest cover decreased in all four communities, with the largest decrease occurring in Sherwood in terms of absolute change (5.2% decrease in land area) and relative change, with over a third of the forest cover area being replaced by other cover in 2005. The agricultural and other lands category decreased in three of the communities and in the case of Sherwood it decreased appreciably (15.5%). Newport experienced gains in the forest transition and agricultural and other lands categories, the only community to demonstrate an increase in either category.

The transition rates to developed land uses were greatest for Damascus and Sherwood. These two communities are located near the Portland metropolitan area, Oregon's most populated region. This proximity to Oregon's largest metropolitan area likely provided the largest influence on the pronounced development we observed in these communities. The most dramatic transition rate was within Sherwood, which had 22.1% of its non-urban lands replaced by developed lands between 1994 and 2005. The City of Damascus has only recently been incorporated (2004) and experienced a loss of 8.2% of its non-urban lands in 2005. The rate of transition in Damascus may increase in the near future as the recent incorporation is likely to encourage accelerated urban development.

Transition rates to urban land cover types were more modest for the other communities, Grants Pass and Newport. For both communities, the loss of non-urban land cover was less that 4% of the total land area within the UGB. Nonetheless, these losses represent 128 ha of land within Grants Pass, and 98 ha within Newport, where landscape functions are now focused on an urban environment rather than on a rural one. These communities are both located in relative unpopulated regions, with no major population centers in close proximity.

Our research into forest spatial pattern change involved characterizing all forested lands within each of the communities into a gradient of forest sub-categories that reflected forest contiguity and spatial proximity to non-forest land cover types. Overall, we found that as developed land categories increased in the communities, spatial forest patterns were affected and tended to become more fragmented. Patch forest, the most fragmented of the forest sub-categories increased in three of the communities, and remained steady in a fourth community (Grants Pass). Edge was the second most fragmented forest spatial pattern and decreased by an amount that was equal or very nearly equal in terms of an absolute percentage to the increase in patch forest in each of the three communities experiencing patch forest gains. Fragmentation patterns experienced the greatest change in Damascus, with patch and edge forest types exhibiting strong differences in 2005 when compared to 1994. Patch, the most fragmented of the four forested sub-categories increased in total area by 13% in Damascus in 2005 while edge forest types decreased by 9%. Interestingly, core increased slightly by 2% in Damascus. We examined the orthophotographs and classified imagery to better understand the core area increase which appeared to occur primarily in a northern portion of the Damascus UGB. We found that an area that was originally classified as agricultural and other lands in 1994 developed into a forest in 2005. There was also a decrease in edge forest in 2005 within Damascus that contributed to core area and patch increases. Grants Pass also exhibited an increase of core areas with 6% of the forest land being designated as core in 2005 compared to 2% in 1994. We again inspected orthophotographs and classified imagery to understand the increase. Similarly to Damascus, areas that were classified as agricultural and other lands in 1994 had transformed into forest in 2005. The

community with the least amount of forested area was Sherwood. In terms of forest pattern, Sherwood was dominated by patch forest area more than any other community. In addition, patch forest within Sherwood increased from 70% in 1994 to 80% in 2005. Land cover transitions occurred with the greatest variability in Sherwood and change was most pronounced in terms of increases in developed medium intensity and decreases in forest and agricultural and other lands categories. The result of these land cover changes was increased forest fragmentation in 2005 in Sherwood.

We also considered the four forest sub-categories as they were configured in 1994 and calculated which land covers existed in these areas in 2005. When the forested sub-categories were replaced by other land cover types, developed low intensity and medium intensity were the most common replacement cover, a result that we also observed when comparing land cover transitions among communities.

## References

Alberti, M., Weeks, R. and Coe, S. *Urban Land-Cover Change Analysis in Central Puget Sound.* Photogrammetric Engineering and Remote Sensing. 2004. 70 (9) 1043-1052.

Alig, R., Plantinga, A., Ahn, S. and Kline, J., 2003: *Land Use Changes Involving Forestry in the United States: 1952 to 1997, With Projections to 2050.* General Technical Report PNW-GTR-587, Portland, OR: USDA Forest Service, Pacific Northwest Research Station. 92.

Alig, R., Lewis, D. and Swenson, J. *Is Forest Fragmentation Driven by the Spatial Configuration of Land Quality? The Case of Western Oregon.* Forest Management and Ecology. 2005. 217 (2-3) 266-274.

Alig, R. and White, E. *Projections of Forestland and Developed Land Areas in Western Washington.* Western Journal of Applied Forestry. 2007. 22 (1) 29-35.

Anderson, J.R., Hardy, E.E., Roach, J.T. and Witmer, R.E., 1976: *A Land Use and Land Cover Classification System for Use with Remote Sensor Data.* Geological Survey Professional Paper. 964.

Askins, R.A, Philbrick, M.J. and Sugeno, D.S. *Relationship between the Regional Abundance of Forest and the Composition of Forest Bird Communities.* Biological Conservation. 1987. 39; 129-152.

Azuma, D., Birch, K., Herstrom, A., Kline, J. and Lettman, G.J., 2009: *Forest Farms and People: Land Use Change on Non-Federal Land in Western Oregon, 1973-2005.* USDA Forest Service and Oregon, Department of Forestry. 48.

Butler, B.J., Swenson, J.J., and Alig, R.J. *Forest Fragmentation in the Pacific Northwest: Quantification and Correlations.* Forest Ecology and Management. 189; 363-373.

City of Damascus, 2010: Community: History. *http://www.ci.damascus.or.us/comm unity history.aspx/* (Accessed 4 April 2011).

City of Sherwood, 2010: City History. *http://www.ci.sherwood.or.us/city-history* (Accessed 4 April 2011).

Cohen, W.B., Fiorella, M., Gray, J., Helmer, E. and Anderson, K. *An Efficient and Accurate Method for Mapping Forest Clearcuts in the Pacific Northwest Using Landsat Imagery.* Photogrammetric Engineering and Remote Sensing. 1998. 64 (4) 293-300.

Congalton, R.G. and Green, K., 1999: *Assessing the Accuracy of Remotely Sensed Data: Principles and Practices*. Boca Rotan, Florida: Lewis Publishers.

ERDAS, 2008: ERDAS Field Guide. Vol. 2. Atlanta, Georgia: ERDAS Inc.

Forman, R. *Estimate of the Area Affected Ecologically by the Road System in the United States.* Conservation Biology. 1999. 14 (1) 31-35.

Grants Pass, 2010: Our Community. *http://www.grantspassoregon.gov/422/Population-Area-Statistics* (Accessed 10 December 2014).

Gibbs, J.P. *Distribution of Woodland Amphibians along a Forest Fragmentation Gradient.* Landscape Ecology. 1998. 13; 263-268.

Gray, A.N., Venklase, C.F. and Rhoads, R.D., 2005: *Timber Resource Statistics for Non-national Forest Land in Western Washington, 2001.* USDA For. Serv. Res. Bull. PNW-RB-246. 117.

Kline, J.D., and Alig, R.J. *Does Land Use Planning Slow the Conversion of Forest and Agricultural Land*? Growth Change. 1999. 30 (1) 3-22.

Lowell, K. and Jaton, A., 1999: *Spatial Accuracy Assessment: Land Information Uncertainty in Natural Resources.* Chelsea, Michigan: Ann Arbor Press.

Mladenoff, D.J., Sickley, T.A., Haight, R.G. and Wydeven, A.P. *A Regional Landscape Analysis and Prediction of Favorable Gray Wolf Habitat in the Northern Great Lakes Region.* Conservation Biology. 1995. 9; 279-294.

Multi-Resolution Land Characteristics Consortium (MRLC), 2010: *2001 National Land Cover Data (NLCD 2001). http://www.epa.gov/mrlc/nlcd-2001.html* (Accessed 4 April 2011).

Nagendra, H., Munroe, D.K. and Southworth, J. *From Pattern to Process: Landscape Fragmentation and the Analysis of Land Use/Land Cover Change.* Agriculture, Ecosystems & Environment. 2004. 101 (2-3) 111-115.

Newport, Oregon, 2010: *Newport Facts. http://discovernewport.com/about/* (Accessed 10 December 2014).

Nowak, D.J. and Walton, J.T. *Projected Urban Growth (2000-2050) and Its Estimated Impact on the US Forest Resource.* Journal of Forestry. 2005. 103 (8) 383-389.

Oregon State University (OSU), 2010: *Oregon Imagery Explorer. http://www.oregonexplorer.info/imagery/* (Accessed 4 April 2011).

Polyakov, M. and Zhang, D. *Population Growth and Land Use Dynamics.* Journal of Agricultural and Applied Economics. 2008a. 40 (2) 649-666.

Polyakov, M. and Zhang, D. *Property Tax Policy and Land-Use Change*. Land Economics. 2008b. 8 (3) 396-408.

Ramsey, F.L. and Schafer, D., 2002: *The Statistical Sleuth: A Course in Methods of Data Analysis.* Second Edition. Belmont, California: Brooks/Cole. 103.

Stanfield, B., Bliss, J. and Spies, T. *Land Ownership and Landscape Structure: A Spatial Analysis of Sixty-Six Oregon (USA) Coast Range Watersheds.* Landscape Ecology. 2002. 17; 685-697.

Theobald, D.M. *Landscape Patterns of Exurban Growth in the USA from 1980 to 2020.* Ecology and Society. 2005. 10 (1) 32.

United States Geological Survey (USGS), 2010: *Global Visualization Viewer (GLOVIS). http://glovis.usgs.gov/* (Accessed 4 April 2011).

U.S. Department of Agriculture, Natural Resource Conservation Service (USDA NRCS), 2009: *Summary Report: 2007 National Resources Inventory. http://www.nrcs.usda.gov/technical/NRI/2007/2007_NRI_Summary.pdf* (Accessed 4 April 2011).

USDC Census Bureau, 2010: *Population and Household Economic Tips. http://www.census.gov/people/* (Accessed 10 December 2014).

Vogt, P., Ritters, K., Estreguil, C., Kozak, J., Wade, T. and Wikcham, J. *Mapping Spatial Patterns with Morphological Image Processing.* Landscape Ecology. 2007. 22; 171-177.

White, E.M., Morzillo, A. and Alig, R. *Past and Projected Rural Land Conversion in the US at State, Regional, and National Levels.* Landscape and Urban Planning. 2009. 89; 37-48.

Wickham, J.D., Riiters, K.H., Wade, T.G. and Coulston, J.W. *Temporal Change in Forest Fragmentation at Multiple Scales.* Landscape Ecol. 2007. 22; 481-489.

Wimberly, M.C. and Ohmann, J. *A Multi-Scale Assessment of Human and Environmental Constraints on Forest Land Cover Change on the Oregon (USA) Coast Range.* Landscape Ecology. 2004. 19; 631-646.

Wulder, M.A., White, J.C. and Coops, N.C. *Fragmentation Regimes of Canada's Forests.* Canadian Geographer/Le Géographe Canadien. 2011. 55.

Xiuwan, C. *Using Remote Sensing and GIS to Analyze Land Cover Change and Its Impacts on Regional Sustainable Development.* International Journal of Remote Sensing. 2002. 23 (1) 107-124.

Yang, L., Xian, G., Klaver, J. and Deal, B. *Urban Land-Cover Change Detection through Sub-Pixel Imperviousness Mapping using Remotely Sensed Data.* Photogrammetric Engineering and Remote Sensing. 2003. 69 (9) 1003-1010.

Yaun, F., Sawaya, K., Loeffelholz, B. and Bauer, M. *Land Cover Classification and Change Analysis of the Twin Cities (Minnesota) Metropolitan Area by Multitemporal Landsat Remote Sensing.* Remote Sensing of Environment. 2005. 98; 317-328.

**Cloud Publications**
International Journal of Advanced Remote Sensing and GIS
2014, Volume 3, Issue 1, pp. 807-816, Article ID Tech-326
ISSN 2320 - 0243

Research Article | Open Access

# GIS Mapping in Urban Slum Water Supply

**Mohammad Saiful Islam[1], Mohammad Sultan Mahmud[2], and Rashed Mustafa[3]**

[1]Department of Computer Science and Engineering, Jahangirnagar University, Dhaka, Bangladesh
[2]Faculty of Information Technology, King Mongkut's University of Technology North Bangkok, Bangkok, Thailand
[3]Department of Computer Science and Engineering, University of Chittagong, Chittagong, Bangladesh

Correspondence should be addressed to Mohammad Saiful Islam, saiful_i@outlook.com

Publication Date: 22 December 2014

Article Link: http://technical.cloud-journals.com/index.php/IJARSG/article/view/Tech-326



**Abstract** Water supply in slum area has been one of the most complicated tasks owing to a complexity in land tenure and rapidly changes in geography, population growth, and the uncertainties in the parameters influencing the time series and also due to the non-availability of adequate supply. Recently, geographical information system (GIS) has become quite popular and widely applied in various fields. This paper demonstrates the use of GIS to water supply in urban slum area to help and improve their quality of life (QoL). In particular, use of GIS technology to build a water supply management model in slum area. At present, in Chittagong city there are no proper water supply networks to supply the water in slum area. To illustrate the applicability and capability of the GIS, the Chittagong city, Bangladesh, was used as a case study. It is envisaged that, the proposed system can save much time, cost, and minimize the mistakes in managing operation and maintenance systems for water distribution networks.
**Keywords** *Geographical Information System (GIS); Quality of Life (QoL); Water Supply in Slum Area*

## 1. Introduction

In developing country like Bangladesh, water supply systems represent an important part in the urban infrastructure and critical factor of public health issue and economic development. The effectiveness of any resource management depends upon the nature of a sequence of measures preceding the decision. Information regarding location, at any given point of interest is necessary in the analysis and design of several resources management projects such as dam construction, pipe-lining, water reservoir operation, water distribution and wastewater disposal (Johnson, 2009).

Water is a scarce commodity, getting scarcer day by day. The humanitarian crises are not just the quantity of water available but the basis on which distribution networks are worked out. In the developing nation, most of municipalities distribution networks are have been grossly over stripped by rapid growth population. Neither the quantity of water available, nor the supplied mode is adequate for the inhabitants of these cities. The people who bear the brunt of this, however, are the poor. People

living in over-crowded shanty towns are not supplied an assured or clean supply of water. A primary impact is threats to life through diffusion of infectious diseases including anaemia arsenicosis, ascariasis diarrhea, cholera, typhoid, scabies (Pond, 2005). Other impacts includes reduces benefits for recreation, diminished health of aquatic ecosystems, could open the door to door corruption and increases violence between water user due to water scarcity, pricing and uncertainty. Water supply in the slum area is not financially beneficial for organization in developing country due to very low cost and at time free of cost. In this circumstance, authorities in every town of the developing world need to devise systems of water supply and distribution that accommodate the needs of the growing number of urban poor.

In recent years, geographic information system (GIS) is a widely used tool in the field of engineering, environmental science and related discipline. GIS is rapidly changing the ways that engineering planning, design, and management of resources are conducted (Johnson, 2009). Water resources system can analyze mathematical model. However supply system are complex involving both physical and human dimensions, thus may not be defined accurately by mathematical method. GIS analysis and linked mathematical models can provide wide-ranging capabilities to examine plans and designs because of mapping visualization help to connect complex information. The goal of this study is to design a GIS based water distribution system to deliver potable water especially in slum areas in required quantities and in satisfactory level to improve the quality of life. This may introduce a significant advantage in water consumption in slum area.

This paper consists of five sections. Section 2 describes some related works on GIS based water supply, section 3 is about propose model, section 4 is about analysis of simulation result and finally section 5 concludes the paper with summary.

## 2. Related Work

### 2.1. Geographical Information System

The introduction of geographical information system technology brings with it a period of change. This is common with information systems and other innovations that changes working practices. Maguire (1991) suggested that by the end of the century everyone in the developed world would use GIS every day for routine operations. Truly, the range of application of GIS has increased in last two decades, in response to the expansion of the necessity for GIS and applications to which it has been applied.

GIS based analysis of the pattern of urban development over the demographic change and land use modifications has indicated that urban growth has mainly taken place linearly (Carver, 1991; Straume, 2014). This tools widely used in urban landscape planning and design (Yi-chuan and Li-fang, 2008; Mirats Tur et al., 2009; Zunying et al., 2010; Sihua, 2011). Sundararaman et al. (2012) explained the demand of sewerage network and scarcity of water supply system using remote sensing and GIS techniques.

Application of GIS technology in the emergency monitoring of sudden air pollution accident is proposed by Chen and Suozhong (2010). The research helps to respond sudden air pollution accident more rapidly for the emergency monitoring staff. Research also done on application technology of GIS data in intelligent transportation system (Xin-hai and Yu-juan, 2010), development of railway asset management systems (Guler and Jovanovic, 2004), and fire prevention supports (Higgins et al., 2014). Moreover, GIS technology has been applied in support of decision-making in the petroleum exploration by Lian and Yan (2010).

### 2.2. Water Supply in Chittagong

According to Chittagong water supply improvement project interim report (2012), the total water production capacity of 219,000 $m^3$/d, which caters about 47 percent of the present demand in the Chittagong city corporation area. The sector development plan (FY2011-25) estimates that in Chittagong, 41 percent of the population is served by a piped water supply, which is increased to 46 percent if supply via water points is included. The Atlas of poor settlements in Chittagong City Corporation notes that only 31.6 percent of the poor households in Chittagong have access to water (Chadder, 2013). However, in many cases this water is obtained from contaminated hand-dug wells or other unprotected sources, has high iron concentrations and salinity and can take considerable time to collect and convey to home. Many of these water sources may also be illegal connections to the Chittagong WASA (CWASA) distribution system. As noted above, the current rules and regulations of CWASA do not allow piped connections to customers without land tenure or notarized permission from the owner. However, over last decade and through intervention of a number of national NGOs, CWASA has started to supply water to low income communities (LICs) without land tenure on the provision that the connection is, at least initially, in the name of the NGO.

Although this is a positive development but progress is slow and in last five years only 26 connections has been made. Referring to CWASA bills for these connections indicates that the average monthly amount charged is BDT 364. This is equivalent to 60 $m^3$ per month or 2 $m^3$ per day per connection. For the 26 working connections the total volume of water provided per day is therefore 52 $m^3$. Considering that CWASA produces in the order of 219,000 $m^3$ per day this amount is negligible, yet it has transformed the lives of many people. It is understood that approximately half of the connections have now been transferred and are under the name of the concerned community based organization (CBO).

### 2.3. Low Income Communities Population and Characteristics in Bangladesh

The slums of urban Bangladesh, mapping and census (2005) estimated that there were a total of 9,048 slums in six cities; Dhaka, Chittagong, Rajshahi, Khulna, Sylhet and Barisal of these 1,810 or 20 percent, were located in Chittagong. It was estimated that 35 percent of the population of these six cities lived in slum areas on only four percent of the available city land. Population density in the slums was estimated at 205,000 people per square kilometer, which is 200 times the average figure for Bangladesh. Other key findings included:

- Approximately 40 percent of the slums had 10 to 20 households
- 80 percent were on private land
- 40 percent of the slums identified in 2005 were established before 1981
- 80 percent of the slums were at least 10 years old, and
- All slums were single stored

In the case of Chittagong it was estimated that the total slum population was 1.46 million, although this was also reported as being 35.4 percent of the population of the city, which does not tie in with current population estimation. If 35.4 percent is correct then the population living in the slums was probably closer to 878,000. This can be explained to some degree by the fact that estimates of the Bangladesh population for the period 2001 to 2011 were considerably higher than the preliminary results given by the 2011 census. It also found that 42 percent of Chittagong slums had no support of an NGO, which was the worst situation in any of the six cities studied.

The WHO/UNICEF joint monitoring programme 2010 (JMP) estimated that the population of Bangladesh to be 149 million of which 28 percent or 41.7 million were classified as urban. Access to improve sources of drinking water during the time is summarized in Table 1.

***Table 1:*** *Improved Water Supply in Bangladesh in 2010 (Chadder, 2013)*

| Facility | Urban (%) | Rural (%) | Total (%) |
|---|---|---|---|
| Piped | 20 | 1 | 6 |
| Other improved | 66 | 79 | 77 |
| Improved total | 85 | 80 | 81 |
| Unimproved | 15 | 20 | 19 |

## 3. Methodology

This research focuses on to investigate a reliable GIS based water supply model in Chittagong city to ensure water in the urban slum area. The methodology presented here is in the form of a general model for the analysis and specification of GIS requirements. Figure 1 presents the overall workflow of the proposed model.

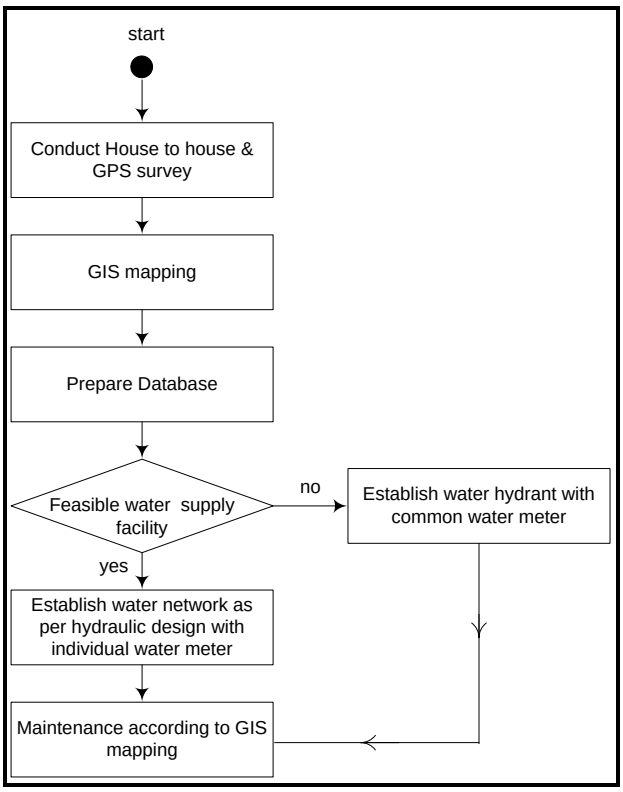


***Figure 1:*** *Workflow of Proposed GIS Based Water Supply Model*

**Step 1:** Global positioning system (GPS) and house to house survey

A survey should be conducted to determine the capabilities of GIS system. For GIS implementation there needs two types of survey: (a) Field verification survey by GPS, and (b) House to House survey.

### (a) Field Verification Survey by GPS

The GPS is a space-based satellite navigation system that provides location and time information in all weather, anywhere on or near the earth, where there is an unobstructed line of sight to four or more GPS satellites. The main objective of GPS survey is to clarify conflicts among the drawings which are collected, and to identify current situation because the information was not present. To identify exact position of planned distribution network and its facilities in real world, for example: gate valve, reducer,

T-connection, hydrant etc. Moreover, to establish the GIS based digital mapping and database for operation and maintenance work. In GPS survey the steps are following:

- Prepare pre survey map
- Identification of pipe lines interventions and water service facilities
- Marking and fix up the points
- Taking GPS reading
- Submit the survey data for GIS mapping
- Recheck the transferred data and mapping
- Distribution network drawing and database design

**(b) House To House Survey:**

House to house surveys are to identify the exact location of CWASA customers. The identification of proper location of water meter installation because the information has not been present. The Work flow of house to house survey includes:

- Prepare an image map
- Marking and fix-up the plot in image map
- Collection of data and
- Transfer for GIS mapping

**Step 2:** GIS Mapping

For GIS mapping “Arc GIS 10” has been used. Survey form data digitized on GIS map using two features: (1) Line feature, for structure and proposed service line; and (2) Point feature, only for proposed water meter connection. Steps for GIS mapping are:

- Preparation of initial GIS datasets by editing work
- Preparation of ground control points (GCP) between CWASA coordinate system and satellite image
- Transform GIS data to WGS1984 coordinate system
- Spatial adjustment to correct strong distortions in GIS data on image data on WGS1984 coordinate system update GIS data.

**Step 3:** Prepare Database

Microsoft access / Excel and post SQL can be use as backend database. Database contains spatial data which is connected to GIS software. And software display different attributes of water supply facility like water meter, pipe lines, valve etc.

**Step 4:** Feasibility Checking

Based on considered factors including landscape, population density, nearest water supply network, cost effectiveness the authority can make decision on whether they establish new water networks for water supply with individual water meter or they establish water hydrant with common water meter.

**Step 5:** GIS based Maintenance

GIS is the prime tools for maintenance of water supply networks. It is easy to locate the service area; it may count individual structure and calculate water consumption by using GIS tools. Future system capabilities also depend on GIS map. GIS records enables repair, replacement and analysis the

inspection results also information about new facilities can be entered into the GIS when that facilities are repaired and rename. We are totally ignored about water supply for slum area due to absent of GIS and spatial data.

## 4. Simulation Result and Discussion

### 4.1. Data Collection

To understand the views of poor communities in Chittagong, here worked alongside Chittagong WASA. For survey have visited forty one (41) settlements (ward) of the urban poor and spoke to representatives of the communities. They were asked from where they collect water, how far this are from their settlements, how much time have spent in the process, how much they collects each day, where they stored the water, what are the quality of the water obtained, how much they have to pay for it, and how much they feels they would ideally like. Furthermore, discussed to officials in the WASA, obtained all the available data of water supply and distribution and the schemes devised for the urban poor.

The study estimated that in the 2010 population of Chittagong was 2.7 million living in 562,000 households. The study also estimated that there were 5,778 LICs in Chittagong containing 301,527 poor households. The study therefore concluded that 53.6 percent or 1.45 million of the total population of Chittagong are poor. The reported classification is presented in Table 2.

***Table 2:*** *Distribution of Households by Ward*

| Ward Ref. | Ward Name | No. of Households | | | | |
|---|---|---|---|---|---|---|
| | | Extremely Poor | Very Poor | Moderately Poor | Marginally Poor | Total Poor |
| 1 | South Pahartali | 3,580 | 888 | 1,411 | 1,077 | 6,956 |
| 2 | Jalalbad | 4,379 | 4,728 | 7,945 | 3,940 | 20,992 |
| 3 | Panchlaish | 2,349 | 2,754 | 4,065 | 2,186 | 11,354 |
| 4 | Chandgaon | 1,670 | 3,830 | 3,400 | 2,601 | 11,501 |
| 5 | Mohara | 4,621 | 5,230 | 3,125 | 1,632 | 14,608 |
| 6 | East Sholakbawar | 814 | 2,330 | 1,924 | 363 | 5,431 |
| 7 | West Sholakbawar | 28,172 | 3,018 | 1,320 | 755 | 33,265 |
| 8 | Sholakbawar | 1,880 | 3,494 | 2,024 | 1,036 | 8,434 |
| 9 | North Pahartali | 7,951 | 3,065 | 1,124 | 69 | 12,209 |
| 10 | North Kattali | 5,710 | 506 | 363 | 652 | 7,231 |
| 11 | South Kattali | 115 | 612 | 1,906 | 7,248 | 9,881 |
| 12 | Saraipara | 25,170 | 2,055 | 13,147 | 2,737 | 43,109 |
| 13 | Pahartali | 3.993 | 4,604 | 2,152 | 3,686 | 14,435 |
| 14 | Lalkhan Bazar | 2,006 | 1,631 | 1,727 | 297 | 5,661 |
| 15 | Bagmoniram | 281 | 299 | 380 | 102 | 1,062 |
| 16 | Chanik Bazar | 219 | 73 | 132 | 349 | 773 |
| 17 | West Bakalia | 5,023 | 2,599 | 1,007 | 1,333 | 9,962 |
| 18 | East Bakalia | 4,417 | 1,032 | 1,613 | 293 | 7,355 |
| 19 | South Bakalia | 2,989 | 2,418 | 1,840 | 765 | 8,012 |
| 20 | Dewan Bazar | 322 | 25 | 20 | 0 | 367 |
| 21 | Jamalkhan | 629 | 96 | 654 | 48 | 1,427 |
| 22 | Enayet Bazar | 2,036 | 4 | 183 | 608 | 2,831 |
| 23 | North Pathantuli | 330 | 131 | 295 | 226 | 982 |
| 24 | North Agrabad | 58 | 582 | 1,699 | 1,620 | 3,959 |
| 25 | Rampur | 498 | 607 | 1,211 | 203 | 2,519 |
| 26 | North Halishahar | 88 | 130 | 905 | 448 | 1,571 |
| 27 | South Agrabad | 2,988 | 988 | 181 | 0 | 4,157 |

| | | | | | | |
|---|---|---|---|---|---|---|
| 28 | Pathantuli | 1,295 | 2,250 | 1,250 | 280 | 5,075 |
| 29 | West Madarbari | 223 | 347 | 311 | 16 | 897 |
| 30 | East Madarbari | 1,404 | 1,561 | 382 | 601 | 3,948 |
| 31 | Alkaran | 10 | 5 | 138 | 300 | 453 |
| 32 | Anderkilla | 35 | 34 | 122 | 170 | 361 |
| 33 | Finghee Bazar | 155 | 85 | 305 | 1,809 | 2,354 |
| 34 | Patharghata | 852 | 1,258 | 740 | 907 | 3,757 |
| 35 | Boxirhat | 7,358 | 198 | 7 | 0 | 7,563 |
| 36 | Gosalldanga | 1,035 | 935 | 169 | 86 | 2,225 |
| 37 | Halishahar Munir Nagar | 317 | 120 | 374 | 593 | 1,404 |
| 38 | South Middle Halishahar | 3,332 | 3,022 | 413 | 138 | 6,905 |
| 39 | South Halishahar | 3,920 | 339 | 396 | 245 | 4,900 |
| 40 | North Patenga | 1,421 | 1,478 | 1,939 | 1,579 | 6,417 |
| 41 | South Patenga | 950 | 1,535 | 1,678 | 1,061 | 5,224 |
| **Total** | | **134,595** | **60,896** | **63,977** | **42,059** | **301,527** |

All LICs are classified as (1) extremely poor, (2) very poor, (3) moderately poor or (4) marginally poor. LICs are generally inhabited by industrial labourers, rickshaw pullers, waste pickers etc. It has been found that there are now over 500,000 garment workers in Chittagong, many of whom live in the LICs. Table 3 illustrates the survey result of LIC of the population of Chittagong.

***Table 3:*** *LICs of the Total Population of Chittagong*

| Type | Settlements | | Households | | Population | |
|---|---|---|---|---|---|---|
| | No. | % | No. | % | No. | % |
| Extremely Poor | 1,574 | 27.2 | 134,595 | 44.6 | 645,450 | 44.6 |
| Very Poor | 1,360 | 23.5 | 60,896 | 20.2 | 292,330 | 20.2 |
| Moderately Poor | 1,561 | 27.0 | 63,977 | 21.2 | 306,810 | 21.2 |
| Marginally Poor | 1,283 | 22.2 | 42,059 | 14.0 | 202,610 | 14.0 |
| **Total** | **5,778** | **100.0** | **301,527** | **100.0** | **1,447,200** | **100.0** |

### 4.2. GIS Database Design

According to survey data, GIS database has been designed. In this research Arc GIS 10 has been the input data including settlement ID, settlement name, FID, shape, perimeter, area, slum id, ward, zone, category and settle_Id etc. Figure 2 illustrates the output information about the proposed model.

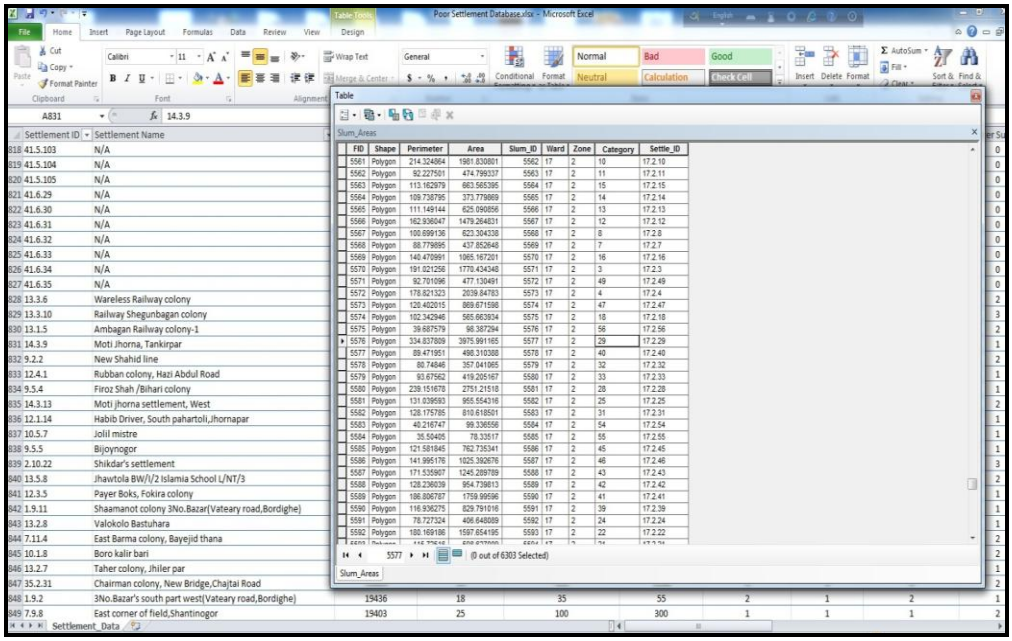

***Figure 2:*** *Attribute Table of GIS Data*

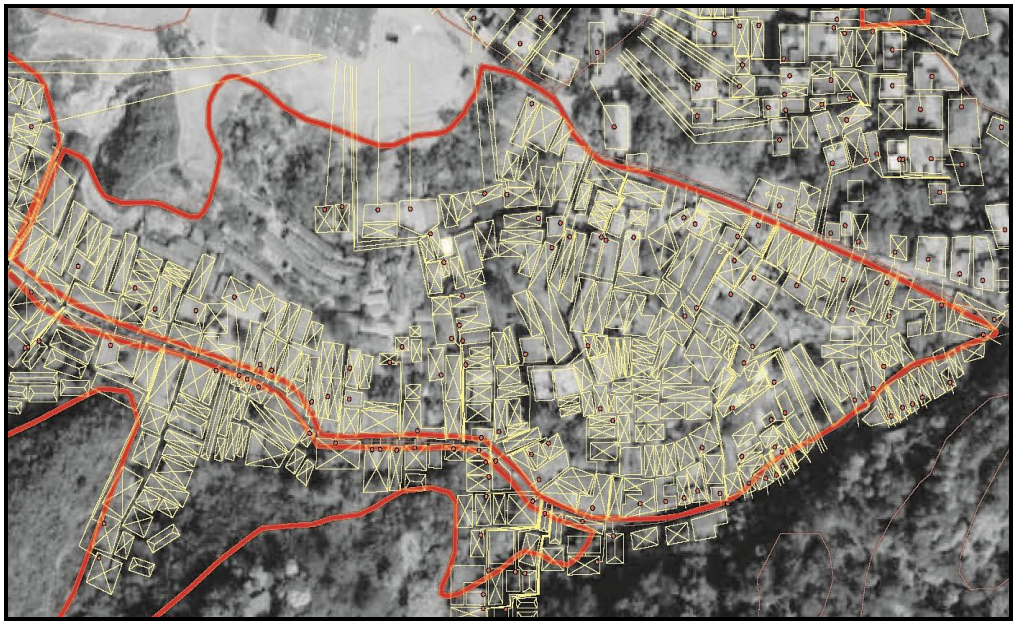

***Figure 3:*** *GIS Based Water Supply Model (Output map)*

The Figure 3 displays overall mapped information about a household or proposed meter. The information including shape of structure, proposed service connection (pipe lines) and water meter.

### 4.3. Discussion

Another name of water is life. Pure drinking water is basic rights of the entire citizen. The peoples of slum area suffering many hydrant diseases including skin diseases due to poor quality water used. To ensure minimum pure water is only option to release those diseases. Some NGO takes the water distribution as a business. Therefore, slum peoples suffering and government losses their revenue, GIS can enhance the maintenance and management. In summary, GIS implementation has a list of effect including:

- Will more easily to inspection, repair, replacement and evaluation
- Future system capabilities
- Income of distributed water company will increase
- Quality of life of slum area will improve due to potable water

## 5. Conclusion

GIS concept and tools plays an important role in all aspect of data collection and archiving, support for condition assessment through display and modeling and message dissemination. Water is a scarce commodity for the urban poor, partially due to the inequity of water distribution within the city. The contribution of this study is to ensure potable water demand for peoples of slum area in legal way. Knowledge of population density and establishment of mapping promise for ensure supply as demand thereby greatly aided to improve the quality of life in slum area. The result shown that comparing with traditional methods, this research helps to respond operation and maintenance water supply more rapidly for the emergency monitoring staff.

The study covers vital aspects on the issue of water supply and distribution for poor communities in a large urban city Chittagong, Bangladesh. There are many more aspects of water supply, quality and distribution that need to be studied in greater depth. For instance, the local authorities should need to take the responsibility for their maintenance.

## References

Carver, S.J. *Integrating Multi-Criteria Evaluation with Geographical Information Systems*. International Journal of Geographical Information Systems. 1991. 5 (3) 321-339.

Chen, W., and Suozhong, C., 2010: *Application of GIS Technology in the Emergency Monitoring of Sudden Air Pollution Accident*. 2nd International Conference on Information Science and Engineering (ICISE). 3550-3555.

Guler, H., and Jovanovic, S. *The Application of Modern GIS Technology in the Development of Railway Asset Management Systems*. International Conference on Systems, Man and Cybernetics. 2004. 5; 4153-4158.

Higgins, E., Taylor, M., Francis, H., Jones, M., and Appleton, D. *The Evolution of Geographical Information Systems for Fire Prevention Support*. Fire Safety Journal. 2014. 69; 117-125.

Johnson, L.E., 2009: *Geographic Information Systems in Water Resources Engineering*. CRC Press.

Lian, W., and Yan, Q., 2010: *The Application of GIS Technology in the Petroleum Exploration*. International Conference on Environmental Science and Information Application Technology (ESIAT). 257-259.

Maguire, D.J., Goodchild, M.F., and Rhind, D. *An Overview and Definition of GIS*. Geographical Information Systems: Principles and Applications. 1991. 1; 9-12.

Mirats Tur, J.M., Zinggerling, C., and Murtra, A.C., 2009: *Geographical Information Systems for Map Based Navigation in Urban Environments.* Robotics and Autonomous Systems. 922-930.

Neil Chadder, 2013: *Institutional Development Consultancy Service under Karnaphuli Water Supply Project Final Report on Water Supply for the Slum Dwellers.*

Pond, K., 2005: *Water Recreation and Disease.* London, UK: IWA Publishing.

Sihua, L., 2011: *GIS Technology Application to Analyzing Landscape Pattern of Zhangjiajie City.* International Conference on Intelligent Computation Technology and Automation (ICICTA). 556-558.

Straume, K. *The Social Construction of a Land Cover Map and its Implications for Geographical Information Systems (GIS) as a Management Tool.* Land Use Policy. 2014. 39; 44-53.

Sundararaman, B., Vinothan, K.G., and Lalwin, M. *Urban Hydrology - A Case Study on Water Supply and Sewage Network for Madurai Region, Using Remote Sensing & GIS Techniques*. International Journal of Engineering and Science. 2012. 1 (8) 7-12.

Xin-hai, L., and Yu-juan, L., 2010: *Research on Application Technology of GIS Data in Intelligent Transportation System (ITS)*. International Conference on Mechanic Automation and Control Engineering (MACE). 2787-2790.

Yi-chuan, Z., and Li-fang, Q., 2008: *The Application of GIS Technology in Urban Landscape Planning and Design in China*. International Workshop on Education Technology & Training and International Workshop on Geoscience & Remote Sensing (ETT and GRS). 95-98.

Zunying, H., Fengxia, G., and Wenbao, L., 2010: *The Application of Spatial Analysis Functions of GIS Technology in Urban Planning*. 2nd International Conference on Information Science and Engineering (ICISE). 4125-4128.